



UNIVERSITAT DE  
BARCELONA

# Síntesis biocatalíticas concurrentes de compuestos quirales multifuncionales. Cascadas de aldosas con transaminasas o cetoreductasas

Carlos José Moreno Fontalba

**ADVERTIMENT.** La consulta d'aquesta tesi queda condicionada a l'acceptació de les següents condicions d'ús: La difusió d'aquesta tesi per mitjà del servei TDX ([www.tdx.cat](http://www.tdx.cat)) i a través del Dipòsit Digital de la UB ([diposit.ub.edu](http://diposit.ub.edu)) ha estat autoritzada pels titulars dels drets de propietat intel·lectual únicament per a usos privats emmarcats en activitats d'investigació i docència. No s'autoritza la seva reproducció amb finalitats de lucre ni la seva difusió i posada a disposició des d'un lloc aliè al servei TDX ni al Dipòsit Digital de la UB. No s'autoritza la presentació del seu contingut en una finestra o marc aliè a TDX o al Dipòsit Digital de la UB (framing). Aquesta reserva de drets afecta tant al resum de presentació de la tesi com als seus continguts. En la utilització o cita de parts de la tesi és obligat indicar el nom de la persona autora.

**ADVERTENCIA.** La consulta de esta tesis queda condicionada a la aceptación de las siguientes condiciones de uso: La difusión de esta tesis por medio del servicio TDR ([www.tdx.cat](http://www.tdx.cat)) y a través del Repositorio Digital de la UB ([diposit.ub.edu](http://diposit.ub.edu)) ha sido autorizada por los titulares de los derechos de propiedad intelectual únicamente para usos privados enmarcados en actividades de investigación y docencia. No se autoriza su reproducción con finalidades de lucro ni su difusión y puesta a disposición desde un sitio ajeno al servicio TDR o al Repositorio Digital de la UB. No se autoriza la presentación de su contenido en una ventana o marco ajeno a TDR o al Repositorio Digital de la UB (framing). Esta reserva de derechos afecta tanto al resumen de presentación de la tesis como a sus contenidos. En la utilización o cita de partes de la tesis es obligado indicar el nombre de la persona autora.

**WARNING.** On having consulted this thesis you're accepting the following use conditions: Spreading this thesis by the TDX ([www.tdx.cat](http://www.tdx.cat)) service and by the UB Digital Repository ([diposit.ub.edu](http://diposit.ub.edu)) has been authorized by the titular of the intellectual property rights only for private uses placed in investigation and teaching activities. Reproduction with lucrative aims is not authorized nor its spreading and availability from a site foreign to the TDX service or to the UB Digital Repository. Introducing its content in a window or frame foreign to the TDX service or to the UB Digital Repository is not authorized (framing). Those rights affect to the presentation summary of the thesis as well as to its contents. In the using or citation of parts of the thesis it's obliged to indicate the name of the author.

**Síntesis biocatalíticas concurrentes de compuestos  
quirales multifuncionales. Cascadas de aldosas con  
transaminasas o cetoreductasas.**

Instituto de Química Avanzada de Cataluña (IQAC)  
Consejo Superior de Investigaciones Científicas (CSIC)

Universidad de Barcelona  
Facultad de Farmacia.  
Programa de Doctorado de Biotecnología.

**Carlos José Moreno Fontalba**  
**2023**

UNIVERSIDAD DE BARCELONA  
FACULTAD DE FARMACIA Y CIENCIAS DE LA ALIMENTACIÓN  
PROGRAMA DE DOCTORADO DE BIOTECNOLOGÍA

INSTITUTO DE QUÍMICA AVANZADA DE CATALUÑA

**Síntesis biocatalíticas concurrentes de compuestos quirales multifuncionales: Cascadas de aldosas con transaminasas o cetoreductasas.**

Memoria presentada por Carlos José Moreno Fontalba para optar al título de Doctor por la Universidad de Barcelona.

Directores:

Dr. Pere Clapés Saborit

Dr. Karel Hernández Sánchez

Tutora:

Dra. Josefa Badia Palacín

Doctorando:

Carlos José Moreno Fontalba

**Carlos José Moreno Fontalba  
2023**

**Dedicatoria**

A toda mi familia, amigos y personas que siempre han creído en mí.

## **Agradecimientos.**

Quiero agradecer a mis directores de Tesis, los Dres. Pere Clapés y Karel Hernández por todo el apoyo, dedicación, confianza y paciencia durante toda la Tesis. Esto definitivamente no hubiera sido posible sin ustedes. Pere, gracias por los buenos consejos (académicos y personales), por permitirme formar parte del equipo, por estar siempre dispuesto y por tratar de encontrar siempre una solución a todo. Karel, no sé ni por donde empezar. Cuando llegue no sabía en lo que me estaba metiendo, menos mal que siempre estuviste presente, gracias por tantas cosas, sobre todo por la paciencia y el apoyo en los altos y bajos de la Tesis y de la vida.

A todas las personas relacionadas con esta Tesis, ya sea a través de colaboraciones científicas (Simon Charnok, Samantha Gittings, Michael Bolte, Dieter Schollmeyer, Teodor Parella y Jordi Bujons) o con actividades y trámites académicos y/o universitarios (Josefa Badia Palacín) mil gracias por su apoyo y siempre su buena disposición.

A todas las personas que me acompañaron durante todo este proceso, amigos y compañeros de trabajo, muchas gracias por hacer agradable y confortable cada día. Hay una muy especial, fue un apoyo en todo momento, gracias por estar en los días duros en el laboratorio, pero, muchas gracias también por estar en los buenos momentos, que fueron muchos. Gracias por escucharme y confiar en mí, Roser mil gracias.

A mi padre y hermanos por todas las lecciones de vida, por todo el cariño y palabras de aliento, algunos de mis hermanos me dieron la oportunidad de ser tío de unos seres maravillosos, esto también es de ustedes.

A mi esposa por todo el tiempo, comprensión y amor durante todos estos años, por todas las cosas que hemos tenido que pasar, y ahora con la ilusión y el sentimiento maravilloso de ser padres, un millón de gracias por tanto.

# **Síntesis biocatalíticas concurrentes de compuestos quirales multifuncionales. Cascadas de aldosas con transaminasas o cetoreductasas.**

## **Resumen.**

Las reacciones enzimáticas en cascada concurrentes o consecutivas han sido objeto de especial atención en el desarrollo de estrategias sintéticas de moléculas complejas. La ventaja de estas estrategias radica en que eliminan la necesidad de purificar los compuestos intermediarios, haciendo más eficiente el proceso sintético. En esta Tesis, se estudia el diseño de rutas biocatalíticas para la síntesis de compuestos quirales a partir de precursores sencillos, en el que cada reacción enzimática contribuye a aumentar el grado de complejidad de las moléculas finales. Con este enfoque, se sintetizaron derivados de  $\gamma$ -hidroxi- $\alpha$ -aminoácidos, 2-hidroxi-4-butirolactonas y del ácido 2-hidroxi-4-*aril*but-3-enóico. Los  $\gamma$ -hidroxi- $\alpha$ -aminoácidos por sus propiedades biológicas son relevantes en la industria farmacéutica. Por ejemplo, la (2*S*,3*R*,4*S*)-4-hidroxiisoleucina, la 4-hidroxi-L-norvalina y el ácido 4-hidroxi-*pipecólico* se utilizan en el tratamiento de la diabetes mellitus. Además, estos compuestos son precursores quirales de moléculas bioactivas, como antibióticos, fungicidas y herbicidas, tales como, las  $\alpha$ -amino- $\gamma$ -butirolactonas, la 4,5-dihidroxinorvalina o el ácido 4-hidroxi-*pirog glutámico* y sus derivados. En este sentido, en el capítulo 3.1 nos planteamos la síntesis diastereoselectiva de  $\gamma$ -hidroxi- $\alpha$ -aminoácidos a través de reacciones enzimáticas consecutivas acoplando una aldolasa y varios sistemas de transaminación con excelente enantioselectividad. Los  $\gamma$ -hidroxi- $\alpha$ -aminoácidos fueron transformados por medios químicos en  $\alpha$ -amino- $\gamma$ -butirolactonas (12 compuestos). Por otra parte, los derivados de 2-hidroxiácidos y las 2-hidroxi-4-butirolactonas son sintones relevantes para la síntesis de moléculas con actividad biológica, tanto naturales como sintéticas, así como auxiliares quirales en síntesis orgánica asimétrica. Para la obtención de estas moléculas, se han desarrollado diversos métodos de síntesis, como la reducción asimétrica con complejos metálicos, reacciones aldólicas estereoselectivas con metal u organocatálisis, y reducción enzimática, entre otros. En el capítulo 3.2 se aborda la síntesis diastereoselectiva de 2-hidroxi-4-butirolactonas mediante reacciones aldólicas catalizadas por una aldolasa estereoselectiva, seguida de reducción del grupo carbonilo de los productos aldólicos utilizando deshidrogenasas estereocomplementarias. En total se sintetizaron 29 productos:

los enantiómeros de la 2-hidroxi-4-butirolactona (>99% ee), 2-hidroxi-3-alkil-4-butirolactonas con configuración (2*R*,3*S*), (2*S*,3*S*), (2*R*,3*R*), o (2*S*,3*R*) con razones diastereomérica entre 60:40 a 98:2. y 2-hidroxi-4-alkil-4-butirolactonas con configuración (2*S*,4*R*) con 87:13 a 98:2 razón diastereomérica).

Finalmente, los derivados del ácido 2-hidroxi-4-arylbut-3-enóico son precursores relevantes en la síntesis de fármacos (p. ej. Enalapril, lisinopril, Cilapril o Benazepril) inhibidores de la enzima convertidora de angiotensina, usados en el tratamiento de disminuyen de la presión arterial. En el capítulo 3.3, se aprovecha la actividad promiscua de la enzima  $\Delta^1$ -piperidina-2-carboxilato/ $\Delta^1$ -pirrolina-2-carboxilato reductasa de *Pseudomonas syringae* pv. tomato DSM 50315 (DpkA) para lograr la síntesis estereoselectiva de ácidos 2-hidroxi-4-arylbut-3-enóicos. La estrategia sintética consistió en reacciones enzimáticas consecutivas entre la aldolasa HBPA, que catalizó reacciones de condensación aldólica entre piruvato y aldehídos aromáticos, seguida de la reducción estereoselectiva catalizada por la DpkA. En total, se sintetizaron 9 derivados del ácido 2-hidroxi-4-arylbut-3-enóico con configuración (*S,E*) con un 87-99% de pureza enantiomérica.

**Palabras claves:** Biocatalizadores, 4-hidroxi-2-oxácidos, Aminación reductiva, 2-Oxoácidos Aldolasa y Promiscuidad enzimática.

# Concurrent biocatalytic syntheses of multifunctional chiral compounds. Aldoses cascades with transaminases or ketoreductases.

## Abstract.

Concurrent or consecutive enzymatic cascade reactions have received special attention in the development of synthetic strategies for complex molecules. The advantage of these strategies is that they eliminate the need to purify the intermediate compounds, making the synthetic process more efficient. In this thesis, we study the design of biocatalytic routes for the synthesis of chiral compounds from simple precursors, in which each enzymatic reaction contributes to increase the degree of complexity of the final molecules. With this approach, derivatives of  $\gamma$ -hydroxy- $\alpha$ -amino acids, 2-hydroxy-4-butyrolactones and 2-hydroxy-4-arylbut-3-enoic acid were synthesized. The  $\gamma$ -hydroxy- $\alpha$ -amino acids are relevant in the pharmaceutical industry due to their biological properties. For example, (2*S*,3*R*,4*S*)-4-hydroxyisoleucine, 4-hydroxy-L-norvaline and 4-hydroxypipericolic acid are used in the treatment of diabetes mellitus. In addition, these compounds are chiral precursors of bioactive molecules such as antibiotics, fungicides and herbicides, such as  $\alpha$ -amino- $\gamma$ -butyrolactones, 4,5-dihydroxynorvaline or 4-hydroxypyroglutamic acid and its derivatives. In this sense, in chapter 3.1 we approached the diastereoselective synthesis of  $\gamma$ -hydroxy- $\alpha$ -amino acids through consecutive enzymatic reactions coupling an aldolase and several transamination systems with excellent enantioselectivity. The  $\gamma$ -hydroxy- $\alpha$ -amino acids were chemically transformed into  $\alpha$ -amino- $\gamma$ -butyrolactones (12 compounds). On the other hand, 2-hydroxy acid derivatives and 2-hydroxy-4-butyrolactones are relevant synthons for the synthesis of biologically active molecules, both natural and synthetic, as well as chiral auxiliaries in asymmetric organic synthesis. To obtain these molecules, several synthesis methods have been developed, such as asymmetric reduction with metal complexes, stereoselective aldol reactions with metal or organocatalysis, and enzymatic reduction, among others. Chapter 3.2 deals with the diastereoselective synthesis of 2-hydroxy-4-butyrolactones by aldol reactions catalyzed by a stereoselective aldolase, followed by reduction of the carbonyl group of the aldol products using stereocomplemental dehydrogenases. In total 29 products were synthesized: the enantiomers of 2-hydroxy-4-butyrolactone (>99% ee), 2-hydroxy-3-alkyl-4-butyrolactones with (2*R*,3*S*), (2*S*,3*S*), (2*R*,3*R*), or (2*S*,3*R*)



configuration with diastereomeric ratios between 60:40 to 98:2. and 2-hydroxy-4-alkyl-4-butyrolactones with (2*S*,4*R*) configuration with 87:13 to 98:2 diastereomeric ratio. Finally, 2-hydroxy-4-arylbut-3-enoic acid derivatives are relevant precursors in the synthesis of angiotensin-converting enzyme inhibitors (e.g. Enalapril, lisinopril, Cilapril or Benazepril) used in the treatment of blood pressure lowering. In chapter 3.3, the promiscuous activity of the enzyme  $\Delta^1$ -piperidine-2-carboxylate/ $\Delta^1$ -pyrroline-2-carboxylate reductase from *Pseudomonas syringae* pv. tomato DSM 50315 (DpkA) is exploited to achieve the stereoselective synthesis of 2-hydroxy-4-arylbut-3-enoic acids. The synthetic strategy consisted of consecutive enzymatic reactions between HBPA aldolase, which catalyzed aldol condensation reactions between pyruvate and aromatic aldehydes, followed by stereoselective reduction catalyzed by DpkA. In total, 9 2-hydroxy-4-arylbut-3-enoic acid derivatives with (*S,E*)-configuration and 87-99% enantiomeric purity were obtained.

**Keywords:** Biocatalysts, 4-hydroxy-2-oxoacids, Reductive amination, 2-Oxoacid Aldolase and Enzyme Promiscuity.

## **Lista de abreviatura usadas frecuentemente en esta Tesis.**

**ACN:** Acetonitrilo.

**AcOEt:** Acetato de etilo.

**API:** Principio activo farmacéutico.

**CIA:** Cromatografía de intercambio aniónico.

**CIC:** Cromatografía de intercambio catiónico.

**DMAP:** 4-Dimetilaminopiridina

**DMF:** Dimetilformamida.

**DMSO:** Dimetilsulfóxido.

**dr:** Relación de diastereoisómeros.

**EC:** Número de la comisión de enzimas.

**EDAC:** 1-etil-3-(3-dimetilaminopropil)carbodiimida, clorhidrato

**ee:** Exceso enantiomérico.

**HPLC:** Cromatografía Líquida de Alta Eficacia.

**HOBt:** Hidroxibenzotriazol.

**IBX:** Ácido 2-iodobenzoico.

**IPTG:** Isopropil- $\beta$ -D-1-tiogalactopiranosido.

**IUBMB:** Unión Internacional de Bioquímica y Biología Molecular.

**PDB:** Banco de datos de proteínas

**PLP:** Piridoxal fosfato.

**RMN:** Resonancia magnética nuclear.

**TA:** Transaminasas.

**TEA:** Trietilamina.

**THF:** Tetrahidrofurano.

**TLC:** Cromatografía de capa fina

**ThDP:** Pirofosfato de tiamina.

## **Abreviaturas de grupos protectores usados**

**Boc:** *tert*-butiloxicarbonilo

**Cbz:** Benciloxicarbonil.

**PheAc:** Fenilacetil

**Ts:** *p*-toluenosulfonilo

## **SUMARIO.**

**Sección I:** Introducción general, contiene una revisión de los aspectos teóricos y antecedentes más relevantes para esta Tesis, por ejemplo: biocatálisis, reacciones y promiscuidad enzimáticas, cascadas biocatalíticas, generalidades de las enzimas utilizadas en esta Tesis: aldosas, transaminasas y óxido-reductasas. Referencias bibliográficas.

**Sección II:** Objetivos, expone la meta general de esta Tesis. Se incluye una lista de objetivos específicos, cada uno de ellos corresponde a un artículo científico que serán presentados en capítulos posteriores.

**Sección III:** Contiene las publicaciones (Capítulos 3.1 y 3.2) y un manuscrito para una publicación (Capítulo 3.3) productos del trabajo experimental realizado en esta Tesis.

- **Capítulo 3.1** Síntesis de derivados de 4-hidroxi aminoácidos mediante reacciones enzimáticas en tándem de adición aldólica y transaminación.
- **Capítulo 3.2** Síntesis estereoselectiva de 2-hidroxi-4-butirolactonas mediante reacciones enzimáticas en tándem de adición aldólica y reducción.
- **Capítulo 3.3** Ampliación de las aplicaciones sintéticas de la  $\Delta^1$ -piperidina-2-carboxilato/ $\Delta^1$ -pirrolina-2-carboxilato reductasa de *Pseudomonas syringae* (DpkA). Síntesis estereoselectiva de derivados del ácido (*S,E*)-2-hidroxi-4-amilbut-3-enoico.

**Sección IV:** Se presenta un análisis y discusión integrativa de los resultados de la Tesis.

**Sección V:** En este apartado se presentan las conclusiones finales de la Tesis.

**Sección VI:** Materiales y métodos de cada capítulo, en este apartado se presentan los procedimientos y condiciones experimentales de cada una de las síntesis químicas o enzimáticas realizadas en esta Tesis. Además, añaden los experimentos de cristalización y difracción de rayos X para determinar la estereoquímica absoluta de los productos sintetizados, así como, modelos moleculares de complejos Enzima-Sustrato.

**Anexos:** Comprende los espectros de RMN ( $^1\text{H}$ ,  $^{13}\text{C}$ , COSY, HSQC, HMBC y NOESY) de los compuestos purificados: material de partida, productos intermediarios y productos finales. Esta información se encuentra en el CD (o lápiz de memoria) adjunto en este trabajo.

## Tabla de contenido

## SECCIÓN I

<b>INTRODUCCIÓN GENERAL</b> .....	1
<b>1.1.</b> Biocatálisis .....	1
<b>1.2.</b> Clasificación de las enzimas .....	2
<b>1.3.</b> Promiscuidad enzimática .....	3
<b>1.4.</b> Sistemas enzimáticos acoplados .....	6
<b>1.5.</b> Clasificación de las cascadas enzimáticas .....	8
<b>1.6.</b> Aldolasas.....	14
<b>1.7.</b> Piruvato aldolasas .....	16
<b>1.8.</b> Transaminasas.....	24
<b>1.9.</b> Óxido-reductasas .....	28
Referencias.....	34

## SECCIÓN II

<b>OBJETIVOS</b> .....	40
<b>2.1</b> Objetivo general.....	40
<b>2.2</b> Objetivos específicos .....	40

## SECCIÓN III

<b>Capítulo 3.1:</b> Synthesis of $\gamma$ -Hydroxy- $\alpha$ -amino Acid Derivatives by Enzymatic Tandem Aldol Addition–Transamination Reactions.....	42
<b>Capítulo 3.2:</b> Biocatalytic synthesis of homochiral 2-hydroxy-4-butyrolactone derivatives by tandem aldol addition and carbonyl reduction. ....	54
<b>Capítulo 3.3:</b> Expanding synthetic applications of $\Delta^1$ -Piperidine-2-carboxylate/ $\Delta^1$ -pyrroline-2-carboxylate reductase from <i>Pseudomonas syringae</i> (DpkAPsyrin). Biocatalytic asymmetric synthesis of (S,E)-2-hydroxy-4-arylbut-3-enoic acid derivatives. ....	66

## SECCIÓN IV

<b>DISCUSIÓN DE RESULTADOS</b> .....	75
--------------------------------------	----

Referencias bibliográficas ..... 120

**SECCIÓN V**

**CONCLUSIONES** ..... 123

**SECCIÓN VI**

**Materiales y métodos del Capítulo 3.1** ..... 124

**Materiales y métodos del Capítulo 3.2** ..... 214

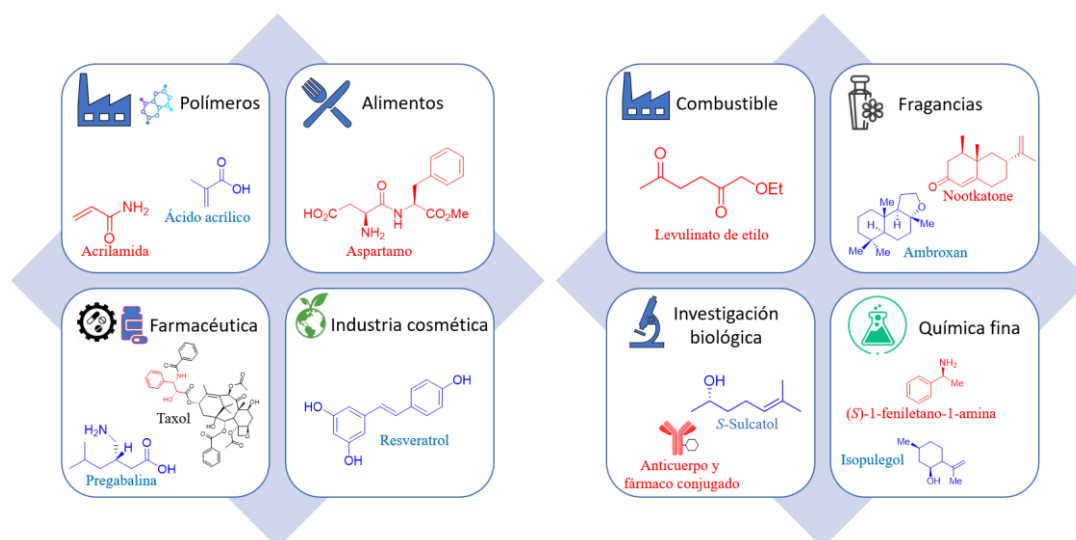
**Materiales y métodos del Capítulo 3.3** ..... 278

## 1.1. Biocatálisis

La biocatálisis es un campo entre la química, bioquímica y biología que comprende el uso de enzimas como catalizadores en reacciones orgánicas que no se dan en su entorno natural. Las enzimas, como cualquier otro catalizador artificial, aumenta la velocidad de una reacción química, disminuyendo la energía de activación del proceso.<sup>1</sup> Durante la catálisis enzimática se pueden dar varios mecanismos catalíticos como: catálisis ácido-base, covalente, mediada por cationes metálicos (ácidos de Lewis), electrostática, por efectos de proximidad y orientación y por estabilización preferencial del estado de transición de la reacción.<sup>2</sup> A diferencia de los catalizadores desarrollados por el hombre, las enzimas poseen una elevada eficiencia catalítica determinada por la especificidad en la unión del sustrato, combinado con una óptima distribución de los grupos catalíticos en el centro activo y una elevada reactividad del sustrato en el complejo enzima-sustrato.<sup>3</sup>

La disposición de los residuos de aminoácidos que participan en la unión del sustrato y la catálisis es, por supuesto, el resultado de procesos de evolución. La naturaleza ha tenido muchas oportunidades de perfeccionar las enzimas como biocatalizadores, por ejemplo: enzimas como la catalasa (CAT, EC: 1.11.1.6), superóxido dismutasa (SOD, EC: 1.15.1.1), fumarasa (FH, EC: 4.2.1.2) o la acetilcolinesterasa (EC: 3.1.1.7) han alcanzado la *perfección catalítica* al presentar valores de  $k_{cat}/K_m$  en el rango de  $10^8$ - $10^9$  M<sup>-1</sup> lo que hace que la catálisis esté controlada por los procesos de difusión.<sup>1c</sup>

La catálisis enzimática es esencial para que ocurra la mayoría de las reacciones o transformaciones químicas presentes en el metabolismo, funcionando con elevada eficiencia y selectividad.<sup>4</sup> Durante el proceso evolutivo, los organismos han adquirido la capacidad de metabolizar una enorme variedad de compuestos químicos<sup>5</sup>, lo que ha generado una gran diversidad de actividades enzimáticas.<sup>5b,6</sup> Los avances en biología molecular e ingeniería de proteínas han permitido aislar estos catalizadores del medio biológico y modificar su reactividad y selectividad con el objetivo de aplicarlos en síntesis orgánica.<sup>3,7</sup> La elevada eficiencia catalítica de las enzimas, así como, su alta regio y estereoselectividad hace que se disminuya los tiempos de reacción y se simplifique la purificación de los productos finales. Estas ventajas han permitido la implantación de diferentes procesos biocatalíticos en la síntesis de valiosos compuestos de interés industrial (**Figura 1**).<sup>3,7-8</sup>

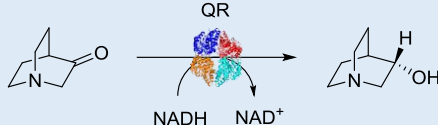
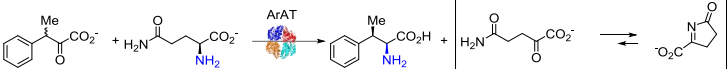
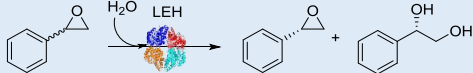
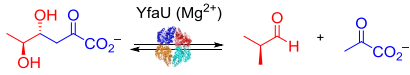
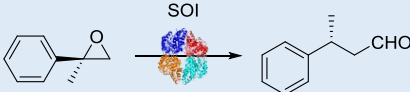
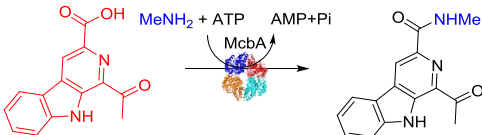


**Figura 1.** Ejemplos de compuestos sintetizados utilizando estrategias enzimáticas o quimioenzimáticas: Polímeros.<sup>8a,d</sup> Alimentos.<sup>8e,f</sup> Combustible.<sup>8g,h</sup> Fragancias.<sup>8i</sup> Farmacéutica.<sup>3</sup> Industria cosmética.<sup>8j</sup> Investigación biológica.<sup>8k,l</sup> Química fina.<sup>8d</sup>

## 1.2. Clasificación de las enzimas

Las enzimas son moléculas de origen biológico constituidas por aminoácidos, conectados entre sí mediante enlaces amida y que adoptan estructuras tridimensionales precisas responsable de su actividad catalítica.<sup>1c</sup> Para estudiar el uso de estas biomoléculas en la síntesis orgánica es necesario, conocer los diferentes tipos de actividades enzimáticas presentes en la naturaleza y su clasificación. Por convención de la Unión Internacional de Bioquímica y Biología Molecular (IUBMB, de sus siglas en inglés *International Union of Biochemistry and Molecular Biology*)<sup>9</sup>, las enzimas se pueden clasificar según el tipo de reacción que catalizan. Se dividen en 7 clases principales: óxido-reductasas, transferasas, hidrolasas, liasas, isomerasas, ligasas (**Tabla I**).<sup>10</sup> Cabe destacar que en 2018 se añadió una séptima clase: las translocasas,<sup>10c</sup> siendo hasta ahora poco relevantes para la biocatálisis. Según la comisión de enzimas (EC por sus siglas en inglés *Enzyme Commission*) estas se identifican mediante números EC que se compone de cuatro elementos separados por puntos (EC a.b.c.d). El primero identifica la clase de reacción catalizada. El segundo número (la subclase) contiene generalmente información sobre el tipo de compuesto o grupo químico implicado la reacción. El tercer número, especifica además el tipo de reacción implicada; y el cuarto número designa el orden en la lista de enzimas descrita de este tipo.<sup>9,10c</sup>

**Tabla I.** Clasificación de las enzimas según IUBMB y ejemplos de uso en Biocatálisis.

Clases de enzimas	Ejemplos de aplicación en Biocatálisis
<p><b>Óxido-reductasas (EC 1.b.c.d)</b></p> <p>Este grupo de enzimas catalizan reacciones de transferencia de electrones.</p>	<p>Reducción estereoselectiva de 3-quinuclidinona catalizado por la 3-Quinuclidinona Reductasa (QR, EC 1.1.1.B52) de <i>Microbacterium luteolum</i>.<sup>11</sup></p> 
<p><b>Transferasas (EC 2.b.c.d)</b></p> <p>Este grupo de enzimas catalizan reacciones de transferencia de grupos funcionales entre moléculas.</p>	<p>Síntesis estereoselectiva de <math>\alpha</math>-aminoácido-<math>\beta</math>-ramificados catalizado por la transaminasa de aminoácidos aromáticos de <i>E. coli</i>. (ArAT, EC 2.6.1.57).<sup>12</sup></p> 
<p><b>Hidrolasas (EC 3.b.c.d)</b></p> <p>Catalizan reacciones de hidrólisis de enlaces C-X (X=C, O, S, y P).</p>	<p>Hidrólisis estereoselectiva de epóxidos catalizado por la limoneno 1,2-epóxido hidrolasa de <i>Rhodococcus erythropolis</i> DCL14 (LEH, EC 3.3.2.8).<sup>13</sup></p> 
<p><b>Liasas (EC 4.b.c.d)</b></p> <p>Catalizan reversiblemente la formación de enlaces C-X (X=C, O ó N) mediante mecanismos diferentes a las Hidrolasas.</p>	<p>Reacción de retro-aldólisis catalizadas por la 2-ceto-3-desoxi-L-ramnonato aldolasa de <i>E coli</i> (YfaU, EC 4.1.2.53).<sup>14</sup></p> 
<p><b>Isomerasas (EC 5.b.c.d)</b></p> <p>Catalizan el reordenamiento intramolecular de grupos.</p>	<p>Isomerización estereoselectiva del (<i>R</i>)-2-metil-2-feniloxirano a (<i>R</i>)-3-fenilbutanal catalizado por la estireno oxido isomerasa de <i>Pseudomonas</i> sp. VLB120 (SOI; EC 5.3.99.7).<sup>15</sup></p> 
<p><b>Ligasas (EC 6.b.c.d)</b></p> <p>Catalizan la formación de enlaces C-X (X = C, O, S, N y P) y P-O. Requieren de energía asociada a la hidrólisis de un enlace de alta energía (ejemplo ATP, AMP).</p>	<p>Reacción de amidación catalizada por la sintasa formadora de enlaces amida –ATP dependiente de <i>Marinactinospora thermotolerans</i> (McbA, EC 6.2.1.-).<sup>16</sup></p> 

Número de enzimas catalogadas por cada tipo a Marzo 2023 (óxido-reductasas 2497, transferasas 2200, Hidrolasas 1815, liasas 854, isomerasas 334, ligasas, 259).<sup>9</sup>

### 1.3. Promiscuidad enzimática.

De acuerdo con Frances H. Arnold, premio Nobel de Química (2018), la promiscuidad catalítica se refiere a la capacidad de una enzima para catalizar, además de su *reacción natural*, reacciones no esperadas que proceden a través de diferentes estados de transición y/o intermediarios reactivos.<sup>17</sup> En 1976, Jensen propuso que las enzimas ancestrales se caracterizaban por un amplio espectro de sustratos y reacciones, y que la selección natural



recogía y afinaba estas diferentes actividades para generar las enzimas actuales con funciones catalíticas específicas.<sup>18</sup> Sin embargo, incluso hoy en día, las enzimas no son tan específicas como se suele pensar. Muchas pueden catalizar otras transformaciones en sus centros activos, lo que se conoce como promiscuidad catalítica.<sup>19</sup> Estas nuevas actividades enzimáticas, a menudo encontradas gracias a una serendipia, resultan muy ventajosas a la hora de extender el uso de las enzimas en síntesis orgánica.<sup>17b,19c</sup>

Por ejemplo, la L-serina hidroximetiltransferasa de *Streptococcus thermophilus* (SHMT, EC 2.1.2.1), *in vivo*, cataliza la formación de L-Ser a partir de  $N^5,N^{10}$ -metilentetrahidrofolato ( $N^5,N^{10}$ -metilenTHF) y Gly.<sup>20</sup> Sin embargo, se ha descrito que *in vitro* esta enzima es capaz de catalizar la adición aldólica de Gly y D-Ala a diferentes aldehídos (**Figura 2**).<sup>21</sup>

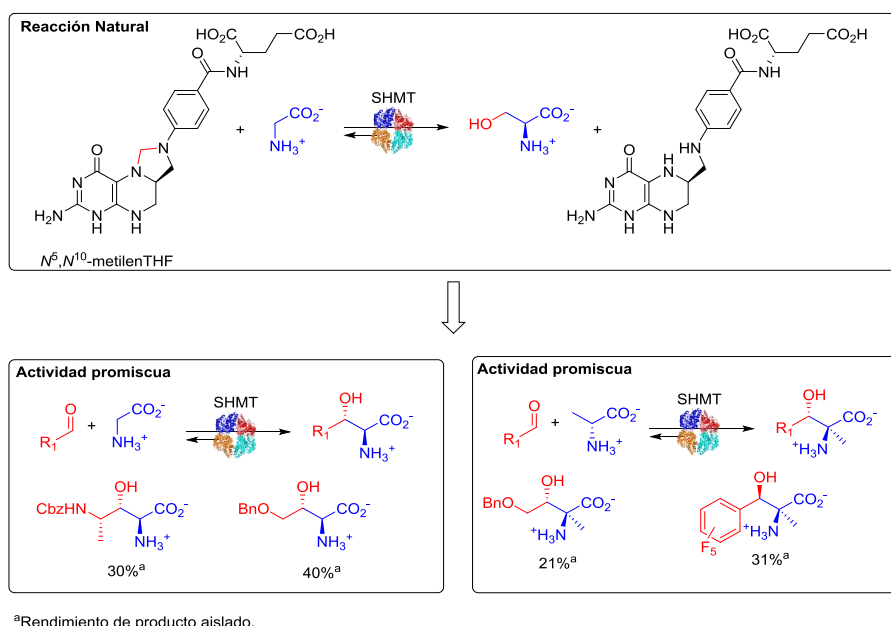


**Figura 2.** La SHMT cataliza *in vivo* la síntesis de L-Ser a partir de  $N^5,N^{10}$ -metilenTHF y Gly. Sin embargo, *in vitro* cataliza la adición aldólica de Gly y D-Ala a aldehídos no naturales.

Otro ejemplo donde se ha encontrado promiscuidad catalítica es la *Trans*-o-hidroxibenzilidenpiruvato hidratasa-aldolasa de *Pseudomonas putida* (HBPA, EC 4.1.2.45) que cataliza la condensación aldólica de piruvato al 2-hidroxibenzaldehído seguido de la deshidratación del aldol.<sup>22</sup> La HBPA es capaz de catalizar la misma reacción con una variedad de aldehídos mostrando promiscuidad hacia el sustrato electrófilo. Sin embargo, en su centro activo solo reconoce al piruvato como sustrato nucleófilo, no pudiendo catalizar reacciones con otros 2-oxoácidos (**Figura 3**).<sup>22-23</sup>

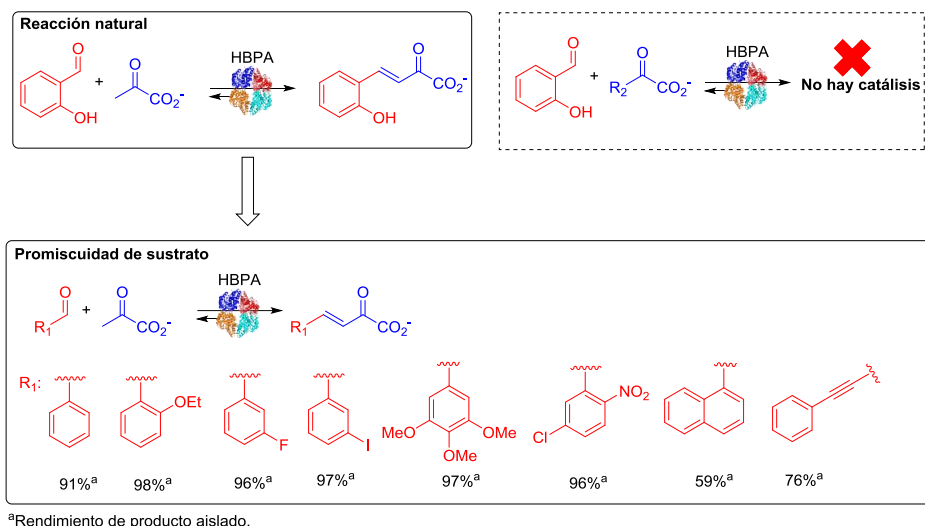


**Figura 3.** Reacción de condensación aldólica catalizada por la HPBA y diversos aldehídos. Se muestra la promiscuidad por el electrófilo de la enzima.

En esta misma enzima se ha reportado promiscuidad hacia el tipo de reacción a catalizar. Esto ocurre cuando existen transformaciones químicas que comparten mecanismos de reacción similares. En este sentido, la HPBA es capaz de catalizar adiciones de Michael de piruvato a  $\beta$ -nitroestirenos, rindiendo después de una descarboxilación oxidativa, ácidos  $\beta$ -aril- $\gamma$ -nitrobutíricos. En este caso, la enzima al catalizar una condensación aldólica tiene como intermediario de reacción la enamina del piruvato (reacción natural) que también puede adicionarse a un compuesto carbonílico  $\alpha,\beta$ -insaturado dando una adición de Michael, promiscuidad catalítica (**Figura 4**).<sup>24</sup>

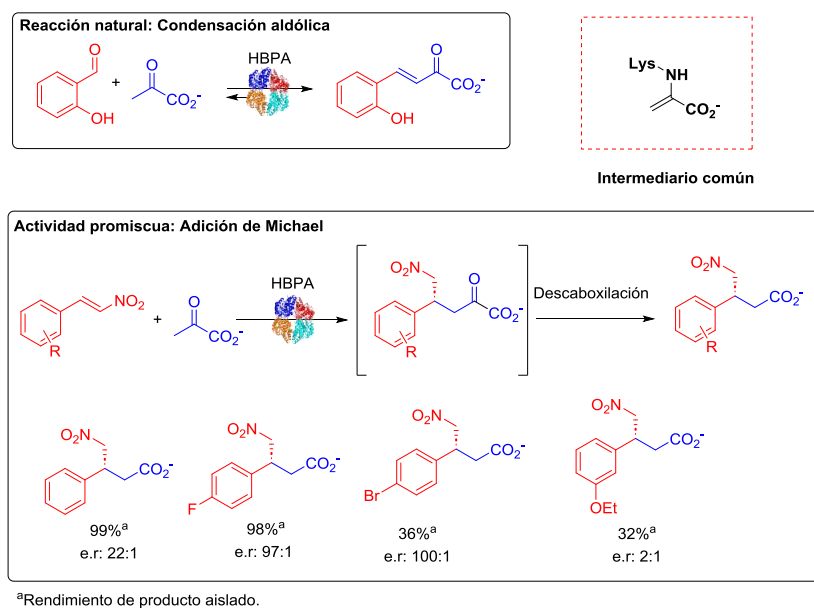


**Figura 4.** Ejemplo de promiscuidad catalítica. Reacción de adición de Michael de piruvato a  $\beta$ -nitroestirenos catalizada por la HPBA.

Esta variación en el comportamiento catalítico natural de las enzimas, se puede optimizar mediante técnicas de biología molecular (p. ej. Evolución dirigida), abriendo un abanico de posibilidades de aplicaciones sintéticas desde el laboratorio hasta la industria.<sup>25</sup> Esta estrategia se utilizó con la halohidrina deshalogenasa de *Agrobacterium radiobacter* AD1 (HHDH, E.C. 4.5.1.-), enzima que cataliza la síntesis de etil (*R*)-4-ciano-3-hidroxi-butanoato, un valioso intermediario en la producción de atorvastatina (fármaco utilizado en el tratamiento de la hipercolesterolemia) a partir del etil (*S*)-4-cloro-3-hidroxi-butanoato, pero, con una baja productividad (**Figura 5**). Utilizando técnicas de evolución dirigida se incrementó la actividad de la enzima hacia el sustrato obteniéndose una variante enzimática que aumenta la productividad del proceso (de 144 mg L<sup>-1</sup> de producto de interés a 576 g L<sup>-1</sup> en 24 h) después de 18 rondas de mutagénesis (**Figura 5**).<sup>19c,25</sup>

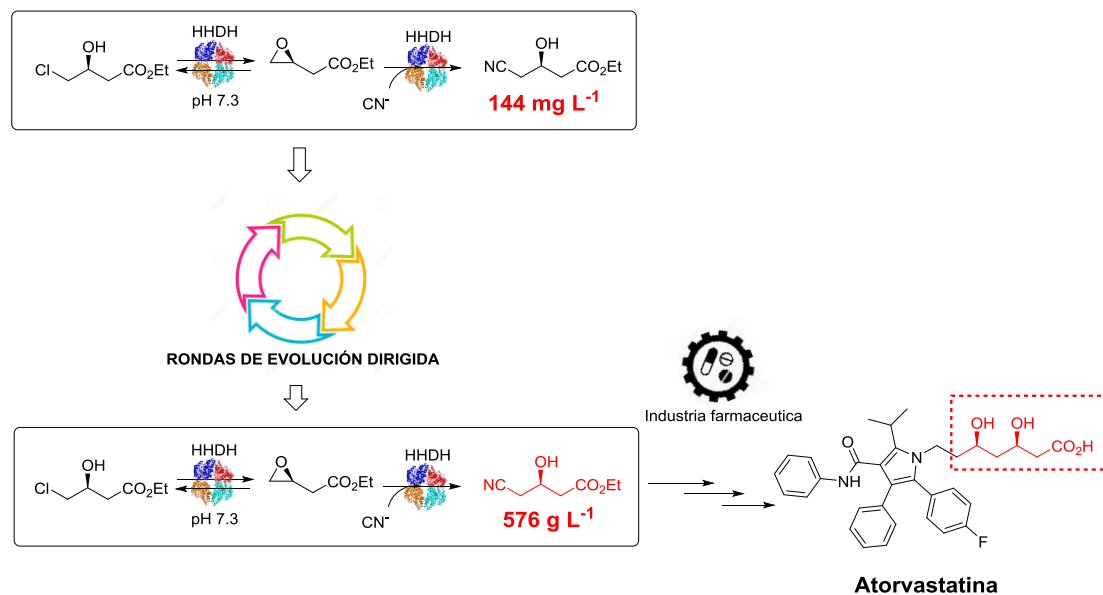
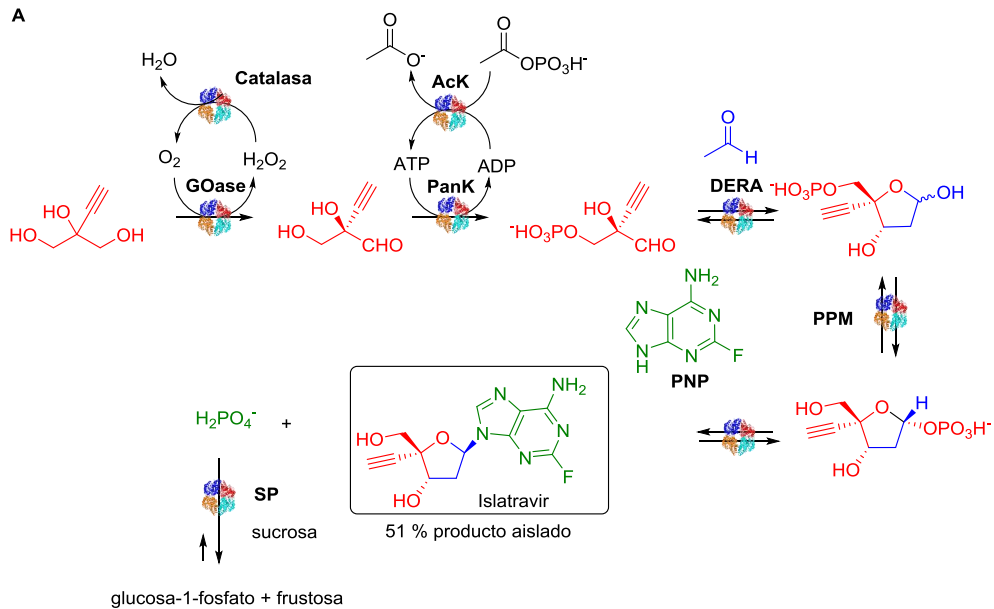


**Figura 5.** Ejemplo de aplicaciones sintéticas desde el laboratorio a escala industrial. La actividad promiscua de una enzima puede ser potenciada a través de rondas de evolución dirigida imitando al proceso evolutivo que se da en la naturaleza durante millones de años. En este ejemplo, se logró una mejora sustancial del biocatalizador que puede ser utilizado en un proceso industrial.

#### 1.4. Sistemas enzimáticos acoplados.

La naturaleza ha permitido, a través de la evolución, acoplar secuencialmente reacciones enzimáticas que se alimentan unas a otras, originando complejas rutas enzimáticas que en su conjunto se conocen como Metabolismo.<sup>1c</sup> *In vitro* las reacciones enzimáticas acopladas, también conocidas como cascadas enzimáticas o concurrentes presentan como ventajas el hecho de poder condensar en un único medio de reacción múltiples etapas de

síntesis, sin necesidad de aislar los compuestos intermediarios, lo que supone una elevada economía atómica (**Figura 6A**).<sup>26</sup> Además, se puede aumentar los rendimientos de productos finales al combinar pasos de síntesis irreversibles que compensen reacciones que estén próximas al equilibrio químico.<sup>48</sup>



**GOase**, galactosa oxidasa (EC 1.1.3.9) ingenierizada de *Fusarium graminearum*.

**Pank**, patotenato quinasa (EC 2.7.1.33) ingenierizada de *E. coli*.

**AcK**, acetate quinasa (EC 2.7.2.1) de *Thermotoga maritima*.

**DERA**, desoxiribosa-5-fosfato aldolasa (EC 4.1.2.4) ingenierizada de *Shewanella halifaxensis*.

**PPM**, fosfopentomutasa (EC 5.4.2.8) ingenierizada de *E. coli*.

**PNP**, purina nucleótido fosforilasa (EC 2.4.2.1) ingenierizada de *E. coli*.

**SP**, sucrosa fosforilasa (EC 2.4.1.1) de *Alloscardovia omnicolens*.

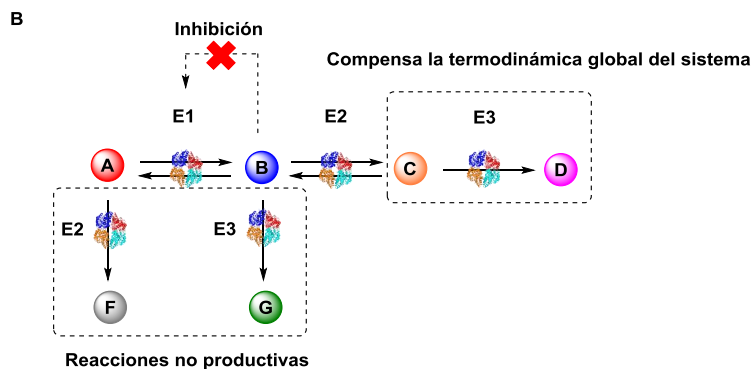


**Figura 6.** Una cascada enzimática permite la síntesis secuencial de moléculas complejas. **A.** Cascada enzimática diseñada para la síntesis del islatravir, retroviral utilizado en el tratamiento del VIH. La reacción catalizada por la sacarosa fosforilasa permite desplazar los equilibrios de las reacciones anteriores. **B.** En una cascada enzimática se minimiza la inhibición por productos y se mejora la termodinámica global del proceso al incluir etapas alejadas del equilibrio químico. Si la especificidad de las enzimas por sus sustratos no es lo suficientemente alta pueden ocurrir reacciones no productivas que atentan contra el rendimiento global del proceso.

La reacción catalizada por la sacarosa fosforilasa (SP, EC 2.4.1.1) permite desplazar los equilibrios en la síntesis enzimática del islatravir (**Figura 6A**). También repercute en un incremento del rendimiento del producto final, el hecho de minimizar la inhibición por producto de una enzima de la cascada al ser eliminado del sistema por el siguiente biocatalizador (**Figura 6B**).<sup>27</sup> Sin embargo, para poder acoplar varios biocatalizadores de manera secuencial, formando una cascada enzimática, tienen que cumplirse dos condiciones fundamentales: *i*) las enzimas que forman la cascada biocatalítica deben mostrar una especificidad de sustrato muy alta, minimizándose reacciones cruzadas que originen rutas estériles y *ii*) las condiciones de reacción (tipo de buffer, pH, fuerza iónica, concentración de co-solventes, temperatura, cofactores, etc) deben permitir una actividad óptima de todos los biocatalizadores del sistema.<sup>3,28</sup>

Las cascadas biocatalíticas no sólo pueden estar formadas por enzimas, también se pueden combinar etapas de síntesis química originando cascadas quimio-enzimáticas. En estos casos se debe seleccionar convenientemente las condiciones de reacción para evitar la inactivación del biocatalizador.<sup>29</sup>

Las reacciones enzimáticas concurrentes son cada vez más comunes en síntesis orgánicas, representando así una tendencia sostenida en la investigación académica y aplicaciones industriales, por esta razón y por las capacidades sintéticas que tienen cada una de las enzimas que se describirán en los siguientes apartados, el desarrollo de esta Tesis constituye una oportunidad para contribuir en diversas áreas, entre ellas la química orgánica, biología, bioquímica, y la biocatálisis, además de permitir el desarrollo de novedosas estrategias sintéticas de compuestos altamente funcionalizados.

## **1.5. Clasificación de las cascadas enzimáticas.**

Las reacciones enzimáticas en cascadas, se pueden clasificar en función de varios criterios, los más utilizados son el entorno donde ocurre la reacción y el número de enzimas que participan en la ruta biosintética. Atendiendo al primer criterio, las cascadas pueden clasificarse en: *in vivo*, cuando los biocatalizadores están confinados dentro de la célula viables o *in vitro*, cuando se trabaja con extractos libres de células o con enzimas purificadas.<sup>28</sup>

En el siguiente ejemplo en nuestro grupo de investigación, se llevó a cabo la síntesis estereoselectiva de D y L-homoserina utilizando un sistema *in vitro* y una cascada cíclica formada por dos enzimas: una piruvato aldolasa y una transaminasa. Como dador de grupos aminos de las transaminasas se utilizó D o L-Ala que permite regenerar el piruvato que volverá a ser utilizado por la aldolasa cerrando el ciclo catalítico (**Figura 7A**).<sup>30</sup> Por su parte, en el sistema *in vivo*, se usó células de *E. coli* enteras liofilizadas, en las que se han co-expresados ambas enzimas. Este sistema compartimentalizado dentro de la célula posee como peculiaridad que utiliza como sustrato la L-Ala generada por el metabolismo celular (**Figura 7B**).<sup>31</sup>

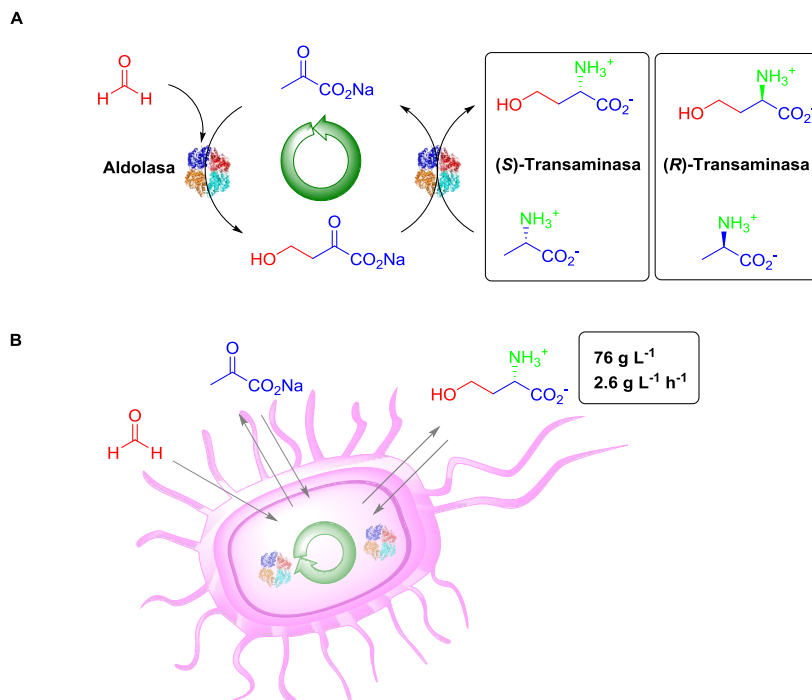


**Figura 7.** Cascada enzimática cíclica utilizada en la síntesis de D y L-homoserina. **A.** Síntesis *in vitro*.<sup>30</sup> **B.** Síntesis *in vivo*.<sup>31</sup>

El segundo criterio para catalogar las cascadas enzimáticas permite clasificarlas en: **monoenzimática y multienzimáticas**. En las cascadas **monoenzimáticas** una sola enzima es capaz de catalizar varias reacciones enzimáticas consecutivas. Por ejemplo, la enzima galactosa oxidasa de *Pichia sp* (GOasa, EC 1.1.3.9) previamente ingenierizada<sup>32</sup>, puede oxidar alcoholes a ácidos carboxílicos, a través del aldehídos producido en una primera reacción, seguido de la oxidación del *gem*-diol a ácidos carboxílicos (**Figura 8**).<sup>33</sup>

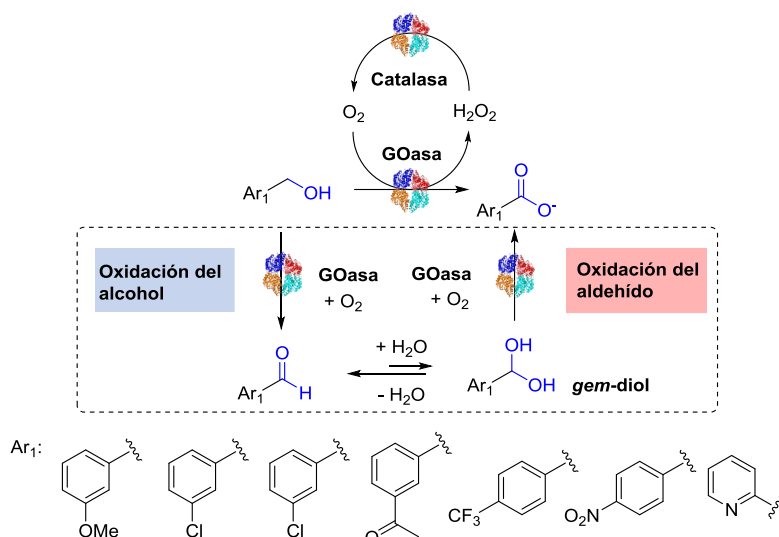


**Figura 8.** Ejemplo de cascada **monoenzimática**. La variante de la GOasa es capaz de realizar una doble oxidación, de alcohol a aldehído, y posteriormente a ácido carboxílico.

Cuando en la ruta biosintética participan dos o más enzimas con diferentes actividades, se denomina cascadas multienzimáticas y pueden distinguirse cinco tipos principales: las cascadas **lineales**, **paralelas**, **ortogonales**, **cíclicas** y **triangulares**.

En las cascadas **lineales**, las enzimas actúan consecutivamente hasta llegar al producto final (**Figura 9A**).<sup>28</sup> Para ilustrar este tipo de cascada, se presenta una alternativa biocatalítica para la síntesis de  $\beta$ -aminoalcoholes quirales, que son motivos estructurales frecuentes en moléculas biológicamente activas. La cascada enzimática comprende la participación de cuatro enzimas que actúan consecutivamente para transformar el estireno en (*S*)-2-amino-2-fenil etanol. La primera reacción es catalizada por la estireno monooxigenasa de *Pseudomonas sp* (SMO, EC 1.14.14.11), que cataliza una epoxidación enantioselectiva generando el (*S*)-epóxido correspondiente. Este compuesto, es convertido a (*S*)-1,2-diol, por acción de una epóxido hidrolasa de *Sphingomonas sp* (SpEH, EC 3.3.2.10). La oxido-reductasa de *Gluconobacter oxydans* (GoSCR, EC 1.1.1.14), oxida al diol y forma la  $\alpha$ -hidroxicetona. Finalmente, la  $\omega$ -transaminasa de *Bacillus megaterium* (BmTA, EC 2.6.1.19) cataliza la transaminación de la  $\alpha$ -hidroxicetona a  $\beta$ -aminoalcohol que forma parte de la molécula del Taxol (**Figura 9B**).<sup>28,34</sup>

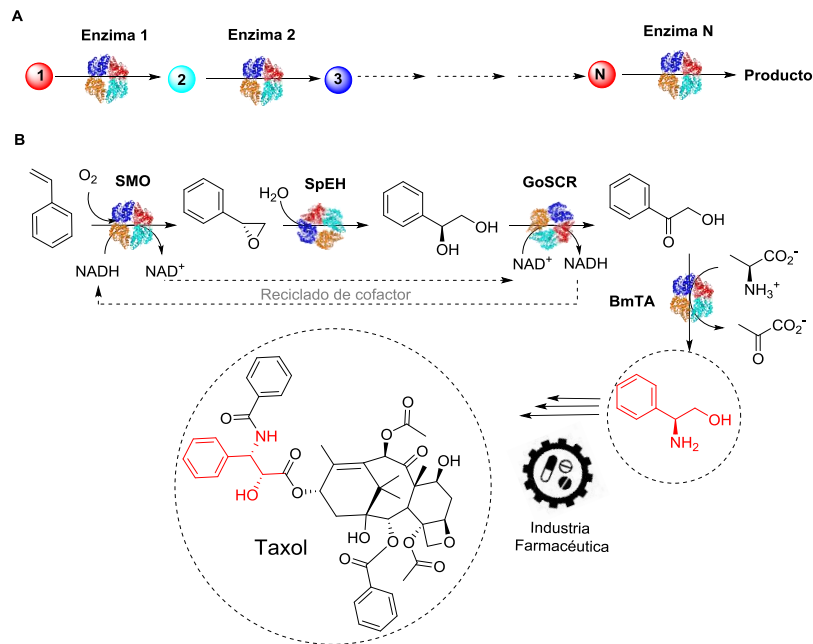


**Figura 9.** Cascadas enzimáticas lineales. **A.** Representación general de una cascada enzimática lineal con participación de N enzimas. **B.** Biotransformación del estireno en (S)-2-amino-2-fenil etanol utilizando una cascada lineal formada por cuatro enzimas. En este sistema se recicla el cofactor ( $NADH/NAD^+$ ) entre la reacción de oxidación y reducción.

Las cascadas **paralelas**, están formadas por pasos enzimáticos complementarios, y en caso de tener un requerimiento específico de un cofactor pueden suplirlo sin la participación de enzimas auxiliares (**Figura 10A**).<sup>28</sup> En la síntesis del ácido L-pipecólico se utilizó este tipo de diseño de cascada enzimática. Para ello, se acopló la lisina deshidrogenasa dependiente de  $NAD^+$  de *Geobacillus stearothermophilus* (*GsLysDH*, EC 1.4.1.15), a una iminoreductasa de *Halomonas elongata* (*HeP5C* EC 1.5.1.2) dependiente de  $NADH$ . La demanda de cofactor entre las dos reacciones es recíproca lo que permite establecer un sistema cerrado de regeneración de cofactores, en la síntesis del intermediario de la Ropivacaina, un fármaco utilizado como anestésico (**Figura 10B**).<sup>35</sup>



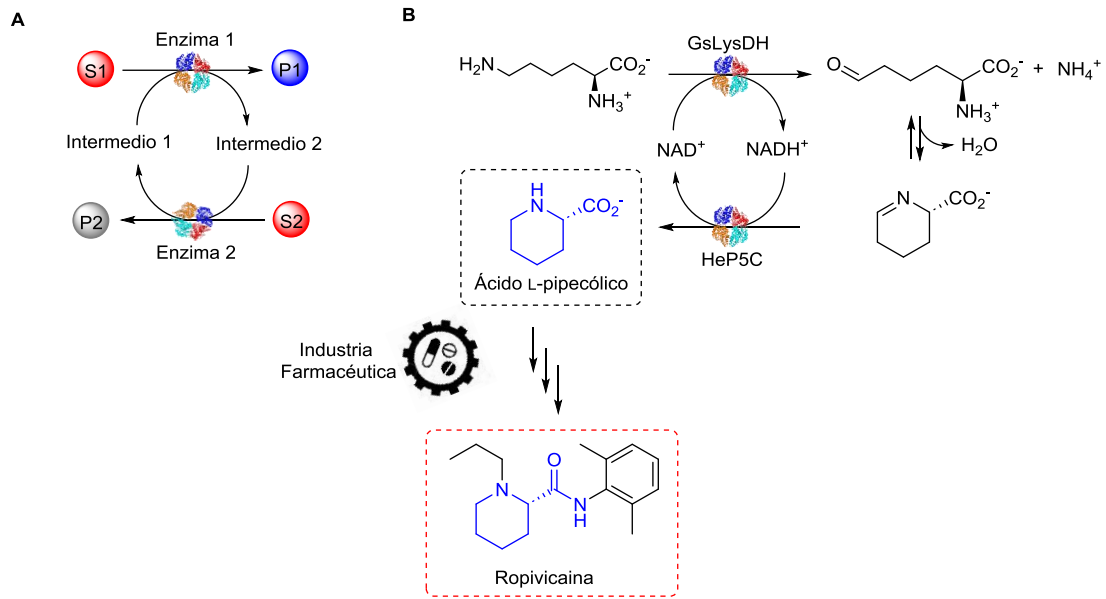


**Figura 10.** Cascadas enzimáticas paralelas. **A.** Esquema general de una cascada enzimática paralela. **B.** Esquema biocatalítico para la síntesis de ácido L-pipecólico. La estrategia consiste en dos etapas enzimáticas paralelas, donde ocurre una desaminación de la Lys en la posición  $\epsilon$  catalizado por la GsLysDH acoplada a la reducción de la imina cíclica catalizado por la HeP5C.<sup>35</sup>

En las cascadas **ortogonales** es necesario incorporar una o más enzimas auxiliares, bien para regenerar algún cofactor, eliminar subproducto(s), mantener estables las condiciones de la reacción o para desplazar equilibrios hacia la formación de producto.<sup>28</sup> Si comparamos las cascadas paralelas con las ortogonales, en las primeras, ambos productos se consideran compuestos valiosos, mientras que, en las cascadas ortogonales, los subproductos generados no lo son, por tanto, se desechan (**Figura 11A**).<sup>36</sup>

El dominio de adenilación de la reductasa de ácidos carboxílicos de *Mycobacterium marinum* (CAR, EC 1.2.1.-) se empleó en reacciones de monoacilación selectiva de diaminas. Sin embargo, la enzima requiere cantidades estequiométricas de ATP para activar al ácido carboxílico en forma de anhídridos mixtos, lo que dificulta notablemente su aplicación incluso a escala de laboratorio. Por ello se ha utilizado en una cascada enzimática ortogonal acoplada a la polifosfato quinasa de clase III de *Cytophaga hutchinsonii* (CHU, EC. 2.7.7.-) que regenera el ATP a partir de polifosfato, lo que permite utilizar cantidades catalíticas del agente activante (**Figura 11B**).<sup>37</sup>

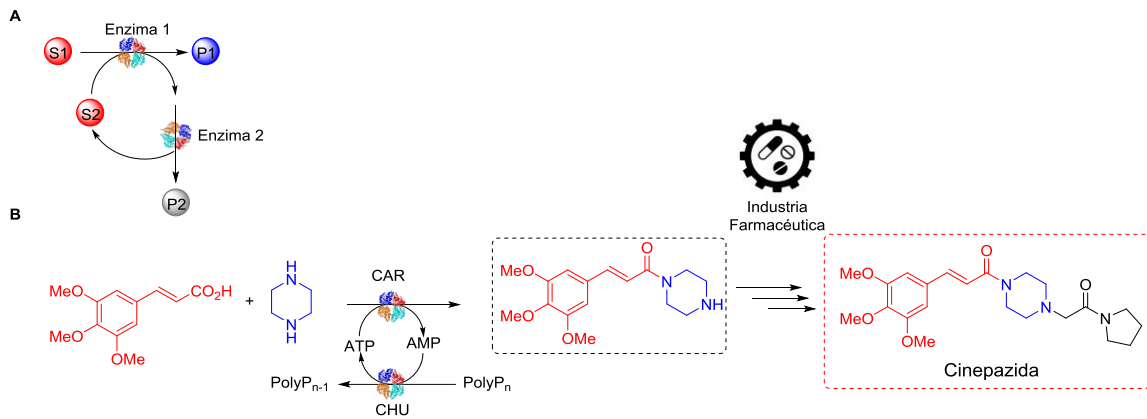


**Figura 11.** Cascadas enzimáticas ortogonales. **A.** Esquema general de la cascada ortogonal. **B.** Reacción de monoacilación selectiva de diaminas.<sup>37</sup>

Por su parte, en las cascadas **cíclicas** hay un reciclado de moléculas, que después de un ciclo de reacción uno de los productos generados se convierte nuevamente en material de partida, favoreciendo la formación del producto de interés que se va acumulando por la repetición del ciclo (**Figura 12A**).<sup>28</sup> En el ejemplo de este tipo de cascada, se utilizó la acetohidroxiácido sintasa I de *E. coli* (AHAS-I, EC 2.2.1.6) para catalizar la adición benzoínica cruzada entre piruvato y benzaldehído, generando (*R*)-fenilacetilcarbinol que posteriormente se transformó en (*1R,2R*)-norpseudoefedrina y (*1R,2S*)-norefedrina mediante transaminasas estereoselectivas de *Aspergillus terreus* (*R*-TA EC 2.6.1.-) y de *Chromobacterium violaceum* (*S*-TA EC 2.6.1.18) respectivamente. Como dador de grupos aminos se utilizó Ala lo que genera piruvato que es reciclado en un nuevo ciclo catalítico (**Figura 12B**).<sup>38</sup>

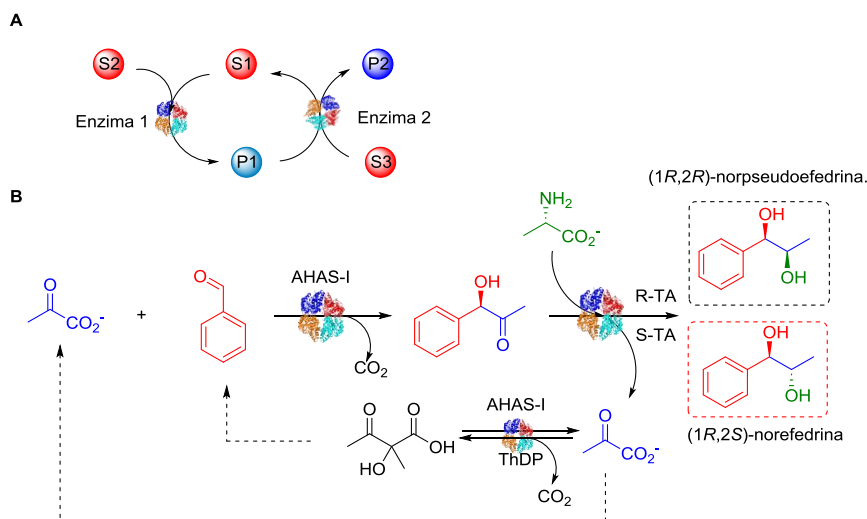


**Figura 12.** Cascadas enzimáticas cíclicas. **A.** Esquema general de una cascada enzimática cíclica. **B.** Síntesis de (*1R,2R*)-norpseudoefedrina y (*1R,2S*)-norefedrina a partir de piruvato y benzaldehído con de reciclaje del piruvato.

Finalmente, las cascadas **triangulares** consisten en sistemas enzimáticos donde el producto de la primera reacción enzimática reacciona con el sustrato inicial por acción de una segunda enzima, dándose un proceso de síntesis convergente (**Figura 13A**).<sup>28</sup> Para ilustrar este tipo de cascadas, se presenta la síntesis de alcaloides derivados de la tetrahydroisoquinolinas, utilizando una transaminasa de *Chromobacterium violaceum* (TAm EC 2.6.1.-) y la norcoclaurina sintasa de origen vegetal (NCS, EC 4.2.1.78), enzima que cataliza una reacción de Pictet–Spengler (**Figura 13B**).<sup>39</sup>

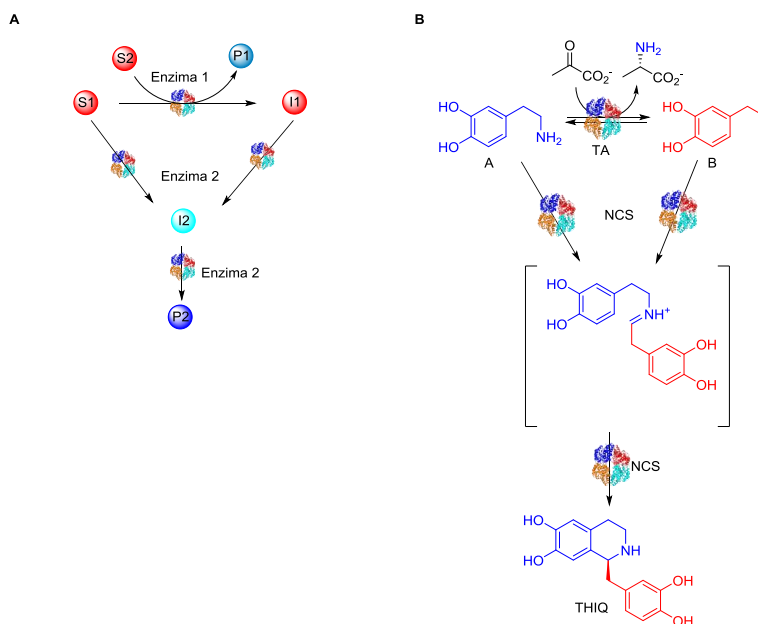


**Figura 13.** Cascadas enzimáticas triangulares. **A.** Esquema general de una cascada enzimática triangular. **B.** Estrategia de síntesis de una tetrahydroisoquinolina (THIQ) utilizando una cascada triangular. El producto del primer paso, reacciona con el sustrato inicial por acción de la NCS, una de las características de este tipo de esquema sintético.

Es de resaltar, que esta clasificación no es estricta, ya que los diseños en cascada pueden combinarse de formas diferentes. Por ejemplo, en una cascada lineal, se podría requerir reacciones enzimáticas auxiliares, con un enfoque ortogonal, para regenerar cofactores, o para eliminar subproductos y desplazar así el equilibrio hacia la formación del producto deseado.<sup>28</sup>

## 1.6. Aldolasas.

La construcción de moléculas bioactivas naturales u homologas sintéticas en términos de tamaño y estereoquímica, requiere de métodos eficientes para la formación asimétrica de enlaces carbono-carbono (C-C). La formación estereoselectiva de este tipo de enlaces es una reacción estratégica en síntesis orgánica que permite la construcción de esqueletos carbonados complejos a partir de moléculas más sencillas y aquirales.<sup>40</sup>

La naturaleza dispone de biocatalizadores capaces de establecer enlaces C-C, las denominadas aldolasas, estas enzimas son consideradas un grupo específicos de liasas (EC 4), presentes en prácticamente todas las ramas del árbol de la vida, y son ampliamente conocidas por su participación en rutas del metabolismo central.<sup>40c</sup> Estas enzimas, catalizan la formación reversible de enlaces C-C a través de la adición de un nucleófilo (enolato) a un electrófilo (un aldehído o una cetona).<sup>41</sup>

Estas enzimas en función del mecanismo catalítico pueden ser clasificadas en dos clases: aldolasas de **Clase I**, estabilizan al intermediario reactivo por medio de una base de Shift (enamina), haciendo uso de un residuo de Lys altamente conservada en el centro activo de la proteína. Esta enamina nucleófila ataca a un electrófilo formando así el enlace C-C (**Figura 14**), con la incorporación de funcionalidades y hasta un máximo de dos centros estereogénicos, cuya estereoquímica relativa es controlada generalmente por el enzima.<sup>42</sup>

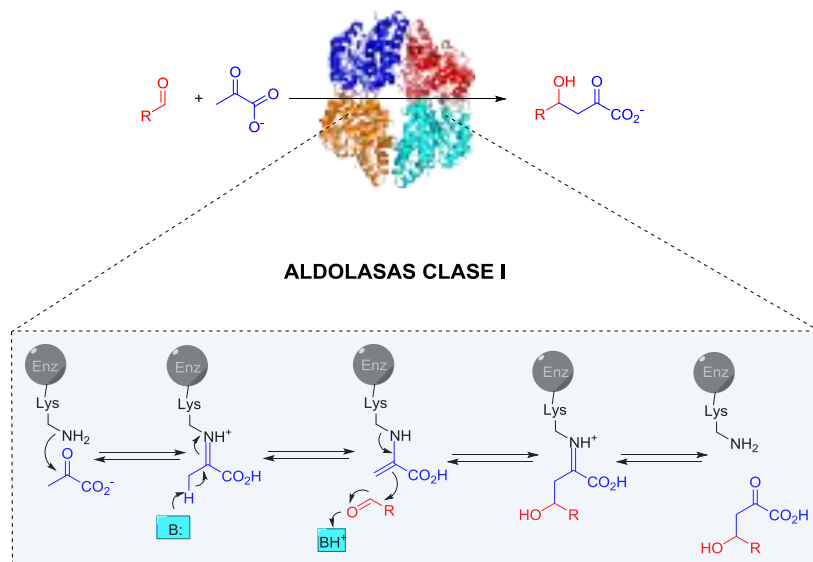


**Figura 14.** Clasificación de las aldolasas según su mecanismo catalítico. **Clase I**, estabilizan al intermediario reactivo por medio de una base de Shift. La reacción se inicia cuando la especie nucleófila forma una imina con la Lys del centro activo. Esto disminuye el  $pK_a$  de los protones en  $\alpha$  lo que facilita su abstracción por un residuo ácido base del centro activo. La enamina generada realiza un ataque nucleofílico al sustrato aceptor (electrófilo) generándose el aldol correspondiente.

Las aldolasas de **Clase II** precisan de cationes metálicos (usualmente  $Mg^{2+}$  ó  $Zn^{2+}$  en el medio biológico) para estabilizar el enolato.<sup>42-43</sup> El catión actúa como ácido de Lewis, facilitando la formación del enolato por abstracción del protón  $\alpha$  del carbonilo (**Figura 15**).<sup>75</sup> El enolato, puede atacar al electrófilo formando así el aducto aldólico como en el caso de las de Clase I

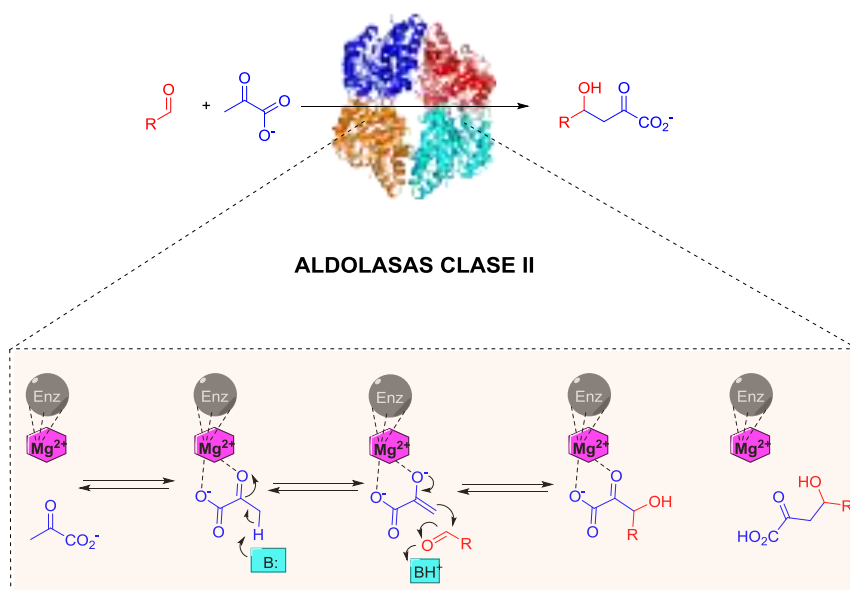


**Figura 15.** Clasificación de las aldolasas según su mecanismo catalítico. **Clase II**, estabilizan el enolato a través de un catión metálico que actúa como ácido de Lewis.

### 1.7. Piruvato aldolasas.

Las piruvato aldolasas catalizan de forma reversible la adición aldólica de un 2-oxoácido a un aldehído, obteniéndose 4-hidroxi-2-oxoácidos,<sup>44</sup> o 2-oxoácido- $\alpha,\beta$ -insaturado cuando ocurre la deshidratación del producto aldólico.<sup>22-23</sup> Dentro las piruvato aldolasas más interesantes desde un punto de vista sintético destacan: la aldolasa del ácido *N*-acetilneuraminico (NeuA, EC 4.1.3.3), también conocida como aldolasa del ácido siálico, la 2-ceto-3-deoxi-D-manno-octosonato aldolasa (KdoA, EC 4.1.2.23), la 2-ceto-3-deoxi-6-fosfo-D-gluconato (KDPGlc aldolasa o GlcA; EC 4.1.2.14), y la 2-ceto-3-deoxi-6-fosfo-D-galactonato aldolasa (KDPGal aldolasa o GalA; EC 4.1.2.21). En nuestro grupo de investigación se han desarrollado en síntesis orgánica tres piruvato aldolasas, a dos de ellas las hemos denominamos 2-oxoácido aldolasas por su amplia tolerancia por el componente nucleofílico, la 3-metil-2-oxobutanoato hidroximetiltransferasa de *E. coli* K-12 (KPHMT, EC 2.1.2.11), que no es realmente una aldolasa, pero, que por promiscuidad catalítica cataliza una adición aldólica, y la 2-ceto-3-deoxi-L-ramnonato aldolasa de *E. coli* (YfaU, EC 4.1.2.53). Y la tercera la *trans*-*o*-hidroxibenzilidenepiruvato hidratasa-aldolasa (HBPA, EC 4.1.2.45) que puede catalizar reacciones de adición y condensación aldólica de piruvato a aldehídos. Estas aldolasas han sido empleadas exhaustivamente en esta Tesis y, por tanto, la descripción de sus características y detalles de su aplicación en síntesis orgánica se describe a continuación.

***Trans*-o-hidroxibenzilidenpiruvato hidratasa-aldolasa (HBPA, EC 4.1.2.45).**

La HBPA, codificada por el gen *NahE* en el operón *Nah7* de *Pseudomonas putida* es un ejemplo de piruvato aldolasa de **Clase I (Figura 16)**, la lisina K183 de su centro activo, es crucial para que ocurra la catálisis enzimática en esta enzima.<sup>45</sup> La enzima fue descubierta en la ruta metabólica de degradación de naftalenosulfonatos<sup>46</sup> y naftaleno.<sup>22,47</sup> Catalizando la hidratación del ácido (*E*)-4-(2-hidroxifenil)-2-oxobut-3-enoico, seguido de la retro-aldólisis del hidroxiaácido a piruvato y 2-hidroxibenzaldehído (**Figura 17**).

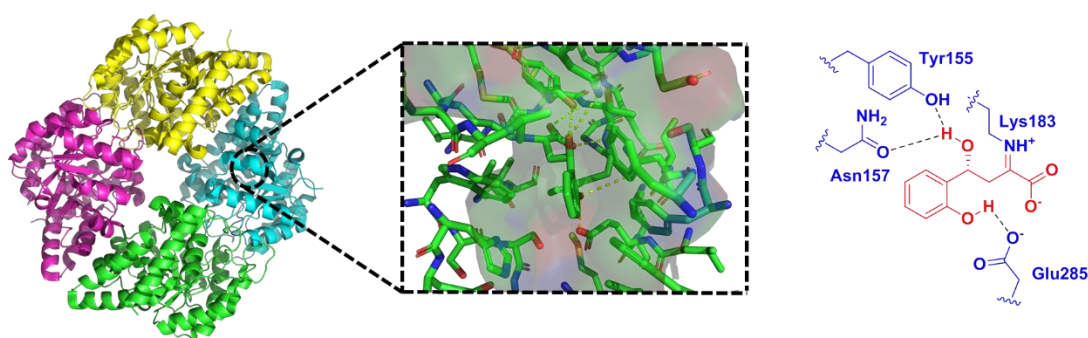


**Figura 16.** Representación de la estructura de la HBPA obtenida por difracción de Rayos X. La enzima posee una estructura homotetramérica (las subunidades se representan en diferentes colores). La enzima se cristalizó con el producto de adición aldólica del piruvato al 2-hidroxibenzaldehído. El aldol, (*R*)-4-hidroxi-4-(2-hidroxifenil)-2-butanato, aparece formando una imina con la Lys183, esencial para la catálisis. La Tyr155 participa como grupo ácido base en la adición aldólica y deshidratación del aldol.<sup>45</sup> Se utilizó el PDB 8DO5<sup>48</sup> para generar las estructuras de la HBPA utilizando el programa PyMOL versión 2.3.2.

La HBPA *in vitro* puede catalizar adiciones o condensaciones aldólicas.<sup>49</sup> En este sentido, Eaton y col. (2000), estudiaron la capacidad esta enzima de utilizar aldehídos aromáticos como sustratos en reacciones de condensación aldólica, reportando que la enzima reconoce una amplia gama de electrófilos. El autor sugiere que la etapa de deshidratación del aldol está mediada por la enzima.<sup>22</sup> Estos resultados fueron corroborados por otros grupos de investigación.<sup>50</sup> Más tarde, Sello y Di Gennaro en el (2013), mostraron que la HBPA es estrictamente dependiente de piruvato.<sup>50</sup> En un trabajo más reciente, Fansher y colaboradores (2023), indicaron que la enzima puede aceptar más de 35 aldehídos (hetero)aromáticos y alifáticos en reacciones de condensaciones aldólicas (**Figura 3**).<sup>23</sup>

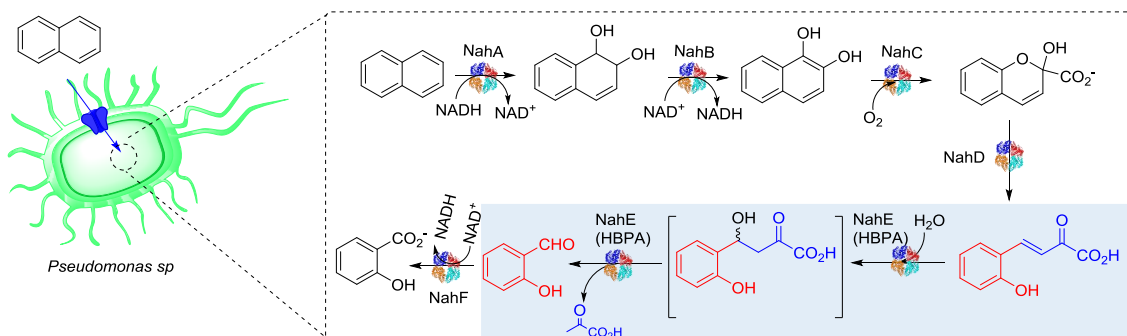


**Figura 17.** Ruta de degradación del naftaleno en *Pseudomonas sp.* Constituida por 7 enzimas actuando secuencialmente.<sup>47</sup> *NahA*: naftaleno 1,2-dioxigenasa (EC 1.14.12.12), *NahB*: *cis*-1,2-dihidro-1,2-dihidroinaftaleno deshidrogenasa (EC 1.3.1.29), *NahC*: 1,2-dihidroinaftaleno dioxigenasa (EC 1.13.11.56), *NahD*: 2-hidroxicromeno-2-carboxilato isomerasa (EC 5.99.1.4), *NahE*: *trans*-*o*-hidroxibenzilidenepiruvato hidratasa-aldolasa (EC 4.1.2.45) y *NahF*: salicilaldehído deshidrogenasa (EC 1.2.1.65). En recuadro azul (HBPA, utilizada en esta Tesis).

A pesar que la HBPA parecía mostrar una elevada especificidad de sustrato por el piruvato, Howard y colaboradores (2016), reportaron que la enzima puede utilizar fluoropiruvato como sustrato frente a una variedad de aldehídos (hete)aromáticos con la peculiaridad de que no se detecta producto de deshidratación. En la reacción de adición aldólica la enzima mostró una elevada estereoselectividad (**Figura 18**).<sup>49a 49b</sup>

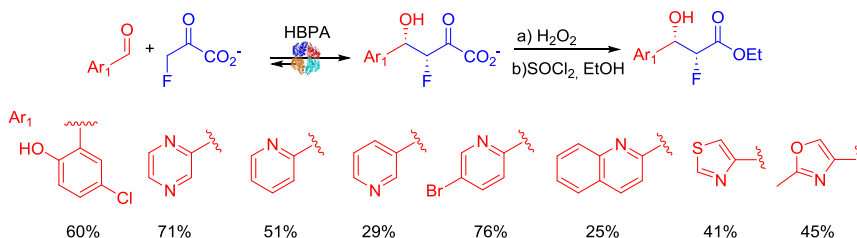


**Figura 18.** Reacción de adición aldólica del fluoropiruvato a aldehídos (hete)aromáticos catalizada por la HBPA. En la figura se muestra el rendimiento de producto aislado. En todos los casos el ee > 98%.

A pesar de las aplicaciones en biocatálisis reportadas para la HBPA (**Figura 19**), los estudios de sus potencialidades sintéticas como aldolasa frente a aldehídos alifáticos no ha sido reportado, por lo que será tema de esta Tesis. Además, se desarrollarán métodos de síntesis biocatalíticas donde se combinará esta enzima con transaminasas y oxido-reductasas en reacciones secuenciales o en cascadas enzimáticas.

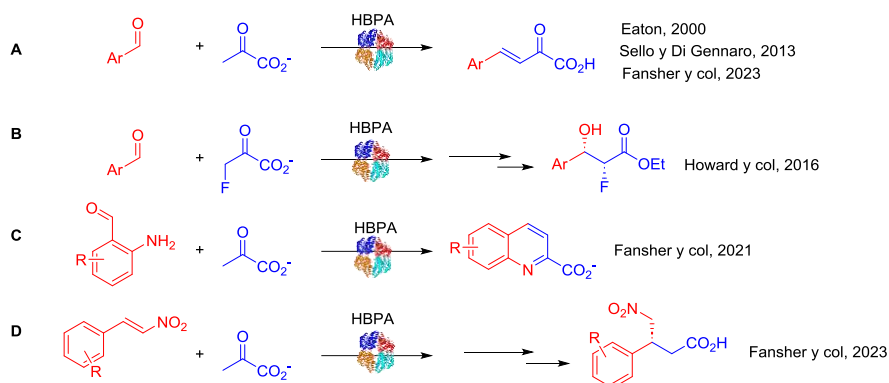
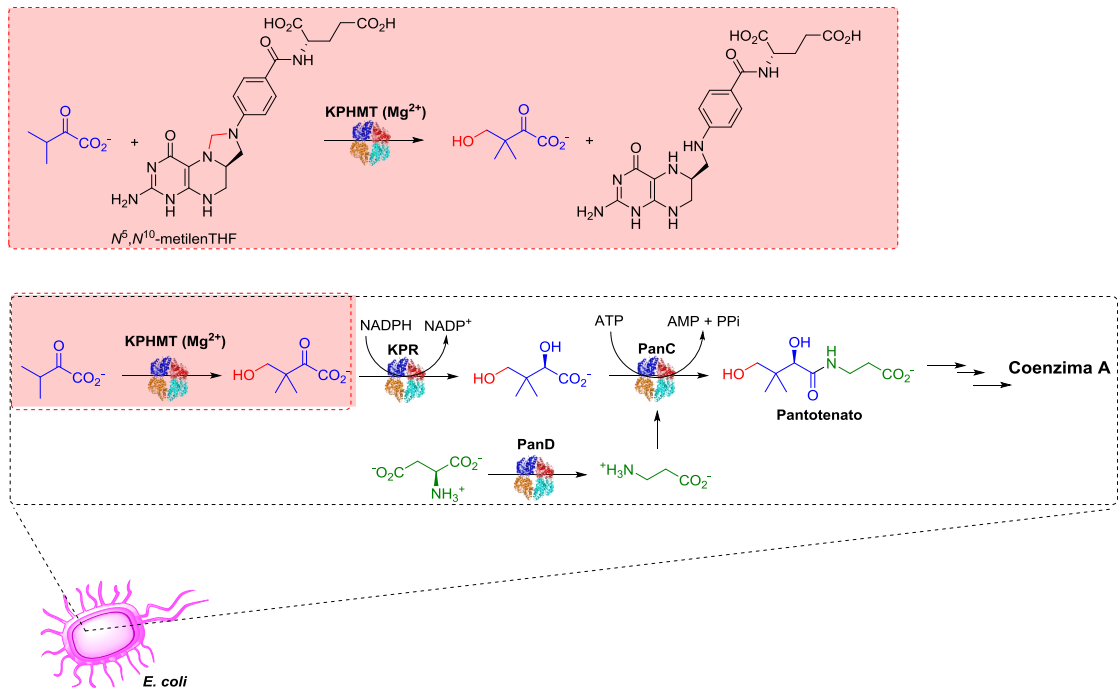


**Figura 19.** Ejemplos de aplicaciones de la HBPA en Biocatálisis. **A.** Síntesis de 2-oxoácidos- $\alpha,\beta$ -insaturado.<sup>22-23,50</sup> **B.** Síntesis enzimática de 3-hidroxiésteres fluorados.<sup>49a</sup> **C.** Síntesis de quinolinas sustituidas.<sup>51</sup> **D.** Síntesis biocatalítica de ácidos 3-aryl-4-nitrobutíricos.<sup>52</sup>

### Metil-2-oxobutanoato hidroximetiltransferasa (KPHMT, EC 2.1.2.11).

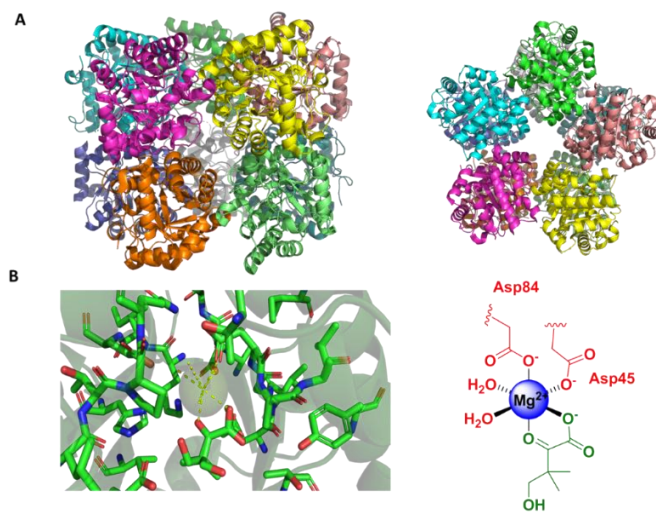
Esta enzima está codificada por el gen *panB* y forma parte de la ruta biosintética del pantotenato o vitamina B5, precursor de la coenzima A y de la proteína transportadora de acilo en bacterias.<sup>53</sup> Es la primera enzima de la ruta metabólica y cataliza la síntesis del 4-hidroxi-3,3-dimetil-2-oxobutanoato (cetopantoato) a partir del 3-metil-2-oxobutanoato (2-oxoisovalerato), y ( $N^5,N^{10}$ -metilenTHF). Posteriormente el producto del gen *panE*, la cetopantoato reductasa (KPR, EC 1.1.1.169), reduce el carbonilo del cetopantoato para formar hidroxipantoato, y finalmente la pantotenato sintasa (EC 2.7.1.169) codificada por *panC*, cataliza la condensación dependiente de ATP de pantoato y  $\beta$ -alanina, previamente generada por la descarboxilación del ácido aspártico catalizado por la aspartato 1-d Descarboxilasa (PanD, EC 4.1.1.11) (**Figura 20**).<sup>53</sup>





**Figura 20.** Ruta biosintética del pantotenato en *E. coli*. Constituida por 4 enzimas: la 3-metil-2-oxobutanoato hidroximetiltransferasa (KPHMT, EC 2.1.2.11) codificada por el gen *panB*, la ketopantoato reductasa (KPR, EC 1.1.1.169) codificada por el gen *panE*, la pantoato quinasa (EC 2.7.1.169) codificada por el gen *panC* y aspartato 1-decarboxilasa (EC 4.1.1.11) codificada por el gen *panD*.

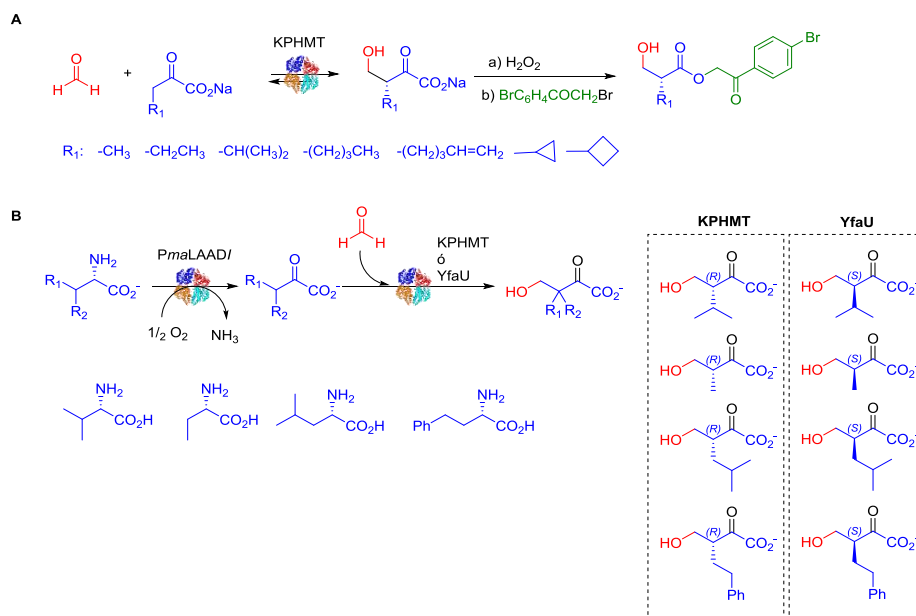
La KPHMT cataliza la transferencia de un grupo hidroximetil (HOCH<sub>2</sub>) del N<sup>5</sup>,N<sup>10</sup>-metilenTHF al 2-oxoisovalerato a través de un mecanismo de reacción muy similar al de una aldólica aldólica. Esto explica que la enzima muestre como actividad promiscua la adición aldólicas de 3-metil-2-oxobutanoato a formaldehído.<sup>53</sup> La activación del 2-oxoácido en el centro activo ocurre a través de un catión metálico que actúa como ácido de Lewis, tal como lo descrito para las aldolasas de **Clase II (Figura 21)**.<sup>54</sup>



**Figura 21.** Representación de la estructura de la KPHMT obtenida por difracción de Rayos X. **A.** Estructura decamérica de la enzima. Las subunidades se representan en diferentes colores. **B.**

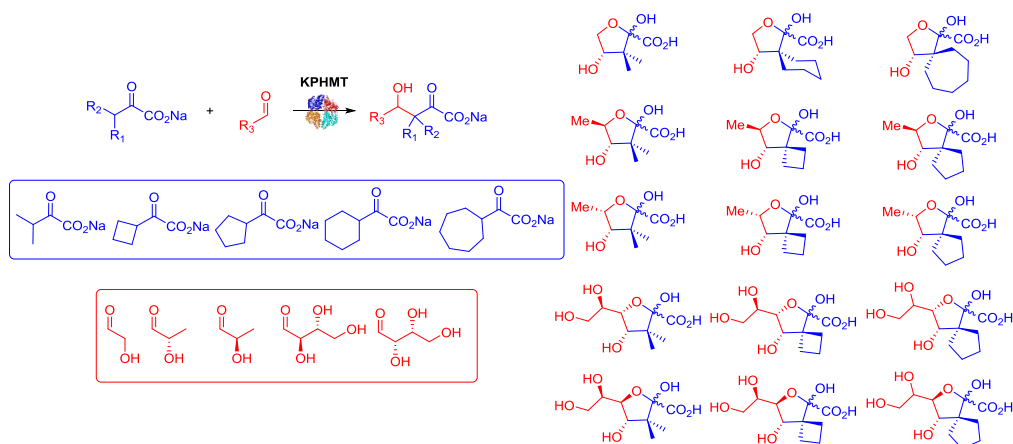
Representación del sitio de coordinación del catión metálico ( $Mg^{2+}$ ) y el producto de la reacción enzimática, 4-hidroxi-3,3-metil-2-oxobutanoato, en una subunidad. El  $Mg^{2+}$  se encuentra hexacoordinado con los grupos carboxilato del Asp45 y 84 y dos moléculas de agua. Además, coordina al sustrato (3,3-metil-2-oxobutanoato) y producto de la reacción a través del grupo carboxilo y carbonilo de estos.<sup>54</sup> Se utilizó el PDB 1M3U para generar las estructuras de la KPHMT utilizando el programa PyMOL versión 2.3.2.

Nuestro grupo de investigación ha evaluado el potencial uso de esta enzima en biocatálisis, por ello en el (2019), se reportó el uso de la KPHMT en la síntesis estereoselectiva de 2-alkil-3-hidroxiésteres (**Figura 22A**). Los autores reportaron rendimientos de productos aislados que oscilan entre 57-88% con un 88-98% de ee, para la KPHMT. En ese trabajo, se demostró que la enzima mostraba una mayor actividad con  $Co^{2+}$  como cofactor en lugar de  $Mg^{2+}$  que es el catión metálico utilizado por la enzima en el entorno biológico.<sup>55</sup> En otro estudio se informó una alternativa biocatalítica para la síntesis de 4-hidroxi-2-oxoácidos 3-sustituidos. En este esquema sintético, se transformó L- $\alpha$ -aminoácidos mediante una L- $\alpha$ -aminoácido deaminasa (AAOs, E.C. 1.4.3.2) dando lugar a 2-oxoácidos intermedios, sustratos de aldolasas estereoselectivas la KPHMT y la YfaU (**Figura 22B**) la formación de aductos aldólicos osciló entre 36 y 98 % y el exceso enantiomérico reportado fue de 91 a 98%.<sup>56</sup>



**Figura 22. A.** Síntesis quimio-enzimáticas de 2-alkil-3-hidroxiésteres. La KPHMT nativa y las variantes I202A, I212A y L42A/I212A catalizaron reacciones de adición aldólica de diferentes 2-oxoácidos al formaldehído.<sup>55</sup> **B.** Síntesis de 4-hidroxi-2-oxoácidos 3-sustituidos. La enzima PmaLAADI catalizó la deaminación oxidativa de L-aminoácidos para formar *in situ* 2-oxoácidos. Las aldolasas (KPHMT y la YfaU) y sus variantes catalizaron reacciones de adición aldólica de diferentes 2-oxoácidos al formaldehído.<sup>56</sup>

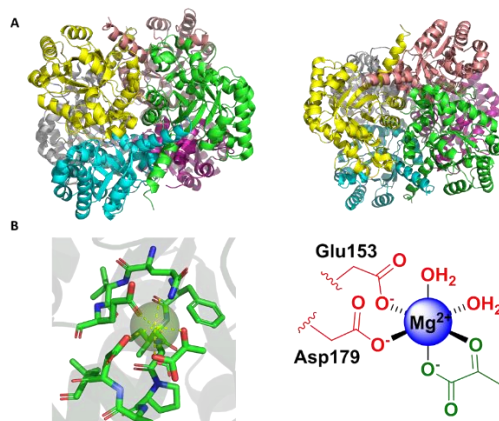
Así mismo, se mostró el uso de la KPHMT y sus variantes mutagénicas en la construcción estereoselectiva de carbonos cuaternarios para una variedad de compuestos con este motivo en su estructura (*gem*-dimetil, *gem*-cicloalquil y compuestos spirocíclicos, siendo estos últimos el centro de atención del desarrollo de fármacos modernos<sup>57</sup>). La estrategia sintética comprendía la adición aldólica de 2-oxoácidos 3,3-disustituídos a aldehídos catalizada por KPHMT, demostrándose la notable tolerancia a los sustratos y el estereocontrol de este biocatalizador (**Figura 23**).<sup>58</sup>



**Figura 23.** Ejemplo de síntesis biocatalítica de moléculas con centros cuaternarios. La KPHMT nativa y las variantes I202A, I212A, L42A/I212A y V214G catalizaron la adición aldólica de diferentes 2-oxoácidos a varios hidroxialdehídos, generando derivados de ácido ulosónico.<sup>58</sup>

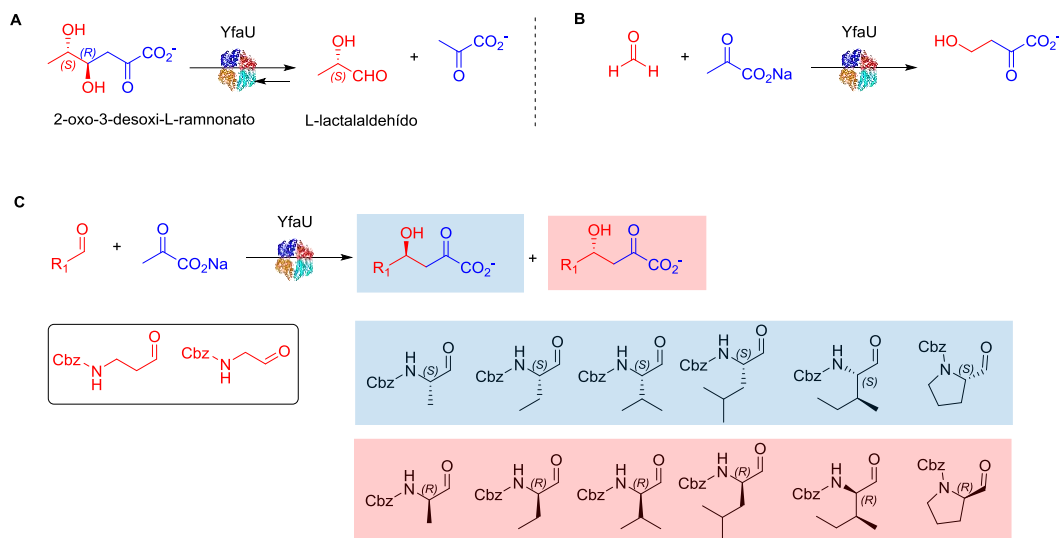
#### oxo-3-desoxi-L-ramnonato aldolasa de *E. coli* (YfaU, EC 4.1.2.53).

La YfaU, codificada por el gen *rhmA* de *E. coli*, es una aldolasa de **Clase II** por lo que requiere de un catión metálico como cofactor (**Figura 24**).<sup>14</sup>



**Figura 24.** Representación de la estructura de la YfaU obtenida por difracción de Rayos X. **A.** Estructura hexamérica de la enzima. Las subunidades se representan en diferentes colores. **B.** Representación del sitio de coordinación del catión metálico ( $Mg^{2+}$ ) y el sustrato de la reacción enzimática, piruvato, en una subunidad. El  $Mg^{2+}$  se encuentra hexacoordinado con los grupos carboxilato del Glu153 y el Asp179 junto a dos moléculas de agua. Además, coordina al sustrato de la reacción a través del grupo carboxilo y carbonilo de este.<sup>14</sup> Se utilizó el PDB 2VWT para generar las estructuras de la YfaU utilizando el programa PyMOL versión 2.3.2.

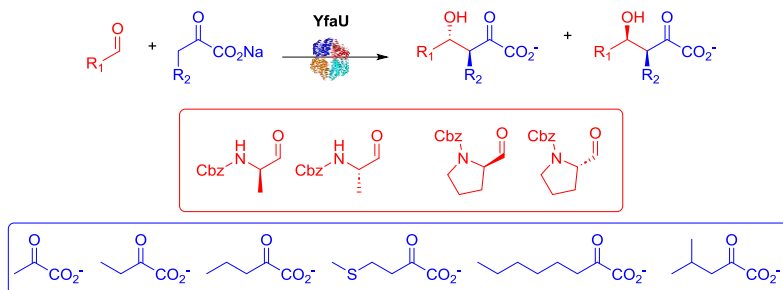
En el metabolismo bacteriano, esta aldolasa tiene una participación directa catalizando la escisión reversible del 2-oxo-3-desoxi-L-ramnonato a partir de piruvato y L-lactaldehído (**Figura 25A**).<sup>14</sup> *In vitro*, la YfaU puede catalizar la adición aldólica de piruvato a una gran variedad de aldehídos que van desde el formaldehído (**Figura 25B**) hasta *N*-Cbz-aminoaldehídos (**Figura 25C**). En todos los casos la enzima mostró una mayor actividad con Ni<sup>2+</sup> como cofactor en comparación con el Mg<sup>2+</sup> que es el encontrado en el entorno celular. Es de destacar, la capacidad que tiene la enzima de tolerar altas concentraciones de un aldehído tan reactivo como el formaldehído (IC<sub>50</sub> =1.5 M). Esto ha permitido utilizar la enzima en reacciones con 1M de concentración sustratos, condiciones en las cuales se inactivarían la mayoría de las enzimas.<sup>30</sup> Otra peculiaridad que mostró este biocatalizador, es que cuando se utilizan sustratos aquirales se obtienen los productos aldólicos como mezclas racémicas. Sin embargo, con sustratos quirales como los (*S*) y (*R*)-*N*-Cbz-aminoaldehídos se da una inducción de quiralidad durante el curso de la reacción, obtiene preferentemente el aldol con configuración *R* y *S* respectivamente (**Figura 25C**).<sup>59</sup>



**Figura 25.** Reacciones de adición aldólica catalizadas por la YfaU. **A.** *In vivo* la enzima cataliza la retro-aldólisis de 2-oxo-3-desoxi-L-ramnoato. **B.** Reacción de adición aldólica de piruvato a formaldehído catalizada de por la YfaU. **C.** Reacción de adición aldólica de piruvato a *N*-Cbz-aminoaldehídos. La estereoquímica de los productos finales dependerá de la configuración de los sustratos de partida.

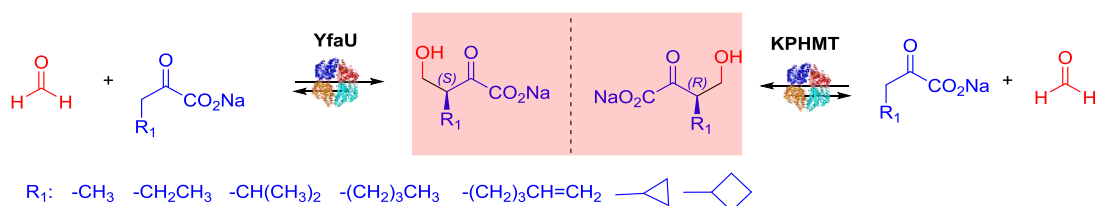
Las potencialidades sintéticas de la YfaU se extendieron con el uso de 2-oxoácidos diferentes al piruvato en reacciones de adición aldólica. En este caso, la tolerancia de la enzima fue menor si se compara con la gran variedad de aldehídos que es capaz de aceptar. Para potenciar la promiscuidad de la enzima por los 2-oxoácidos se diseñaron

variantes enzimáticas capaces de catalizar la adición aldólica de análogos del piruvato con cadenas laterales voluminosas a *N*-Cbz-aminoaldehídos. En estas reacciones la enzima mostró un control de la estereoquímica sobre el centro quiral proveniente del nucleófilo (**Figura 26**).<sup>60</sup>



**Figura 26.** Adición aldólica de análogos del piruvato a *N*-Cbz-aminoaldehídos catalizado por la YfaU nativa y las variantes W23A y W23A/L216A.

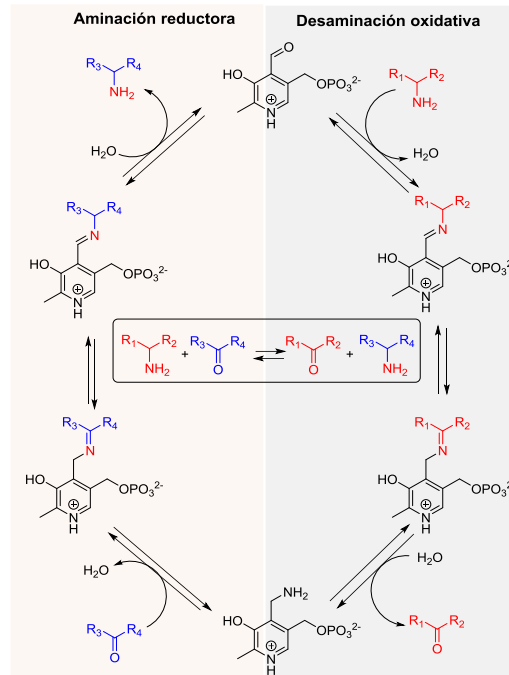
Es de destacar que las enzimas YfaU y KPHMT, son biocatalizadores estereocomplementarios, permitiendo disponer de los enantiómeros de un producto aldólico en dependencia del biocatalizador utilizado (**Figura 27**). Esto representa una ventaja sintética que será explorada en esta Tesis en la síntesis de moléculas quirales a partir de precursores aquirales sencillos utilizando sistemas enzimáticos acoplados.



**Figura 27.** Reacciones de adición aldólica de 2-oxoácidos al formaldehído catalizado por dos aldolasas estereocomplementarias, la YfaU y la KPHMT.

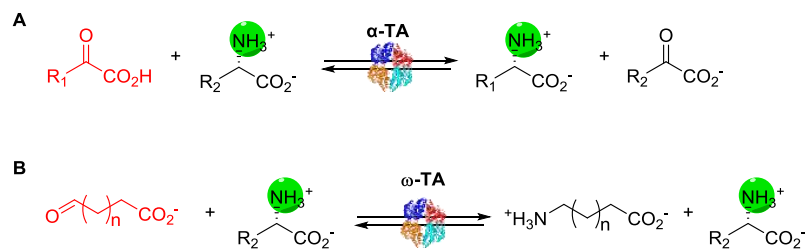
## 1.8. Transaminasas.

Las transaminasas son un grupo específico de transferasas (EC 2.6.1.d), que catalizan la migración de un grupo amino de una molécula donadora a un grupo carbonilo de un compuesto aceptor.<sup>61</sup> Todas las enzimas de esta clase utilizan como cofactor el derivado de la vitamina B6, el piridoxal-5'-fosfato (PLP). El proceso de transaminación consta de dos etapas, una desaminación oxidativa de un donante de amino seguida de una aminación reductora de un aceptor de aminos (**Figura 27**).<sup>62</sup>



**Figura 27.** Mecanismo transaminación mediado por PLP. En la primera etapa, el grupo amino se transfiere de un dador de amino al PLP, dando lugar a la generación de una formación de la piridoxamina-5' fosfato (PMP) y liberando la cetona correspondiente. En la aminación reductiva, el grupo amino de la PMP se transfiere a un sustrato aceptor, permitiendo la regeneración de PLP.

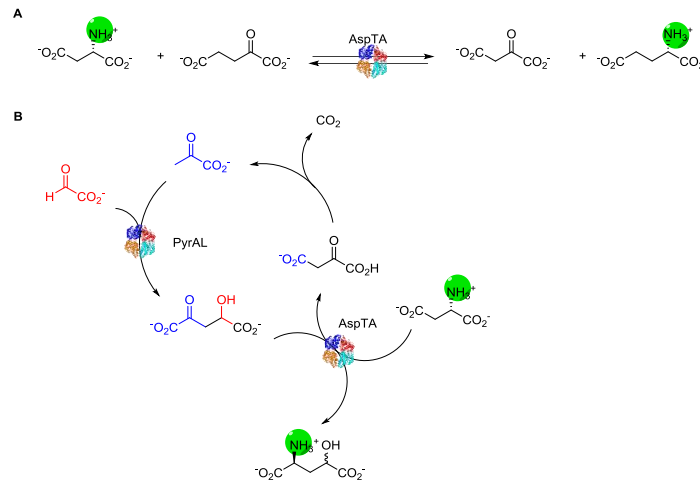
A la fecha se han descrito 124 tipos de transaminasas, (IUBMB fecha de consulta marzo 2023) siendo en la naturaleza su principal función la transferencia de grupo aminos de  $\alpha$ -aminoácidos a 2-oxoácidos.<sup>63</sup> Estas enzimas pueden clasificarse en dos grande grupos en función de la distancia del grupo amino respecto al grupo carboxilo, así tenemos: las  $\alpha$ -transaminasas ( $\alpha$ -TA) que requieren la presencia del grupo amino en la posición  $\alpha$ -respecto al grupo carboxilo, por lo que catalizan síntesis de  $\alpha$ -aminoácidos (**Figura 28A**) y las  $\omega$ -transaminasas ( $\omega$ -TA) capaces de transferir grupos aminos que están más alejados de un grupo carboxilato (p. ej. en posición  $\gamma$ ,  $\delta$  o  $\epsilon$ ) e incluso pueden llegar a prescindir de la función carboxílica (**Figura 28B**).



**Figura 28.** Clasificación de las transaminasas. **A.** Reacción catalizada por una  $\alpha$ -transaminasas ( $\alpha$ -TA) **B.** Reacción catalizada por una  $\omega$ -transaminasas ( $\omega$ -TA).

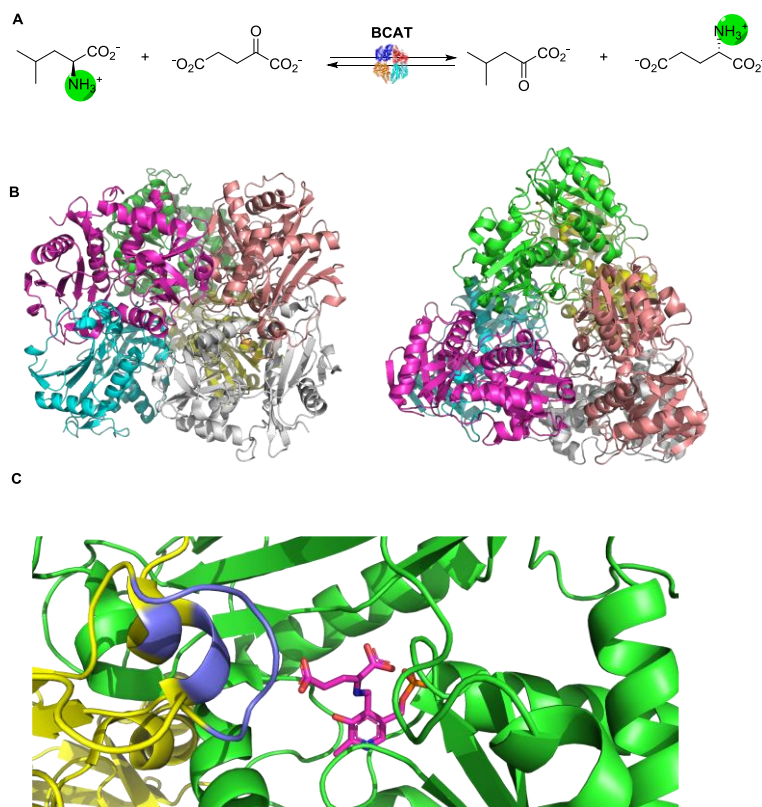
Un ejemplo típico de las  $\alpha$ -TA, es la aspartato transaminasa de *E. coli* (AspTA, EC 2.6.1.1), enzima que cataliza la transferencia de un grupo amino desde el Asp al 2-

oxoglutarato, generando oxalacetato y Glu (**Figura 29A**). Esta capacidad de transferencia de grupo amino de esta enzima se ha utilizado en biocatálisis, un ejemplo de ello se muestra en la estrategia de síntesis de ácido  $\gamma$ -hidroxiglutámico mediante una cascadas cíclicas entre una piruvato aldolasa PyrAL y la AspTa (**Figura 29B**).<sup>64</sup>



**Figura 29.** Reacción catalizada por la aspartato transaminasa de *E. coli* (AspTA). **A.** Reacción natural catalizada por la AspTA. **B.** Cascada enzimática cíclica entre una piruvato aldolasa (PyrAL) y la AspTA utilizada en la síntesis de ácido  $\gamma$ -hidroxiglutámico.

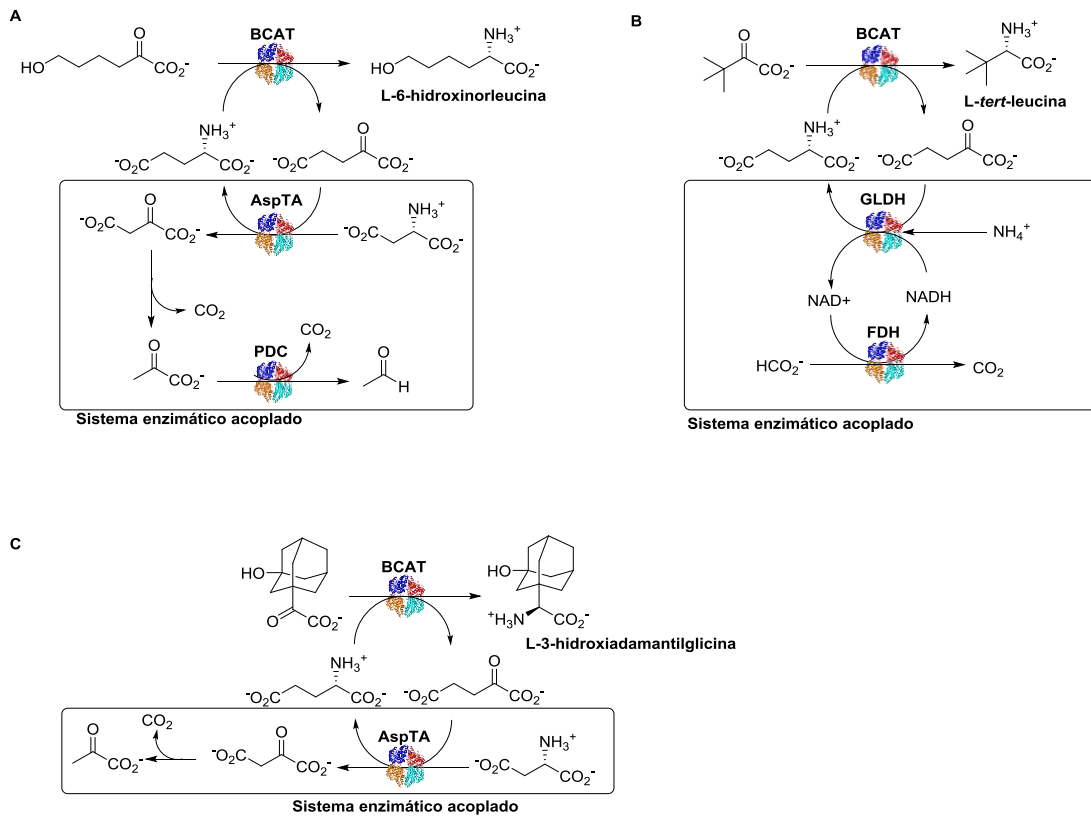
Otro ejemplo, de este tipo de enzimas es la aminotransferasa de aminoácidos ramificados de *E. coli* (BCAT, EC 2.6.1.42) codificada por el gen *ilvE*. En los sistemas biológicos desempeña un papel clave en la biosíntesis de aminoácidos hidrofóbicos. De forma general, la enzima cataliza de manera reversible la transferencia del grupo amino desde un aminoácido hidrofóbico al 2-oxoglutarato para formar el 2-oxoácido y el correspondiente aminoácido correspondiente (**Figura 30A**). Por lo tanto, el centro activo de esta enzima debe ser capaz de gestionar el reconocimiento tanto del grupo carboxilato del Glu como la cadena lateral hidrofóbica del otro sustrato. Este reconocimiento dual que presenta esta transaminasa es debido a la plasticidad del centro activo para acomodarse a los requerimientos del sustrato. La enzima es un homohexámero y los centros activos se encuentran en la región entre cada subunidad, participando en su arquitectura aminoácidos de dos subunidades. Esto genera una región interdominio con flexibilidad para permitir los cambios necesarios para acomodar sustratos con diferentes requerimientos estructurales (**Figura 30B y C**).<sup>65</sup>



**Figura 30.** Reacción natural de la BCAT y representación su estructura cristalina obtenida por difracción de Rayos X. **A.** Reacción enzimática catalizada naturalmente por la BCAT (EC 2.6.1.42). **B.** La enzima posee una estructura homohexamérica (las subunidades se representan en diferentes colores). **C.** En el centro activo se muestra al Glu unido al cofactor PLP a través de una imina entre el grupo  $\alpha$ -amino del primero y el grupo carbonilo del PLP. En la arquitectura del centro activo participan dos subunidades (representadas en amarillo y verde). En azul aparece la región interdominio que muestra flexibilidad y es responsable del reconocimiento dual que muestra la transaminasa, siendo capaz de unir en esta zona tanto el grupo  $\gamma$ -carboxilato del Glu como un residuo hidrofóbico de su segundo sustrato (Val, Leu e Ile).<sup>65</sup> Se utilizó el PDB 1IYE para generar las estructuras de la BCAT utilizando el programa PyMOL versión 2.3.2.

*In vitro*, la BCAT se ha utilizado en la síntesis estereoselectiva (ee > 99%) de aminoácidos no naturales como la L-6-hidroxinorleucina (**Figura 31A**).<sup>66</sup>, la L-*tert*-leucina (**Figura 31B**) o la L-3-hidroxiadamantilglicina (**Figura 31C**).<sup>67</sup> La aplicación de BCAT en biocatálisis requiere utilizar un sistema acoplado que desplace los equilibrios de reacción y permita emplear cantidades catalíticas del sustrato dador de aminos (Glu) puesto que el producto de su transaminación, el 2-oxoglutarato, es un inhibidor de la enzima (se ha reportado que a concentraciones de 10 mM de 2-oxoglutarato la BCAT solo retiene el 20% de su actividad inicial).<sup>67</sup>

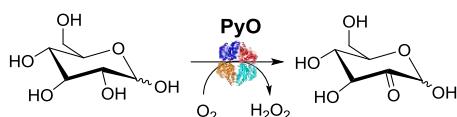
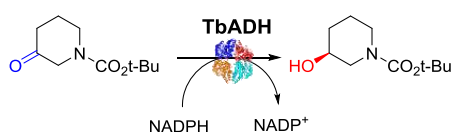
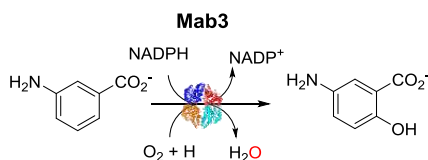
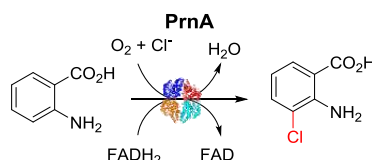
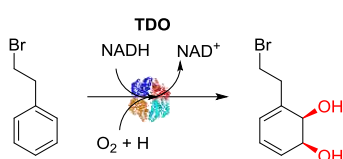
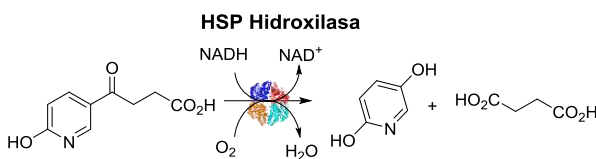




**Figura 31.** Síntesis de aminoácidos no naturales catalizado por la BCAT. **A.** Síntesis de L-6-hidroxinorleucina.<sup>66</sup> **B.** Síntesis de L-tert-leucina y **C.** Síntesis de L-3-hidroxiadamantilglicina.<sup>67</sup> En todos los esquemas de síntesis se necesita un sistema enzimático acoplado que permita utilizar cantidades catalíticas de Glu para minimizar la inhibición por producto de la transaminasa. PDC, piruvato descarboxilasa de *Zymomonas mobilis* (EC 4.1.1.1), GLDH, L-glutamato deshidrogenasa (EC 1.4.1.3) y FDH, formiato deshidrogenasa (EC 1.2.1.2).

## 1.9. Óxido-reductasas.

A la fecha el IUBMB ha clasificado 2497 enzimas como óxido-reductasas (EC 1---).<sup>68</sup> Como su nombre indica estas enzimas catalizan reacciones redox donde participan sustratos con diferentes funcionalidades químicas como: alcoholes, aldehídos, cetonas, ácidos carboxílicos, compuestos aromáticos, aminas, etc. Estas enzimas requieren de un grupo (cofactor) que medie el proceso de transferencia de electrones durante la catálisis, pudiendo ser un catión metálico (Cu<sup>2+</sup>, Fe<sup>2+/3+</sup>, Mn<sup>2+</sup>, etc.) o moléculas orgánicas como el NAD(P)H, el FAD o el grupo hemo (**Figura 33**).<sup>69</sup>

**Oxidación de alcoholes****Reducción de grupos carbonilos****Hidroxilación de anillos aromáticos****Reacción de halogenación de anillos aromáticos****Dihidroxilación de anillos aromáticos****Oxidación descarboxilativa**

**Figura 33.** Ejemplos de reacciones catalizadas por óxido-reductasas. Oxidación de alcoholes, catalizado por la PyO: Piranos oxidasa (EC 1.1.3.10). Hidroxilación de anillos aromáticos catalizado por la Mab3: 3-hydroxybenzoate 2-monooxygenase (EC 1.14.99.23). Dihidroxilación de anillos aromáticos catalizado por la TDO, tolueno dioxigenasa (EC 1.14.12.11). Reducción de grupos carbonilos catalizado por la TbADH, alcohol deshidrogenasa (EC 1.1.1.2). Halogenación de anillos aromáticos catalizado por la PrnA: Triptófano halogenasa (EC 1.14.19.9). Oxidaciones descarboxilativas catalizadas por la HSP Hidroxilasa (EC 1.14.13.163).

Dentro de las óxido-reductasas encontramos las deshidrogenasas (EC. 1.1.1.d) que son enzimas capaces de oxidar a un sustrato a expensas de reducir a un aceptor de electrones, usualmente  $\text{NAD}^+/\text{NADP}^+$  o  $\text{FAD}/\text{FMN}$  de manera reversible. Estas desempeñan un papel fundamental en la biocatálisis, ya que generan productos quirales con nuevas funcionalidades.<sup>70</sup> Uno de estos compuestos, son las 2-hidroxi-4-butirolactonas, debido a que son importantes bloques estructurales de compuestos con: actividad biológica (p. ej. *N*-sulfonilado o  $\alpha$ -amino- $\gamma$ -butirolactonas, implicadas en la regulación del *quórum sensing* en bacterias.<sup>71</sup>,  $\gamma$ -butirolactonas-1, como componentes clave en la síntesis de compuestos con actividad citotóxica (p. ej. Etopósidos<sup>72</sup> y Anfidinólido B1<sup>73</sup>), antibióticos (lactivivina)<sup>74</sup> y Cinatrin<sup>75</sup> un fármaco antiinflamatorio) o auxiliares quirales en síntesis asimétrica. Entre las estrategias de síntesis empleadas para su síntesis destacan: hidrogenación asimétrica catalizada por complejos de Ru y Rh (**Figura 34A**), adiciones aldólicas catalizadas por ácidos de Lewis o utilizando organocatalizadores (**Figura 34B**) y resolución enzimática de lactonas (**Figura 34C**). Sin embargo, la reducción estereoselectiva de derivados de 4-hidroxi-2-oxoácidos para producir derivados de 2-hidroxi-4-butirolactonas sigue inexplorada, por esta razón, en el capítulo

3.2 de este trabajo nos planteamos diseñar una estrategia enzimática que permita acceder a este tipo de compuestos mediante una vía sintética novedosa que involucra aldolasas estereocomplementarias (KPHMT e YfaU descritas previamente) y dos óxido-reductasas estereoselectivas, las cuales se describen en detalles a continuación.

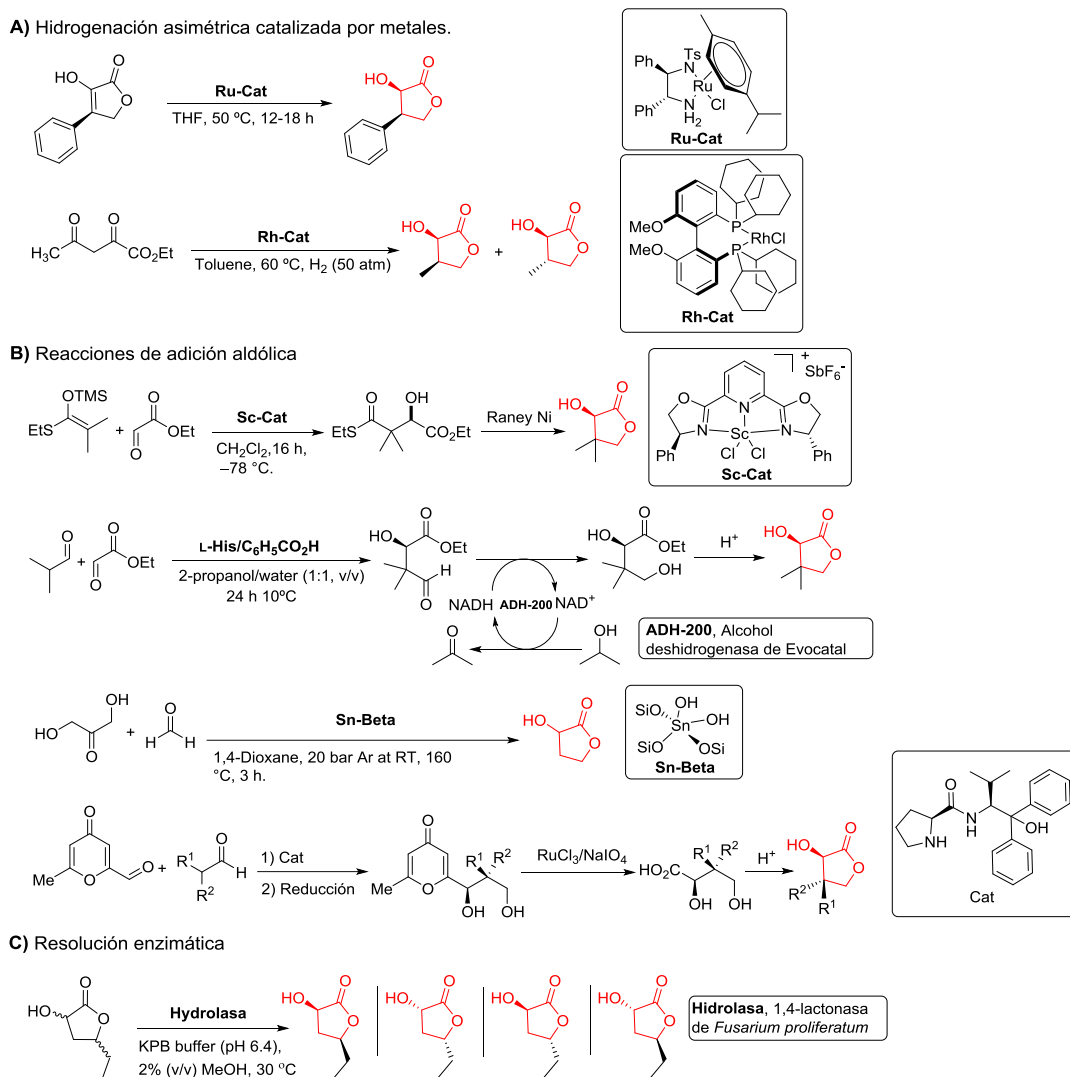


**Figura 34.** Estrategias sintéticas para la obtención de derivados de 2-hidroxi-4-butirolactona. **A.** Reducción asimétrica catalizada por metales<sup>76</sup>; **B.** Reacciones de adición aldólica<sup>77</sup> y **C.** Resolución enzimática.<sup>78</sup>

### 2-dehidropantoate 2-reductasa (KPR, EC 1.1.1.169).

La KPR es una enzima homodimérica de 34 kDa, codificada por el gen *panE* de *E. coli*, forma parte de la ruta biosintética del Pantotenato descrita anteriormente (**Figura 20**).<sup>53,79</sup> Esta enzima cataliza la reducción dependiente de NADPH del ketopantoato para formar pantoato. En un primer paso de la catálisis, el NADPH se une al centro activo de la enzima, seguido de la unión del ketopantoato mediante un mecanismo bi-bi ordenado, lo

que permite que ocurra la transferencia de hidruro que da lugar al alcohol y al cofactor oxidado. En este mecanismo intervienen la Lys176 como residuo ácido/base y Glu256 y Asn98 que contribuyen a la estabilización del sustrato en el centro activo (**Figura 35**).<sup>79</sup>

80

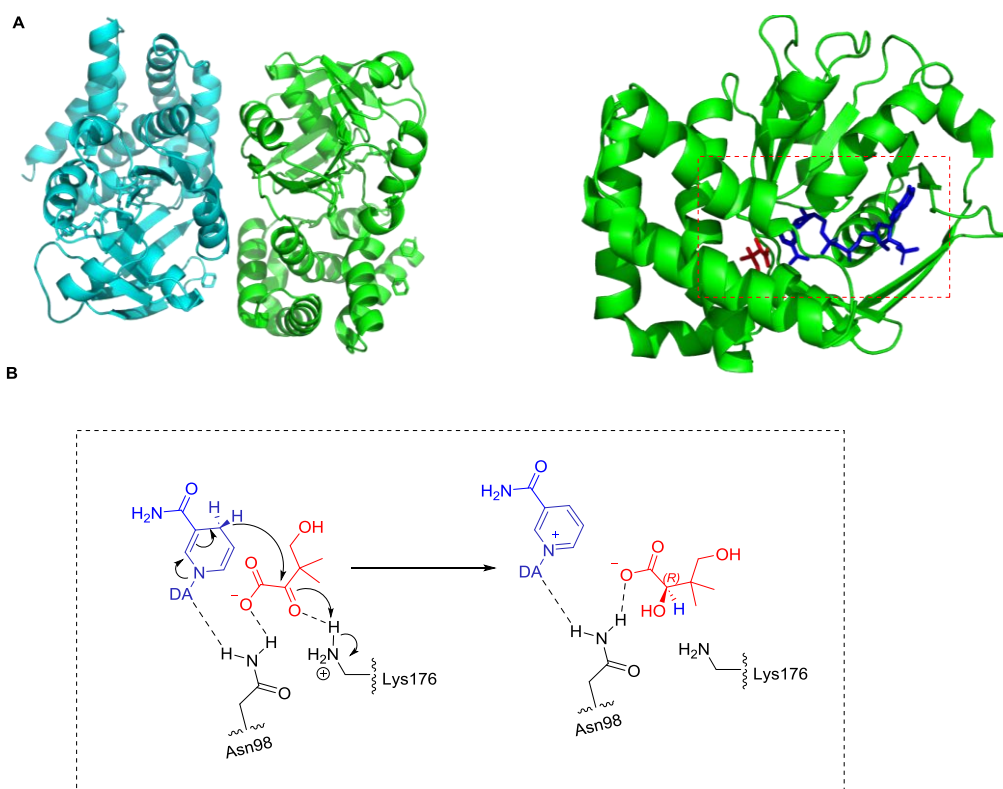


**Figura 35.** Representación de la estructura de la KPR obtenida por difracción de Rayos X. **A.** Estructura dimérica de la enzima con el cetopantoato y el NADPH unidos al centro activo. Las subunidades se representan en diferentes colores, azul y verde. **B.** Mecanismo catalítico propuesto en la reducción del cetopantoato catalizado por la KPR. Un protón del C4 del NADPH es transferido al sustrato generándose un alcóxido que es re-protonado la Lys176, obteniéndose así el pantoato y el NADP<sup>+</sup> como productos de la reacción.<sup>79</sup> Se utilizó el PDB 2OFP para generar las estructuras de la KPR utilizando el programa PyMOL versión 2.3.2.

Cabe resaltar, que en la literatura no hay evidencia del uso de la KPR en síntesis orgánicas. En este sentido, en esta Tesis la usaremos en la síntesis biocatalítica concurrente de derivados de 2-hidroxi-4-butirolactona, capítulo 3.2.

### $\Delta^1$ -piperidina-2-carboxilato/ $\Delta^1$ -pirrolina-2-carboxilato reductasa (DpkA, EC 1.5.1.21).

La DpkA está codificada por el gen *dpka* de *Pseudomonas syringae*.<sup>81</sup> formando parte de la ruta de degradación de la D-Lys.<sup>82</sup> Esta ruta metabólica está formada por 5 enzimas e implica una serie de reacciones enzimáticas a través de intermediarios cíclicos de seis

carbonos. La DpkA, cataliza la reducción dependiente de NADPH del ácido pipecolínico ( $\Delta^1$ -Piperideine-2-carboxilato, Pip2C) formando L-Pipecolato (**Figura 36**).<sup>81</sup>

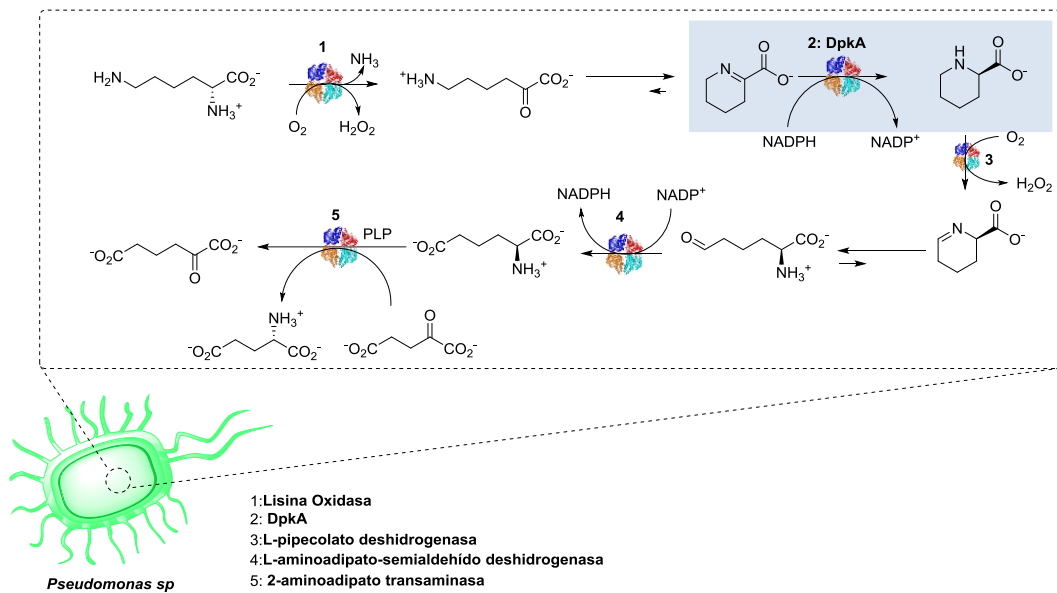


**Figura 36.** Ruta de degradación de D-Lys en *Pseudomonas sp*. Para transformar la Lys a 2-oxoadipato intervienen 5 enzimas (1) D-lisina oxidasa (EC 1.4.3.14), cataliza la  $\alpha$  desaminación de la D-lisina, generando 6-Amino-2-oxohexanoate que se deshidrata espontáneamente y forma el ácido pipecolínico, (2) la DpkA reduce el ácido pipecolínico y forma L-Pipecolato, luego, (3) la L-pipecolato deshidrogenasa (EC 1.5.99.3) en presencia de oxígeno genera el  $\Delta^1$ -Piperideina-6-L-carboxylato que es oxidado por la (4) L-aminoadipato-semialdehído deshidrogenasa (EC 1.2.1.31) dependiente de NADP<sup>+</sup> que lo transforma en L- $\alpha$ -aminoadipato que finalmente por acción de una (5) transaminasa (EC 2.6.1.39) genera el 2-oxoadipato que es incorporado en otra ruta metabólica para generar 2-oxoglutarato uno de los intermediarios del Ciclo de Krebs.

La DpkA es una enzima dimérica peso molecular de 36.3 kDa que ha sido cristalizada lo que permitido analizar la estructura de su centro activo. Así, se identificó la tríada catalítica Asp:Ser:His, como responsable de su mecanismo de acción. Los puentes de hidrógeno entre los tres aminoácidos permiten que la His54 actúe como aceptor o donador de protones para facilitar la transferencia de hidruros entre el cofactor y el sustrato (**Figura 37**).<sup>81</sup>

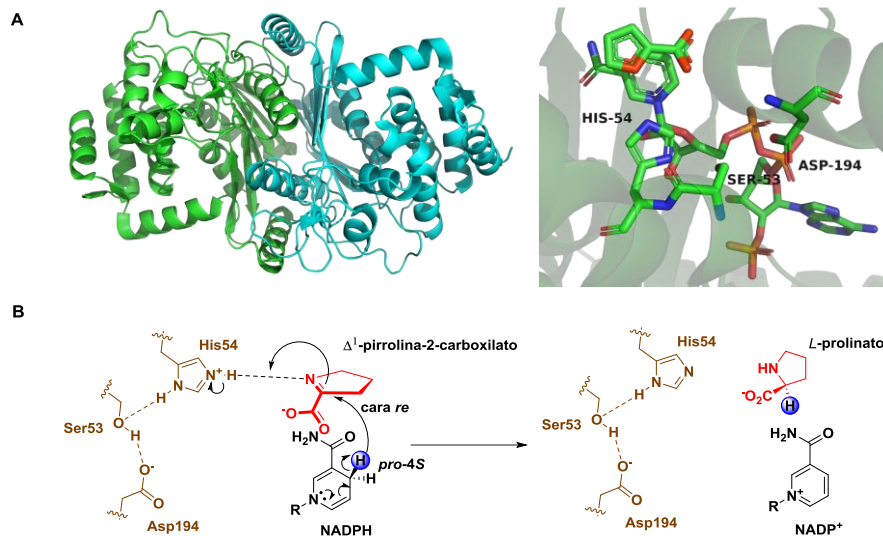


**Figura 37.** Representación de la estructura de la DpkA obtenida por difracción de Rayos X. **A.** Estructura dimérica de la enzima con el pirrol-2-carboxilato (P2C, análogo del sustrato) y el NADP<sup>+</sup> unidos al centro activo. Las subunidades se representan en diferentes colores, verde y azul. Además, se muestran los aminoácidos que participan en la catálisis (Ser53, His54 y Asp194). **B.** Mecanismo catalítico propuesto en la reducción del  $\Delta^1$ -pirrolina-2-carboxilato catalizado por la DpkA. El hidrógeno *pro-4S* del NADPH es transferido a la cara *re* del grupo imina del sustrato dándose una protonación del nitrógeno mediado por la His54, obteniéndose así, los productos de la reacción: L-prolinato y NADP<sup>+</sup>.<sup>81</sup> Se utilizó el PDB 2CWH para generar las estructuras de la DpkA utilizando el programa PyMOL versión 2.3.2.

La DpkA cataliza la reducción de iminas cíclicas como el  $\Delta^1$ -Piperideine-2-carboxilato y el  $\Delta^1$ -pirroline-2-carboxilato formando L-pipecolato y L-prolina, respectivamente (**Figura 37A**).<sup>81</sup> Por otra parte, DpkA es capaz de reducir estereoselectivamente iminas formadas entre 2-oxoácidos y metilamina obteniéndose *N*-metil-L-aminoácidos (**Figura 38**).

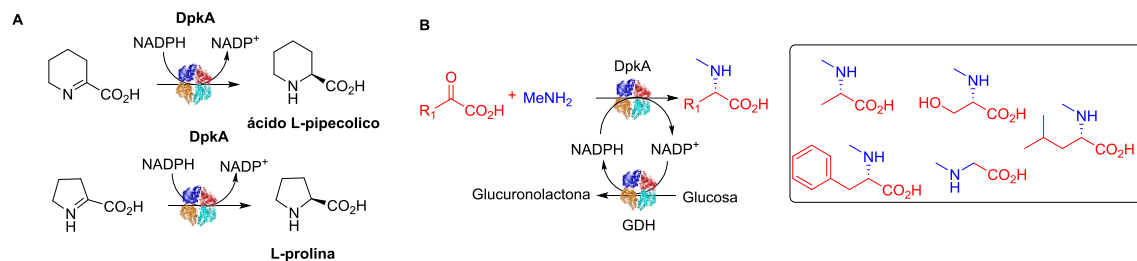


**Figura 38.** Reacciones enzimáticas catalizadas por la DpkA. **A.** Reacciones naturales catalizada por la enzima. **B.** Síntesis de *N*-metil-L-aminoácidos a partir de metilamina y diversos 2-oxoácidos acoplada con GDH (glucosa deshidrogenasa) para el reciclado de cofactores.

A pesar de esto, todas las potencialidades sintéticas de la DpkA no han sido estudiadas. Por ello, en esta Tesis nos planteamos introducir esta enzima en cascadas enzimáticas junto con aldolasas estereoselectivas, lo que permitiría crear moléculas quirales a partir de precursores aquirales sencillos.

## Referencias.

1. (a) Kumar, A.; Gudiukaite, R.; Gricajeva, A.; Sadauskas, M.; Malunavicius, V.; Kamyab, H.; Sharma, S.; Sharma, T.; Pant, D., Microbial lipolytic enzymes—promising energy-efficient biocatalysts in bioremediation. *Energy* **2020**, *192*, 116674; (b) Arsalan, A.; Younus, H., Enzymes and nanoparticles: Modulation of enzymatic activity via nanoparticles. *International journal of biological macromolecules* **2018**, *118*, 1833-1847; (c) Voet, D.; Voet, J. G., *Biochemistry*. John Wiley & Sons: 2010; (d) Bell, E. L.; Finnigan, W.; France, S. P.; Green, A. P.; Hayes, M. A.; Hepworth, L. J.; Lovelock, S. L.; Niikura, H.; Osuna, S.; Romero, E., Biocatalysis. *Nature Reviews Methods Primers* **2021**, *1* (1), 46.
2. Copeland, R. A., A brief history of enzymology. *Enzymes: A practical introduction to structure, mechanism, and data analysis* **2000**, *2*, 1-10.
3. Winkler, C. K.; Schrittwieser, J. H.; Kroutil, W., Power of biocatalysis for organic synthesis. *ACS central science* **2021**, *7* (1), 55-71.
4. (a) Grunwald, P., *Biocatalysis: biochemical fundamentals and applications*. World Scientific: 2009; (b) Zhao, L.; Jing, X.; Li, X.; Guo, X.; Zeng, L.; He, C.; Duan, C., Catalytic properties of chemical transformation within the confined pockets of Werner-type capsules. *Coordination Chemistry Reviews* **2019**, *378*, 151-187.
5. (a) Náráy-Szabó, G.; Mika, L. T., Conservative evolution and industrial metabolism in Green Chemistry. *Green chemistry* **2018**, *20* (10), 2171-2191; (b) Wheeler, G.; Ishikawa, T.; Pornsaksit, V.; Smirnov, N., Evolution of alternative biosynthetic pathways for vitamin C following plastid acquisition in photosynthetic eukaryotes. *Elife* **2015**, *4*, e06369.
6. Fani, R.; Fondi, M., Origin and evolution of metabolic pathways. *Physics of Life Reviews* **2009**, *6* (1), 23-52.
7. Pyser, J. B.; Chakrabarty, S.; Romero, E. O.; Narayan, A. R., State-of-the-art biocatalysis. *ACS Central Science* **2021**, *7* (7), 1105-1116.
8. (a) Guajardo, N.; Domínguez de María, P., Continuous biocatalysis in environmentally- friendly media: a triple synergy for future sustainable processes. *ChemCatChem* **2019**, *11* (14), 3128-3137; (b) Sheldon, R. A.; Pereira, P. C., Biocatalysis engineering: the big picture. *Chemical Society Reviews* **2017**, *46* (10), 2678-2691; (c) Tripathi, P.; Sinha, S., Industrial biocatalysis: An insight into trends and future directions. *Current Sustainable/Renewable Energy Reports* **2020**, *7*, 66-72; (d) Wu, S.; Snajdrova, R.; Moore, J. C.; Baldenius, K.; Bornscheuer, U. T., Biocatalysis: enzymatic synthesis for industrial applications. *Angewandte Chemie International Edition* **2021**, *60* (1), 88-119; (e) Stoineva, I. B.; Galunsky, B. P.; Lozanov, V. S.; Ivanov, I. P.; Petkov, D. D., Enzymic synthesis design and enzymic synthesis of aspartame. *Tetrahedron* **1992**, *48* (6), 1115-1122; (f) Alsoufi, M. A.; Aziz, R. A., Production of aspartame by immobilized thermolysin. *Iraqi Journal of Science* **2019**, 1232-1239; (g) Tang, G.; Deng, K.; Li, P.; Huang, J.; Dao, F.; Jiang, H.; Wang, J.; Jiang, J., One-pot method of recyclable lipase-nanocatalyst based on chitosan magnetic nanomaterial for ethyl levulinate synthesis. *Composites Science and Technology* **2023**, 110002; (h) Jia, B.; Liu, C.; Qi, X., Selective production of ethyl levulinate from levulinic acid by lipase-immobilized mesoporous silica nanoflowers composite. *Fuel Processing Technology* **2020**, *210*, 106578; (i) Armanino, N.; Charpentier, J.; Flachsmann, F.; Goeke, A.; Liniger, M.; Kraft, P., What's hot, what's not: the trends of the past 20 years in the chemistry of odorants. *Angewandte Chemie International Edition* **2020**, *59* (38), 16310-16344; (j) Jeandet, P.; Sobarzo-Sánchez, E.; Silva, A. S.; Clément, C.; Nabavi, S. F.; Battino, M.; Rasekhian, M.; Belwal, T.; Habtemariam, S.; Koffas, M., Whole-cell biocatalytic, enzymatic and green chemistry methods for the production of resveratrol and its derivatives. *Biotechnology advances* **2020**, *39*, 107461; (k) Kaminska, J.; Markowicz, L.; Stolarska, J.; Gora, J., Bakers' yeast mediated preparation of s (+)- 6-methyl- 5- hepten- 2- ol, the pheromone of an ambrosia beetle. *Acta biotechnologica* **1991**, *11* (1), 63-66; (l) Steele, A. D.; Kiefer, A. F.; Hwang, D.; Yang, D.; Teijaro, C. N.; Adhikari, A.; Rader, C.; Shen, B., Application of a Biocatalytic Strategy for the Preparation of Tiansimycin-Based Antibody-Drug Conjugates Revealing Key Insights into Structure-Activity Relationships. *Journal of medicinal chemistry* **2023**.
9. McDonald, A. G.; Boyce, S.; Tipton, K. F., ExplorEnz: the primary source of the IUBMB enzyme list. *Nucleic acids research* **2009**, *37* (suppl\_1), D593-D597.
10. (a) Ringborg, R. H.; Woodley, J., The application of reaction engineering to biocatalysis. *Reaction Chemistry & Engineering* **2016**, *1* (1), 10-22; (b) McDonald, A. G.; Tipton, K. F., Fifty- five years of

- enzyme classification: advances and difficulties. *The FEBS journal* **2014**, *281* (2), 583-592; (c) Probst, D.; Manica, M.; Nana Teukam, Y. G.; Castrogiovanni, A.; Paratore, F.; Laino, T., Biocatalysed synthesis planning using data-driven learning. *Nature communications* **2022**, *13* (1), 964.
11. Chen, Q.; Xie, B.; Zhou, L.; Sun, L.; Li, S.; Chen, Y.; Shi, S.; Li, Y.; Yu, M.; Li, W., A tailor-made self-sufficient whole-cell biocatalyst enables scalable enantioselective synthesis of (R)-3-quinuclidinol in a high space-time yield. *Organic Process Research & Development* **2019**, *23* (9), 1813-1821.
12. Li, F.; Yang, L. C.; Zhang, J.; Chen, J. S.; Renata, H., Stereoselective Synthesis of  $\beta$ - Branched Aromatic  $\alpha$ - Amino Acids by Biocatalytic Dynamic Kinetic Resolution. *Angewandte Chemie International Edition* **2021**, *60* (32), 17680-17685.
13. Sun, Z.; Lonsdale, R.; Wu, L.; Li, G.; Li, A.; Wang, J.; Zhou, J.; Reetz, M. T., Structure-guided triple-code saturation mutagenesis: efficient tuning of the stereoselectivity of an epoxide hydrolase. *ACS Catalysis* **2016**, *6* (3), 1590-1597.
14. Rea, D.; Hovington, R.; Rakus, J. F.; Gerlt, J. A.; Fülöp, V.; Bugg, T. D.; Roper, D. I., Crystal structure and functional assignment of YfaU, a metal ion dependent class II aldolase from Escherichia coli K12. *Biochemistry* **2008**, *47* (38), 9955-9965.
15. Choo, J. P.; Li, Z., Styrene Oxide Isomerase Catalyzed Meinwald Rearrangement Reaction: Discovery and Application in Single-Step and One-Pot Cascade Reactions. *Organic Process Research & Development* **2022**, *26* (7), 1960-1970.
16. Petchey, M. R.; Rowlinson, B.; Lloyd, R. C.; Fairlamb, I. J.; Grogan, G., Biocatalytic synthesis of moclobemide using the amide bond synthetase McbA coupled with an ATP recycling system. *ACS Catalysis* **2020**, *10* (8), 4659-4663.
17. (a) Rix, G.; Watkins-Dulaney, E. J.; Almhjell, P. J.; Boville, C. E.; Arnold, F. H.; Liu, C. C., Scalable continuous evolution for the generation of diverse enzyme variants encompassing promiscuous activities. *Nature communications* **2020**, *11* (1), 5644; (b) Chen, K.; Arnold, F. H., Engineering new catalytic activities in enzymes. *Nature Catalysis* **2020**, *3* (3), 203-213; (c) Bloom, J. D.; Arnold, F. H., In the light of directed evolution: pathways of adaptive protein evolution. *Proceedings of the National Academy of Sciences* **2009**, *106* (supplement\_1), 9995-10000.
18. Jensen, R. A., Enzyme recruitment in evolution of new function. *Annual review of microbiology* **1976**, *30* (1), 409-425.
19. (a) O'Brien, P. J.; Herschlag, D., Catalytic promiscuity and the evolution of new enzymatic activities. *Chemistry & biology* **1999**, *6* (4), R91-R105; (b) Copley, S. D., Enzymes with extra talents: moonlighting functions and catalytic promiscuity. *Current Opinion in Chemical Biology* **2003**, *7* (2), 265-272; (c) Renata, H.; Wang, Z. J.; Arnold, F. H., Expanding the enzyme universe: accessing non- natural reactions by mechanism- guided directed evolution. *Angewandte Chemie International Edition* **2015**, *54* (11), 3351-3367.
20. Schirch, V.; Szebenyi, D. M., Serine hydroxymethyltransferase revisited. *Current Opinion in Chemical Biology* **2005**, *9* (5), 482-487.
21. (a) Gutierrez, M. L.; Garrabou, X.; Agosta, E.; Servi, S.; Parella, T.; Joglar, J.; Clapés, P., Serine Hydroxymethyl Transferase from Streptococcus thermophilus and l- Threonine Aldolase from Escherichia coli as Stereocomplementary Biocatalysts for the Synthesis of  $\beta$ - Hydroxy-  $\alpha$ ,  $\omega$ - diamino Acid Derivatives. *Chemistry—A European Journal* **2008**, *14* (15), 4647-4656; (b) Hernandez, K.; Zelen, I.; Petrillo, G.; Usón, I.; Wandtke, C. M.; Bujons, J.; Joglar, J.; Parella, T.; Clapés, P., Engineered L- Serine Hydroxymethyltransferase from Streptococcus thermophilus for the Synthesis of  $\alpha$ ,  $\alpha$ - dialkyl-  $\alpha$ - amino acids. *Angewandte Chemie* **2015**, *127* (10), 3056-3060.
22. Eaton, R. W., trans-o-Hydroxybenzylidenepyruvate Hydratase-Aldolase as a Biocatalyst. *Applied and environmental microbiology* **2000**, *66* (6), 2668-2672.
23. Fansher, D. J.; Ngwira, N.; Salehi, A. R.; Woods, J.; Cascao, A.; Palmer, D. R., Biocatalytic Synthesis of  $\alpha$ ,  $\beta$ -Unsaturated 2-Keto Acids and Derivatives Using the Promiscuous Aldolase, NahE. *Synthesis* **2023**, *55* (01), 75-89.



24. Fansher, D. J.; Palmer, D. R., A Type 1 Aldolase, NahE, Catalyzes a Stereoselective Nitro- Michael Reaction: Synthesis of  $\beta$ - Aryl-  $\gamma$ - nitrobutyric Acids. *Angewandte Chemie, International Edition* **2023**, *62* (6), e202214539.
25. Fox, R. J.; Davis, S. C.; Mundorff, E. C.; Newman, L. M.; Gavrilovic, V.; Ma, S. K.; Chung, L. M.; Ching, C.; Tam, S.; Muley, S., Improving catalytic function by ProSAR-driven enzyme evolution. *Nature biotechnology* **2007**, *25* (3), 338-344.
26. (a) Huffman, M. A.; Fryszkowska, A.; Alvizo, O.; Borra-Garske, M.; Campos, K. R.; Canada, K. A.; Devine, P. N.; Duan, D.; Forstater, J. H.; Grosser, S. T., Design of an in vitro biocatalytic cascade for the manufacture of islatravir. *Science* **2019**, *366* (6470), 1255-1259; (b) Nicolaou, K.; Edmonds, D. J.; Bulger, P. G., Cascade reactions in total synthesis. *Angewandte Chemie International Edition* **2006**, *45* (43), 7134-7186.
27. Schrittwieser, J. H.; Velikogne, S.; Hall, M. I.; Kroutil, W., Artificial biocatalytic linear cascades for preparation of organic molecules. *Chemical Reviews* **2018**, *118* (1), 270-348.
28. Benítez-Mateos, A. I.; Roura Padrosa, D.; Paradisi, F., Multistep enzyme cascades as a route towards green and sustainable pharmaceutical syntheses. *Nature chemistry* **2022**, *14* (5), 489-499.
29. (a) González-Granda, S.; Albarrán-Velo, J.; Lavandera, I.; Gotor-Fernández, V., Expanding the Synthetic Toolbox through Metal–Enzyme Cascade Reactions. *Chemical reviews* **2023**; (b) Zhou, Y.; Wu, S.; Bornscheuer, U. T., Recent advances in (chemo) enzymatic cascades for upgrading bio-based resources. *Chemical communications* **2021**, *57* (82), 10661-10674; (c) Schwendenwein, D.; Ressmann, A. K.; Entner, M.; Savic, V.; Winkler, M.; Rudroff, F., Chemo-enzymatic cascade for the generation of fragrance aldehydes. *Catalysts* **2021**, *11* (8), 932; (d) Calderini, E.; Süß, P.; Hollmann, F.; Wardenga, R.; Schallmeyer, A., Two (Chemo)-enzymatic cascades for the production of opposite enantiomers of chiral azidoalcohols. *Catalysts* **2021**, *11* (8), 982; (e) Risi, C.; Zhao, F.; Castagnolo, D., Chemo-enzymatic metathesis/aromatization cascades for the synthesis of furans: Disclosing the aromatizing activity of laccase/TEMPO in oxygen-containing heterocycles. *ACS Catalysis* **2019**, *9* (8), 7264-7269; (f) Zhao, F.; Masci, D.; Tomarelli, E.; Castagnolo, D., Biocatalytic and Chemo-Enzymatic Approaches for the Synthesis of Heterocycles. *Synthesis* **2020**, *52* (20), 2948-2961; (g) Özgen, F. F.; Runda, M. E.; Schmidt, S., Photo-biocatalytic Cascades: Combining Chemical and Enzymatic Transformations Fueled by Light. *ChemBioChem* **2021**, *22* (5), 790-806; (h) Wu, S.; Zhou, Y.; Gerngross, D.; Jeschek, M.; Ward, T. R., Chemo-enzymatic cascades to produce cycloalkenes from bio-based resources. *Nature communications* **2019**, *10* (1), 5060.
30. Hernandez, K.; Bujons, J.; Joglar, J. s.; Charnock, S. J.; Dominguez de Maria, P.; Fessner, W. D.; Clapés, P., Combining aldolases and transaminases for the synthesis of 2-amino-4-hydroxybutanoic acid. *ACS Catalysis* **2017**, *7* (3), 1707-1711.
31. Česnik Katulić, M.; Sudar, M.; Hernández, K.; Qi, Y.; Charnock, S. J.; Vasić-Rački, Đ.; Clapés, P.; Findrik Blažević, Z., Cascade Synthesis of l-Homoserine Catalyzed by Lyophilized Whole Cells Containing Transaminase and Aldolase Activities: The Mathematical Modeling Approach. *Industrial & Engineering Chemistry Research* **2021**, *60* (38), 13846-13858.
32. Escalettes, F.; Turner, N. J., Directed evolution of galactose oxidase: generation of enantioselective secondary alcohol oxidases. *ChemBioChem* **2008**, *9* (6), 857-860.
33. Birmingham, W. R.; Turner, N. J., A single enzyme oxidative “cascade” via a dual-functional galactose oxidase. *ACS Catalysis* **2018**, *8* (5), 4025-4032.
34. Zhang, J.; Yang, X.; Dong, R.; Gao, L.; Li, J.; Li, X.; Huang, S.; Zhang, C.; Chang, H., Cascade biocatalysis for regio- and stereoselective aminohydroxylation of styrenyl olefins to enantiopure arylglycinols. *ACS sustainable chemistry & engineering* **2020**, *8* (49), 18277-18285.
35. Padrosa, D. R.; Benítez-Mateos, A. I.; Calvey, L.; Paradisi, F., Cell-free biocatalytic syntheses of l-pipecolic acid: A dual strategy approach and process intensification in flow. *Green chemistry* **2020**, *22* (16), 5310-5316.
36. Ricca, E.; Brucher, B.; Schrittwieser, J. H., Multi- enzymatic cascade reactions: overview and perspectives. *Advanced Synthesis & Catalysis* **2011**, *353* (13), 2239-2262.

37. Lubberink, M.; Schnepel, C.; Citoler, J.; Derrington, S. R.; Finnigan, W.; Hayes, M. A.; Turner, N. J.; Flitsch, S. L., Biocatalytic monoacylation of symmetrical diamines and its application to the synthesis of pharmaceutically relevant amides. *ACS Catalysis* **2020**, *10* (17), 10005-10009.
38. Sehl, T.; Hailes, H. C.; Ward, J. M.; Wardenga, R.; von Lieres, E.; Offermann, H.; Westphal, R.; Pohl, M.; Rother, D., Two steps in one pot: enzyme cascade for the synthesis of nor (pseudo) ephedrine from inexpensive starting materials. *Angewandte Chemie International Edition* **2013**, *52* (26), 6772-6775.
39. Lichman, B.; Lamming, E.; Pesnot, T.; Smith, J.; Hailes, H.; Ward, J., One-pot triangular chemoenzymatic cascades for the syntheses of chiral alkaloids from dopamine. *Green Chemistry* **2015**, *17* (2), 852-855.
40. (a) Desmons, S.; Fauré, R.; Bontemps, S., Formaldehyde as a promising C1 source: the instrumental role of biocatalysis for stereocontrolled reactions. *ACS Catalysis* **2019**, *9* (10), 9575-9588; (b) Miao, Y.; Rahimi, M.; Geertsema, E. M.; Poelarends, G. J., Recent developments in enzyme promiscuity for carbon-carbon bond-forming reactions. *Current Opinion in Chemical Biology* **2015**, *25*, 115-123; (c) Windle, C. L.; Müller, M.; Nelson, A.; Berry, A., Engineering aldolases as biocatalysts. *Current Opinion in Chemical Biology* **2014**, *19*, 25-33.
41. (a) Walters, M. J.; Toone, E. J., Pyruvate aldolases in chiral carbon-carbon bond formation. *Nature Protocols* **2007**, *2* (7), 1825-1830; (b) Clapés, P.; Fessner, W.-D.; Sprenger, G. A.; Samland, A. K., Recent progress in stereoselective synthesis with aldolases. *Current Opinion in Chemical Biology* **2010**, *14* (2), 154-167.
42. Flechner, A.; Gross, W.; Martin, W. F.; Schnarrenberger, C., Chloroplast class I and class II aldolases are bifunctional for fructose- 1, 6- biphosphate and sedoheptulose- 1, 7- biphosphate cleavage in the Calvin cycle. *FEBS Letters* **1999**, *447* (2-3), 200-202.
43. Hernández, K.; Szekrenyi, A.; Clapés, P., Nucleophile promiscuity of natural and engineered aldolases. *ChemBioChem* **2018**, *19* (13), 1353-1358.
44. (a) Hernández, K.; Joglar, J.; Bujons, J.; Parella, T.; Clapés, P., Nucleophile promiscuity of engineered class II pyruvate aldolase YfaU from *E. coli*. *Angewandte Chemie, International Edition* **2018**, *57* (14), 3583-3587; (b) Laurent, V.; Gourbeyre, L.; Uzel, A.; Hélaïne, V.; Nauton, L.; Traïkia, M.; de Berardinis, V.; Salanoubat, M.; Gefflaut, T.; Lemaire, M., Pyruvate aldolases catalyze cross-aldol reactions between ketones: Highly selective access to multi-functionalized tertiary alcohols. *ACS Catalysis* **2020**, *10* (4), 2538-2543; (c) Royer, S. F.; Gao, X.; Groleau, R. R.; Van der Kamp, M. W.; Bull, S. D.; Danson, M. J.; Crennell, S. J., Structurally Informed Mutagenesis of a Stereochemically Promiscuous Aldolase Produces Mutants That Catalyze the Diastereoselective Syntheses of All Four Stereoisomers of 3-Deoxy-hexulonic Acid. *ACS Catalysis* **2022**, *12* (18), 11444-11455.
45. Lancaster, E. B.; Johnson Jr, W. H.; LeVieux, J. A.; Hardtke, H. A.; Zhang, Y. J.; Whitman, C. P., A mutagenic analysis of NahE, a hydratase-aldolase in the naphthalene degradative pathway. *Archives of Biochemistry and Biophysics* **2023**, *733*, 109471.
46. Stolz, A., Degradation of substituted naphthalenesulfonic acids by *Sphingomonas xenophaga* BN6. *Journal of Industrial Microbiology and Biotechnology* **1999**, *23*, 391-399.
47. Davies, J.; Evans, W., Oxidative metabolism of naphthalene by soil pseudomonads. The ring-fission mechanism. *Biochemical Journal* **1964**, *91* (2), 251.
48. LeVieux, J. A. Structure-based mechanism of hydratase-aldolases in the Type I aldolase superfamily and structures of tautomerase superfamily members. 2017.
49. (a) Howard, J. K.; Müller, M.; Berry, A.; Nelson, A., An Enantio- and Diastereoselective Chemoenzymatic Synthesis of  $\alpha$ -Fluoro  $\beta$ -Hydroxy Carboxylic Esters. **2016**; (b) Windle, C. L.; Berry, A.; Nelson, A., Aldolase-catalysed stereoselective synthesis of fluorinated small molecules. *Current Opinion in Chemical Biology* **2017**, *37*, 33-38.
50. Sello, G.; Di Gennaro, P., Aldol Reactions of the trans-*o*-Hydroxybenzylidenepyruvate Hydratase-Aldolase (t HBP-HA) from *Pseudomonas fluorescens* N3. *Applied biochemistry and biotechnology* **2013**, *170*, 1702-1712.
51. Fansher, D. J.; Granger, R.; Kaur, S.; Palmer, D. R., Repurposing an aldolase for the chemoenzymatic synthesis of substituted quinolines. *ACS Catalysis* **2021**, *11* (12), 6939-6943.

52. Fansher, D. J.; Palmer, D. R., A Type 1 Aldolase, NahE, Catalyzes a Stereoselective Nitro- Michael Reaction: Synthesis of  $\beta$ - Aryl-  $\gamma$ - nitrobutyric Acids. *Angewandte Chemie International Edition* **2023**, *62* (6), e202214539.
53. Sugantino, M.; Zheng, R.; Yu, M.; Blanchard, J. S., Mycobacterium tuberculosis ketopantoate hydroxymethyltransferase: Tetrahydrofolate-independent hydroxymethyltransferase and enolization reactions with  $\alpha$ -keto acids. *Biochemistry* **2003**, *42* (1), 191-199.
54. von Delft, F.; Inoue, T.; Saldanha, S. A.; Ottenhof, H. H.; Schmitzberger, F.; Birch, L. M.; Dhanaraj, V.; Witty, M.; Smith, A. G.; Blundell, T. L., Structure of E. coli ketopantoate hydroxymethyl transferase complexed with ketopantoate and Mg<sup>2+</sup>, solved by locating 160 selenomethionine sites. *Structure* **2003**, *11* (8), 985-996.
55. Marín-Valls, R.; Hernandez, K.; Bolte, M.; Joglar, J. s.; Bujons, J.; Clapes, P., Chemoenzymatic hydroxymethylation of carboxylic acids by tandem stereodivergent biocatalytic aldol reaction and chemical decarboxylation. *ACS Catalysis* **2019**, *9* (8), 7568-7577.
56. Pickl, M.; Marín- Valls, R.; Joglar, J.; Bujons, J.; Clapés, P., Chemoenzymatic Production of Enantiocomplementary 2- Substituted 3- Hydroxycarboxylic Acids from 1-  $\alpha$ - Amino Acids. *Advanced Synthesis & Catalysis* **2021**, *363* (11), 2866-2876.
57. Hiesinger, K.; Dar'in, D.; Proschak, E.; Krasavin, M., Spirocyclic scaffolds in medicinal chemistry. *Journal of medicinal chemistry* **2020**, *64* (1), 150-183.
58. Marín-Valls, R.; Hernández, K.; Bolte, M.; Parella, T.; Joglar, J. s.; Bujons, J.; Clapés, P., Biocatalytic construction of quaternary centers by aldol addition of 3, 3-disubstituted 2-oxoacid derivatives to aldehydes. *Journal of the American Chemical Society* **2020**, *142* (46), 19754-19762.
59. Hernández, K.; Gómez, A.; Joglar, J.; Bujons, J.; Parella, T.; Clapés, P., 2- Keto- 3- Deoxy- 1- Rhamnonate Aldolase (YfaU) as Catalyst in Aldol Additions of Pyruvate to Amino Aldehyde Derivatives. *Advanced Synthesis & Catalysis* **2017**, *359* (12), 2090-2100.
60. Hernández, K.; Joglar, J.; Bujons, J.; Parella, T.; Clapés, P., Nucleophile promiscuity of engineered class II pyruvate aldolase YfaU from E. coli. *Angewandte Chemie International Edition* **2018**, *57* (14), 3583-3587.
61. (a) Ghislieri, D.; Turner, N. J., Biocatalytic approaches to the synthesis of enantiomerically pure chiral amines. *Topics in Catalysis* **2014**, *57*, 284-300; (b) Slabu, I.; Galman, J. L.; Lloyd, R. C.; Turner, N. J., Discovery, engineering, and synthetic application of transaminase biocatalysts. *ACS Catalysis* **2017**, *7* (12), 8263-8284.
62. Eliot, A. C.; Kirsch, J. F., Pyridoxal phosphate enzymes: mechanistic, structural, and evolutionary considerations. *Annual review of biochemistry* **2004**, *73* (1), 383-415.
63. (a) Kelly, S. A.; Pohle, S.; Wharry, S.; Mix, S.; Allen, C. C.; Moody, T. S.; Gilmore, B. F., Application of  $\omega$ -transaminases in the pharmaceutical industry. *Chemical Reviews* **2018**, *118* (1), 349-367; (b) de la Torre, F.; Santis, L. D.; Suárez, M. F.; Crespillo, R.; Cánovas, F. M., Identification and functional analysis of a prokaryotic- type aspartate aminotransferase: implications for plant amino acid metabolism. *The Plant Journal* **2006**, *46* (3), 414-425.
64. Guérard-Hélaine, C.; Heuson, E.; Ndiaye, M.; Gourbeyre, L.; Lemaire, M.; Hélaine, V.; Charmantray, F.; Petit, J.-L.; Salanoubat, M.; de Berardinis, V., Stereoselective synthesis of  $\gamma$ -hydroxy- $\alpha$ -amino acids through aldolase–transaminase recycling cascades. *Chemical communications* **2017**, *53* (39), 5465-5468.
65. Goto, M.; Miyahara, I.; Hayashi, H.; Kagamiyama, H.; Hirotsu, K., Crystal structures of branched-chain amino acid aminotransferase complexed with glutamate and glutarate: true reaction intermediate and double substrate recognition of the enzyme. *Biochemistry* **2003**, *42* (13), 3725-3733.
66. Seo, Y.-M.; Kim, A.; Bea, H.-S.; Lee, S.-H.; Yun, H., Asymmetric synthesis of 1-6-hydroxynorleucine from 2-keto-6-hydroxyhexanoic acid using a branched-chain aminotransferase. *Biocatalysis and Biotransformation* **2012**, *30* (2), 171-176.
67. Young Hong, E.; Cha, M.; Yun, H.; Kim, B.-G., Asymmetric synthesis of L-tert-leucine and L-3-hydroxyadamantylglycine using branched chain aminotransferase. *Journal of Molecular Catalysis B: Enzymatic* **2010**, *66* (1-2), 228-233.

68. McDonald, A., The Enzyme List Class 1—Oxidoreductases. *Nomenclature Committee of the International Union of Biochemistry and Molecular Biology (NC-IUBMB)* **2019**.
69. Monti, D.; Ottolina, G.; Carrea, G.; Riva, S., Redox reactions catalyzed by isolated enzymes. *Chemical reviews* **2011**, *111* (7), 4111-4140.
70. Hollmann, F.; Opperman, D. J.; Paul, C. E., Biocatalytic reduction reactions from a chemist's perspective. *Angewandte Chemie International Edition* **2021**, *60* (11), 5644-5665.
71. (a) Galloway, W. R.; Hodgkinson, J. T.; Bowden, S. D.; Welch, M.; Spring, D. R., Quorum sensing in Gram-negative bacteria: small-molecule modulation of AHL and AI-2 quorum sensing pathways. *Chemical Reviews* **2011**, *111* (1), 28-67; (b) Cavanaugh, C. L.; Nicewicz, D. A., Synthesis of  $\alpha$ -benzyloxyamino- $\gamma$ -butyrolactones via a polar radical crossover cycloaddition reaction. *Organic letters* **2015**, *17* (24), 6082-6085.
72. Yang, J.; Bogni, A.; Schuetz, E. G.; Ratain, M.; Dolan, M. E.; McLeod, H.; Gong, L.; Thorn, C.; Relling, M. V.; Klein, T. E., Etoposide pathway. *Pharmacogenetics and genomics* **2009**, *19* (7), 552-553.
73. Korpak, M.; Pietruszka, J., Chemoenzymatic one-pot synthesis of  $\gamma$ -butyrolactones. *Advanced Synthesis & Catalysis* **2011**, *353* (9), 1420-1424.
74. NOZAKI, Y.; KATAYAMA, N.; HARADA, S.; ONO, H.; OKAZAKI, H., Lactivicin, a naturally occurring non- $\beta$ -lactam antibiotic having  $\beta$ -lactam-like action: biological activities and mode of action. *The Journal of antibiotics* **1989**, *42* (1), 84-93.
75. Tanaka, K.; Itazaki, H.; Yoshida, T., Cinatrins, a novel family of phospholipase A2 inhibitors ii. Biological activities. *The Journal of antibiotics* **1992**, *45* (1), 50-55.
76. (a) Hu, Z.-Q.; Li, X.; Liu, L.-X.; Yu, C.-B.; Zhou, Y.-G., Ruthenium-Catalyzed Asymmetric Transfer Hydrogenation of  $\beta$ -Substituted  $\alpha$ -Oxobutyrolactones. *The Journal of organic chemistry* **2021**, *86* (23), 17453-17461; (b) Blandin, V.; Carpentier, J. F.; Mortreux, A., Asymmetric Hydrogenation of 2, 4- Dioxo Esters: Selective Synthesis of 2- Hydroxy- 4- oxo Esters and Direct Access to Chiral 2- Hydroxy- 4- butyrolactones. *European Journal of Organic Chemistry* **1999**, *1999* (8), 1787-1793.
77. Evans, D. A.; Wu, J.; Masse, C. E.; MacMillan, D. W., A general method for the enantioselective synthesis of pantolactone derivatives. *Organic letters* **2002**, *4* (20), 3379-3382.
78. Chen, B.; Yin, H. F.; Wang, Z. S.; Xu, J. H.; Fan, L. Q.; Zhao, J., Facile Synthesis of Enantiopure 4-Substituted 2- Hydroxy- 4- butyrolactones using a Robust Fusarium Lactonase. *Advanced Synthesis & Catalysis* **2009**, *351* (17), 2959-2966.
79. Ciulli, A.; Chirgadze, D. Y.; Smith, A. G.; Blundell, T. L.; Abell, C., Crystal structure of Escherichia coli ketopantoate reductase in a ternary complex with NADP<sup>+</sup> and pantoate bound: substrate recognition, conformational change, and cooperativity. *Journal of Biological Chemistry* **2007**, *282* (11), 8487-8497.
80. Matak-Vinković, D.; Vinković, M.; Saldanha, S. A.; Ashurst, J. L.; von Delft, F.; Inoue, T.; Miguel, R. N.; Smith, A. G.; Blundell, T. L.; Abell, C., Crystal structure of Escherichia coli ketopantoate reductase at 1.7 Å resolution and insight into the enzyme mechanism. *Biochemistry* **2001**, *40* (48), 14493-14500.
81. Goto, M.; Muramatsu, H.; Mihara, H.; Kurihara, T.; Esaki, N.; Omi, R.; Miyahara, I.; Hirotsu, K., Crystal structures of  $\Delta$ 1-piperideine-2-carboxylate/ $\Delta$ 1-pyrroline-2-carboxylate reductase belonging to a new family of NAD (P) H-dependent oxidoreductases: conformational change, substrate recognition, and stereochemistry of the reaction. *Journal of Biological Chemistry* **2005**, *280* (49), 40875-40884.
82. (a) Muramatsu, H.; Mihara, H.; Kakutani, R.; Yasuda, M.; Ueda, M.; Kurihara, T.; Esaki, N., The putative malate/lactate dehydrogenase from Pseudomonas putida is an NADPH-dependent  $\Delta$ 1-piperideine-2-carboxylate/ $\Delta$ 1-pyrroline-2-carboxylate reductase involved in the catabolism of d-lysine and d-proline. *Journal of Biological Chemistry* **2005**, *280* (7), 5329-5335; (b) Miller, D. L.; Rodwell, V. W., Metabolism of basic amino acids in Pseudomonas putida: Catabolism of lysine by cyclic and acyclic intermediates. *Journal of Biological Chemistry* **1971**, *246* (9), 2758-2764.

**Sección II**

# **OBJETIVOS**

### **1.1. Objetivo general:**

Desarrollar estrategias biocatalíticas concurrentes de compuestos quirales multifuncionales en ensayos enzimáticos acoplados entre aldolasas con transaminasas o deshidrogenasas.

### **1.2. Objetivos específicos:**

Establecer estrategias para la síntesis diastereoselectiva de  $\gamma$ -hidroxi- $\alpha$ -aminoácidos mediante la combinación de una piruvato-aldolasa enantioselectiva HBPA y transaminasas *S*-selectivas.

Diseñar estrategias de síntesis biocatalítica de derivados de 2-hidroxi-4-butirolactona utilizando aldolasas y deshidrogenasas.

Ampliar las aplicaciones sintéticas de la  $\Delta^1$ -piperidina-2-carboxilato/ $\Delta^1$ -pirrolina-2-carboxilato reductasa de *Pseudomonas syringae* (DpkA) que permitan la síntesis asimétrica de derivados del ácido (*S,E*)-2-hidroxi-4-amilbut-3-enoico.



**Informe sobre las publicaciones generadas en esta Tesis de Doctorado:**

Como Director y co-Director de la Tesis de Doctorado presentada por el estudiante **Carlos José Moreno Fontalba**, el Prof. Pere Clapès Saborit y el Dr. Kárel Hernández Sánchez, respectivamente hacen constar que dos de los trabajos presentados en la sección de Resultados y Discusión han sido publicados en la revista *ACS Catalysis*:

- **Moreno, C. J., Hernández, K., Charnok, S. J., Gittings, S., Bolte, M., Joglar, J., ... & Clapés, P. (2021).** Synthesis of  $\gamma$ -hydroxy- $\alpha$ -amino acid derivatives by enzymatic tandem aldol addition–transamination reactions. *ACS catalysis*, 11(8), 4660-4669. (<https://doi.org/10.1021/acscatal.1c00210>)
- **Moreno, C. J., Hernández, K., Gittings, S., Bolte, M., Joglar, J., ... & Clapés, P. (2023).** Biocatalytic Synthesis of Homochiral 2-Hydroxy-4-butyrolactone Derivatives by Tandem Aldol Addition and Carbonyl Reduction. *ACS catalysis*, 13, 5348–5357. (<https://doi.org/10.1021/acscatal.3c00367>)

*ACS Catalysis* es una revista que cubre el área de la Catálisis (Q1) y la Química (miscelánea) (Q1) publicada por la *American Chemical Society*. Factor de impacto 2021-2022: 13.700.

En la realización de los trabajos publicados en esta Tesis de Doctorado el estudiante Carlos Jose Moreno Fontalba trabajó bajo la supervisión del Prof. Pere Clapès Saborit y el Dr. Kárel Hernández Sánchez participando directamente en:

- Análisis bibliográfico.
- Trabajos de Biología Molecular relacionados con la clonación, mutagénesis y expresión de proteínas.
- Trabajos de Química Orgánica relacionados con la síntesis, purificación y caracterización estructural de sustratos precursores y productos obtenidos por medios biocatalíticos.
- Elaboración de los materiales suplementarios y revisión de los diferentes trabajos publicados.

**Los artículos anteriormente mencionados han sido utilizados exclusivamente en la elaboración de la memoria de esta Tesis de Doctorado y en ninguna otra.**

Director de la Tesis,

Porf. Pere Clapès Saborit

Barcelona, a 11 de Abril de 2023

co-Director de la Tesis

Dr. Kárel Hernández Sánchez

**Sección III**

## **Capítulo 3.1**

Synthesis of  $\gamma$ -Hydroxy- $\alpha$ -amino Acid Derivatives by  
Enzymatic Tandem Aldol Addition–Transamination  
Reactions.



# Synthesis of $\gamma$ -Hydroxy- $\alpha$ -amino Acid Derivatives by Enzymatic Tandem Aldol Addition–Transamination Reactions

## Resumen

Los  $\gamma$ -hidroxi- $\alpha$ -aminoácidos son compuestos con importantes aplicaciones en la industria farmacéutica debido a sus actividades biológicas. Por ejemplo: la (2*S*,3*R*,4*S*)-4-hidroxiisoleucine, la 4-hidroxi-L-norvalina y el ácido 4-hidroxipecolico son utilizados para el tratamiento de la diabetes. Además, forman parte de precursores quirales de moléculas bioactivas como antibióticos, fungicidas y herbicidas, por ejemplo: las  $\alpha$ -amino- $\gamma$ -butirolactonas, la 4,5-dihidroxinorvaline o el ácido 4-hidroxi-piroglutamico y sus derivados. Debido a la importancia de estos compuestos en este capítulo nos planteamos la síntesis diastereoselectiva de  $\gamma$ -hidroxi- $\alpha$ -aminoácidos a través de reacciones enzimáticas consecutivas acoplando una aldolasa y varios sistemas enzimáticos de transaminación. La reacción aldólica consistió en la adición estereoselectiva de piruvato a aldehídos alifáticos catalizado por la *trans*-*O*-hidroxibenziliden piruvato hidratasa-aldolasa (HBPA) de *Pseudomonas putida*. Los (*R*)-4-hidroxi-2-oxoácidos obtenidos fueron aminados utilizando diferentes *S*-transaminasas: panel de  $\omega$ -transaminasas suministrado por la empresa Prozomix Ltd a través de una colaboración público-privada y  $\alpha$ -transaminasas clonadas, expresadas y purificadas en nuestro laboratorio. Bajo este enfoque la HBPA generó 4-hidroxi-oxoácidos con una eficiencia notable, amplia tolerancia al sustrato y alta estereoselectividad. Al acoplar esta enzima con los sistemas de transaminación bencilamina/T039 y BCAT/AspAT quedó claro que constituyen una alternativa complementaria para la síntesis de  $\gamma$ -hidroxi- $\alpha$ -aminoácidos quirales.

# Synthesis of $\gamma$ -Hydroxy- $\alpha$ -amino Acid Derivatives by Enzymatic Tandem Aldol Addition–Transamination Reactions

Carlos J. Moreno,<sup>1</sup> Karel Hernández,<sup>1</sup> Simon J. Charnok, Samantha Gittings, Michael Bolte, Jesús Joglar, Jordi Bujons, Teodor Parella, and Pere Clapés\*



Cite This: *ACS Catal.* 2021, 11, 4660–4669



Read Online

ACCESS |



Metrics & More



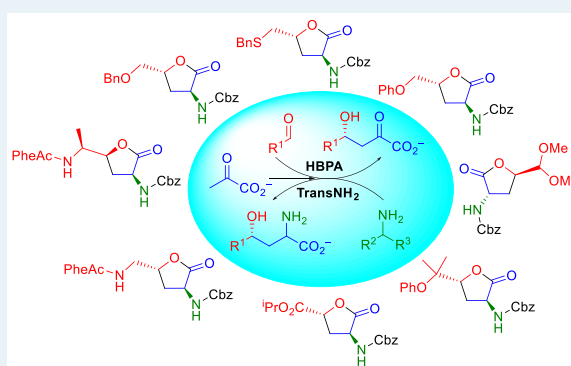
Article Recommendations



Supporting Information

**ABSTRACT:** Three enzymatic routes toward  $\gamma$ -hydroxy- $\alpha$ -amino acids by tandem aldol addition–transamination one-pot two-step reactions are reported. The approaches feature an enantioselective aldol addition of pyruvate to various nonaromatic aldehydes catalyzed by *trans*-*o*-hydroxybenzylidene pyruvate hydratase-aldolase (HBPA) from *Pseudomonas putida*. This affords chiral 4-hydroxy-2-oxo acids, which were subsequently enantioselectively aminated using *S*-selective transaminases. Three transamination processes were investigated involving different amine donors and transaminases: (i) L-Ala as an amine donor with pyruvate recycling, (ii) a benzylamine donor using benzaldehyde lyase from *Pseudomonas fluorescens* Biovar I (BAL) to transform the benzaldehyde formed into benzoin, minimizing equilibrium limitations, and (iii) L-Glu as an amine donor with a double cascade comprising branched-chain  $\alpha$ -amino acid aminotransferase (BCAT) and aspartate amino transferase (AspAT), both from *E. coli*, using L-Asp as a substrate to regenerate L-Glu. The  $\gamma$ -hydroxy- $\alpha$ -amino acids thus obtained were transformed into chiral  $\alpha$ -amino- $\gamma$ -butyrolactones, structural motifs found in many biologically active compounds and valuable intermediates for the synthesis of pharmaceutical agents.

**KEYWORDS:** biocatalysis, 2-oxoacid aldolase, transaminases, aldol addition, reductive amination,  $\gamma$ -hydroxy- $\alpha$ -amino acids



## INTRODUCTION

$\gamma$ -Hydroxy- $\alpha$ -amino acids represent compounds with relevant biological and pharmacological importance.<sup>1</sup> Examples include antidiabetics such as (2*S*,3*R*,4*S*)-4-hydroxyisoleucine, 4-hydroxy-L-norvaline, and 4-hydroxypipicolinic acid and nutritional supplements in the food industry, e.g. *trans*-4-hydroxy-L-proline.<sup>1*a*,2</sup> Moreover, they constitute structural motifs of more complex naturally occurring and synthetic molecules, namely antibiotics,<sup>3</sup> antimitotics,<sup>4</sup> and (bio)-herbicides,<sup>5</sup> as well as chiral building blocks for the production of active ingredients, e.g.  $\alpha$ -amino- $\gamma$ -butyrolactones, 4,5-dihydroxynorvaline, and 4-hydroxypyroglutamic acid and derivatives (Figure 1).<sup>2*b*,d,6</sup>

Therefore, substantial research efforts have been devoted to their synthesis using multistep catalytic or stoichiometric chemical approaches (Figure 2).<sup>1*a*,2*g*,7</sup> Biocatalytic access to these compounds is regarded as a powerful strategy because of their simplicity and stereoselectivity starting from simple achiral materials (Figure 2).<sup>2*c*,e,8</sup>

In this sense, the sequential combination of carbonylases and transaminases in one-pot one-step or one-pot two-step reactions with or without substrate recycling offers broad synthetic possibilities. Using this route, chiral L- and D-homoserine, D-*anti*-dihydroxynorvaline, 4-hydroxyisoleucine, norpseudoephedrine, and norephedrine were prepared.

However, the number of examples is scarce and, although they represent a remarkable achievement, they are often limited by the poor stereoselectivity profile of pyruvate aldolases as catalysts to generate the corresponding 4-hydroxy-2-oxo acid precursors or the lack of transaminase selectivity toward the aldol adduct.

Herein, we report three strategies for the biocatalytic diastereoselective synthesis of  $\gamma$ -hydroxy- $\alpha$ -amino acids by combining an enantioselective pyruvate-aldolase and *S*-selective transaminases,<sup>8*b*</sup> starting from pyruvate and diverse aldehyde substrates.

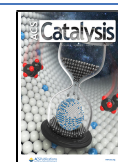
## RESULTS AND DISCUSSION

**Stereoselective Aldol Addition of Pyruvate to Aldehydes Catalyzed by *trans*-*o*-Hydroxybenzylidene Pyruvate Hydratase-Aldolase (HBPA).** The *trans*-*o*-hydroxybenzylidene pyruvate hydratase-aldolase (HBPA, EC 4.1.2.45) from *Pseudomonas putida* was discovered in the

Received: January 15, 2021

Revised: March 20, 2021

Published: April 2, 2021



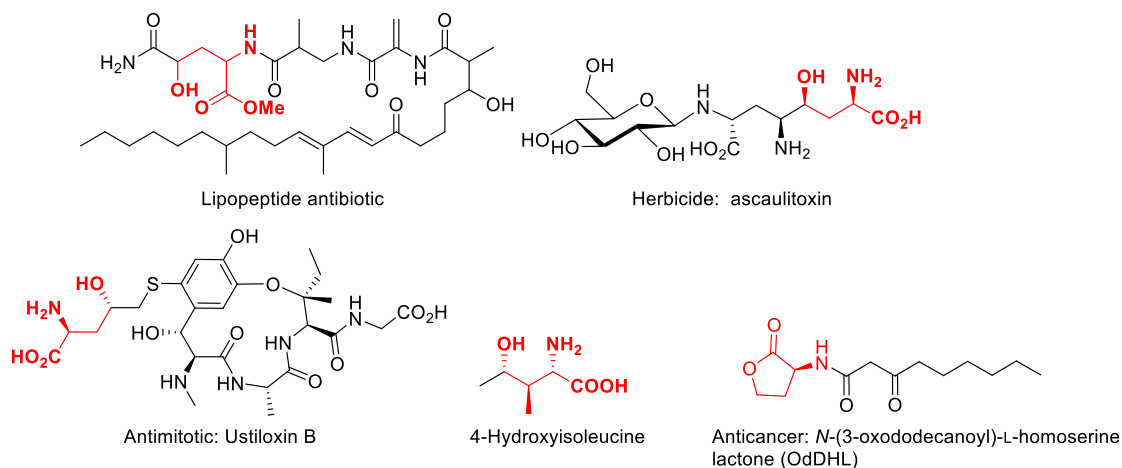


**Figure 1.** Examples of bioactive compounds bearing a  $\gamma$ -hydroxy- $\alpha$ -amino acid moiety or  $\alpha$ -amino- $\gamma$ -butyrolactone.

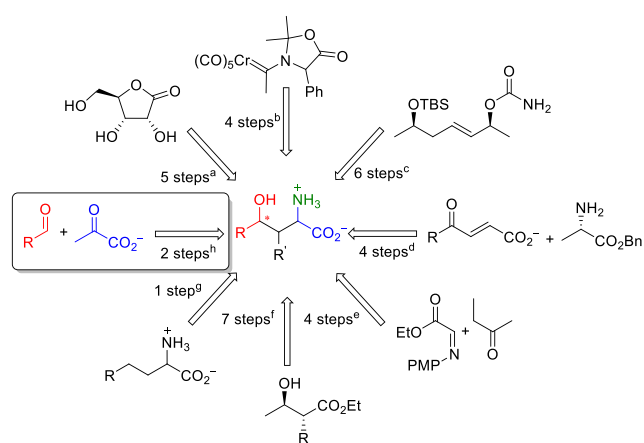


**Figure 2.** Examples of strategies for the synthesis  $\gamma$ -hydroxy- $\alpha$ -amino acids: (a) synthesis from *D*-ribonolactone as a chiral precursor and stereocontrolled transformation;<sup>7d</sup> (b) aldol reaction with oxazolidonyl chromium carbene complex and photocyclization;<sup>7c</sup> (c) cyanate to isocyanate rearrangement and enzymatic kinetic resolution;<sup>1a</sup> (d) aza-Michael additions controlled by a crystallization-induced asymmetric transformation;<sup>7f</sup> (e) Mannich condensation and catalytic epimerization;<sup>7b</sup> (f) palladium(II)-catalyzed aza Claisen rearrangements;<sup>7a</sup> (g) direct  $\beta$  or  $\gamma$ -hydroxylation of amino acids via  $\alpha$ -ketoglutarate-dependent dioxygenases;<sup>2c,8a</sup> (h) enzymatic synthesis via carbonylase-transaminase reactions.<sup>2e,8b,e,9</sup>

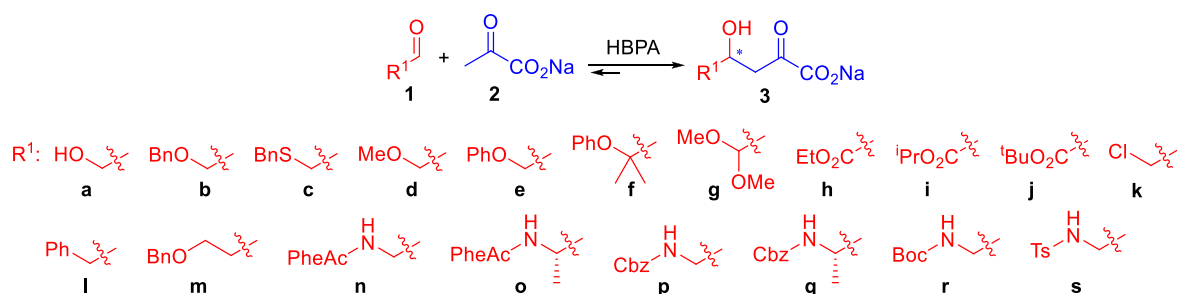
metabolic degradative pathway of naphthalene and naphthalenesulfonates.<sup>10</sup> *In vivo*, HBPA catalyzes the reversible aldol condensation of pyruvate to salicylaldehyde in two steps: an

aldol addition and a subsequent dehydration, both steps being catalyzed by the enzyme. Interestingly, it has been reported that HBPA catalyzes the aldol addition of fluoropyruvate to aromatic aldehydes with high stereoselectivity, in which the fluorine atom precludes the dehydration step by the enzyme.<sup>11</sup> We envisioned that HBPA could catalyze aldol additions of pyruvate to nonaromatic electrophiles, in which the dehydration activity could be largely minimized or even suppressed, rendering aldol adducts with high enantioselectivity. We assayed various nonaromatic electrophiles (**1a–s**; Scheme 1) as substrates of HBPA in the aldol addition of pyruvate.

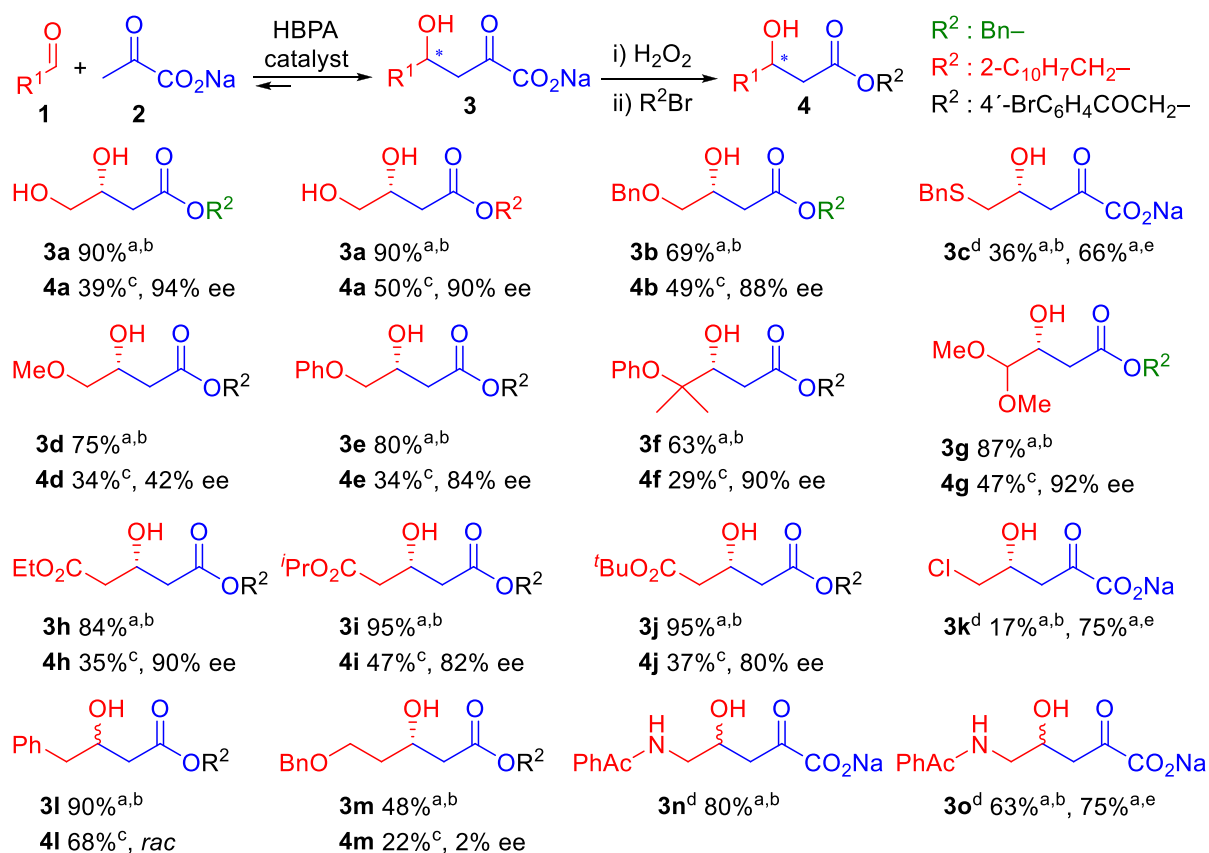
Good to excellent conversions to 4-hydroxy-2-oxo acids **3** (70–95%) were achieved for most of the electrophiles, indicating an excellent structural substrate tolerance of HBPA (Scheme 2). A single residue mutation, the HBPA H205A variant, greatly improved the catalyst efficiency toward **1c,k,o**, yielding **3c,k,o**, respectively, in 66–75% conversion.

Molecular models of the complex of pyruvate-enamine-bound HBPA with aldehydes **1c,o** suggest that the H205A mutation generates a new cavity in the HBPA active site, which reduces the steric hindrance. This cavity can be occupied by the phenyl moiety of the incoming aldehyde (Figure 3 and Figure S93), thus facilitating the interactions with residues Trp224 and Phe269. Moreover, an analysis of the HBPA structure shows that the carboxylic groups of Glu206, Asp207, Asp208, and Asp265 are within 5 Å of the  $\delta$  and  $\epsilon$ -N atoms of the imidazole group of His205, stabilizing its protonated state

**Scheme 1.** Panel of Aldehyde Substrates **1** Assayed in the Aldol Addition of Pyruvate **2** Catalyzed by Wild-Type HBPA and Its H205A Variant



**Scheme 2. HBPA Wild-Type and H205A Variant Catalyzed Aldol Addition of Pyruvate to Aldehydes 1 and Transformation of Aldol Adducts 3 into 3-Hydroxy Ester Derivatives 4, for Enantiomeric Ratio Measurement<sup>f</sup>**



<sup>a</sup>Conversions measured by HPLC. <sup>b</sup>HBPA wild-type. <sup>c</sup>Isolated yield. <sup>d</sup>ee not determined; the material was submitted directly to the enzymatic transamination reaction and the stereochemistry inferred from the corresponding 14c (for 3c), 15k (for 3k), 14n (for 3n), and 14o (for 3o) derivatives; see Schemes 7 and 8. <sup>e</sup>HBPA H205A variant. <sup>f</sup>The ee values were determined by HPLC on a chiral stationary phase.

(Figure 4). This positive charge is also stabilized by a  $\pi$ -cation interaction with the aromatic moiety of Trp224. Therefore, removal of this protonated imidazole, which is  $\sim 8$  Å from the  $\epsilon$ -amino group of the essential Lys183, by the H205A mutation modifies the electrostatic environment of the active site, which could also contribute to the enhanced activity of this mutant toward the selected substrates.

Enantiomeric ratios were determined by HPLC on a chiral stationary phase after transforming the aldol adducts 3 into 3-hydroxy ester derivatives 4 (Scheme 2 and Figures S74–S85). The corresponding authentic racemic samples were produced by employing 2-oxo-3-deoxy-L-rhamnonate aldolase (YfaU), which yielded aldol adducts 3 as racemic mixtures with the selected electrophiles (see the Supporting Information). Excellent levels of enantioselectivity were achieved for 3a,f–h (96–90% ee), while they were good to moderate for 3b,e,i,j (88–80% ee). This is significant considering the low stereoselective profile of wild-type pyruvate aldolases toward low-molecular-weight electrophiles.<sup>12</sup> Low enantioselectivity was attained with the methoxy derivative 3d (42% ee), whereas racemates were obtained with phenylacetaldehyde (3l) and 3-(benzyloxy)propanal (3m). Cbz-, Boc-, and Ts-protected aminoethanal compounds 1p,r,s, respectively, and (S)-Cbz-2-aminopropanal (1q) were not converted. Thus, PhAc was the amino protecting group of choice for aminoaldehydes in the planned HBPA catalysis. Interestingly,

PheAc has the advantage that it can be removed by penicillin G acylase, a mild and orthogonal protection compatible with most common amino masking groups.<sup>13</sup>

Single-crystal X-ray diffraction studies of compounds 4e,f,j indicate that HBPA renders aldol adducts having an *R* configuration as the major products (Figure 5). This is consistent with the reported stereochemical outcome of the reactions between fluoropyruvate and (hetero)aromatic aldehydes.<sup>11</sup> Therefore, an *R* configuration may safely be assumed for the major enantiomers of 3a–k (Scheme 2).

Molecular models of the complexes of HBPA were obtained with (i) the covalently bound pyruvate enamine and the electrophile molecules (Figures S88–S93) and (ii) the imines derived from the aldol adducts (Figures S94–S99). These models suggest that there is no steric restriction to the *re*- or *si*-face approach of the electrophile to the enamine. Thus, it is not clear why there is a preference for the *re*-face approach, which would generate the *R*-aldol adducts as major products of the reaction. A more in depth theoretical study would be required to determine the source of this preference; however, this is beyond the scope of this paper.

**Synthesis of  $\gamma$ -Hydroxy- $\alpha$ -amino Acid Derivatives Using a Biocatalytic One-Pot Cyclic Cascade Approach with L-Ala as an Amine Donor.** We began to screen a transaminase panel (T001–T050) provided by Prozomix Ltd. toward the selected aldol adduct examples 3a,b,e,g,h, produced

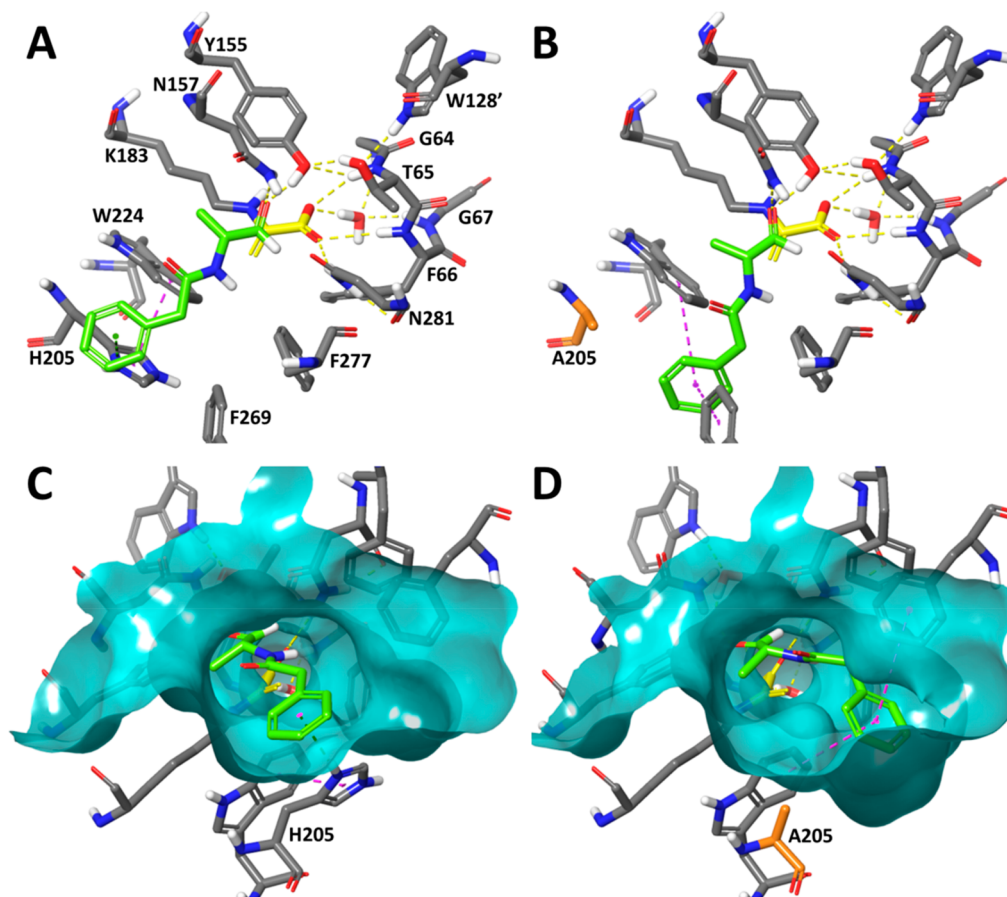


**Figure 3.** Models of the prereactive complexes of wild-type HBPA (A, C) and HBPA H205A (B, D) with the covalently bound pyruvate enamine (yellow C atoms) and aldehyde **1o** (green C atoms). The mutated residue is highlighted in orange. Interactions are shown with dashed lines: H bonds in yellow,  $\pi$ -stacking in magenta, and  $\pi$ -cation in dark green. A comparison of the surface of the active sites of both proteins (C, D) (transparent cyan) reveals that the H205A mutation generates an expanded cavity near residue A205, which can be occupied by the phenyl moiety of **1o**. These models were obtained by QM/MM optimization of the structure of the complexes at the DFT (B3LYP/6-31G\*\*) level of theory, as detailed in the Supporting Information.

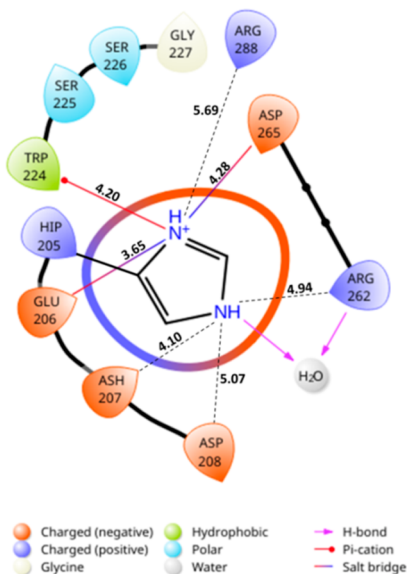


**Figure 4.** Scheme showing the interactions established by the imidazole group of residue His205 of HBPA. Distances (dashed lines) to nearby residues are indicated.

with good conversions and enantioselectivities by HBPA catalysis (Figures S8–S12). We used *L*-Ala (**5**) as an amino donor in a one-pot two-step reaction sequence (Scheme 3). Thus, for the screening, the enzymatic aldol addition was run first and, once the formation of **3** reached a maximum, *L*-Ala (**5**) (500 mM,  $\geq 10$  equiv with respect to **3**) and the transaminase (T###) were added, allowing the reaction to proceed for 24 h. Since unpurified aldol adducts **3** were supplied for the screening reactions, HPLC analysis was the method of choice to detect false positives caused by transamination of the remaining unreacted aldehyde **1**. Compounds **6b,e**, bearing aromatic moieties, were directly detected by HPLC. The percentages of **6a,g,h** formed were estimated by measuring the consumption of **3a,g,h** by HPLC, after precolumn derivatization of the carbonyl group via oxime formation (see the Supporting Information).

Roughly, 4 out of the 50 different transaminases were selected as promising candidates for the transamination reaction (Figures S8–S12). For scale-up experiments, we capitalize on a strategy developed by our group consisting of a one-pot reaction recycling of pyruvate **2**, formed in the transamination reaction, into the aldol reaction (Scheme 4).<sup>8b</sup> This approach effectively shifts the equilibrium of the transamination to the product, since the pyruvate is continuously removed by the aldol reaction.

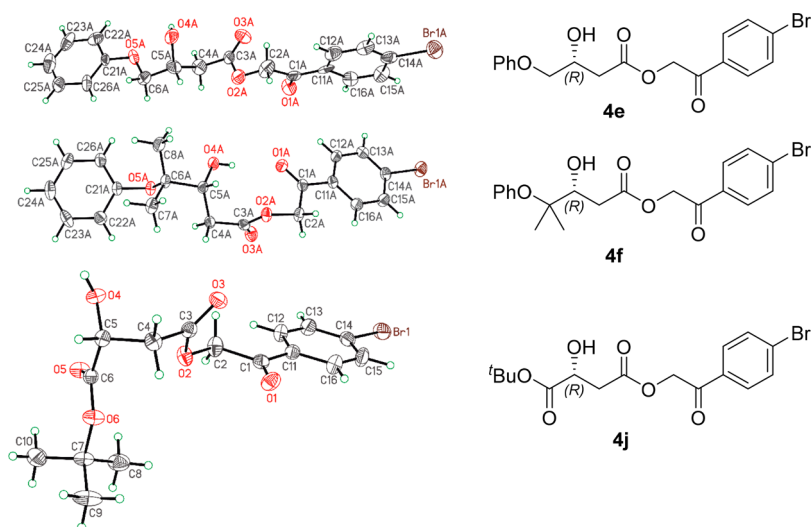
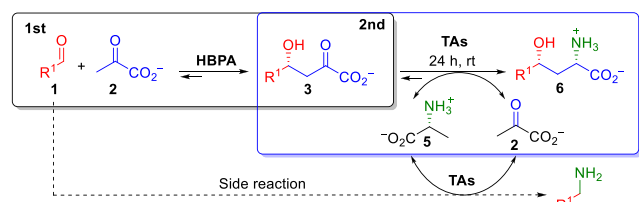


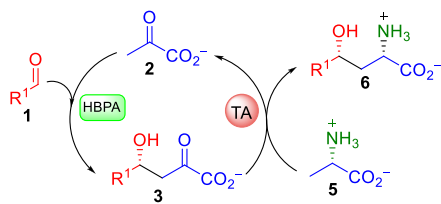
**Figure 5.** X-ray structures of (R)-**4e**, (R)-**4f**, and (R)-**4j** as ORTEP-type plots displaying one molecule with 50% probability ellipsoids. The data can be obtained free of charge from The Cambridge Crystallographic Data Centre via [www.ccdc.cam.ac.uk/data\\_request/cif](http://www.ccdc.cam.ac.uk/data_request/cif).

**Scheme 3. One-Pot Two-Step Screening Reaction for the Synthesis of  $\gamma$ -Hydroxy- $\alpha$ -amino Acid Derivatives **6**, Using L-Ala (**5**) as an Amine Donor for the Enzymatic Transamination Reaction<sup>a</sup>**



<sup>a</sup>The dotted line indicates an enzymatic transamination of the aldehyde remaining in the system.

**Scheme 4. One-Pot Biocatalytic Cascade Synthesis of  $\gamma$ -Hydroxy- $\alpha$ -amino Acid Derivatives **6** Starting from Aldehydes **1** and an Amine Donor **5** with Pyruvate (**2**) Recycling**



To successfully perform this strategy, the transamination of the aldehydes **1** must be largely avoided or minimized. To evaluate the degree of conversion for each aldehyde and establish suitable reaction conditions for the one-pot cascade process, we ran control experiments incubating aldehydes **1a,b,e,g,h** (100 mM) with selected transaminases (Figures S13–S18). Having established the suitable conditions, we started testing a range of starting pyruvate (**2**) concentrations between 5 and 100 mM, against 100 mM of L-Ala. Using **1g** (100 mM) as the electrophile and HBPA/T039 catalysts, 42 mM of **6g** (42% yield) was formed at 5 mM pyruvate concentration, indicating pyruvate recycling (Figure 6A and Figure S21). At 50 mM of pyruvate, **6g** reached a maximum

(55 mM, 55% yield), with no effective pyruvate recycling. Further increasing the initial pyruvate concentration (i.e., up to 100 mM) caused an increase in **3g** production, but **6g** decreased, likely due to an equilibrium limitation of the transamination. Using **1a** (200 mM) and HBPA/T039, the best initial pyruvate concentration was 100 mM (Figure 6B and Figure S19). Under these conditions, 47 mM of **6a** (47% yield, with respect to the limiting substrate **5**) was formed, but no pyruvate recycling occurred. Aldol adduct **3a** was most probably in an equilibrium between the cyclic hemiketal and the acyclic form. It is likely that the hemiketal was not a substrate for the transaminase and its activity was limited by the actual concentration of the acyclic adduct. Disappointingly, this strategy failed to produce the corresponding  $\gamma$ -hydroxy- $\alpha$ -amino acid derivatives **6** for the rest of the aldehydes with the selected transaminases and aldol adducts **3** were the only species detected (see Figure S20 for an example).

One problem that jeopardizes the pyruvate recycling strategy was that the aldolase and transaminase were not sufficiently active toward the aldehyde and aldol adduct, respectively, in comparison with the system reported by us for the synthesis of homoserine.<sup>8b</sup> This makes a rapid conversion difficult for both the initial pyruvate and the aldol adduct formed, compromising the efficiency of the recycling process. Therefore, the one-pot two-step reaction sequence appears to be the most convenient route in dealing with aldolases and/or transaminases with kinetic and thermodynamic limitations. In this case, however, an effective method to overcome the equilibrium limitations of the transaminase must be implemented.

**Synthesis of  $\gamma$ -Hydroxy- $\alpha$ -amino Acid Derivatives Using a Biocatalytic One-Pot Two-Step Approach Using Benzylamine as an Amine Donor.** Another strategy was devised for the synthesis of the selected target  $\gamma$ -hydroxy- $\alpha$ -amino acid derivatives using benzylamine (**7**) as an alternative amine donor (Scheme 5). The effective shift of the equilibrium of the transamination was accomplished by converting the benzaldehyde (**8**) formed into benzoin (**9**) by benzaldehyde lyase from *Pseudomonas fluorescens* Biovar I (BAL) (Scheme 5). BAL is highly selective toward benzaldehyde, ensuring an almost quantitative conversion

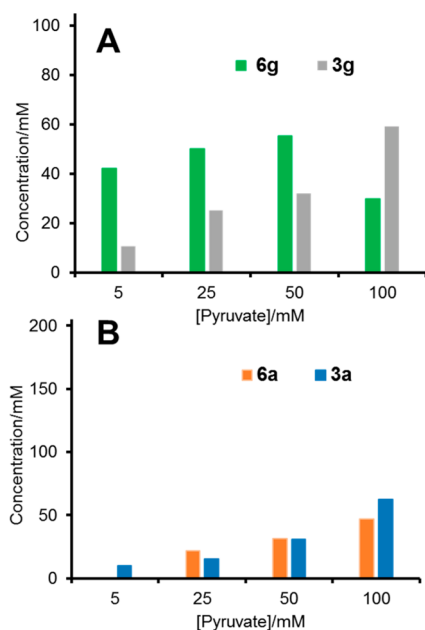


**Figure 6.** One-pot biocatalytic synthesis of **6g** (A) and **6a** (B), starting from aldehydes **1g** (100 mM), **1a** (200 mM), and **5** (100 mM) in both experiments: concentration of the components after 24 h of reaction as a function of the initial concentration of pyruvate using HBPA/T039 catalysts.

into the mostly insoluble benzoin, which benefits the reaction equilibrium.<sup>14</sup> Benzylamine has been reported to be a suitable amine donor, and different strategies to eliminate the benzaldehyde were proposed: e.g. conversion into benzoic acid under 1 atm of oxygen,<sup>15</sup> extraction with hexane in an aqueous–organic two-phase system,<sup>16</sup> and reduction to benzyl alcohol during a cascade synthesis of  $\omega$ -amino fatty acids and  $\alpha,\omega$ -diamines from  $\omega$ -hydroxy fatty acids and  $\alpha,\omega$ -diols, respectively.<sup>17</sup>

For this strategy, an extended panel of 194 transaminases from Prozymix Ltd. was screened in a one-pot two-step sequence (Figure S22 and Table S7) using the crude reaction products of adducts **3a,b,e,g,h** as starting materials.

Next, we rescreened 27 positive hits from the first screening in the two-step sequence, removing the HBPA before starting the transamination reaction aldolase to avoid retroaldolysis (see the Supporting Information). In this case, the aldol adducts **3**, products **6**, benzaldehyde (**8**), and benzoin (**9**) were analyzed and quantified by HPLC. Only transaminase

T039 was able to convert the aldol adducts **3a,b,e,g** into the corresponding products **6** (Figure S24). The reaction with aldehyde **1h** resulted in a false positive, because no product could be detected in scale-up experiments.

The same two-step reaction sequence was then repeated with and without removing HBPA, using T039 and including aldehydes **1i,j** (Figure 7A). The HBPA did not affect the yield

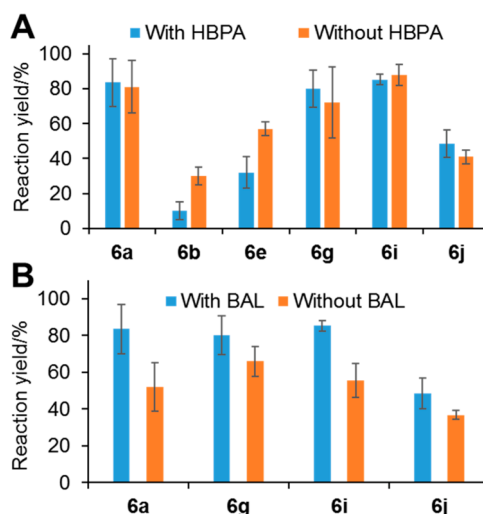
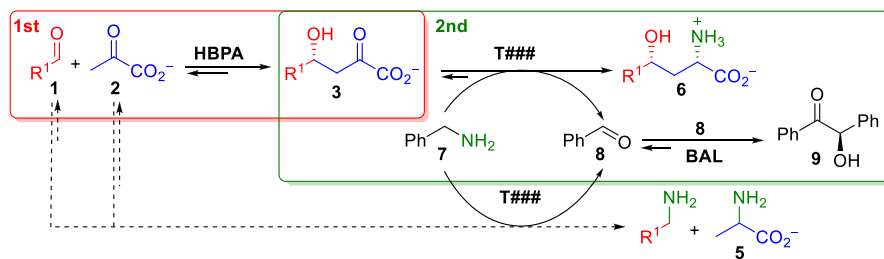


**Figure 7.** One-pot two-step stereoselective synthesis of  $\gamma$ -hydroxy- $\alpha$ -amino acids (**6a,b,e,g,i,j**), using the HBPA/T039 system and benzylamine (**7**) as amine donor: influence of the presence of HBPA (A) and BAL (B) on the reaction yield of products **6**. Error bars are the values of the estimated standard error of the mean of two independent experiments under the same reaction conditions.

of **6a,g,i,j**, indicating that T039 was rather selective toward the corresponding aldol adducts and that no retroaldolysis was taking place. On the other hand, elimination of HBPA benefited **6b,e** in comparison with those products without aromatic substituents. Next, we investigated the effect of BAL on the yield of **6a,g,i,j** (Figure 7B). The addition of BAL was largely positive for **6a,i** and less so for **6g,j**. Overall, this depends on each individual case and should be considered for establishing the optimal operational conditions. Moreover, no aldol condensation of pyruvate to benzaldehyde catalyzed by HBPA was detected.

The low conversion of aldol adducts with aromatic substituents, **3b,e**, and the need for a highly selective transaminase for the 4-hydroxy-2-oxo acids **3** prompted us to

**Scheme 5. One-Pot Two-Step Stereoselective Synthesis of  $\gamma$ -Hydroxy- $\alpha$ -Amino Acids **6**, Using Benzylamine (**7**) as an Amine Donor for the Enzymatic Transamination Reaction and BAL to Transform the Benzaldehyde Formed (**8**) into Benzoin (**9**)<sup>a</sup>**

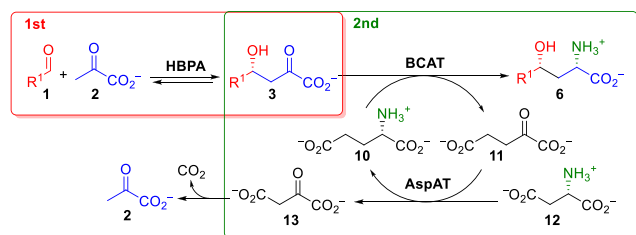


<sup>a</sup>Dotted lines indicate a transamination reaction of the aldehydes **1** and pyruvate **2**, favoring the retroaldolysis of **3** catalyzed by the HBPA present in the system.

explore another methodology based on branched-chain  $\alpha$ -amino acid aminotransferases (BCATs).<sup>18</sup>

**Synthesis of  $\gamma$ -Hydroxy- $\alpha$ -amino Acid Derivatives Using a Biocatalytic One-Pot Two-Step Approach with the PLP-Dependent Branched-Chain Amino Acid Aminotransferase (BCAT) from *E. coli*.** The branched-chain  $\alpha$ -amino acid aminotransferase (BCAT) from *E. coli* was selected to convert **3** into **6**, employing L-Glu (**10**) as an amine donor and delivering 2-oxoglutarate (**11**), which is a strong inhibitor of BCAT (e.g., 10 mM of **11** reduces the activity up to 80%).<sup>19</sup> Thus, the regeneration of L-Glu was needed, which was accomplished by coupling with aspartate aminotransferase (AspAT) from *E. coli* that employed L-Asp (**12**) as the substrate (Scheme 6). The resulting oxaloacetate **13** spontaneously decomposes into CO<sub>2</sub> and pyruvate, shifting the transamination equilibrium to the formation of  $\gamma$ -hydroxy- $\alpha$ -amino acids **6**.

**Scheme 6. One-Pot Two-Step Stereoselective Synthesis of  $\gamma$ -Hydroxy- $\alpha$ -amino Acids **6** using L-Glu (**10**) as an Amine Donor<sup>a</sup>**



<sup>a</sup>The 2-oxoglutarate (**11**) formed was transaminated to L-Glu (**10**) by AspAT using L-Asp (**12**) as an amine donor. The oxaloacetate (**13**) decomposes into CO<sub>2</sub> and pyruvate, shifting the equilibrium of the transamination to  $\gamma$ -hydroxy- $\alpha$ -amino acids **6**.

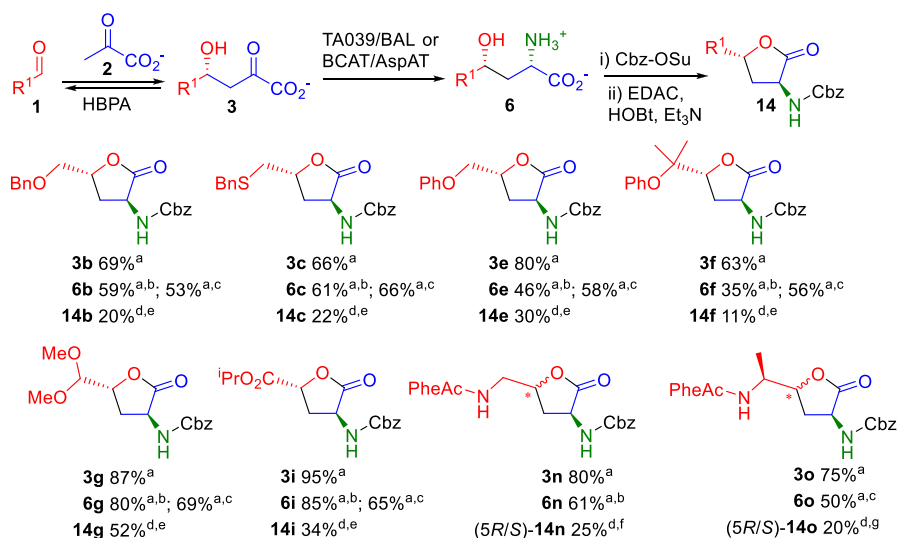
The reaction system worked successfully with the aldol adducts **3**, with better performances for some examples in

comparison to those with the benzylamine/T039 system (Scheme 7). For instance, this reaction system converted the aldol adduct **3k**, which was not a substrate for T039 (Scheme 8). On the other hand, benzylamine/T039 afforded product **6n**, whereas its precursor **3n** was not converted by the BCAT/AspAT system. Therefore, both methodologies are somehow complementary. Despite the fact that pyruvate is released because of the decarboxylation of oxaloacetate **13**, attempts to run the reaction with one-pot pyruvate recycling failed to provide the corresponding  $\gamma$ -hydroxy- $\alpha$ -amino acids **6** (Figure S25).

Finally, for the laboratory-scale preparation of  $\gamma$ -hydroxy- $\alpha$ -amino acids **6** we chose a system with better performance for conversion, isolation, and product purification. Products **6** were converted into the corresponding Cbz-*N* <sup>$\alpha$</sup> - $\gamma$ -butyrolactone derivatives **14** (Scheme 7).  $\alpha$ -Amino- $\gamma$ -butyrolactones are structural motifs found in biologically active compounds in addition to being valuable chiral intermediates for the synthesis of pharmaceutical agents.<sup>6a,20</sup> The optimal lactonization conditions were established, and particular attention was paid to avoid eroding the enantiopurity of **14** (Table S7). The *R* configuration for aldol adducts **3b,c,e-g,i** (Scheme 2) and the *S* configuration generated by the transaminases<sup>8b,19c</sup> afforded the expected 2*S*,4*R*-configured hydroxy amino acid derivatives **6**, which were confirmed by a NMR diastereochemical analysis of products **14**. Exceptions were the products **6n,o**. In this case, the aldol addition reaction was not stereoselective, yielding a mixture of diastereoisomers (*S**R*/*S**S*)-**14n** and (*S**R*/*S**S*)-**14o**, respectively.

Interestingly, the enzymatic transamination reaction of aldol adducts **3k,h** led to the formation of (2*S*,4*R*)-(-)-*trans*-4-hydroxyproline (**15k**) (Scheme 8 A) and  $\gamma$ -hydroxypyroglutamic acid (**15h**) (Scheme 8 B), respectively. The first product could be formed by an intramolecular nucleophilic substitution of the terminal Cl at C5 by the amine group after the transamination reaction.

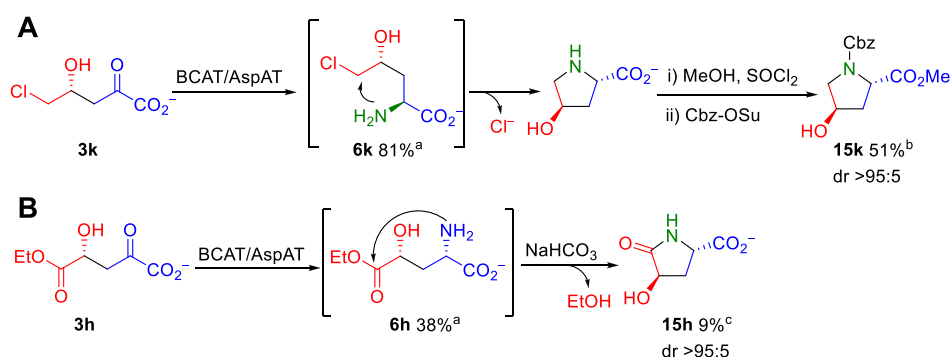
**Scheme 7. Synthesis of  $\gamma$ -Hydroxy- $\alpha$ -amino Acids **6** by Tandem HBPA/Transaminase Catalyzed Reactions and Conversion to  $\alpha$ -Amino- $\gamma$ -butyrolactone Derivatives **14****



<sup>a</sup>Conversions determined by HPLC. <sup>b</sup>Transaminase T039/BAL (see Scheme 5). <sup>c</sup>BCAT/AspAT system (see Scheme 6). <sup>d</sup>Isolated yield. <sup>e</sup>dr >95:5 as measured by NMR; no other diastereomers were detected. <sup>f</sup>dr 50:50 as measured by NMR. <sup>g</sup>dr 60:40 (*S*/*R*) as measured by NMR.



**Scheme 8. (A) Formation of (2*S*,4*R*)-(-)-*trans*-4-Hydroxyproline Derivative 15k by Tandem Enzymatic Aldol Reaction/Transamination and Intramolecular Nucleophilic Substitution with the Amine Group<sup>d</sup> and (B) Formation of  $\gamma$ -Hydroxypyroglutamic Acid (15h) by Intramolecular Aminolysis of the Ethyl Ester Group under Basic Conditions**

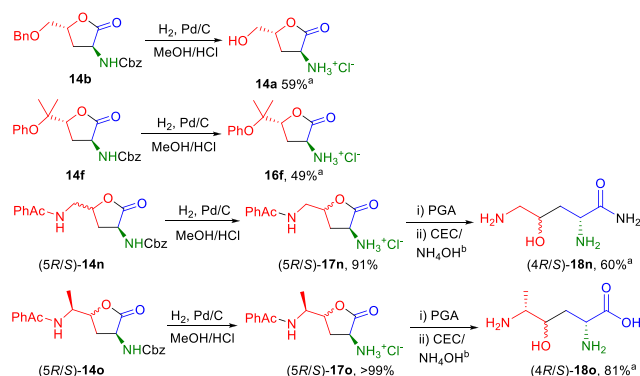


<sup>a</sup>Percentage of product formed determined by HPLC. <sup>b</sup>Isolated yield from **1k**. <sup>c</sup>Isolated yield from **1h**. The material contained L-Asp and L-Glu as major impurities. <sup>d</sup>The stereochemistry of **15k** was established unequivocally by a comparison with authentic samples (see Figure S26).

The  $\gamma$ -hydroxypyroglutamic acid **15h** was probably formed by intramolecular aminolysis of the ethyl ester group during the attempts to protect the amino group by Cbz. The basic conditions necessary to conduct the reaction with CbzOSu likely favored the reaction (Scheme 8 B). On the other hand, the corresponding isopropyl ester derivative of Cbz-*N*<sup>α</sup>- $\gamma$ -butyrolactone **14i** could be isolated, most likely due to the steric hindrance imposed by the isopropyl group, which precluded an intramolecular aminolysis.

Deprotection of the Cbz group of butyrolactones **14** was accomplished by catalytic hydrogenolysis with H<sub>2</sub> in the presence of Pd/C, while PheAc was removed by enzymatic hydrolysis mediated by penicillin G acylase (PGA) (Scheme 9). Hydrogenolysis of (5*R*/5*S*)-**14n** and (5*R*/5*S*)-**14o**

**Scheme 9. Protection Group Removal of Selected  $\alpha$ -Amino- $\gamma$ -butyrolactone Derivatives 14**



<sup>a</sup>Isolated yield. <sup>b</sup>Cation exchange chromatography (CEC) eluted with an aqueous solution of NH<sub>4</sub>OH.

furnished the lactones (5*R*/5*S*)-**17n** and (5*R*/5*S*)-**17o**, which upon treatment with PGA and purification by cation exchange chromatography, with NH<sub>4</sub>OH as eluent, led to the corresponding amide derivatives (4*R*/4*S*)-**18n** and carboxylates (4*R*/4*S*)-**18o**.

## CONCLUSIONS

A tandem enantioselective aldol addition–transamination approach was established for the production of chiral

$\gamma$ -hydroxy- $\alpha$ -amino acids. The *trans*-*o*-hydroxybenzylidene pyruvate hydratase-aldolase afforded chiral 4-hydroxy-2-oxo acids with a remarkable efficiency, broad substrate tolerance, and unparalleled stereoselectivity, far beyond those of the pyruvate aldolases hitherto reported. Thus, the HBPA/benzylamine/T039 and HBPA/Glu/BCAT/AspAT systems are adequate complementary approaches for the asymmetric synthesis of chiral  $\gamma$ -hydroxy- $\alpha$ -amino acids **6**. Overall, the HBPA/Glu/BCAT/AspAT system renders, in some instances, better results mainly due to the selectivity of the  $\alpha$ -transaminase BCAT for the 2-oxo acids and its inability to catalyze the transamination of the remaining aldehyde from the aldol addition. Moreover, the reaction can be carried out in whole cells. The HBPA/benzylamine/T039 system is more unspecific, allowing the conversion of various structurally different substrates, such as that of the aldehydes **1** into primary amines. The HBPA/L-Ala/T039 approach with pyruvate recycling is not straightforward and needs an optimization of the activities of the aldolase and transaminase involved to develop an effective process.

Using the strategy developed in this work, an unprecedented number of chiral  $\gamma$ -hydroxy- $\alpha$ -amino acids and the corresponding  $\alpha$ -amino- $\gamma$ -butyrolactones were constructed in two steps with high stereoselectivity from small functionalized aldehydes.

## ASSOCIATED CONTENT

### Supporting Information

The Supporting Information is available free of charge at <https://pubs.acs.org/doi/10.1021/acscatal.1c00210>.

General methods and protocols for the screening and synthesis, activity determinations, synthesis of starting materials, synthesis of  $\gamma$ -hydroxy- $\alpha$ -amino acids and  $\alpha$ -amino- $\gamma$ -butyrolactones, NMR spectra, and computation methods and modeling (PDF)

## AUTHOR INFORMATION

### Corresponding Author

Pere Clapés – Institute for Advanced Chemistry of Catalonia, Department of Biological Chemistry, IQAC-CSIC, Barcelona 08034, Spain; [orcid.org/0000-0001-5541-4794](https://orcid.org/0000-0001-5541-4794); Email: [pere.clapes@iqac.csic.es](mailto:pere.clapes@iqac.csic.es)

## Authors

**Carlos J. Moreno** – Institute for Advanced Chemistry of Catalonia, Department of Biological Chemistry, IQAC-CSIC, Barcelona 08034, Spain

**Karel Hernández** – Institute for Advanced Chemistry of Catalonia, Department of Biological Chemistry, IQAC-CSIC, Barcelona 08034, Spain

**Simon J. Charnok** – Prozomix Ltd. West End Industrial Estate, Haltwhistle, Northumberland NE49 9HA, U.K.

**Samantha Gittings** – Prozomix Ltd. West End Industrial Estate, Haltwhistle, Northumberland NE49 9HA, U.K.

**Michael Bolte** – Institut für Anorganische Chemie, J.-W.-Goethe-Universität, Frankfurt/Main, Germany;

orcid.org/0000-0001-5296-6251

**Jesús Joglar** – Institute for Advanced Chemistry of Catalonia, Department of Biological Chemistry, IQAC-CSIC, Barcelona 08034, Spain

**Jordi Bujons** – Institute for Advanced Chemistry of Catalonia, Department of Biological Chemistry, IQAC-CSIC, Barcelona 08034, Spain; orcid.org/0000-0003-2944-2905

**Teodor Parella** – Servei de Resonància Magnètica Nuclear, Universitat Autònoma de Barcelona, Bellaterra, Spain;

orcid.org/0000-0002-1914-2709

Complete contact information is available at:  
<https://pubs.acs.org/10.1021/acscatal.1c00210>

## Author Contributions

<sup>†</sup>C.J.M. and K.H. contributed equally.

## Funding

This project has received funding from the Ministerio de Ciencia e Innovación (MICIN), cofinanced by the Fondo Europeo de Desarrollo Regional (FEDER) (grants RTI2018-094637-B-I00 to P.C. and PGC2018-095808-B-I00 to T.P.), and Programación Conjunta Internacional (PCI2018-092937), through the EU initiative ERA CoBioTech under grant agreement No [722361] to P.C and S.J.Ch.) (Tralaminol).

## Notes

The authors declare no competing financial interest.

## ACKNOWLEDGMENTS

The authors gratefully acknowledge the “Consorti de Serveis Universitaris de Catalunya” (CSUC) for allowing the use of its software and hardware resources.

## REFERENCES

(1) (a) Szcześniak, P.; Październiak-Holewa, A.; Klimczak, U.; Stecko, S. Synthesis of  $\beta$ - and  $\gamma$ -Hydroxy  $\alpha$ -Amino Acids via Enzymatic Kinetic Resolution and Cyanate-to-Isocyanate Rearrangement. *J. Org. Chem.* **2014**, *79*, 11700–11713. (b) Plaza, A.; Viehrig, K.; Garcia, R.; Müller, R. Jahnellamides,  $\alpha$ -Keto- $\beta$ -Methionine-Containing Peptides from the Terrestrial Myxobacterium *Jahnella* sp.: Structure and Biosynthesis. *Org. Lett.* **2013**, *15*, 5882–5885. (2) (a) Zafar, M. I.; Gao, F. 4-Hydroxyisoleucine: A Potential New Treatment for Type 2 Diabetes Mellitus. *BioDrugs* **2016**, *30*, 255–262. (b) Sun, D. Y.; Cheng, X. T.; Gao, D. K.; Xu, P. P.; Guo, Q. Q.; Zhu, Z. L.; Zhu, M. L.; Wang, X. Y.; Qin, H. M.; Lu, F. P. Properties, Biosynthesis, and Catalytic Mechanisms of Hydroxy-Amino-Acids. *IOP Conference Series: Earth and Environmental Science* **2018**, *188*, 012084. (c) Jing, X.; Wang, X.; Zhang, W.; An, J.; Luo, P.; Nie, Y.; Xu, Y. Highly Regioselective and Stereoselective Hydroxylation of Free Amino Acids by a 2-Oxoglutarate-Dependent Dioxygenase from *Kutzneria albida*. *ACS Omega* **2019**, *4*, 8350–8358. (d) Simon, R. C.; Busto, E.; Schrittwieser, J. H.; Sattler, J. H.; Pietruszka, J.; Faber, K.; Kroutil, W. Stereoselective Synthesis of  $\alpha$ -Hydroxynorvaline Through

Combination of Organo- And Biocatalysis. *Chem. Commun.* **2014**, *50*, 15669–15672. (e) Guérard-Hélaine, C.; Heuson, E.; Ndiaye, M.; Gourbeyre, L.; Lemaire, M.; Hélaine, V.; Charmantray, F.; Petit, J.-L.; Salanoubat, M.; de Berardinis, V.; Gefflaut, T. Stereoselective Synthesis of  $\gamma$ -Hydroxy- $\alpha$ -Amino Acids Through Aldolase-Transaminase Recycling Cascades. *Chem. Commun.* **2017**, *53*, 5465–5468. (f) Zhang, Y.; Farrants, H.; Li, X. Adding a Functional Handle to Nature's Building Blocks: The Asymmetric Synthesis of  $\beta$ -Hydroxy- $\alpha$ -Amino Acids. *Chem. - Asian J.* **2014**, *9*, 1752–1764. (g) Enoki, J.; Meisborn, J.; Müller, A.-C.; Kourist, R. A Multi-Enzymatic Cascade Reaction for the Stereoselective Production of  $\gamma$ -Oxyfunctionalized Amino Acids. *Front. Microbiol.* **2016**, *7*, 1–8. (h) Bunch, L.; Pickering, D. S.; Gefflaut, T.; Vinatier, V.; Helaine, V.; Amir, A.; Nielsen, B.; Jensen, A. A. 4,4-Dimethyl- and Diastereomeric 4-Hydroxy-4-methyl-(2S)-Glutamate Analogues Display Distinct Pharmacological Profiles at Ionotropic Glutamate Receptors and Excitatory Amino Acid Transporters. *ChemMedChem* **2009**, *4*, 1925–1929. (i) Alaux, S.; Kusk, M.; Sagot, E.; Bolte, J.; Jensen, A. A.; Bräuner-Osborne, H.; Gefflaut, T.; Bunch, L. Chemoenzymatic Synthesis of a Series of 4-Substituted Glutamate Analogues and Pharmacological Characterization at Human Glutamate Transporters Subtypes 1–3. *J. Med. Chem.* **2005**, *48*, 7980–7992. (j) Singh, A. B.; Khaliq, T.; Chaturvedi, J. P.; Narender, T.; Srivastava, A. K. Anti-diabetic and anti-oxidative effects of 4-hydroxypipercolic acid in C57BL/KsJ-db/db mice. *Hum. Exp. Toxicol.* **2012**, *31*, 57–65.

(3) (a) Ohyama, T.; Kurihara, Y.; Ono, Y.; Ishikawa, T.; Miyakoshi, S.; Hamano, K.; Araei, M.; Suzuki, T.; Igari, H.; Suzuki, Y. Arborcandins A, B, C, D, E and F, novel 1, 3- $\beta$ -glucan synthase inhibitors: production and biological activity. *J. Antibiot.* **2000**, *53*, 1108–1116. (b) Sugawara, T.; Tanaka, A.; Tanaka, K.; Nagai, K.; Suzuki, K.; Suzuki, T. YM-170320, a novel lipopeptide antibiotic inducing morphological change of colonies in a mutant of *Candida tropicalis* pK233. *J. Antibiot.* **1998**, *51*, 435–438.

(4) (a) Wang, X.; Wang, J.; Lai, D.; Wang, W.; Dai, J.; Zhou, L.; Liu, Y. Ustiloxin G, a New Cyclopeptide Mycotoxin from Rice False Smut Balls. *Toxins* **2017**, *9*, 54. (b) Lin, X.; Bian, Y.; Mou, R.; Cao, Z.; Cao, Z.; Zhu, Z.; Chen, M. Isolation, Identification, and Characterization of Ustilaginoidea Virens from Rice False Smut Balls with High Ustilotoxin Production Potential. *J. Basic Microbiol.* **2018**, *58*, 670–678. (c) Hunter, L.; McLeod, M. D.; Hutton, C. A. Synthesis of the  $\beta$ -hydroxydopa- $\gamma$ -hydroxy- $\delta$ -sulfinylnorvaline component of ustiloxins A and B. *Org. Biomol. Chem.* **2005**, *3*, 732–734.

(5) (a) Bassarello, C.; Bifulco, G.; Evidente, A.; Riccio, R.; Gomez-Paloma, L. Stereochemical studies on ascaulitoxin: a J-based NMR configurational analysis of a nitrogen substituted system. *Tetrahedron Lett.* **2001**, *42*, 8611–8613. (b) Vurro, M.; Andolfi, A.; Boari, A.; Zonno, M. C.; Caretto, S.; Avolio, F.; Evidente, A. Optimization of the Production of Herbicidal Toxins by the Fungus *Ascochyta Caulina*. *Biol. Control* **2012**, *60*, 192–198.

(6) (a) Cavanaugh, C. L.; Nicewicz, D. A. Synthesis of  $\alpha$ -Benzoyloxylamino- $\gamma$ -Butyrolactones via a Polar Radical Crossover Cycloaddition Reaction. *Org. Lett.* **2015**, *17*, 6082–6085. (b) Avenoz, A.; Cativiela, C.; Paris, M.; Peregrina, J. M.; Saenz-Torre, B. Synthesis of enantiomerically pure constrained  $\gamma$ -hydroxy- $\alpha$ -amino acids by directed hydroxylation. *Tetrahedron: Asymmetry* **1997**, *8*, 1123–1129. (c) Mondal, D.; Schweizer, F. Synthesis of Allosteric-Templated Hydroxyornithine and Hydroxyarginine Analogs. *Carbohydr. Res.* **2010**, *345*, 1533–1540. (d) Ren, J.-L.; Zhang, X.-Y.; Yu, B.; Wang, X.-X.; Shao, K.-P.; Zhu, X.-G.; Liu, H.-M. Discovery of Novel AHLs as Potent Antiproliferative Agents. *Eur. J. Med. Chem.* **2015**, *93*, 321–329. (e) Mattmann, M. E.; Geske, G. D.; Worzalla, G. A.; Chandler, J. R.; Sappington, K. J.; Greenberg, E. P.; Blackwell, H. E. Synthetic Ligands that Activate and Inhibit a Quorum-Sensing Regulator in *Pseudomonas Aeruginosa*. *Bioorg. Med. Chem. Lett.* **2008**, *18*, 3072–3075.

(7) (a) Swift, M. D.; Sutherland, A. Stereocontrol of palladium(II)-catalysed aza-Claisen rearrangements using a combination of 1,3-allylic strain and a solvent mediated directing effect. *Org. Biomol. Chem.* **2006**, *4*, 3889–3891. (b) De Lamo Marin, S.; Catala, C.;

- Kumar, S. R.; Valleix, A.; Wagner, A.; Mioskowski, C. A Practical and Efficient Total Synthesis of Potent Insulinotropic (2S,3R,4S)-4-Hydroxyisoleucine through a Chiral *N*-Protected  $\gamma$ -Keto- $\alpha$ -amino-ester. *Eur. J. Org. Chem.* **2010**, *2010*, 3985–3989. (c) Schmeck, C.; Hegedus, L. S. Synthesis of Optically Active 4-Substituted 2-Aminobutyrolactones and Homoserines by Combined Aldol/Photocyclization Reactions of Chromium Aminocarbene Complexes. *J. Am. Chem. Soc.* **1994**, *116*, 9927–9934. (d) Ariza, J.; Font, J.; Ortuño, R. M. Enantioselective synthesis of hydroxy  $\alpha$ -amino acids. (–)-erythro- and (–)-threo- $\gamma$ -hydroxyornivalines. *Tetrahedron* **1990**, *46*, 1931–1942. (e) Berkeš, D.; Kolarovič, A.; Považanec, F. Stereoselective sodium borohydride reduction, catalyzed by manganese(II) chloride, of  $\gamma$ -oxo- $\alpha$ -amino acids. A practical approach to syn- $\gamma$ -hydroxy- $\alpha$ -amino acids. *Tetrahedron Lett.* **2000**, *41*, S257–S260. (f) Jakubec, P.; Berkeš, D.; Kolarovič, A.; Považanec, F. Asymmetric Synthesis of Aliphatic  $\alpha$ -Amino and  $\gamma$ -Hydroxy  $\alpha$ -Amino Acids and Introduction of a Template for Crystallization-Induced Asymmetric Transformation. *Synthesis* **2006**, *2006*, 4032–4040.
- (8) (a) Baud, D.; Saaidi, P.-L.; Monfleur, A.; Harari, M.; Cuccaro, J.; Fossey, A.; Besnard, M.; Debard, A.; Mariage, A.; Pellouin, V.; Petit, J.-L.; Salanoubat, M.; Weissenbach, J.; de Berardinis, V.; Zapparucha, A. Synthesis of Mono- and Dihydroxylated Amino Acids with New  $\alpha$ -Ketoglutarate-Dependent Dioxygenases: Biocatalytic Oxidation of C-H Bonds. *ChemCatChem* **2014**, *6*, 3012–3017. (b) Hernández, K.; Bujons, J.; Joglar, J.; Charnock, S. J.; Domínguez de María, P.; Fessner, W. D.; Clapés, P. Combining Aldolases and Transaminases for the Synthesis of 2-Amino-4-hydroxybutanoic Acid. *ACS Catal.* **2017**, *7*, 1707–1711. (c) Hara, R.; Yamagata, K.; Miyake, R.; Kawabata, H.; Uehara, H.; Kino, K. Discovery of Lysine Hydroxylases in the Clavaminc Acid Synthase-Like Superfamily for Efficient Hydroxylysine Bioproduction. *Appl. Environ. Microbiol.* **2017**, *83*, e00693–e00617. (d) Hibi, M.; Kawashima, T.; Kodera, T.; Smirnov, S. V.; Sokolov, P. M.; Sugiyama, M.; Shimizu, S.; Yokozeki, K.; Ogawa, J. Characterization *Bacillus thuringiensis* L-Isoleucine Dioxygenase for Production of Useful Amino Acids. *Appl. Environ. Microbiol.* **2011**, *77*, 6926. (e) Smirnov, S. V.; Samsonova, N. N.; Novikova, A. E.; Matrosov, N. G.; Rushkevich, N. Y.; Kodera, T.; Ogawa, J.; Yamanaka, H.; Shimizu, S. A novel strategy for enzymatic synthesis of 4-hydroxyisoleucine: identification of an enzyme possessing HMKP (4-hydroxy-3-methyl-2-keto-pentanoate) aldolase activity. *FEMS Microbiol. Lett.* **2007**, *273*, 70–77. (f) Ogawa, J.; Yamanaka, H.; Mano, J.; Doi, Y.; Horinouchi, N.; Kodera, T.; Nio, N.; Smirnov, S. V.; Samsonova, N. N.; Kozlov, Y. I.; Shimizu, S. Synthesis of 4-hydroxyisoleucine by the aldolase-transaminase coupling reaction and basic characterization of the aldolase from *Arthrobacter simplex* AKU 626. *Biosci., Biotechnol., Biochem.* **2007**, *71*, 1607–1615. (g) Xu, L.; Wang, L.-C.; Su, B.-M.; Xu, X.-Q.; Lin, J. Multi-Enzyme Cascade for Improving  $\beta$ -Hydroxy- $\alpha$ -Amino Acids Production by Engineering L-Threonine Transaldolase and Combining Acetaldehyde Elimination System. *Bioresour. Technol.* **2020**, *310*, 123439.
- (9) Sehl, T.; Hailes, H. C.; Ward, J. M.; Wardenga, R.; von Lieres, E.; Offermann, H.; Westphal, R.; Pohl, M.; Rother, D. Two Steps in One Pot: Enzyme Cascade for the Synthesis of Nor(pseudo)ephedrine from Inexpensive Starting Materials. *Angew. Chem., Int. Ed.* **2013**, *52*, 6772–6775.
- (10) (a) Stolz, A. Degradation of substituted naphthalenesulfonic acids by *Sphingomonas xenophaga* BN6. *J. Ind. Microbiol. Biotechnol.* **1999**, *23*, 391–399. (b) Eaton, R. W. *trans*-o-Hydroxybenzylidene-pyruvate Hydratase-Aldolase as a Biocatalyst. *Appl. Environ. Microbiol.* **2000**, *66*, 2668–2672.
- (11) Howard, J. K.; Müller, M.; Berry, A.; Nelson, A. An Enantio- and Diastereoselective Chemoenzymatic Synthesis of  $\alpha$ -Fluoro  $\beta$ -Hydroxy Carboxylic Esters. *Angew. Chem., Int. Ed.* **2016**, *55*, 6767–6770.
- (12) (a) Lamble, H. J.; Danson, M. J.; Hough, D. W.; Bull, S. D. Engineering stereocontrol into an aldolase-catalysed reaction. *Chem. Commun.* **2005**, 124–126. (b) Lamble, H. J.; Royer, S. F.; Hough, D. W.; Danson, M. J.; Taylor, G. L.; Bull, S. D. A thermostable aldolase for the synthesis of 3-deoxy-2-ulosonic acids. *Adv. Synth. Catal.* **2007**, *349*, 817–821. (c) Woodhall, T.; Williams, G.; Berry, A.; Nelson, A. Creation of a tailored aldolase for the parallel synthesis of sialic acid mimetics. *Angew. Chem., Int. Ed.* **2005**, *44*, 2109–2112. (d) Schurink, M.; Wolterink-Van Loo, S.; van der Oost, J.; Sonke, T.; Franssen, M. C. R. Substrate Specificity and Stereoselectivity of Two *Sulfolobus* 2-Keto-3-deoxygluconate Aldolases towards Azido-Substituted Aldehydes. *ChemCatChem* **2014**, *6*, 1073–1081. (e) Baker, P.; Seah, S. Y. K. Rational Design of Stereoselectivity in the Class II Pyruvate Aldolase Bphl. *J. Am. Chem. Soc.* **2012**, *134*, 507–513. (f) Archer, R. M.; Royer, S. F.; Mahy, W.; Winn, C. L.; Danson, M. J.; Bull, S. D. Syntheses of 2-Keto-3-deoxy-D-xylosonate and 2-Keto-3-deoxy-L-arabinonate as Stereochemical Probes for Demonstrating the Metabolic Promiscuity of *Sulfolobus solfataricus* Towards D-Xylose and D-Arabinose. *Chem. - Eur. J.* **2013**, *19*, 2895–2902. (g) Clapés, P.; Garrabou, X. Current Trends in Asymmetric Synthesis With Aldolases. *Adv. Synth. Catal.* **2011**, *353*, 2263–2283.
- (13) Pathak, T.; Waldmann, H. Enzymes and protecting group chemistry. *Curr. Opin. Chem. Biol.* **1998**, *2*, 112–120.
- (14) (a) Demir, A. S.; Şeşenoglu, Ö.; Eren, E.; Hosrik, B.; Pohl, M.; Janzen, E.; Kolter, D.; Feldmann, R.; Dünkelmann, P.; Müller, M. Enantioselective Synthesis of  $\alpha$ -Hydroxy Ketones via Benzaldehyde Lyase-Catalyzed C-C Bond Formation Reaction. *Adv. Synth. Catal.* **2002**, *344*, 96–103. (b) González, B.; Vicuña, R. Benzaldehyde lyase, a novel thiamine PPI-requiring enzyme, from *Pseudomonas fluorescens* biovar I. *J. Bacteriol.* **1989**, *171*, 2401. (c) Brandt, G. S.; Nemeria, N.; Chakraborty, S.; McLeish, M. J.; Yep, A.; Kenyon, G. L.; Petsko, G. A.; Jordan, F.; Ringe, D. Probing the Active Center of Benzaldehyde Lyase with Substitutions and the Pseudosubstrate Analogue Benzoylphosphonic Acid Methyl Ester. *Biochemistry* **2008**, *47*, 7734–7743.
- (15) Cheng, Y.; Shan, Q.; Zhang, Y.; Quan, Z.; Zhang, K.; Wang, B. A Highly Efficient One-Enzyme Protocol Using  $\omega$ -Transaminase and an Amino Donor Enabling Equilibrium Displacement Assisted by Molecular Oxygen. *Org. Chem. Front.* **2018**, *5*, 1633–1638.
- (16) Shin, J.-S.; Kim, B.-G. Transaminase-Catalyzed Asymmetric Synthesis of L-2-Aminobutyric Acid from Achiral Reactants. *Biotechnol. Lett.* **2009**, *31*, 1595–1599.
- (17) Sung, S.; Jeon, H.; Sarak, S.; Ahsan, M. M.; Patil, M. D.; Kroutil, W.; Kim, B.-G.; Yun, H. Parallel Anti-Sense Two-Step Cascade for Alcohol Amination Leading to  $\omega$ -Amino Fatty Acids and  $\alpha,\omega$ -Diamines. *Green Chem.* **2018**, *20*, 4591–4595.
- (18) Aki, K.; Ogawa, K.; Ichihara, A. Transaminases of branched chain amino acids: IV. Purification and properties of two enzymes from rat liver. *Biochim. Biophys. Acta - Enzymology* **1968**, *159*, 276–284.
- (19) (a) Seo, Y.-M.; Yun, H. Enzymatic Synthesis of L-tert-Leucine with Branched Chain Aminotransferase. *J. Microbiol. Biotechnol.* **2011**, *21*, 1049–1052. (b) Hong, E. Y.; Cha, M.; Yun, H.; Kim, B.-G. Asymmetric Synthesis of L-tert-Leucine and L-3-Hydroxyadamantylglycine using Branched Chain Aminotransferase. *J. Mol. Catal. B: Enzym.* **2010**, *66*, 228–233. (c) Xian, M.; Alaux, S.; Sagot, E.; Gefflaut, T. Chemoenzymatic synthesis of glutamic acid analogues: substrate specificity and synthetic applications of branched chain aminotransferase from *Escherichia coli*. *J. Org. Chem.* **2007**, *72*, 7560–7566.
- (20) (a) Galloway, W. R. J. D.; Hodgkinson, J. T.; Bowden, S. D.; Welch, M.; Spring, D. R. Quorum Sensing in Gram-Negative Bacteria: Small-Molecule Modulation of AHL and AI-2 Quorum Sensing Pathways. *Chem. Rev.* **2011**, *111*, 28–67. (b) Anedi, S. C.; Biabani, F.; Poduch, E.; Mannargudi, B. M.; Majumder, K.; Wei, L.; Khayat, R.; Tong, L.; Kotra, L. P. Engineering D-amino acid containing novel protease inhibitors using catalytic site architecture. *Bioorg. Med. Chem.* **2006**, *14*, 214–236.

## **Capítulo 3.2**

Biocatalytic synthesis of homochiral 2-hydroxy-4-butyrolactone derivatives by tandem aldol addition and carbonyl reduction.

## Biocatalytic synthesis of homochiral 2-hydroxy-4-butyrolactone derivatives by tandem aldol addition and carbonyl reduction.

### Resumen.

Los derivados de 2-hidroxiácidos y las 2-hidroxi-4-butyrolactonas son sintones importantes en la síntesis de moléculas naturales y sintéticas con actividad biológica. Además, son utilizadas como auxiliares quirales en síntesis orgánica asimétrica. Muchos métodos de síntesis se han desarrollado para la síntesis de estas moléculas, como: reducción asimétrica utilizando complejos metálicos, reacciones aldólicas estereoselectivas utilizando metal u organocatálisis, reducción enzimática entre otros. En este capítulo nos planteamos la síntesis diastereoselectiva de 2-hidroxi-4-butyrolactonas a través de una reacción aldólica catalizado por una aldolasa y la reducción del grupo carbonilo del producto aldólico utilizando deshidrogenasas. La reacción aldólica se realizó utilizando diferentes C-C liasas: dos aldolasas de *E. coli*, 3-metil-2-oxobutanoato hidroximetiltransferasa (KPHMT), 2-oxo-3-desoxi-L-rhamnonate aldolasa (YfaU) y la *trans*-O-hidroxibenziliden piruvato hidratasa-aldolasa (HBPA) de *Pseudomonas putida* que catalizaron la adición aldólica de 2-oxoácidos a diferentes aldehídos. La reducción de los aldoles obtenidos se realizó con dos deshidrogenasas: la 2-deshidropantoato 2-reductasa de *E. coli* (KPR) y la  $\Delta^1$ -piperidina-2-carboxilato/ $\Delta^1$ -pirrolina-2-carboxilato reductasa de *Pseudomonas syringae* pv. tomato DSM 50315 (DpkA). Esta última enzima se ha descrito como imina reductasa, en este trabajo dejamos constancia que también puede catalizar eficazmente la reducción de 2-oxoácidos a 2-hidroxiácidos. Curiosamente, el resultado estereoquímico de esta deshidrogenasa resultó ser complementario al de la cetopantoato reductasa KPR.

# Biocatalytic Synthesis of Homochiral 2-Hydroxy-4-butyrolactone Derivatives by Tandem Aldol Addition and Carbonyl Reduction

Carlos J. Moreno, Karel Hernández, Samantha Gittings, Michael Bolte, Jesús Joglar, Jordi Bujons, Teodor Parella, and Pere Clapés\*



Cite This: *ACS Catal.* 2023, 13, 5348–5357



Read Online

ACCESS |

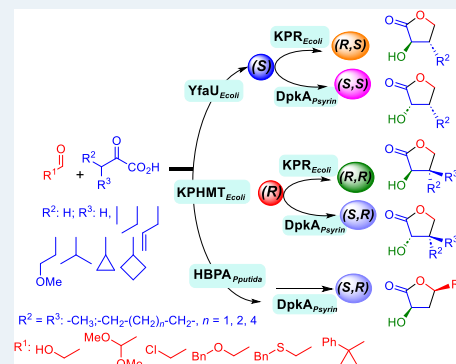
Metrics & More

Article Recommendations

Supporting Information

**ABSTRACT:** Chiral 2-hydroxy acids and 2-hydroxy-4-butyrolactone derivatives are structural motifs often found in fine and commodity chemicals. Here, we report a tandem biocatalytic stereodivergent route for the preparation of these compounds using three stereoselective aldolases and two stereocomplementary ketoreductases using simple and achiral starting materials. The strategy comprises (i) aldol addition reaction of 2-oxoacids to aldehydes using two aldolases from *E. coli*, 3-methyl-2-oxobutanoate hydroxymethyltransferase (KPHMT<sub>Ecoli</sub>), 2-keto-3-deoxy-L-rhamnonate aldolase (YfaU<sub>Ecoli</sub>), and *trans*-*o*-hydroxybenzylidene pyruvate hydratase-aldolase from *Pseudomonas putida* (HBPA<sub>Pputida</sub>) and (ii) subsequent 2-oxogroup reduction of the aldol adduct by ketopantoate reductase from *E. coli* (KPR<sub>Ecoli</sub>) and a  $\Delta^1$ -piperidine-2-carboxylate/ $\Delta^1$ -pyrroline-2-carboxylate reductase from *Pseudomonas syringae* pv. tomato DSM 50315 (DpkA<sub>Psyrim</sub>) with uncovered promiscuous ketoreductase activity. A total of 29 structurally diverse compounds were prepared: both enantiomers of 2-hydroxy-4-butyrolactone (>99% ee), 21 2-hydroxy-3-substituted-4-butyrolactones with the (2*R*,3*S*), (2*S*,3*S*), (2*R*,3*R*), or (2*S*,3*R*) configuration (from 60:40 to 98:2 dr), and 6 2-hydroxy-4-substituted-4-butyrolactones with the (2*S*,4*R*) configuration (from 87:13 to 98:2 dr). Conversions of aldol adducts varied from 32 to 98%, while quantitative conversions were achieved by both ketoreductases, with global isolated yields between 20 and 45% for most of the examples. One-pot one-step cascade reactions were successfully conducted achieving isolated yields from 30 to 57%.

**KEYWORDS:** biocatalysis, 2-oxoacid aldolase, ketoreductases, aldol addition, 2-hydroxy acids, 2-hydroxy-4-butyrolactones



## INTRODUCTION

Chiral 2-hydroxy acids and 2-hydroxy-4-butyrolactone derivatives are interesting compounds frequently found in naturally occurring biologically active products, synthetic drugs, and biodegradable polymers (e.g., poly  $\alpha$ -hydroxy acids for biomedical and pharmaceutical applications) (Figure 1).<sup>1</sup> Moreover, they constitute an important class of building blocks and chiral auxiliaries (e.g., (*R*)- or (*S*)-pantolactone derivatives) in asymmetric organic synthesis.<sup>2</sup>

Many efforts have been dedicated to the synthesis of 2-hydroxy-4-butyrolactone derivatives.<sup>1g,2e,3</sup> As examples of methods for their synthesis, it is worth mentioning (Scheme 1): enzymatic or metal-catalyzed asymmetric reduction,<sup>1b,4</sup> resolution procedures,<sup>5</sup> oxidation of vicinal diols,<sup>6</sup> and stereoselective aldol addition using metal- or organocatalysts in combination with enzymatic reduction.<sup>1j,2b,7</sup> Although organocatalysis and metal-catalyzed asymmetric approaches have reached a high degree of efficiency, in many instances, organocatalysts still suffer from low turnover numbers, and metal catalysis still needs extreme temperatures, sophisticated metal ligands, expensive heavy metals, and high hydrogen pressure. However, although enzymatic carbonyl reduction of 2-oxoacid derivatives has been reported,<sup>8</sup> the stereoselective

reduction of 4-hydroxy-2-oxoacid derivatives to produce 2-hydroxy-4-butyrolactone derivatives remains unexplored.

We have envisioned a straightforward asymmetric construction of 2-hydroxy-4-butyrolactone derivatives by a synthetic route consisting of a stereoselective enzymatic aldol addition of 2-oxoacids to aldehydes and subsequent asymmetric biocatalytic reduction of the 2-carbonyl group (Scheme 1). Herein, we demonstrated the feasibility of this approach by using a selection of 2-oxoacids (2) and aldehydes (1) to enzymatically generate 3- and 4-substituted 4-hydroxy-2-oxoacids 3 and 6, respectively, with defined stereochemistry. Then, a stereoselective biocatalytic reduction of the 2-carbonyl group was conducted to produce 2-hydroxyacids 4 and 7, which, after intramolecular esterification (i.e., lactonization) taking place during the workup and purification steps, rendered

Received: January 25, 2023

Revised: March 9, 2023

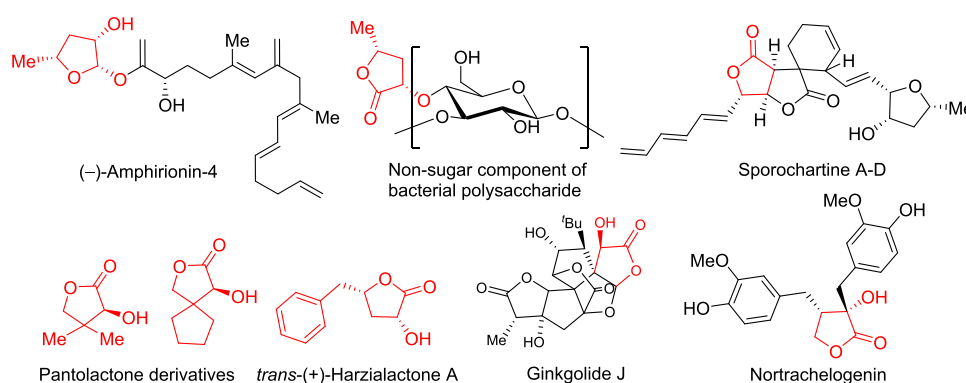


**Figure 1.** Examples of biologically relevant compounds bearing 2-hydroxy-4-butyrolactone derivatives.

3- and 4-substituted-2-hydroxy-4-butyrolactones **5** and **8**, respectively (Scheme 2).

Three stereoselective 2-oxoacid aldolases were selected as biocatalysts for the aldol reactions, namely, 3-methyl-2-oxobutanoate hydroxymethyltransferase (KPHMT<sub>Ecoli</sub>) and 2-keto-3-deoxy-L-rhamnonate aldolase (YfaU<sub>Ecoli</sub>) and its W23V variant, both from *E. coli*.<sup>9</sup> These were employed for the aldol addition of 2-oxoacids **2a–2n** to formaldehyde **1a**. The third one, *trans*-*o*-hydroxybenzylidene pyruvate hydratase-aldolase from *Pseudomonas putida* (HBPA<sub>Pputida</sub>), and its H205A variant were selected as the catalyst for the stereoselective aldol addition of sodium pyruvate **2a** to aldehydes **1a–1g**.<sup>10</sup> In addition, two reductases were employed to convert the carbonyl group into a hydroxyl group. The ketopantoate reductase from *E. coli* (KPR<sub>Ecoli</sub>) in vivo catalyzes the NADPH-dependent reduction of ketopantoate to pantoate as part of the pantothenate biosynthetic pathway.<sup>11</sup> Ketopantoate bears a *gem*-dimethyl quaternary center, and therefore, we envision that KPR<sub>Ecoli</sub> could be active toward 3-substituted-2-oxo acids **3**. The second one,  $\Delta^1$ -piperidine-2-carboxylate/ $\Delta^1$ -pyrroline-2-carboxylate reductase from *Pseudomonas syringae* pv. tomato DSM 50315 (DpkA<sub>Psyrin</sub>), was described as an imine reductase transforming 3,4,5,6-tetrahydropyridine-2-carboxylic acid and 3,4-dihydro-2*H*-pyrrole-5-carboxylic acid into *L*-pipecolic acid and *L*-proline, respectively.<sup>12</sup> In this case, during our ongoing investigation on iminoreductases, we serendipitously found that DpkA<sub>Psyrin</sub> had a promiscuous ketoreductase activity, and consequently, we consider it interesting to exploit its synthetic capabilities. Moreover, both reductases have been underdeveloped for the synthesis of 2-hydroxy acids.

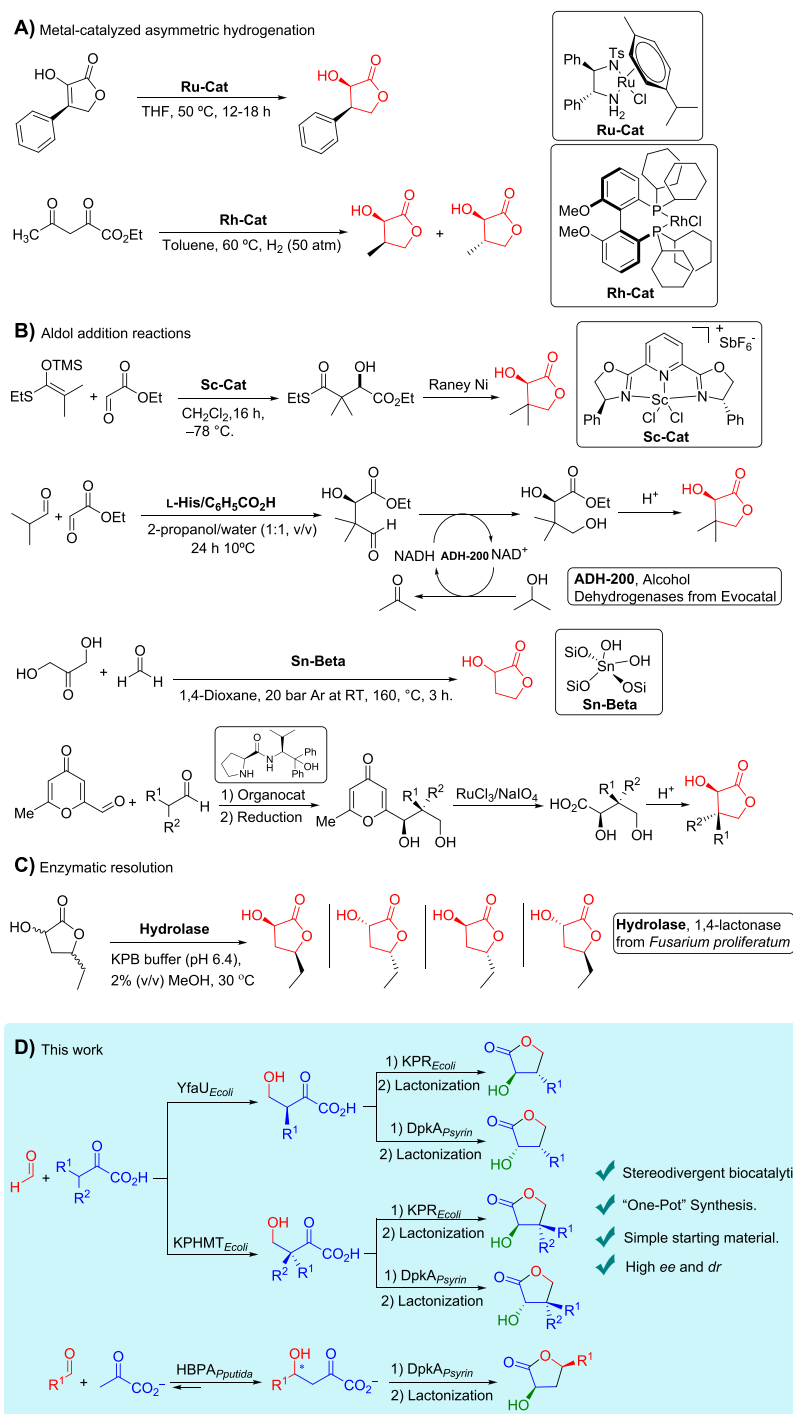
## RESULTS AND DISCUSSION

**Synthesis and Product Characterization.** We began our investigations assaying KPR<sub>Ecoli</sub> and DpkA<sub>Psyrin</sub> as catalysts for the reduction of the 4-hydroxy-2-ketoacids **3** and **6**, obtained from the enzymatic aldol addition of 2-oxoacids **2** to aldehydes **1** (Scheme 2). To this end, the aldol reaction was first run under the conditions described in our previous studies.<sup>9,10</sup> When the aldol adduct attained the maximum concentration (i.e., steady state), YfaU<sub>Ecoli</sub> and KPHMT<sub>Ecoli</sub> were inactivated by adding EDTA to avoid enzymatic retroaldololysis, whereas in the case of HBPA, this was unnecessary. Then, DpkA<sub>Psyrin</sub> or KPR<sub>Ecoli</sub>, glucose, glucose dehydrogenase [GDH, from ProZomix, see the Supporting Information (SI)], and NADP<sup>+</sup> were added. The enzymatic aldol and reduction reactions were monitored by reverse-phase high-performance liquid chromatography (HPLC), and once the reaction did not further

evolve, they were worked up, purified, and characterized as 3-substituted-2-hydroxy-4-butyrolactones **5** and 4-substituted-2-hydroxy-4-butyrolactones derivatives **8** (Schemes 3, 4 and 5) (see the SI). The butyrolactones were formed during the lyophilization of the product after the anion exchange purification procedure in the presence of formic acid. This transformation was favored by the water elimination during the freeze-drying process. However, the efficiency of this process was limited, and as a consequence, another purification step was required, implying low isolated yields (Schemes 3, 4 and 5). Moreover, the yields were not improved by performing the lactonization in the presence of catalytic amounts of TsOH in toluene using a Dean–Stark apparatus. This step was not optimized neither the workup nor the purification processes.

The biocatalytic reduction of the aldol adducts always gave quantitative substrate conversions after 24 h of reaction either with DpkA<sub>Psyrin</sub> or KPR<sub>Ecoli</sub>. Interestingly, KPR<sub>Ecoli</sub> showed ample substrate tolerance on 3-substituted-4-hydroxy-2-oxoacids **3**, including those bearing *gem*-cycloalkyl quaternary centers **3k–n**, homologues to the natural substrate **3j**. An exception was **3i**, which was not converted (Schemes 3 and 4) probably due to the steric limitations imposed by the active-site cavity. DpkA<sub>Psyrin</sub> tolerated all examples assayed of 4-substituted-4-hydroxy-2-oxoacids **6b–g**, whereas they were not substrates for KPR<sub>Ecoli</sub>. DpkA<sub>Psyrin</sub> has a more stringent substrate selectivity toward 3-substituted-4-hydroxy-2-oxoacids **3**, accepting only the unsubstituted **3a** or short C3-substituents such as methyl or ethyl, **3b** and **3c**, respectively, with a preference for those 3*S* configured.

The stereochemical outcome of the aldol addition of 2-oxoacids to formaldehyde has already been reported in previous studies on MBP-YfaU<sub>Ecoli</sub>, KPHMT<sub>Ecoli</sub> and HBPA<sub>Pputida</sub> catalysis.<sup>9,10</sup> An identical stereochemical outcome was found for substrates **2e** and **2f**, which have not been previously reported. Compounds **5b–h** and **8b–g** contain one chiral center with known absolute stereochemistry defined by the aldolase.<sup>9b,10</sup> This chiral center was used as a reference for the assessment of the overall relative configuration of these compounds by nuclear magnetic resonance (NMR) (see the SI). In addition, the absolute configuration for *R*-**5a** and *S*-**5a** was confirmed by comparing their specific rotation values with those reported (see the SI).<sup>13</sup> Furthermore, authentic commercial samples and X-ray diffraction were used to unequivocally assign *R*-**5j**<sup>13a</sup> (see the SI) and *R*-**5l** (Figure S33), respectively. The stereochemical configuration of *R*-**5k**, *R*-**5m**, and *R*-**5n** was inferred considering the high enantioselectivity observed for KPR<sub>Ecoli</sub> found in the examples

Scheme 1. Synthetic Methodologies for the Preparation of 2-Hydroxy-4-butylolactone Derivatives<sup>a</sup>

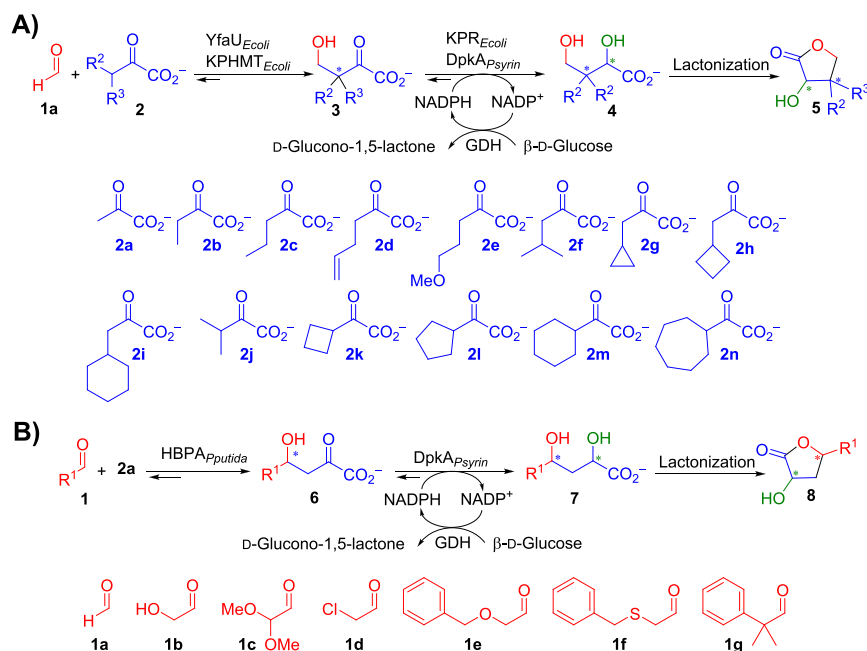
<sup>a</sup>(A) Metal-catalyzed asymmetric.<sup>1b,4a</sup> (B) Aldol reaction.<sup>2j,7b,1j,7a,c</sup> (C) Enzymatic resolution.<sup>5</sup> (D) This work: stereodivergent biocatalytic approach. Stereoselective aldol addition of 2-oxoacid derivatives to aldehydes catalyzed by 2-oxoacid aldolases, namely, 3-methyl-2-oxobutanoate hydroxymethyltransferase ( $KPHMT_{E.coli}$  EC 2.1.2.11), 2-keto-3-deoxy-L-rhamnonate aldolase ( $YfaU_{E.coli}$  EC 4.1.2.53), both from *E. coli*, and *trans*-o-hydroxybenzylidene pyruvate hydratase-aldolase from *Pseudomonas putida* ( $HBPA_{P.putida}$  EC 4.1.2.45) followed by asymmetric enzymatic reduction using ketopantoate reductase from *E. coli* ( $KPR_{E.coli}$  EC 1.1.1.169) and an NAD(P)H-dependent  $\Delta^1$ -piperidine-2-carboxylate/ $\Delta^1$ -pyrroline-2-carboxylate reductase from *Pseudomonas syringae* pv. tomato DSM50315 (GenBank: DQ017704.1) ( $DpkA_{P.syringae}$  EC 1.5.1.21).

thereof. Thus, the absolute stereochemistry at C3 coming from the  $KPR_{E.coli}$  reduction was mainly *R* and that from  $DpkA_{P.syringae}$  was preferentially *S*.

Molecular modeling of the 4-hydroxy-2-oxoacid substrates 3 bound to both reductases provided an explanation for these stereochemical results. Both enzymes are known to exist in

open and closed forms, whose interconversion is triggered by substrate binding. In the closed forms, substrates and NADPH are buried in a deep and relatively narrow cavity (Figure 2A,B). The optimized energy model of 4-hydroxy-2-oxoacid 3a bound into the active site of  $KPR_{E.coli}$  shows that the pre-reactive conformation of the substrate is stabilized by multiple H-bond



**Scheme 2. Biocatalytic Synthesis of 2-Hydroxy-4-butyrolactones by Tandem Aldolase and Ketoreductase Starting from Aldehydes 1 and 2-Oxoacids 2<sup>a</sup>**


<sup>a</sup>(A) Synthesis of 3-substituted-2-hydroxy-4-butyrolactones: aldolases: YfaU<sub>Ecoli</sub> and KPHMT<sub>Ecoli</sub>; ketoreductases: KPR<sub>Ecoli</sub> and DpkA<sub>Psyrin</sub>. (B) Synthesis of 4-substituted-2-hydroxy-4-butyrolactones: aldolase HBPA<sub>Pputida</sub> and ketoreductase DpkA<sub>Psyrin</sub>. GDH: glucose dehydrogenase from Prozomix.

interactions (Figure 2C). Thus, the 3a carboxylate accepts H-bonds from the 4-OH group (intramolecular), the amide group of Asn184, and the backbone-NH of Ser244, while the 4-OH group does the same from the sidechains of Asn194 and Asn241. In addition, the 2-oxo group is fixed by H-bonds with the sidechains of Asn98 and the catalytic Lys176, which is properly disposed to transfer its proton to the developing C2-kalkoxide, when reduction takes place. In this way, this 2-oxo group exposes its *si*-face to the nicotinamide moiety of the reduced NADPH cofactor, which delivers its pro-4S hydrogen to render the corresponding intermediate 2R-4a, the precursor of 2R-5a.<sup>11c,d</sup> Similar interactions and binding modes can be proposed for the rest of 4-hydroxy-2-oxoacid substrates 3 (Figure S69), which correlates with the observed 2R-stereochemical outcome for their KPR<sub>Ecoli</sub> reduction products. On the other hand, the corresponding models with DpkA<sub>Psyrin</sub> show that the carboxylate group of the substrates accepts H-bonds from the sidechains of Arg58 and Thr166, as well as from the backbone-NH of His192 and Gly193, and that it also establishes a salt bridge with the protonated guanidine group of Arg58 (Figures 2D and S70). In addition, the 2-oxo group accepts H-bonds from the 4-OH group (intramolecular) and from the protonated imidazole of His54, which acts as a general acid catalyst.<sup>12</sup> This substrate binding mode forces the exposure of the *re*-face of the 2-oxo group to the reduced NADPH, rendering the 2S-4 products, precursors of the 2-hydroxy-4-butyrolactones 2S-5. The same can be extended to DpkA<sub>Psyrin</sub> substrates 6b–g (Figure S70).

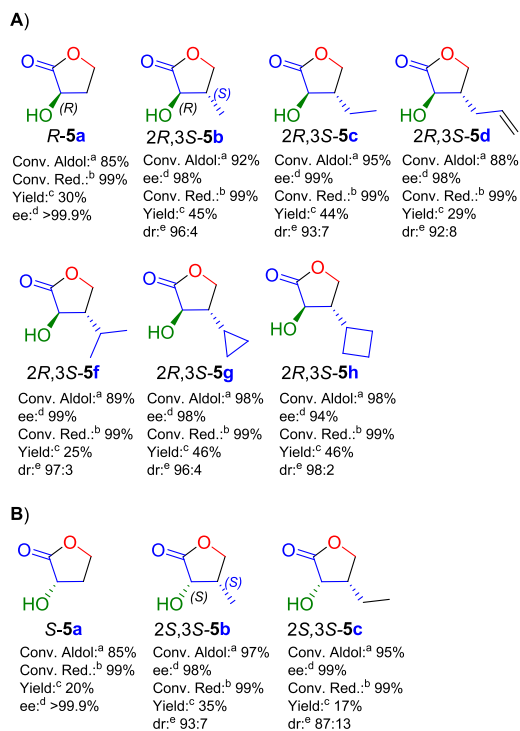
The degree of stereoselectivity of both reductases depended on the ketoacid. Thus, the 3S-configured 3-substituted-4-hydroxy-2-oxoacids (3S-3) gave very good diastereomeric ratios with KPR<sub>Ecoli</sub> catalysis, i.e., 92:8 to 98:2 inferred from the (2R,3S):(2S:3S) ratios of compounds 5 (Scheme 3A). For the 3R-configured ones, the diastereomeric ratios were high toward

3b, 3e, and 3f (93:7–96:4) and moderate with 3c and 3g (72:28–84:16) (Scheme 4A). A particular case was 3h because the low dr (60:40) value was essentially due to the moderate 75% ee of the preceding aldol addition reaction. For the unsubstituted 4-hydroxy-2-oxoacid 3a and the ones containing *gem*-cycloalkyl substituents, 3j–n, excellent enantiomeric excesses >99% were achieved. DpkA<sub>Psyrin</sub> gave excellent stereoselectivities with 2-oxoacids 3a, 3b, and 6b–d,g, whereas 3S-3c, with a C3-ethyl substituent, 6e, and 6f rendered moderate diastereomeric ratios (87:13–89:11) (Schemes 3B and 5).

**Kinetic Analysis.** The kinetics of the enzymatic reduction of 4-hydroxy-2-oxoacids with KPR<sub>Ecoli</sub> and DpkA<sub>Psyrin</sub> were determined using the products obtained from the aldol addition (Table 1). To avoid artifacts during the assay, the aldolase and metal excess were previously removed (see the SI).

As expected, the natural substrate of KPR<sub>Ecoli</sub>, i.e., ketopantoate 3j, gave the highest specificity constant ( $k_{cat}/K_m$ )<sup>app</sup>, exceeding by 1 to 4 orders of magnitude those of the rest of the 2-oxoacids. The introduction of cyclobutyl (3k) and cyclopentyl (3l) moieties, similar to 3j, gave ( $k_{cat}/K_m$ )<sup>app</sup> values of the same order of magnitude as that of the natural substrate. It is noteworthy the inhibition of KPR<sub>Ecoli</sub> by its natural substrate (3j) that has not been noticed in previous reports likely due to the limited range of substrate concentration analyzed.<sup>11d</sup> Besides, in another publication on KPR from *Staphylococcus aureus*, an apparent substrate inhibition constant was reported to be around 270 μM, one order of magnitude lower than that found in this study for KPR<sub>Ecoli</sub>.<sup>15</sup> As suspected, substrate inhibition was also detected for the corresponding cycloalkyl analogues 3k and 3l. Compared with the natural substrate, 3j, the  $k_{si}^{app}$  of the analogue bearing a cyclobutyl moiety, 3k, increased 1.7-fold, whereas for the one with the

**Scheme 3. One-Pot Two-Step Synthesis of 3-Substituted-2-hydroxy-4-butyrolactones **5** by Tandem Biocatalytic Aldol-Reduction Reactions Catalyzed by Tandem YfaU<sub>Ecoli</sub> and (A) KPR<sub>Ecoli</sub> and (B) DpkA<sub>Psyrin</sub>**

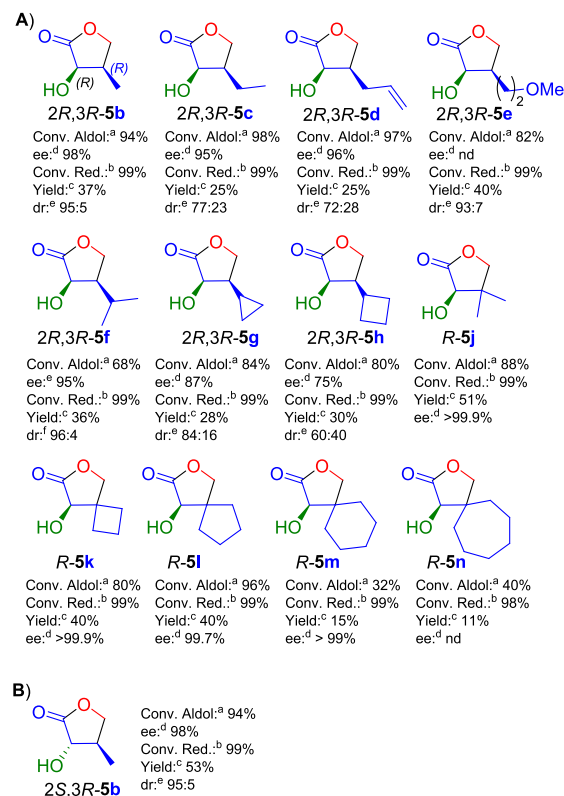


<sup>a</sup>Conditions: 1 mmol scale, total volume (10 mL) at 25 °C, and magnetically stirred at 250 rpm; YfaU<sub>Ecoli</sub> wt (3 mg purified protein mL<sup>-1</sup>) in plain water (4 mL), 2-oxoacids (**2a–i**) (0.1 M), and NiCl<sub>2</sub> (1 mM) were added. The reaction was started by adding formaldehyde (**1**, 0.1 M). After 24 h, the reduction reaction (20 mL final volume) was carried out by adding EDTA (5 mM), glucose (0.2 M), GDH (3.4 U mL<sup>-1</sup>), KPR<sub>Ecoli</sub> (4.7 U mL<sup>-1</sup>) or DpkA<sub>Psyrin</sub> (10<sup>-3</sup> U mL<sup>-1</sup>), and finally NADP<sup>+</sup> (5 mM). After purification by anion exchange chromatography and eluting with HCO<sub>2</sub>H (1 M), the lactonization occurred during freeze drying the pure fraction pool. The product was then further purified by column chromatography on silica with a step gradient of hexane/EtOAc (see the SI). HPLC monitoring conditions: RP-HPLC XBridge C18, 5 μm, 4.6 × 250 mm column. The solvent system: solvent (A): 0.1% (v/v) trifluoroacetic acid (TFA) in H<sub>2</sub>O and solvent (B): 0.095% (v/v) TFA in CH<sub>3</sub>CN/H<sub>2</sub>O 4:1, flow rate 1 mL min<sup>-1</sup>, detection at 215 nm at 30 °C. Precolumn derivatization with BnONH<sub>2</sub> elution conditions: gradient from 10 to 100% B over 30 min (reaction with compounds **2a–l**) and 10 to 100% B over 60 min (reaction with compounds **2m,n**). <sup>b</sup>Conversion of aldol addition. <sup>c</sup>Conversion of the reduction. <sup>d</sup>Isolated yields. <sup>e</sup>Enantiomeric excess of the reduction determined by HPLC on chiral stationary phases. <sup>f</sup>Diastereomeric ratio determined by NMR.

cyclopentyl substituent, **3l**, it increased 7.3-fold. The impact of substrate inhibition, i.e., ( $k_{si}/K_m$ )<sup>app</sup>,<sup>16</sup> is larger for the dimethyl and cyclobutyl analogues (**3k**, ( $k_{si}/K_m$ )<sup>app</sup> = 4.3 ± 1.8) (**3j**, ( $k_{si}/K_m$ )<sup>app</sup> = 9.3 ± 4.8) and much lower for the cyclopentyl (**3l**, ( $k_{si}/K_m$ )<sup>app</sup> = 140 ± 91). This is consistent with the fact that **3k** and **3j** may have similar steric and electronic interactions with the enzyme, whereas **3l** is bulkier and might establish fewer interactions in the active site.

The ( $k_{cat}/K_m$ )<sup>app</sup> values of KPR<sub>Ecoli</sub> for 3S-substituted-2-oxoacids increase with the size of the C3-alkyl chain up to two carbon atoms (3S-**3b** vs 3S-**3c**) and then decrease following

**Scheme 4. One-Pot Two-Step Synthesis of 3-Substituted-2-hydroxy-4-butyrolactones **5** by Tandem Biocatalytic Aldol-Reduction Reactions Catalyzed by Tandem KPHMT<sub>Ecoli</sub> and (A) KPR<sub>Ecoli</sub> and (B) DpkA<sub>Psyrin</sub>**

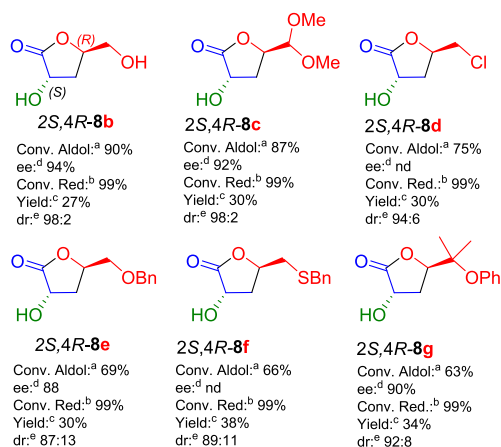


<sup>a</sup>Conditions: 1 mmol scale, total volume (10 mL) at 25 °C, and magnetically stirred at 250 rpm; KPHMT<sub>Ecoli</sub> wild-type (1 mg purified protein mL<sup>-1</sup>) in plain (6.8 mL) water, CoCl<sub>2</sub> (1 mM), and 2-oxoacids (**2a–i**) (0.1 M) were added. The reaction was started by adding formaldehyde (0.1 M). After 24 h, the reduction reaction, workup, lactonization, purification, and HPLC reaction monitoring were conducted as described in Scheme 3 (see also the SI). <sup>b</sup>Conversion of aldol addition. <sup>c</sup>Conversion of the reduction. <sup>d</sup>Isolated yields. <sup>e</sup>Enantiomeric excess of the reduction determined by HPLC on chiral stationary phases. <sup>f</sup>Diastereomeric ratio determined by NMR.

the order of isopropyl (3S-**3f**), cycloalkyl (3S-**3g**, 3S-**3h**), and allyl (3S-**3d**) substituents (Table 1 and Figure 3). On the other hand, ( $k_{cat}/K_m$ )<sup>app</sup> for the 3R-substituted-2-oxoacids decreased with the size of the C3-alkyl chain substituent being the methoxypropyl one with the lowest value. In the case of DpkA<sub>Psyrin</sub> ( $k_{cat}/K_m$ )<sup>app</sup> remained nearly constant for the 3-substituted-4-hydroxy-2-oxoacids 3S-**3b,c** and 3R-**3b** (Table 1). Kinetic parameters for DpkA<sub>Psyrin</sub> using 4-substituted-4-hydroxy-2-oxoacids **6** indicate that 4R-**6b** and 4R-**6c** are around 10-fold better substrates than the 3-substituted-4-hydroxy-2-oxoacids. Unfortunately, kinetic parameters for 4R-**6d–g** could not be measured, owing to the unconverted pyruvate of aldol reactions (>20 mM) that strongly alters their  $k_{cat}$  and  $K_m$  values.

The stereochemical configuration of the C3-methyl substituent has strong influence on the ( $k_{cat}/K_m$ )<sup>app</sup> for KPR<sub>Ecoli</sub>: 3R-**3b** functions 40-fold better than that of 3S-**3b** being the best one among the 3-substituted chiral substrates for KPR<sub>Ecoli</sub> (Figure 3). In contrast, the 3S-isomers of **3c** and **3h** showed moderately better ( $k_{cat}/K_m$ )<sup>app</sup> values than their 3R-

**Scheme 5. One-Pot Two-Step Synthesis of 4-Substituted-2-hydroxy-4-butyrolactones **8** by Tandem Biocatalytic Aldol-Reduction Reactions Catalyzed by Tandem HBPA<sub>Pputida</sub> and DpkA<sub>Psyriin</sub><sup>a</sup>**



<sup>a</sup>Conditions: 1 mmol scale, 8.3 mL total volume at 25 °C, and orbitally stirred at 250 rpm. Sodium pyruvate **2b** (0.1 M), aldehyde **1b–g** (0.1 M), HBPA wild-type and H205A variant for substrates **1d** and **1f** (1 mg protein mL<sup>-1</sup>). After 24 h, the reduction reaction, workup, lactonization, purification, and HPLC reaction monitoring were conducted as described in Scheme 3, except the EDTA addition (see also the SI). <sup>b</sup>Conversion of aldol addition. <sup>c</sup>Conversion of the reduction. <sup>d</sup>Isolated yields. <sup>e</sup>Enantiomeric excess of the reduction determined by HPLC on chiral stationary phases. <sup>f</sup>Diastereomeric ratio determined by NMR.

homologues. The rest of the 3R-2-oxoacids gave similar results as compared to those of the S-configuration. The kinetic parameters of DpkA<sub>Psyriin</sub> for 3S- and 3R-**3b** substrates indicate that the 3S-configuration was preferred for this enzyme (Table 1). Comparing both reductases within the same substrates assayed, KPR<sub>Ecoli</sub> ( $k_{cat}/K_m$ )<sup>APP</sup> values are ca. 10<sup>1</sup>- to 10<sup>4</sup>-fold higher than those of DpkA<sub>Psyriin</sub>. On the other hand, 4-substituted-4-hydroxy-2-oxoacids **6b–g** were not substrates of KPR<sub>Ecoli</sub>.

It is interesting to note that in all cases, complete conversions were reached after 24 h, even though the much lower  $k_{cat}$ <sup>APP</sup> values of some of the substrates, relative to **3j**.

**Enzymatic Cascade Synthesis.** Results for the cascade process were successful in some examples with isolated yields ranging from 20 to 57% (Scheme 6). Additional examples were tested, but the results were unsuccessful, and no product formation was detected by HPLC. Instead, we observed that formaldehyde was not converted while the starting 2-oxoacid was consumed, indicating that it was reduced by the ketoreductase. Hence, we reasoned that the successful one-pot one-step process depends on the rates of aldol and retroaldol reactions and the 2-oxoacid reduction.

## CONCLUSIONS

A biocatalytic route for the synthesis of chiral 3- and 4-substituted-2-hydroxy-4-butyrolactone derivatives was developed. The methodology provides structurally diverse compounds from the achiral starting material in a stereodivergent fashion using stereocomplementary 2-oxoacid aldolases and ketoreductases as catalysts. A total of 33 substrates were tested

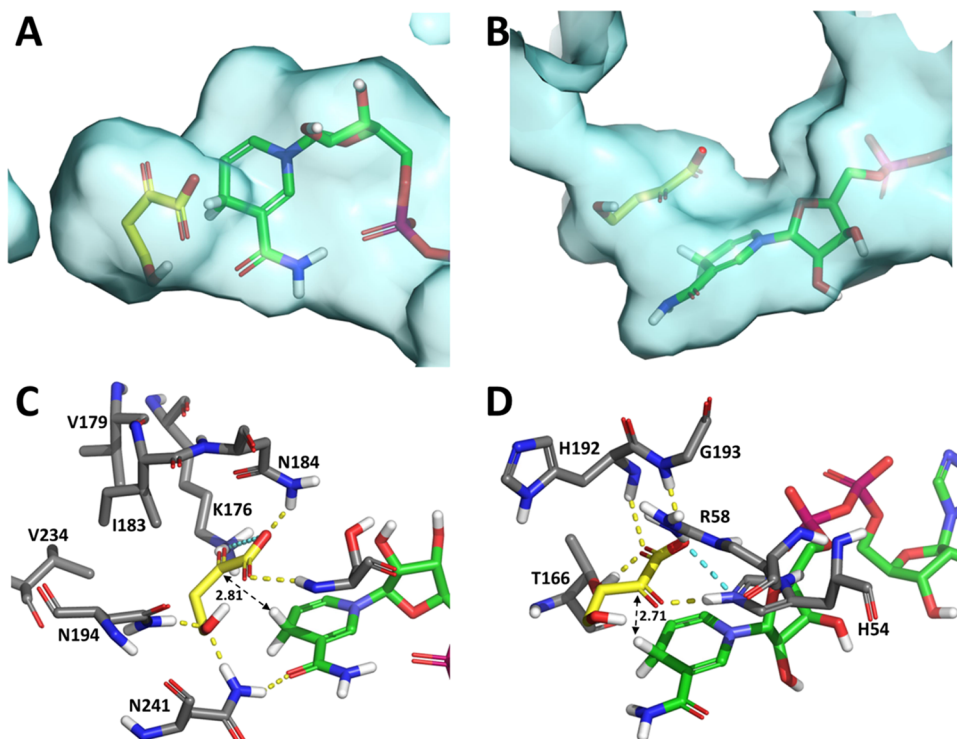


**Figure 2.** Molecular models of **3a** bound to KPR<sub>Ecoli</sub> (A,C) and DpkA<sub>Psyriin</sub> (B,D). These models were built starting from PDB structures 2OFP (A) and 2CWH<sup>14</sup> (B), and their structure was optimized by QM/MM methods (QM part optimized at the DFT B3LYP/6-31G\*\* level of theory and MM part optimized with the OPLS2005 force field, see the SI). The substrate, NADPH, and close protein residues are shown with yellow, green, and gray C-atoms; H-bonds and salt bridges are shown with yellow and cyan dashed lines; the protein surface of the active-site cavities is shown in cyan (A,B); the distances between the reactive carbonyl C-atom and the NADPH pro-4S hydrogen are also displayed (C,D).

**Table 1. Kinetic Parameters for KPR<sub>Ecoli</sub> and DpkA<sub>Psyrrin</sub> Catalyzed 2-Carbonyl Reduction of C3-Substituted 4-Hydroxy-2-oxoacids (3 and 6)<sup>a</sup>**

substrate 3	KPR <sub>Ecoli</sub> <sup>b</sup>				DpkA <sub>Psyrrin</sub> <sup>b</sup>		
	$k_{\text{cat}}^{\text{app}}$	$K_m^{\text{app}}$	$(k_{\text{cat}}/K_m)^{\text{app}}$	$k_{\text{si}}^{\text{app}}$	$k_{\text{cat}}^{\text{app}}$	$K_m^{\text{app}}$	$(k_{\text{cat}}/K_m)^{\text{app}}$
3a	7.1 ± 0.5	4.9 ± 1.2	1.5 ± 0.4		1.7 ± 0.2	33 ± 7	0.052 ± 0.013
3S-3b	348 ± 15	12.9 ± 1.4	27 ± 3		1.1 ± 0.1	19 ± 4	0.058 ± 0.012
3S-3c	926 ± 37	3.0 ± 0.5	314 ± 52		0.23 ± 0.01	14 ± 2	0.016 ± 0.002
3S-3d	89 ± 6	9.5 ± 1.7	9.4 ± 1.8				
3S-3f	1021 ± 69	13 ± 2	77 ± 12				
3S-3g	350 ± 20	15 ± 2	24 ± 4				
3S-3h	820 ± 150	65.5 ± 13.4	13 ± 3	8.4 ± 1.8			
3R-3b	5350 ± 138	4.8 ± 0.4	1109 ± 86		0.0024 ± 0.0002	7.5 ± 1.9	0.047 ± 0.013
3R-3c	700 ± 34	7 ± 1	106 ± 18				
3R-3d	90 ± 5	9.5 ± 1.5	9.4 ± 1.6				
3R-3e	5.9 ± 0.5	18 ± 3	0.34 ± 0.10				
3R-3g	87 ± 4	2.3 ± 0.4	37 ± 6				
3R-3h	40 ± 4	11 ± 3	3.7 ± 1.0				
3j	4457 ± 813	0.4 ± 0.2	10,747 ± 4587	3.9 ± 1.3			
3k	6791 ± 1022	1.5 ± 0.5	4427 ± 1668	6.6 ± 1.5			
3l	1166 ± 67	0.2 ± 0.1	5569 ± 3737	28 ± 4			
4R-6b					3.00 ± 0.02	11 ± 1	0.28 ± 0.039
4-R-6c					84 ± 27 <sup>c</sup>	97 ± 43 <sup>c</sup>	0.87 ± 0.48

<sup>a</sup> $k_{\text{cat}}^{\text{app}} = \text{min}^{-1}$ ;  $K_m^{\text{app}} = \text{mM}$ ;  $(k_{\text{cat}}/K_m)^{\text{app}} = \text{min}^{-1} \text{mM}^{-1}$ ;  $k_{\text{si}} = \text{mM}$ . <sup>b</sup>The kinetic parameters for KPR<sub>Ecoli</sub> and DpkA<sub>Psyrrin</sub> were determined in a continuous assay method monitoring the oxidation of NADPH to NADP<sup>+</sup> at 340 nm. The reactions were monitored during 15 min measuring every 30 s. The assay mixture (0.3 mL) consisted of 50 mM Tris–HCl buffer pH 8.0, containing NADPH (0.16 mM), aldol adducts (1–60 mM), and appropriate amounts of enzymes. One unit of activity was defined as the amount of ketoreductases that catalyzes the formation of 1 μmol NADP<sup>+</sup> per min at 30 °C. Measurements were carried out in triplicate independent experiments. To determine the kinetic parameters, data were fitted to the Michaelis–Menten kinetic model using the software GraphPad Prism version 5.0 (see Figures S11–S32). <sup>c</sup>Estimated parameters because the activity vs concentration curve did not reach a plateau within the range of concentrations studied (12–50 mM) (Figure S32).

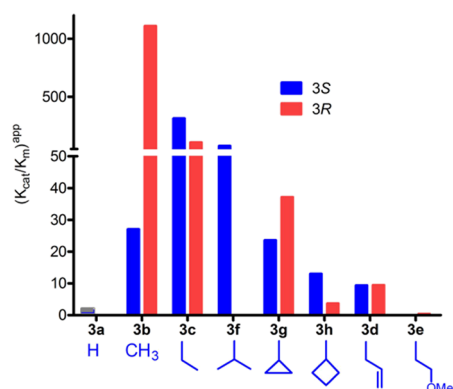
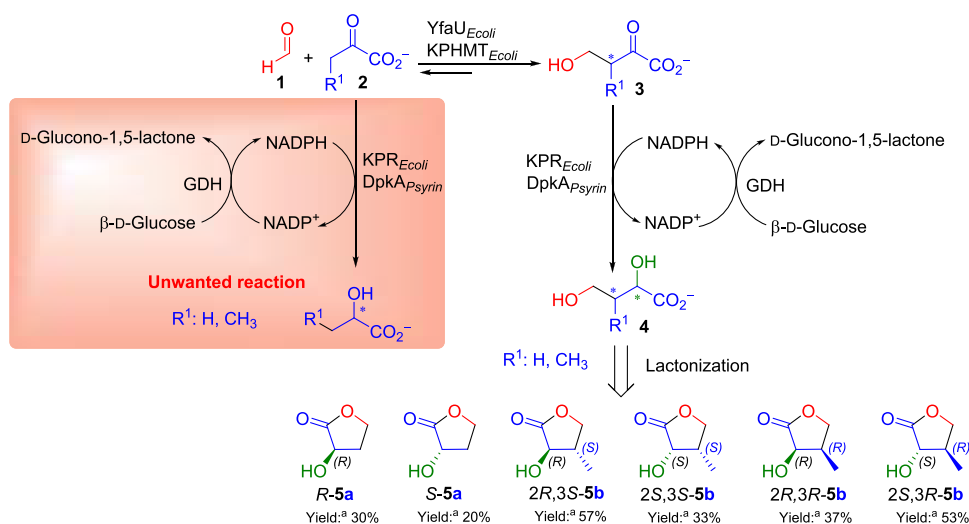


**Figure 3.** Values of  $(k_{\text{cat}}/K_m)^{\text{app}}$  for the KPR<sub>Ecoli</sub> catalysis vs the C3-substituent structure of both enantiomers of the 4-hydroxy-2-oxoacids. The  $(k_{\text{cat}}/K_m)^{\text{app}}$  values were taken from Table 1 and are given in  $\text{min}^{-1}$ .

for both reactions, furnishing 29 different 3- and 4-substituted 2-hydroxy-4-butyrolactones achieving conversions of aldol addition from 32 (only one example) to 98% and ketoreduction >95%, diastereomeric ratios from 60:40 to 98:2, and ee >99%. Apart from the aldol reaction, both KPR<sub>Ecoli</sub> and DpkA<sub>Psyrrin</sub> gave quantitative conversions after 24 h of incubation, even for substrates with  $k_{\text{cat}}^{\text{app}}$  values much lower as compared with 3j in the case of KPR<sub>Ecoli</sub>. KPR<sub>Ecoli</sub> showed broad substrate tolerance toward the C3-substituted 2-oxoacids, including those bearing *gem*-cycloalkyl quaternary centers, homologues to the natural substrate ketopantoate (3j). Moreover, substrate inhibition was observed for ketopantoate as well as for its *gem*-cycloalkyl homologues. On the other hand, KPR<sub>Ecoli</sub> does not tolerate the 4-substituted-4-hydroxy-2-oxoacids 6. Concerning DpkA<sub>Psyrrin</sub> it accepted all examples of 4-substituted-4-hydroxy-2-oxoacids (6), whereas it has stringent substrate selectivity for the 3-substituted-4-hydroxy-2-oxoacids 4 accepting only methyl and ethyl C3-substituents, with a strong preference for the 3S-configured aldol adducts.

**Scheme 6. Enzymatic Cascade Process for the Synthesis of the Two Enantiomers of 2-Hydroxy-4-butyrolactones, R-5a and S-5a, and the Four Possible Stereoisomers of 3-Methyl-2-hydroxy-4-butyrolactones 5b<sup>a</sup>**



<sup>a</sup>Isolated yields.

Concerning the stereochemical preference,  $KPR_{Ecoli}$  gave 2*R*-configured 2-hydroxyacids, whereas  $DpkA_{Psynin}$  furnished the corresponding 2*S* enantiomers. Finally, we conducted the synthesis of some 2-hydroxy-4-butyrolactones in a one-pot one-step (i.e., aldol addition + ketoreduction) reaction system. This was possible when the rate of the aldol addition reaction was much faster than that of ketoreduction of the starting 2-oxoacid. Under these conditions, the yields were similar to those achieved in a one-pot two-step fashion. Both methodologies are of practical value to carry out the synthesis of the corresponding products in 20–57% isolated yields.

## ■ ASSOCIATED CONTENT

### Supporting Information

The Supporting Information is available free of charge at <https://pubs.acs.org/doi/10.1021/acscatal.3c00367>.

General methods and protocols for the screening and synthesis, activity determinations, kinetics determination, synthesis of starting materials, synthesis of 2-hydroxy-4-butyrolactone derivatives, NMR spectra, and computational methods and modeling (PDF)

## ■ AUTHOR INFORMATION

### Corresponding Author

Pere Clapés – Dept. of Biological Chemistry, Institute for Advanced Chemistry of Catalonia, IQAC-CSIC, 08034 Barcelona, Spain; [orcid.org/0000-0001-5541-4794](https://orcid.org/0000-0001-5541-4794); Email: [pere.clapes@iqac.csic.es](mailto:pere.clapes@iqac.csic.es)

### Authors

Carlos J. Moreno – Dept. of Biological Chemistry, Institute for Advanced Chemistry of Catalonia, IQAC-CSIC, 08034 Barcelona, Spain  
 Karel Hernández – Dept. of Biological Chemistry, Institute for Advanced Chemistry of Catalonia, IQAC-CSIC, 08034 Barcelona, Spain  
 Samantha Gittings – Proxomix Ltd., Northumberland NE49 9HA, United Kingdom

Michael Bolte – Institut für Anorganische Chemie, J.-W.-Goethe-Universität, Frankfurt/Main, D-60438 Frankfurt/Main, Germany

Jesús Joglar – Dept. of Biological Chemistry, Institute for Advanced Chemistry of Catalonia, IQAC-CSIC, 08034 Barcelona, Spain

Jordi Bujons – Dept. of Biological Chemistry, Institute for Advanced Chemistry of Catalonia, IQAC-CSIC, 08034 Barcelona, Spain; [orcid.org/0000-0003-2944-2905](https://orcid.org/0000-0003-2944-2905)

Teodor Parella – Servei de Resonància Magnètica Nuclear, Universitat Autònoma de Barcelona, 08193 Bellaterra, Spain; [orcid.org/0000-0002-1914-2709](https://orcid.org/0000-0002-1914-2709)

Complete contact information is available at: <https://pubs.acs.org/10.1021/acscatal.3c00367>

### Author Contributions

The manuscript was written through contributions of all authors. All authors have given approval to the final version of the manuscript. C.J.M. and K.H. contributed equally.

### Funding

Grant PID2021-122166OB-I00 funded by MCIN/AEI/10.13039/501100011033 and “ERDF A way of making Europe”.

### Notes

The authors declare no competing financial interest.

## ■ ACKNOWLEDGMENTS

Grant PID2021-122166OB-I00 funded by MCIN/AEI/10.13039/501100011033 and “ERDF A way of making Europe”. C.J.M. acknowledges a PhD contract (i.e., Ayudas para Contratos Predoctorales para la Formación de Doctores) BES-2016-079447 funded by MCIN/AEI/10.13039/501100011033. The authors wish to thank Dr. Lothar Fink, from Frankfurt University, for the X-ray structure determination with Cu  $K\alpha$  radiation. The authors thankfully acknowledge the use of the computational resources of the Consorci de Serveis Universitaris de Catalunya (CSUC).

## REFERENCES

- (1) (a) Yin, Q.; Yin, L.; Wang, H.; Cheng, J. Synthesis and Biomedical Applications of Functional Poly( $\alpha$ -hydroxy acids) via Ring-Opening Polymerization of O-Carboxyanhydrides. *Acc. Chem. Res.* **2015**, *48*, 1777–1787. (b) Hu, Z.-Q.; Li, X.; Liu, L.-X.; Yu, C.-B.; Zhou, Y.-G. Ruthenium-Catalyzed Asymmetric Transfer Hydrogenation of  $\beta$ -Substituted  $\alpha$ -Oxobutyrolactones. *J. Org. Chem.* **2021**, *86*, 17453–17461. (c) Ley, S. V.; Sheppard, T. D.; Myers, R. M.; Chorghade, M. S. Chiral Glycolate Equivalents for the Asymmetric Synthesis of  $\alpha$ -Hydroxycarbonyl Compounds. *Bull. Chem. Soc. Jpn.* **2007**, *80*, 1451–1472. (d) Sewell, A. L.; Villa, M. V. J.; Matheson, M.; Whittingham, W. G.; Marquez, R. Fast and Flexible Synthesis of Pantothenic Acid and CJ-15,801. *Org. Lett.* **2011**, *13*, 800–803. (e) Sun, X.; Li, W.; Zhou, L.; Zhang, X. Matching and Mismatching Effects of Hybrid Chiral Biaxial Bisphosphine Ligands in Enantioselective Hydrogenation of Ketoesters. *Chem. – Eur. J.* **2009**, *15*, 7302–7305. (f) Lalot, J.; Stasik, I.; Demailly, G.; Beaupère, D. An improved synthesis of 5-thio-d-ribose from d-ribose-1,4-lactone. *Carbohydr. Res.* **2002**, *337*, 1411–1416. (g) Gröger, H. Enzymatic Routes to Enantiomerically Pure Aromatic  $\alpha$ -Hydroxy Carboxylic Acids: A Further Example for the Diversity of Biocatalysis. *Adv. Synth. Catal.* **2001**, *343*, 547–558. (h) Wilson, K. E.; Burk, R. M.; Biftu, T.; Ball, R. G.; Hoogsteen, K. Zaragozic acid A, a potent inhibitor of squalene synthase: initial chemistry and absolute stereochemistry. *J. Org. Chem.* **1992**, *57*, 7151–7158. (i) Puthuraya, K. P.; Oomura, Y.; Shimizu, N. Effects of endogenous sugar acids on the ventromedial hypothalamic nucleus of the rat. *Brain Res.* **1985**, *332*, 165–168. (j) Heidlindemann, M.; Hammel, M.; Scheffler, U.; Mahrwald, R.; Hummel, W.; Berkessel, A.; Gröger, H. Chemoenzymatic Synthesis of Vitamin B5-Intermediate (R)-Pantolactone via Combined Asymmetric Organ- and Biocatalysis. *J. Org. Chem.* **2015**, *80*, 3387–3396. (k) Kagayama, T.; Sakaguchi, S.; Ishii, Y. Synthesis of  $\alpha$ -hydroxy- $\gamma$ -butyrolactones from acrylates and 1,3-dioxolanes using N-hydroxyphthalimide (NHPI) as a key catalyst. *Tetrahedron Lett.* **2005**, *46*, 3687–3689. (l) Ikemoto, T.; Sakashita, K.; Kageyama, Y.; Onuma, F.; Shibuya, Y.; Ichimura, K.; Mori, K. Relationship between Molecular Structure and Induced Spontaneous Polarization for Chiral Dopants Containing an Optically Active Lactone. *Mol. Cryst. Liq. Cryst.* **1994**, *250*, 247–256.
- (2) (a) Camps, P.; Munoz-Torrero, D. Synthesis and Applications of (R)- and (S)-Pantolactone as Chiral Auxiliaries. *Curr. Org. Chem.* **2004**, *8*, 1339–1380. (b) Bourgeois, F.; Medlock, J. A.; Bonrath, W.; Sparr, C. Catalyst Repurposing Sequential Catalysis by Harnessing Regenerated Prolineamide Organocatalysts as Transfer Hydrogenation Ligands. *Org. Lett.* **2020**, *22*, 110–115. (c) Coppola, G. M.; Schuster, H. F.,  *$\alpha$ -Hydroxy acids in enantioselective syntheses*; Wiley-VCH: Weinheim, 1997. (d) Hanessian, S., *Total synthesis of natural products, the "Chiron" approach*; Pergamon Press: Oxford, 1983. (e) Yamaguchi, S.; Matsuo, T.; Motokura, K.; Miyaji, A.; Baba, T. Cascade Synthesis of Five-Membered Lactones using Biomass-Derived Sugars as Carbon Nucleophiles. *Chem. – Asian J.* **2016**, *11*, 1731–1737. (f) Phukan, P.; Sasmal, S.; Maier, Martin E. Flexible Routes to the 5-Hydroxy Acid Fragment of the Cryptophycins. *Eur. J. Org. Chem.* **2003**, *2003*, 1733–1740. DOI: 10.1002/ejoc.200210695; (g) White, J. D.; Hrcnciar, P. Synthesis of Polyhydroxylated Pyrrolizidine Alkaloids of the Alexine Family by Tandem Ring-Closing Metathesis–Transannular Cyclization. (+)-Australine. *J. Org. Chem.* **2000**, *65*, 9129–9142. (h) Mulzer, J.; Mantoulidis, A.; Ohler, E. Total Syntheses of Epithilones B and D. *J. Org. Chem.* **2000**, *65*, 7456–7467. (i) Eggersdorfer, M.; Laudert, D.; Létinois, U.; McClymont, T.; Medlock, J.; Netscher, T.; Bonrath, W. One Hundred years of vitamins—A success story of the natural sciences. *Angew. Chem., Int. Ed.* **2012**, *51*, 12960–12990. (j) Evans, D. A.; Wu, J.; Masse, C. E.; MacMillan, D. W. C. A General Method for the Enantioselective Synthesis of Pantolactone Derivatives. *Org. Lett.* **2002**, *4*, 3379–3382.
- (3) (a) Burgener, S.; Cortina, N. S.; Erb, T. J. Oxalyl-CoA Decarboxylase Enables Nucleophilic One-Carbon Extension of Aldehydes to Chiral  $\alpha$ -Hydroxy Acids. *Angew. Chem., Int. Ed.* **2020**, *59*, 5526–5530. (b) Wang, P.; Tao, W.-J.; Sun, X.-L.; Liao, S.; Tang, Y. A Highly Efficient and Enantioselective Intramolecular Cannizzaro Reaction under TOX/Cu(II) Catalysis. *J. Am. Chem. Soc.* **2013**, *135*, 16849–16852. (c) Ganta, A.; Shamshina, J. L.; Cafiero, L. R.; Snowden, T. S. Stereoselective synthesis of cis- or trans-2,4-disubstituted butyrolactones from Wynberg lactone. *Tetrahedron* **2012**, *68*, 5396–5405. (d) Jung, J. E.; Ho, H.; Kim, H.-D. Bidentate chelation-controlled asymmetric synthesis of  $\alpha$ -hydroxy esters based on the glycolate enolate alkylation. *Tetrahedron Lett.* **2000**, *41*, 1793–1796. (e) Pansare, S. V.; Bhattacharyya, A. Enantioselective synthesis of  $\beta,\beta$ -dialkyl  $\alpha$ -hydroxy  $\gamma$ -butyrolactones. *Tetrahedron Lett.* **2001**, *42*, 9265–9267. (f) Pansare, S. V.; Bhattacharyya, A. Enantioselective synthesis of pantolactone analogues from an ephedrine-derived morpholine-dione. *Tetrahedron* **2003**, *59*, 3275–3282. (g) Yamaguchi, S.; Motokura, K.; Sakamoto, Y.; Miyaji, A.; Baba, T. Tin-catalyzed conversion of biomass-derived triose sugar and formaldehyde to  $\alpha$ -hydroxy- $\gamma$ -butyrolactone. *Chem. Commun.* **2014**, *50*, 4600–4602.
- (4) (a) Blandin, V.; Carpentier, J.-F.; Mortreux, A. Asymmetric Hydrogenation of 2,4-Dioxo Esters: Selective Synthesis of 2-Hydroxy-4-oxo Esters and Direct Access to Chiral 2-Hydroxy-4-butylolactones. *Eur. J. Org. Chem.* **1999**, 1787–1793. (b) Shimizu, S.; Yamada, H.; Hata, H.; Morishita, T.; Akutsu, S.; Kawamura, M. Novel Chemoenzymatic Synthesis of d(–)-Pantoyl Lactone. *Agric. Biol. Chem.* **1987**, *51*, 289–290. (c) Pansare, S. V.; Ravi, R. G. Asymmetric reactions of  $\alpha$ -ketoacid-derived hemiacetals: Stereoselective synthesis of  $\alpha$ -hydroxy acids. *Tetrahedron* **1998**, *54*, 14549–14564.
- (5) Chen, B.; Yin, H.-F.; Wang, Z.-S.; Xu, J.-H.; Fan, L.-Q.; Zhao, J. Facile Synthesis of Enantiopure 4-Substituted 2-Hydroxy-4-butylolactones using a Robust Fusarium Lactonase. *Adv. Synth. Catal.* **2009**, *351*, 2959–2966.
- (6) (a) Shen, L.; Chen, Z.-N.; Zheng, Q.; Wu, J.; Xu, X.; Tu, T. Selective Formation of Vicinal Glycols to  $\alpha$ -Hydroxy Acetates in Water via a Dehydrogenation and Oxidation Relay Process by a Self-Supported Single-Site Iridium Catalyst. *ACS Catal.* **2021**, *11*, 12833–12839. (b) Furukawa, K.; Shibuya, M.; Yamamoto, Y. Chemoselective Catalytic Oxidation of 1,2-Diols to  $\alpha$ -Hydroxy Acids Controlled by TEMPO–ClO<sub>2</sub> Charge-Transfer Complex. *Org. Lett.* **2015**, *17*, 2282–2285.
- (7) (a) Van de Vyver, S.; Odermatt, C.; Romero, K.; Prasomsri, T.; Román-Leshkov, Y. Solid Lewis Acids Catalyze the Carbon–Carbon Coupling between Carbohydrates and Formaldehyde. *ACS Catal.* **2015**, *5*, 972–977. (b) Bielitz, M.; Pietruszka, J. An Enantioselective Mukaiyama Aldol Reaction as the Key Step towards the Tetrahydropyran Core of Psymberin via a  $\gamma$ -Butyrolactone Intermediate. *Synlett* **2012**, *23*, 1625–1628. (c) Smirnov, M. V.; Kucherenko, A. S.; Gridnev, I. D.; Korlyukov, A. A.; Zlotin, S. G.  $\gamma$ -Pyronecarbaldehyde-Based Practical Asymmetric Catalytic Synthesis of Chiral 2,4-Dihydroxycarboxylic Acids and  $\alpha$ -Hydroxy- $\gamma$ -lactones. *Adv. Synth. Catal.* **2022**, *364*, 3245–3262.
- (8) (a) de Wildeman, S.; Sereinig, N., *Enzymatic reduction of carbonyl groups. In Science of Synthesis, Stereoselective Synthesis 2. Stereoselective Reactions of Carbonyl and Imino Groups*; Molander, G. A., Ed.; Georg Thieme Verlag: Stuttgart, 2011; Vol. 2, pp 133–208. (b) Kim, M. J.; Whitesides, G. M. L-Lactate dehydrogenase: substrate specificity and use as a catalyst in the synthesis of homochiral 2-hydroxy acids. *J. Am. Chem. Soc.* **1988**, *110*, 2959–2964. (c) Simon, E. S.; Plante, R.; Whitesides, G. M. D-lactate dehydrogenase. *Appl. Biochem. Biotechnol.* **1989**, *22*, 169–179. (d) Yamazaki, Y.; Maeda, H. Enzymatic Synthesis of Optically Pure (R)-(-)-Mandelic Acid and Other 2-Hydroxycarboxylic Acids: Screening for the Enzyme, and Its Purification, Characterization and Use. *Agric. Biol. Chem.* **1986**, *50*, 2621–2631. (e) Bur, D.; Luyten, M. A.; Wynn, H.; Provencher, L. R.; Jones, J. B.; Gold, M.; Friesen, J. D.; Clarke, A. R.; Holbrook, J. J. Enzymes in organic synthesis. 45. An evaluation of the substrate specificity and asymmetric synthesis potential of the cloned L-lactate dehydrogenase from *Bacillus stearothermophilus*. *Can. J. Chem.* **1989**, *67*, 1065–1070. (f) Wu, C.-Y.; Chen, S.-T.; Chiou, S.-H.; Wang, K.-T. Facile synthesis of chiral 2-hydroxy acids catalyzed by a stable duck  $\epsilon$ -crystallin with endogenous l-lactate dehydrogenase activity. *FEBS Lett.* **1992**, *301*, 219–222.

(9) (a) Marín-Valls, R.; Hernández, K.; Bolte, M.; Parella, T.; Joglar, J.; Bujons, J.; Clapés, P. Biocatalytic Construction of Quaternary Centers by Aldol Addition of 3,3-Disubstituted 2-Oxoacid Derivatives to Aldehydes. *J. Am. Chem. Soc.* **2020**, *142*, 19754–19762. (b) Marín-Valls, R.; Hernández, K.; Bolte, M.; Joglar, J.; Bujons, J.; Clapés, P. Chemoenzymatic Hydroxymethylation of Carboxylic Acids by Tandem Stereodivergent Biocatalytic Aldol Reaction and Chemical Decarboxylation. *ACS Catal.* **2019**, *9*, 7568–7577.

(10) Moreno, C. J.; Hernández, K.; Charnok, S. J.; Gittings, S.; Bolte, M.; Joglar, J.; Bujons, J.; Parella, T.; Clapés, P. Synthesis of  $\gamma$ -Hydroxy- $\alpha$ -amino Acid Derivatives by Enzymatic Tandem Aldol Addition–Transamination Reactions. *ACS Catal.* **2021**, *11*, 4660–4669.

(11) (a) Sanchez, J. E.; Gross, P. G.; Goetze, R. W.; Walsh, R. M.; Peebles, W. B.; Wood, Z. A. Evidence of Kinetic Cooperativity in Dimeric Ketopantoate Reductase from *Staphylococcus aureus*. *Biochemistry* **2015**, *54*, 3360–3369. (b) von Delft, F.; Inoue, T.; Saldanha, S. A.; Ottenhof, H. H.; Schmitzberger, F.; Birch, L. M.; Dhanaraj, V.; Witty, M.; Smith, A. G.; Blundell, T. L.; Abell, C. Structure of *E. coli* Ketopantoate Hydroxymethyl Transferase Complexed with Ketopantoate and Mg<sup>2+</sup>, Solved by Locating 160 Selenomethionine Sites. *Structure* **2003**, *11*, 985–996. (c) Matak-Vinković, D.; Vinković, M.; Saldanha, S. A.; Ashurst, J. L.; von Delft, F.; Inoue, T.; Miguel, R. N.; Smith, A. G.; Blundell, T. L.; Abell, C. Crystal Structure of *Escherichia coli* Ketopantoate Reductase at 1.7 Å Resolution and Insight into the Enzyme Mechanism†. *Biochemistry* **2001**, *40*, 14493–14500. (d) Zheng, R.; Blanchard, J. S. Kinetic and Mechanistic Analysis of the *E. coli* panE-Encoded Ketopantoate Reductase. *Biochemistry* **2000**, *39*, 3708–3717. (e) Zheng, R.; Blanchard, J. S. Identification of Active Site Residues in *E. coli* Ketopantoate Reductase by Mutagenesis and Chemical Rescue. *Biochemistry* **2000**, *39*, 16244–16251. (f) Aberhart, D. J.; Russell, D. J. Steric course of ketopantoate hydroxymethyltransferase in *E. coli*. *J. Am. Chem. Soc.* **1984**, *106*, 4902–4906.

(12) Goto, M.; Muramatsu, H.; Mihara, H.; Kurihara, T.; Esaki, N.; Omi, R.; Miyahara, I.; Hirotsu, K. Crystal Structures of  $\Delta$ 1-Piperidine-2-carboxylate/ $\Delta$ 1-Pyrroline-2-carboxylate Reductase Belonging to a New Family of NAD(P)H-dependent Oxidoreductases: Conformational Change, Substrate Recognition, and Stereochemistry of the Reaction. *J. Biol. Chem.* **2005**, *280*, 40875–40884.

(13) (a) Nakata, K.; Gotoh, K.; Ono, K.; Futami, K.; Shiina, I. Kinetic Resolution of Racemic 2-Hydroxy- $\gamma$ -butyrolactones by Asymmetric Esterification Using Diphenylacetic Acid with Pivalic Anhydride and a Chiral Acyl-Transfer Catalyst. *Org. Lett.* **2013**, *15*, 1170–1173. (b) Zhang, Z.; Collum, D. B. Wittig Rearrangements of Boron-Based Oxazolidinone Enolates. *J. Org. Chem.* **2019**, *84*, 10892–10900. (c) Denmark, S. E.; Yang, S.-M. Total Synthesis of (+)-Brasilenyne. Application of an Intramolecular Silicon-Assisted Cross-Coupling Reaction. *J. Am. Chem. Soc.* **2004**, *126*, 12432–12440. (d) Abraham, C. J.; Paull, D. H.; Bekele, T.; Scerba, M. T.; Dudding, T.; Lectka, T. A Surprising Mechanistic “Switch” in Lewis Acid Activation: A Bifunctional, Asymmetric Approach to  $\alpha$ -Hydroxy Acid Derivatives. *J. Am. Chem. Soc.* **2008**, *130*, 17085–17094. (e) Shuey, S. J.; Partridge, J. J.; Uskokovic, M. R. Triply convergent synthesis of 1.alpha.,25-dihydroxy-24(R)-fluorocholecalciferol. *J. Org. Chem.* **1988**, *53*, 1040–1046.

(14) Ciulli, A.; Chirgadzé, D. Y.; Smith, A. G.; Blundell, T. L.; Abell, C. Crystal Structure of *Escherichia coli* Ketopantoate Reductase in a Ternary Complex with NADP<sup>+</sup> and Pantoate Bound: substrate recognition, conformational change, and cooperativity. *J. Biol. Chem.* **2007**, *282*, 8487–8497.

(15) Zhu, L.; Xu, X.; Wang, L.; Dong, H.; Yu, B. The D-Lactate Dehydrogenase from *Sporolactobacillus inulinus* Also Possessing Reversible Deamination Activity. *PLoS One* **2015**, *10*, No. e0139066.

(16) Kokkonen, P.; Beier, A.; Mazurenko, S.; Damborsky, J.; Bednar, D.; Prokop, Z. Substrate inhibition by the blockage of product release and its control by tunnel engineering. *RSC Chem. Biol.* **2021**, *2*, 645–655.

## Recommended by ACS

### Synthesis of Novel 1,4-Diketone Derivatives and Their Further Cyclization

Hacer Can Üsküp, Belma Hasdemir, *et al.*

APRIL 07, 2023  
ACS OMEGA

READ 

### Light-Driven Reduction of CO<sub>2</sub> to CO in Water with a Cobalt Molecular Catalyst and an Organic Sensitizer

Pui-Yu Ho, Marc Robert, *et al.*

APRIL 18, 2023  
ACS CATALYSIS

READ 

### Structural Understanding of Fungal Terpene Synthases for the Formation of Linear or Cyclic Terpene Products

Rehka T, Congqiang Zhang, *et al.*

MARCH 27, 2023  
ACS CATALYSIS

READ 

### Flipping the Substrate Creates a Highly Selective Halohydrin Dehalogenase for the Synthesis of Chiral 4-Aryl-2-oxazolidinones from Readily Available Epoxides

Chuanhua Zhou, Dunming Zhu, *et al.*

MARCH 24, 2023  
ACS CATALYSIS

READ 

Get More Suggestions >

## Capítulo 3.3

Expanding synthetic applications of  $\Delta^1$ -Piperidine-2-carboxylate/ $\Delta^1$ -pyrroline-2-carboxylate reductase from *Pseudomonas syringae* (DpkA<sub>*Psyrin*</sub>). Biocatalytic asymmetric synthesis of (*S,E*)-2-hydroxy-4-arylbut-3-enoic acid derivatives.



Expanding synthetic applications of  $\Delta^1$ -Piperidine-2-carboxylate/ $\Delta^1$ -pyrroline-2-carboxylate reductase from *Pseudomonas syringae* (DpkA<sub>P<sub>syrin</sub></sub>). Biocatalytic asymmetric synthesis of (*S,E*)-2-hydroxy-4-arylbut-3-enoic acid derivatives.

**Resumen.**

Los derivados del ácido 2-hidroxi-4-arylbut-3-enoico son precursores clave para la síntesis de inhibidores de la enzima convertidora de angiotensina, estos inhibidores reducen la presión arterial al impedir que el cuerpo produzca la hormona angiotensina. Entre este tipo de fármacos se encuentran: el Enalapril, Lisinopril, Cilapril y Benazepril. En las últimas décadas se han dedicado muchos esfuerzos en desarrollar estrategias para la síntesis asimétrica de este tipo de moléculas, entre ellas destacan la deracemización del ácido ( $\pm$ )-2-hidroxi-4-fenilbut-3-enoico<sup>1</sup>, y la hidrogenación asimétrica de derivados del ácido 2-oxo-4-arylbut-3-enoico. En este trabajo, se presenta una alternativa sintética basada en la actividad promiscua de la  $\Delta^1$ -piperidina-2-carboxilato/ $\Delta^1$ -pirrolina-2-carboxilato reductasa de *Pseudomonas syringae* pv. tomato DSM 50315 (DpkA) que se muestra como una herramienta útil para la síntesis estereoselectiva de ácidos 2-hidroxi-4-arylbut-3-enoicos. En este capítulo, se describe la síntesis de estos ácidos utilizando una cascada enzimática concurrente, formada por la *trans*-*O*-hidroxibenziliden piruvato hidratasa-aldolasa (HBPA) que permitió la construcción de los esqueletos carbonados de los productos finales a partir de precursores sencillos (piruvato y aldehídos aromáticos) seguido de la reducción estereoselectiva catalizado por la DpkA.

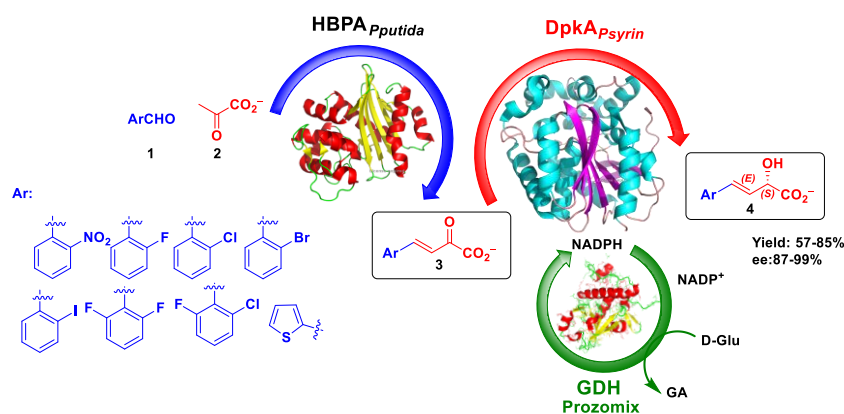
**Expanding synthetic applications of  $\Delta^1$ -Piperidine-2-carboxylate/ $\Delta^1$ -pyrroline-2-carboxylate reductase from *Pseudomonas syringae* (DpkA<sub>Psyrin</sub>). Biocatalytic asymmetric synthesis of (*S,E*)-2-hydroxy-4-arylbut-3-enoic acid derivatives.**

Carlos J. Moreno,<sup>a,‡</sup> Samantha Gittings,<sup>b</sup> Dieter Schollmeyer,<sup>c</sup> Jesús Joglar,<sup>a</sup> Jordi Bujons,<sup>a</sup> Karel Hernández,<sup>a\*</sup> Pere Clapés<sup>a\*</sup>

<sup>a</sup>Institute for Advanced Chemistry of Catalonia, Dept. of Biological Chemistry, IQAC-CSIC, Jordi Girona 18-26, 08034 Barcelona, Spain.

<sup>b</sup>Prozomix Ltd. West End Industrial Estate, Haltwhistle, Northumberland, NE49 9HA, United Kingdom. <sup>c</sup>Johannes Gutenberg-Universitaet Mainz, Department Chemie, Zentrale Analytik, Duesbergweg 10-14, 55099 Mainz.

Graphical abstract



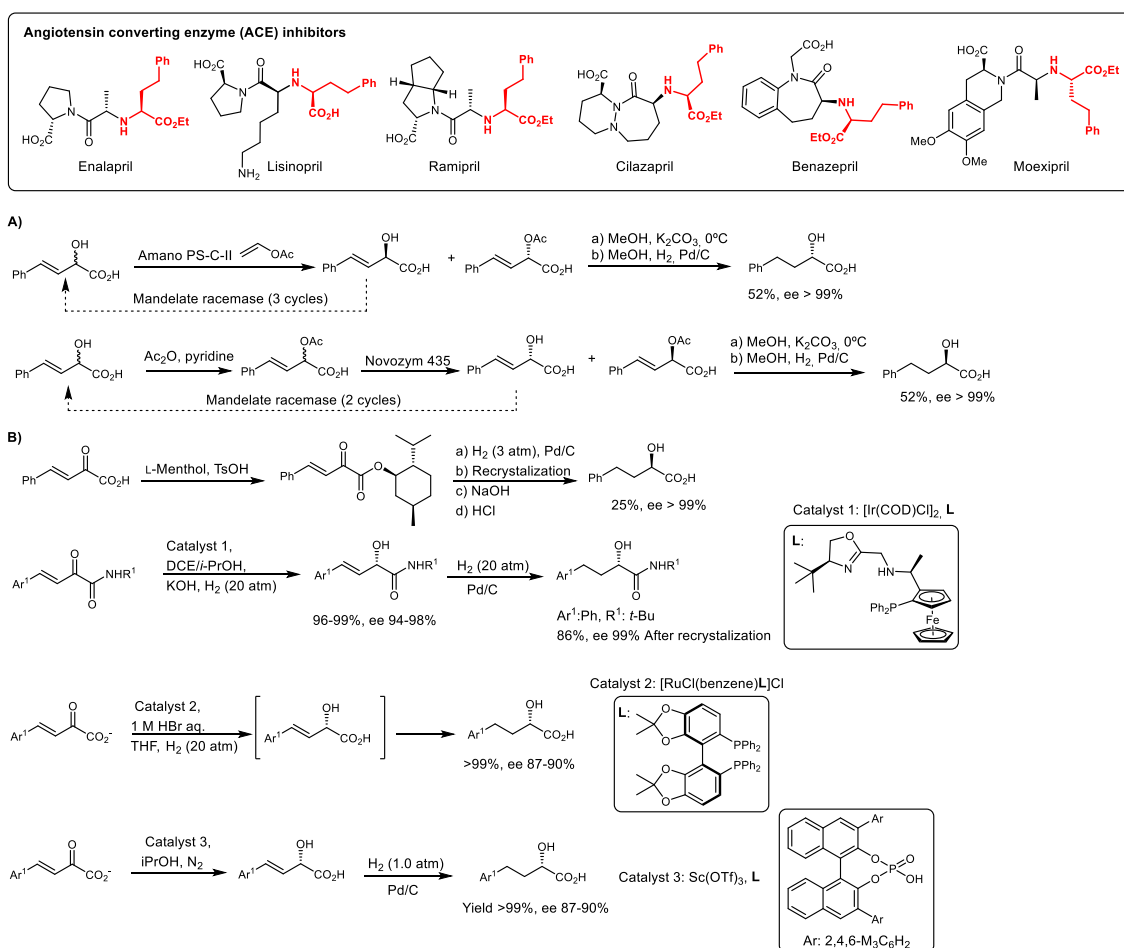
**KEYWORDS.** Biocatalysis, Aldol condensation, Ketoreductases, 2-hydroxy-4-arylbut-3-enoic acid.

**ABSTRACT**

Chiral 2-hydroxy-4-arylbut-3-enoic acid derivatives are important precursors for the synthesis of angiotensin converting enzyme (ACE) inhibitors such as enalapril, lisinopril, cilapril or benazepril. Here we take advantage of the unexplored promiscuous ketoreductase activity of  $\Delta^1$ -piperidine-2-carboxylate/ $\Delta^1$ -pyrroline-2-carboxylate reductase from *Pseudomonas syringae* pv. tomato DSM 50315 (DpkA<sub>Psyrin</sub>) for the synthesis of 2-hydroxy-4-arylbut-3-enoic acids. The strategy was designed as a cascade enzymatic process comprising aldol addition, for the construction of carbon scaffold catalyzed by the *trans*-o-hydroxybenzylidene pyruvate hydratase-aldolase from *Pseudomonas putida* (HBPA<sub>Pputida</sub>), and subsequent symmetric reduction of the carbonyl group catalyzed by DpkA<sub>Psyrin</sub>. A total of 9 structurally diverse 2-hydroxy-4-arylbut-3-enoic acids were prepared with (*S,E*) configuration in 87-99% ee. Quantitative conversions were achieved for this cascade process, with global isolated yields between 57-85%. A total of nine structurally diverse 2-hydroxy-4-arylbut-3-enoic acids were prepared with (*S,E*) configuration in 87-99% ee.

## INTRODUCTION

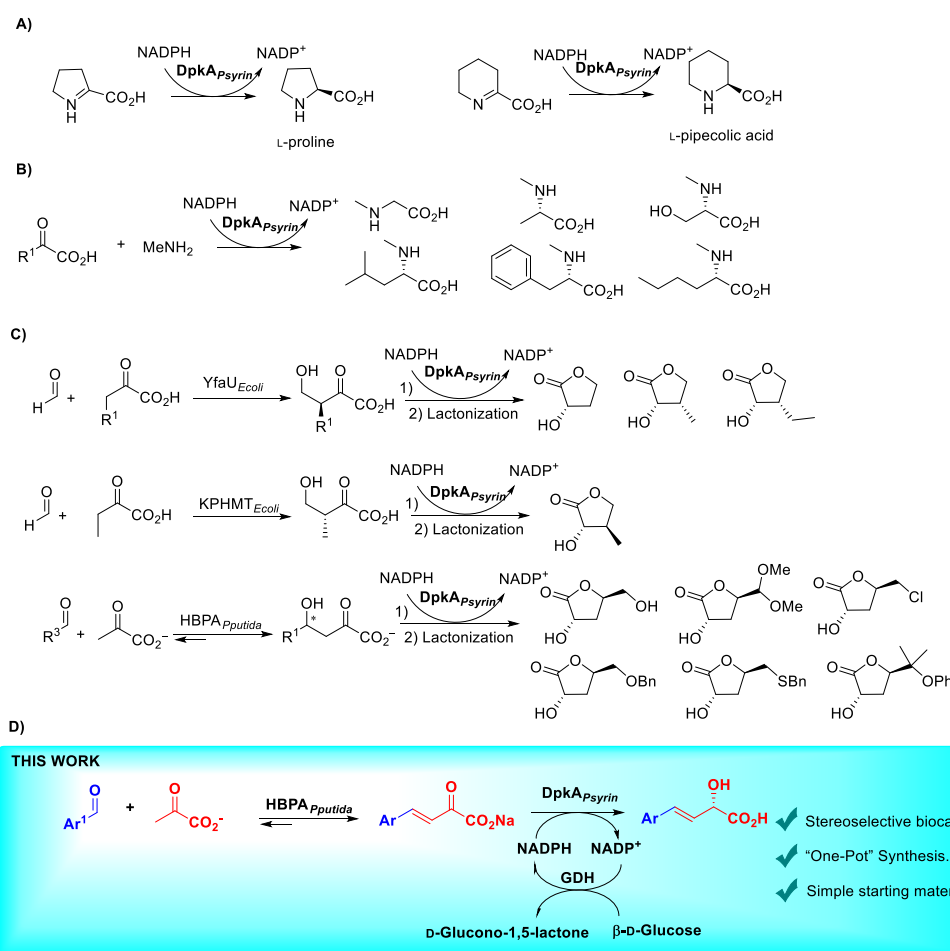
Chiral 2-hydroxy-4-arylbut-3-enoic acid derivatives are important precursors for the preparation of relevant biologically active compounds such as angiotensin converting enzyme (ACE) inhibitors (e.g. enalapril, lisinopril, cilapril or benazepril).<sup>1-4</sup> Many efforts have been devoted to develop strategies for the asymmetric synthesis of these type of molecules (Scheme 1).<sup>1-4</sup>



**Scheme 1.** Asymmetric synthetic methodologies for the preparation of 2-hydroxy-4-arylbutanoic acid using 2-hydroxy-4-arylbut-3-enoic acid derivatives as intermediates. **A)** Deracemization of (±)-2-hydroxy-4-phenylbut-3-enoic acid<sup>1</sup> and **B)** asymmetric hydrogenation of 2-oxo-4-arylbut-3-enoic acid derivatives.<sup>2-4</sup>

Asymmetric reduction on esters of 2-oxo-4-arylbut-3-enoic acids have a significant role in the synthesis of 2-hydroxy-4-arylbutyrates, however, hydrolysis and recrystallization of the corresponding acids is necessary for improving the enantiomeric purity of the product.<sup>3, 5</sup> Therefore, it is desirable to develop an efficient and asymmetric method for the reduction of 2-oxo-4-arylbut-3-enoic acids<sup>3</sup> and then hydrogenation of the double bond by conventional methods. In this line of thinking, we focus our attention on the

enzyme  $\Delta^1$ -piperidine-2-carboxylate/ $\Delta^1$ -pyrroline-2-carboxylate reductase from *Pseudomonas syringae* pv. tomato DSM 50315 (DpkA<sub>Psyrin</sub>, EC 1.5.1.21), described as an imino reductase<sup>6-13</sup> (Scheme 2 A and B). In previous work, we observed that DpkA<sub>Psyrin</sub> also exhibited promiscuous ketoreductase activity (Scheme 2C).<sup>14</sup> Thus, we envision a straightforward enzymatic cascade process for the asymmetric synthesis of 2-hydroxy-4-arylbut-3-enoic acid derivatives consisting of an aldol condensation reaction catalyzed by *trans*-o-hydroxybenzylidene pyruvate hydratase-aldolase from *Pseudomonas putida* (HBPA<sub>Pputida</sub>, EC 4.1.2.45)<sup>15</sup> and an ensuing asymmetric reduction of the carbonyl group catalyzed by DpkA<sub>Psyrin</sub>. (Scheme 2D). Cascade strategies are advantageous to improve the overall synthetic efficiency and avoid intermediate purification steps, with the consequent reduction of waste generation. Further benefits include reducing the need to handle unstable intermediaries and shifting unfavorable reaction equilibrium toward products.<sup>16-17</sup>



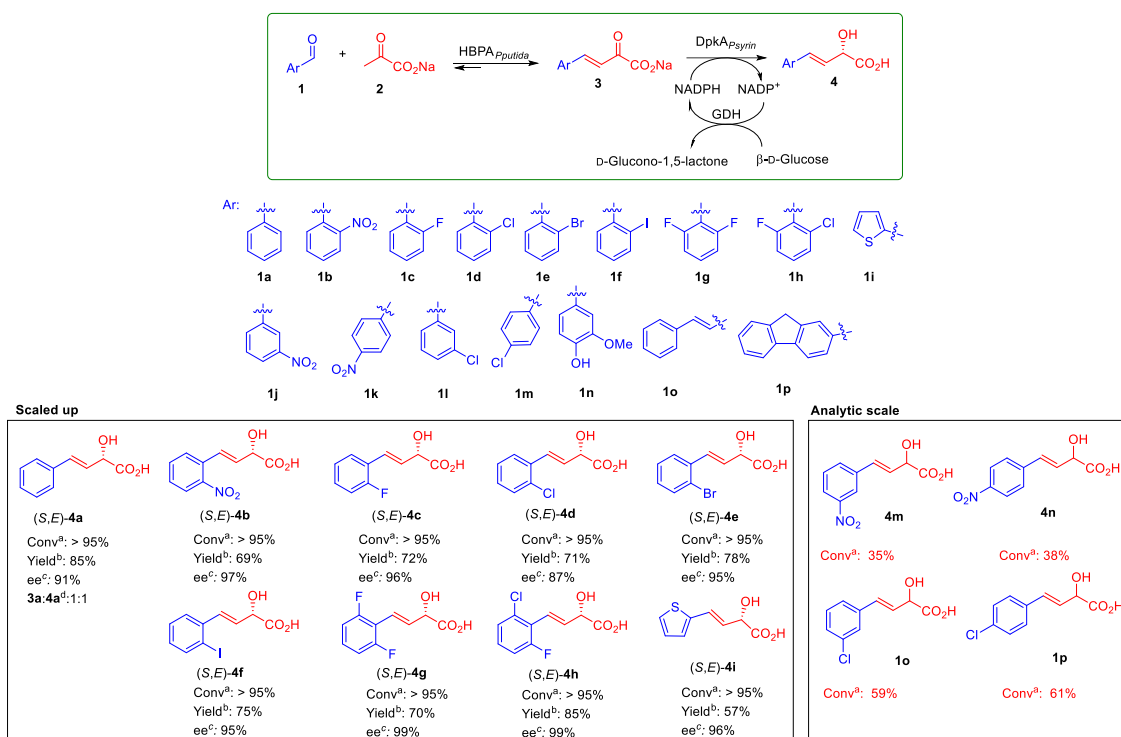
**Scheme 2.** Reaction catalyzed by DpkA<sub>Psyrin</sub>. **A)** natural imine reductase activity.<sup>6-7, 9, 11</sup> **B)** synthesis of *N*-methyl-*L*-amino acids from methylamine and various 2-oxo acids.<sup>8, 10, 12-13</sup> **C)** ketoreductase activity describe in our group.<sup>14</sup> **D)** this work: enzymatic cascade process in the asymmetric synthesis of (*S,E*)-2-hydroxy-4-arylbut-3-enoic acid derivatives by a cascade of aldol

condensation catalyzed by HBPA<sub>Pputida</sub> and asymmetric biocatalytic reduction of the carbonyl group catalyzed by DpkA<sub>Psyrin</sub>.

## RESULTS AND DISCUSSION

We previously report that DpkA<sub>Psyrin</sub> is able to reduce carbonyl group in different 2-oxoacid.<sup>14</sup> Thus, as a continuation of our synthetic study we select conformationally constrained compounds as substrates such as arylbut-3-enoic acids, **3a-p** (Scheme 3), for the ketoreductase. The asymmetric biocatalytic reduction of (*E*)-2-oxo-4-phenylbut-3-enoic acid (**3a**) (see SI, page S12) proceeded in quantitative yields (conv > 95%) after 24 h of reaction with 85 % of isolated yield of *S*-**4a** and 91% ee. However, in the enzymatic cascade process we obtained a mixture of **3a** and *S*-**4a** (**3a**:*S*-**4a**, 1:1 determined by <sup>1</sup>H NMR, see SI, page S11) after purification (Scheme 3). Pyruvate is a substrate of DpkA<sub>Psyrin</sub> (estimated kinetic parameters for pyruvate reduction  $K_m^{app} = 101$  mM and  $k_{cat}^{app} = 0.4$  min<sup>-1</sup>,  $1 \leq [\text{pyruvate}] \leq 60$  mM, see Figure S10) and competes with the reduction of **3a**. Moreover, the reversibility of the aldol condensation reaction can also affect the final yield of *S*-**4a**. Thus, the successful cascade process depends on both the favorable aldol condensation reaction equilibrium and the relative reduction rates of **2** and **3**.

Gratifyingly, the cascade reactions with substrates **1b-i** rendered quantitative formation of the reduced product (*S*-**4b-i**), with complete consumption of the starting material (**1**) and the intermediate precursors (**3b-i**) (Scheme 3 scale up panel). Conversion was incomplete or even sluggish with aryl groups with *meta* and *para* substituents (e.g., **3j-m**) (Scheme 3 analytical scale). On the other hand, DpkA<sub>Psyrin</sub> was inactive toward aryl groups with both *ortho* and *para* substituents (e.g., **3n**), 2-oxo-dienoic acids (e.g., **3o**) and fused aromatic rings (e.g., **3p**), probably due to the steric limitations imposed by the active site cavity. After two purification steps: basic/acidic aqueous–organic solvent extraction and a reverse phase chromatography (Isolera Biotage<sup>®</sup> System, see SI, page S6), **4b-i** were obtained as carboxylic acids with isolated yields between 57-85% (Scheme 3).



**Scheme 3.** Enzymatic cascade process for the synthesis of (*S,E*)-2-hydroxy-4-arylbut-3-enoic acid *S-4* by means of a cascade process of aldol condensation and reduction reactions catalyzed by HBPA<sub>Pputida</sub> and DpkA<sub>Psyrin</sub> respectively. GDH, Glucose dehydrogenase was provided by Prozomix Ltd (PRO-GDH(001)).

<sup>a</sup>Conversion of reduction reaction. No starting materials or aldol condensation products were detected by HPLC. <sup>b</sup>Isolated yields. <sup>c</sup>Enantiomeric excess of the reduction determined by HPLC on chiral stationary phases. <sup>d</sup>In the enzymatic cascade process, a mixture of **3a** and **4a** was obtained after purification. The **3a**:**S-4a** ratio was determined by <sup>1</sup>H NMR (see Figure S23).

Enantiomeric ratios of 2-hydroxy-4-arylbut-3-enoic acid (*S-4*) were determined by HPLC on a chiral stationary phase. The corresponding authentic racemic samples were prepared by Luche reduction<sup>18-20</sup> from  $\alpha,\beta$ -unsaturated ketones (**3a-i**) produced by HBPA<sub>Pputida</sub> catalysis (see SI page S10, compound *rac-4b*). Excellent levels of enantioselectivity were achieved for *S-4b,c,e-i* (95–99% ee), and good for *S-4d* (87% ee). Consistent with our previous study<sup>14</sup> single-crystal X-ray diffraction of *S-4c-e* indicated that DpkA<sub>Psyrin</sub> renders 2-hydroxyacids having an *S* configuration as the major stereoisomer (Figure 1). Therefore, an *S* configuration may be assumed for the major enantiomers of *S-4b, f-i* (Scheme 3).

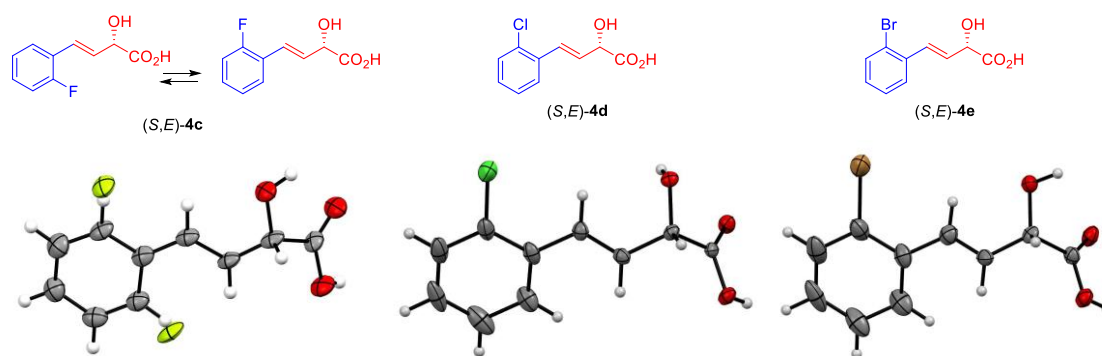


**Figure 1.** X-ray structures of (*E,S*)-**4c**, (*E,S*)-**4d**, and (*E,S*)-**4e** as ORTEP-type plots displaying one molecule with 50% probability ellipsoids. In compound (*S,E*)-**4c** it was observed that the position of the F-atom was disordered (ring-flipping). The data can be obtained free of charge from The Cambridge Crystallographic Data Centre via [www.ccdc.cam.ac.uk/data\\_request/cif](http://www.ccdc.cam.ac.uk/data_request/cif).

## CONCLUSIONS

In summary, we expanded the synthetic application of DpkA<sub>Psyrin</sub> through its promiscuous ketoreductase activity for the asymmetric reduction of 2-oxo-4-arylbut-3-enoic acid derivatives. The cascade enzymatic system using HBPA<sub>Pputida</sub> as catalyst for the construction of carbon scaffold and DpkA<sub>Psyrin</sub> for carbonyl reduction providing homochiral (*S,E*)-2-hydroxy-4-arylbut-3-enoic acid derivatives with diverse aromatic moieties from achiral starting material. Nine products were obtained in isolated yields from 57% to 85% and ee from 87 to 99%. DpkA<sub>Psyrin</sub> gave quantitative conversions after 24 h of incubation tolerating substrates with substitutions at *ortho* positions of the aromatic ring. Incomplete conversions were observed with aryl groups bearing substituents in with *meta* and *para* substituents, whereas it was completely inactive towards substrates bearing aryl groups with both *ortho* and *para* substituents, 2-oxo-dienoic acids and fused aromatic rings.

## References.

1. Larissegger-Schnell, B.; Kroutil, W.; Faber, K., Chemo-Enzymatic Synthesis of (R)- and (S)-2-Hydroxy-4-phenylbutanoic Acid via Enantio-Complementary Deracemization of (±)-2-Hydroxy-4-phenyl-3-butenic Acid Using a Racemase-Lipase Two-Enzyme System. *Synlett* **2005**, *2005* (12), 1936-1938.
2. Yanagisawa, H.; Ishihara, S.; Ando, A.; Kanazaki, T.; Miyamoto, S.; Koike, H.; Iijima, Y.; Oizumi, K.; Matsushita, Y.; Hata, T., Angiotensin-converting enzyme inhibitors. perhydro-1, 4-thiazepin-5-one derivatives. *Journal of medicinal chemistry* **1987**, *30* (11), 1984-1991.
3. Zhu, L.; Meng, Q.; Fan, W.; Xie, X.; Zhang, Z., Direct asymmetric hydrogenation of 2-oxo-4-arylbut-3-enoic acids. *The Journal of Organic Chemistry* **2010**, *75* (17), 6027-6030.
4. Wang, S.; Yu, Y.; Wen, J.; Zhang, X., Iridium/f-Amphox-catalyzed asymmetric hydrogenation of styrylglyoxylamides. *Synlett* **2018**, *29* (16), 2203-2207.
5. Meng, Q.; Zhu, L.; Zhang, Z., Highly Enantioselective Sequential Hydrogenation of Ethyl 2-Oxo-4-arylbut-3-enoate to Ethyl 2-Hydroxy-4-arylbutyrate. *J. Org. Chem.* **2008**, *73* (18), 7209-7212.
6. Xu, Y.; Zhou, D.; Luo, R.; Yang, X.; Wang, B.; Xiong, X.; Shen, W.; Wang, D.; Wang, Q., Metabolic engineering of *Escherichia coli* for polyamides monomer  $\delta$ -valerolactam production from feedstock lysine. *Applied Microbiology and Biotechnology* **2020**, *104*, 9965-9977.
7. Muramatsu, H.; Mihara, H.; Kakutani, R.; Yasuda, M.; Ueda, M.; Kurihara, T.; Esaki, N., The putative malate/lactate dehydrogenase from *Pseudomonas putida* is an NADPH-dependent  $\Delta$ 1-piperidine-2-carboxylate/ $\Delta$ 1-pyrroline-2-carboxylate reductase involved in the catabolism of d-lysine and d-proline. *J. Biol. Chem.* **2005**, *280* (7), 5329-5335.
8. Mindt, M.; Risse, J. M.; Grub, H.; Sewald, N.; Eikmanns, B. J.; Wendisch, V. F., One-step process for production of N-methylated amino acids from sugars and methylamine using recombinant *Corynebacterium glutamicum* as biocatalyst. *Scientific Reports* **2018**, *8* (1), 12895.
9. Goto, M.; Muramatsu, H.; Mihara, H.; Kurihara, T.; Esaki, N.; Omi, R.; Miyahara, I.; Hirotsu, K., Crystal structures of  $\Delta$ 1-piperidine-2-carboxylate/ $\Delta$ 1-pyrroline-2-carboxylate reductase belonging to a new family of NAD (P) H-dependent oxidoreductases: conformational change, substrate recognition, and stereochemistry of the reaction. *J. Biol. Chem.* **2005**, *280* (49), 40875-40884.
10. Kerbs, A.; Mindt, M.; Schwardmann, L.; Wendisch, V. F., Sustainable production of N-methylphenylalanine by reductive methylation of phenylpyruvate using engineered *Corynebacterium glutamicum*. *Microorganisms* **2021**, *9* (4), 824.
11. Cheng, J.; Huang, Y.; Mi, L.; Chen, W.; Wang, D.; Wang, Q., An economically and environmentally acceptable synthesis of chiral drug intermediate L-pipecolic acid from biomass-derived lysine via artificially engineered microbes. *Journal of Industrial Microbiology and Biotechnology* **2018**, *45* (6), 405-415.
12. Mindt, M.; Hannibal, S.; Heuser, M.; Risse, J. M.; Sasikumar, K.; Nampoothiri, K. M.; Wendisch, V. F., Fermentative production of N-alkylated glycine derivatives by recombinant *Corynebacterium glutamicum* using a mutant of imine reductase DpkA from *Pseudomonas putida*. *Front. Bioeng. Biotechnol.* **2019**, *7*, 232.
13. Mindt, M.; Walter, T.; Kugler, P.; Wendisch, V. F., Microbial engineering for production of N-functionalized amino acids and amines. *Biotech. J.* **2020**, *15* (7), 1900451.
14. Moreno, C. J.; Hernández, K.; Gittings, S.; Bolte, M.; Joglar, J. s.; Bujons, J.; Parella, T.; Clapés, P., Biocatalytic Synthesis of Homochiral 2-Hydroxy-4-butyrolactone Derivatives by Tandem Aldol Addition and Carbonyl Reduction. *ACS Catalysis* **2023**, *13*, 5348-5357.
15. Fansher, D. J.; Ngwira, N.; Salehi, A. R.; Woods, J.; Cascao, A.; Palmer, D. R., Biocatalytic Synthesis of  $\alpha$ ,  $\beta$ -Unsaturated 2-Keto Acids and Derivatives Using the Promiscuous Aldolase, NahE. *Synthesis* **2023**, *55* (01), 75-89.
16. Wang, Y.; Ren, H.; Zhao, H., Expanding the boundary of biocatalysis: design and optimization of in vitro tandem catalytic reactions for biochemical production. *Critical reviews in biochemistry and molecular biology* **2018**, *53* (2), 115-129.



17. Muschiol, J.; Peters, C.; Oberleitner, N.; Mihovilovic, M. D.; Bornscheuer, U. T.; Rudroff, F., Cascade catalysis—strategies and challenges en route to preparative synthetic biology. *Chemical Communications* **2015**, *51* (27), 5798-5811.
18. Luche, J. L., Lanthanides in organic chemistry. 1. Selective 1, 2 reductions of conjugated ketones. *Journal of the American Chemical Society* **1978**, *100* (7), 2226-2227.
19. Luche, J.-L.; Rodriguez-Hahn, L.; Crabbé, P., Reduction of natural enones in the presence of cerium trichloride. *Journal of the Chemical Society, Chemical Communications* **1978**, (14), 601-602.
20. Gemal, A. L.; Luche, J. L., Lanthanoids in organic synthesis. 6. Reduction of. alpha.-enones by sodium borohydride in the presence of lanthanoid chlorides: synthetic and mechanistic aspects. *Journal of the American Chemical Society* **1981**, *103* (18), 5454-5459.

**Sección IV**

# **Discusión de resultados.**

La síntesis enzimática de compuestos orgánicos complejos y multifuncionales mediante reacciones concurrentes ha recibido una gran atención en los últimos años.<sup>1</sup> Aldolasas, transaminasas y óxido-reductasas han tenido un papel protagónico en este enfoque. Su combinación ha demostrado ser altamente efectiva en la construcción de moléculas de interés biotecnológico debido a su eficiencia y selectividad en la formación de enlaces C-C, C-N y/o C-O.<sup>2</sup> En esta Tesis, se exploró el diseño de estrategias de síntesis asimétricas multienzimáticas de compuestos altamente funcionalizados, con carboligasas (p. ej. Aldolasas como HBPA, YfaU y la transferasa KPHMT), transaminasas (p. ej. BCAT y una librería de 194 enzimas proporcionadas por la empresa Prozomix<sup>®</sup>), óxido-reductasas (p. ej. Deshidrogenasas como KPR y DpkA) y enzimas auxiliares para la regeneración de cofactores o transformación de productos secundarios de las reacciones (p. ej. BAL, GDH y AspTA) (**Tabla 4.1**).

**Tabla 4.1.** Resumen de las enzimas utilizadas en esta Tesis.

Enzima	Nombre	Uso en esta Tesis
<b>HBPA</b>	<i>trans</i> -o-hidroxibenzilidenepiruvato hidratasa-aldolasa	-Reacción de adición aldólica estereoselectiva de piruvato a aldehídos alifáticos y aromáticos -Sistemas multienzimáticos aldolasa-deshidrogenasa.
<b>YfaU</b>	2-oxo-3-desoxi-L-ramnonato aldolasa	-Reacción de adición aldólica estereoselectiva de 2-oxoácidos a formaldehído. -Sistemas multienzimáticos aldolasa-deshidrogenasa. -Reacción de adición aldólica no estereoselectiva de piruvato a aldehídos alifáticos.
<b>KPHMT</b>	3-metil-2-oxobutanoato hidroximetiltransferasa	-Reacción de adición aldólica estereoselectiva de 2-oxoácidos a formaldehído. Sistemas multienzimáticos aldolasa-deshidrogenasa.
<b>BAL</b>	Benzaldehído Liasa	-Enzima auxiliar utilizada en sistemas enzimáticos donde participan transaminasas.
<b>BCAT</b>	Aminotransferasa de $\alpha$ -aminoácidos con cadenas ramificadas	-Transaminasa utilizada en la síntesis de $\gamma$ -hidroxi- $\alpha$ -aminoácidos.
<b>AspTA</b>	Aspartato transaminasa	-Enzima auxiliar en la reacción con BCAT.
<b>T39</b>	Transaminasa 39	-Transaminasa empleada en la síntesis de $\gamma$ -hidroxi- $\alpha$ -aminoácidos
<b>DpkA</b>	$\Delta^1$ -piperidina-2-carboxilato/ $\Delta^1$ -pirrolina-2-carboxilato reductasa	-Deshidrogenasa utilizada en los sistemas multienzimáticos combinada con aldolasas. Síntesis de derivados quirales de 2-hidroxi-4-butirolactonas.
<b>KPR</b>	Cetopantoato reductasa	-Deshidrogenasa utilizada en los sistemas multienzimáticos combinada con aldolasas. Síntesis de derivados quirales de 2-hidroxi-4-butirolactonas.
<b>GDH</b>	Glucosa deshidrogenasa	-Enzima auxiliar utilizada en la regeneración NADPH.

Los genes de las enzimas utilizadas en este trabajo fueron aislados a partir de genomas bacterianos de *E. coli* o *Pseudomonas syringae* (catálogo de microorganismos del Instituto Leibniz-DSMZ) y ADN sintético (servicio de síntesis de genes de la compañía GenScript®) (**Figura 4.1**).

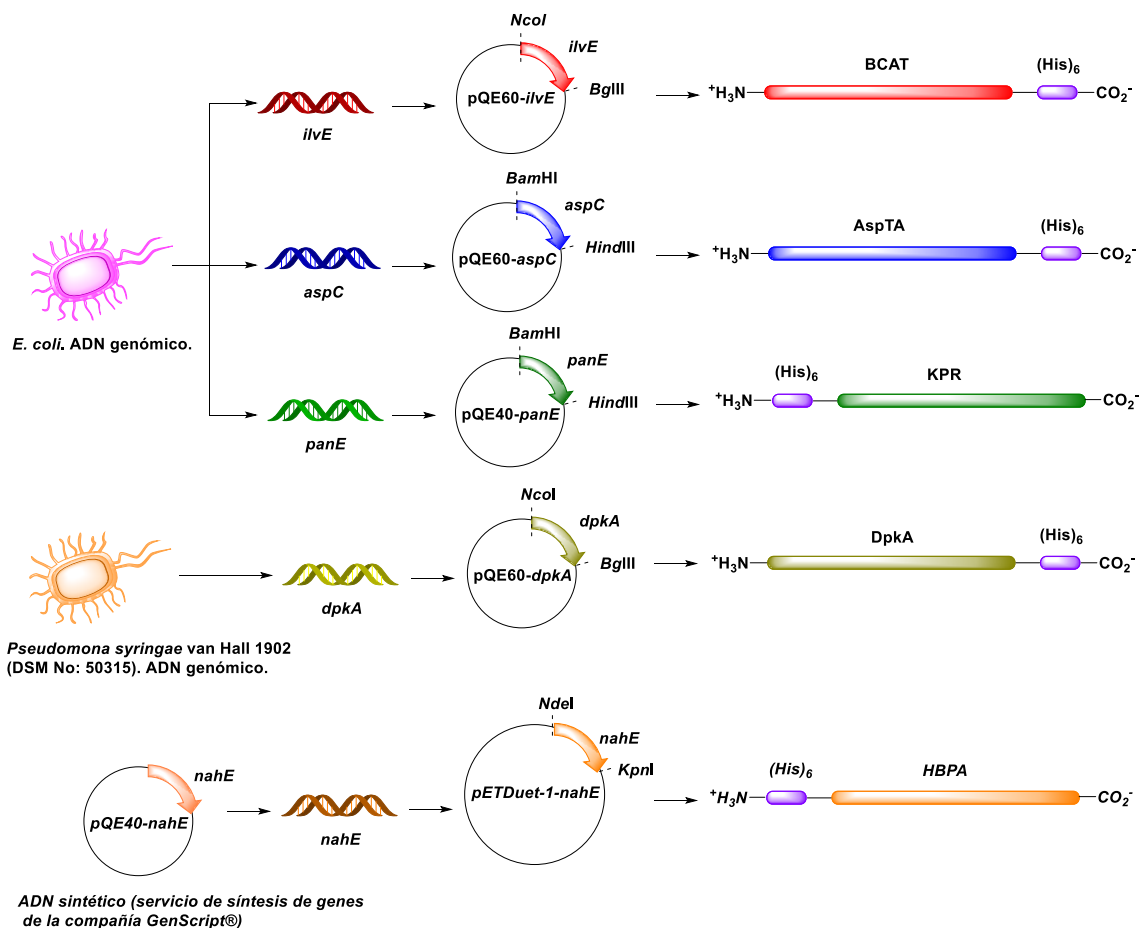


**Figura 4.1.** Representación esquemática de las estrategias de clonación para la BCAT, AspTA, KPR, DpkA y HBPA. Los genes de las diferentes enzimas fueron aislados de varias fuentes: ADN genómico de *E. coli* (genes *ilvE*, *aspC* y *panE*), ADN genómico de *Pseudomonas syringae* (gen *dpkA*) y ADN sintético (gen *nahE*).

Las enzimas: BAL, YfaU y KPHMT fueron clonadas en trabajos anteriores en nuestro grupo de investigación (**Figura 4.2**)<sup>2e,f,4</sup>, no obstante, serán utilizadas en esta Tesis. Por otra parte, la transaminasa (T39) y la glucosa deshidrogenasa (GDH) fueron obtenidas en colaboración con la compañía Prozomix® como “cell free extract”.

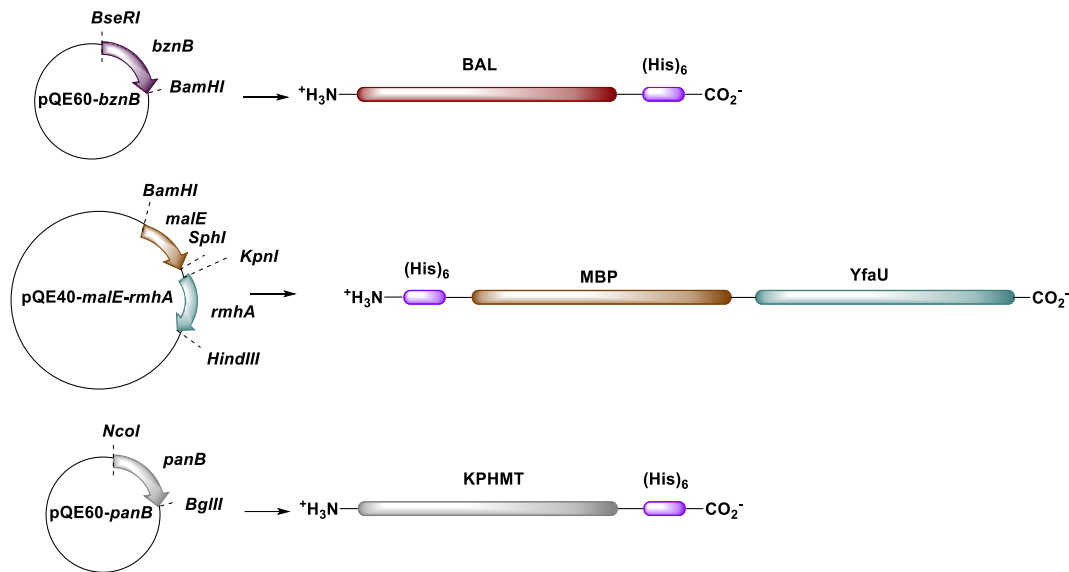


**Figura 4.2.** Representación esquemática de las estrategias de clonación para la BAL, YfaU y KPHMT. La YfaU fue expresada como proteína de fusión junto a la MBP (proteína de unión a maltosa) con el objetivo de disminuir la formación de cuerpos de inclusión.

A todas las enzimas se les añadió una secuencia de 6 histidina (His)<sub>6</sub> en el extremo N o C terminal (**Figuras 4.1 y 4.2**) con el objetivo de facilitar su aislamiento y purificación utilizando una cromatografía de afinidad con metal inmovilizado (resina *Ni Sepharose*<sup>®</sup> *TM High Performance*). En cada caso, el proceso de purificación se analizó por SDS-PAGE (**Figura 4.3**).

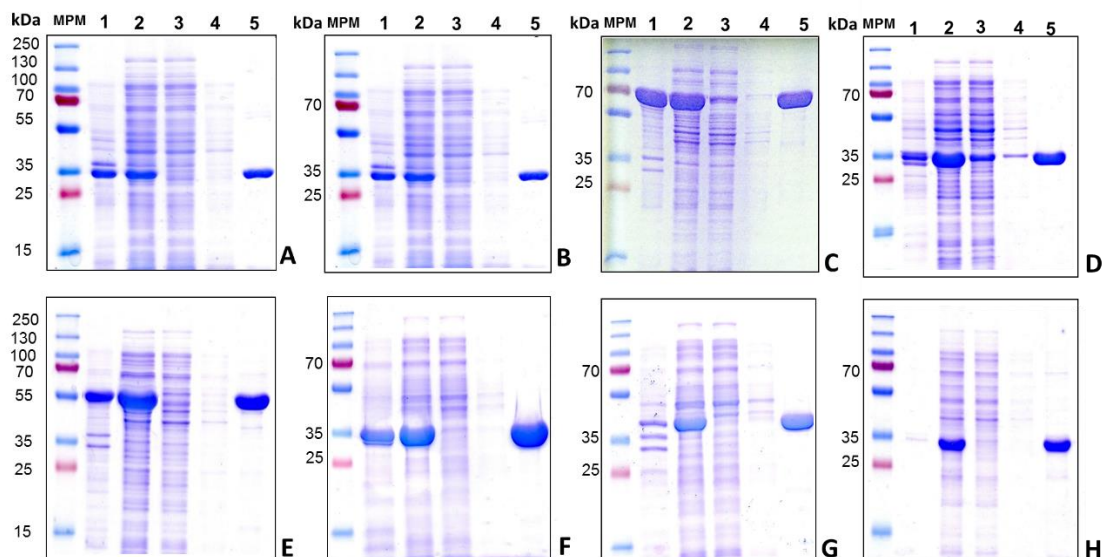


**Figura 4.3.** Análisis por SDS-PAGE de las etapas de purificación de las enzimas utilizadas en este trabajo. **A.** HBPA (38 kDa) nativa, **B.** HBPA H205A (38 kDa), **C.** MBP-YfaU (72 kDa), **D.** DpkA (36 kDa), **E.** BAL (60 kDa), **F.** BCAT (35 kDa), **G.** AspTA (45 kDa) y **H.** KPR (34 kDa). 1-pellet después de la lisis, 2-sobrenadante después de la lisis, 3- proteínas no unidas a la resina, 4- lavado y 5- proteína eluída. MPM, mercador de peso molecular.

## Estudio de las potencialidades sintéticas de la HBPA como biocatalizador en la adición aldólica estereoselectiva de piruvato a aldehídos alifáticos y la condensación aldólica entre piruvato y aldehídos aromáticos.

Para determinar las potencialidades sintéticas de la HBPA se evaluó a escala analítica la reacción de adición y condensación aldólica de piruvato de sodio a diferentes electrófilos (p. ej. aldehídos alifáticos y aromáticos respectivamente) catalizadas por la enzima (Figura 4.4A y 4.4B).

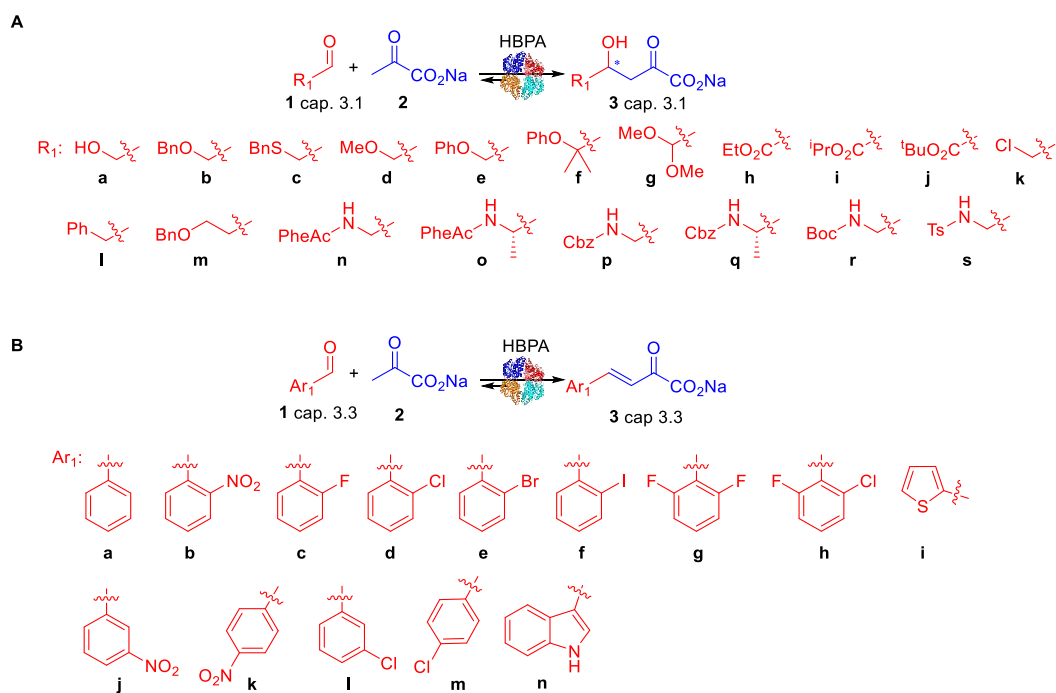


**Figura 4.4.** Esquemas de reacciones enzimáticas catalizadas por la HBPA estudiadas en esta Tesis. **A.** Reacción de adición aldólica de piruvato a aldehídos alifáticos generando 4-hidroxi-2-oxoácidos. **B.** Reacción de condensación aldólica de piruvato a aldehídos aromáticos obteniéndose 2-oxoácido- $\alpha,\beta$ -insaturados.

El objetivo fue seleccionar aquellos sustratos con los mejores porcentajes de conversión aldólica a las 24 h, y seleccionar electrófilos adecuados para escalar las reacciones y caracterizar los 4-hidroxi-2-oxoácidos y 2-oxoácido- $\alpha,\beta$ -insaturados, así como, evaluar la tolerancia de la HBPA para el electrófilo. Disponer de electrófilos adecuados para la HBPA, y caracterizar estructuralmente sus productos aldólicos, fue importante debido a que estos constituyen productos intermedios en reacciones enzimáticas acopladas con transaminasas (capítulo 3.1) y óxido-reductasas (capítulos 3.2 y 3.3) (Figura 4.5).

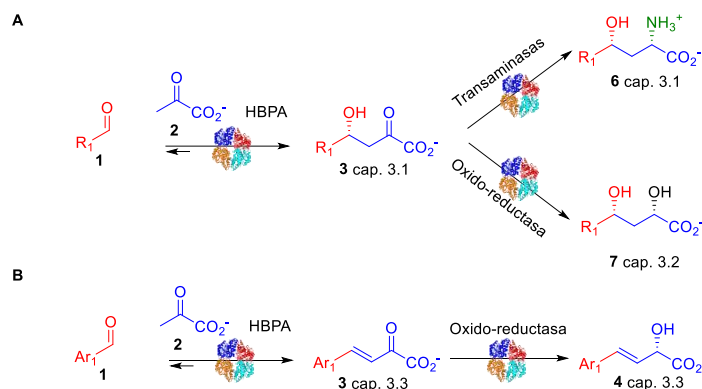


**Figura 4.5.** Estrategias de síntesis multienzimáticas planteadas en esta Tesis utilizando la HBPA como primera enzima. **A.** Síntesis enantioselectiva de 4-hidroxi- $\alpha$ -aminoácidos (capítulo 3.1) y 2,4-dihidroxiácidos (capítulo 3.2). **B.** Síntesis enantioselectiva de 2-hidroxiácidos  $\alpha,\beta$ -insaturados (capítulo 3.3).

Los aldehídos **1c**, **d-f**, **i**, **j**, **m**, **n-s** (capítulo 3.1, **Figura 4.4A**) no están disponibles comercialmente, por tanto, fueron sintetizados en nuestro laboratorio (**Figura 4.6**). Una de las estrategias sintéticas seguidas fue la oxidación del alcohol correspondiente utilizando ácido 2-yodobenzoico (IBX) (oxidación directa del alcohol, **1c**, **1e** y **1m** mientras que en otros casos fueron necesarios etapas anteriores de protección y reducción, **1f**, **1o**, **1p**, **1q** y **1r**). Los aldehídos **1d**, **1n** y **1s** fueron sintetizados a partir del acetal, por desprotección del grupo carbonilo en medio ácido. Debido al carácter hidrófilo de **1d** no pudo ser aislado del medio acuoso, por lo que se utilizó en solución acuosa después de neutralizar el  $\text{H}_2\text{SO}_4$  con  $\text{CaCO}_3$  y eliminar las sales precipitadas por filtración. Los aldehídos **1i**, **j** se sintetizaron por ruptura oxidativa de dioles con ácido orto-peryódico a partir de los ésteres correspondientes del ácido L-tartárico (**Figura 4.6**).

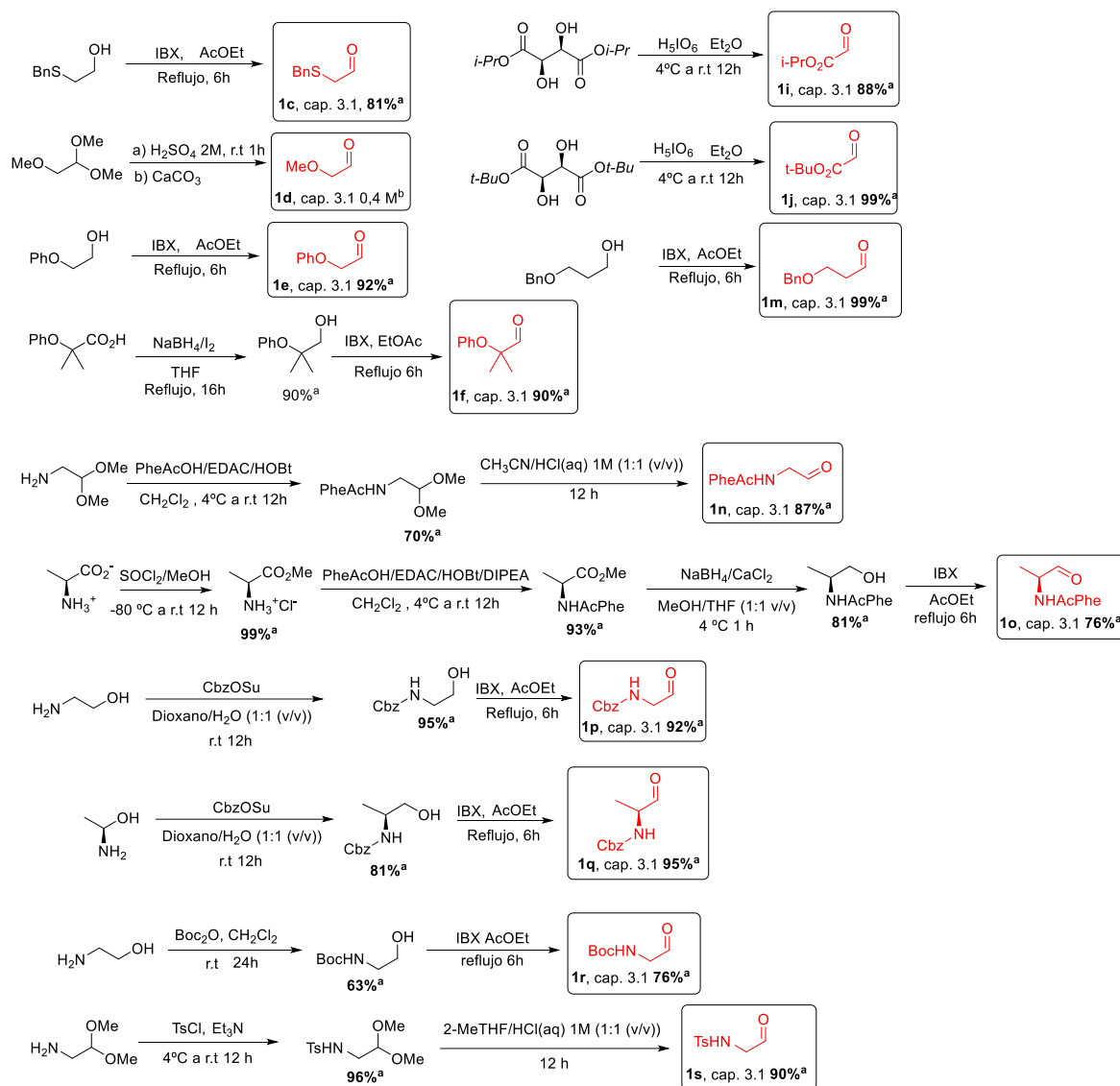
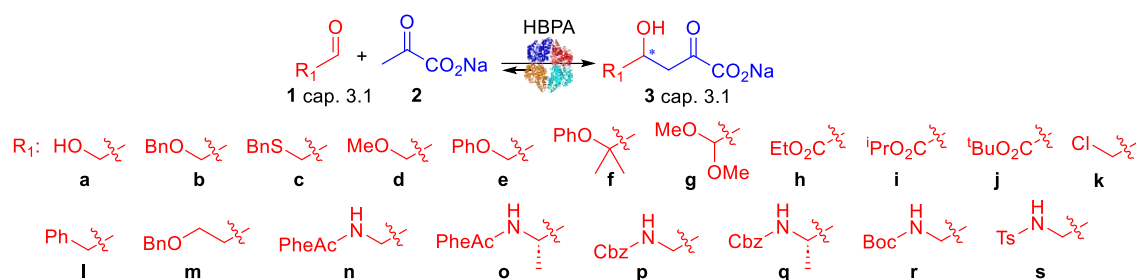


**Figura 4.6.** Estrategias de síntesis de aldehídos **1c**, **d-f**, **i**, **j**, **m**, **n-s** (capítulo 3.1). <sup>a</sup>Rendimiento de producto aislado. <sup>b</sup>**1d** no fue aislado y la concentración fue estimada por HPLC utilizando propionaldehído como patrón.

Las conversiones de las adiciones aldólicas de piruvato a los aldehídos (**1a-s**, cap. 3.1) catalizado por la HBPA se reportan en la **Tabla 4.2**. Las reacciones se siguieron por HPLC.



**Tabla 4.2.** Reacción de adición aldólica de piruvato (**2**) a diferentes aldehídos (**1**) catalizado por la HBPA nativa y la variante H205A (Capítulo 3.1).



Aldehído	Producto aldólico	Variante HBPA	Conversión <sup>a</sup> (%)
<b>1a</b>	<b>3a</b>	nativa	90
<b>1b</b>	<b>3b</b>	nativa	69
<b>1c</b>	<b>3c</b>	nativa/H205A	36/75
<b>1d</b>	<b>3d</b>	nativa	75
<b>1e</b>	<b>3e</b>	nativa	80
<b>1f</b>	<b>3f</b>	nativa/H205A	63/75
<b>1g</b>	<b>3g</b>	nativa	87
<b>1h</b>	<b>3h</b>	nativa	84
<b>1i</b>	<b>3i</b>	nativa	95
<b>1j</b>	<b>3j</b>	nativa	95
<b>1k</b>	<b>3k</b>	nativa/H205A	17/75
<b>1l</b>	<b>3l</b>	nativa	90
<b>1m</b>	<b>3m</b>	nativa/H205A	48/50
<b>1n</b>	<b>3n</b>	nativa	80
<b>1o</b>	<b>3o</b>	nativa/H205A	63/75
<b>1p</b>	<b>3p</b>	nativa/H205A	NP
<b>1q</b>	<b>3q</b>	nativa/H205A	NP
<b>1r</b>	<b>3r</b>	nativa/H205A	NP
<b>1s</b>	<b>3s</b>	nativa/H205A	NP

<sup>a</sup>Conversión de la reacción (24h) como porcentaje de formación de **3** determinado por HPLC. NP: Producto no detectado.

En estos experimentos se consiguieron conversiones de adición aldólica del 63 al 95% para la mayoría de los aldehídos, lo que evidencia la promiscuidad de la enzima hacia el sustrato electrófilo en la reacción. En el caso de los aminoaldehídos (**1n-s**) la selección del grupo protector fue clave para obtener altas conversiones en la reacción catalizada por la enzima. Los aldehídos con los grupos protectores de la función amino Cbz (**1p** y **1q**), Boc (**1r**) y Ts (**1s**), no fueron sustratos de la enzima, mientras que con el grupo protector fenilacetil (PheAc, **1n** y **1o**) se alcanzaron conversiones de reacción de alrededor del 80% después de 24h.

Por otra parte, se observaron bajas conversiones para los aldehídos **1c** (36%) y **1k** (17%) (**Tabla 4.2**). Con el objetivo de mejorar estos resultados se realizó un análisis de mutantes disponibles en el laboratorio, encontrándose que la variante H205A incrementó la

conversión de la reacción aldólica para los aldehídos **1c** (75%) y **1k** (75%). Durante la realización de esta Tesis, se publicó la estructura cuaternaria de la enzima HBPA (PDB: 6DAO)<sup>5</sup> lo que permitió realizar una interpretación estructural de estos resultados. El centro activo de la HBPA se encuentra formando una cavidad profunda y angosta, donde el grupo  $\epsilon$ -amino de la Lys183 catalítica está a unos 11 Å de la superficie, con varios residuos aromáticos (H205, W224, F269 y F277) flanqueando la entrada y residuos predominantemente polares (G64, T65, G67, Y155, N157 y N281) al final de la cavidad, cerca de la Lys catalítica (**Figura 4.7**).

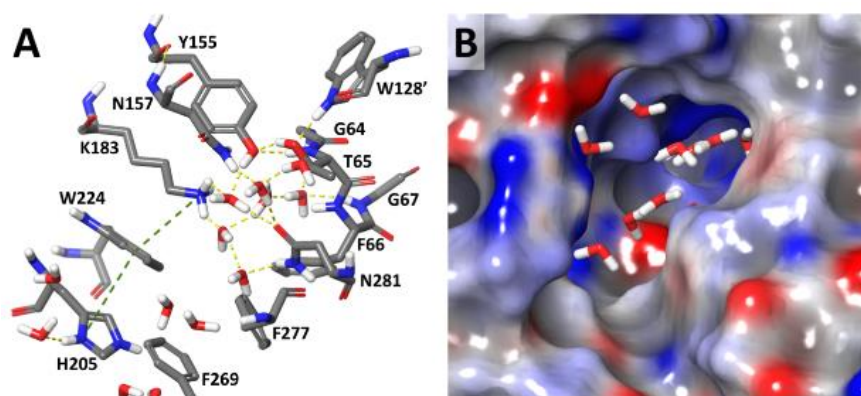


**Figura 4.7.** Estructura del centro activo del HBPA **A.** muestra el residuo de Lys (K183) esencial para la catálisis, y los residuos que conforman la cavidad, y **B.** Superficie de potencial electrostático de la enzima. Se observa la cavidad en forma de túnel que delimita el centro activo y molécula de agua en su interior.

El análisis de los modelos moleculares de los complejos de HBPA (piruvato formando la enamina con la K183) y los aldehídos **1c** y **1o** del cap. 3.1, realizados por el Dr. Jordi Bujons, sugieren que la sustitución de la His 205 por una Ala genera más espacio en el centro activo de la enzima, lo que minimiza el impedimento estérico que presentan **1c** y **1k** (**Figura 4.8**).

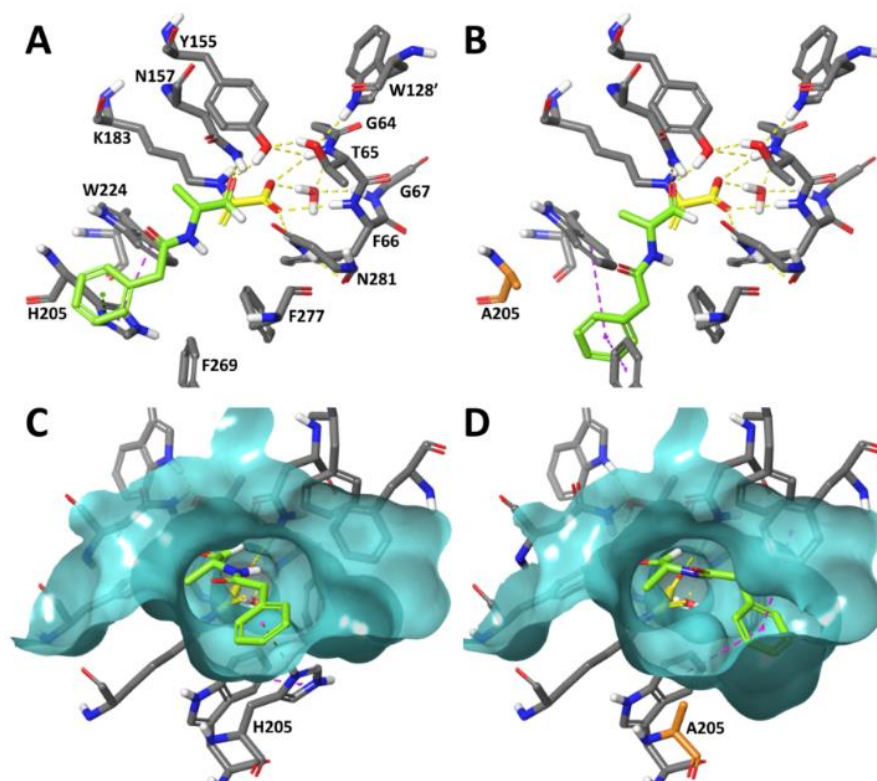


**Figura 4.8.** Modelos de los complejos pre-reactivos de la HBPA nativa (**A** y **C**) y la variante H205A (**B** y **D**) con la enamina piruvato (en amarillo) y el aldehído **1o** (en verde). La Ala 205 aparece resaltado en naranja. Las interacciones se muestran con líneas discontinuas: puentes de hidrógeno en amarillo, interacciones  $\pi$ - $\pi$  en magenta y  $\pi$ -catión en verde oscuro. La comparación de la superficie de los centros activos de ambas proteínas (**C** y **D**) revela que la variante H205A genera una cavidad expandida cerca del residuo A205.

Por otra parte, un análisis de la estructura del HBPA muestra que los grupos carboxilos del Glu206, Asp207, Asp208 y Asp265 están a menos de 5 Å de los átomos  $\delta$  y  $\epsilon$ -N del grupo imidazol de la His205, estabilizando su estado protonado (**Figura 4.9**). Esta carga positiva también está estabilizada por una interacción  $\pi$ -catión con el grupo indol del residuo Trp224. La eliminación de este imidazol protonado, que se encuentra a  $\sim 8$  Å del grupo  $\epsilon$ -amino de la Lys183 esencial modifica el entorno electrostático del centro activo, lo que también podría contribuir a la mayor eficacia de la catálisis enzimática hacia estos aldehídos.

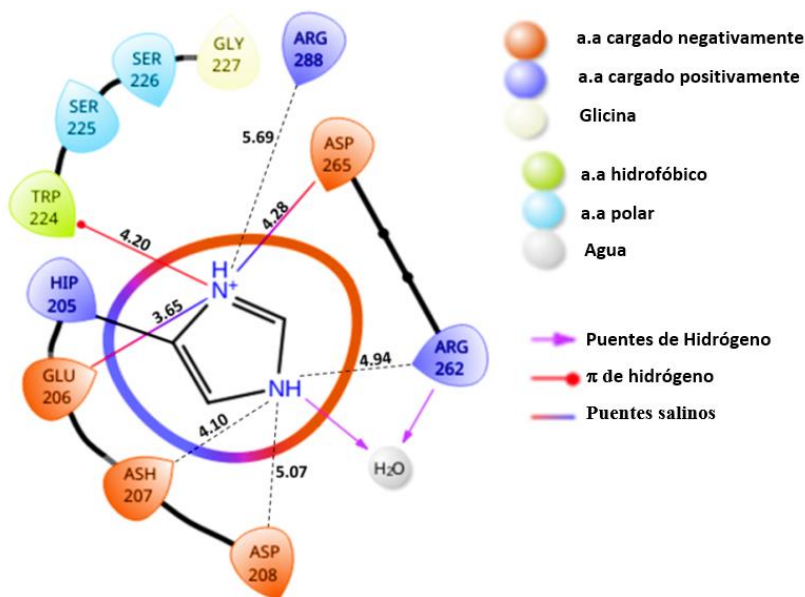


**Figura 4.9.** Esquema que muestra las interacciones establecidas por el grupo imidazol del residuo H205 de la HBPA. Se indican las distancias (líneas discontinuas) a los residuos cercanos.

Una vez determinado el espectro de sustratos que puede aceptar la HBPA, se pasó a la síntesis y purificación de los productos de adición aldólica para su caracterización estructural. En esta etapa nos encontramos que los aldoles forman mezclas complejas de analizar en medio ácido (**Figura 4.10**), por lo que fue necesario realizar una descarboxilación oxidativa transformándolos en 3-hidroxiácidos que pudieron ser aislados como ésteres (**Figura 4.11**).

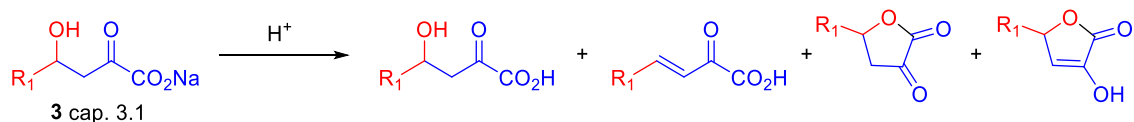


**Figura 4.10.** Al exponer a medio ácido los aldoles **3** pueden darse reacciones de deshidratación, lactonización y enolización que dificultan el aislamiento y purificación del producto de interés.

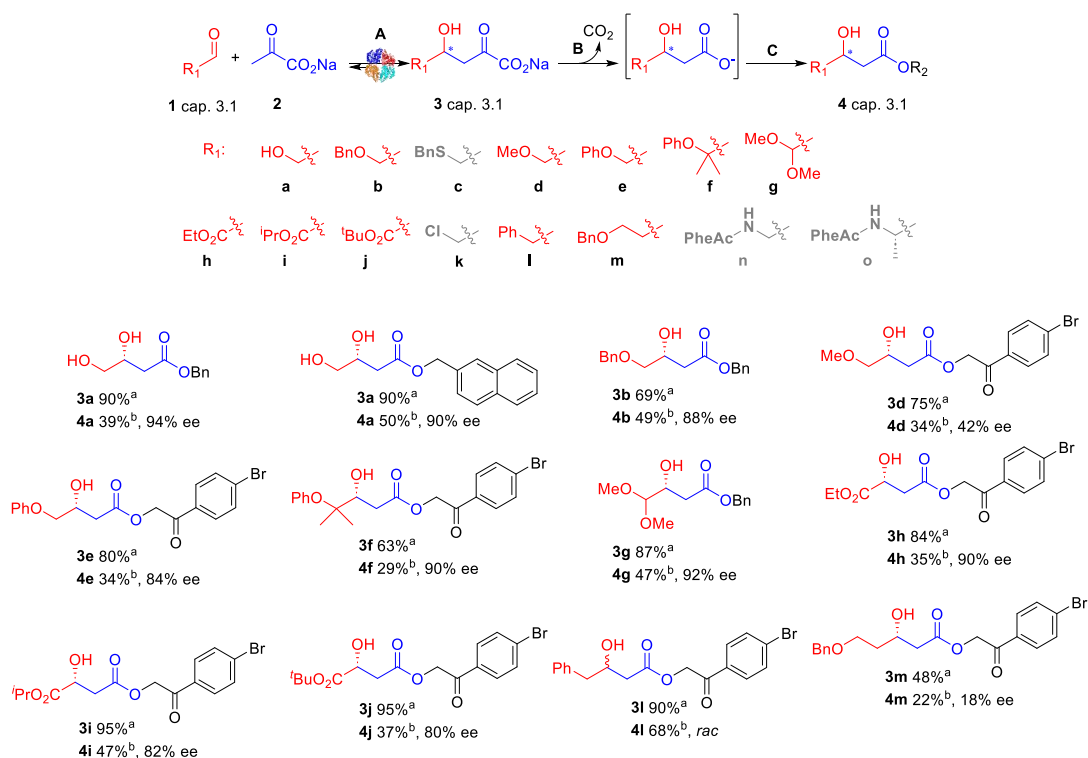


**Figura 4.11.** Estrategia de síntesis de los 3-hidroxiésteres **4** del capítulo 3.1. **A.** Adición aldólica HBPA nativa o variante H205A. **B.** *i*) H<sub>2</sub>O<sub>2</sub> *ii*) Catalasa. **C.** Esterificación: *i*) Bromuro de bencilo/CsCl (0.1 eq) / DMF r.t 12h. *ii*) 2-bromometilnaftaleno/CsCl (0.1 eq)/DMF r.t 12h *iii*) 2,4-dibromoacetofenona/ DMF r.t 12h. <sup>a</sup>Conversión de la reacción aldólica determinada por HPLC. <sup>b</sup>Rendimiento de producto aislado después de 3 etapas de reacción. Las mezclas racémicas se sintetizaron siguiendo el mismo procedimiento, pero, utilizando YfaU como biocatalizador. La estereoquímica de los aldoles **3c**, **3k**, **3n** y **3o** se describirán más adelante (pág. 113).

La HBPA en reacciones aldólicas de piruvato **2** a los electrófilos **1a**, **1f-h** del cap. 3.1 mostró una buena enantioselectividad (90%-95% ee), mientras que, para **1b**, **1e** y **1i-j** (cap.3.1) se alcanzaron niveles moderados (80-88% ee). Estos resultados demuestran el buen desempeño estereoquímico del biocatalizador puesto que por lo general las piruvato aldolasas muestran un perfil poco estereoselectivo hacia los electrófilos de bajo peso molecular.<sup>6</sup> Además de ser el primer reporte de una reacción aldólica estereoselectiva catalizada por la HBPA. Sin embargo, se alcanzaron bajos niveles de enantioselectividad con el metoxiacetaldehído (**1d** cap. 3.1) y 3-(benciloxi)propanal (**1m** cap. 3.1) (43 y 18% ee, respectivamente) mientras que se obtuvo una mezcla racémica usando fenilacetaldehído (**1l** cap. 3.1). Esto evidencia que la estereoselectividad de la enzima depende de la naturaleza del electrófilo.

Para conocer la estereoquímica absoluta que produce la HBPA, se generaron cristales de los compuestos **4e**, **4f** y **4i** (cap. 3.1). Estos cristales fueron analizados con difracción de

rayos X, en colaboración con el Dr. Michael Bolte del Instituto de Química Inorgánica, Universidad J.-W.-Goethe, Frankfurt/Main, Alemania. Los análisis, indicaron que HBPA genera aductos aldólicos con configuración *R* como productos mayoritarios (**Figura 4.12**). Esto concuerda con los resultados estereoquímico reportado de las reacciones entre fluoro piruvato y aldehídos (hetero)aromáticos,<sup>7</sup> así como, la reacción entre el  $\beta$ -nitroestireno y piruvato catalizado por la misma enzima.<sup>8</sup>

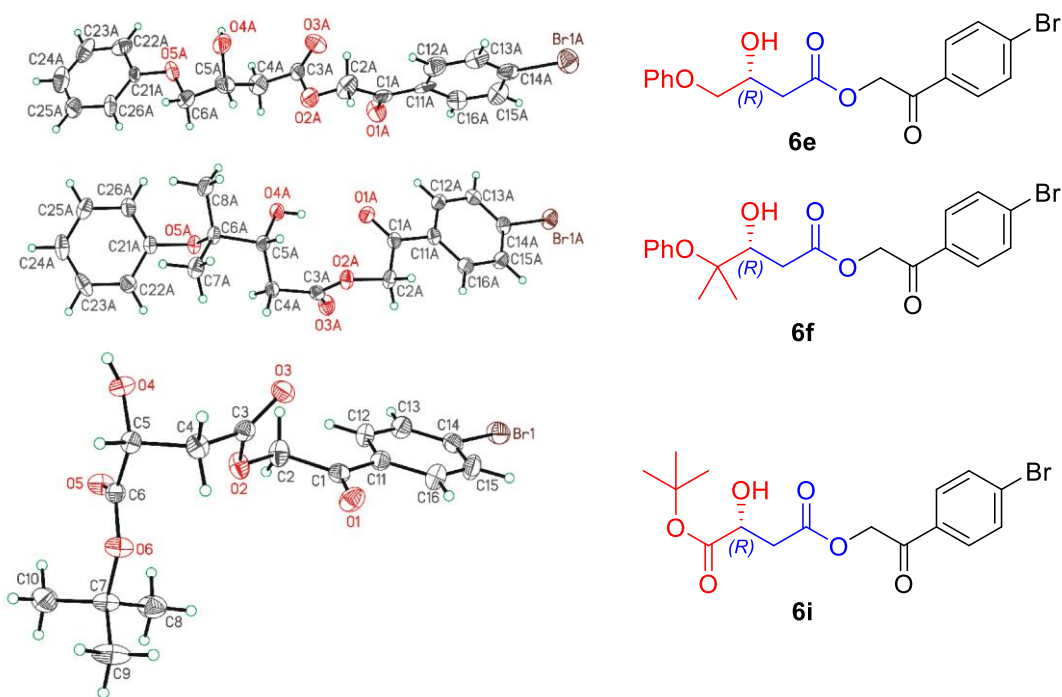


**Figura 4.12.** Estructuras de rayos X de (*R*)-**6e**, (*R*)-**6f** y (*R*)-**6i**. Gráfico de tipo ORTEP que muestra una molécula con elipsoides de probabilidad del 50%. Los datos pueden obtenerse gratuitamente en: Cambridge Crystallographic Data Centre a través de [www.ccdc.cam.ac.uk/data\\_request/cif](http://www.ccdc.cam.ac.uk/data_request/cif)

De análisis de los modelos moleculares de la HBPA con (i) la enamina de piruvato en el centro activo y las moléculas de electrófilo (**Figuras S88-S93**, cap. 3.1) y (ii) las iminas derivadas de los aductos aldólicos (**Figuras S94-S99** cap. 3.1) no se aprecia restricción estérica entre la aproximación esterofacial “*re*- o *si*” del electrófilo a la enamina. Por lo tanto, no está claro por qué hay una preferencia por la aproximación a la “*re*”, que genera los aductos con configuración *R*. Esta preferencia de la enzima se ha reportado en estudios previos sin que quede clara las razones por la cual ocurre.<sup>7-8</sup>

Seguidamente se analizó la promiscuidad de la HBPA hacia electrófilos aromáticos. Para ello se realizaron reacciones de condensación aldólica entre piruvato y aldehídos aromáticos (**Figura 4.13**) los aldehídos evaluados fueron buenos sustratos para la enzima utilizando 1 eq de **2**, con conversiones entre un 50 y 95%. Utilizando un exceso de piruvato (3 eq) se logró alcanzar conversiones superiores al 95% debido a que se desplazó el equilibrio de la reacción hacia la formación de producto (**Figura 4.13**). Coincidiendo con trabajos previos, sólo se detectó producto de condensación aldólica, en la reacción entre el piruvato y aldehídos aromáticos catalizada por la HBPA.<sup>9</sup> La formación del producto deshidratado está mediada por la enzima puesto que se han descrito reacciones de adición aldólica de piruvato a aldehídos aromáticos catalizado por piruvato aldolasas donde se obtiene el producto de adición aldólica.<sup>10</sup> Además, en nuestro grupo de investigación hemos visto que la reacción de adición aldólica de **2** a **1a** catalizada por la YfaU produce exclusivamente el aldol correspondiente (resultados no mostrados).

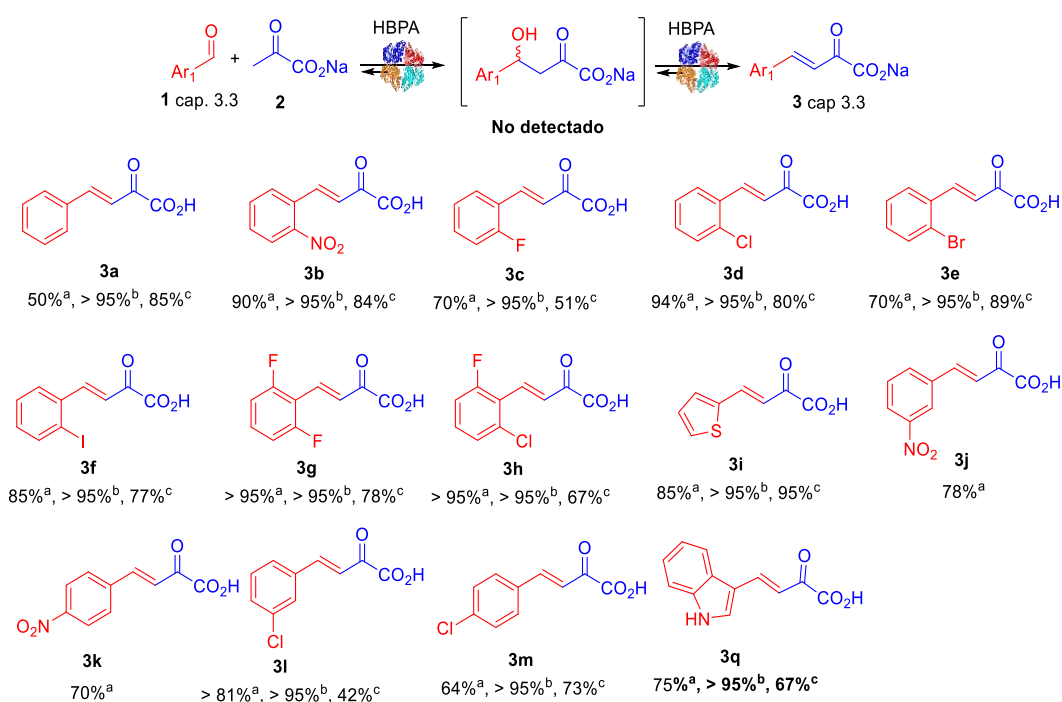


**Figura 4.13.** Reacción de condensación aldólica entre piruvato y aldehídos aromáticos catalizadas por la HBPA. <sup>a</sup>Conversión de la reacción (1 eq de **2**) como porcentaje de formación de **3** (24h) determinado por HPLC. <sup>b</sup>Conversión de la reacción (3 eq de **2**) como porcentaje de formación de **3** (24h) determinado por HPLC <sup>c</sup>Rendimiento de producto aislado. Los productos **1j** y **1k** no fueron aislados.

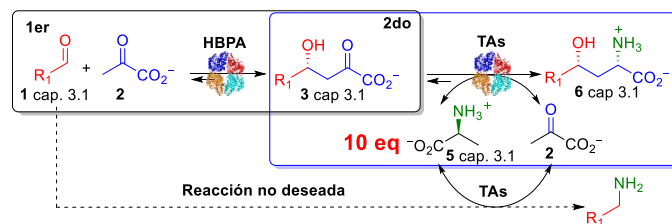
En esta primera etapa se evaluó las habilidades sintéticas de la HBPA nativa y su variante H205A, caracterizando los productos de adición y condensación aldólicas generado por este biocatalizador. Estos compuestos fueron sustratos de otras enzimas en reacciones

enzimáticas secuenciales donde se generó  $\gamma$ -hidroxi- $\alpha$ -aminoácidos (cap. 3.1) y derivados del ácido (*S,E*)-2-hidroxi-4-arylbut-3-enoico respectivamente (cap. 3.3).

**Síntesis de derivados de  $\gamma$ -hidroxi- $\alpha$ -aminoácidos (6, cap. 3.1) utilizando sistemas enzimáticos formados por la HBPA y transaminasas estereoselectivas.**

Iniciamos la búsqueda y selección de transaminasas estereoselectivas capaces de transformar los aductos aldólicos generados por la HBPA (**3a-b, 3e, 3g-h** cap. 3.1) a partir de un panel de 194 transaminasas (T1- T194) proporcionado por Prozomix Ltd. Para el análisis de las transaminasas se seleccionó dos donadores de grupos amino diferentes: L-Ala (**5** cap. 3.1) y bencilamina (**7** cap. 3.1) (**Figura 4.14A y 4.14B**, respectivamente). Para desplazar los equilibrios de reacción en el caso de **5** se utilizó un exceso de este sustrato (10 eq) **Figura 4.14A**, mientras que con **7** se utilizó una enzima auxiliar acoplada al sistema, la benzaldehído liasa (BAL) que transforma el benzaldehído formado en (*R*)-benzoína (**9** cap. 3.1) que precipita en el medio de reacción por su baja solubilidad en agua (**Figura 4.14B**).

A Uso de L-Ala (**5** cap 3.1) como donador de grupos aminos.



B Uso de bencilamina (**7** cap 3.1) como donador de grupos aminos.

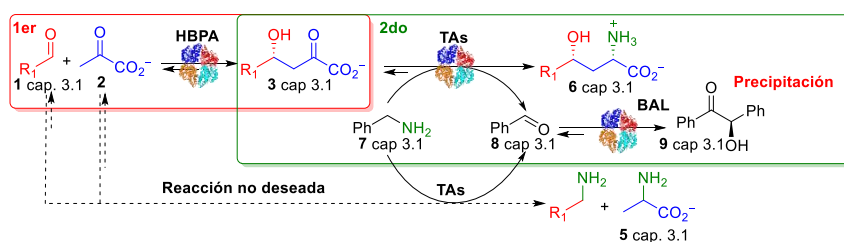


**Figura 4.14.** Estrategia de búsqueda y selección de transaminasas capaces de transformar los aductos aldólicos generados por la HBPA (**3a-b, 3e, 3g-h** cap. 3.1). **A.** L-Ala **5** como dador de grupo amino. **B.** Bencilamina **7** como dador de grupo amino.

En ambas estrategias, primero se llevó a cabo la adición aldólica catalizada por la HBPA y, una vez la formación de **3** (cap. 3.1) alcanzó un máximo de conversión, se puso en marcha la reacción de transaminación añadiendo a la mezcla aldólica L-Ala (**5** cap. 3.1, 10 eq respecto a **3** (cap. 3.1) y la transaminasa (TA) a evaluar) o la bencilamina (**7** cap.



3.1, junto con la BAL y la transaminasa (TA) a evaluar). En la primera estrategia las reacciones se siguieron por HPLC, bien por consumo del área correspondiente al aducto aldólico (**3a**, **3g** y **3h** cap. 3.1) o por formación de producto aminado (**6** cap. 3.1) cuando **3** presentaba motivos aromáticos (**6b** y **6e** cap. 3.1). Por su parte, en la segunda estrategia se hizo el seguimiento evaluando por HPLC la formación de benzaldehído **8** (cap. 3.1) y/o benzoína **9** (cap. 3.1). La **figura 4.15** muestra un ejemplo de los resultados de la primera estrategia de selección de transaminasas (T1-T50) utilizando el aldol **3a**. Las flechas verdes indican las enzimas capaces de disminuir el área del aducto aldólico o aldehído remanente en la mezcla, indicando así, una reacción positiva. El análisis completo se puede ver en las **Figuras S8-S12** de la sección de Materiales y Métodos del capítulo 3.1.

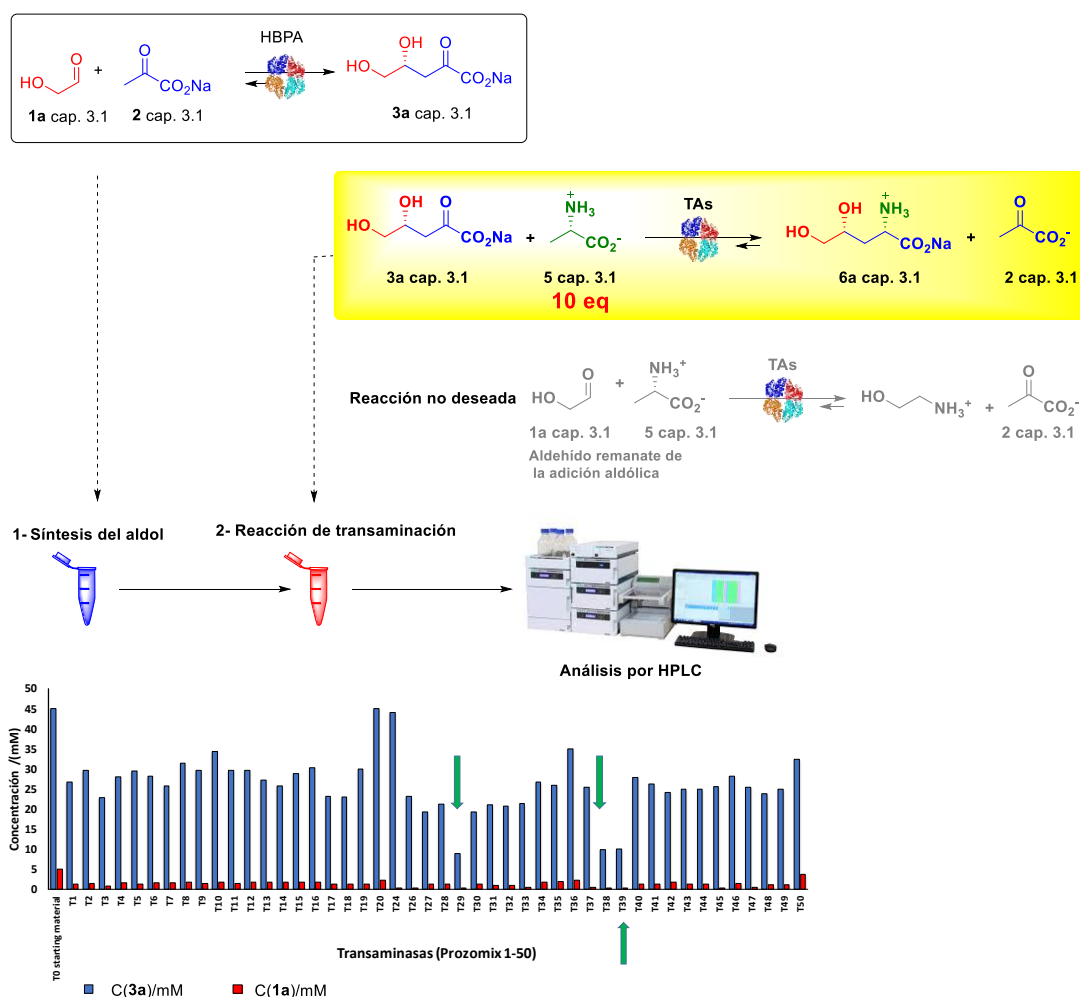


**Figura 4.15.** Análisis de un panel de transaminasas de Prozymix (cap. 3.1), utilizando L-Ala (**5**) como donante de grupo amino para obtener **6a**. Condiciones: **3a** (45 mM), **1a** (5 mM, remanente de la adición aldólica), HBPA (0,5 mg mL<sup>-1</sup>, presente en la adición aldólica), L-Ala (500 mM), T1-T50 (2 a 3 mg de sólido por reacción).

De las 50 enzimas evaluadas con la primera estrategia, se seleccionó la transaminasa T39 como candidata para la reacción de transaminación de diferentes aldeos, en una cascada enzimática cíclica (**Figura 4.16A**). La principal característica de este sistema es que permitiría utilizar cantidades sub-estequiométricas de **2** al ser regenerado por la reacción de transaminación.

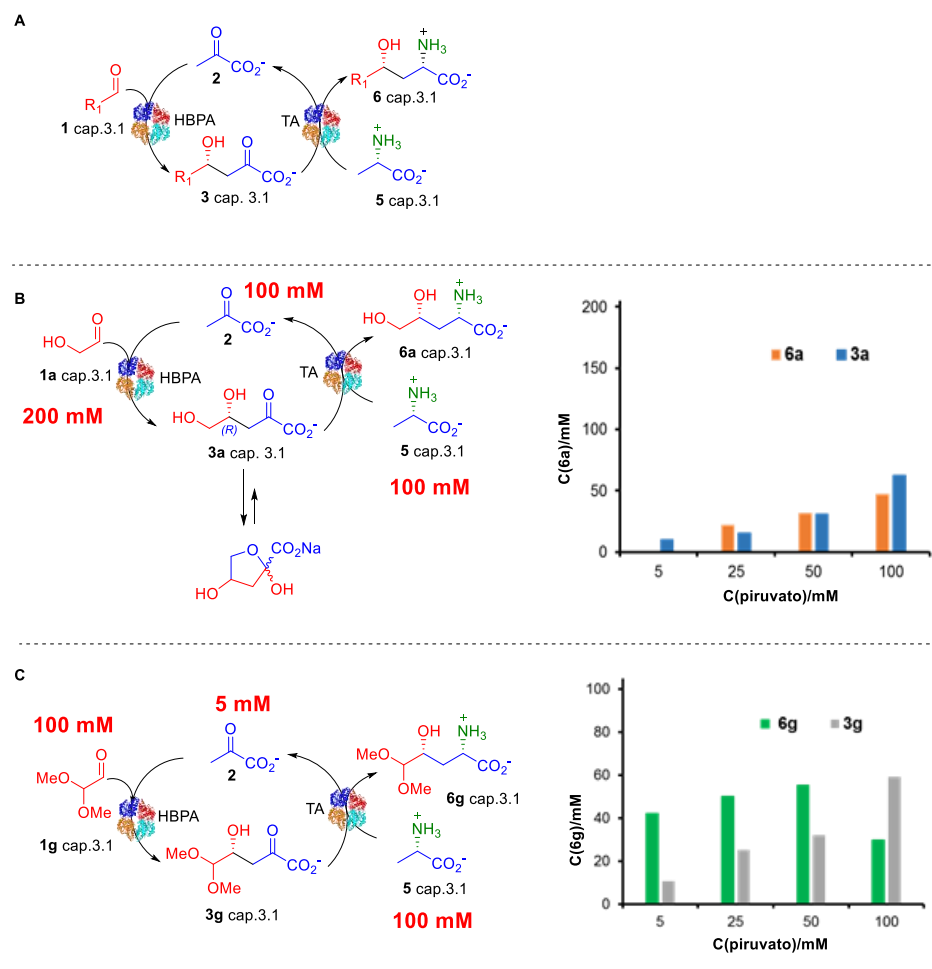


**Figura 4.16.** Síntesis biocatalítica en cascada de derivados de  $\gamma$ -hidroxi- $\alpha$ -aminoácidos (**6**, cap. 3.1) a partir de aldeídos (**1**, cap. 3.1), piruvato (**2**) y L-Ala (**5** cap. 3.1). **A.** Representación general de la cascada enzimática utilizada en la síntesis de  $\gamma$ -hidroxi- $\alpha$ -aminoácidos (**6a**, cap. 3.1). **B.** Cascada enzimática con glicolaldehído como sustrato. **C.** Cascada enzimática con dimetoxiacetaldehído como sustrato.

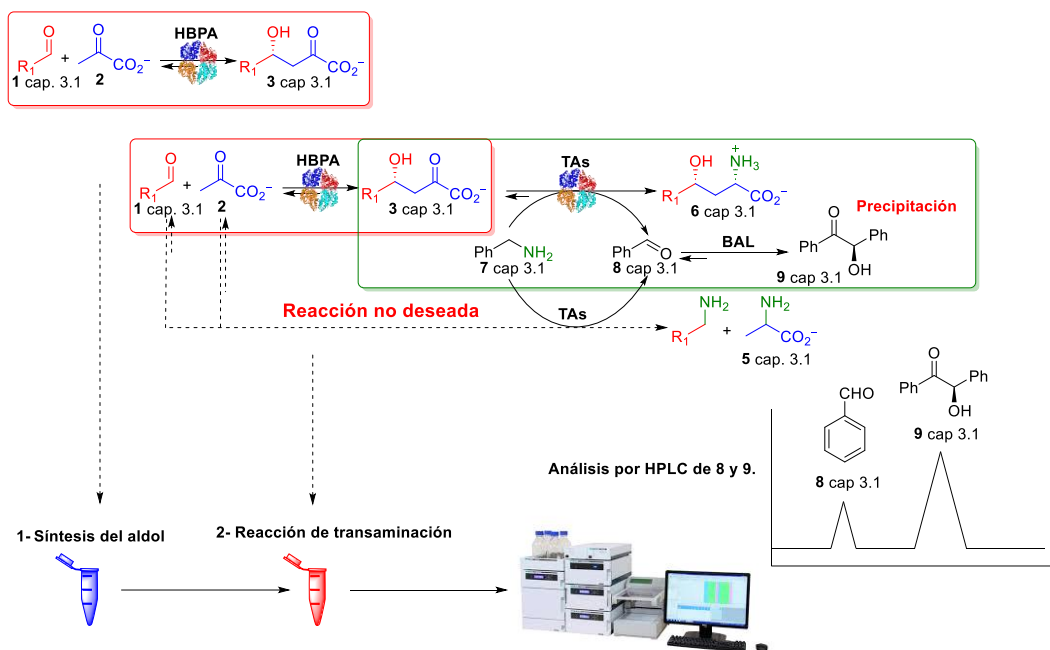
Utilizando glicolaldehído **1a** (cap. 3.1) (200 mM) y el sistema enzimático HBPA/T39, se alcanzó la máxima formación de **6a** (47 mM, 47% de rendimiento) a una concentración de piruvato de 100 mM (**Figura 4.16B**). En estas condiciones, no se produjo un reciclado de piruvato por lo que el sistema biocatalítico no funciona como una cascada enzimática cíclica. Esto pudiera explicarse porque el aducto aldólico está en equilibrio con el

hemiacetal cíclico, lo que contribuye a disminuir la concentración efectiva de la forma abierta que es el sustrato de la T39, situación que ha sido descrita anteriormente.<sup>2b</sup>

Sin embargo, con el sustrato **1g** (cap. 3.1) a una concentración de 100 mM se logró un 42% de conversión de producto aminado **6g** (cap. 3.1) partiendo de 5mM de piruvato (**2**) sugiriendo un reciclado del oxoácido. Al aumentar la concentración de **2** a 50 mM de obtuvo un 55% de (**6g**) sin reciclaje de **2** y una concentración de piruvato de 100 mM provocó un aumento de producto aldólico **3** (cap. 3.1), pero, la conversión de producto aminado disminuyó probablemente por problemas de equilibrio en la reacción de transaminación (**Figura 4.16C**).

Desafortunadamente, la estrategia sintética que emplea una cascada cíclica de reacciones con reciclado de piruvato no produjo los derivados  $\gamma$ -hidroxi- $\alpha$ -aminoácidos deseados con todos los aldehídos probados, y solo se detectaron los aductos de aldol **3** del cap. 3.1 (**Figura S20** cap. 3.1). La aldolasa y las transaminasas no mostraron suficiente actividad hacia el aldehído y el aducto aldol, respectivamente, lo que dificultó la conversión rápida tanto del piruvato inicial como del aducto aldol formado y comprometió la eficiencia del proceso de reciclado y por ende la producción del producto aminado.

Utilizando bencilamina como dador de grupo amino, se seleccionaron 27 enzimas candidatas entre las 194 transaminasas que disponíamos (**Figura 4.17**, celdas de color amarillo). Para minimizar el esfuerzo en el análisis de la librería de transaminasas se siguió la reacción sólo a través de la formación de benzaldehído (**8**) y (*R*)-benzoína (**9**). Este método presenta como inconveniente que en la mezcla de la reacción de transaminación existen otros sustratos (**1**) y (**2**) que también pueden contribuir a su formación. Esto es potencialmente problemático al tener HBPA en la mezcla puesto que la enzima puede catalizar la retro-aldólisis de **3** favorecido por la irreversibilidad de la reacción de transaminación en estas condiciones (**Figura 4.17**).



Aldol adduct	T18	T19	T20	T21	T22	T23	T24	T26	T31	T33
3a	10	27	16	40	9	55	54	66	61	35
3b	4	6	17	9	36	17	11	43	59	0
3e	5	5	15	16	18	13	17	34	26	0
3g	16	6	28	20	31	21	32	58	55	48
3h	7	9	0	9	15	0	8	14	11	6

Aldol adduct	T37	T39	T45	T47	T48	T53	T59	T77	T81	T82
3a	0	44	9	58	15	22	0	12	71	0
3b	0	28	0	59	0	0	0	4	37	0
3e	0	33	10	37	0	0	0	0	27	8
3g	54	58	20	48	0	0	14	10	42	6
3h	0	31	0	16	0	0	0	4	14	0

Aldol adduct	T87	T88	T93	T130	T150	T152	T166	T168	T169	T170
3a	23	15	35	69	0	14	90	25	34	33
3b	0	0	15	23	5	0	42	16	40	17
3e	0	0	19	24	8	5	48	14	39	18
3g	0	0	39	8	2	6	43	15	33	17
3h	0	0	12	5	18	6	16	10	16	11

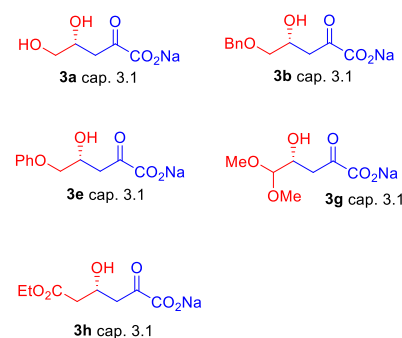
  

Aldol adduct	T171	T172	T173	T174	T176	T177	T178	T179	T180	T187
3a	0	38	12	53	73	45	23	66	67	23
3b	0	15	0	36	43	12	8	0	17	0
3e	18	0	0	37	40	17	17	7	21	0
3g	6	7	0	40	40	12	18	25	32	20
3h	0	8	0	38	16	0	8	8	14	0

Aldol adduct	T188	T189	T190	T191	T192	T193	T194
3a	78	89	15	100	49	39	94
3b	56	57	9	52	10	0	68
3e	64	65	6	68	14	16	72
3g	47	41	18	43	40	29	48
3h	17	18	9	20	11	10	19

Sustratos evaluados



**Figura 4.17.** Primera ronda de selección de las TAs de Prozomix (T1-T194) capaces de transaminar los aductos aldólicos (6a-b, 6e, 6g-h cap. 3.1) utilizando benzilamina (7) como dador de grupo amino. Los números dentro de las celdas representan el porcentaje de formación de benzaldehído/benzoína al cabo de 24 h determinado por HPLC. Condiciones: Reacción aldólica: 1 (100 mM), 2 (100 mM) y HBPA (1 mg mL<sup>-1</sup>); Reacción de Transaminación: 3 (~50 mM) y 7 (75 mM), BAL (10U) y TAs (2-3 mg de sólido en reacción). Con las transaminasas que no aparecen en la tabla no se detectó reacción de transaminación. Teniendo en cuenta las cantidades iniciales de benzilamina y 3 en las mezclas de reacción, se consideró que un porcentaje >67% (celdas en rojo) procedía del consumo parcial de benzilamina debido a las reacciones de transaminación de aldehídos (1) y piruvato (2), que quedaban sin reaccionar de la reacción de adición aldólica o se formaban por retro-aldólisis durante la reacción de transaminación. Las transaminasas en amarillo son las que se seleccionaron como potenciales candidatas para estudiar la transaminación los aductos aldólicos.

Teniendo en cuenta este inconveniente se realizó un segundo análisis de las reacciones de transaminación catalizadas por las 27 enzimas encontradas, pero ahora eliminado la HBPA para evitar el efecto de retro-aldolisis. Bajo estas condiciones solamente la transaminasa T39 fue capaz de convertir los aductos aldólicos (**3a-b**, **3e**, **3g-h** cap. 3.1) en los productos aminados buscados (**6a-b**, **6e**, **6g-h** cap. 3.1) (**Figura 4.18**).

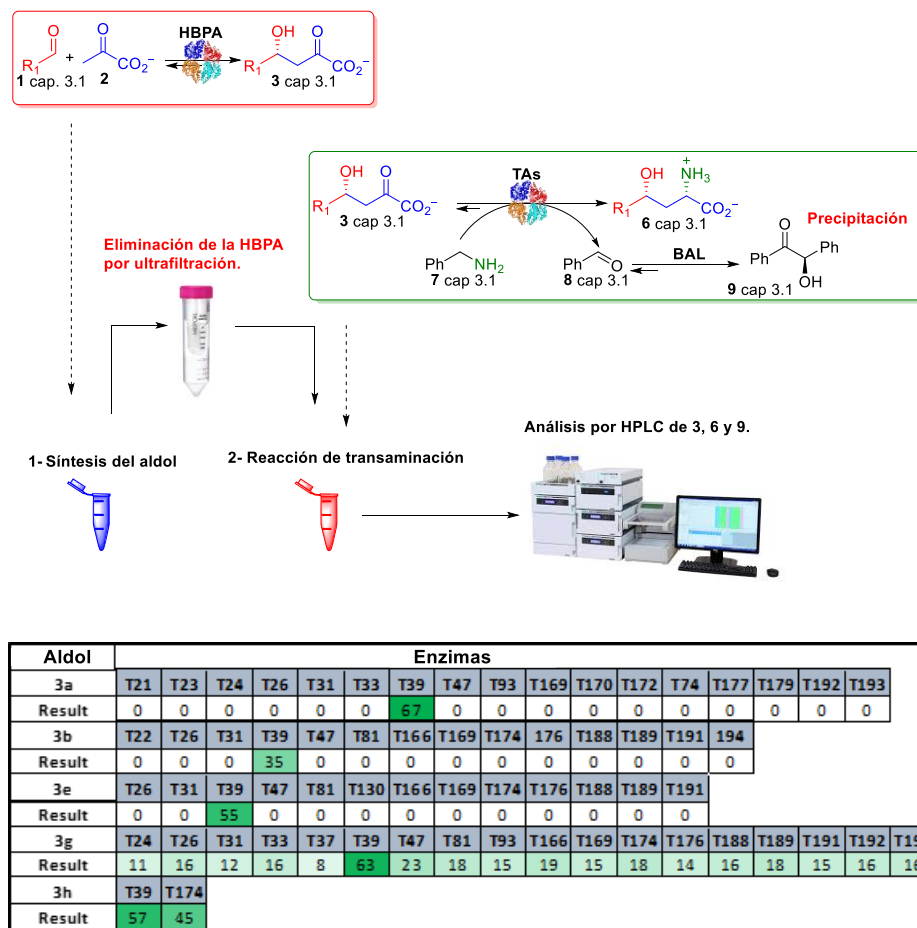


**Figura 4.18.** Segunda ronda de selección de enzimas TAs de Prozomix (27 candidatas del análisis anterior). Se muestra la conversión de la reacción teniendo considerando el aducto aldólico consumido (**3**, cap. 3.1), el producto transaminado formado (**6**, cap. 3.1) y la (*R*)-benzoína formada (**9**, cap. 3.1).

Adicionalmente al estudio del panel de transaminasas de Prozomix se trabajó con la aminotransferasa de  $\alpha$ -aminoácidos de cadena ramificada (BCAT) de *E. coli* puesto que los productos formados (**6**, cap. 3.1) son derivados de  $\alpha$ -aminoácido. Esta enzima utiliza L-Glu (**10**, cap. 3.1) como dador de grupo amino (**Figura 4.19**). En la reacción se genera 2-oxoglutarato (**11**, cap. 3.1), que es inhibidor de la enzima.<sup>11</sup> Por lo tanto, es necesario utilizar cantidades sub-estequiométricas de **10** y un sistema de regeneración utilizando la

aspartato aminotransferasa (AspTA) de *E. coli*. Esta segunda enzima utiliza L-Asp (**12** cap. 3.1) como sustrato dador de grupo amino, generando oxaloacetato (**13** cap. 3.1), el cual se descarboxila espontáneamente contribuyendo a desplazar el equilibrio de la reacción<sup>11</sup> de transaminación hacia la formación del  $\gamma$ -hidroxi- $\alpha$ -aminoácidos (**6** cap. 3.1).

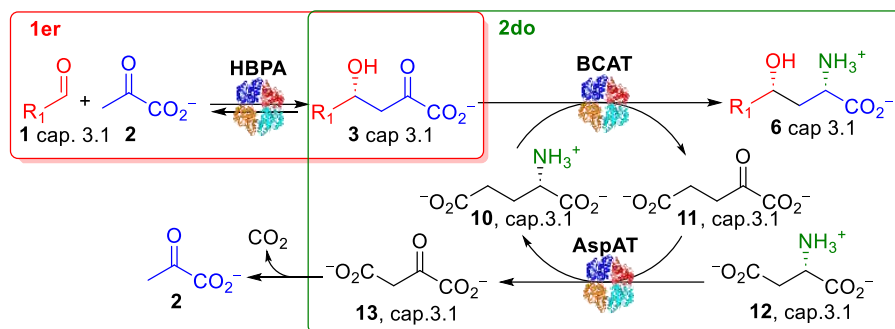
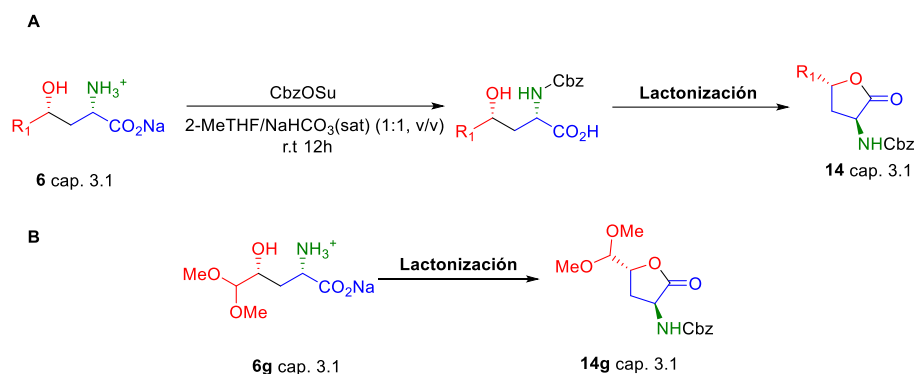


**Figura 4.19.** Síntesis estereoselectiva en dos pasos de  $\gamma$ -hidroxi- $\alpha$ -aminoácidos (**6**) del cap. 3.1, utilizando L-Glu (**10**) como dador de grupo amino. El 2-oxoglutarato (**11**) formado fue transaminado a L-Glu por la AspTA usando L-Asp (**12**) como segundo dador de grupo amino. El oxaloacetato (**13**) formado se descompone en CO<sub>2</sub> y piruvato desplazando el equilibrio de la transaminación hacia el  $\gamma$ -hidroxi- $\alpha$ -aminoácidos.

Es importante mencionar que a pesar de que se libera piruvato debido a la descarboxilación de **13**, los intentos de llevar a cabo la reacción con reciclaje de piruvato en un sistema enzimático en cascada cíclica fueron infructuosos. No se logró obtener los correspondientes  $\gamma$ -hidroxi- $\alpha$ -aminoácidos (**6**, cap. 3.1) dándose una disminución del aldehído (**1**, cap. 3.1) acumulación del aldol (**3**, cap. 3.1) pero sin la formación del producto aminado (**6**, cap. 3.1), (**Figura S25** materiales y métodos cap. 3.1) Sin embargo, cuando se utilizó el sistema enzimático HBPA/BCAT/AspTA en una secuencia de dos etapas enzimáticas se logró la transaminación de la mayoría de los aldoles estudiados. Este sistema permitió transaminar el aldol **3k** (cap.3.1) que no fue sustrato para la T39. Sin embargo, el aducto aldólico **3n** (cap.3.1) no fue transaminado por el sistema BCAT/AspTA y si por la T39 por lo que ambas estrategias de transaminación son complementarias.

La síntesis de los  $\gamma$ -hidroxi- $\alpha$ -aminoácidos **6** del cap. 3.1, se llevó a cabo con el mejor sistema de enzimático encontrado (HBPA/T039 o HBPA/BCAT/AspTA) para cada sustrato. Para el aislamiento y purificación de los productos se escogió como estrategia proteger el grupo amino con el grupo Cbz y posteriormente lactonizar intramolecularmente el  $\gamma$ -hidroxi- $\alpha$ -aminoácido *N*-protegido utilizando la esterificación

de Steglich (**Figura 4.20A**).<sup>12</sup> El  $\gamma$ -hidroxi- $\alpha$ -aminoácido **6g** (cap. 3.1) se utilizó para optimizar las condiciones de lactonización intramolecular (**Figura 4.20B**).



**Procedimiento 1:** EDAC (1,5eq), DMAP (0,03 eq), DMF 60 mL 4°C a r.t 16h

**Procedimiento 2:** EDAC (1,5eq), HOBt, (1,5 eq), DMF 60 mL 4°C a r.t 16h

**Procedimiento 3:** EDAC (1,5eq), HOBt, (1,5 eq), Et<sub>3</sub>N (2,0 eq), CH<sub>2</sub>Cl<sub>2</sub> 60 mL 4°C a r.t 16h

Procedimiento	Conversión Aldólica/(%) <sup>a</sup>	Conversión Transaminación/(%) <sup>b</sup>	Rendimiento (%) <sup>c</sup>	[ $\alpha$ ] <sup>d</sup>
1	80	98	27	- 20
2	86	90	35	- 21
3	87	94	52	- 20

<sup>a</sup> Conversión reacción aldólica (24 h) determinada por HPLC (**3g** cap. 3.1). <sup>b</sup>

Conversión reacción de transaminación (24 h) determinada por HPLC (**6g** cap. 3.1).

<sup>c</sup>Rendimiento de producto aislado (**14g** cap. 3.1). <sup>d</sup>c=1 in CHCl<sub>3</sub>.

**Figura 4.20.** Los  $\gamma$ -hidroxi- $\alpha$ -aminoácidos fueron aislados y purificados como lactonas *N*-protegidas (**14** cap 3.1). **A.** Estrategia general seguida en la síntesis de lactonas derivadas de  $\gamma$ -hidroxi- $\alpha$ -aminoácido. **B.** Efecto de las condiciones de lactonización intramolecular sobre el rendimiento de producto aislado y la estereoquímica del producto final. Se utilizó a **6g** (cap. 3.1) para estudiar diferentes condiciones de reacción.

Para el procedimiento 1, se utilizó como base la 4-dimetilaminopiridina (DMAP) en cantidades catalíticas para acelerar la esterificación intramolecular tratando de disminuir la reorganización de la *O*-acilisourea intermediaria hacia la *N*-acilurea, sin embargo, el rendimiento del producto aislado fue del 27% (**Figura 4.20B**). Para mejorar el rendimiento en la reacción de lactonización se ensayaron otras condiciones donde se incluyó hidroxibenzotriazol (HOBt) y un exceso de base (Et<sub>3</sub>N) lográndose mejorar los rendimientos de la lactona aislada hasta un 52% (**Figura 4.20B**, procedimiento 3). A pesar del riesgo de racemización que supone el uso de bases en las reacciones de  $\alpha$ -aminoácidos con carbodiimidas<sup>12b</sup>, no se observó variaciones en la rotación óptica de las

lactonas en las condiciones de reacción ensayadas (**Figura 4.20B**) por lo que se asumió que no se afectaba la integridad del centro estereogénico originado durante la reacción de transaminación.

Utilizando el procedimiento 3 se sintetizaron los correspondientes derivados de  $\gamma$ -butirolactonas (**14**, cap. 3.1 **Figura 4.21**). La configuración  $2S,4R$  esperada se confirmó mediante el análisis por RMN, aprovechando la estructura cíclica de los productos **14** (cap.3.1) y la estereoquímica del centro quiral originando en la reacción aldólica que se había determinado previamente. Las excepciones fueron los productos **6n** y **6o** (cap. 3.1), en estos casos la reacción de adición aldólica no fue estereoselectiva originándose una mezcla de diastereoisómeros ( $5R/S$ )-**14n** y ( $5R/S$ )-**14o**, respectivamente como productos finales.

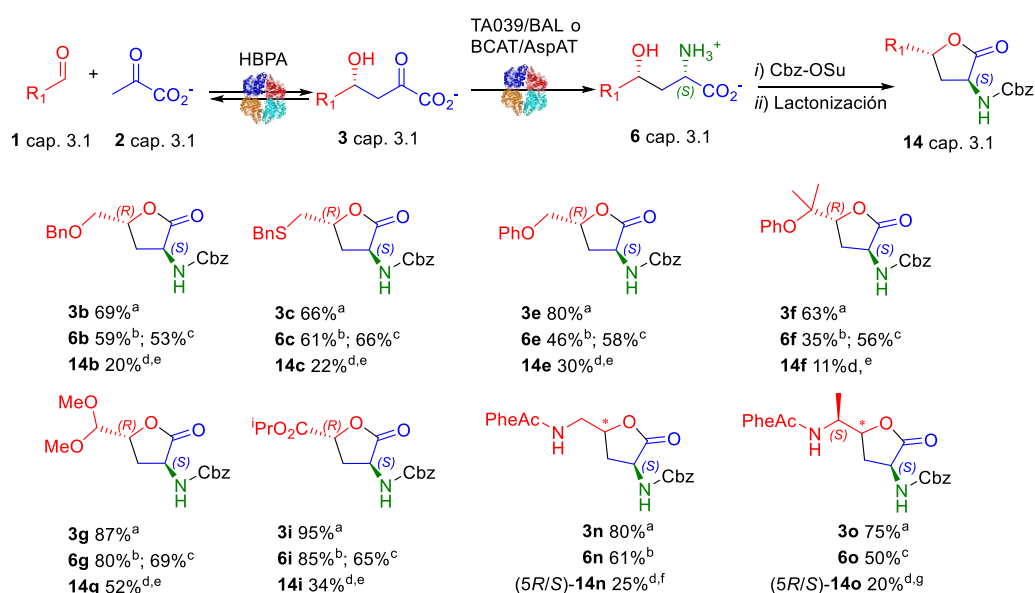


**Figura 4.21.** Síntesis de las  $\gamma$ -butirolactonas (**14**, cap. 3.1) derivadas de  $\gamma$ -hidroxi- $\alpha$ -aminoácidos. <sup>a</sup>Conversión reacción aldólica (24 h) determinada por HPLC. <sup>b</sup>Conversión de la reacción de transaminación (24 h) determinada por HPLC. Sistema T039/BAL. <sup>c</sup>Conversión de la reacción de transaminación (24 h) determinada por HPLC. Sistema BCAT/AspTA. <sup>d</sup>Rendimiento de producto aislado. <sup>e</sup>dr >95:5 determinado por RMN. <sup>f</sup>dr 50:50 determinado por RMN; <sup>g</sup>dr 60:40 ( $S$ : $R$ ) determinado por RMN.

La configuración del centro estereogénico de los productos aldólicos **3c**, **3n-o**, cap. 3.1 se determinó a partir de las estereoquímicas de las correspondientes lactonas finales conociendo el comportamiento estereoquímicos de las reacciones de transaminación (**Figura 3.4.20**). La estereoquímica del producto aldólico **3k**, cap. 3.1 se determinó también de manera indirecta, pero en este caso después de la reacción de transaminación



se obtuvo el derivado de (2*S*,4*R*)-4-hydroxyproline **15k** cap. 3.1, al darse una reacción de sustitución nucleofílica intramolecular después de la incorporación del grupo amino (**Figura 4.22**).

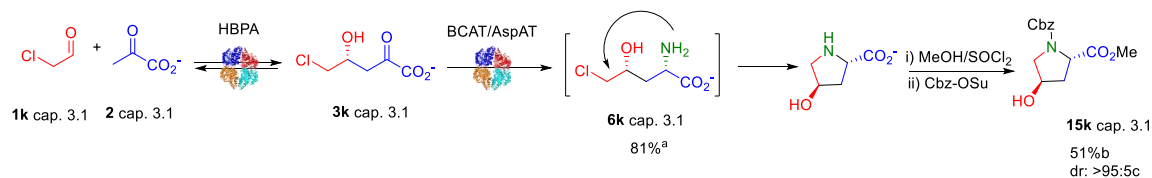


**Figura 4.22.** Síntesis de (2*S*,4*R*)-4-hydroxyproline a partir del aldol **3k**, cap.3.1.<sup>a</sup>Conversión de la reacción de transaminación (24 h) determinada por HPLC. <sup>b</sup>Rendimiento de producto aislado. <sup>c</sup>La caracterización estereoquímica de **15k**, cap. 3.1 se realizó inequívocamente por HPLC con fase estacionaria quiral utilizando los diastereómeros comercialmente disponibles de la hidroxiprolina.

La ventaja de utilizar el grupo protector Cbz es que puede ser eliminado fácilmente bajo hidrogenación catalítica. Así, se obtuvo **16a** (cap. 3.1) con un 59% de rendimiento de producto aislado a partir de **14b**, cap. 3.1 (**Figura 4.23A**). Por su parte, el grupo protector PheAc de las lactonas (5*R*/*S*-**14n** y **14o**) se eliminó mediante hidrólisis enzimática catalizada por la penicilina G acilasa (PGA, EC 3.5.1.11, Roche diagnostics GmbH, Mannheim, donada a nuestro grupo de investigación por el Prof. Wolf-Dieter Fessner de la Universidad de Darmstadt), obteniéndose los aminoácidos **18n**, cap. 3.1 y **18o**, cap. 3.1 con rendimientos de producto aislado de 60 y 81% respectivamente (**Figura 4.23B**).

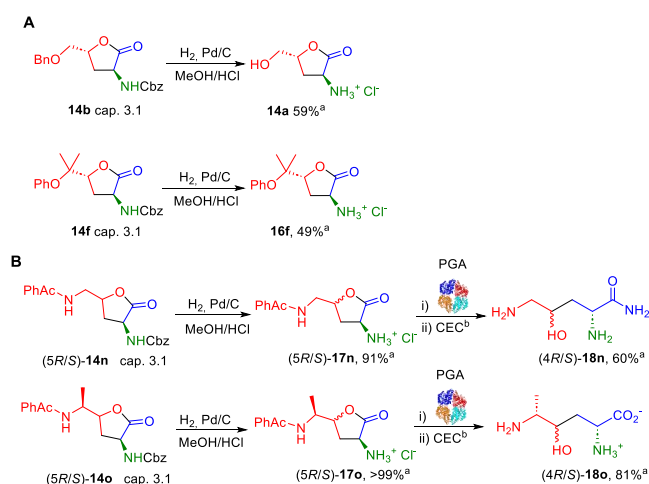


**Figura 4.23.** Eliminación de los grupos protectores de aminos de las  $\gamma$ -butirolactonas **14**, cap. 3.1. **A.** Hidrogenación catalítica. **B.** Desprotección quimio-enzimática: hidrogenación catalítica e hidrólisis enzimática catalizada por la PGA. <sup>a</sup>Rendimiento de producto aislado. <sup>b</sup>Cromatografía de intercambio catiónico (CEC). Macro-Prep<sup>®</sup> High S Media (BioRad), condiciones de elusión:  $\text{NH}_4\text{OH}$  (1M).

### Estudios de sistemas multienzimáticos aldolasa-deshidrogenasa.

La DpkA de *Pseudomonas syringae* pv. Tomato DSM 50315 se describió como una imino reductasa que cataliza la reducción de iminas cíclicas como el  $\Delta^1$ -Piperideine-2-carboxilato y el  $\Delta^1$ -pirroline-2-carboxilato formando L-pipecolato y L-prolina, respectivamente (**Figura 4.24A**).<sup>13</sup> Sin embargo, en nuestro laboratorio nos percatamos que esta enzima era capaz de reducir grupos carbonilos de 2-oxoácidos como el piruvato. Por lo que decidimos estudiar esta actividad promiscua de la enzima y aplicarla en síntesis orgánica (**Figura 4.24B**).

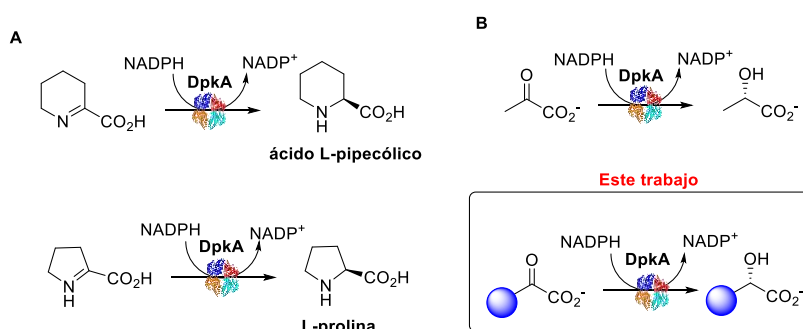


**Figura 4.24.** Reacciones enzimáticas catalizadas por la DpkA. **A.** Actividad natural de la enzima como imino-reductasa. **B.** Actividad promiscua como ceto-reductasa sobre la que se centrará este trabajo.

Otra de las deshidrogenasas estudiada en esta Tesis es la 2-dehidropantoate 2-reductasa de *E coli*. (KPR). Esta enzima cataliza la reducción estereoselectiva del cetopantoato (4-hidroxi-3,3-dimetil-2-oxobutanoato) para formar (*R*)-pantoato ((*R*)-2,4-dihidroxi-3,3-dimetilbutanoato) (**Figura 4.25A**). La elevada estereoselectividad del biocatalizador en su reacción natural y el hecho de no existir ningún reporte sobre su aplicación en biocatálisis no hizo plantearnos la tarea de estudiar sus potenciales aplicaciones en síntesis orgánica (**Figura 4.25B**).

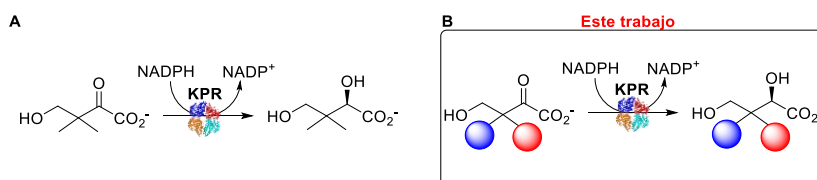


**Figura 4.25.** Reacciones enzimáticas catalizadas por la KPR. **A.** Actividad natural de la enzima con el cetopantoato. **B.** Actividad promiscua sobre análogos del sustrato natural sobre la que se centrará este trabajo.

En una estrategia biocatalítica de dos reacciones enzimáticas consecutivas se evaluó la reducción catalizada por la DpkA de los aductos aldólicos generados por la adición aldólica de piruvato a aldehídos alifáticos catalizados por HBPA (se escogieron las reacciones con mejores ee). Los 2-hidroxiácidos (**7** del cap. 3.2) sintetizados se aislaron como lactonas al sufrir una esterificación intramolecular en las condiciones ácidas generadas durante la purificación. Los derivados de 2-hidroxi-4-butirolactonas (**8** del cap. 3.2) se obtuvieron con rendimientos de productos aislados entre 27 y 34% y relación diastereomérica desde 87:13 hasta 98:2 (**Figura 4.26**). Los aldoles generados por la HBPA fueron ensayados como sustratos de la KPR, pero no se detectó la formación del producto reducido.

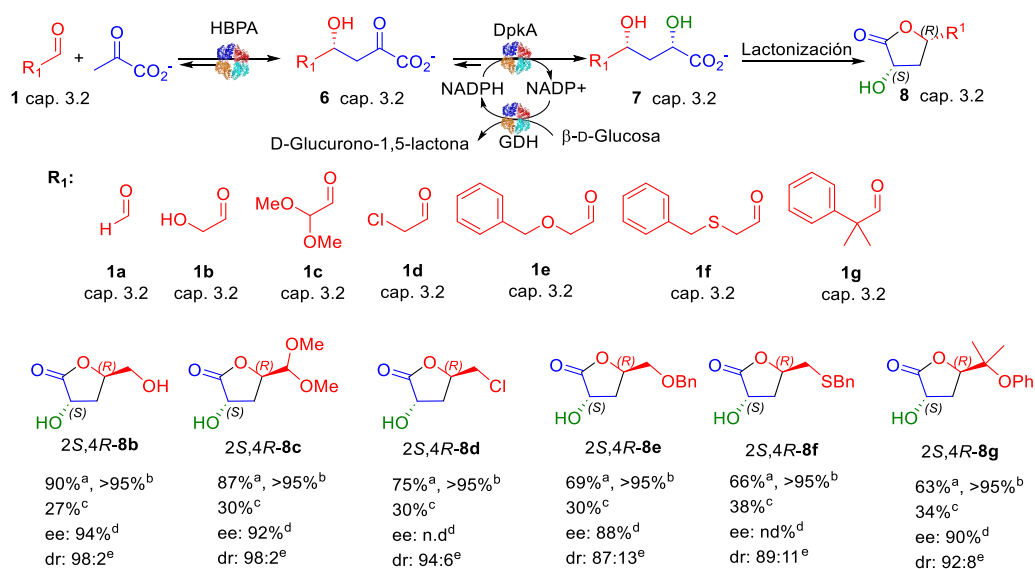


**Figura 4.26.** Síntesis biocatalítica multienzimática de derivados de 2-hidroxi-4-butirolactonas **8** (cap. 3.2), catalizados por la HBPA y la deshidrogenasa DpkA. <sup>a</sup>Conversión reacción aldólica (24 h) determinada por HPLC. <sup>b</sup>Conversión reacción de reducción (24 h) determinada por HPLC. <sup>c</sup>Rendimientos de producto aislados. <sup>d</sup>Exceso enantiomérico de la reacción aldólica determinado anteriormente por HPLC en fase estacionaria quiral. <sup>e</sup>Relación diastereomérica determinada por RMN.

Así mismo, la deshidrogenasa DpkA fue capaz de aceptar como sustratos los derivados del ácido (*E*)-2-oxo-4-arilbut-3-enoico, producto de las condensaciones aldólicas entre piruvato y aldehídos aromáticos catalizado por la HBPA (**Figura 4.27**). Sin embargo, los aldehídos (**1n-p**, cap. 3.3) no fueron transformados por el sistema HBPA/DpkA probablemente debido a que estos aldehídos aromáticos son malos sustratos para la aldolasa y la DpkA reduce irreversiblemente al piruvato antes de que este pueda participar en la reacción de condensación aldólica catalizado por la HBPA (**Figura 4.27**). A estos

resultados hay que añadir que ninguno de los productos de condensación entre el piruvato y aldehídos aromáticos (**3** cap. 3.3) fue sustrato de la KPR.

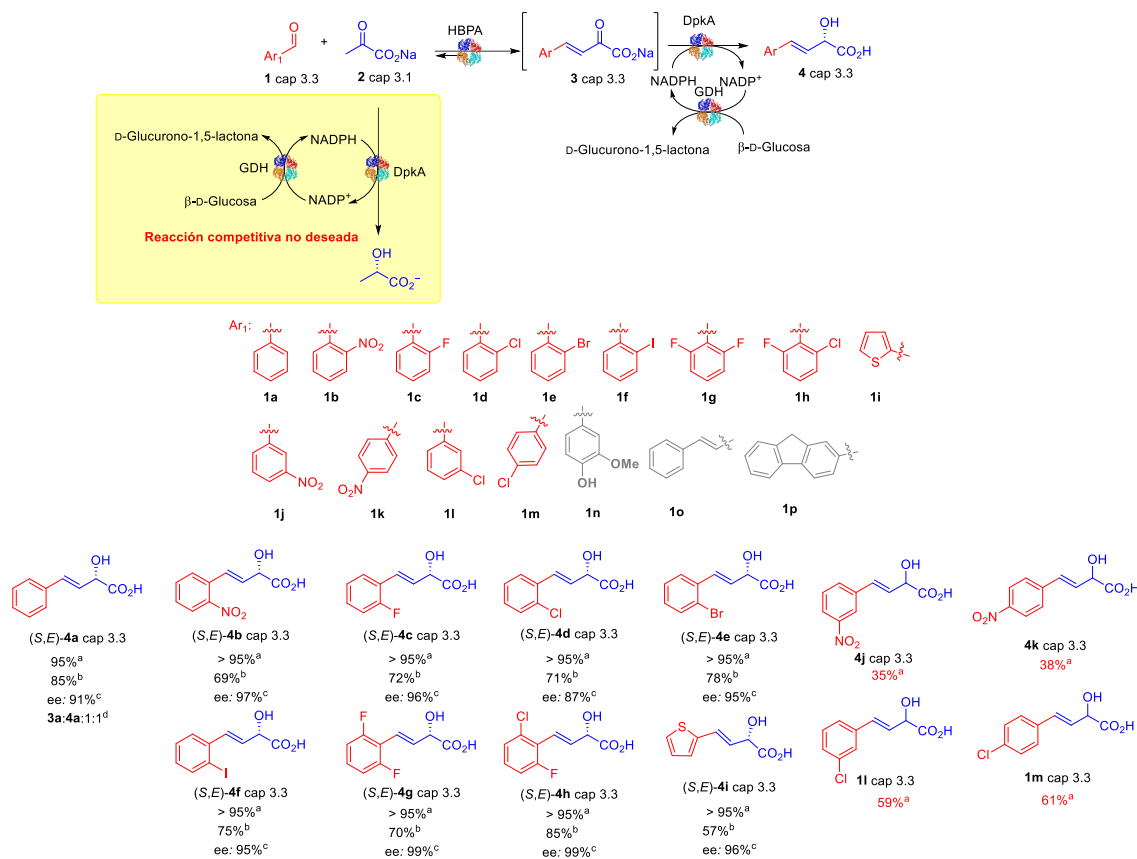


**Figura 4.27.** Sistema enzimático acoplado entre la HBPA y la DpkA en la síntesis de derivados del ácido (*S,E*)-2-hidroxi-4-arilbut-3-enoico (**4**, cap. 3.3). <sup>a</sup>Conversión de la reacción de reducción (24h) determinado por HPLC. No se detectó material de partida ni productos de condensación aldólica. <sup>b</sup>Rendimientos aislados. <sup>c</sup>Exceso enantiomérico de la reducción determinado por HPLC con fase estacionaria quiral. Las mezclas racémicas se obtuvieron por reducción de **3** cap 3.3 con NaBH<sub>4</sub>/CeCl<sub>3</sub>.<sup>14</sup> <sup>d</sup>Se obtuvo mezcla de **3a** y **4a** después de la purificación. La relación **3a:4a** se determinó por RMN. Los productos **4j**, **k** y **4l**, **m** no fueron aislados.

La DpkA toleró sustratos con sustituciones voluminosas en las posiciones 2 y 6 del anillo aromático (**3b**, **d-h**, cap. 3.3) y heterociclos como el tiofeno (**3i**, cap. 3.3). Sin embargo, La conversión fue incompleta con grupos aril o con sustituyentes en otras posiciones del anillo aromático (p. ej. **3j-m**, cap. 3.3). En esta cascada enzimática la enzima mostró excelentes niveles de enantioselectividad para **4b-c**, **e-i** (cap. 3.3) (95-99% ee), y buenos para **4d** (cap. 3.3) (87% ee) (**Figura 4.27**).

La estereoquímica absoluta de la catálisis con DpkA se determinó por difracción de rayos X de monocristal de los compuestos **4c-f** (cap. 3.3). El análisis se llevó a cabo en colaboración con el Dr. Dieter Schollmeyer, del Instituto de Química Orgánica, Universidad Gutenberg de Mainz, Alemania. Los análisis, indicaron que la DpkA genera 2-hidroxiácidos mayoritariamente con configuración *S* (**Figura 4.28**).

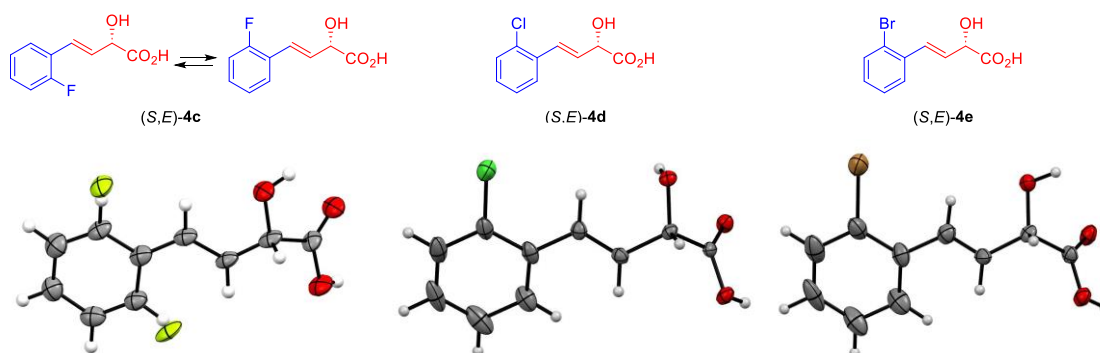


**Figura 4.28.** Estructuras de rayos X de (S,E)-**4c**, (S,E)-**4d** y (S,E)-**4e** del cap. 3.3. Se representan los gráficos de tipo ORTEP que muestran una molécula con elipsoides de probabilidad del 50%. Los datos cristalográficos fueron depositados en: Cambridge Crystallographic Data Centre a través de [www.ccdc.cam.ac.uk/data\\_request/cif](http://www.ccdc.cam.ac.uk/data_request/cif).

Además de la HBPA, en nuestro grupo de investigación se tiene una amplia experiencia en el trabajo con otras piruvato aldolasas como la YfaU y la KPHMT ambas de *E. coli*. Estas enzimas son estereocomplementarias y son estereoselectivas en la adición aldólica de 2-oxoácidos a formaldehído,<sup>2f,15</sup> por lo que se diseñaron sistemas multienzimáticos combinando estas aldolasas con la DpkA o la KPR (**Figura 4.29**).

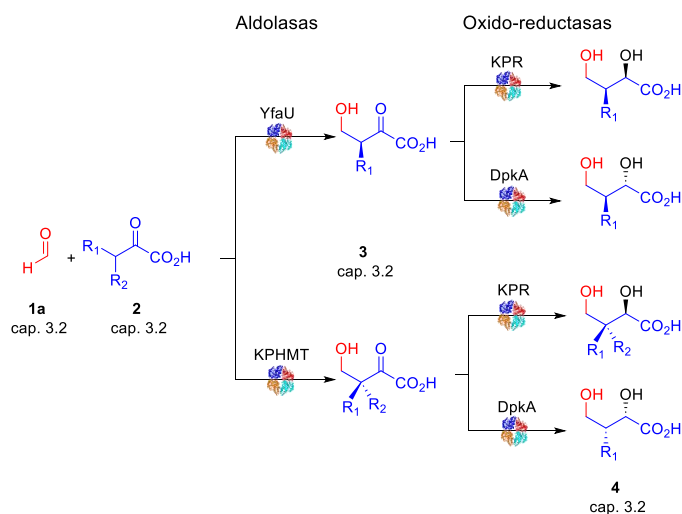


**Figura 4.29.** Estrategia general de síntesis biocatalítica consecutiva de 2-hidroxiácidos (**4** cap. 3.2).

A partir de la adición aldólica de 2-oxoácidos (**2a-n**, cap. 3.2) a formaldehído (**1a**, cap. 3.2) se generaron los 4-hidroxi-2-oxoácidos (**3a-n**, cap. 3.2) catalizadas por las aldolasas de Clase II, la KPHMT y YfaU. Terminada la reacción aldólica (máxima formación de producto aldólico) se inactivaron las enzimas con EDTA para prevenir la retro-aldólisis favorecida por la reducción irreversible del 2-oxoácido catalizado por las deshidrogenasas. Posteriormente, se inició la reducción biocatalítica incorporando las oxido-reductasas (DpkA o KPR). Los 2-hidroxiácidos (**4**, cap. 3.2) se purificaron primeramente por cromatografía de intercambio aniónico (CIA) y se sometieron a un proceso de liofilización en medio ácido, lo que favoreció la esterificación intramolecular formando derivados de 2-hidroxi-4-butirolactonas que finalmente fueron purificadas por sílica (**5a-n**, cap. 3.2. **Figura 4.30**).

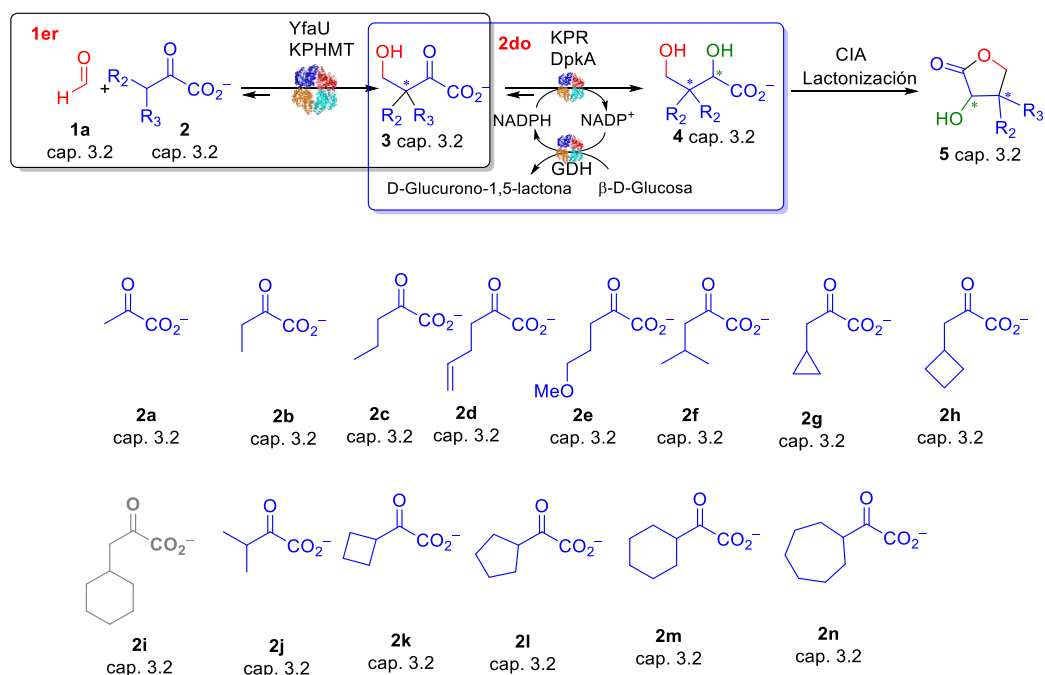


**Figura 4.30.** Estrategia de síntesis biocatalítica de 2-hidroxi-4-butirolactonas (**5a-n**, cap. 3.2). **1er**. Adición aldólica catalizada por YfaU o KPHMT. **2do**. Reducción enzimática catalizada por KPR o DpkA. **CIA**: Cromatografía de intercambio aniónico (DOWEX 1X8). Elusión: HCO<sub>2</sub>H 1M.

Los 2-oxoácidos **2d-e**, **2g-i**, **2k-n** (capítulo 3.2) fueron sintetizados siguiendo las estrategias descritas en trabajos previos de nuestro grupo de investigación (**Figura 4.31**).<sup>2f,15</sup> A partir de los 2-oxoácidos se prepararon soluciones acuosas a pH 7,0 para

hacerlos compatibles con las actividades de las aldolasas (Tabla S1 materiales y métodos cap. 3.2).

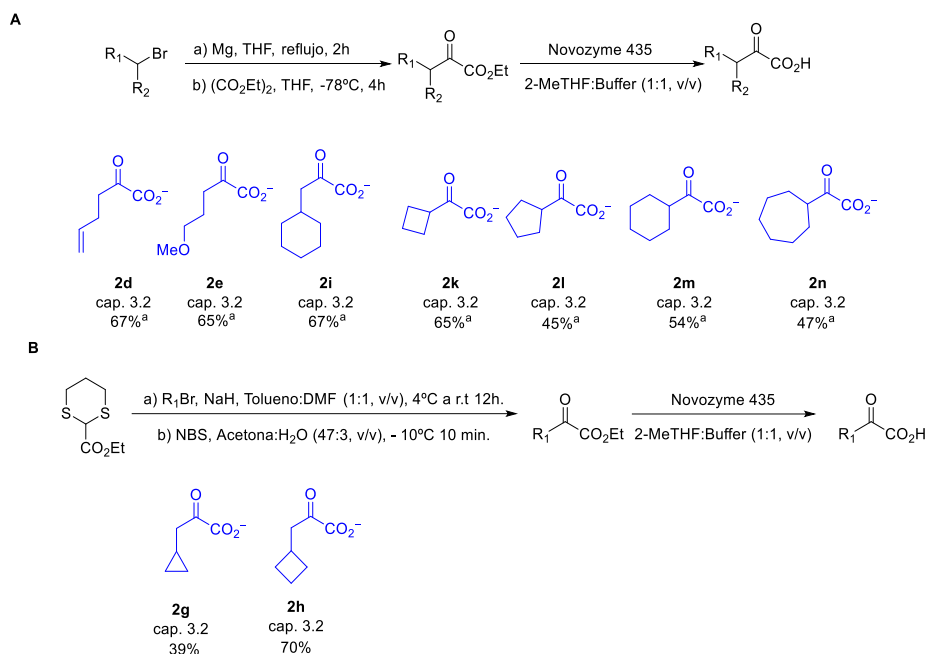


**Figura 4.31.** Estrategias de síntesis de los 2-oxoácidos **2d-e**, **2g-i**, **2k-n** (capítulo 3.2) utilizados como sustratos en esta Tesis. **A.** Síntesis de los compuestos **2d-e**, **2i**, **2k-n** (capítulo 3.2) a partir de la adición del correspondiente magnesiano al oxalato de etilo y posterior hidrólisis enzimática del éster. **B.** Síntesis de los compuestos **2g**, **h** a través de la alquilación del 1,3-ditiano-2-carboxilato de etilo utilizando el correspondiente bromuro de alquilo, seguido de la ruptura oxidativa del ditiano con N-bromosuccinimida (NBS) y posterior hidrólisis enzimática del 2-oxoéster.<sup>16-17</sup>

Las diferentes combinaciones de lactonas sintetizadas se muestran en la **Figura 4.32**. Para todos los sustratos estudiados las deshidrogenasas resultaron ser biocatalizadores estereocomplementarios, así, la DpkA origina estereoquímica *S*, mientras que KPR estereoquímica *R*. Sin embargo, la actividad de la DpkA disminuyó a medida que se incrementó el tamaño del sustituyente en posición 3 sin importar la estereoquímica de este centro (la enzima solo tolera un grupo metilo y etilo en esta posición, **Figura 4.32B y D**).

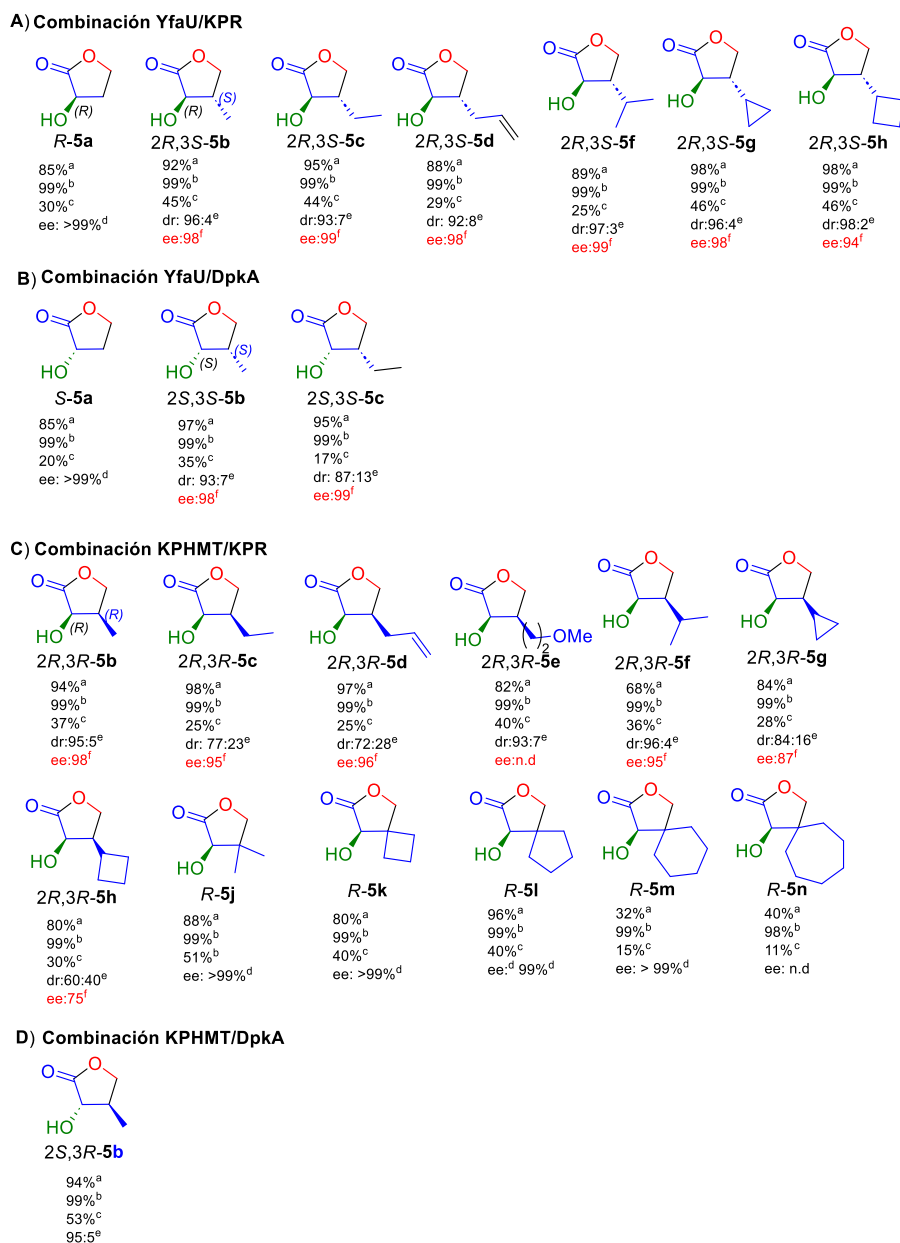


**Figura 4.32.** Síntesis biocatalítica en dos etapas enzimáticas (Aldolasa-deshidrogenasa) de 3-hidroxi-4-butirolactonas (**5**, cap. 3.2). **A.** YfaU y KPR, **B.** YfaU o DpkA, **C.** KPHMT y KPR y **D.** KPHMT y DpkA. <sup>a</sup>Conversión de la reacción de adición aldólica (24h) determinado por HPLC. <sup>b</sup>Conversión de la reacción de reducción enzimática (24h) determinado por HPLC. <sup>c</sup>Rendimiento de producto aislado. <sup>d</sup>Exceso enantiomérico de la reacción de reducción determinado por HPLC en fase estacionaria quiral. <sup>e</sup>Relación diastereomérica determinada por RMN. <sup>f</sup>Exceso enantiomérico de la reacción de adición aldólica determinado por HPLC en fase estacionaria quiral en trabajos previos. n.d: no determinado.

Por otro lado, la KPR mostró una amplia tolerancia a los sustratos, incluidos los 4-hidroxi-2-oxoácidos con centros cuaternarios (**3k-n**, cap. 3.2) análogos al sustrato natural de la enzima (**3j**, cap. 3.2). Una excepción fue **3i** que no fue sustrato de la enzima. Para las lactonas con un sólo estereocentro (**R-5a**, **S-5a**, **R-5j-n**) ambas enzimas muestran ee >



99% demostrando la elevada estereoselectividad de los biocatalizadores; para el resto de productos las relaciones diastereoméricas pueden verse comprometidas por la estereoselectividad de las aldolasas<sup>2f</sup> (**Figura 4.32**). De manera general los bajos rendimientos observados en la mayoría de las combinaciones enzimáticas empleadas pueden deberse a la eficacia de la lactonización durante la liofilización y la etapa de purificación adicional que fue necesario realizar.

Adicionalmente, fue posible combinar las aldolasas y las deshidrogenasas en un sistema en cascada enzimática concurrente. Esta estrategia permitió la síntesis de los enantiómeros del 2-hidroxi-4-butirolactona (*R*-**5a** y *S*-**5** cap. 3.2) y los cuatro estereoisómeros de 3-metil-2-hidroxi-4-butirolactona (*2R,3S*-**5b**, *2S,3S*-**5b**, *2R,3R*-**5b** y *2S,3R*-**5b**, cap. 3.2) con rendimientos de productos aislados entre 20 y 57% (**Figura 4.33**).

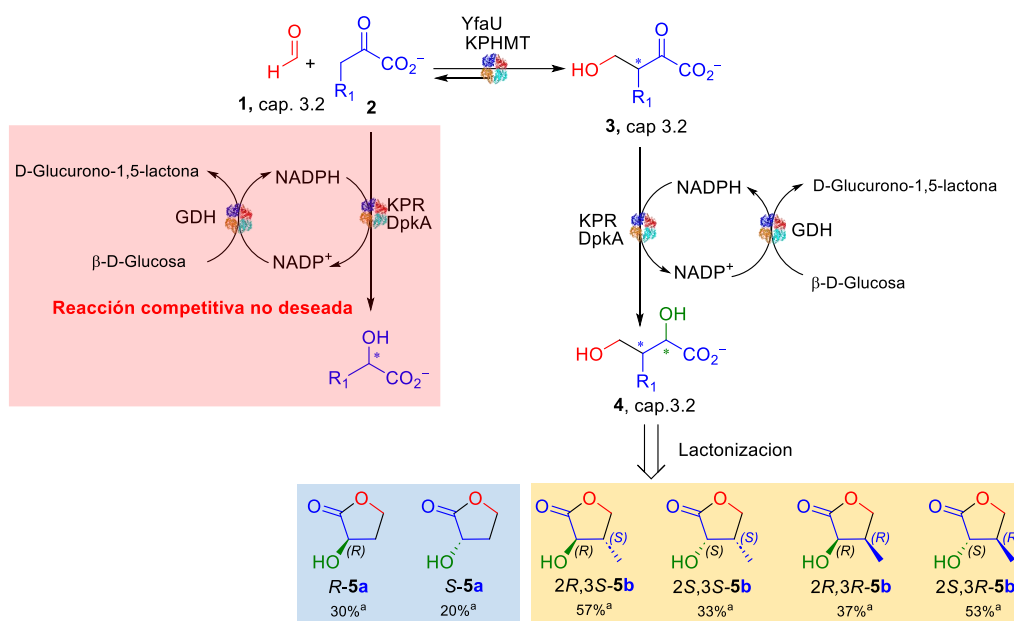


**Figura 4.33.** Síntesis biocatalítica en cascada de los enantiómeros de la 2-hidroxi-4-butirolactona **5a**, y los estereoisómeros de la 3-metil-2-hidroxi-4-butirolactonas **5b**.<sup>a</sup>Rendimiento de producto aislado.

Con el resto de los 2-oxoácidos ensayados los resultados fueron infructuosos, no observándose disminución simultánea del material de partida. Es decir, no se apreció consumo de formaldehído (**1**) mientras que el 2-oxoácido (**2**) de partida se consumía. Esto indicaba su reducción por la deshidrogenasa, hecho que se corroboró con experimentos controles de reducción de cetoácido aislado. El consumo del 2-oxoácido por las deshidrogenasas compromete el rendimiento de la reacción aldólica cuando el 2-oxoácido

no es un buen sustrato para la aldolasa. En otras palabras, se establece una competencia entre los 2-oxoácidos presentes en el sistema: el sustrato de la reacción aldólica y su producto por la reducción. El balance entre las velocidades de estos dos procesos de reducción es la que determina la eficiencia del sistema enzimático en cascada. Esto lo corroboramos en varios experimentos donde detectamos el consumo de **2** por HPLC sin que se afectara al formaldehído presente en el sistema.

Respecto a la estereoquímica de estas reacciones, de trabajos previos de nuestro grupo de investigación, la adición aldólica de 2-oxoácidos a formaldehído catalizada por MBP-YfaU nativa y la variante W23V, así como, para la KPHMT nativa y sus variantes I202A y I212A conocemos que la síntesis procedía con elevada estereoselectividad y que por tanto los compuestos **5b-h** (cap. 3.2) contienen un centro quiral con estereoquímica absoluta conocida (*R* para MBP-YfaU nativa y variantes y *S* KPHMT nativa y sus variantes).<sup>2f</sup> Este centro quiral se utilizó como referencia para la evaluación de la configuración relativa global de estos compuestos mediante RMN. En esta Tesis inferimos un resultado estereoquímico idéntico para el aldol **3e** (cap. 3.2) que no se había descrito previamente para la KPHMT I212A

La configuración absoluta de *R-5a*, *S-5a* y *R-5j* se confirmó comparando sus valores de rotación específica con las de muestras comerciales auténticas. Por otra parte, el compuesto *R-5l* del cap. 3.2 fue analizado con difracción de rayos X. Los análisis indicaron que la estereoquímica absoluta en C3 procedente de la reducción de la KPR era *R* (**Figura 4.34**). De estos resultados se infirió la estereoquímica absoluta de *R-5k*, *R-5m* y *R-5n* del cap. 3.2.

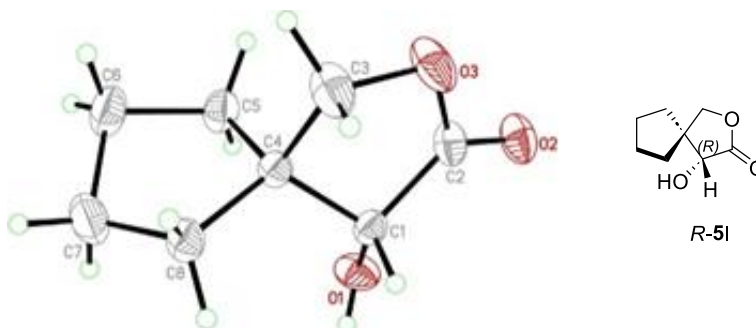


**Figura 4.34.** Estructura de rayos X de *R-5l*, cap. 3.2. Gráfico de tipo ORTEP que muestra una molécula con elipsoides de probabilidad del 50%. Los datos pueden obtenerse gratuitamente en: Cambridge Crystallographic Data Centre a través de [www.ccdc.cam.ac.uk/data\\_request/cif](http://www.ccdc.cam.ac.uk/data_request/cif).

El análisis de los modelos moleculares de los complejos de ambas deshidrogenasas con los aldoles **3** (cap. 3.2) realizados por el Dr. Jordi Bujons proporcionó una explicación para estos resultados estereoquímicos descritos anteriormente.

Muchas enzimas moldean sus estructuras para mantener los sustratos en los centros activos durante la catálisis, de modo que puede ser necesaria una remodelación conformacional durante cada ciclo catalítico.<sup>18</sup> En este sentido, la KPR y la DpkA presentan dos posibles estados conformacionales: las formas abiertas y cerradas, cuya interconversión se desencadena por la unión del sustrato.<sup>13,19</sup> En las formas cerradas, los sustratos (**3**, cap. 3.2 y el NADPH) están enterrados en una cavidad profunda y relativamente estrecha (**Figura 4.35A** y **4.35B**, KPR y DpkA, respectivamente). En el caso de la KPR, el modelo de **3a** (cap. 3.2) unido en el centro activo de la enzima muestra que la conformación pre-reactiva del sustrato está estabilizada por múltiples interacciones de puentes de hidrógeno (**Figura 4.35C**), de este modo, el grupo 2-oxo expone su lado *si* a la fracción nicotinamida del cofactor NADPH, que entrega su hidrógeno pro-4*S* para dar lugar al correspondiente intermediario *2R-4a*, precursor de *2R-5a*, catalizado por la K176, lo que se correlaciona con el resultado *2R*-estereoquímico observado para sus productos reducidos por la KPR. El resto de los análisis se pueden ver materiales y métodos del capítulo 3.2 (Figura S69).

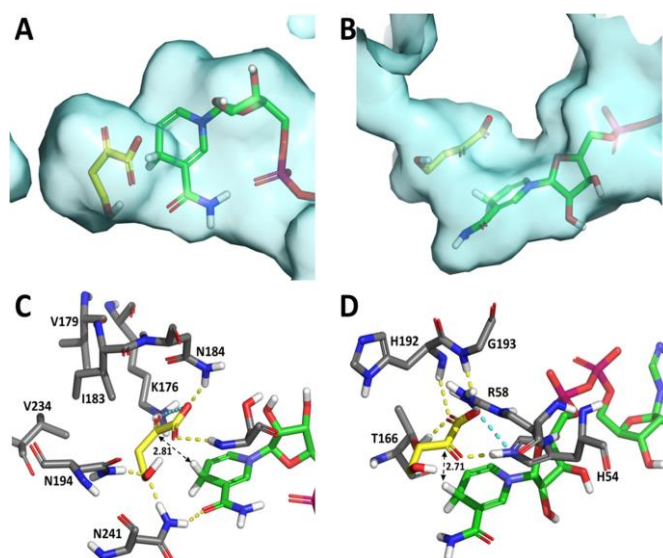


**Figura 4.35.** Modelos moleculares de **3a** (cap. 3.2) unido a la KPR (**A** y **C**) y DpkA (**B** y **D**). Los modelos se construyeron a partir de las estructuras PDB (2OFP)<sup>23</sup> (**A**) y (2CWH)<sup>13</sup> (**B**) y su estructura se optimizó mediante métodos QM/MM. El sustrato **3a**, el NADPH y los residuos cercanos se muestran con átomos C amarillos, verdes y grises; los enlaces H y los puentes salinos se muestran con líneas discontinuas amarillas y azules; la superficie proteica de las cavidades del centro activo se muestra en azul (**A** y **B**). Se muestran las distancias entre el átomo C del carbonilo reactivo y el hidrógeno pro-4*S* del NADPH (**C** y **D**).

Por otro lado, los modelos correspondientes con DpkA muestran que el grupo carboxilato de los sustratos acepta enlaces H de las cadenas laterales de R58 y T166, así como, de la porción-NH de H192 y la G193, (**Figura 4.35D** y **S69**, cap. 3.2). Además, el grupo 2-oxo acepta enlaces H desde el grupo 4-OH (intramolecular) y desde el imidazol protonado de H54, que actúa como residuo ácido en la catálisis. Este modo de unión al sustrato fuerza la exposición de la cara posterior del grupo 2-oxo al NADPH reducido, dando lugar a los productos 2*S*-**4**, precursores de las 2-hidroxi-4-butirolactonas 2*S*-**5**. El resto de los análisis con los otros sustratos se pueden ver materiales y métodos del capítulo 3.2 (**Figura S69**).

A manera de resumen podemos plantear que la DpkA muestra actividad promiscua hacia la reducción de 4-hidroxi-2-oxoácidos tolerando sustituyentes en la posición 4 y originando productos con estereoquímica *S*. Mientras que, la KPR, reduce 4-hidroxi-2-oxoácidos análogos a su sustrato natural mostrando tolerancia a una gran variedad de grupos en posición 3, pero, no es capaz de reducir 2-oxoácidos con sustituyentes en posición 4 ni sustratos conformacionalmente restringidos. Esta enzima durante la reducción origina productos con estereoquímica *R* (**Figura 4.36**).

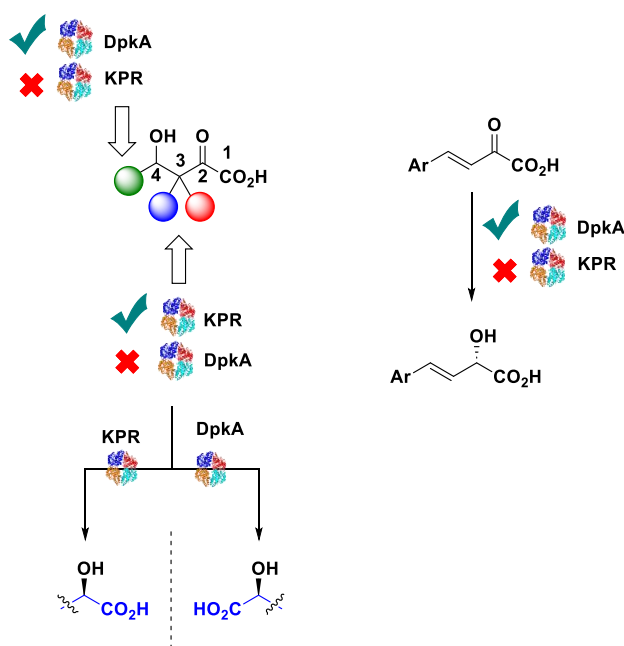


**Figura 4.36.** La DpkA muestra actividad promiscua hacia la reducción de 4-hidroxi-2-oxoácidos tolerando sustituyentes en la posición 4 mientras la KPR acepta una gran variedad de grupos en posición 3, pero no es capaz de reducir 2-oxoácidos con sustituyentes en posición 4 ni sustratos conformacionalmente restringidos. Ambas enzimas son estereocomplementarias.

### Estudio cinético de la DpkA y la KPR utilizando los 4-hydroxi-2-oxoácidos (3 y 6) sintetizados en este trabajo.

Para completar nuestro estudio con las deshidrogenasas se determinaron los parámetros cinéticos de las enzimas en la reducción de los 4-hydroxi-2-oxoácidos sintetizados en esta Tesis. En la literatura se ha reportado que la DpkA y la KPR presenta una cinética bisustrato ordenada (Bi-Bi ordenado de acuerdo a la nomenclatura planteada por Cleland (Figura 4.37).<sup>3,19-20</sup>

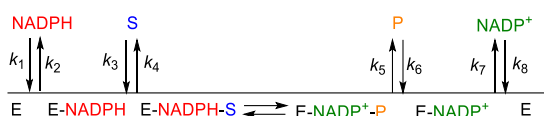


**Figura 4.37.** Notación de Cleland para representar el mecanismo Bi-Bi ordenado de una deshidrogenasa y ecuación de la velocidad inicial bajo un régimen de estado estacionario.<sup>3</sup>

$$V_0 = \frac{k_{\text{cat}}[E]_0[\text{NADPH}][\text{S}]}{K_{\text{NADPH}}K_{\text{S}} + K_{\text{S}}[\text{NADPH}] + K_{\text{NADPH}}[\text{S}] + [\text{NADPH}][\text{S}]}$$

$$k_{\text{cat}} = \frac{k_5 k_7}{k_5 + k_7} \quad K_{\text{NADPH}} = \frac{k_2}{k_1} \quad K_{\text{NADPH}} = \frac{k_5 k_7}{k_1(k_5 + k_7)} \quad K_{\text{S}} = \frac{k_7(k_4 + k_5)}{k_3(k_5 + k_7)}$$

Debido al número de sustratos utilizados en esta Tesis se decidió simplificar los ensayos enzimáticos utilizando una concentración fija de NADPH (0.16 mM) lo que permite reducir el sistema a la siguiente ecuación de velocidad inicial:

$$V_0 = \frac{k_{\text{cat}}^{\text{app}}[E]_0[\text{S}]}{K_{\text{m}}^{\text{app}} + [\text{S}]}$$

$$k_{\text{cat}}^{\text{app}} = k_{\text{cat}} \underbrace{\left[ \frac{[\text{NADPH}]}{K_{\text{NADPH}} + [\text{NADPH}]} \right]}_{\text{Constante}} \quad K_{\text{m}}^{\text{app}} = K_{\text{S}} \underbrace{\left[ \frac{K_{\text{NADPH}} + [\text{NADPH}]}{K_{\text{NADPH}} + [\text{NADPH}]} \right]}_{\text{Constante}}$$

Los ensayos enzimáticos se realizaron en experimentos continuos, monitorizando la oxidación del NADPH a NADP<sup>+</sup> a 340 nm (NADPH  $\epsilon_{340} = 6,22 \text{ mM}^{-1} \text{ cm}^{-1}$ ).<sup>21</sup> Con los sustratos **3a-1** (cap. 3.2) y **6b-c** (cap. 3.2). Para ello se sintetizaron los productos aldólicos con aldolasas específicas (Tabla 4.3). Terminada la reacción se eliminó el componente enzimático por ultrafiltración (Amicon Ultra-15 cut off 3 kDa) y el exceso de metal con EDTA, evitándose posibles interferencias durante los ensayos cinéticos.

**Tabla 4.3.** Aductos aldólicos utilizados como sustratos en los ensayos enzimáticos de la DpkA y la KPR. Los sustratos se utilizaron en solución después de remover la enzima y quelar el exceso de metal cuando se utilizó una aldolasa clase II.

Sustratos	Aldolasa	[S]/mM <sup>a</sup>	<i>r.e</i> <sup>b</sup> /%	
<b>3a</b>	YfaU nativa	85	- <sup>c</sup>	
<i>S-3b</i>	YfaU W23V	92	99:1	
<i>S-3c</i>		95	99,5:0,5	
<i>S-3d</i>		88	99:1	
<i>S-3f</i>		89	99,5:0,5	
<i>S-3g</i>		98	99:1	
<i>S-3h</i>		98	97:3	
<i>R-3b</i>		KPHMT nativa	94	97,5:2,5
<i>R-3c</i>		KPHMT nativa	98	97,5:2,5
<i>R-3d</i>	KPHMT I212A	97	98:2	
<i>R-3e</i>	KPHMT I212A	82	- <sup>d</sup>	
<i>R-3g</i>	KPHMT nativa	84	93,5:6,5	
<i>R-3h</i>	KPHMT I202A	80	87,5:12,5	
<b>3j</b>	KPHMT nativa	88	- <sup>c</sup>	
<b>3k</b>	KPHMT nativa	80	- <sup>c</sup>	
<b>3l</b>	KPHMT nativa	96	- <sup>c</sup>	
<i>R-6b</i>	HBPA nativa	82	97:3	
<i>R-6c</i>	HBPA nativa	85	93,5:6,5	

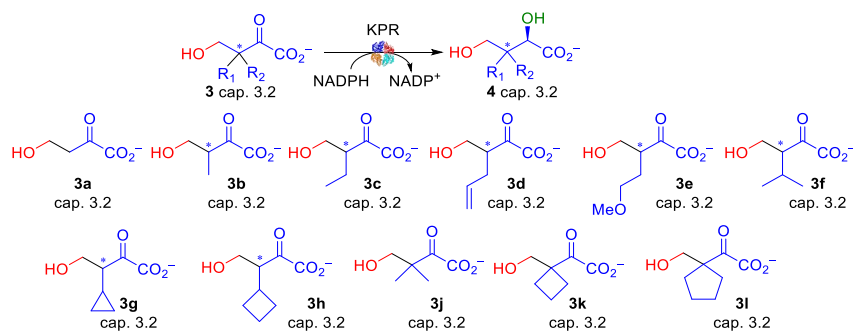
<sup>a</sup>Concentración de sustrato determinada por HPLC. <sup>b</sup>Razón enantiomérica determinado por HPLC con fase estacionaria quiral.<sup>2f</sup> <sup>c</sup>Sustrato aquiral. <sup>d</sup>No determinado.

Al realizar los ensayos de actividad enzimática notamos que los 2-oxoácidos presentan absorción de luz a 340 nm. Esto hizo que la máxima concentración de sustrato (**3** y **6**, cap. 3.2) utilizada en nuestro estudio fuese de 60 mM, dado que a concentraciones superiores se da una saturación en la señal del espectrofotómetro a dicha longitud de onda (contribución del NADPH y el 2-oxoácido). Por otro lado, concentraciones inferiores a 1 mM en nuestras manos dieron resultados con baja reproducibilidad, por ello, el rango de concentración de sustrato utilizado en este trabajo fue de 1 a 60 mM.

Para determinar los parámetros cinéticos aparentes  $V_{\max}^{\text{app}}$  y  $K_m^{\text{app}}$  se siguió las recomendaciones de Copeland, evitando los inconvenientes que surgen al linealizar la ecuación de Michaelis –Menten.<sup>22</sup> Las velocidades iniciales se graficaron en función de la concentración de cada sustrato y se realizó un ajuste no lineal al modelo de Michaelis-Menten utilizando el software GraphPad Prims v 5.0. Las determinaciones se realizaron

por triplicado en experimentos independientes. En este sentido, la **Tabla 4.4** muestra los parámetros cinéticos calculados para la KPR.

**Tabla 4.4.** Parámetros cinéticos calculados para la KPR en la reducción de los 4-hidroxi-2-oxoácidos (**3**, cap. 3.2).



Substratos	Parámetros cinéticos				Rango [S]
	$k_{cat}^{app}$	$K_m^{app}$	$(k_{cat}/K_m)^{app}$	$K_i^{app}$	
<b>3a</b>	7,1±0,5	4,9±1,2	1,4±0,4		0,2Km <sup>app</sup> ≤ [S] ≤ 12Km <sup>app</sup>
<i>S-3b</i>	348±15	12,9±1,4	27±3		0,1Km <sup>app</sup> ≤ [S] ≤ 5Km <sup>app</sup>
<i>S-3c</i>	926±37	3,0±0,5	319±52		0,3Km <sup>app</sup> ≤ [S] ≤ 22Km <sup>app</sup>
<i>S-3d</i>	89±6	9,5±1,7	9,4±1,8		0,1Km <sup>app</sup> ≤ [S] ≤ 6Km <sup>app</sup>
<i>S-3f</i>	1021±69	13±2	77±12		0,1Km <sup>app</sup> ≤ [S] ≤ 4Km <sup>app</sup>
<i>S-3g</i>	350±20	15±2	24±4		0,1Km <sup>app</sup> ≤ [S] ≤ 4Km <sup>app</sup>
<i>S-3h</i>	820±50	65±13	13±3	8,4 ±1,8	0,2Km <sup>app</sup> ≤ [S] ≤ Km <sup>app</sup>
<i>R-3b</i>	5350±138	4,8±0,4	1114±86		0,2Km <sup>app</sup> ≤ [S] ≤ 13Km <sup>app</sup>
<i>R-3c</i>	700±34	7±1	108±18		0,2Km <sup>app</sup> ≤ [S] ≤ 10Km <sup>app</sup>
<i>R-3d</i>	90±5	9,5±1,5	9,4±1,6		0,1Km <sup>app</sup> ≤ [S] ≤ 7Km <sup>app</sup>
<i>R-3e</i>	5,9±0,5	18±3	0,34±0,10		0,1Km <sup>app</sup> ≤ [S] ≤ 3Km <sup>app</sup>
<i>R-3g</i>	87±4	2,3±0,4	38±6		0,4Km <sup>app</sup> ≤ [S] ≤ 24Km <sup>app</sup>
<i>R-3h</i>	40±4	11±3	3,7±1,0		0,1Km <sup>app</sup> ≤ [S] ≤ 5Km <sup>app</sup>
<b>3j</b>	4457±813	0,4±0,2	11141±4587	3,9±1,3	2,5Km <sup>app</sup> ≤ [S] ≤ 148Km <sup>app</sup>
<b>3k</b>	6791±1022	1,5±0,5	4527±1668	6,6±1,5	0,7Km <sup>app</sup> ≤ [S] ≤ 35Km <sup>app</sup>
<b>3l</b>	1166±67	0,2±0,1	5831±3737	28±4	5Km <sup>app</sup> ≤ [S] ≤ 320Km <sup>app</sup>

$$k_{cat}^{app} = \text{min}^{-1}; K_m^{app} = \text{mM}; (k_{cat}/K_m)^{app} = \text{min}^{-1}.\text{mM}^{-1}, K_i^{app} = \text{mM}$$

Para la mayoría de los aldoles ensayados se pudo utilizar un rango de concentración de sustratos de 0,25-5,0 veces el valor de la  $K_m$  (entre el 20 y  $\approx$  80% de  $V_{max}$ ) garantizando una distribución de puntos en todas las zonas de la hipérbola, permitiendo un buen ajuste al modelo de la ecuación de Michealis–Menten.<sup>22</sup> Si comparamos los valores de la constante de especificidad para **R-3b** y **3j** (sustrato natural de la KPR) observamos que la eliminación de un grupo metilo en **R-3b** causa una disminución de un orden de magnitud de  $(k_{cat}/K_m)^{app}$  respecto al sustrato natural (teniendo una mayor contribución la  $K_m^{app}$ ). Este efecto es más dramático cuando se cambia la estereoquímica del sustrato, así **3j** muestra una constante de especificidad casi 400 veces mayor que la de **S-3b** (se afecta tanto la  $k_{cat}^{app}$  como la  $K_m^{app}$ ). De igual forma la  $(k_{cat}/K_m)^{app}$  del sustrato natural resultó ser 7000 veces mayor que la del sustrato **3a** donde se han eliminado todos los grupos metilo del carbono contiguo al grupo carbonilo (se afecta tanto la  $k_{cat}^{app}$  como la  $K_m^{app}$ ) (**Tabla 4.4**).

Estos resultados demuestran que en el centro activo de la enzima existen dos regiones que contribuyen de manera diferente a la catálisis (influyen sobre  $k_{cat}^{app}$  y  $K_m^{app}$ ) a través de las interacciones con los grupos metilo (aproximadamente contribuyen en 1,4 y 3,5 kcal mol<sup>-1</sup> a la estabilización del ES<sup>‡</sup> bajo las condiciones de nuestro ensayo cinético), resultando más importante la cavidad determinada por los residuos de V179, I183, V234 y T238 (**Figura 4.38** residuos en azul).



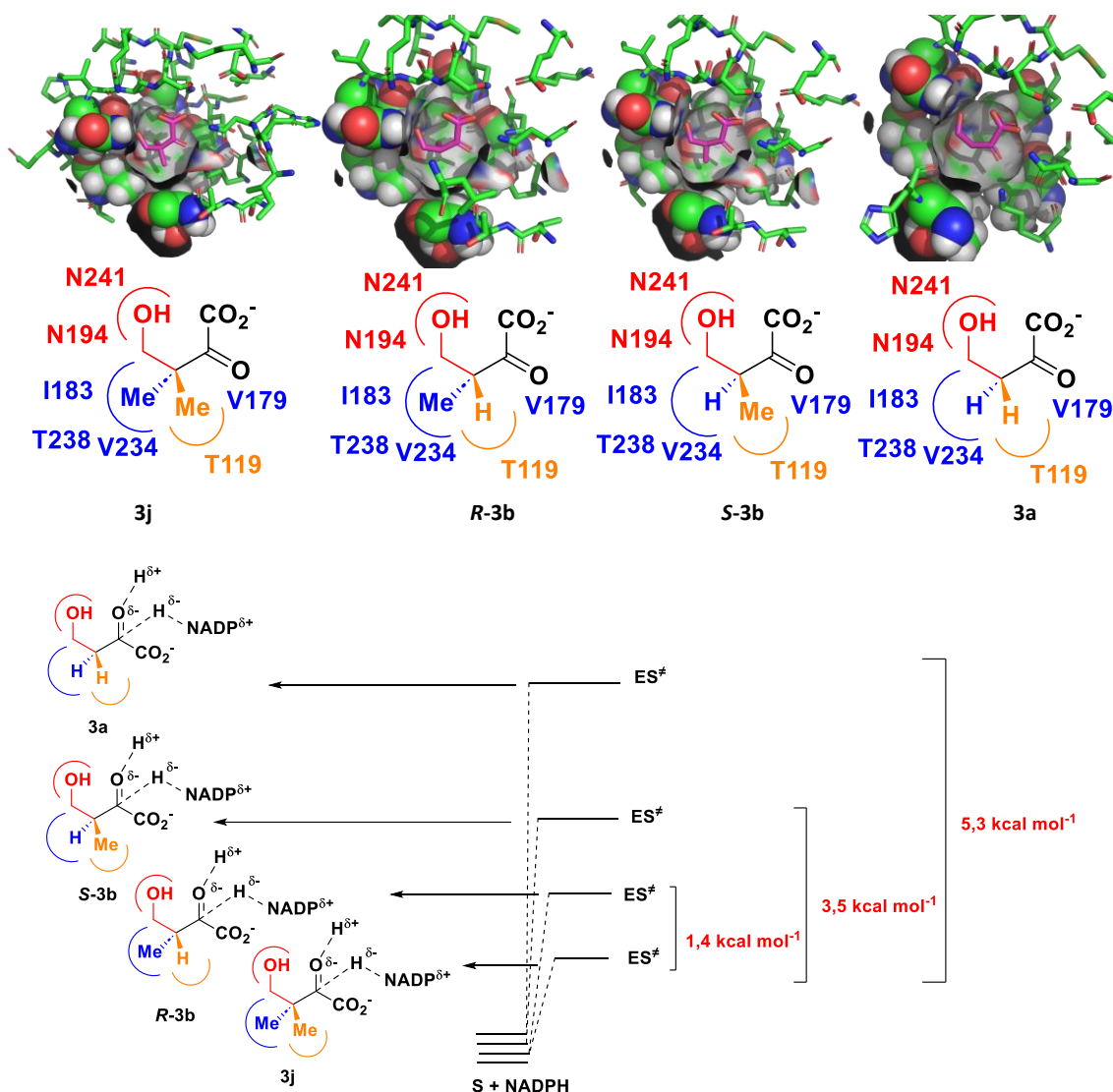


**Figura 4.38.** Modelos moleculares de los sustratos **3j**, **R-3b**, **S-3b** y **3a** en el centro activo de la KPR. Al eliminar los grupos metilo del C3 del sustrato natural (**3j**) se suprimen las interacciones en el centro activo de la enzima que se reflejan en una disminución de la constante de especificidad. Las diferencias en las energías de los estados de transición se calcularon utilizando la ecuación:  $\Delta\Delta G_{ES^{\ddagger}} = -RT \ln[(k_{cat}/K_m)^{app} / (k_{cat}/K_m)^{app}_{3j}]$ ,  $R = 8,1 \text{ J mol}^{-1} \text{ K}^{-1}$  y  $T = 303 \text{ K}$ .<sup>22-23</sup> Los modelos fueron realizados por el Dr. Jordi Bujons a partir de la estructura PDB 2OFP.<sup>24</sup>

Los sustratos **3k**, **l**, al igual que **3j**, poseen en su estructura un centro cuaternario que les permite mantener las interacciones entre los dos sitios de unión del centro activo de la enzima. A pesar de esto, presentan una disminución de la constante de especificidad con respecto a **3j** probablemente debido a la rigidez conformacional de los anillos de ciclobutano y ciclopentano (**Figura 4.39**). La disminución de los valores de  $(k_{cat}/K_m)^{app}$  de **3k** y **3l** con respecto al sustrato natural es menos dramática que la observada para los sustratos **S-3b** y **3a**, lo que demuestra la importancia de las interacciones de los sustituyentes del C3 del 2-oxoácido para la catálisis.

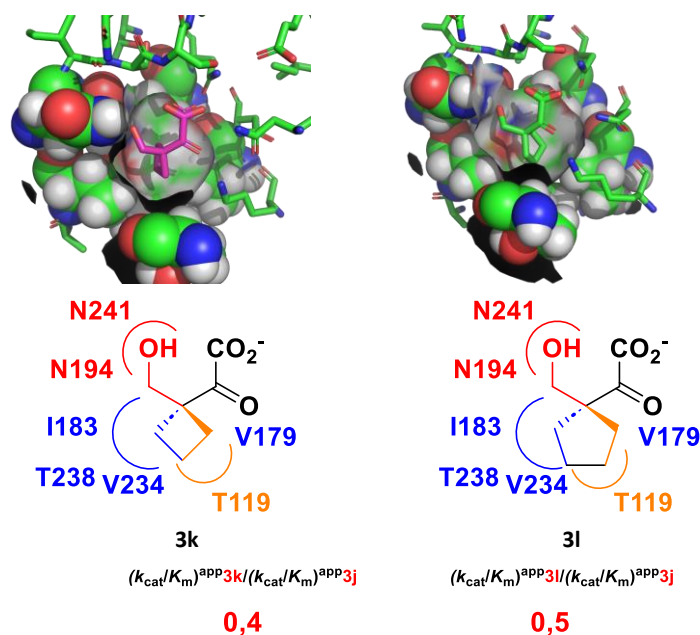


**Figura 4.39.** Modelos moleculares de los sustratos **3k**, **l** en el centro activo de la KPR. Las restricciones conformacionales de los anillos de ciclobutano y ciclopentano causan una disminución de la constante de especificidad con respecto al sustrato natural (**3j**). Los modelos fueron realizados por el Dr. Jordi Bujons a partir de la estructura PDB 2OFP.<sup>24</sup>

Para el resto de los sustratos la enzima mostró una disminución de  $(k_{\text{cat}}/K_m)^{\text{app}}$  a medida que aumenta el tamaño del sustituyente en el C3 del 2-oxoácido debido a interacciones estéricas desfavorables en el centro activo de la enzima (**Figura 4.40**). Una excepción la tenemos con los sustratos *S*-**3b** al *S*-**3c** donde se observó un incremento de 12 veces en la constante de especificidad determinado tanto por un aumento de la  $k_{\text{cat}}^{\text{app}}$  como una disminución de la  $K_m^{\text{app}}$  al pasar de un grupo metil a etilo en el sustrato (**Figura 4.40**, **Tabla 4.4**).

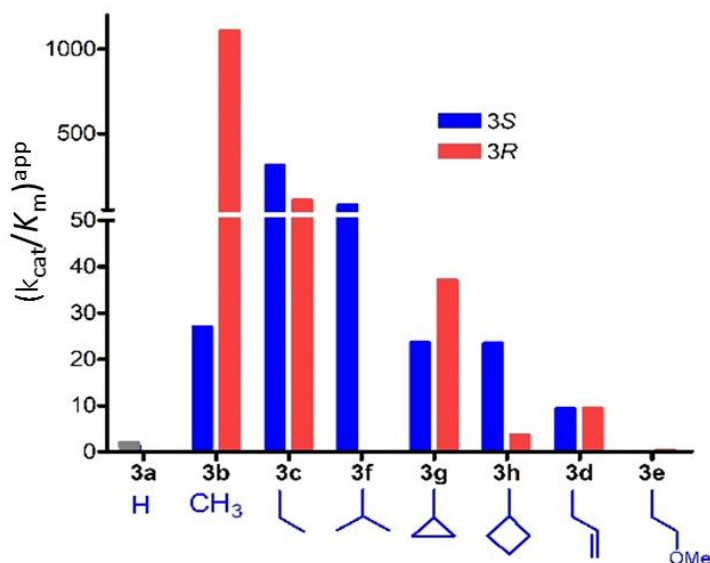
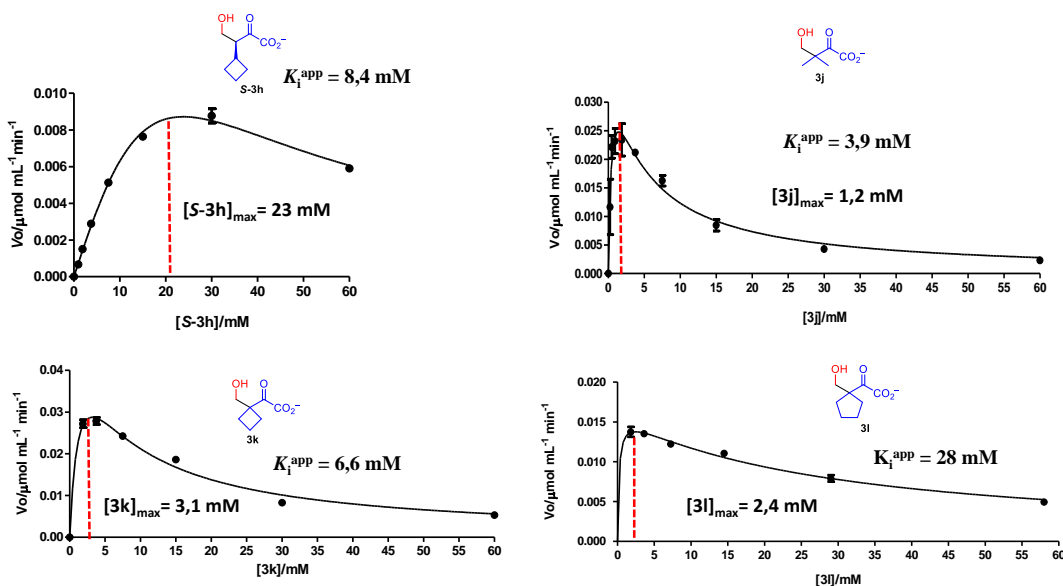


**Figura 4.40.** Los valores de  $(k_{cat}/K_m)^{app}$  disminuyen a medida que se hace más voluminoso el sustituyente del C3 del sustrato (**3a-h**, cap.3.2) en ambos enantiómeros para la catálisis de la KPR.

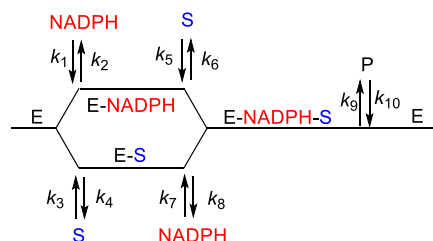
Los datos cinéticos obtenidos para los sustratos **S-3h** y **3j, k, l** se ajustaron a un modelo de inhibición por sustrato (**Figura 4.41**). El fenómeno de una aparente inhibición por sustrato se ha descrito para otras enzimas con cinética bisustrato.<sup>25</sup>



$$V_0 = \frac{V_{max}^{app}[S]}{K_m^{app} + [S](1 + [S]/K_i^{app})} \quad [S]_{max} = \sqrt{K_m^{app} K_i^{app}}$$

**Figura 4.41.** Los datos cinéticos obtenidos para los sustratos **S-3h** y **3j, k, l** se justaron a un modelo de inhibición por sustrato utilizando el software GraphPad Prims v 5.0. Se muestra la constante de inhibición y la concentración de sustrato a la cual se alcanza la máxima velocidad inicial.

Un máximo en la curva cinética ( $V_0$  vs  $[S]$ ) es una consecuencia de la complejidad de un mecanismo Bi-Bi al azar bajo un régimen de estado estacionario cuando se dan determinadas relaciones entre las constantes de velocidad de cada etapa.<sup>25a,26</sup> En este sentido, los resultados obtenidos para la KPR con los sustratos **S-3h** y **3j, k, l** se pueden explicar a través de este complejo modelo cinético (**Figura 4.42**).



$$V_0 = \frac{(K_1[\text{NADPH}][\text{S}] + K_2[\text{NADPH}]^2[\text{S}] + K_3[\text{NADPH}][\text{S}]^2)[\text{E}]_0}{K_4 + K_5[\text{NADPH}] + K_6[\text{S}] + K_7[\text{NADPH}][\text{S}] + K_8[\text{NADPH}]^2 + K_9[\text{S}]^2 + K_{10}[\text{NADPH}]^2[\text{S}] + K_{11}[\text{NADPH}][\text{S}]^2}$$

$$K_1 = k_1k_4k_5k_9 + k_2k_3k_7k_9$$

$$K_2 = k_1k_5k_7k_9$$

$$K_3 = k_2k_5k_7k_9$$

$$K_4 = k_2k_4k_6 + k_2k_4k_8 + k_2k_4k_9$$

$$K_5 = k_1k_4k_6 + k_1k_4k_8 + k_1k_4k_9 + k_2k_6k_7 + k_2k_7k_9$$

$$K_6 = k_2k_3k_6 + k_2k_3k_8 + k_2k_3k_9 + k_4k_5k_8 + k_4k_5k_9$$

$$K_7 = k_1k_4k_5 + k_2k_3k_7 + k_1k_5k_8 + k_3k_6k_7 + k_5k_7k_9$$

$$K_8 = k_1k_6k_7 + k_1k_7k_9$$

$$K_9 = k_3k_5k_8 + k_3k_5k_9$$

$$K_{10} = k_1k_5k_7$$

$$K_{11} = k_3k_5k_7$$

Si:  $[\text{NADPH}] = \text{constante}$  y  $K_2[\text{NADPH}]^2 \gg K_3[\text{NADPH}][\text{S}]$ , entonces:

$$V_0 = \frac{k_{\text{cat}}^{\text{app}}[\text{E}]_0[\text{S}]}{K_m^{\text{app}} + [\text{S}](1 + [\text{S}]/K_i^{\text{app}})}$$

Donde:

$$k_{\text{cat}}^{\text{app}} = \frac{K_1[\text{NADPH}] + K_2[\text{NADPH}]^2}{K_6 + K_7[\text{NADPH}] + K_{10}[\text{NADPH}]^2} \quad K_m^{\text{app}} = \frac{K_4 + K_5[\text{NADPH}] + K_8[\text{NADPH}]^2}{K_6 + K_7[\text{NADPH}] + K_{10}[\text{NADPH}]^2} \quad K_i^{\text{app}} = \frac{K_6 + K_7[\text{NADPH}] + K_{10}[\text{NADPH}]^2}{K_9 + K_{11}[\text{NADPH}]}$$

**Figura 4.42.** Ecuación de velocidad obtenida por el método de King–Altman para un mecanismo Bi-UNI al azar bajo un régimen de estado estacionario en ausencia de productos.<sup>26</sup> Bajo determinadas condiciones la ecuación de velocidad se reduce a una aparente inhibición por sustrato. Deducir la ecuación para un mecanismo Bi-Bi al azar bajo régimen de estado estacionario es en extremo complejo por ello se utilizó el sistema Bi-UNI como una simplificación del modelo.

Otra hipótesis que explicaría la aparente inhibición por sustrato sería la existencia de un segundo sitio de unión en la enzima para el 2-oxoácido, pero no se dispone de ninguna evidencia estructural que lo confirme por lo que ha sido descartada.<sup>19,20b,27</sup> Estos resultados discrepan con los descritos para la KPR de *E. coli* (no se reportan desviaciones del modelo hiperbólico) probablemente debido a que se han utilizado concentraciones de **3j** inferiores a 1 mM no llegando a observarse la disminución de la actividad enzimática con la concentración de sustrato ( $[\text{3j}]_{\text{max}} = 1,2 \text{ mM}$ , **Figura 4.41**). Esto también puede sesgar los patrones de inhibición por producto que hacen concluir que la enzima sigue

una cinética Bi-Bi ordenada.<sup>19,20b,27</sup> Sin embargo, para la KPR de *Staphylococcus aureus* se informó de una constante de inhibición por sustrato aparente ( $K_i^{\text{app}}$ ) de 270  $\mu\text{M}$  para **3j**, un orden de magnitud inferior a la encontrada en este trabajo.<sup>28</sup>

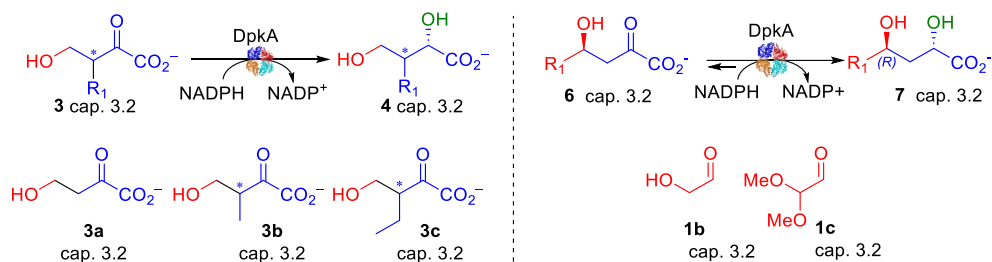
Debido al comportamiento cinético de la KPR con los sustratos **3j**, **k**, **l** (máxima actividad en el sistema cuando  $[\text{S}]_{\text{max}} = 1,2\text{-}3,1\text{mM}$ , **Figura 4.41**) se añadió una mayor concentración de enzima en las reacciones biocatalíticas ( $[\text{E}]_0^{\text{biocatálisis}} = 1 \text{ mg mL}^{-1}$  vs  $[\text{E}]_0^{\text{ensayo enzimático}} = 0,0003 \text{ mg mL}^{-1}$ ) para contrarrestar el hecho de trabajar a concentraciones de sustrato (50 mM) alejadas del máximo en la curva cinética. Además, utilizar una concentración de NADPH de 5 mM ( $[\text{NADPH}]^{\text{biocatálisis}} = 1250 K_m^{\text{NADPH}}$ ,  $K_m^{\text{NADPH}} = 4,0 \mu\text{M}$ )<sup>20b</sup>, unido a un sistema de regeneración que mantiene su concentración “constante” durante la reacción, contribuye a potenciar la actividad de la deshidrogenasa. Todo esto contribuye a una elevada formación del producto reducido (**4j**, **k**, **l**).

En el caso de la DpkA los ensayos enzimáticos sólo se pudieron realizar con los sustratos **3a**, **S-3b,c** y **R-3b,c** debido que la deshidrogenasa muestra una baja tolerancia por 4-hidroxi-2-oxoácidos con sustituyentes en el C3. En el caso de los sustratos **6** sólo se estudiaron el **R-6b** y **R-6c** dado que, para el resto, la conversión de la reacción aldólica comprometió su uso (el piruvato remanente en el medio de reacción (>20 mM) altera los resultados cinéticos del ensayo al ser también sustrato de la enzima) (**Tabla 4.5**).

Con los sustratos **3a**, **S-3b** y **R-6c** no se pudo utilizar un rango de concentración de sustratos de 0,25-5,0 veces el valor de la  $K_m$  (entre el 20 y  $\approx 80\%$  de  $V_{\text{max}}$ )<sup>22</sup> por lo que obtuvimos parámetros cinéticos estimados (**Tabla 4.5**).

La DpkA no mostró variaciones significativas en la constante de especificidad para los sustratos **3a**, **S-3b** y **R-3b**, lo que la diferencia de la KPR. Al aumentar el tamaño del sustituyente del C3 (pasar de un metilo a un etilo) se da una disminución de casi 4 veces en la  $(k_{\text{cat}}/K_m)^{\text{app}}$  determinado mayormente por una disminución en la  $k_{\text{cat}}^{\text{app}}$  (sustratos **S-3b** y **S-3c**, **Tabla 4.5**).

**Tabla 4.5.** Parámetros cinéticos en la reducción de los 4-hidroxi-2-oxoácidos (**3**, cap. 3.2) y (**6b-c**, cap. 3.2) catalizado por la DpkA.



Substratos	Parámetros cinéticos			Rango [S]
	$k_{cat}^{app}$	$K_m^{app}$	$(k_{cat}/K_m)^{app}$	
<b>3a</b>	1,7±0,2	33±7	0,052±0,013	0,03Km <sup>app</sup> ≤ [S] ≤ 2Km <sup>app</sup>
<i>S</i> - <b>3b</b>	1,1±0,1	19±4	0,058±0,012	0,05Km <sup>app</sup> ≤ [S] ≤ 3Km <sup>app</sup>
<i>S</i> - <b>3c</b>	0,23±0,01	14±2	0,016±0,002	0,07Km <sup>app</sup> ≤ [S] ≤ 5Km <sup>app</sup>
<i>R</i> - <b>3b</b>	0,36±0,0002	7,5±1,9	0,047±0,013	0,13Km <sup>app</sup> ≤ [S] ≤ 8Km <sup>app</sup>
<i>R</i> - <b>6b</b>	3,00±0,02	11±1	0,28±0,039	0,1Km <sup>app</sup> ≤ [S] ≤ 5Km <sup>app</sup>
<i>R</i> - <b>6c</b>	85±27 <sup>C</sup>	97±43 <sup>C</sup>	0,87±0,48	0,01Km <sup>app</sup> ≤ [S] ≤ 0,6Km <sup>app</sup>

$$k_{cat}^{app} = \text{min}^{-1}; K_m^{app} = \text{mM}; (k_{cat}/K_m)^{app} = \text{min}^{-1}\text{mM}^{-1}$$

Utilizando los datos cinéticos para comparar la catálisis de la DpkA y la KPR, se observa que con los sustratos **3a**, *S*-**3b**, *S*-**3c** y *R*-**3b** la segunda enzima alcanza una estabilización del estado de transición de la reacción ( $ES^\ddagger$ ) de 2; 3; 6 y 6 kcal mol<sup>-1</sup> respectivamente respecto al primer biocatalizador bajo las condiciones de los ensayos cinéticos realizados en esta Tesis (**Figura 4.43**).

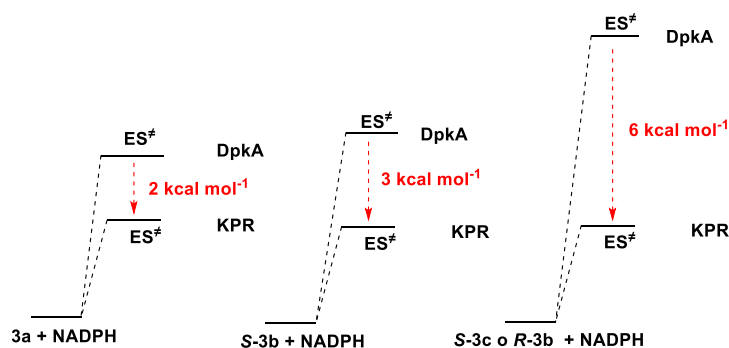


**Figura 4.43.** Para los sustratos **3a**, *S*-**3b**, *S*-**3c** y *R*-**3b** la KPR alcanza una mayor estabilización de los  $ES^\ddagger$  en comparación con la DpkA. Las diferencias en las energías de los estados de transición se calcularon utilizando la ecuación:  $\Delta\Delta G_{ES^\ddagger} = -RT\ln[(k_{cat}/K_m)^{app}_{DpkA}/(k_{cat}/K_m)^{app}_{KPR}]$ ,  $R = 8,1 \text{ J mol}^{-1} \text{ K}^{-1}$  y  $T = 303 \text{ K}$ .<sup>22-23</sup>

Finalmente, para los sustratos **R-6b** y **R-6c** la DpkA mostró valores de  $(k_{cat}/K_m)^{app}$  superiores a los de los sustratos **3** (por ejemplo: 5 y 16 veces respectivamente si se compara con **S-3b**). A pesar que el sustrato **R-6c** posee un grupo voluminoso en su estructura la constante de especificidad fue mayor que para el sustrato **R-6b** (3 veces mayor), esto se debió a un mayor incremento de la  $k_{cat}^{app}$  en comparación con el aumento de la  $K_m^{app}$ . En este análisis hay que tener en cuenta que los parámetros cinéticos obtenidos para **R-6b** son estimados, debido a su elevado valor de  $K_m^{app}$ . Desafortunadamente no se pudo disponer de más sustratos de la serie **6** que nos permitan obtener un mayor número de datos cinéticos para realizar un estudio más completo de esta actividad promiscua de la DpkA.

## Referencias.

1. (a) Schrittwieser, J. H.; Velikogne, S.; Hall, M. I.; Kroutil, W., Artificial biocatalytic linear cascades for preparation of organic molecules. *Chemical Reviews* **2018**, *118* (1), 270-348; (b) Benítez-Mateos, A. I.; Roura Padrosa, D.; Paradisi, F., Multistep enzyme cascades as a route towards green and sustainable pharmaceutical syntheses. *Nature chemistry* **2022**, *14* (5), 489-499; (c) Ricca, E.; Brucher, B.; Schrittwieser, J. H., Multi-enzymatic cascade reactions: overview and perspectives. *Advanced Synthesis & Catalysis* **2011**, *353* (13), 2239-2262; (d) Vázquez-González, M.; Wang, C.; Willner, I., Biocatalytic cascades operating on macromolecular scaffolds and in confined environments. *Nature Catalysis* **2020**, *3* (3), 256-273; (e) France, S. P.; Hepworth, L. J.; Turner, N. J.; Flitsch, S. L., Constructing biocatalytic cascades: in vitro and in vivo approaches to de novo multi-enzyme pathways. *Acs Catalysis* **2017**, *7* (1), 710-724; (f) Citoler, J.; Derrington, S. R.; Galman, J. L.; Bevinakatti, H.; Turner, N. J., A biocatalytic cascade for the conversion of fatty acids to fatty amines. *Green chemistry* **2019**, *21* (18), 4932-4935; (g) Bell, E. L.; Finnigan, W.; France, S. P.; Green, A. P.; Hayes, M. A.; Hepworth, L. J.; Lovelock, S. L.; Niikura, H.; Osuna, S.; Romero, E., Biocatalysis. *Nature Reviews Methods Primers* **2021**, *1* (1), 46; (h) Gandomkar, S.; Żądło-Dobrowolska, A.; Kroutil, W., Extending designed linear biocatalytic cascades for organic synthesis. *ChemCatChem* **2019**, *11* (1), 225-243; (i) Kumar Roy, T.; Sreedharan, R.; Ghosh, P.; Gandhi, T.; Maiti, D., Ene-Reductase: a multifaceted biocatalyst in organic synthesis. *Chemistry—A European Journal* **2022**, *28* (21), e202103949; (j) Sheldon, R. A.; Brady, D., Broadening the scope of biocatalysis in sustainable organic synthesis. *ChemSusChem* **2019**, *12* (13), 2859-2881.
2. (a) Hernandez, K.; Bujons, J.; Joglar, J. s.; Charnock, S. J.; Dominguez de Maria, P.; Fessner, W. D.; Clapés, P., Combining aldolases and transaminases for the synthesis of 2-amino-4-hydroxybutanoic acid. *ACS Catalysis* **2017**, *7* (3), 1707-1711; (b) Guérard-Hélaine, C.; Heuson, E.; Ndiaye, M.; Gourbeyre, L.; Lemaire, M.; Hélaine, V.; Charmantray, F.; Petit, J.-L.; Salanoubat, M.; de Bernardinis, V., Stereoselective synthesis of  $\gamma$ -hydroxy- $\alpha$ -amino acids through aldolase-transaminase recycling cascades. *Chemical Communications* **2017**, *53* (39), 5465-5468; (c) Slabu, I.; Galman, J. L.; Lloyd, R. C.; Turner, N. J., Discovery, engineering, and synthetic application of transaminase biocatalysts. *ACS Catalysis* **2017**, *7* (12), 8263-8284; (d) Pickl, M.; Ebner, M.; Gittings, S.; Clapés, P.; Kroutil, W., Biocatalytic Transamination of Aldolase-Derived 3-Hydroxy Ketones. *Advanced Synthesis & Catalysis*; (e) Hernández, K.; Gómez, A.; Joglar, J.; Bujons, J.; Parella, T.; Clapés, P., 2-Keto-3-Deoxy-l-Rhamnonate Aldolase (YfaU) as Catalyst in Aldol Additions of Pyruvate to Amino Aldehyde Derivatives. *Advanced Synthesis & Catalysis* **2017**, *359* (12), 2090-2100; (f) Marín-Valls, R.; Hernandez, K.; Bolte, M.; Joglar, J. s.; Bujons, J.; Clapes, P., Chemoenzymatic hydroxymethylation of carboxylic acids by tandem stereodivergent biocatalytic aldol reaction and chemical decarboxylation. *ACS Catalysis* **2019**, *9* (8), 7568-7577; (g) Oroz-Guinea, I.; García-Junceda, E., Enzyme catalysed tandem reactions. *Current opinion in chemical biology* **2013**, *17* (2), 236-249.
3. Cleland, W. W., The kinetics of enzyme-catalyzed reactions with two or more substrates or products: I. Nomenclature and rate equations. *Biochimica et Biophysica Acta (BBA)-Specialized Section on Enzymological Subjects* **1963**, *67*, 104-137.
4. Hernández, K.; Parella, T.; Joglar, J.; Bujons, J.; Pohl, M.; Clapés, P., Expedient Synthesis of C-Aryl Carbohydrates by Consecutive Biocatalytic Benzoin and Aldol Reactions. *Chemistry—A European Journal* **2015**, *21* (8), 3335-3346.
5. LeVieux, J. A.; Medellin, B.; Johnson Jr, W. H.; Erwin, K.; Li, W.; Johnson, I. A.; Zhang, Y. J.; Whitman, C. P., Structural characterization of the hydratase-aldolases, NahE and PhdJ: implications for the specificity, catalysis, and N-acetylneuraminase lyase subgroup of the aldolase superfamily. *Biochemistry* **2018**, *57* (25), 3524-3536.
6. (a) Woodhall, T.; Williams, G.; Berry, A.; Nelson, A., Creation of a tailored aldolase for the parallel synthesis of sialic acid mimetics. *Angewandte Chemie* **2005**, *117* (14), 2147-2150; (b) Lambale, H. J.; Danson, M. J.; Hough, D. W.; Bull, S. D., Engineering stereocontrol into an aldolase-catalysed reaction. *Chemical communications* **2005**, (1), 124-126; (c) Lambale, H. J.; Royer, S. F.; Hough, D. W.; Danson, M. J.; Taylor, G. L.; Bull, S. D., A thermostable aldolase for the synthesis



- of 3-deoxy-2-ulosonic acids. *Advanced Synthesis & Catalysis* **2007**, *349* (6), 817-821; (d) Baker, P.; Seah, S. Y., Rational design of stereoselectivity in the class II pyruvate aldolase BphI. *Journal of the American Chemical Society* **2012**, *134* (1), 507-513; (e) Archer, R. M.; Royer, S. F.; Mahy, W.; Winn, C. L.; Danson, M. J.; Bull, S. D., Syntheses of 2-Keto-3-deoxy-D-xylonate and 2-Keto-3-deoxy-L-arabinonate as Stereochemical Probes for Demonstrating the Metabolic Promiscuity of *Sulfolobus solfataricus* Towards D-Xylose and L-Arabinose. *Chemistry—A European Journal* **2013**, *19* (8), 2895-2902; (f) Clapes, P.; Garrabou, X., Current trends in asymmetric synthesis with aldolases. *Advanced Synthesis & Catalysis* **2011**, *353* (13), 2263-2283.
7. Howard, J. K.; Müller, M.; Berry, A.; Nelson, A., An Enantio- and Diastereoselective Chemoenzymatic Synthesis of  $\alpha$ -Fluoro  $\beta$ -Hydroxy Carboxylic Esters. **2016**.
8. Fansher, D. J.; Palmer, D. R., A Type 1 Aldolase, NahE, Catalyzes a Stereoselective Nitro-Michael Reaction: Synthesis of  $\beta$ -Aryl- $\gamma$ -nitrobutyric Acids. *Angewandte Chemie International Edition* **2023**, *62* (6), e202214539.
9. (a) Fansher, D. J.; Ngwira, N.; Salehi, A. R.; Woods, J.; Cascao, A.; Palmer, D. R., Biocatalytic Synthesis of  $\alpha$ ,  $\beta$ -Unsaturated 2-Keto Acids and Derivatives Using the Promiscuous Aldolase, NahE. *Synthesis* **2023**, *55* (01), 75-89; (b) Eaton, R. W., trans-o-Hydroxybenzylidenepyruvate Hydratase-Aldolase as a Biocatalyst. *Applied and environmental microbiology* **2000**, *66* (6), 2668-2672; (c) Sello, G.; Di Gennaro, P., Aldol Reactions of the trans-o-Hydroxybenzylidenepyruvate Hydratase-Aldolase (t HBP-HA) from *Pseudomonas fluorescens* N3. *Applied biochemistry and biotechnology* **2013**, *170*, 1702-1712.
10. (a) Henderson, D. P.; Shelton, M. C.; Cotterill, I. C.; Toone, E. J., Stereospecific preparation of the N-terminal amino acid moiety of nikkomycins Kx and Kz via a multiple enzyme synthesis. *The Journal of Organic Chemistry* **1997**, *62* (23), 7910-7911; (b) Walters, M. J.; Srikannathasan, V.; McEwan, A. R.; Naismith, J. H.; Fierke, C. A.; Toone, E. J., Characterization and crystal structure of *Escherichia coli* KDPGal aldolase. *Bioorganic & medicinal chemistry* **2008**, *16* (2), 710-720; (c) Griffiths, J. S.; Cheriyan, M.; Corbell, J. B.; Pocivavsek, L.; Fierke, C. A.; Toone, E. J., A bacterial selection for the directed evolution of pyruvate aldolases. *Bioorganic & medicinal chemistry* **2004**, *12* (15), 4067-4074; (d) Henderson, D. P.; Cotterill, I. C.; Shelton, M. C.; Toone, E. J., 2-Keto-3-deoxy-6-phosphogalactonate Aldolase as a Catalyst for Stereocontrolled Carbon-Carbon Bond Formation. *The Journal of Organic Chemistry* **1998**, *63* (4), 906-907.
11. young Hong, E.; Cha, M.; Yun, H.; Kim, B.-G., Asymmetric synthesis of L-tert-leucine and L-3-hydroxyadamantylglycine using branched chain aminotransferase. *Journal of Molecular Catalysis B: Enzymatic* **2010**, *66* (1-2), 228-233.
12. (a) Neises, B.; Steglich, W., Simple method for the esterification of carboxylic acids. *Angewandte Chemie International Edition in English* **1978**, *17* (7), 522-524; (b) Magano, J., Large-Scale Amidations in Process Chemistry: Practical Considerations for Reagent Selection and Reaction Execution. *Organic Process Research & Development* **2022**, *26* (6), 1562-1689.
13. Goto, M.; Muramatsu, H.; Mihara, H.; Kurihara, T.; Esaki, N.; Omi, R.; Miyahara, I.; Hirotsu, K., Crystal structures of  $\Delta$ 1-piperideine-2-carboxylate/ $\Delta$ 1-pyrroline-2-carboxylate reductase belonging to a new family of NAD (P) H-dependent oxidoreductases: conformational change, substrate recognition, and stereochemistry of the reaction. *Journal of Biological Chemistry* **2005**, *280* (49), 40875-40884.
14. Luche, J. L., Lanthanides in organic chemistry. 1. Selective 1, 2 reductions of conjugated ketones. *Journal of the American Chemical Society* **1978**, *100* (7), 2226-2227.
15. Marín-Valls, R.; Hernández, K.; Bolte, M.; Parella, T.; Joglar, J. s.; Bujons, J.; Clapés, P., Biocatalytic construction of quaternary centers by aldol addition of 3, 3-disubstituted 2-oxoacid derivatives to aldehydes. *Journal of the American Chemical Society* **2020**, *142* (46), 19754-19762.
16. Weinstock, L. M.; Currie, R. B.; Lovell, A. V., A general, one-step synthesis of  $\alpha$ -keto esters. *Synthetic Communications* **1981**, *11* (12), 943-946.
17. Ortiz, C.; Ferreira, M. L.; Barbosa, O.; dos Santos, J. C.; Rodrigues, R. C.; Berenguer-Murcia, Á.; Briand, L. E.; Fernandez-Lafuente, R., Novozym 435: the "perfect" lipase immobilized biocatalyst? *Catalysis Science & Technology* **2019**, *9* (10), 2380-2420.

18. Hanson, J. A.; Duderstadt, K.; Watkins, L. P.; Bhattacharyya, S.; Brokaw, J.; Chu, J.-W.; Yang, H., Illuminating the mechanistic roles of enzyme conformational dynamics. *Proceedings of the National Academy of Sciences* **2007**, *104* (46), 18055-18060.
19. Ciulli, A.; Chirgadze, D. Y.; Smith, A. G.; Blundell, T. L.; Abell, C., Crystal structure of Escherichia coli ketopantoate reductase in a ternary complex with NADP<sup>+</sup> and pantoate bound: substrate recognition, conformational change, and cooperativity. *Journal of Biological Chemistry* **2007**, *282* (11), 8487-8497.
20. (a) Muramatsu, H.; Mihara, H.; Kakutani, R.; Yasuda, M.; Ueda, M.; Kurihara, T.; Esaki, N., The putative malate/lactate dehydrogenase from Pseudomonas putida is an NADPH-dependent  $\Delta^1$ -piperidine-2-carboxylate/ $\Delta^1$ -pyrroline-2-carboxylate reductase involved in the catabolism of d-lysine and d-proline. *Journal of Biological Chemistry* **2005**, *280* (7), 5329-5335; (b) Zheng, R.; Blanchard, J. S., Kinetic and mechanistic analysis of the E. coli panE-encoded ketopantoate reductase. *Biochemistry* **2000**, *39* (13), 3708-3717.
21. Dawson, R. M. C.; Elliott, D. C.; Elliott, W. H.; Jones, K. M., *Data for biochemical research*. Clarendon press: 2002.
22. Copeland, R. A., *Enzymes: a practical introduction to structure, mechanism, and data analysis*. John Wiley & Sons: 2000.
23. Wilkinson, A. J.; Fersht, A. R.; Blow, D. M.; Winter, G., Site-directed mutagenesis as a probe of enzyme structure and catalysis: tyrosyl-tRNA synthetase cysteine-35 to glycine-35 mutation. *Biochemistry* **1983**, *22* (15), 3581-3586.
24. Matak-Vinković, D.; Vinković, M.; Saldanha, S. A.; Ashurst, J. L.; von Delft, F.; Inoue, T.; Miguel, R. N.; Smith, A. G.; Blundell, T. L.; Abell, C., Crystal structure of Escherichia coli ketopantoate reductase at 1.7 Å resolution and insight into the enzyme mechanism. *Biochemistry* **2001**, *40* (48), 14493-14500.
25. (a) Ferdinand, W., The interpretation of non-hyperbolic rate curves for two-substrate enzymes. A possible mechanism for phosphofructokinase. *Biochemical Journal* **1966**, *98* (1), 278; (b) Jensen, R. A.; Trentini, W. C., Alternative allosteric effects exerted by end products upon a two-substrate enzyme in Rhodospirillum rubrum. *Journal of Biological Chemistry* **1970**, *245* (8), 2018-2022.
26. Leskovac, V., *Comprehensive enzyme kinetics*. Springer Science & Business Media: 2003.
27. Zheng, R.; Blanchard, J. S., Substrate specificity and kinetic isotope effect analysis of the Escherichia coli ketopantoate reductase. *Biochemistry* **2003**, *42* (38), 11289-11296.
28. Sanchez, J. E.; Gross, P. G.; Goetze, R. W.; Walsh Jr, R. M.; Peeples, W. B.; Wood, Z. A., Evidence of kinetic cooperativity in dimeric ketopantoate reductase from Staphylococcus aureus. *Biochemistry* **2015**, *54* (21), 3360-3369.

Sección V

# Conclusiones

## Conclusiones generales

-La *trans*-o-hidroxi-bencilideno piruvato hidratasa-aldolasa (HBPA) catalizó la síntesis enantioselectiva de 4-hidroxi-2-oxoácidos quirales a partir de aldehídos alifáticos. Se acopló su actividad catalítica con otras actividades enzimáticas como: transaminasas (cap. 3.1). y deshidrogenasas (cap. 3.2) evitándose los pasos de purificación de los intermediarios de síntesis.

-Los sistemas biocatalíticos HBPA/T039 y HBPA/BCAT/AspTA representan enfoques complementarios adecuados para la síntesis asimétrica de  $\gamma$ -hidroxi- $\alpha$ -aminoácidos quirales con moderados rendimientos y excelente estereocontrol por parte de las enzimas implicadas (cap. 3.1).

- La HBPA catalizó la síntesis de 2-oxoácidos  $\alpha,\beta$ -insaturados con buenos rendimientos a partir de aldehídos aromáticos (cap. 3.3), permitiendo la síntesis en cascada de derivados quirales del ácido 2-hidroxi-4-arylbut-3-enoico cuando se acoplo con la deshidrogenasas DpkA (cap. 3.3).

-La estrategia biocatalítica que combina 2-oxoácido aldolasas estereoselectivas (YfaU y KPHMT) con dos deshidrogenasas estereocomplementarias (KPR y DpkA) permitió la síntesis de 2-hidroxiácidos quirales y derivados de 2-hidroxi-4-butirolactonas, en una síntesis de dos pasos enzimáticos y en un sistema en cascada (cap. 3.2).

-La deshidrogenasa KPR mostró una amplia tolerancia al sustrato frente a los 4-hidroxi-2-oxoácidos, incluyendo aquellos con centros cuaternarios en C3, homólogos al sustrato natural. Sin embargo, se observó inhibición por sustrato para el cetopantoato y sus análogos, sin afectar esto al proceso biocatalítico (cap. 3.2).

-La DpkA presentó una actividad promiscua hacia la reducción del grupo carbonilo de 2-oxoácidos y 4-hidroxi-2-oxoácidos. Sin embargo, tiene una baja tolerancia a sustrato con sustituyentes en el C3 del sustrato, aceptando sólo metilo y etilo como sustituyentes, con preferencia el aldol con configuración 3*S* (cap. 3.2).

**Sección VI**

**Materiales y métodos.**  
**Capítulo 3.1**

## Supporting Information

### Synthesis of $\gamma$ -Hydroxy- $\alpha$ -Amino Acid Derivatives by Enzymatic Tandem Aldol Addition-Transamination Reactions

Carlos J. Moreno<sup>a</sup>, Karel Hernández<sup>a</sup>, Simon J. Charnok<sup>b</sup>, Samantha Gittings<sup>b</sup>, Michael Bolte<sup>c</sup>, Jesús Joglar<sup>a</sup>, Jordi Bujons<sup>a</sup>, Teodor Parella<sup>d</sup>, Pere Clapés<sup>a</sup>

<sup>a</sup>Institute for Advanced Chemistry of Catalonia, Dept. of Biological Chemistry, IQAC-CSIC, Spain.

<sup>b</sup>Prozomix Ltd. West End Industrial Estate, Haltwhistle, Northumberland, NE49 9HA, UK.

<sup>c</sup>Institut für Anorganische Chemie, J.-W.-Goethe-Universität, Frankfurt/Main, Germany.

<sup>d</sup>Servei de Ressonància Magnètica Nuclear. Universitat Autònoma de Barcelona, Bellaterra, Spain.

#### Table of Contents

<b>Materials.....</b>	<b>3</b>
<b>Methods. ....</b>	<b>4</b>
<b>Protein production and purification.....</b>	<b>8</b>
<b>TLC analysis. ....</b>	<b>14</b>
<b>Specific rotation.....</b>	<b>14</b>
<b>HPLC analysis. ....</b>	<b>14</b>
<b>NMR analysis. ....</b>	<b>15</b>
<b>Activity determination of HBPA. ....</b>	<b>15</b>
<b>Activity determination of (S)-selective transaminases.....</b>	<b>16</b>
<b>Synthesis of starting material (1c-f, 1i-j, 1l-s). ....</b>	<b>17</b>
<b>General procedure for the aldol addition of sodium pyruvate to aldehydes (1a-s) catalyzed by HBPA .....</b>	<b>22</b>
<b>Synthesis of 4-hydroxyesters (R-4a-m). ....</b>	<b>23</b>
<b>X-Ray structures of R-4e, R-4f and R-4j .....</b>	<b>34</b>
<b>Enzymatic transamination of 4-hydroxy-2-oxoacids (3). Screening of transaminases from Prozomix, using L-Ala and benzyl amine as amino donors. ....</b>	<b>37</b>
<b>Assay of one-pot biocatalytic cascade synthesis of 4-hydroxy-amino with substrate recycling. ...</b>	<b>44</b>
<b>Assay of one-pot two steps 4-hydroxy-amino acids derivatives using a biocatalytic one-pot two-steps approach using the PLP-Dependent branched-chain amino acid aminotransferase (BCATs) from <i>Escherichia coli</i>. ....</b>	<b>50</b>

<b>Assay of one-pot biocatalytic cascade synthesis of 4-hydroxy-amino acid derivatives with substrate recycling BCAT/L-Glu/L-Asp/AspAT. ....</b>	<b>51</b>
<b>Synthesis of 4-hydroxy-amino acids by tandem HBPA/transaminase and conversion to <math>\alpha</math>-amino-<math>\gamma</math>-butyrolactone derivatives. ....</b>	<b>52</b>
<b>Chemical synthesis of 1-Benzyl 2-methyl (2<i>S</i>,4<i>R</i>)- and (2<i>S</i>,4<i>S</i>)-4-hydroxypyrrolidine-1,2-dicarboxylate ((2<i>S</i>,4<i>R</i>)-15k and (2<i>S</i>,4<i>S</i>)-15k). ....</b>	<b>63</b>
<b>Chemoenzymatic synthesis of 1-benzyl 2-methyl (2<i>S</i>,4<i>R</i>)-4-hydroxypyrrolidine-1,2-dicarboxylate (15k). ....</b>	<b>64</b>
<b>Analysis of the diastomeric excess of 15k. ....</b>	<b>65</b>
<b>NMR spectra*. ....</b>	<b></b>
<b>Chromatograms of the HPLC analysis on chiral stationary phases. ....</b>	<b>67</b>
<b>Computational Modeling. ....</b>	<b>74</b>
<b>Computational Methods. ....</b>	<b>88</b>
<b>References. ....</b>	<b>89</b>

\* Se encuentra como material electrónico

**Materials.**

Glycolaldehyde dimer, sodium pyruvate, benzaldehyde, 2,2-dimethoxyacetaldehyde, chloroacetaldehyde, ethyl glyoxylate, indole-3-carboxaldehyde, L-Ala, L-Asp, L-Glu, L-Val, benzylamine, 2,4'-dibromoacetophenone, benzyl bromide, and 2-(bromomethyl)naphthalene were purchased from Sigma-Aldrich. (*S*)-Cbz-*N*-2-Aminopropanal (**1q**) used in this study was synthesized in our lab using procedures published in previous works.<sup>1</sup> Synthetic oligonucleotides were purchased from Eurofins Genomics. All reagents for molecular biology were from Life Thermo Scientific. Culture media components for *E. coli* were from Pronadisa (Madrid, Spain). Antibiotics, IPTG and L-arabinose were from Carl Roth. High-density IDA-Agarose 6BCL nickel charged was from GE Healthcare Life Science. Water for analytical HPLC was obtained from an Arium Pro ultrapure water purification system (Sartorius Stedim Biotech) and the rest of solvents used in this work were of analytical or HPLC grade. Bacterial strains, oligonucleotides, and plasmids used in this study are listed in **Table S1**.

**Table S1.** Strains, plasmids, and oligonucleotides used in this study.

<b>Strains</b>	<b>Relevant genotype</b>
<i>E. coli</i> Nova Blue (used for plasmid preparation)	<i>endA1</i> , <i>hdsR17</i> (rB <sup>+</sup> , mB <sup>+</sup> ), <i>supE44</i> , <i>thi1</i> , <i>recA1</i> , <i>gyrA96</i> , <i>relA1</i> , <i>lac F'</i> [proA <sup>+</sup> B <sup>+</sup> , <i>lacI</i> <sup>q</sup> ZΔM15::Tn10] ( <i>Tet</i> <sup>R</sup> ).
<i>E. coli</i> B121-AI (used for protein expression)	F <sup>-</sup> <i>ompT gal dcm lon hdsS<sub>B</sub>(r<sub>B</sub><sup>-</sup>m<sub>B</sub><sup>-</sup>)</i> [ <i>malB</i> <sup>+</sup> ] <sub>K-12</sub> (λ <sup>S</sup> ) <i>araB::T7RNAP-tetA</i>
<i>E. coli</i> M15 [pREP4] (used for protein expression)	<i>nal</i> <sup>s</sup> , <i>str</i> <sup>s</sup> , <i>rif</i> <sup>s</sup> , <i>thi</i> <sup>-</sup> , <i>lac</i> <sup>-</sup> , <i>ara</i> <sup>+</sup> , <i>gal</i> <sup>+</sup> , <i>mtl</i> <sup>-</sup> , F <sup>-</sup> , <i>recA</i> <sup>+</sup> , <i>uvr</i> <sup>+</sup> , <i>lon</i> <sup>+</sup> , KmR.
<b>Oligonucleotides</b>	<b>Sequences</b>
Primer 1 (HBPA)	Forward: 5'ATGTCGTCATATGAGAGGATCGC 3'
Primer 2 (HBPA)	Reverse:5'GAACCGATGGTACCTTATTTGCTATACTTCG 3'
Primer 3 (HBPA)	Forward: 5'ATGAGAGGATCGCATCACC 3'
Primer 4 (HBPA)	Reverse:5'TTATTGCTATACTTCG 3'
HBPA H205A	CAC(H)→GCG(A) Forward: 5'CGAACATCCGTTTTCTGCCG <b>GCG</b> GAGGACGATTACTATGCCG3'
BCAT(53)	Forward: 5' ATGCATGCCATGGGAATGACCACGAAGAAAGCTG 3'
BCAT(35)	Reverse:5'ATACGATAGATCTTTGATTAAGTTGATCTAACCAGCCCC 3'
AspAT(53)	Forward: 5' AGTCAGCTGGATCCATGTTTGAGAACATTACCGC 3'
AspAT(35)	Reverse: 5'CATACTAAGCTTTAGTGATGGTGATGGTGATGAGATCTCAGCACTG CCACAATCGC 3'
<b>Plasmids</b>	<b>Relevant genetic characteristics</b>
pETDuet-1	The vector encodes two multiple cloning sites, each of which is preceded by a T7 promoter, <i>lac</i> operator and ribosome binding site. The vector also



	carries the pBR322-derived ColE1 replicon, <i>lacI</i> gene and ampicillin resistance gene.
pETDuet-1- <i>HBPA</i>	Plasmid containing the synthetic gene <i>nahE</i> (1008 bp), codes for <i>trans-O</i> -hydroxybenzylidenepyruvate hydratase-aldolase (HBPA , EC 4.1.2.45) from <i>Pseudomonas putida</i> .This study.
pETDuet-1- <i>HBPA H205A</i>	Plasmid containing the <i>nahE</i> (CAC→GCG) gene, codes for HBPA H205A. This study.
pQE-60	The vector encodes one multiple cloning site preceded by a T5 promoter, <i>lac</i> operator and ribosome binding site. The vector also carries the ColE1 replicon and ampicillin resistance gene.
pQE60 <i>BCAT</i>	Plasmid containing the <i>ilvE</i> gene (960 bp), codes for branched-chain amino acid aminotransferase (BCAT EC 2.6.1.42) from <i>E. coli</i> K-12. This study.
pQE60 <i>AspAT</i>	Plasmid containing the <i>aspC</i> gene (1227 bp), code for aspartate amino transferase ( <i>AspAT</i> EC 2.6.1.1) from <i>E. coli</i> K-12. This study.
pQE60 <i>BAL</i>	Previous work. <sup>2</sup>
pQE40 MBP-YfaU	Previous work. <sup>3</sup>

## Methods.

**Enzymes cloning. HBPA:** The optimized synthetic gene *nahE* (**Figure S1**) insert in a pQE 40 (GenScript's gene synthesis service) was re-cloned into the second cloning site of a pETDuet-1 plasmid, using the restriction enzymes *NdeI* and *KpnI* (**Figure S2**). All DNA manipulation were performed using routine procedures of molecular biology.<sup>3</sup>

### A)

```

ATGCTGAACAAGGTGATCAAAAACACCCGCTCTGACCGCGGAGGACATCAACGGTGCGTGGACCATTATGCCGACC
CCGAGCACCCCGGATGCGAGCGATTGGCGTAGCACCAACACCGTTGACCTGGATGAAACCGCGCGTATCGTGGAG
GAACTGATGCGCGCGGTGTTAACGGCATTCTGAGCATGGGCACCTTTGGCGAGTGCGCGACCTGACCTGGGAG
GAAAAGCGTGACTACGTGAGCACCGTGGTTGAAACCATCCGTGGTGCGTGTCCCGTATTTCTGCCGCACCACCGCG
CTGAACACCCGTGAGGTGATCCGTCAGACCCGTGAACTGATCGATATTGGTGCGAACGGCACCATGCTGGGTGTG
CCGATGTGGGTAAAGATGGACCTGCCGACCGCGGTTCAATTTTACCGTGATGTTGCGGGTGCGGTTCCGGAGGCG
GCGATCGCGATTTATGCGAACCCGGAAGCGTTCAAATTTGATTTCCCGCGTCCGTTCTGGGCGGAGATGAGCAAG
ATCCCGCAGGTGGTTACCGCGAAATACCTGGGTATTGGCATGCTGGACCTGGATCTGAACTGGCGCCGAACATC
CGTTTTCTGCCGCACGAGGACGATTACTATGCGGCGGCGGTATCAACCCGGAACGTATTACCGGTTCTGGAGC
AGCGGTGCGATGTGCGGTCCGGCGACCGCGATTATGCTGCGTGACGAGGTGGAACGTGCGAAGAGCACCGGTGAT
TGGATCAAGGCGAAAGCGATTAGCGACGATATGCGTGCGGCGGACAGCACCCCTGTTTCCGCGTGGTGATTTTAGC
GAGTTCAGCAAGTACAACATCGGCCTGGAAAAGCGCGTATGGATGCGGCGGGTTGGCTGAAAAGCGGGTCCGTCG
CGTCCGCGTACAACCTGGTGCCGGAAGATTATCTGGTTGGTGCGCAAAAGACGCGTAAAGCGTGGGCGGCGCTG
CACGCGAAGTATAGCAA

```

### B)

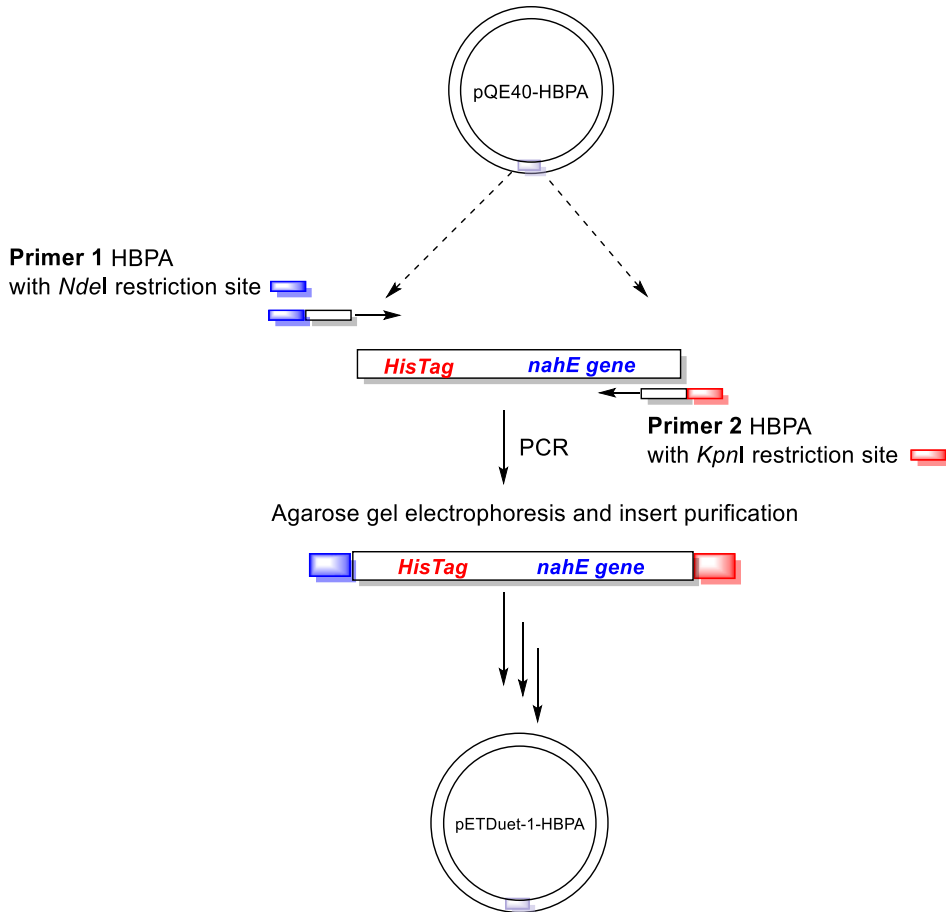
```

MLNKVIKTRRLTAEDINGAWTIMPTSPDASDWRSTNTVDLDETARIVEELIAAGVNGILSMGTFGECATLTWEEKRDYV
STVVETIRGRVPYFCGTTALNTREVIRQTRELIDIGANGTMLGVPMVWKMDLPTAVQFYRDVAGAVPEAAIAYANPEAFK
FDFPRPFWAEMSKIPQVVTA KYLGIGMLDLDLKLAPNIRFLPHEDDYAAARINPERITAFWSSGAMCGPATAIMLRDEVE
RAKSTGDWIKAKAISDDMRAADSTLFRGDFSEFSKYNIGLEKARMDAAGWLKAGPCRPPYNLVPEDYLVAQKSGKAW
AALHAKYSK

```

**Figure S1. A)** Optimized gene sequence (GenScript's gene synthesis service) and **B)** amino acid sequence of HBPA (NCBI database accession number: WP\_011475383.1).

### A)



**B)**

MRGSHHHHHHGSMLNKVIKTTRLTAEDINGAWTIMPTSTPDASDWRSTNTVDLDETARIVEELIAAGVNGILSMGTFGEC  
 ATLTWEEKRDYVSTVVEITIRGRVPYFCGTTALNTREVIRQTRELIDIGANGTMLGVPMWVKMDLPTAVQFYRDVAGAVP  
 EAAIAIYANPEAFKFDPRPFWAEMSKIPQVVTA KYLGIGMLDLDLKLAPNIRFLPHEDDYAAAARINPERITAFWSSGAMC  
 GPATAIMLRDEVERAKSTGDWIKAKAISDDMRAADSTLFRGDFSEFSKYNIGLEKARMDAAGWLKAGPCRPPYNLVPED  
 YLVGAQKSGKAWAALHAKYSK

**Figure S2. A)** Schematic representation of the cloning method of HBPA in the pETDuet-1 plasmid. **B)** Protein sequence of His tag-HBPA. 6x His tag (red) and HBPA (blue).

**BCAT** and **AspAT** (NCBI database accession number ABD20288.1 and NP\_415448 respectively). The genes *ilvE* and *aspC* from *E. coli* K-12 were amplified by PCR from genomic DNA and cloned into pQE 60 using *NcoI/BglIII* restriction enzymes (primers BCAT(53) and BCAT(35)) and *BamHI/HindIII* restriction enzymes (primers AspAT(53) and AspAT(35)) respectively (**Table S3**). All DNA manipulation were performed using routine procedures of molecular biology.<sup>3</sup>

**A)**

MGMTTKKADYIWFNGEMVVRWEDAKVHVMSHALHYGTSVFEGIRCYDSHGKGPVFRHREHMQR LHDSAKIYRFPVSQSI  
 DELMEACRDVIRKNNLTSAYIRPLIFVGDVGMGVNPPAGYSTDVIIAAPPWGAYLGAEALEQGIDAMVSSWNRAAPNTIPT  
 AAKAGGNYLSSLLVGSEARRHGYQEGIALDVNGYISEGAGENLFEVKDGVLFPPFTSSALPGITRDIIKLAKELGIEVRE  
 QVLSRESLYLADEVFMSGTAAEITPVRSVDGIQVGEGRCPVTKRIQQAFFGLFTGETEDKVGWLDQVNQRS **HHHHHH**

**B)**

MGGSMFENITAAPADPILGLADLFRADERPGKINLGIGVYKDETGKTPVLT SVKKAEQYLLENETTKNYLGIDGIPEFGRCT  
 QELLFGKGSALINDKRARTAQTPGGTGALRVAADFLAKNTSVKRVVWSNPSWPNHKS VFNSAGLEVREYAYYDAENHTL  
 DFDALINSLNEAQAGDVVLFHGCCHNPTGIDPTLEQWQTLAQLSVEKGWLP LDFAYQGFARGLEEDAEG LRAFAAMHK  
 ELIVASSYSKNFGLYNERVGACTLVAADSETVDRAFSQMKA AIRANYSNPPAHGASVVATILSNDALRAIWEQELTDMRQ  
 RIQRM RQLFVNTLQEKGANRDFSFIKQNGMFSFSGLTKEQVLR LREEFGVYAVASGRVNVAGMTPDNMAPLCEAIVAVL  
 RSHHHHHH

**Figure S3.** A) Protein sequence of BCAT-His tag and B) protein sequence of AspAT-His tag. BCAT (blue), AspAT (green) and 6x His tag (red).

**Site-directed mutagenesis**

The HBPA gene mutation H205A was introduced with the Megaprimer site-directed mutagenesis strategies (**Figure S4**) with PCR procedure described in **Table S2**.

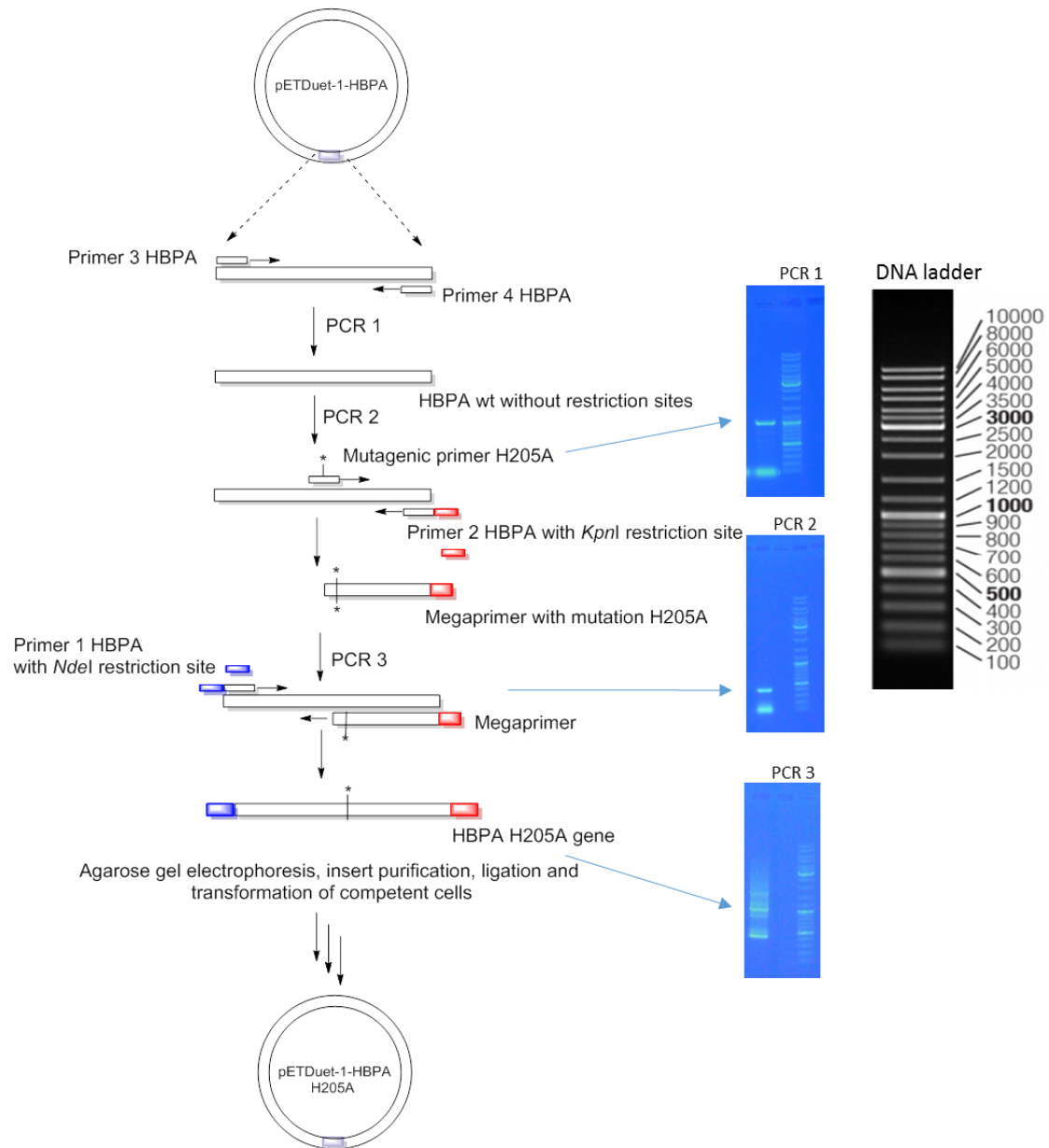


**Figure S4.** Schematic illustration of the megaprimer method for site-directed mutagenesis. The first-round PCR (PCR 1) was performed using external forward (Primer 3 HBPA) and reverse primer (Primer 4 HBPA), neither of one with restriction site. The second-round PCR (PCR 2) was performed using the internal mutagenic primer (Primer HBPA H205A) and external primer (Primer 2 HBPA) with *KpnI* restriction site. The third-round PCR (PCR 3) was performed using external primer (Primer 1 HBPA) with *NdeI* restriction site and the product of PCR2 (“megaprimer”).

**Table S2.** Megaprimer site-directed mutagenesis PCR protocols.**a) PCR 1**

Components	V/ $\mu$ L	Final concentration (50 $\mu$ L total volume)	PCR cycles		
			Step	T/ $^{\circ}$ C	Time/s
Water, nuclease free	35.5		Initial denaturation	98	180
5X Green Buffer <sup>a</sup>	10		35 PCR cycles	98	10
dNTP mix (10 mM each)	1	0.2 mM each		55	30
F1, forward primer (25 $\mu$ M)	1	0.5 $\mu$ M		72	20
R, reverse primer (25 $\mu$ M)	1	0.5 $\mu$ M			
Template DNA (1 ng $\mu$ L <sup>-1</sup> )	1	0.01 ng $\mu$ L <sup>-1</sup>	Final extension	72	600
DNA Polymerase (2 U $\mu$ L <sup>-1</sup> ) <sup>b</sup>	0.5	0.02 U $\mu$ L <sup>-1</sup>		4	Hold

**b) PCR 2**

Components	V/ $\mu$ L	Final concentration (50 $\mu$ L total volume)	PCR cycles		
			Step	T/ $^{\circ}$ C	Time/s
Water, nuclease free	35.5		Initial denaturation	98	180
5X Green Buffer <sup>a</sup>	10		35 PCR cycles	98	10
dNTP mix (10 mM each)	1	0.2 mM each		55	30
F1, forward primer (25 $\mu$ M)	1	0.5 $\mu$ M		72	6
R, reverse primer (25 $\mu$ M)	1	0.5 $\mu$ M			
Template DNA (1 ng $\mu$ L <sup>-1</sup> )	1	0.01 ng $\mu$ L <sup>-1</sup>	Final extension	72	600
DNA Polymerase (2 U $\mu$ L <sup>-1</sup> ) <sup>b</sup>	0.5	0.02 U $\mu$ L <sup>-1</sup>		4	Hold

**c) PCR 3**

Components	V/ $\mu$ L	Final concentration (50 $\mu$ L total volume)	PCR cycles		
			Step	T/ $^{\circ}$ C	Time/s
Water, nuclease free	35.5		Initial denaturation	98	180
5X Green Buffer <sup>a</sup>	10		35 PCR cycles	98	10
dNTP mix (10 mM each)	1	0.2 mM each		55	30
F1, forward primer (25 $\mu$ M)	1	0.5 $\mu$ M		72	300
R, reverse primer (25 $\mu$ M)	1	0.5 $\mu$ M			
Template DNA (1 ng $\mu$ L <sup>-1</sup> )	1	0.01 ng $\mu$ L <sup>-1</sup>	Final extension	72	600
DNA Polymerase (2 U $\mu$ L <sup>-1</sup> ) <sup>b</sup>	0.5	0.02 U $\mu$ L <sup>-1</sup>		4	Hold

<sup>a</sup>5X Phusion Green HF Buffer (Thermo Scientific). <sup>b</sup>The concentration of Megaprimer depends on the efficiency of the PCR2. Megaprimer size: 418 bp (H205A). <sup>c</sup>Fusion Green High-Fidelity DNA Polymerase (Thermo Scientific).

**Protein production and purification**

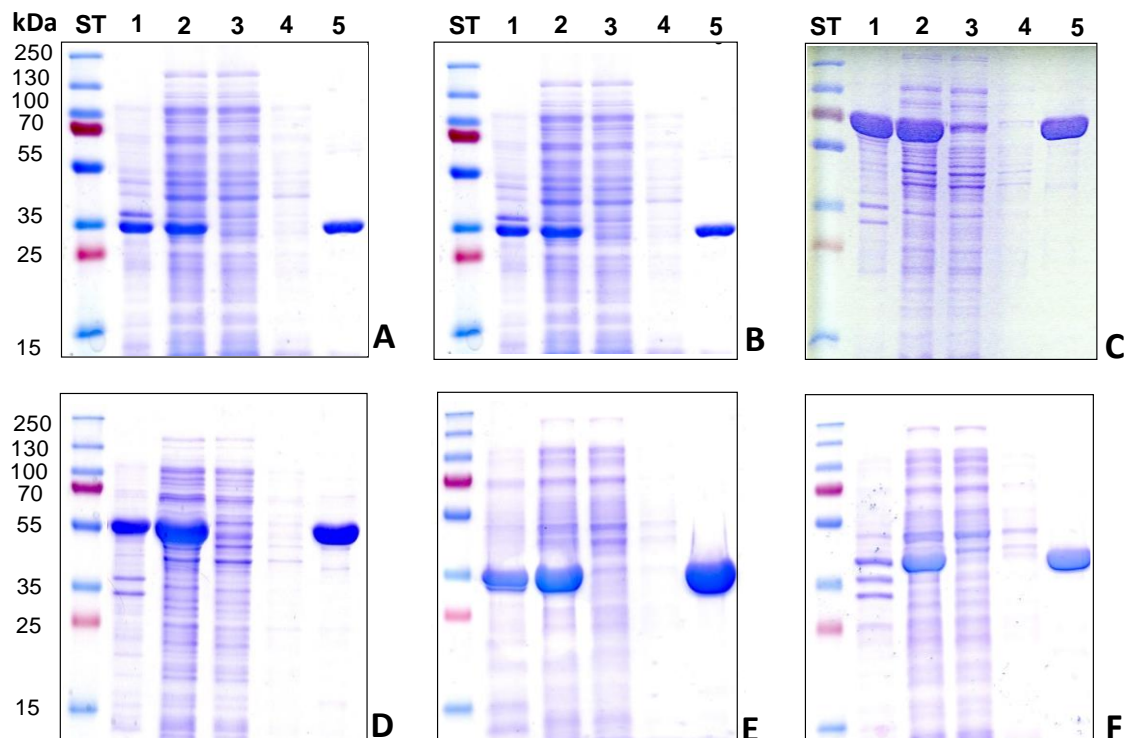
General procedure for HBPA, BCAT and AspAT: Competent *E. coli* strain cells were transformed with the correspondent plasmid (**Table S3**) and grown in LB medium with

selected antibiotics at 37 °C on a rotary shaker at 200 rpm. A final optical density at 600 nm ( $OD_{600}$ ) of 2–3 was usually achieved. An aliquot of the pre-culture (20 mL) was transferred into a baffled shaker flask (2 L) containing LB medium (1 L) plus selected antibiotics and antifoam SE-15 (0.02% (v/v)), and incubated at 37 °C with shaking at 200 rpm. During the middle exponential phase growth ( $DO_{600} \approx 0.5-0.8$ ), the temperature was lowered to 30 °C to minimize inclusion bodies formation and then proteins expression were induced (**Table S3**). After 12-16 h, cells from the induced-culture broths (5 L, 16-22 g of cells) were centrifuged (2500  $g$  for 45 min at 4 °C). The pellet was re-suspended in the lysis buffer (400 mL). Cells were lysed using a cell disrupter (Constant Systems) and cellular debris were removed by centrifugation (35000  $g$  for 45 min at 4 °C). The clear supernatant was applied to a cooled HR 16/40 column (GE Healthcare) packed with Nickel Sepharose™ High Performance (50 mL bed volume, GE Healthcare) at 6 mL min<sup>-1</sup> and washed with lysis buffer (400 mL) at 6 mL min<sup>-1</sup>. The protein was eluted with elution buffer (200 mL) at a flow rate of 6 mL min<sup>-1</sup> (**Table S3, Figure S5**). The recombinant proteins were dialyzed against 1 L of dialysis buffer (3x1 L 24 h each). The dialyzed solution obtained (90-140 mL) was stored at - 20 °C. The glycerol in dialysis buffer minimizes protein precipitation after purification. Protein concentrations were determined by absorption at 280 nm using extinction coefficients calculated by ProtParam (<http://expasy.org/tools/protparam.html>), HBPA *wt* and H205A variant (1.7 mg mL<sup>-1</sup>), BCAT (1.40 mg mL<sup>-1</sup>) and AspAT (0.98 mg mL<sup>-1</sup>), assuming all Cys residues are reduced.

**Table S3.** Conditions for expression and purification of protein using in this work.

Enzyme	Expression conditions		Purification conditions		
	Cellular expression system	Induction conditions and selection antibiotics	Lysis buffer	Elution buffer	Dialysis buffer
HBPA	<i>E. coli</i> BL21 AI	IPTG 1 mM L-arabinose (0.2% m/v) T =30 °C Ampicillin (100 $\mu\text{g mL}^{-1}$ )	50 mM $\text{NaH}_2\text{PO}_4$ buffer pH 8.0, NaCl (300 mM), imidazole (20 mM), glycerol (10 % v/v) and DNase	50mM $\text{NaH}_2\text{PO}_4$ buffer pH 8.0, NaCl (300 mM), imidazole (250mM) and glycerol (10 % v/v).	20 mM TEA buffer pH 6.5, NaCl (50 mM), EDTA (0.5 mM) and glycerol (50% v/v).
BCAT	<i>E. coli</i> M15 [pREP-4]	IPTG 50 $\mu\text{M}$ T = 20°C Ampicillin (100 $\mu\text{g mL}^{-1}$ ) Kanamycin (25 $\mu\text{g mL}^{-1}$ )			50mM $\text{NaH}_2\text{PO}_4$ buffer pH 7.0, NaCl (100 mM), PLP (0.01 mM) and glycerol (50% v/v).
AspAT					

General procedure for MBP-YfaU and BAL. Protein expression and purification were performed as described in previous work.<sup>2-3</sup>

**Figure S5.** Analysis of enzyme purification steps by Coomassie Blue-stained SDS-PAGE. *Wild-type* HBPA (A), H205A variant (B), MBP-YfaU (C), BAL (D), BCAT (E),

and AspAT (F). In each case, the gel was loaded with samples from pellet after lysis (lane 1), supernatant of lysis (lane 2), flow-through fraction (lane 3), wash fraction (lane 4) and elution fraction (lane 5). The molecular masses of the proteins in the Standard Molecular Weight Marker (ST) are as indicated. The predicted molecular mass of HBPA *wild-type* and H205A variant is 38 kDa. MBP-YfaU (72.3 kDa), BAL (60.1 kDa), BCAT (35.3 kDa), and AspAT (45 kDa).

**Table S4.** Yield of enzyme after purification and inclusion bodies formation.

Enzyme	Inclusion bodies formation/(%) <sup>a</sup>	Yield <sup>b</sup>
HBPA <i>wild-type</i>	36	72
HBPA H205A	40	85
MBP-YfaU	47	168
BAL	30	234
BCAT	39	396
AspAT	29	168

<sup>a</sup>Formation of inclusion bodies was estimated by color densitometry in SDS-PAGE using Image J version 1.53a. <sup>b</sup>mg protein L<sup>-1</sup> culture medium.

### Electrospray mass spectrometry of proteins.

Glycerinated proteins were diluted in water/formic acid (0.1% v/v) (1 mg protein mL<sup>-1</sup>, final concentration in the solution) and glycerol and salts were removed with PD MiniTrap G-10 of (GE Healthcare). The samples were eluted in water/formic acid (0.1% v/v, 0.5 mL) and injected (5 µL) to an Acquity UPLC BEH C4, 1.7 µm, 2.1x50 mm column connected to a mass spectrometer ESI-TOF instrument (LCT PremierWaters, Milford, MA, USA), equipped with a 4 GHz time-to-digital converter (TDC) with a dual ESI source (LockSpray). The second sprayer provided the lock mass calibration with leucine enkephalin (m/z 556.2771). The ESI-TOF was operated in the W-optics mode, thus providing a mass resolution of at least 10 000 full width at half maximum (FWHM). The acquisition time per spectrum was set to 0.2 s, and the mass range was from 500 to 1800 Da. Data were acquired using a cone voltage of 50 V, capillary voltage of 3000 V, desolvation temperature of 35 °C, and source temperature of 100 °C. The desolvation gas flow was set at 400 L h<sup>-1</sup> and the cone gas flow was set at 30 L h<sup>-1</sup>. The solvent system used for the elution was: solvent (A): 0.1% formic acid in CH<sub>3</sub>CN/H<sub>2</sub>O (70/30, v/v) and solvent (B): 0.1% (v/v) formic acid in H<sub>2</sub>O, gradient elution from 28% A to 100% A in 25 min, 100% A for 2 min and 28% A for 18 min, flow rate 0.2 mL min<sup>-1</sup>. Mass Lynx

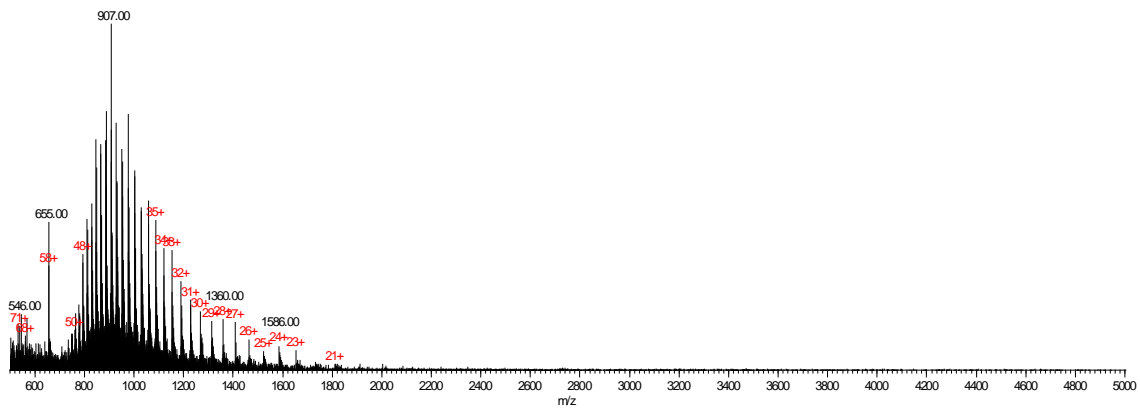
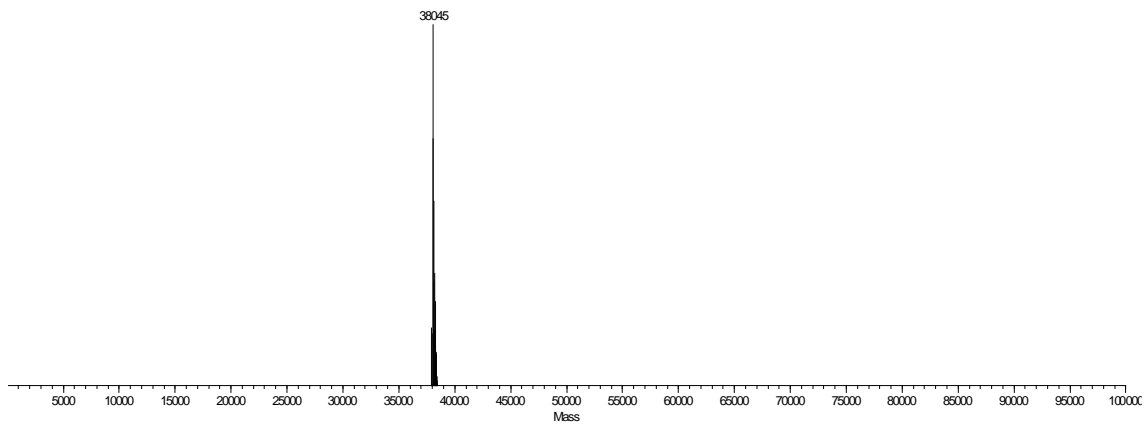


4.1 software (Waters, Milford, MA, USA) was used for data acquisition and processing. Magtran software 4, kindly provided by Dr. Zhongqi Zhang (Amgen, Inc.; Thousand Oaks, CA), was used for molecular weight deconvolution from ESI-MS spectra of proteins (**Table S5/Figure S6**).

**Table S5.** Molecular weight determination by ESI-MS of HBPA.

Enzyme variant	Molecular weight calculated/Da	$\Delta m/Da$ (HBPA <i>wt</i> – HBPA H205A) Theoretical	$\Delta m/Da$ (HBPA <i>wt</i> – HBPA H205A) Experimental
<i>Wild-type</i>	38045		
H205A	37979	66	66

HBPA *wild-type*



HBPA H205A

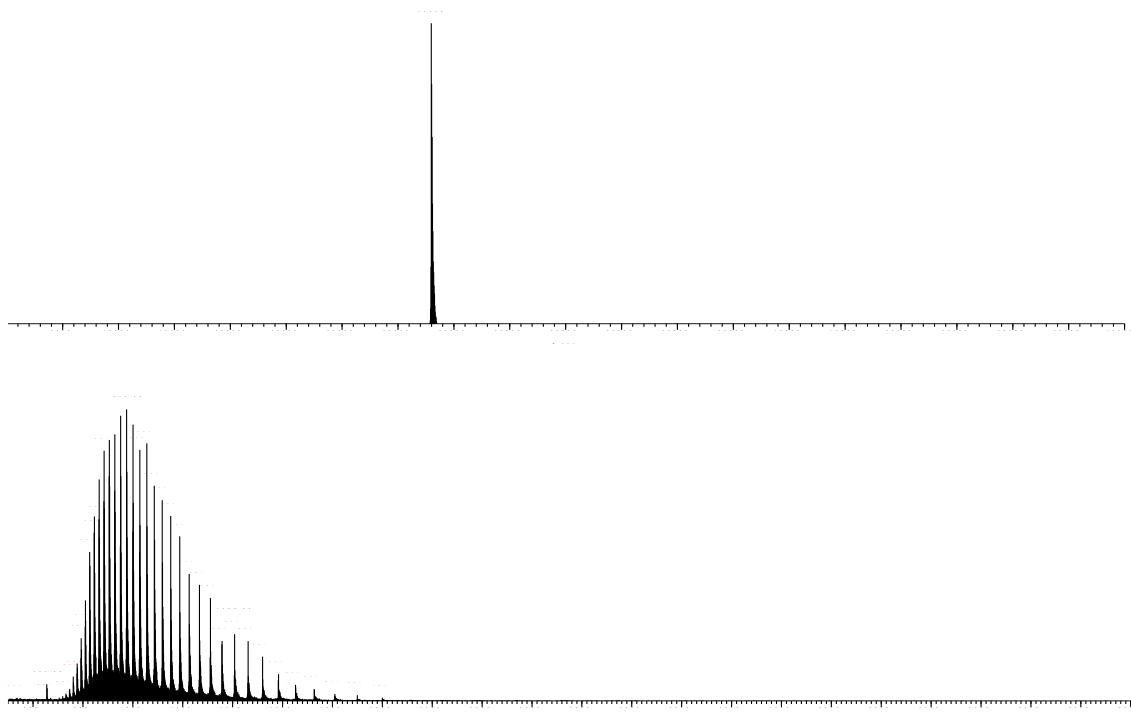


**Figure S6:** ESI/TOF spectra and deconvolution spectra of HBPA and H205A variant.

**TLC analysis.**

Thin layer chromatography was performed using precoated silica gel plates with or without fluorescent indicator UV254 (Macherey-Nagel GmbH & Co. KG, Kieselgel 60). TLC without fluorescent visualization was stained using ceric ammonium molybdate, ninhydrin or *p*-anisaldehyde.

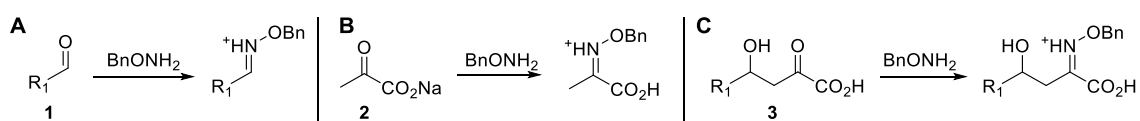
**Specific rotation.**

Specific rotation values were measured with a Perkin Elmer Model 341 (Überlingen, Germany) (Na Lamp, 589 nm). Products (16 to 63 mg) were dissolved in H<sub>2</sub>O, MeOH or CHCl<sub>3</sub> (1.5 mL) and the samples were analyzed at room temperature 1.0 dm cell with polarized light. Rotation values are described in each compound.

**HPLC analysis.**

HPLC analysis was performed on a RP-HPLC XBridge<sup>®</sup> C18, 5 μm, 4.6 × 250 mm column (Waters). The solvent system used was: solvent (A): 0.1% (v/v) trifluoroacetic acid (TFA) in H<sub>2</sub>O and solvent (B): 0.095% (v/v) TFA in CH<sub>3</sub>CN/H<sub>2</sub>O 4:1, flow rate 1 mL min<sup>-1</sup>, detection at 215 nm and column temperature at 30 °C.

The amount of products and substrates were quantified from the peak areas using an external standard methodology. Reaction monitoring for aliphatic aldehydes (**1**), sodium pyruvate (**2**) and aldol adduct (**3**) were carried out as follows:



**a)** Analysis of the compounds bearing carbonyl groups. Samples were withdrawn from the reaction mixture (10 μL) and mixed with a solution of BnONH<sub>2</sub> (50 μL of a 0.13 mM stock solution in pyridine:methanol:water 33:15:2) during 5 min, and then diluted with methanol (500 μL). After centrifugation, they were analyzed by HPLC. Elution conditions: most samples were analyzed using a gradient elution from 10 to 100% B over 30 min.

**b)** Analysis of the compounds bearing aromatic moieties. Samples were withdrawn from the reaction mixture (50 μL) and diluted with methanol (500 μL). After

centrifugation, they were analyzed by HPLC. Elution conditions: most samples were analyzed with a gradient elution from 10 to 100% B over 30 min.

c) Analysis of the compounds bearing amino groups. Samples were withdrawn from the reaction mixture (10  $\mu$ L) and mixed with sodium borate buffer (20  $\mu$ L of a 100 mM stock solution pH 10.0). Then, a solution of *N*-(benzoyloxy)succinimide (Bz-OSu) (50  $\mu$ L of a 150 mM stock solution in CH<sub>3</sub>CN, 7.5  $\mu$ mol, 7.5 eq) was added. After incubation at room temperature for 30 min, samples were diluted with AcOH:CH<sub>3</sub>CN 10:90 (300  $\mu$ L), centrifuged, and subsequently analyzed by HPLC. Elution conditions: most samples were analyzed with a gradient elution from 10 to 100% B over 30 min.

d) Chiral HPLC: Enantiomeric excesses (ee) were determined by HPLC on chiral stationary phase. Compounds **4a** and **4a'** were analyzed on a CHIRALPAK<sup>®</sup> ID, **4b**, **4e-f**, **4h-j** and **4m** on a CHIRALPAK<sup>®</sup> IB, and **4d**, **4g** and **4l** on a CHIRALPAK<sup>®</sup> IC, columns (46 x 250 mm, 5  $\mu$ m). All samples were eluted with hexane/isopropanol mixtures at flow rate 1 mL min<sup>-1</sup>, column temperature 30 °C and diode array detection (215-350 nm). Specific elution conditions are described in each compound.

### NMR analysis.

Routine <sup>1</sup>H (400 MHz) and <sup>13</sup>C (101 MHz) NMR spectra of compounds were recorded with a Varian Mercury-400 spectrometer. Full characterization of the described compounds was performed using typical gradient-enhanced 2D experiments: COSY, HSQC, NOESY, HMBC, and selective 1D nOe recorded under routine conditions.

### Activity determination of HBPA

The activity was determined using the aldol condensation of sodium pyruvate to indole-3-carboxyaldehyde using a continuous assay method.<sup>5</sup> One unit of activity was defined as the amount of HBPA that catalyzes the formation of 1  $\mu$ mol sodium (*E*)-4-(1*H*-indol-3-yl)-2-oxobut-3-enoate per min at 30 °C, in 50 mM sodium phosphate buffer pH 7.0 containing 3% of MeOH (v/v). The assay was performed as follows: to a solution of sodium pyruvate (20  $\mu$ L of a 2 M stock solution in H<sub>2</sub>O pH 6.5-7.0, prepared just before use) and indole-3-carboxyaldehyde (200  $\mu$ L of a 0.075 mM solution in 50 mM sodium phosphate buffer pH 7.0, and 3% of MeOH (v/v)), a solution of the enzyme (80  $\mu$ L, of stock solution between 0.0625 – 4 mg mL<sup>-1</sup> in 20 mM TEA buffer pH 6.8, containing

NaCl (50 mM), EDTA (0.5 mM), and 50% of glycerol (v/v)) was added. The total reaction volume was 0.3 mL. Reaction was monitoring spectrophotometrically at 367 nm during 15 min measuring each 30 s.

#### **Activity determination of (S)-selective transaminases.**

The activity of **T039** was determined using the transamination of  $\alpha$ -ketoglutarate to L-Glu, using L-Ala as amine donor. Pyruvate formed was measured with a coupled assay with lactate dehydrogenase (LDH), measuring the consumption of NADH. One unit of activity was defined as the amount of transaminase that catalyzes the formation of 1  $\mu$ mol of L-Glu per min at 30 °C in 50 mM sodium phosphate buffer pH 7.0, containing PLP (0.05 mM). The assay protocol was as follows: to a solution mixture of  $\alpha$ -ketoglutarate and L-Ala (180  $\mu$ L of a 16.6 mM  $\alpha$ -ketoglutarate, and a 83.3 mM L-Ala stock solutions, containing NADH (0.16 mM) and PLP (0.08 mM) stock solution in 50 mM sodium phosphate buffer pH 7.0), and LDH (20  $\mu$ L of 140 U mL<sup>-1</sup>stock solution, 4.2 U in the reaction), T039 (100  $\mu$ L of a 0.006 – 0.09 mg mL<sup>-1</sup> stock solutions of free cell extract powder in 50 mM sodium phosphate buffer pH 7.0) was added. Total final volume was 0.3 mL. Reaction was monitoring spectrophotometrically at 340 nm during 10 min measuring each 30 s.

Activity of **AspAT** was determined using the transamination of  $\alpha$ -ketoglutarate to L-Glu, using L-Asp as amine donor. Oxalacetic acid formed was measured with a coupled assay with lactate dehydrogenase (LDH) and Malate dehydrogenase (MDH), measuring the consumption of NADH. One unit of activity was defined as the amount of transaminase that catalyzes the formation of 1  $\mu$ mol of L-Glu per min at 30 °C in 50 mM sodium phosphate buffer pH 7.0, containing PLP (0.05 mM). The assay protocol was as follows: to a solution mixture of  $\alpha$ -ketoglutarate and L-Asp (250  $\mu$ L of a 12 mM  $\alpha$ -ketoglutarate, and 240 mM L-Asp stock solutions, containing NADH (0.19 mM) and PLP (0.12 mM) stock solution in 50 mM sodium phosphate buffer pH 7.0, LDH (2.4  $\mu$ L of 9968 U mL<sup>-1</sup> stock solution, 25 U in the reaction) and MDH (10  $\mu$ L of 6000 U mL<sup>-1</sup>stock solution, 5 U in the reaction), AspAT (50  $\mu$ L, of stock solution between 0.00024 - 1 mg mL<sup>-1</sup> in 50mM NaH<sub>2</sub>PO<sub>4</sub> buffer pH 7.0, NaCl (100 mM), PLP (0.01 mM) and glycerol (50% v/v)) was added. Total final volume was 0.3 mL. Reaction was monitoring spectrophotometrically at 340 nm during 15 min measuring each 30 s.

Activity of **BCAT** was determined using the transamination of  $\alpha$ -ketoglutarate to L-Glu, using L-Val as amine donor. L-Glu formed was measured with a coupled assay with Glutamate dehydrogenase (GDH) measuring the formation of NADH.<sup>6</sup> One unit of activity was defined as the amount of transaminase that catalyzes the formation of 1  $\mu$ mol of L-Glu per min at 30 °C in 100 mM sodium phosphate buffer pH 8.0, containing PLP (0.05 mM). The assay protocol was as follows: to a solution mixture of  $\alpha$ -ketoglutarate and L-Val (250  $\mu$ L of 6 mM  $\alpha$ -ketoglutarate, and 12 mM L-Val stock solution, containing NAD<sup>+</sup> (0.6 mM) and PLP (0.6 mM) in 100 mM sodium phosphate buffer pH 8.0, GDH (1.8 mg of 13 U mg<sup>-1</sup> stock solution, 2 U mL<sup>-1</sup> in the reaction), BCAT (50  $\mu$ L, of stock solution between 0.0078 – 1 mg mL<sup>-1</sup> in 50 mM NaH<sub>2</sub>PO<sub>4</sub> buffer pH 7.0, NaCl (100 mM), PLP (0.01 mM) and glycerol (50% v/v)) was added. Total final volume was 0.3 mL. Reaction was monitoring spectrophotometrically at 340 nm during 15 min measuring each 30 s.

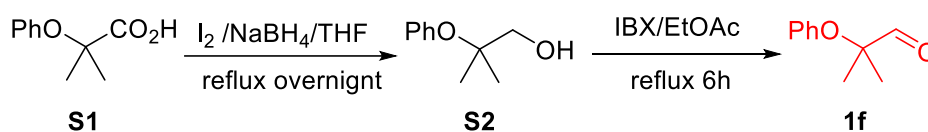
#### Synthesis of starting material (1c-f, 1i-j, 1l-s).

**2-(Benzylthio)acetaldehyde (1c).** Typical procedure: The title compound was prepared by oxidation the corresponding alcohol precursor. 2-(Benzylthio)ethanol (1.2 g, 7.1 mmol) was dissolved in EtOAc (250 mL) and 2-iodoxybenzoic acid (IBX) (4.0 g, 14.3 mmol, 2 eq) was added. The mixture was refluxed for 6 h. Then, the reaction mixture was allowed to cold down to room temperature (rt), filtrated and the filtrate was washed with NaHCO<sub>3</sub> 5%, brine (3 x 100 mL), dried over anhydrous MgSO<sub>4</sub> and concentrated under vacuum to afford the compound **1c** as a yellow oil, (959 mg, 81%). The spectral properties of this product agreed with those reported in the literature.<sup>7</sup> <sup>1</sup>H NMR (400 MHz, CDCl<sub>3</sub>)  $\delta$  9.40 (t,  $J = 2 \times 3.4$  Hz, 1H), 7.34 – 7.21 (m, 5H), 3.61 (s, 2H), 3.07 (d,  $J = 3.4$  Hz, 2H). <sup>13</sup>C NMR (101 MHz, CDCl<sub>3</sub>)  $\delta$  193.8, 129.2, 128.6, 127.4, 40.2, 35.5.

**2-Methoxyacetaldehyde (1d).** To a solution of 1,1,2-trimethoxyethane (5.0 g, 41.6 mmol) in H<sub>2</sub>SO<sub>4</sub> (20 mL, 2 M), was stirred at rt for 1 h. CaCO<sub>3</sub> solid was added until neutralization. After that, reaction mixture was filtrated through Celite<sup>®</sup>. Aldehyde **1d** was used without any further purification. The concentration of the compound in the final solution resulted to be 0.4 M, as determined by HPLC analysis using pre-column derivatization with *O*-benzylhydroxylamine.

**2-Phenoxyacetaldehyde (1e).** The title compound **1e** (oil, 1.4 g, 92%) was prepared following the procedure described for (**1c**) starting from 2-phenoxyethanol (1.5 g, 10.9 mmol). The spectral properties of this product matched those reported in the literature.<sup>8</sup> <sup>1</sup>H NMR (400 MHz, CDCl<sub>3</sub>) δ 9.86 (t, *J* = 2x1.2 Hz, 1H), 7.34 – 7.19 (m, 2H), 7.05 – 6.78 (m, 3H), 1.55 (s, 2H). <sup>13</sup>C NMR (101 MHz, CDCl<sub>3</sub>) δ 199.4, 157.6, 129.6, 122.0, 114.5, 72.6.

**2-Methyl-2-phenoxypropanal (1f).**



To a suspension of 2-methyl-2-phenoxypropanoic acid **S1** (2.0 g, 11.1 mmol) and NaBH<sub>4</sub> (1.3 g, 33.3 mmol, 3 eq) in anhydrous THF (100 mL), I<sub>2</sub> (3.4 g, 13.3 mmol, 1.2 eq) was slowly added under N<sub>2</sub> atmosphere. When all the added I<sub>2</sub> was consumed, the reaction was stirred overnight under reflux. The mixture was allowed to cold down to rt, and methanol was added until there was no gas formation. The solvent was removed under vacuum affording a white solid. To this residue, aqueous NaOH 5% (200 mL) was added and solution was stirred for 3 h, and extracted with CH<sub>2</sub>Cl<sub>2</sub> (3 x 100 mL). The organic phases were combined, washed with water (3x100 mL), NaHCO<sub>3</sub> 20% (3 x 100 mL), brine (3 x 100 mL) and dried over anhydrous magnesium sulfate. The solvent removed under vacuum affording 2-methyl-2-phenoxypropanol **S2** as an oil (1.7 g, 90%). <sup>1</sup>H NMR (400 MHz, CDCl<sub>3</sub>) δ 7.30 – 7.23 (m, 2H), 7.09 (t, *J* = 2x7.4 Hz, 1H), 6.99 (d, *J* = 1.4 Hz, 1H), 6.96 (d, *J* = 1.2 Hz, 1H), 3.58 (s, 2H), 1.26 (s, 6H). <sup>13</sup>C NMR (101 MHz, CDCl<sub>3</sub>) δ 154.5, 129.1, 123.8, 80.6, 70.3, 23.1. The title compound **1f** (oil, 932 mg, 57%) was prepared following the procedure described for **1c** starting from **S2** (1.7 g, 10.0 mmol). <sup>1</sup>H NMR (400 MHz, CDCl<sub>3</sub>) δ 9.84 (s, 1H), 7.29 – 7.19 (m, 2H), 7.02 (t, *J* = 2x7.9 Hz, 1H), 6.85 (d, *J* = 0.8 Hz, 1H), 6.83 (d, *J* = 1.0 Hz, 1H), 1.41 (s, 6H). <sup>13</sup>C NMR (101 MHz, CDCl<sub>3</sub>) δ 203.4, 155.1, 129.4, 122.8, 119.8, 83.1, 21.8.

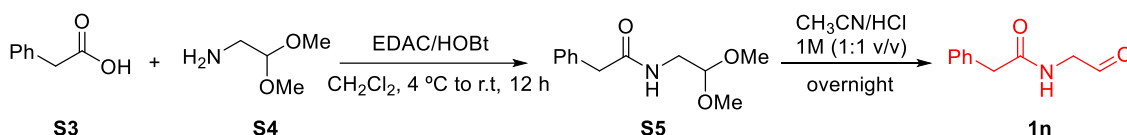
**Isopropyl 2-oxoacetate (1i).** To a solution of diisopropyl-L-(+)-tartrate (5.0 g, 21.4 mmol) in anhydrous ether (100 mL) at 4 °C, H<sub>5</sub>IO<sub>6</sub> (4.9 g, 21.4 mmol, 1 eq) was added under N<sub>2</sub> atmosphere. After stirring at 4 °C for 2 h, the reaction mixture was filtered through Celite® and the filter cake washed with ether (3 x 100 mL). Finally, the solvent

was removed under vacuum affording the title compound (**1i**) as a yellow oil (5 g, 88%). The compound was used without any further purification.  $^1\text{H}$  NMR (400 MHz,  $\text{CD}_3\text{OD}$ )  $\delta$  5.06 – 4.98 (m, 1H), 1.26 (d,  $J = 2.0$  Hz, 3H), 1.25 (d,  $J = 2.0$  Hz, 3H).  $^{13}\text{C}$  NMR (101 MHz,  $\text{CD}_3\text{OD}$ )  $\delta$  168.6, 93.5, 68.9, 20.4.

**tert-Butyl 2-oxoacetate (1j).** Compound **1j** was obtained as a white solid (1 g, 99%) following the procedure described for **1i** starting from di-*tert*-butyl-L-(+)-tartrate (1.0 g 3.8 mmol).  $^1\text{H}$  NMR (400 MHz,  $\text{CD}_3\text{OD}$ )  $\delta$  4.70 (s, 1H), 4.34 (s, 1H), 3.29 (s, 1H), 1.47 (d,  $J = 3.7$  Hz, 9H).  $^{13}\text{C}$  NMR (101 MHz,  $\text{CD}_3\text{OD}$ )  $\delta$  170.8, 168.3, 93.7, 47.98, 81.8, 72.6, 26.8.

**3-(Benzyloxy)propanal (1m).** The title compound **1m** (colorless oil, 1.5 g, 99%) was prepared following the procedure described for **1c** starting from 3-(benzyloxy)propan-1-ol (1.5 g, 9.0 mmol). The NMR data agreed with that reported in the literature.<sup>8</sup>  $^1\text{H}$  NMR (400 MHz,  $\text{CDCl}_3$ )  $\delta$  9.79 (t,  $J = 2 \times 1.9$  Hz, 1H), 7.36 – 7.24 (m, 5H), 4.52 (s, 2H), 3.80 (t,  $J = 2 \times 6.1$  Hz, 2H), 2.69 (td,  $J = 2 \times 6.1$ , 1.9 Hz, 2H).  $^{13}\text{C}$  NMR (101 MHz,  $\text{CDCl}_3$ )  $\delta$  201.1, 137.8, 128.4, 127.8, 127.7, 73.2, 63.8, 43.9.

#### ***N*-(2-Oxoethyl)-2-phenylacetamide (1n).**



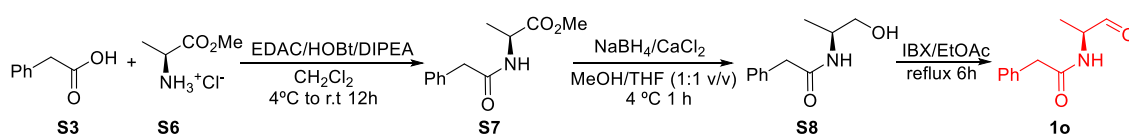
To a solution of 2-phenylacetic acid **S3** (10.0 g, 73.5 mmol) in anhydrous  $\text{CH}_2\text{Cl}_2$  (200 mL) at 4 °C, HOBt (11.9 g 88.4 mmol, 1.2 eq) was added, followed by EDAC (16.9 g, 88.2 mmol, 1.2 eq), and 2,2-dimethoxyethanamine **S4** (9.3 g, 88.1 mmol, 1.2 eq). After stirring for 12 h from 4 °C to rt under  $\text{N}_2$  atmosphere, the solvent was removed under vacuum. The residue was re-suspended in EtOAc (400 mL), washed with citric acid 5% (3 x 200 mL),  $\text{NaHCO}_3$  5% (3 x 200 mL), brine (3 x 200 mL) and dried over anhydrous  $\text{MgSO}_4$  and concentrated under vacuum yielding *N*-(2,2-dimethoxyethyl)-2-phenylacetamide **S5** (11.5 g, 70%).  $^1\text{H}$  NMR (400 MHz,  $\text{CDCl}_3$ )  $\delta$  7.36 – 7.21 (m, 5H), 4.29 (t,  $J = 2 \times 5.4$  Hz, 1H), 3.56 (s, 2H), 3.34 (t,  $J = 2 \times 5.6$  Hz, 2H), 3.31 (s, 6H).  $^{13}\text{C}$  NMR (101 MHz,  $\text{CDCl}_3$ )  $\delta$  171.0, 134.8, 129.3, 128.9, 127.3, 102.6, 54.5, 43.7, 41.1. A solution of **S5** (3.0 g, 13.4 mmol) was dissolved in  $\text{CH}_3\text{CN}/\text{HCl}$  1 M 1:1 (v/v) (150 mL) and the



mixture was stirred at rt overnight. After that, the solvent was evaporated under vacuum until the remaining aqueous phase. Then, solid NaCl was added until saturation, and extracted with CH<sub>2</sub>Cl<sub>2</sub> (3 x 100 mL). The organic phases were combined, dried over anhydrous MgSO<sub>4</sub> and concentrated under vacuum to afford the title compound **1n** as solid (2.1 g, 87%). The NMR data agreed with that reported in the literature.<sup>9</sup> <sup>1</sup>H NMR (400 MHz, CDCl<sub>3</sub>) δ 9.59 (s, 1H), 7.39 – 7.22 (m, 5H), 4.14 (d, *J* = 5.0 Hz, 2H), 3.62 (s, 2H). <sup>13</sup>C NMR (101 MHz, CDCl<sub>3</sub>) δ 196.0, 171.3, 134.2, 129.4, 129.1, 127.5, 50.3, 43.4.

**L-Alanine methyl ester hydrochloride (S6).** To a solution of L-Ala (6.5 g, 73.0 mmol) in anhydrous MeOH (150 mL) cooled at – 80 °C, SOCl<sub>2</sub> (26.0 g, 218.9 mmol, 3 eq) was slowly added under N<sub>2</sub> atmosphere. After the addition, the mixture was stirred overnight allowed to warm up to rt. After that, the solvent was evaporated under vacuum and the residue was dissolved again with MeOH and removed under vacuum. This operation was repeated five times (5 x 100 mL). Finally, the excess of volatile acid was eliminated *in vacuo* over NaOH pellets.<sup>10</sup> L-Alanine methyl ester hydrochloride (10.4 g, 99%) was obtained as a white solid. <sup>1</sup>H NMR (400 MHz, D<sub>2</sub>O) δ 4.06 (q, *J* = 3x7.2 Hz, 1H), 3.70 (d, *J* = 1.0 Hz, 3H), 1.41 (dd, *J* = 7.3, 1.0 Hz, 3H). <sup>13</sup>C NMR (101 MHz, D<sub>2</sub>O) δ 171.2, 53.5, 48.7, 15.0.

**(S)-N-(1-Oxopropan-2-yl)-2-phenylacetamide (1o).**



To a solution of 2-phenylacetic acid **S3** (8.3 g, 61.0 mmol, 1 eq) in anhydrous CH<sub>2</sub>Cl<sub>2</sub> (200 mL) at 4 °C, HOBt (10.0 g 73.2 mmol, 1.2 eq) was added, followed by consecutive the addition of EDAC (10.2 g, 73.2 mmol, 1.2 eq), L-alanine methyl ester hydrochloride **S6** (10.2 g, 73.2 mmol, 1.2 eq) and DIPEA (11.8 g, 91.4 mmol, 1.5 eq). After stirring for 12 h from 4°C to rt under N<sub>2</sub> atmosphere, the reaction mixture was transferred to a separation funnel and the organic phase was washed with HCl 1 M (3 x 200 mL), NaHCO<sub>3</sub> 5% (3 x 200 mL) and brine (3 x 200 mL). Then, the organic phase was dried over anhydrous MgSO<sub>4</sub> and concentrated under vacuum yielding *N*-phenylacetyl-L-alanine methyl ester **S7** (12.6 g, 93%) as a white solid. <sup>1</sup>H NMR (400 MHz, CDCl<sub>3</sub>) δ 7.39 – 7.22 (m, 5H), 4.56 (p, *J* = 2x7.2, 2x7.1Hz, 1H), 3.69 (s, 3H), 3.57 (s, 2H), 1.32 (d, *J* = 7.1 Hz,

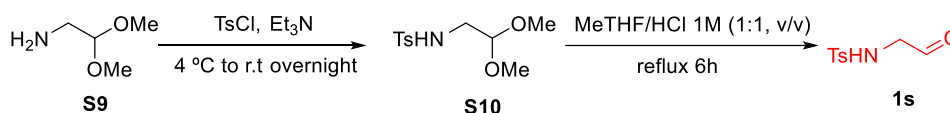
3H).  $^{13}\text{C}$  NMR (101 MHz,  $\text{CDCl}_3$ )  $\delta$  173.3, 170.3, 134.4, 127.4, 129.4, 129.0, 127.4, 52.4, 48.1, 43.6, 18.3. To a solution of **S7** (6.0 g, 27.1 mmol) in anhydrous MeOH/THF mixture (100 mL 1:1 v/v),  $\text{CaCl}_2$  (15.1 g, 135.6 mmol, 5 eq) and  $\text{NaBH}_4$  (5.1 g, 135.6 mmol, 5 eq) were added and the mixture was stirred for 1h at 0 °C under  $\text{N}_2$  atmosphere. Then, HCl 1 M (300 mL) was added at 4°C and stirred until no gas formation was detected. The organic solvent was removed under vacuum, checking that the pH of the aqueous phase was acidic. The product was extracted with  $\text{CH}_2\text{Cl}_2$  (3 x 100 mL) and the combined organic phases dried over anhydrous  $\text{MgSO}_4$  and concentrated under vacuum to afford *N*-phenylacetyl-L-alaninol **S8** as a white solid (4.2 g, 81%).  $^1\text{H}$  NMR (400 MHz,  $\text{CDCl}_3$ )  $\delta$  7.38 – 7.20 (m, 5H), 4.02 (ddt,  $J = 10.5, 6.8, 2 \times 3.6$  Hz, 1H), 3.60 (dd,  $J = 10.9, 3.4$  Hz, 2H), 3.56 (s, 2H), 3.46 (dd,  $J = 11.0, 6.1$  Hz, 2H), 1.07 (d,  $J = 6.8$  Hz, 3H).  $^{13}\text{C}$  NMR (101 MHz,  $\text{CDCl}_3$ )  $\delta$  171.9, 134.7, 129.3, 129.0, 127.4, 67.2, 48.1, 43.7, 16.8. *N*-phenylacetyl-L-alaninol **S8** (2.0 g, 10.4 mmol) was dissolved in EtOAc and oxidized with IBX (5.8 g, 20.7 mmol) using an identical procedure to that described for **1c**, affording the title compound **1o** as a white solid (1.5 g, 76%).  $^1\text{H}$  NMR (400 MHz,  $\text{CDCl}_3$ )  $\delta$  9.48 (s, 1H), 7.39 – 7.21 (m, 5H), 4.47 (p,  $J = 4 \times 7.4$  Hz, 1H), 3.60 (s, 2H), 1.29 (d,  $J = 7.4$  Hz, 3H).  $^{13}\text{C}$  NMR (101 MHz,  $\text{CDCl}_3$ )  $\delta$  198.7, 170.9, 134.4, 129.3, 129.1, 127.5, 54.4, 43.4, 14.4.

***N*-Cbz-2-Aminoethanal (1p)**. The title compound **1p** (oil, 1.8 g, 92%) was prepared following the procedure described for **1c** starting from *N*-Cbz-2-aminoethanol (2.0 g, 10.2 mmol). The spectral properties of this product matched those reported in the literature.<sup>11</sup>  $^1\text{H}$  NMR (400 MHz,  $\text{CDCl}_3$ )  $\delta$  9.64 (s, 1H), 7.40 – 7.26 (m, 5H), 5.12 (s, 2H), 4.14 (d,  $J = 5.1$  Hz, 2H).  $^{13}\text{C}$  NMR (101 MHz,  $\text{CDCl}_3$ )  $\delta$  196.3, 156.2, 136.1, 128.6, 128.3, 128.1, 67.2, 51.7.

***tert*-Butyloxycarbonyl-2-aminoethanal (1r)**. To a solution of 2-aminoethanol (3.0 g, 49.1 mmol) in anhydrous  $\text{CH}_2\text{Cl}_2$  (50 mL), di-*tert*-butyldicarbonate ( $\text{Boc}_2\text{O}$ ) (10.7 g, 49.1 mmol, 1eq) was added under  $\text{N}_2$  atmosphere. After stirring at rt overnight the solvent was removed under vacuum. The residue was re-suspended in EtOAc (300 mL) and washed with citric acid 5% wt/v (3 x 100 mL),  $\text{NaHCO}_3$  5% wt/v (3 x 100 mL) and brine (3 x 100 mL). The organic phase was dried over anhydrous  $\text{MgSO}_4$  and concentrated under vacuum yielding *tert*-butyl (2-hydroxyethyl)carbamate as a yellow oil (5 g, 63%).  $^1\text{H}$  NMR (400 MHz,  $\text{CDCl}_3$ )  $\delta$  3.76 – 3.57 (m, 2H), 3.26 (q,  $J = 2 \times 5.4, 5.3$  Hz, 2H), 1.42 (s, 9H).  $^{13}\text{C}$  NMR (101 MHz,  $\text{CDCl}_3$ )  $\delta$  146.7, 79.7, 62.7, 43.2, 28.3. *Tert*-butyl (2-

hydroxyethyl)carbamate (1.5 g, 10.3 mmol) was dissolved in EtOAc and oxidized with IBX (5.8 g, 52.0 mmol) using an identical procedure to that for compound **1c**, affording the title compound **1r** as an oil (1.1 g, 76%). <sup>1</sup>H NMR (400 MHz, CDCl<sub>3</sub>) δ 9.63 (s, 1H), 4.06 (d, *J* = 5.1 Hz, 2H), 1.43 (s, 9H). <sup>13</sup>C NMR (101 MHz, CDCl<sub>3</sub>) δ 197.0, 146.7, 85.2, 28.2. The NMR data matched that reported in the literature.<sup>12</sup>

#### 4-Methyl-*N*-(2-oxoethyl)benzenesulfonamide (**1s**).



To a solution of 2,2-dimethoxyethanamine (**S9**) (2.0 g, 19.0 mmol) in anhydrous CH<sub>2</sub>Cl<sub>2</sub> (100 mL), TsCl (3.6 g 19.0 mmol, 1 eq) and Et<sub>3</sub>N (2.9 g, 28.5 mmol, 1.5 eq) were added at 4 °C under N<sub>2</sub> atmosphere and then left to warm up to rt. After stirring for 24 h, the reaction mixture was extracted with HCl 1 M (3 x 100 mL). Then, the organic phase was washed with NaHCO<sub>3</sub> 5% (3 x 100 mL) and brine (3 x 100 mL), dried over anhydrous MgSO<sub>4</sub> and concentrated under vacuum yielding *N*-(2,2-dimethoxyethyl)-4-methylbenzenesulfonamide (**S10**) as an oil (4.7 g, 96%). **S10** (4.7 g, 18.2 mmol) was dissolved in MeTHF/HCl 1 M (200 mL 1:1 v/v). After stirring under reflux for 6 h, the mixture was then allowed to cold down to rt and the organic solvent was removed under vacuum. The residue was re-suspended in EtOAc (300 mL), washed with brine (3 x 100 mL), dried over anhydrous MgSO<sub>4</sub>, and concentrated under vacuum to afford the compound **1s** as a white solid (3.4 g, 90%). <sup>1</sup>H NMR (400 MHz, CDCl<sub>3</sub>) δ 9.54 (s, 1H), 7.72 (d, *J* = 8.3 Hz, 1H), 7.30 (dt, *J* = 7.9, 2x0.8 Hz, 2H), 3.91 (d, *J* = 5.1 Hz, 2H), 2.41 (s, 3H). <sup>13</sup>C NMR (101 MHz, CDCl<sub>3</sub>) δ 194.7, 144.0, 136.0, 129.9, 127.2, 52.6, 21.5.

#### General procedure for the aldol addition of sodium pyruvate to aldehydes (**1a-s**) catalyzed by HBPA

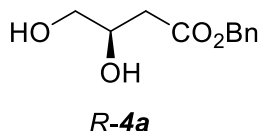
Analytical scale: The reaction (500 μL total volume) was conducted in 1.5 mL Eppendorf tubes. To a solution of the aldehyde (**1a-s**) (dissolved in 50 mM sodium phosphate buffer pH 7.0, 100 mM final concentration in the reaction; in case of partial water solubility, DMF (20% v/v in the reaction was used), a solution of sodium pyruvate (**2**) (25 μL of a 2.0 M aqueous stock solution, pH 6.5-7.0, 100 mM final concentration in the reaction, (*Caution: The solution of sodium pyruvate has to be freshly prepared before use!*) was added.

The reaction was started by adding of HBPA *wild-type* (125  $\mu\text{L}$  of a stock solution 0.029 U  $\text{mL}^{-1}$ , 4 mg  $\text{mL}^{-1}$  in 50 mM TEA buffer, 50 mM NaCl, 0.5 mM EDTA and 50% (v/v) of glycerol, 0.007 U  $\text{mL}^{-1}$ , 1 mg protein  $\text{mL}^{-1}$  final concentration in the reaction). The reaction mixture was placed in a vortex mixer (1000 rpm) at 25 °C for 24 h. Samples were withdrawn immediately after the enzyme addition (0 h) and after 24 h and analyzed by HPLC as described above.

### Synthesis of 4-hydroxyesters (*R-4a-m*)

The aldol additions catalyzed by HBPA, oxidative decarboxylation and the subsequent esterification was carried as follows:

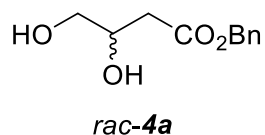
#### Benzyl (*R*)-3,4-dihydroxybutanoate (*R-4a*).



The synthesis of sodium 4-hydroxy-2-oxoacid **3a** was conducted in 50 mL Erlenmeyer flask. The reaction volume was 20 mL. Sodium pyruvate **2** (1.1 g, 10 mmol, 1 eq, 0.5 M in the reaction) and glycolaldehyde dimer (600 mg, 10 mmol monomer, 1 eq, 0.5 M in the reaction) were dissolved in 15 mL of water. Finally, reaction was started by adding the enzyme (HBPA *wild-type*, 5 mL of a stock solution 0.029 U  $\text{mL}^{-1}$ , 4 mg  $\text{mL}^{-1}$  in 50 mM TEA buffer, 50 mM NaCl, 0.5 mM EDTA and 50% (v/v) of glycerol, 0.007 U  $\text{mL}^{-1}$ , 1 mg protein  $\text{mL}^{-1}$  final concentration in the reaction). The mixture was placed in an orbital shaker (250 rpm) at 25 °C for 24 h. Reaction was monitored by HPLC and samples were withdrawn immediately after the enzyme addition (0 h) and after 24 h as described above. When the aldol adduct **3a** formed was maximum, the reaction mixture was transferred in a round-bottom flask of 250 mL capacity to avoid spilling of the reaction media due to the huge amount of foam generated when adding the catalase to eliminate the excess of  $\text{H}_2\text{O}_2$  (see below) and cooled down to 4 °C. To this mixture,  $\text{H}_2\text{O}_2$  (1.4 mL of a stock solution 8.8 M, 1.2 eq) was added under magnetic stirring. The reaction was monitored by HPLC, and when **3a** was not detected by HPLC, catalase from bovine liver (50 mg) dissolved in 100 mM sodium phosphate buffer, pH 7.0 (1 mL) was added. When the mixture stopped bubbling, it was diluted with methanol (10 volumes), filtered through Celite® and the filter cake washed with methanol (3 x 50 mL). The filtrates were pooled and the solvent was removed under vacuum until dryness. The residue was re-suspended in anhydrous DMF (40 mL) under  $\text{N}_2$  atmosphere and CsCl (6.7 mg, 4.0 mmol, 0.4 eq) was added. The

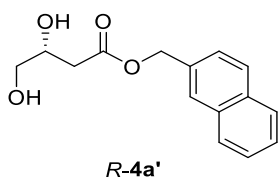
reaction was started by adding BnBr (3.4 g, 20 mmol, 2.0 eq) and stirred at 25 °C for 24 h. Then, EtOAc (200 mL) was added and washed with H<sub>2</sub>O (3 x 100 mL) and brine (3 x 100 mL). The organic phase was dried over anhydrous MgSO<sub>4</sub>, absorbed onto silica gel (100 mL) and loaded in a column chromatography (47x4.5 cm) packed with silica gel (100 g, 35-70 μm, 200-500 mesh). Product was eluted with a step gradient of hexane: EtOAc: 100:0, 200 mL, 80:20, 200 mL, 40:60, 200 mL, 20:80, 200 mL, 0:100, 500 mL. Pure fractions were pooled, and the solvent removed under vacuum affording the title compound *R-4a* as a white solid (401 mg, 19 %).  $[\alpha]_{20}^D = -11.2$  ( $c = 1$ , in MeOH). Chiral HPLC analysis: CHIRALPACK ID, isocratic elution hexane/isopropanol 80/20 (v/v), flow rate 1 mL min<sup>-1</sup>,  $t_r$  (*S*) = 12.774 min,  $t_r$  (*R*) = 11.293 min, 97:3 er. <sup>1</sup>H NMR (400 MHz, D<sub>2</sub>O)  $\delta$  7.34 – 7.21 (m, 5H), 5.04 (s, 2H), 3.98 (ddt,  $J = 8.7, 6.3, 2 \times 4.4$ , Hz, 1H), 3.43 (dd,  $J = 11.7, 4.4$  Hz, 1H), 3.37 (dd,  $J = 11.7, 6.3$  Hz, 1H), 2.51 (dd,  $J = 15.6, 4.4$  Hz, 1H), 2.39 (dd,  $J = 15.6, 8.8$  Hz, 1H). <sup>13</sup>C NMR (101 MHz, D<sub>2</sub>O)  $\delta$  173.4, 135.5, 128.7, 128.7, 128.5, 128.2, 127.4, 68.4, 67.0, 64.7, 38.2. ESI-TOF  $m/z$ : Calcd for  $[M+Na^+]$  C<sub>11</sub>H<sub>14</sub>O<sub>4</sub>Na<sup>+</sup>: 233.0823, found  $[M+Na^+]$ : 2330814.

#### Benzyl 3,4-dihydroxybutanoate (*rac-4a*).



The racemic aldol adduct *rac-3a* was conducted in an Erlenmeyer flask (50 mL). The reaction volume was 10 mL. Sodium pyruvate **2** (1.1 g, 10 mmol, 1 eq, 1.0 M in the reaction) and glycolaldehyde dimer (0.6 g, 10 mmol monomer, 1 eq, 1.0 M in the reaction) were dissolved in 4.9 mL of water and NiCl<sub>2</sub> (100 μL of a 0.1 M stock solution, 1 mM final concentration in the reaction) was added. Finally, reaction was started by adding the enzyme (MBP-YfaU, 55.6 mg of lyophilized powder, dissolved in water (4.9 mL), 2 mg protein mL<sup>-1</sup> final concentration in the reaction). The mixture was placed in an orbital shaker (250 rpm) at 25 °C for 24 h. The aldol reaction was analyzed as describe above. The subsequent oxidative decarboxylation, esterification, and purification were performed as described for *R-4a*, affording the compound *rac-4a* (579 mg, 28%). NMR spectra is indistinguishable from that of *R-4a*.

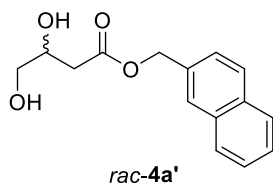
#### Naphthalen-2-ylmethyl (*R*)-3,4-dihydroxybutanoate (*R-4a'*).



Synthesis of **3a** and decarboxylation reaction were performed as described for *R-4a*. The residue from the oxidative decarboxylation was suspended in anhydrous DMF (40 mL) under N<sub>2</sub> atmosphere, and CsCl (336.4 mg, 2.0 mmol, 0.4 eq) was added. To this suspension, 2-(bromomethyl)naphthalene (2.2 g, 10 mmol, 2 eq) was added and the reaction was stirred at 25 °C for 24 h. Work up and purification were carried out as described for *R-4a*. Compound *R-4a'* was obtained as a white solid (650 mg, 50%).  $[\alpha]_{20}^D = +10.6$  ( $c = 1$ , in MeOH). Chiral HPLC analysis: CHIRALPACK ID, isocratic elution hexane/isopropanol 80/20 (v/v), flow rate 1 mL min<sup>-1</sup>, tr (*S*) = 17.145 min, tr (*R*) = 14.157 min, 98:2 er. <sup>1</sup>H NMR (400 MHz, CDCl<sub>3</sub>) δ 7.84 (d,  $J = 3.9$  Hz, 1H), 7.83 – 7.80 (m, 3H), 7.51 – 7.45 (m, 2H), 7.44 (dd,  $J = 8.5, 1.7$  Hz, 1H), 5.31 (s, 2H), 4.15 (ddt,  $J = 8.0, 6.1, 3.8$  Hz, 1H), 3.67 (dd,  $J = 11.3, 3.6$  Hz, 1H), 3.52 (dd,  $J = 11.3, 6.1$  Hz, 1H), 2.63 (dd,  $J = 16.6, 8.6$  Hz, 1H), 2.56 (dd,  $J = 16.6, 4.0$  Hz, 1H). <sup>13</sup>C NMR (101 MHz, CDCl<sub>3</sub>) δ 172.5, 133.1, 132.8, 128.5, 128.0, 127.7, 127.5, 126.4, 125.8, 68.4, 66.9, 65.7, 37.6. ESI-TOF m/z: Calcd for [2M+Na<sup>+</sup>] C<sub>30</sub>H<sub>32</sub>O<sub>8</sub>Na<sup>+</sup>: 543.2015, found [2M+Na<sup>+</sup>]: 543.1995.

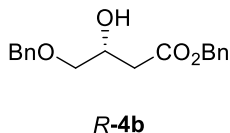
#### Naphthalen-2-ylmethyl 3,4-dihydroxybutanoate (*rac-4a'*).

Synthesis of *rac-3a* and decarboxylation reaction were performed as described for *rac-4a*. Conditions for esterification and product purification were conducted as described for *R-4a'*. The NMR spectra of *rac-4a'* (237 mg, 58%) was indistinguishable from that of *R-4a'*.



#### Benzyl (*R*)-4-(benzyloxy)-3-hydroxybutanoate (*R-4b*).

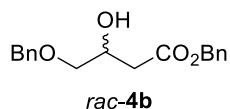
The synthesis of aldol intermediate **3b** was conducted in an Erlenmeyer (50 mL). Reaction volume was 27 mL. Benzyloxyacetaldehyde (**1b**) (0.4 g, 2.7 mmol, 1 eq, 0.1 M in the reaction) was dissolved in DMF (5.4 mL, 20% (v/v) final concentration in the reaction) and sodium pyruvate **2** (293.1 mg, 2.7 mmol, 1 eq, 0.1 M final concentration in the reaction) dissolved in water (15 mL) was added. Finally, reaction was started by adding the enzyme HBPA *wild-type* (6.6 mL of a stock solution 0.029 U mL<sup>-1</sup>, 4 mg mL<sup>-1</sup> in 50 mM TEA buffer, 50 mM NaCl, 0.5 mM EDTA and 50% (v/v) of glycerol, 0.007 U mL<sup>-1</sup>, 1 mg protein mL<sup>-1</sup> final concentration in the reaction). The Erlenmeyer was placed in an orbital shaker (250 rpm) at 25 °C for 24h. Reaction was



monitored by HPLC and samples were withdrawn immediately after the enzyme addition (0 h) and after 24 h as described above. The oxidative decarboxylation and subsequent esterification were carried out as described for *R-4a*. Product was eluted with a step gradient of hexane: EtOAc: 100:0, 200 mL, 90:10, 200 mL, 80:20, 200 mL, 70:30, 500 mL, 60:40, 500 mL. Pure fractions were pooled and the solvent removed under vacuum affording the title compound *R-4b* as a yellow oil (368 mg, 49%).  $[\alpha]_{20}^D = + 8.7$  ( $c = 2$ , in MeOH). Chiral HPLC analysis: CHIRALPACK IB, isocratic elution hexane/isopropanol 80/20 (v/v), flow rate 1 mL min<sup>-1</sup>,  $t_r(S) = 8.292$  min,  $t_r(R) = 9.317$  min, 94:6 er. <sup>1</sup>H NMR (400 MHz, CDCl<sub>3</sub>)  $\delta$  7.36 – 7.27 (m, 10H), 5.12 (s, 2H), 4.53 (s, 2H), 4.25 (qd,  $J = 6.1, 4.4$  Hz, 1H), 3.50 (dd,  $J = 9.6, 4.5$  Hz, 1H), 3.46 (dd,  $J = 9.5, 5.9$  Hz, 1H), 2.59 (d,  $J = 6.6$  Hz, 2H). <sup>13</sup>C NMR (101 MHz, CDCl<sub>3</sub>)  $\delta$  171.9, 137.8, 135.6, 128.6, 128.4, 128.3, 128.2, 127.8, 127.7, 67.2, 66.5, 38.3. ESI-TOF  $m/z$ : Calcd for [2M+Na<sup>+</sup>] C<sub>36</sub>H<sub>40</sub>O<sub>8</sub>Na<sup>+</sup>: 623.2649, found [2M+Na<sup>+</sup>]: 623.2621.

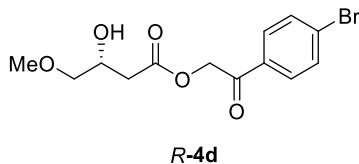
#### Benzyl 4-(benzyloxy)-3-hydroxybutanoate (*rac-4b*).

The synthesis of aldol intermediate *rac-3b* was conducted in an Erlenmeyer flask (50 mL). The reaction volume was 27 mL. Benzyloxyacetaldehyde (**1b**) (0.4 g, 2.7 mmol, 1 eq, 0.1 M in the reaction) was dissolved in DMF (5.4 mL, 20% (v/v) final concentration in the reaction) and sodium pyruvate **2** (293.1 mg, 2.7 mmol, 1 eq, 0.1 M in the reaction) dissolved in water (10.7 mL) was added. Then, NiCl<sub>2</sub> (270  $\mu$ L of a 1 M stock solution, 1 mM final concentration in the reaction) was added and reaction was started by adding the enzyme (MBP-YfaU 150 mg of lyophilized powder dissolved in water (10.7 mL), 2 mg of protein mL<sup>-1</sup> final concentration in the reaction). The flask was placed in an orbital shaker (250 rpm) at 25 °C for 24h. Reaction was monitored by HPLC and samples were withdrawn immediately after



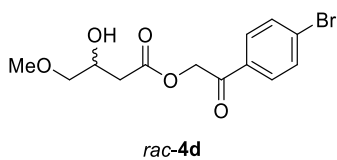
the enzyme addition (0 h) and after 24 h as described above. The oxidative decarboxylation, subsequent esterification, and purification were conducted as described for *R-4b*, affording the compound *rac-4b* (283 mg, 41%). NMR spectra was indistinguishable from that of *R-4b*.

#### 2-(4-Bromophenyl)-2-oxoethyl (*R*)-3-hydroxy-4-methoxybutanoate (*R-4d*).



The precursor **3d** was prepared following the procedure described for *R-4a* starting from **1d** (8.4 mL of 0.4 M aqueous solution, 3.4 mmol, 1 eq, 0.1M) and sodium pyruvate **2** (371.4 mg, 3.4 mmol, 1 eq, 0.1 M final concentration in the reaction). The oxidative decarboxylation of **3d** was performed as described for *R-4a*. The residue from the oxidative decarboxylation was re-suspended with anhydrous DMF (50 mL) under N<sub>2</sub> atmosphere in a round-bottom flask of 100 mL. To this solution, 2,4'-dibromoacetophenone (938 mg, 3.4 mmol, 1 eq) was added. The reaction mixture was stirred at 4 °C for 2 h. Work up and purification were carried out as described for *R-4a*. Product was eluted with a step gradient of hexane:EtOAc: 100:0, 200 mL, 95:5, 200 mL, 90:10, 500 mL 80:20, 500 mL, 70:30, 200 mL, 60:40, 200 mL, 50:50, 800 mL. Pure fractions were pooled, and the solvent removed under vacuum affording compound *R-4d* as a white solid (379 mg, 34%).  $[\alpha]_{20}^D = +0.3$  ( $c = 2$  in CHCl<sub>3</sub>). Chiral HPLC analysis: CHIRALPACK IC, isocratic elution hexane/isopropanol 80/20 (v/v), flow rate 1 mL min<sup>-1</sup>, tr (*S*) = 52.976 min, tr (*R*) = 58.220 min, 71:29 er. <sup>1</sup>H NMR (400 MHz, CDCl<sub>3</sub>)  $\delta$  7.76 (d,  $J = 8.7$  Hz, 2H), 7.63 (d,  $J = 8.6$  Hz, 2H), 5.39 (d,  $J = 16.4$  Hz, 1H), 5.29 (d,  $J = 16.5$  Hz, 1H), 4.35 – 4.24 (m, 1H), 3.47 (d,  $J = 1.7$  Hz, 1H), 3.45 (d,  $J = 2.7$  Hz, 1H), 3.40 (s, 3H), 2.70 (d,  $J = 5.0$  Hz, 1H), 2.69 (d,  $J = 7.7$  Hz, 1H). <sup>13</sup>C NMR (101 MHz, CDCl<sub>3</sub>)  $\delta$  191.4, 171.2, 132.6, 132.3, 129.4, 129.2, 75.4, 67.2, 65.9, 59.2, 38.5. ESI-TOF  $m/z$ : Calcd for [M+Na<sup>+</sup>] C<sub>13</sub>H<sub>30</sub>Br<sub>2</sub>O<sub>10</sub>Na<sup>+</sup>: 527.0103, found [M+Na<sup>+</sup>]: 527.0106.

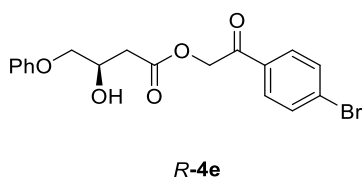
#### 2-(4-Bromophenyl)-2-oxoethyl 3-hydroxy-4-methoxybutanoate (*rac-4d*).



The aldol adduct precursor *rac-3d* was prepared following the procedure described for *rac-4a* (reaction volume was 27 mL) starting from **1d** (6.8 mL of 0.4 M aqueous solution, 2.7 mmol, 1 eq, 0.1M) and sodium pyruvate **2** (297.10 mg, 2.7 mmol, 1 eq). Oxidative decarboxylation, esterification, and purification were carried out as described for *R-4d*, affording compound *rac-4d* (315 mg, 35%). NMR spectra was indistinguishable from that of *R-4d*.

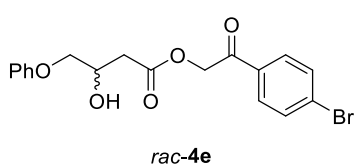
#### 2-(4-Bromophenyl)-2-oxoethyl (*R*)-3-hydroxy-4-phenoxybutanoate (*R-4e*).





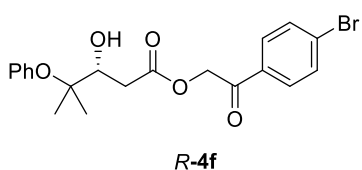
The precursor **3e** was prepared following the procedure described for *R*-**4b**. Reaction volume was 37 mL. Starting from **1e** (0.5 g, 3.7 mmol, 1 eq, 0.1 M) and sodium pyruvate **2** (0.4 g, 3.7 mmol, 1 eq, 0.1 M). Oxidative decarboxylation of **3e** was conducted as described for *R*-**4a** and the esterification as described for *R*-**4d**. Product was eluted with a step gradient of hexane: EtOAc: 100:0, 200 mL, 95:5, 200 mL, 90:10, 500 mL 80:20, 1 L, 50:50, 1 L. Pure fractions were pooled, and the solvent removed under vacuum affording *R*-**4e** as a white solid (495 mg, 34 %).  $[\alpha]_{20}^D = +0.3$  ( $c = 1$ , in  $\text{CHCl}_3$ ). Chiral HPLC analysis: CHIRALPACK IB, isocratic elution hexane/isopropanol 95/5 (v/v), flow rate  $1 \text{ mL min}^{-1}$ ,  $\text{tr}(S) = 89.648 \text{ min}$ ,  $\text{tr}(R) = 83.586 \text{ min}$ , 92:8 er.  $^1\text{H NMR}$  (400 MHz,  $\text{CDCl}_3$ )  $\delta$  7.78 (d,  $J = 1.8 \text{ Hz}$ , 1H), 7.76 (d,  $J = 1.9 \text{ Hz}$ , 1H), 7.64 (d,  $J = 2.0 \text{ Hz}$ , 1H), 7.63 (d,  $J = 1.8 \text{ Hz}$ , 1H), 7.33 – 7.22 (m, 2H), 6.99 – 6.89 (m, 3H), 5.42 (d,  $J = 16.4 \text{ Hz}$ , 1H), 5.32 (d,  $J = 16.5 \text{ Hz}$ , 1H), 4.58 – 4.47 (m, 1H), 4.08 (dd,  $J = 9.5, 5.6 \text{ Hz}$ , 1H), 4.04 (dd,  $J = 9.5, 5.3 \text{ Hz}$ , 1H), 2.90 (dd,  $J = 15.5, 4.2 \text{ Hz}$ , 1H), 2.81 (dd,  $J = 15.5, 8.4 \text{ Hz}$ , 1H).  $^{13}\text{C NMR}$  (101 MHz,  $\text{CDCl}_3$ )  $\delta$  191.4, 171.1, 158.4, 132.5, 132.3, 129.5, 129.3, 121.2, 114.6, 70.5, 67.0, 65.9, 38.7. ESI-TOF  $m/z$ : Calcd for  $[\text{2M}+\text{Na}^+]$   $\text{C}_{36}\text{H}_{34}\text{Br}_2\text{O}_{10}\text{Na}^+$ : 807.0416, found  $[\text{2M}+\text{Na}^+]$ : 807.0412.

#### 2-(4-bromophenyl)-2-oxoethyl 3-hydroxy-4-phenoxybutanoate (*rac*-**4e**).



The precursor *rac*-**3e** was prepared following the procedure described for *rac*-**4b** (reaction volume was 18 mL) starting from **1d** (0.25 g, 1.8 mmol, 1 eq, 0.1 M) and sodium pyruvate **2** (202.1 mg, 1.8 mmol, 1 eq, 0.1 M). Oxidative decarboxylation, esterification, and purification were carried out as described for *R*-**4d**, affording compound *rac*-**4e** (250 mg, 35%). NMR spectra was indistinguishable from that of *R*-**4e**.

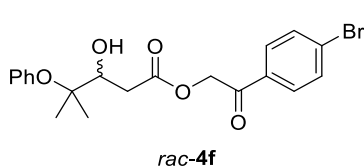
#### 2-(4-bromophenyl)-2-oxoethyl (*R*)-3-hydroxy-4-methyl-4-phenoxybutanoate (*R*-**4f**).



The precursor **3f** was prepared following the procedure described for *R*-**4b**. Reaction volume was 21 mL, starting from **1f** (0.35 mg, 2.1 mmol, 1 eq, 0.1 M) and sodium pyruvate **2** (234.6 mg, 2.1 mmol, 1 eq, 0.1 M). Oxidative decarboxylation of **3e** was conducted as described for *R*-**4a** and the esterification as

described for *R-4d*. Purification by column chromatography: product was eluted with a step gradient of hexane: EtOAc: 100:0, 200 mL, 95:5, 200 mL, 90:10, 500 mL 80:20, 1 L, 50:50, 500 mL. *R-4f* was obtained as a solid (260 mg, 29 %).  $[\alpha]_{20}^D = -1.3$  ( $c = 1$  in MeOH). Chiral HPLC analysis: CHIRALPACK IB, isocratic elution hexane/isopropanol 90/10 (v/v), flow rate 1 mL min<sup>-1</sup>, tr (*S*) = 23.895 min, tr (*R*) = 25.530 min, 95:5 er. <sup>1</sup>H NMR (400 MHz, CDCl<sub>3</sub>)  $\delta$  7.78 (d,  $J = 1.9$  Hz, 1H), 7.77 (d,  $J = 1.9$  Hz, 1H), 7.64 (d,  $J = 2.0$  Hz, 1H), 7.62 (d,  $J = 1.8$  Hz, 1H), 7.30 – 7.21 (m, 2H), 7.08 (t,  $J = 2 \times 7.4$  Hz, 1H), 7.00 – 6.96 (m, 2H), 5.43 (d,  $J = 16.4$  Hz, 1H), 5.31 (d,  $J = 16.5$  Hz, 1H), 4.20 (dd,  $J = 10.2, 2.6$  Hz, 1H), 2.99 (dd,  $J = 15.2, 2.6$  Hz, 1H), 2.75 (dd,  $J = 15.2, 10.2$  Hz, 1H), 1.31 (s, 3H), 1.28 (s, 3H). <sup>13</sup>C NMR (101 MHz, CDCl<sub>3</sub>)  $\delta$  191.6, 172.1, 154.4, 132.3, 129.4, 129.3, 129.0, 124.0, 123.8, 81.7, 74.5, 65.9, 37.0, 23.1, 21.8. ESI-TOF m/z: Calcd for [2M+Na<sup>+</sup>] C<sub>40</sub>H<sub>42</sub>Br<sub>2</sub>O<sub>10</sub>Na<sup>+</sup>: 863.1042, found [2M+Na<sup>+</sup>]: 863.1037.

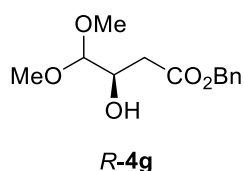
#### 2-(4-Bromophenyl)-2-oxoethyl 3-hydroxy-4-methyl-4-phenoxybutanoate (*rac-4f*).



The precursor *rac-3f* was prepared following the procedure described for *rac-4b*. Reaction volume was 18 mL, starting from **1f** (0.3 g, 1.8 mmol, 1 eq, 0.1 M) and sodium pyruvate **2** (202.1 mg, 1.8 mmol, 1 eq, 0.1 M).

Oxidative decarboxylation, esterification, and purification were carried out as described for *R-4d*, affording compound *rac-4f* (169 mg, 22%). NMR spectra was indistinguishable from that of *R-4f*.

#### Benzyl (*R*)-3-hydroxy-4,4-dimethoxybutanoate (*R-4g*).

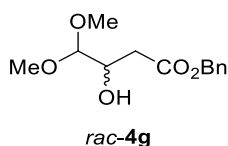


The precursor **3g** was prepared following the procedure described for *R-4a*. Reaction volume was 15 mL starting from **1g** (873  $\mu$ L of a 6.6 M commercial aqueous solution, 5.8 mmol, 1 eq, 0.1M) and sodium pyruvate **2** (0.63 g, 5.8 mmol, 1 eq, 1 M). Oxidative

decarboxylation of **3g** and esterification were carried out as described for *R-4a*. Column chromatography purification: *R-4g* was eluted with a step gradient of hexane:EtOAc: 100:0, 200 mL, 90:10, 200 mL, 80:20, 200 mL, 70:30, 200 mL, 60:40, 500 mL, 50:50, 500 mL affording *R-4g* as a yellow oil (680 mg, 47%).  $[\alpha]_{20}^D = +1.7$  ( $c = 4.2$ , in H<sub>2</sub>O). Chiral HPLC analysis: CHIRALPACK IC, isocratic elution hexane/isopropanol 80/20 (v/v), flow rate 1 mL min<sup>-1</sup>, tr (*S*) = 14.580 min, tr (*R*) = 17.366 min, 96:4 er. <sup>1</sup>H NMR

(400 MHz, CDCl<sub>3</sub>)  $\delta$  7.37 – 7.27 (m, 5H), 5.14 (s, 2H), 4.24 (d,  $J$  = 5.5 Hz, 1H), 4.13 – 4.05 (m, 1H), 3.43 (s, 3H), 3.40 (s, 3H), 2.67 (dd,  $J$  = 16.1, 3.9 Hz, 1H), 2.54 (dd,  $J$  = 16.1, 8.4 Hz, 1H). <sup>13</sup>C NMR (101 MHz, CDCl<sub>3</sub>)  $\delta$  171.9, 135.7, 128.5, 128.2, 128.2, 105.8, 68.3, 66.5, 55.7, 55.1, 36.6. ESI-TOF  $m/z$ : Calcd for [2M+Na<sup>+</sup>] C<sub>26</sub>H<sub>36</sub>O<sub>10</sub>Na<sup>+</sup>: 531.2211, found [2M+Na<sup>+</sup>]: 531.2206.

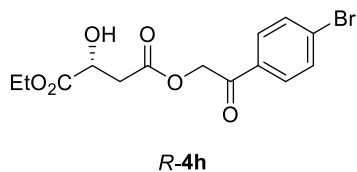
#### Benzyl 3-hydroxy-4,4-dimethoxybutanoate (*rac*-4g).



The aldol adduct precursor *rac*-3g was prepared following the procedure described for *rac*-4a. Reaction volume was 58 mL, starting from **1g** (873  $\mu$ L of a 6.6 M commercial aqueous solution, 5.8 mmol, 1 eq, 0.1 M) and sodium pyruvate **2** (0.63 g, 5.8 mmol, 1 eq, 1 M).

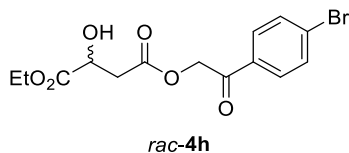
Oxidative decarboxylation of *rac*-3g and esterification were carried out as described for *R*-4a. Purification and the compound characterization were conducted as described for *R*-4g, affording *rac*-4g (1.0 g, 71%). The NMR spectra was indistinguishable from that of *R*-4g.

#### 4-(2-(4-Bromophenyl)-2-oxoethyl)-1-ethyl-(*R*)-2-hydroxysuccinate (*R*-4h).

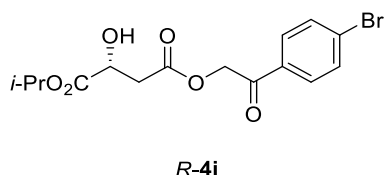


Precursor **3h** was prepared following the procedure described for *R*-4b. Reaction volume was 34 mL, starting from **1h** (700  $\mu$ L of a 4.9 M commercial aqueous solution, 3.4 mmol, 1 eq, 0.1 M) and sodium pyruvate **2** (0.38 g, 3.4

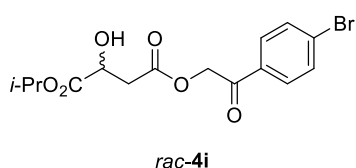
mmol, 1 eq, 0.1 M). Oxidative decarboxylation of **3h** was conducted as described for *R*-4a and the esterification as described for *R*-4d. Purification by column chromatography: product was eluted with a step gradient of hexane:EtOAc: 100:0, 200 mL, 95:5, 200 mL, 90:10, 500 mL 80:20, 2 L, 50:50, 700 mL, affording *R*-4h as a white solid (434 mg, 35 %).  $[\alpha]_{20}^D = +1.8$  ( $c = 1$ , in MeOH). Chiral HPLC analysis: CHIRALPACK IB, isocratic elution hexane/isopropanol 80/20 (v/v), flow rate 1 mL min<sup>-1</sup>,  $t_r$  (*S*) = 18.187 min,  $t_r$  (*R*) = 21.975 min, 95:5 er. <sup>1</sup>H NMR (400 MHz, CDCl<sub>3</sub>)  $\delta$  7.78 – 7.71 (m, 2H), 7.65 – 7.60 (m, 2H), 5.33 (d,  $J$  = 0.9 Hz, 2H), 4.55 (dd,  $J$  = 6.3, 4.3 Hz, 1H), 4.28 (dd,  $J$  = 7.2, 1.9 Hz, 1H), 4.25 (dd,  $J$  = 7.1, 1.8 Hz, 1H), 3.05 (dd,  $J$  = 16.2, 4.3 Hz, 1H), 2.96 (dd,  $J$  = 16.2, 6.2 Hz, 1H), 1.29 (td,  $J$  = 2x7.1, 0.5 Hz, 3H). <sup>13</sup>C NMR (101 MHz, CDCl<sub>3</sub>)  $\delta$  190.9, 173.0, 169.7, 132.6, 132.3, 129.3, 129.2, 67.3, 66.0, 62.1, 38.7, 14.1. ESI-TOF  $m/z$ : Calcd for [2M+Na<sup>+</sup>] C<sub>28</sub>H<sub>30</sub>Br<sub>2</sub>O<sub>12</sub>Na<sup>+</sup>: 739.0002, found [2M+Na<sup>+</sup>]: 739.0008.

**4-(2-(4-Bromophenyl)-2-oxoethyl) 1-ethyl -2-hydroxysuccinate (*rac*-4h).**

The precursor *rac*-3h was prepared following the procedure described for *rac*-4b. Reaction volume was 25 mL, starting from **1h** (500  $\mu$ L of a 4.9 M commercial aqueous solution, 2.5 mmol, 1 eq, 0.1M) and sodium pyruvate **2** (0.27 g, 2.5 mmol, 1 eq, 0.1 M). Oxidative decarboxylation and esterification were carried out as described for *R*-4d. Purification and the compound characterization were conducted as described above, affording *rac*-4g (330 mg, 38%). The NMR spectra was indistinguishable from that of *R*-4h.

**4-(2-(4-Bromophenyl)-2-oxoethyl) 1-isopropyl (*R*)-2-hydroxysuccinate (*R*-4i).**

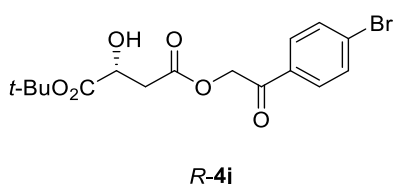
The precursor **3i** was prepared following the procedure described for *R*-4a. Reaction volume was 35 mL starting from **1g** (0.4 g, 3.4 mmol, 1 eq, 0.1 M in the reaction) and sodium pyruvate **2** (0.38 g, 3.4 mmol, 1 eq, 0.1 M). Oxidative decarboxylation of **3i** and esterification were carried out as described for *R*-4d. Column chromatography purification: *R*-4i was eluted with a step gradient of hexane: EtOAc: 100:0, 200 mL, 95:5, 200 mL, 90:10, 500mL 80:20, 1 L, 70:30, 200 mL, 60:40, 200 mL, 50:50, 1 L. The title compound *R*-4i was obtained as a white solid (608 mg, 47%).  $[\alpha]_{20}^D = + 2.2$  ( $c = 4$ , in MeOH). Chiral HPLC analysis: CHIRALPACK IB, isocratic elution hexane/isopropanol 80/20 (v/v), flow rate 1 mL min<sup>-1</sup>,  $t_r$  (*S*) = 14.048 min,  $t_r$  (*R*) = 15.680 min, 91:9 er. <sup>1</sup>H NMR (400 MHz, CDCl<sub>3</sub>)  $\delta$  7.77 – 7.73 (m, 2H), 7.65 – 7.60 (m, 2H), 5.32 (d,  $J = 3.4$  Hz, 2H), 5.11 (p,  $J = 4 \times 6.3$  Hz, 1H), 4.51 (dd,  $J = 6.3, 4.3$  Hz, 1H), 3.04 (dd,  $J = 16.2, 4.3$  Hz, 1H), 2.94 (dd,  $J = 16.1, 6.2$  Hz, 1H), 1.27 (dd,  $J = 6.2, 3.6$  Hz, 6H). <sup>13</sup>C NMR (101 MHz, CDCl<sub>3</sub>)  $\delta$  190.9, 172.5, 169.7, 132.6, 132.3, 129.3, 129.2, 70.1, 67.3, 66.0, 38.7, 21.6. ESI-TOF  $m/z$ : Calcd for [2M+Na<sup>+</sup>] C<sub>30</sub>H<sub>34</sub>Br<sub>2</sub>O<sub>12</sub>Na<sup>+</sup>: 767.0315, found [2M+Na<sup>+</sup>]: 767.0311.

**4-(2-(4-bromophenyl)-2-oxoethyl) 1-isopropyl -2-hydroxysuccinate (*rac*-4i).**

The aldol adduct precursor *rac*-3i was prepared following the procedure described for *rac*-4a. Reaction volume was 22 mL. Starting from **1i** (0.25 g, 2.2 mmol, 1 eq, 0.1 M) and sodium pyruvate **2** (0.24 g, 2.2 mmol, 1 eq, 1 M).

Oxidative decarboxylation of *rac*-**3i** and esterification were carried out as described for *R*-**4d**. Purification and the compound characterization were conducted as described for *R*-**4i**, affording *rac*-**4i** (362 mg, 45%). The NMR spectra was indistinguishable from that of *R*-**4i**.

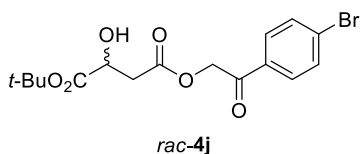
**4-(2-(4-bromophenyl)-2-oxoethyl) 1-(tert-butyl) (*R*)-2-hydroxysuccinate (*R*-**4j**).**



The precursor **3j** was prepared following the procedure described for *R*-**4b**. Reaction volume was 27 mL. Starting from **1j** (0.35 g, 2.7 mmol, 1 eq, 0.1 M) and sodium pyruvate **2** (0.3 g, 2.7 mmol, 1 eq, 0.1 M).

Oxidative decarboxylation of **3j** and esterification were conducted as described for *R*-**4d**. Column chromatography: product was eluted with a step gradient of hexane:EtOAc: 100:0, 200 mL, 95:5, 200 mL, 90:10, 3 L 40:60, 1 L, yielding *R*-**4j** as a white solid (381 mg, 37%).  $[\alpha]_{20}^D = +0.4$  ( $c = 4$ , in MeOH). Chiral HPLC analysis: CHIRALPACK IB, isocratic elution hexane/isopropanol 80/20 (v/v), flow rate 1 mL min<sup>-1</sup>, tr (*S*) = 11.661 min, tr (*R*) = 13.056 min, 90:10 er. <sup>1</sup>H NMR (400 MHz, CDCl<sub>3</sub>)  $\delta$  7.75 (d,  $J = 8.7$  Hz, 2H), 7.62 (d,  $J = 8.7$  Hz, 2H), 5.35 (d,  $J = 16.4$  Hz, 1H), 5.29 (d,  $J = 16.4$  Hz, 1H), 4.42 (q,  $J = 3 \times 5.5$  Hz, 1H), 3.00 (dd,  $J = 16.1, 4.4$  Hz, 1H), 2.91 (dd,  $J = 16.1, 6.2$  Hz, 1H), 1.48 (s, 9H). <sup>13</sup>C NMR (101 MHz, CDCl<sub>3</sub>)  $\delta$  190.9, 172.2, 169.7, 132.7, 132.2, 129.2 (d,  $J = 4.5$  Hz), 83.1, 67.4, 65.9, 38.8, 27.9. ESI-TOF  $m/z$ : Calcd for [2M+Na<sup>+</sup>] C<sub>32</sub>H<sub>38</sub>Br<sub>2</sub>O<sub>12</sub>Na<sup>+</sup>: 795.0627, found [2M+Na<sup>+</sup>]: 795.0621.

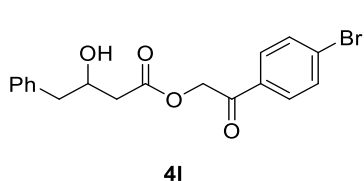
**4-(2-(4-bromophenyl)-2-oxoethyl) 1-(tert-butyl) -2-hydroxysuccinate (*rac*-**4j**).**



The precursor *rac*-**3j** was prepared following the procedure described for *rac*-**4b**. Reaction volume was 23 mL, starting from **1j** (0.3 g, 2.3 mmol, 1 eq, 0.1 M) and sodium pyruvate **2** (0.25 g, 2.3 mmol, 1 eq, 0.1 M). Oxidative

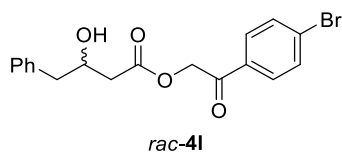
decarboxylation and esterification were carried out as described for *R*-**4d**. Purification and the compound characterization were conducted as described above, affording *rac*-**4j** (285 mg, 32%). The NMR spectra were indistinguishable from that of *R*-**4j**.

**2-(4-bromophenyl)-2-oxoethyl 3-hydroxy-4-phenylbutanoate (**4l**).**



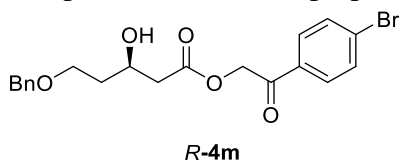
Precursor **3I** was prepared following the procedure described for *R-4b*. Reaction volume was 34 mL, starting from **1I** (0.4 mg, 3.3 mmol, 1 eq, 0.1 M) and sodium pyruvate **2** (0.37 mg, 3.3 mmol, 1 eq, 0.1 M). Oxidative decarboxylation of **3I** and esterification were performed as described for *R-4d*. Column chromatography: product was eluted with a step gradient of hexane: EtOAc: 100:0, 200 mL, 95:5, 200 mL, 90:10, 500 mL, 80:20, 1 L, 50:50, 1 L, rendering **4I** as a yellow solid (337 mg, 27%). Chiral HPLC analysis: CHIRALPACK IC, isocratic elution hexane/isopropanol 80/20 (v/v), flow rate 1 mL min<sup>-1</sup>, tr (*S*) = 30.090 min, tr (*R*) = 25.124 min, 50:50 er. <sup>1</sup>H NMR (400 MHz, CDCl<sub>3</sub>) δ 7.78 – 7.72 (m, 2H), 7.65 – 7.60 (m, 2H), 7.35 – 7.20 (m, 5H), 5.39 (d, *J* = 16.4 Hz, 1H), 5.28 (d, *J* = 16.4 Hz, 1H), 4.36 (ddt, *J* = 13.1, 6.9, 2x3.6 Hz, 1H), 2.93 (dd, *J* = 13.6, 7.0 Hz, 1H), 2.83 (dd, *J* = 13.6, 6.3 Hz, 1H), 2.68 (dd, *J* = 15.3, 3.6 Hz, 1H), 2.59 (dd, *J* = 15.3, 8.8 Hz, 1H). <sup>13</sup>C NMR (101 MHz, CDCl<sub>3</sub>) δ 132.3, 129.5, 129.3, 128.5, 126.6, 69.5, 65.8, 42.9, 41.1. Calcd. for [2M+Na<sup>+</sup>] C<sub>32</sub>H<sub>36</sub>Br<sub>2</sub>O<sub>8</sub>Na<sup>+</sup>: 729.0675, found [2M+Na<sup>+</sup>]: 729.0679.

#### 2-(4-Bromophenyl)-2-oxoethyl (*R*)-3-hydroxy-4-phenylbutanoate (*rac-4I*).



The precursor *rac-3I* was prepared following the procedure described for *rac-4b*. Reaction volume was 25 mL, starting from **1I** (0.3 g, 2.5 mmol, 1 eq, 0.1 M) and sodium pyruvate **2** (0.27 g, 2.5 mmol, 1 eq, 0.1 M). Oxidative decarboxylation and esterification, were carried out as described for *R-4d*. Purification and the compound characterization were conducted as described above, affording *rac-4I* (339 mg, 37%). The NMR spectra was indistinguishable from that of **4I**.

#### 2-(4-Bromophenyl)-2-oxoethyl (*R*)-5-(benzyloxy)-3-hydroxypentanoate (*R-4m*).

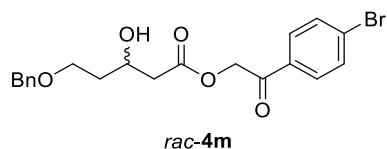


The precursor **3m** was prepared following the procedure described for *R-4b*. Reaction volume was 30 mL. Starting from **1m** (0.5 g, 3.0 mmol, 1 eq, 0.1 M) and sodium pyruvate **2** (0.34 g, 3.0 mmol, 1 eq, 0.1 M). Oxidative decarboxylation of **3m** and esterification were performed as described for *R-4d*. Column chromatography: product was eluted with a step gradient of hexane: EtOAc: 100:0, 200 mL, 95:5, 200 mL, 90:10, 500 mL, 80:20, 1.5 L, 70:30, 200 mL, 50:50, 1 L. *R-4m* was obtained as a solid (278 mg,

22 %).  $[\alpha]_{20}^D = -1.8$  ( $c = 1$ , in MeOH). Chiral HPLC analysis: CHIRALPACK IB, isocratic elution hexane/isopropanol 80/20 (v/v), flow rate  $1 \text{ mL min}^{-1}$ ,  $t_r(S) = 16.139$  min,  $t_r(R) = 17.517$  min, 50:50 er.  $^1\text{H NMR}$  (400 MHz,  $\text{CDCl}_3$ )  $\delta$  7.76 (d,  $J = 8.6$  Hz, 2H), 7.63 (d,  $J = 8.6$  Hz, 2H), 7.36 – 7.23 (m, 5H), 5.39 (d,  $J = 16.4$  Hz, 1H), 5.27 (d,  $J = 16.5$  Hz, 1H), 4.52 (s, 2H), 4.34 (tt,  $J = 2 \times 7.3, 2 \times 5.1$  Hz, 1H), 3.72 (dt,  $J = 9.5, 2 \times 5.9$  Hz, 1H), 3.66 (dt,  $J = 9.4, 2 \times 5.8$  Hz, 1H), 2.67 (d,  $J = 2.1$  Hz, 1H), 2.66 (d,  $J = 4.7$  Hz, 1H), 1.88 (d,  $J = 7.1$  Hz, 1H), 1.85 (d,  $J = 5.8$  Hz, 1H).  $^{13}\text{C NMR}$  (101 MHz,  $\text{CDCl}_3$ )  $\delta$  191.5, 171.4, 138.0, 132.6, 132.3, 129.4, 129.3, 128.4, 127.7, 73.2, 67.9, 67.1, 65.8, 42.0, 36.0. Calcd for  $[\text{2M}+\text{Na}^+]$   $\text{C}_{40}\text{H}_{42}\text{Br}_2\text{O}_{10}\text{Na}^+$ : 863.1042, found  $[\text{2M}+\text{Na}^+]$ : 863.1038.

### 2-(4-bromophenyl)-2-oxoethyl -5-(benzyloxy)-3-hydroxypentanoate (*rac*-4m).

The precursor *rac*-3m was prepared following the procedure described for *rac*-4b.



Reaction volume was 19 mL, starting from **1m** (0.3 g, 1.8 mmol, 1 eq, 0.1 M) and sodium pyruvate **2** (0.2 g, 1.8 mmol, 1 eq, 0.1 M). Oxidative decarboxylation and

esterification were carried out as described for *R*-4d. Purification and the compound characterization were conducted as described above, affording *rac*-4m (176 mg, 23%). The NMR spectra were indistinguishable from that of *R*-4m.

### X-Ray structures of *R*-4e, *R*-4f and *R*-4j

Suitable single crystals for X-ray structural analysis of *R*-4e, *R*-4f, and *R*-4j were obtained at room temperature. Compound *R*-4e (100 mg) was dissolved in MeOH: $\text{CH}_2\text{Cl}_2$  3:1 (v/v) (4 mL), *R*-4f (95 mg) in MeOH: $\text{CH}_2\text{Cl}_2$  1:2 (v/v) (4 mL) and *R*-4j (80 mg) in  $\text{Et}_2\text{O}$ :DMF 9:1 (v/v) (1 mL). Crystals were obtained by evaporation in glass vials (6 mL, 3.5 cm,  $\varnothing$  1.4 cm) after 72 h at 25 °C. Based on the high enantiomeric excesses observed for the enzyme HBPA X-ray diffraction analysis indicates that HBPA render aldol adducts having *R* configuration as major products (**Figure S7**). Data were collected on a STOE IPDS II two-circle diffractometer with a Genix Microfocus tube with mirror optics using MoK $\alpha$  radiation ( $\lambda = 0.71073 \text{ \AA}$ ). The data were scaled using the frame scaling procedure in the X-Area program system (Software X-Area - STOE & Cie GmbH. <https://www.stoe.com/product/software-x-area>). The structures were solved by direct methods using the program SHELXS and refined against  $F^2$  with full-matrix least-squares techniques using the program SHELXL<sup>13</sup> (**Table S6**). The absolute configuration could

be unequivocally determined for all three structures. The H atoms bonded to O atoms in *R-4e* were geometrically allocated and refined with a riding model. In *R-4f*, the H atoms bonded to O atoms were freely refined. In *R-4j*, the H atom bonded to O was refined with a distance restraint of 0.84 (1) Å for the O-H bond.

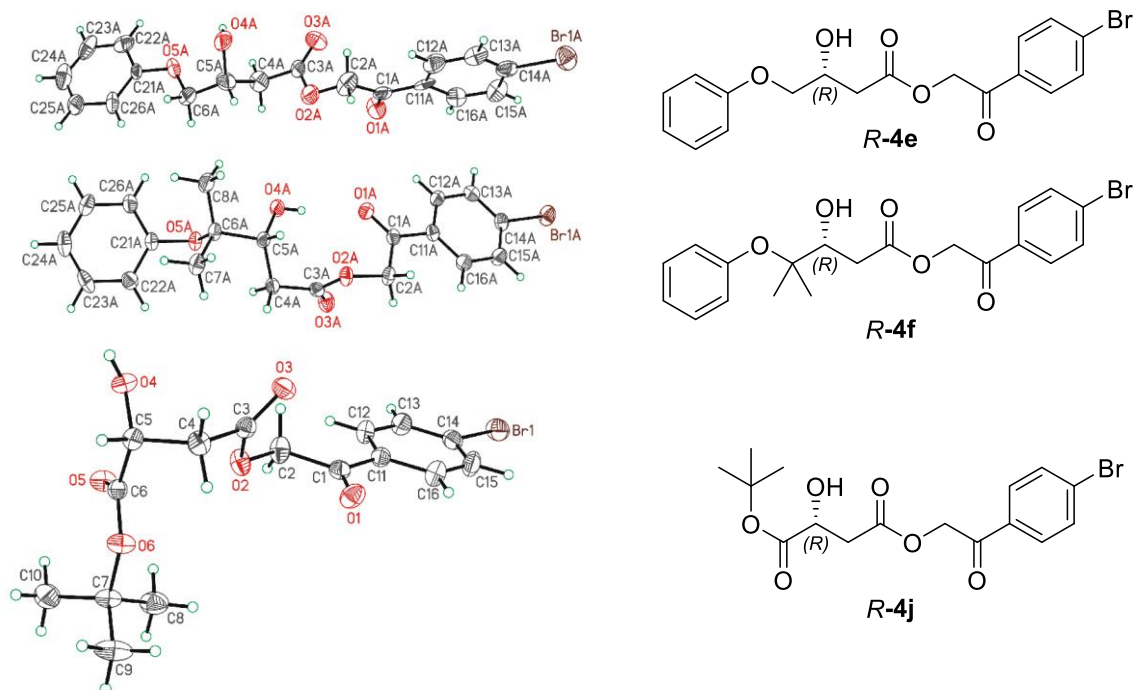


**Figure S7.** X-Ray structures of *R-4e*, *R-4f* and *R-4j*. ORTEP-type plot displaying one molecule with 50% probability ellipsoids. The data can be obtained free of charge from The Cambridge Crystallographic Data Centre via [www.ccdc.cam.ac.uk/data\\_request/cif](http://www.ccdc.cam.ac.uk/data_request/cif)



**Table S6.** X-ray Crystallographic partial data.

Identification code	<b>4e</b>	<b>4f</b>	<b>4j</b>
CCDC number	XXX	XXX	XXX
Empirical formula	C <sub>18</sub> H <sub>17</sub> BrO <sub>5</sub>	C <sub>20</sub> H <sub>21</sub> BrO <sub>5</sub>	C <sub>16</sub> H <sub>19</sub> BrO <sub>6</sub>
Formula weight	393.22	421.28	387.22
Temperature	173(2) K	173(2) K	173(2) K
Wavelength	0.71073 Å	0.71073 Å	0.71073 Å
Crystal system	Orthorhombic	Monoclinic	Orthorhombic
Space group	<i>P</i> 2 <sub>1</sub> 2 <sub>1</sub> 2 <sub>1</sub>	<i>P</i> 2 <sub>1</sub>	<i>P</i> 2 <sub>1</sub> 2 <sub>1</sub> 2 <sub>1</sub>
Unit cell dimensions	a = 5.4464(3) Å, α = 90°. b = 16.6460(7) Å, β = 90°. c = 36.746(2) Å, γ = 90°.	a = 14.6639(7) Å, α = 90°. b = 8.4782(3) Å, β = 108.740(4)°. c = 15.7923(8) Å, γ = 90°.	a = 5.5586(2) Å, α = 90°. b = 12.4492(7) Å, β = 90°. c = 25.3738(11) Å, γ = 90°.
Volume	3331.4(3) Å <sup>3</sup>	1859.27(15) Å <sup>3</sup>	1755.87(14) Å <sup>3</sup>
Z	8	4	4
Density (calculated)	1.568 Mg/m <sup>3</sup>	1.505 Mg/m <sup>3</sup>	1.465 Mg/m <sup>3</sup>
Absorption coefficient	2.493 mm <sup>-1</sup>	2.239 mm <sup>-1</sup>	2.367 mm <sup>-1</sup>
F(000)	1600	864	792
Crystal size	0.130 x 0.030 x 0.030 mm <sup>3</sup>	0.230 x 0.210 x 0.160 mm <sup>3</sup>	0.180 x 0.110 x 0.080 mm <sup>3</sup>
Theta range for data collection	2.064 to 25.027°	3.327 to 27.605°	2.912 to 25.932°
Index ranges	-5<=h<=6, -19<=k<=19, -43<=l<=38	-19<=h<=19, -11<=k<=10, -20<=l<=20	-6<=h<=6, -15<=k<=15, -31<=l<=31
Reflections collected	9721	29057	16242
Independent reflections	5745 [R(int) = 0.0830]	8236 [R(int) = 0.0421]	3411 [R(int) = 0.0294]
Completeness to theta = 25.000°	99.6 %	99.6 %	99.8 %
Absorption correction	Semi-empirical from equivalents	Semi-empirical from equivalents	Semi-empirical from equivalents
Max. and min. transmission	1.000 and 0.657	1.000 and 0.695	1.000 and 0.671
Refinement method	Full-matrix least-squares on F <sup>2</sup>	Full-matrix least-squares on F <sup>2</sup>	Full-matrix least-squares on F <sup>2</sup>
Data / restraints / parameters	5745 / 0 / 433	8236 / 1 / 477	3411 / 1 / 212
Goodness-of-fit on F <sup>2</sup>	1.222	1.136	1.264
Final R indices [I>2σ(I)]	R1 = 0.0915, wR2 = 0.1878	R1 = 0.0552, wR2 = 0.1299	R1 = 0.0389, wR2 = 0.0724
R indices (all data)	R1 = 0.1244, wR2 = 0.2068	R1 = 0.0606, wR2 = 0.1334	R1 = 0.0409, wR2 = 0.0731
Absolute structure parameter	0.028(19)	0.010(11)	-0.008(7)
Largest diff. peak and hole	1.124 and -0.623 e.Å <sup>-3</sup>	0.739 and -0.558 e.Å <sup>-3</sup>	0.423 and -0.341 e.Å <sup>-3</sup>

### Enzymatic transamination of 4-hydroxy-2-oxoacids (**3**). Screening of transaminases from Prozomix, using L-Ala and benzylamine as amino donors.

**Using L-Ala (**5**) as amino donors:** the reaction (500  $\mu$ L total volume) was conducted in Eppendorf tubes (1.5 mL). Sodium salts of 4-hydroxy-2-oxoacids, **3a-b**, **3e**, **3h-g**, were prepared following the procedure described above. A solution (250  $\mu$ L) of transaminase from Prozomix TA as cell free extracts (T01 to T050) (2-3 mg of lyophilized solid in the reaction dissolved in 50 mM sodium phosphate buffer pH 7.0) containing L-Ala (**5**) (10 eq, 0.5 M final concentration in the reaction) and 1 mM PLP in the reaction was prepared. To this solution, a portion of aldol reaction mixture (250  $\mu$ L), containing 4-hydroxy-2-oxoacid (**3**) ( $\approx$  100 mM as the basis of calculation) was added. The reaction mixture was placed in a vortex mixer (1000 rpm) at 25  $^{\circ}$ C for 24 h. Samples were withdrawn immediately after the substrate mix addition (0 h) and after 24 h and analyzed by HPLC as described above. The decrease of the aldol adducts, **3a**, **3g**, and **3h** (Figures S8, S11 and S12, respectively) or the formation of the aminated products, **6b** and **6e** (Figures S9 and S10) were indicative of potential positives.

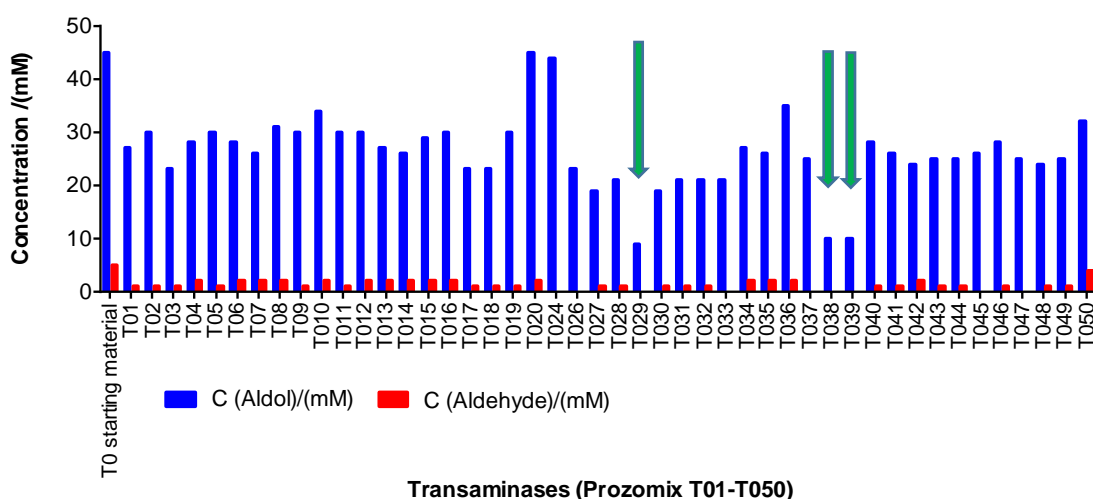
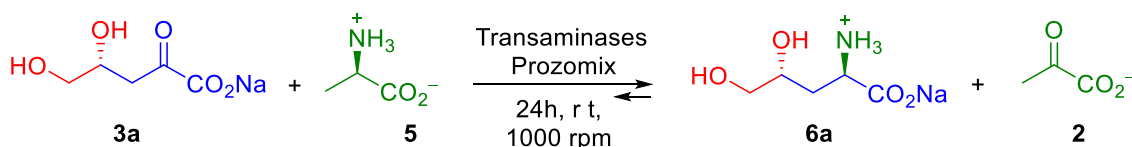


**Figure S8.** Screening of a panel of transaminases from Prozomix, using L-Ala (**5**) as amine donor to furnish **6a**. Conditions: Crude aldol adduct **3a** containing: **3a** (45 mM), **1a** (5 mM), and HBPA (0.5 mg mL<sup>-1</sup>); transamination: L-Ala (500 mM), T01-T050 cell

free extracts (2 to 3 mg). Green arrows indicate enzymes that decrease the area of aldol adduct or aldehyde.

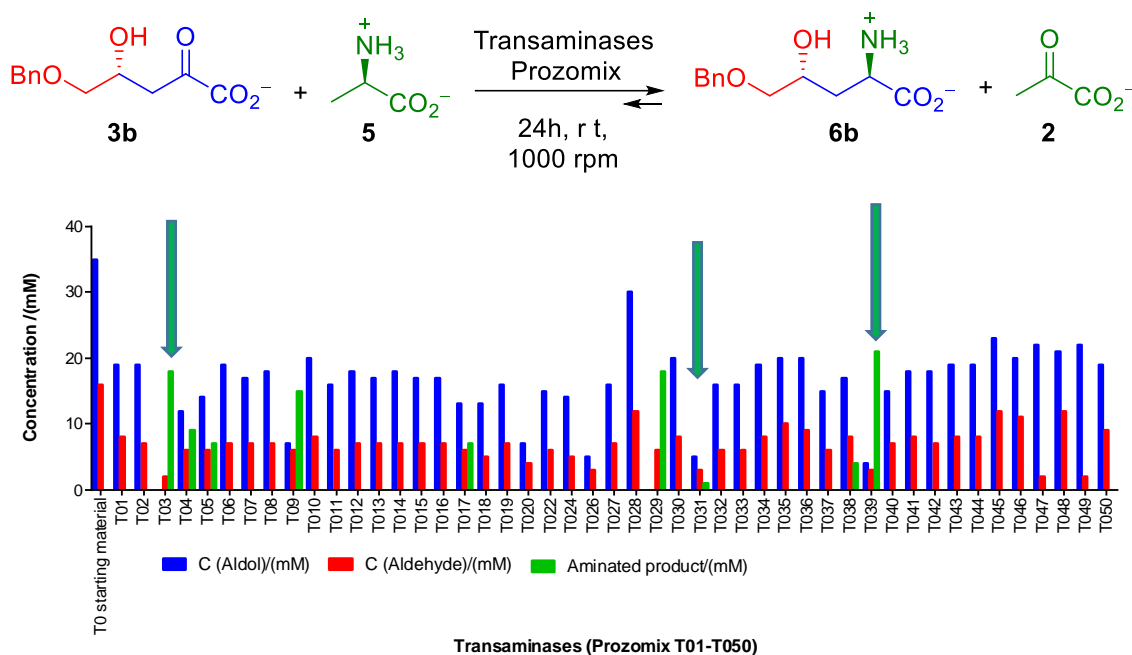


**Figure S9.** Screening of a panel of transaminases from Prozomix, using L-Ala (**5**) as amine donor to furnish **6b**. Conditions: Crude aldol adduct **3b** containing: **3b** (33 mM), **1b** (17 mM), and HBPA (0.5 mg mL<sup>-1</sup>); transamination: L-Ala (500 mM), T01-T050 cell free extracts (2 to 3 mg). Green arrows indicate enzymes that decrease the area of aldol adduct or aldehyde.

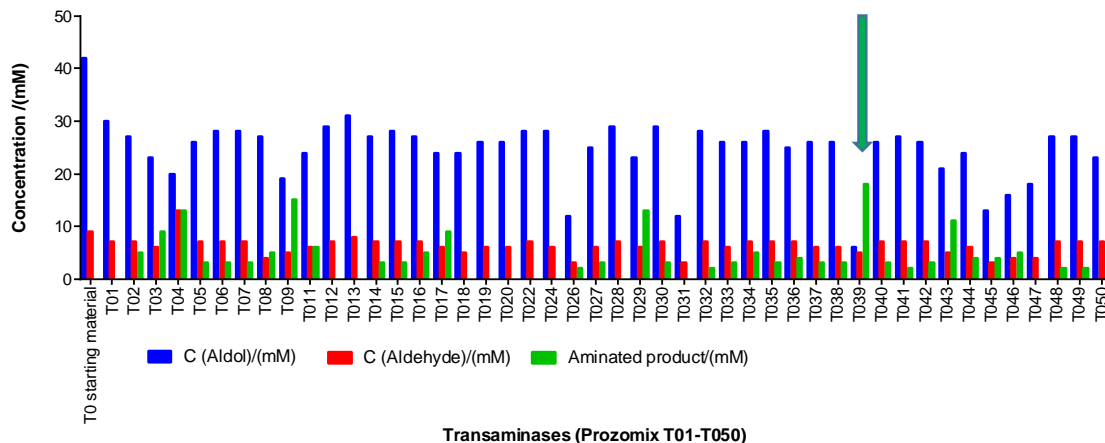
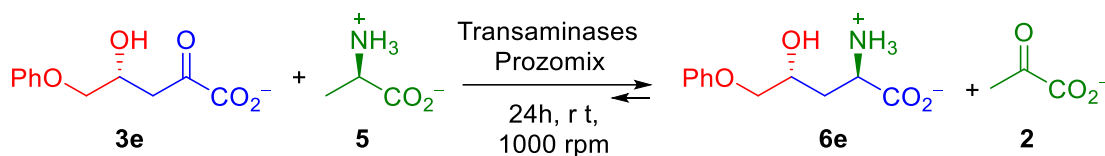


**Figure S10.** Screening of a panel of transaminases from Prozomix, using L-Ala (**5**) as amine donor to furnish **6e**. Conditions: Crude aldol adduct **3e** containing: **3e** (42 mM), **1e** (8 mM), and HBPA ( $0.5 \text{ mg mL}^{-1}$ ); transamination: L-Ala (500 mM), T01-T050 cell free extracts (2 to 3 mg). Green arrows indicate enzymes that decrease the area of aldol adduct or aldehyde.

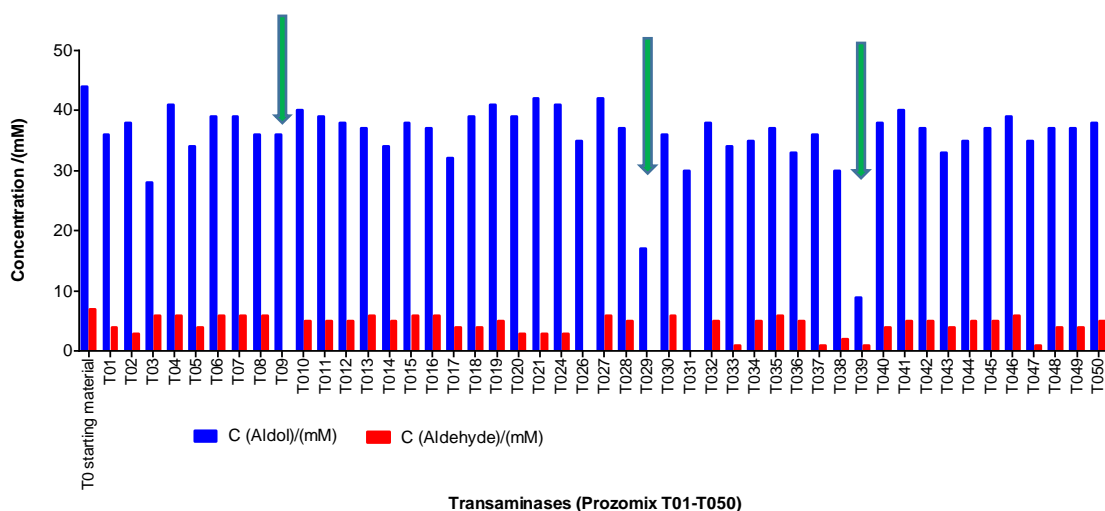
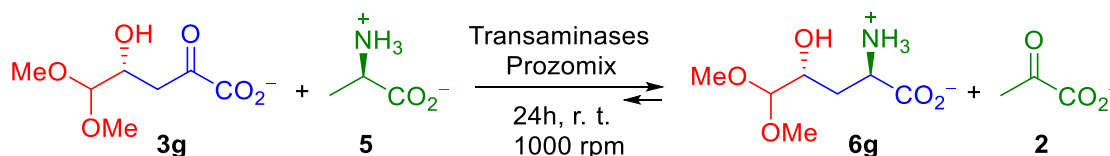


**Figure S11.** Screening of a panel of transaminases from Prozomix, using L-Ala (**5**) as

amine donor to furnish **6g**. Conditions: Crude aldol adduct **3g** containing: **3g** (43 mM) and **1g** (7 mM), HBPA (0.5 mg mL<sup>-1</sup>); transamination: L-Ala (500 mM), T01-T050 cell free extracts (2 to 3 mg). Green arrows indicate enzymes that decrease the area of aldol adduct or aldehyde.

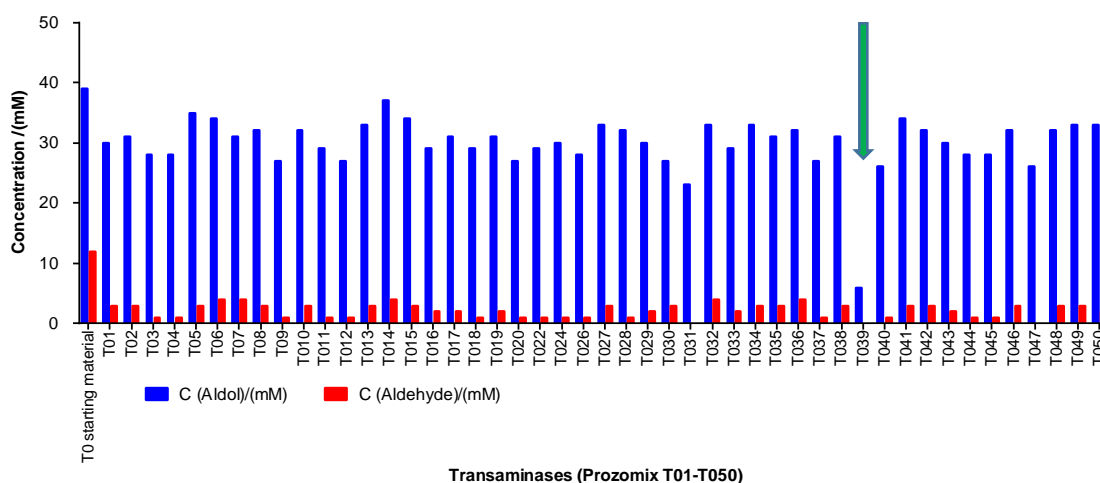
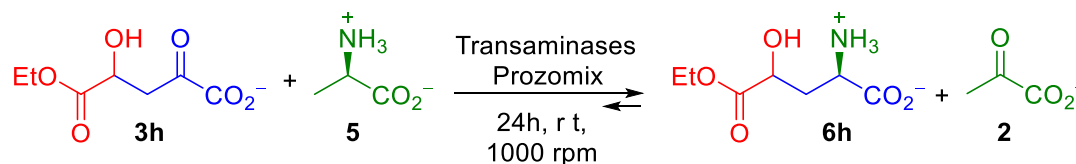


**Figure S12.** Screening of a panel of transaminases from Prozomix, using L-Ala (**5**) as amine donor to furnish **6h**. Conditions: Crude aldol adduct **3h** containing: **3h** (38 mM) and **1g** (12 mM), HBPA (0.5 mg mL<sup>-1</sup>); transamination: L-Ala (500 mM), T01-T050 cell free extracts (2 to 3 mg). Green arrows indicate enzymes that decrease the area of aldol adduct or aldehyde.

### Control experiments for aldehyde (**1**) transamination.

The reactions (500  $\mu$ L total volume) were conducted in Eppendorf tubes (1.5 mL). Transaminases lyophilized cell free extracts from Prozomix (2-3 mg) (T029, T031, T038 and T039 for **1a**; T03, T029, T031 and T039 for **1b**; T031 and T039 for **1g**, **1h** and **1e**) were dissolved in 50 mM sodium phosphate buffer pH 7.0 containing L-Ala (250  $\mu$ L of a 1 M stock solution 500 mM final concentration in the reaction, 10 eq, with 2 mM PLP, 1 mM in the reaction). To this solution, aldehydes (**1a-b**, **1e**, and **1g-h**) (250  $\mu$ L of a 100 mM stock solution in 50 mM sodium phosphate buffer pH 7.0, 50 mM in each reaction,

in case of water insoluble hydrophobic aldehydes DMF (20% in the stock, 10% v/v in the reaction) were added. The reaction mixtures were placed in a vortex mixer (1000 rpm) at 25 °C for 24 h. Samples were withdrawn immediately after the aldehydes addition (0 h) and after 24 h and analyzed by HPLC as described above. Pyruvate formation indicated a positive aldehyde transamination reaction showed that **1a**, **1g** and **1h** were fully converted by T031 and T039 to corresponding amine (**Figures S13**, **S16** and **S17**, respectively). Moreover, the disappearance of aldehydes **1b** and **1e** and the formation of a peak of the amine were indicative of a positive reaction (**Figures S14** and **S15**).

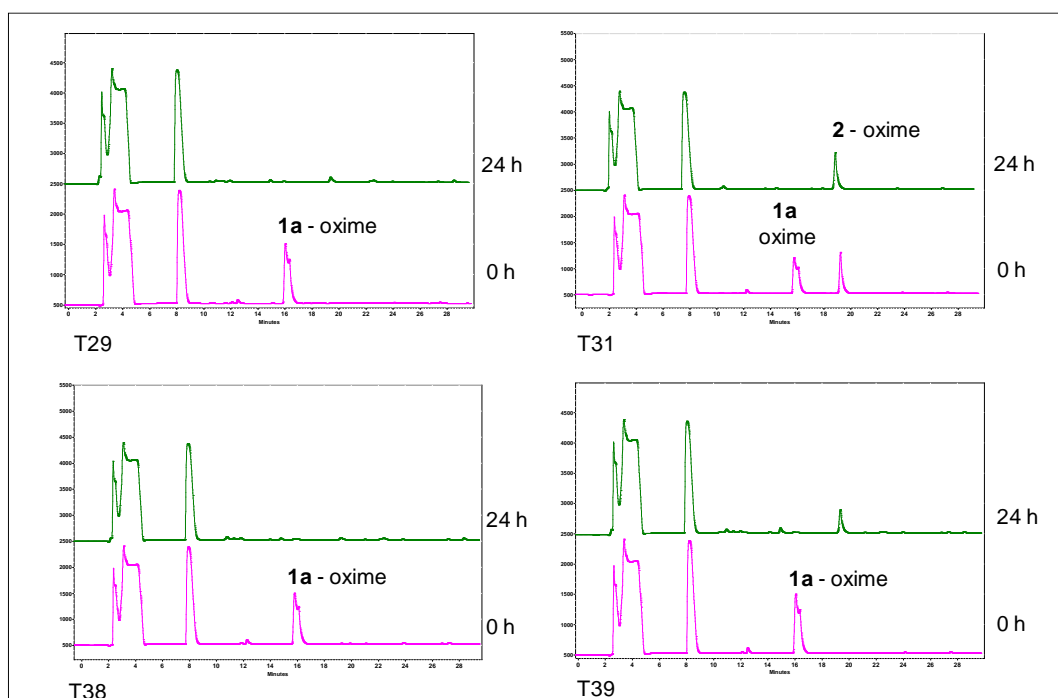
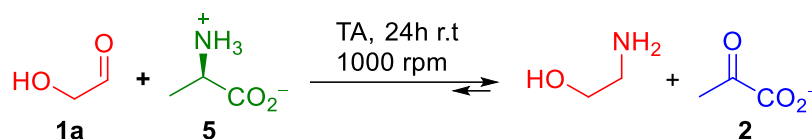


**Figure S13.** HPLC chromatograms of **1a** transamination catalyzed by T029, T031, T038, and T039 at 0 h and after 24 h of incubation.

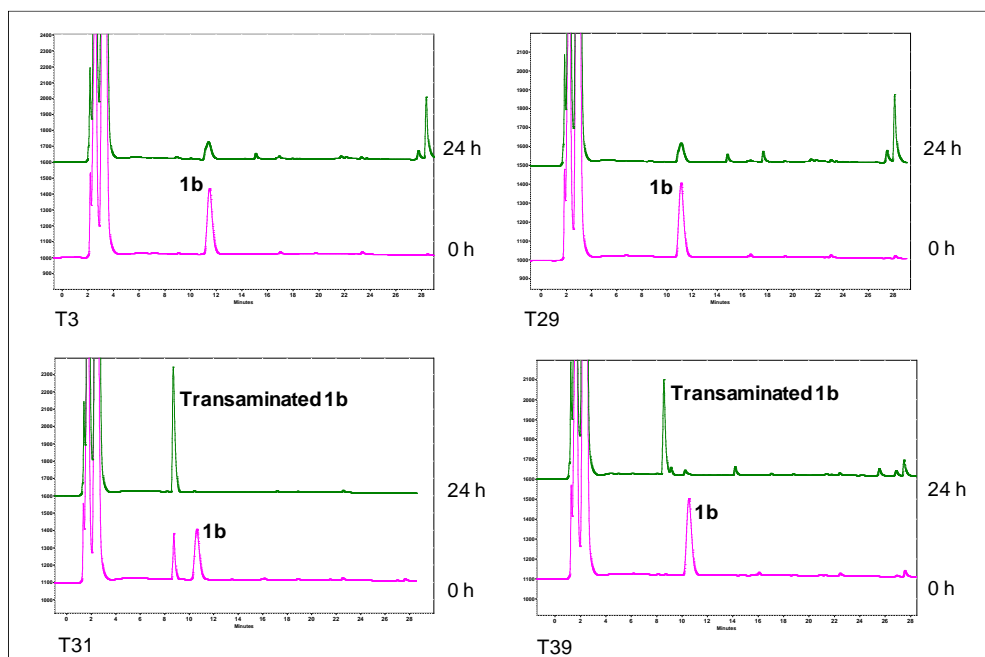
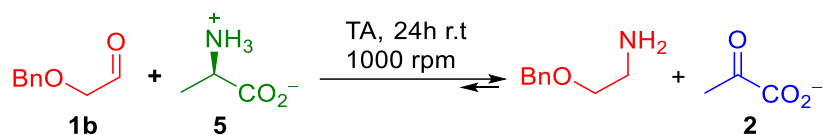


**Figure S14.** HPLC chromatograms of **1b** transamination catalyzed by T03, T029, T031, and T039 at 0 h and after 24 h of incubation.

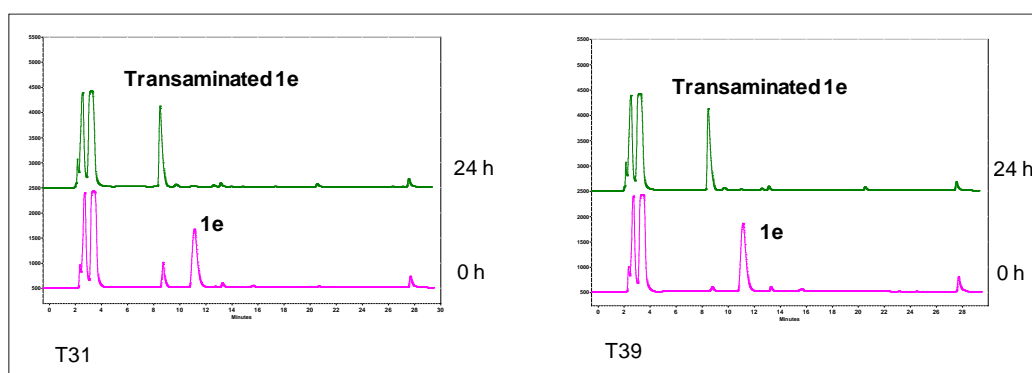
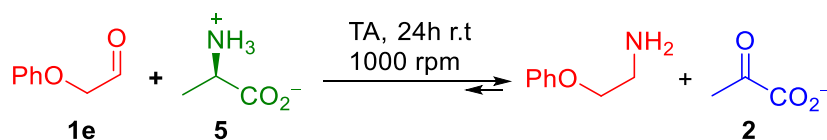


**Figure S15.** HPLC chromatograms of **1e** transamination catalyzed by T031, and T039 at 0 h and after 24 h of incubation.

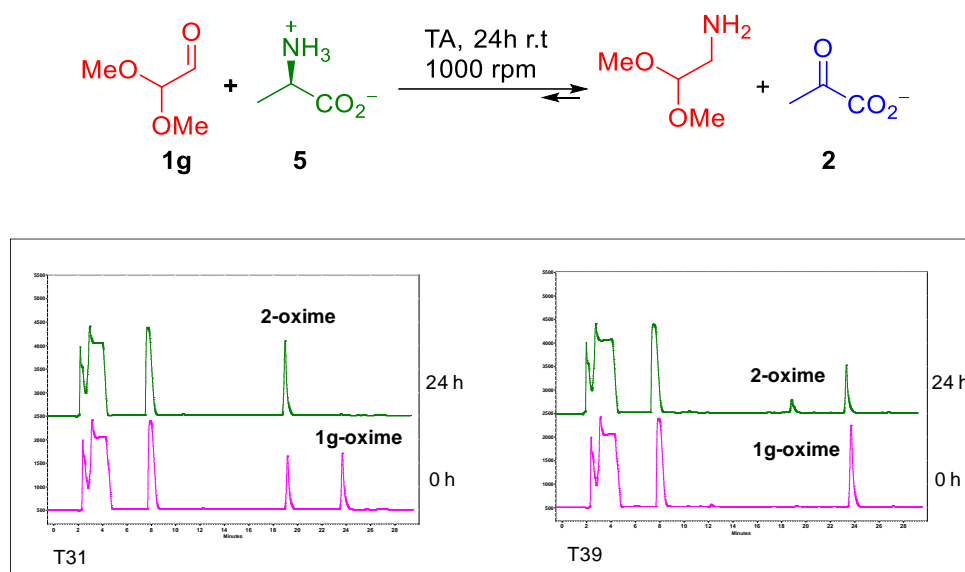


**Figure S16.** HPLC chromatograms of **1g** transamination catalyzed by T029, T031, and T039 24 h at 0 h and after 24 h of incubation.

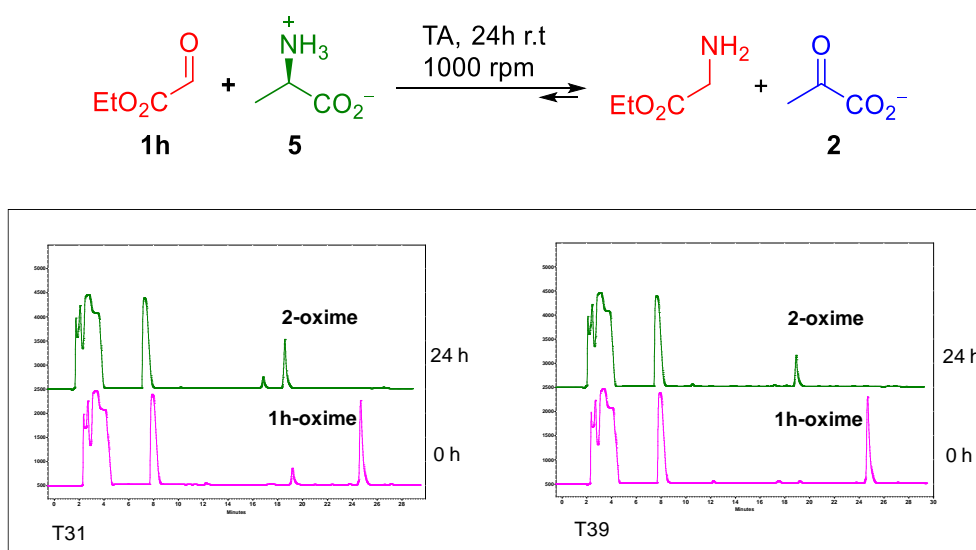


**Figure S17.** HPLC chromatograms of **1h** transamination catalyzed by T031 and T039 at 0 h and after 24 h of incubation.

Two enzymes (T031 and T039) were selected from this assay and evaluated under equimolar conditions of aldehydes **1a-b**, **1e**, **1h-g** (100 mM) and sodium pyruvate **2** (100 mM). Reactions (500  $\mu$ L total volume) were conducted in Eppendorf tubes (1.5 mL). Transaminases lyophilized cell free extracts from Prozomix (2-3 mg) (T031 and T039) were dissolved in 50 mM sodium phosphate buffer pH 7.0 containing L-Ala (100  $\mu$ L of a 0.5 M stock solution 100 mM final concentration in the reaction, 1 eq, with 5 mM PLP,



1 mM in the reaction). To this solution, aldehydes (**1a-b**, **1e**, and **1g-h**) (400  $\mu\text{L}$  of a 125 mM stock solution in 50 mM sodium phosphate buffer pH 7.0, 100 mM final concentration in each reaction, in case of water insoluble hydrophobic aldehydes DMF (20% in the stock, 10% v/v in the reaction) were added. The reaction mixtures were placed in a vortex mixer (1000 rpm) at 25  $^{\circ}\text{C}$  for 24 h. The monitoring and analysis of the reactions was identical as described above. The percentage of transamination of each aldehyde catalyzed by T031 and T039 in the two experimental conditions tested is shown in **Figure S18**.

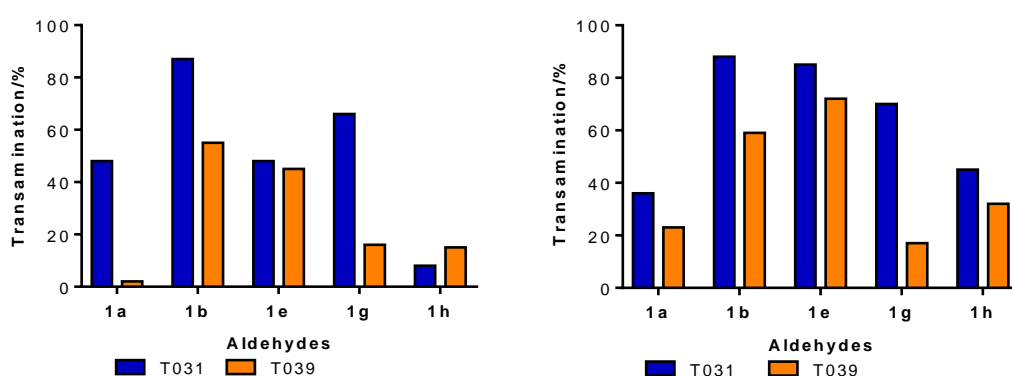


**Figure S18.** Control experiments for aldehyde transamination catalyzed by T031 and T039 at 24 h of incubation. **A)** Aldehyde (**1**) (100 mM) and L-Ala (**5**) (100 mM); **B)** aldehyde (**1**) (50 mM) and L-Ala (**5**) (500 mM).

#### Assay of one-pot biocatalytic cascade synthesis of 4-hydroxy-amino with substrate recycling.

General procedure: the reaction (500  $\mu\text{L}$  total volume) was conducted in Eppendorf tubes (1.5 mL). A solution of transaminase Prozomix T039 cell free extract (2 to 3 mg of 0.12 U  $\text{mg}^{-1}$  lyophilized solid, dissolved in 50 mM sodium phosphate pH 7.0 (250  $\mu\text{L}$ ), 0.50 to 0.75 U  $\text{mL}^{-1}$ , 4 to 6 mg protein  $\text{mL}^{-1}$  in the reaction), L-Ala (50  $\mu\text{L}$  of a stock solution 1 M in 50 mM sodium phosphate buffer pH 7.0, 100 mM final concentration in the reaction), sodium pyruvate (1.25, 6.25, 12.5, 25.0 y 50.0  $\mu\text{L}$  of a 2 M stock solution in plain water pH 7.0, equivalent to 5, 25, 50, 100 and 200 mM final concentrations in the reaction), PLP (20  $\mu\text{L}$  of a 25 mM stock solution in 50 mM sodium phosphate buffer pH 7.0, 1.0 mM final concentration in the reaction) and aldehydes **1** ( $\approx$  100 mM final concentration in the reaction, as the basis of calculation) was prepared. The necessary volume of 50 mM phosphate buffer pH 7.0 to complete 500  $\mu\text{L}$  after adding the enzyme

was added in each case. The reaction was started by the addition of HBPA *wild-type* (125  $\mu\text{L}$  of a stock solution  $0.029 \text{ U mL}^{-1}$ ,  $4 \text{ mg mL}^{-1}$  in  $50 \text{ mM TEA}$  buffer,  $50 \text{ mM NaCl}$ ,  $0.5 \text{ mM EDTA}$  and  $50\% \text{ (v/v)}$  of glycerol,  $0.007 \text{ U mL}^{-1}$ ,  $1 \text{ mg protein mL}^{-1}$  final concentration in the reaction). The reaction mixture was placed in a vortex mixer ( $1000 \text{ rpm}$ ) at  $25 \text{ }^\circ\text{C}$  for  $24 \text{ h}$ . Samples were withdrawn immediately after the aldehydes addition ( $0 \text{ h}$ ) and after  $24 \text{ h}$  and analyzed by HPLC as described above (**Figures S19-S21**).

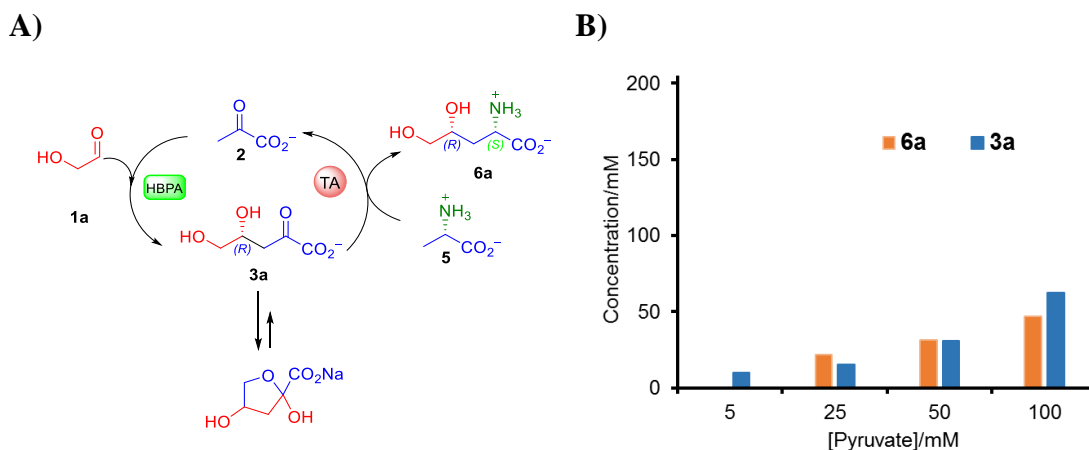


**Figure S19.** A) One-pot biocatalytic cascade synthesis of **6a** with substrate **2** recycling, starting from aldehyde **1a** ( $200 \text{ mM}$ ) and the amine donor **5** ( $100 \text{ mM}$ ). B) Concentration of **3a** and **6a** after  $24 \text{ h}$  of reaction as a function of the initial concentration of pyruvate.

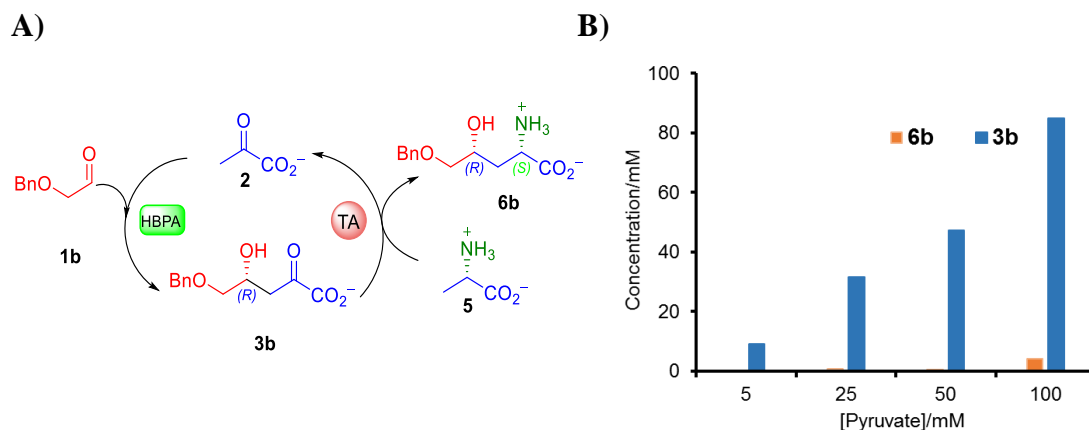


**Figure S20.** A) One-pot biocatalytic cascade synthesis of **6b** with substrate **2** recycling, starting from aldehyde **1b** (100 mM) and the amine donor **5** (100 mM). B) Concentration of **3b** and **6b** after 24 h of reaction as a function of the initial concentration of pyruvate.

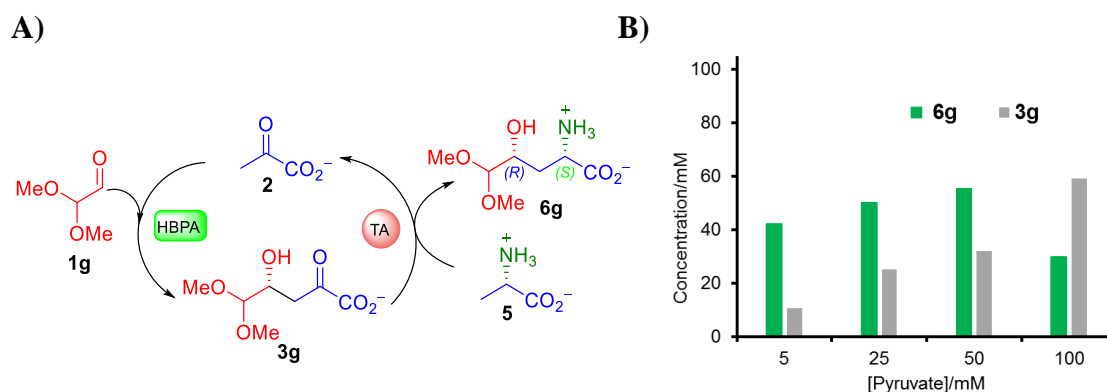


**Figure S21.** A) One-pot biocatalytic cascade synthesis of 4-hydroxy-amino acid derivative **6g** with substrate **2** recycling, starting from aldehyde **1g** (100 mM) and the amine donor **5** (100 mM). B) Concentration of **3g** and **6g** after 24 h of reaction as a function of the initial concentration of pyruvate.

**Using benzyl amine as amino donors:** an extended panel of 194 transaminases from Prozomix Ltd was screened in a one-pot two-step transformation, using benzylamine (**7**) as amine donor and BAL to transform the formed benzaldehyde (**8**) into benzoin (**9**). The reaction (500  $\mu$ L total volume) was conducted in Eppendorf tubes (1.5 mL). 4-Hydroxy-2-oxoacids (**3a-b**, **3e**, **3g-h**) were prepared following the procedure described in section “General procedure for the aldol addition of sodium pyruvate to aldehydes (**1a-s**) catalyzed by HBPA, page S23”. Transaminases from Prozomix TA (T001 to T194 set) (2-3 mg of lyophilized solid) were dissolved in a solution (250  $\mu$ L) containing benzylamine (**7**) (150 mM), PLP (2 mM), ThDP (0.03 mM),  $\text{MgSO}_4$  (5.0 mM), and BAL

(10 U). The reaction was started by the addition of the aldol reaction mixture (250  $\mu\text{L}$ ) containing the aldol adduct **3** and unreacted aldehyde **1** and pyruvate **2** (Table S7).

**Table S7.** Composition ( $\mu\text{mol}$ ) of the crude aldol reaction mixture (250  $\mu\text{L}$ ) used in the screening reaction for the selected **3a**, **3b**, **3e**, **3g**, and **3h** aldol adducts

	<b>3</b> (%)	<b>3</b> ( $\mu\text{mol}$ )	Unreacted <b>2</b> ( $\mu\text{mol}$ )	Unreacted <b>1</b> ( $\mu\text{mol}$ )	Expected consumption benzylamine ( <b>7</b> ) <sup>a</sup> (%)	Maximum consumption benzylamine ( <b>7</b> ) <sup>b</sup> (%)
<b>a</b>	90	22.5	2.5	2.5	60.0	73.3
<b>b</b>	89	22.3	2.8	2.8	59.3	74.0
<b>e</b>	80	20.0	5.0	5.0	53.3	80.0
<b>g</b>	87	21.8	3.3	3.3	58.0	75.3
<b>h</b>	84	21.0	4.0	4.0	56.0	77.3

<sup>a</sup>Only transamination of aldol adduct **3**. <sup>b</sup>Transamination of aldol adduct **3** plus unreacted pyruvate **2** and aldehyde **1**.

Thus, the final amounts of benzylamine and adducts **3** in the initial reaction mixture were 37.5  $\mu\text{mol}$  and between 20 and 22.5  $\mu\text{mol}$ , respectively (Table S7). The reaction mixture was placed in a vortex mixer (1000 rpm) at 25 °C for 24 h. Samples were withdrawn immediately after the substrate mix addition (0 h) and after 24 h and analyzed by HPLC as described above. In the first screening round, the benzylamine (**7**) consumption was analyzed (i.e. measured analyzing the benzaldehyde and benzoin (**8+9**) formation). Samples (20  $\mu\text{L}$ ) were diluted in methanol (500  $\mu\text{L}$ ) and analyzed by HPLC; elution conditions: 55% B over 10 min.

Aldol adduct	T18	T19	T20	T21	T22	T23	T24	T26	T31	T33
3a	10	27	16	40	9	55	54	66	61	35
3b	4	6	17	9	36	17	11	43	59	0
3e	5	5	15	16	18	13	17	34	26	0
3g	16	6	28	20	31	21	32	58	55	48
3h	7	9	0	9	15	0	8	14	11	6

Aldol adduct	T37	T39	T45	T47	T48	T53	T59	T77	T81	T82
3a	0	44	9	58	15	22	0	12	71	0
3b	0	28	0	59	0	0	0	4	37	0
3e	0	33	10	37	0	0	0	0	27	8
3g	54	58	20	48	0	0	14	10	42	6
3h	0	31	0	16	0	0	0	4	14	0

Aldol adduct	T87	T88	T93	T130	T150	T152	T166	T168	T169	T170
3a	23	15	35	69	0	14	90	25	34	33
3b	0	0	15	23	5	0	42	16	40	17
3e	0	0	19	24	8	5	48	14	39	18
3g	0	0	39	8	2	6	43	15	33	17
3h	0	0	12	5	18	6	16	10	16	11

Aldol adduct	T171	T172	T173	T174	T176	T177	T178	T179	T180	T187
3a	0	38	12	53	73	45	23	66	67	23
3b	0	15	0	36	43	12	8	0	17	0
3e	18	0	0	37	40	17	17	7	21	0
3g	6	7	0	40	40	12	18	25	32	20
3h	0	8	0	38	16	0	8	8	14	0

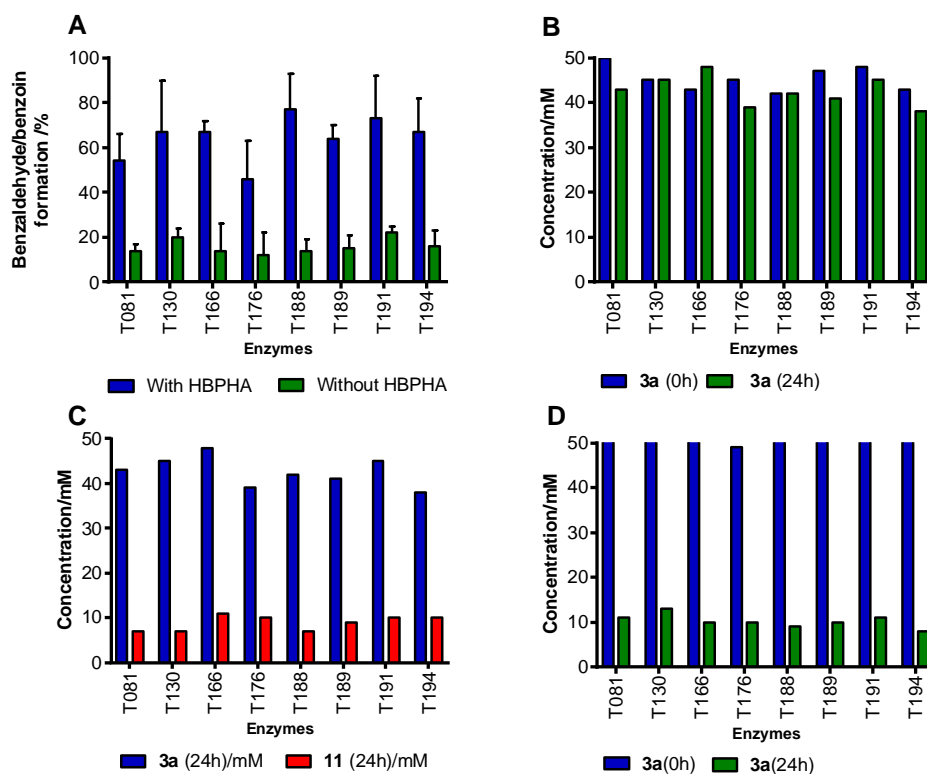
  

Aldol adduct	T188	T189	T190	T191	T192	T193	T194
3a	78	89	15	100	49	39	94
3b	56	57	9	52	10	0	68
3e	64	65	6	68	14	16	72
3g	47	41	18	43	40	29	48
3h	17	18	9	20	11	10	19

**Figure S22.** Percentage of benzaldehyde/benzoin formed (i.e., benzylamine consumed) for the screening of 194 transaminases from Prozomix (T001-T194), against aldol adducts **3a-b**, **3e** and **3g-h** using benzylamine (**7**) as amine donor. Conditions: Aldol addition: **1** (100 mM), **2** (100 mM) and HBPA (1 mg mL<sup>-1</sup>); transamination: **3** (~50 mM) and **7** (75 mM), and T### cell free extract (2-3 mg). The percentage of benzaldehyde/benzoin formed (i.e., benzylamine consumed) after 24 h was determined by HPLC from the peak areas by an external standard method. Transaminases not appearing on the table gave zero-conversion with all substrates. Taking into account the initial amounts of benzylamine and **3** in the reaction mixtures, a percentage >67% (red-backgrounded cells) was considered to come from partial consumption of benzylamine because of the transamination reactions of aldehydes (**1**) and pyruvate (**2**), which remained unreacted from the aldolic reaction or were formed by retroaldolysis during the transamination reaction. The yellow-backgrounded transaminases are those that were selected as potential positive transaminases, i.e. those that showed percentages between 33% and 67% at least for one of the substrates.

### Determination of the effect of the retroaldolysis reaction on the yield of **6a** as example.

In some cases of the first screening round, an excess of benzaldehyde/benzoin production (>67%, red spots) was detected. To assess if HBPA mediated retroaldolysis favored by the transamination of the remaining aldehyde, independent experiments were performed using **3a** as example. Transamination assays were carried out with and without previously removing HBPA of the aldol reaction mixture (**Figure S23**).



**Figure S23.** One-pot two-step synthesis of synthesis of **6a**, using benzylamine (**7**) as amine donor. A) Benzaldehyde/benzoin formed in transamination experiments with and without HBPA. B) Decrease of the aldol adduct at 24 h for the transamination system without HBPA. C) Concentration of the aldol adduct (**3a**) and benzaldehyde/benzoin (**11**) at 24 h for the transamination system without HBPA. D) Decrease of the aldol adduct at 24 h for the transamination system with HBPA. Example to demonstrate that the transamination of the aldehyde may activate the retroaldolysis of **3** mediated by HBPA, generating aldehyde and pyruvate and causing the excess of benzoin formation.

### Second screening removing the HBPA before running the transamination reaction.

A second screening transamination round was done, removing previously the aldolase from the aldolic mixtures using amicon® Ultra-15 centrifugal filter devices (Nominal Molecular Weight Limit 3.000 Da), 7000 rpm, for 10 minutes at 4 °C. Transamination of **3** was performed following the procedure described above. The percentages of transamination for **3a**, **3g** and **3h** were determined using three measurements: a) from the aldol adducts **3** consumed with precolumn derivatization (10 µL of samples were withdrawn from the reaction mixtures and derivatized with BnONH<sub>2</sub> and analyzed by HPLC as described above), b) from the transaminated product formed (**6a**, **6g** and **6h**) previous precolumn derivatization with Bz-OSu as described above, and c) from benzoin produced (**11**) as it was described above. Transamination of **3b** and **3e** were determined

from the aldol adduct **3** consumed and **6b** and **6e** formed, respectively (50  $\mu\text{L}$  of samples were withdrawn from the reaction mixtures and diluted in 500  $\mu\text{L}$  of MeOH and directly analyzed with a gradient elution from 10 to 100% B over 30 min) (**Figure S24**).

Aldol adduct	Enzymes																	
<b>3a</b>	T21	T23	T24	T26	T31	T33	T39	T47	T93	T169	T170	T172	T74	T177	T179	T192	T193	
Result	0	0	0	0	0	0	67	0	0	0	0	0	0	0	0	0	0	
<b>3b</b>	T22	T26	T31	T39	T47	T81	T166	T169	T174	176	T188	T189	T191	194				
Result	0	0	0	35	0	0	0	0	0	0	0	0	0	0				
<b>3e</b>	T26	T31	T39	T47	T81	T130	T166	T169	T174	T176	T188	T189	T191					
Result	0	0	55	0	0	0	0	0	0	0	0	0	0					
<b>3g</b>	T24	T26	T31	T33	T37	T39	T47	T81	T93	T166	T169	T174	T176	T188	T189	T191	T192	T194
Result	11	16	12	16	8	63	23	18	15	19	15	18	14	16	18	15	16	16
<b>3h</b>	T39	T174																
Result	57	45																

**Figure S24.** Second screening round analyzing the percentage of transamination measuring the aldol adduct consumed (**3**), the transaminated product formed (**6**) and benzoin produced (**11**).

#### Evaluation of the effect of HBPA and BAL in the yield of **6a-b**, **6e** and **6g-j**

4-Hydroxy-2-oxoacids (**3a-b**, **3e**, **3h-g**) were prepared as previously described. Transamination reactions of **3** were performed as above without removing HBPA, using Prozomix T039 transaminase. To evaluate the effect of BAL on the formation of **6**, we run the same two-step reaction sequence without removing HBPA using T039, and without adding BAL in the transamination reaction. Reactions were monitored by HPLC as described for the second screening round.

#### Assay of one-pot two steps 4-hydroxy- $\alpha$ -amino acids derivatives using a biocatalytic one-pot two-steps approach using the PLP-Dependent branched-chain amino acid aminotransferase (BCATs) from *Escherichia coli*.

Reactions were conducted in Eppendorf tubes (1.5 mL) with 500  $\mu\text{L}$  total reaction volume. To an aldolic reaction mixture containing aldol adduct (**3**) (250  $\mu\text{L}$ ,  $\approx 100$  mM, as the basis of calculation), L-Glu and L-Asp solution mixture (65  $\mu\text{L}$  of stock solution in 50 mM sodium phosphate buffer pH 8.0 containing L-Glu **12** (77 mM), L-Asp **14** (385 mM) and PLP (8 mM), 10 mM, 50 mM and 1 mM final concentration in the reaction respectively), BCAT (28  $\mu\text{L}$  of a stock solution  $0.0538$  U  $\text{mL}^{-1}$ ,  $18$  mg  $\text{mL}^{-1}$  in 50 mM  $\text{NaH}_2\text{PO}_4$  buffer pH 7.0, NaCl (100 mM), PLP (0.01 mM) and glycerol (50% v/v), 0.003

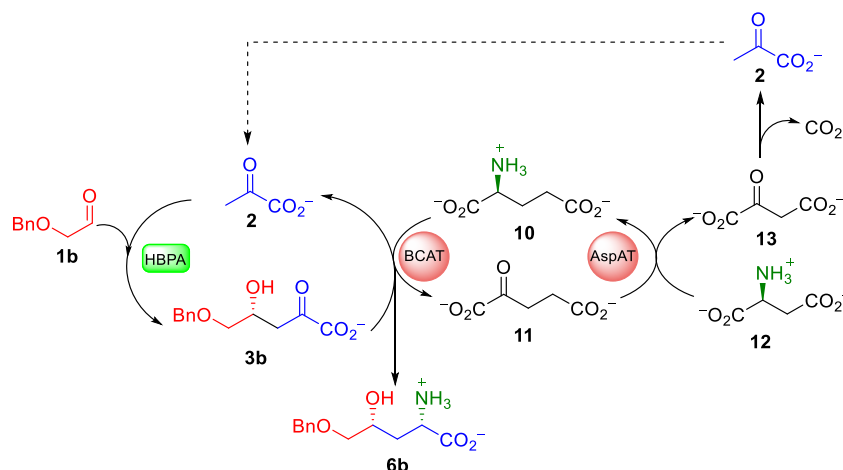
U mL<sup>-1</sup>, 1 mg protein mL<sup>-1</sup> final concentration in the reaction), reaction was started by adding the enzyme (AspAT, 42 μL of a stock solution 2.1615 U mL<sup>-1</sup>, 12 mg mL<sup>-1</sup> in 50mM NaH<sub>2</sub>PO<sub>4</sub> buffer pH 7.0, NaCl (100 mM), PLP (0.01 mM) and glycerol (50% v/v), 0.18 U mL<sup>-1</sup>, 1 mg protein mL<sup>-1</sup> final concentration in the reaction). The necessary volume of 50 mM phosphate buffer pH 7.0 to complete 500 μL was added. The reaction mixture was placed in a vortex mixer (1000 rpm) at 25 °C for 24 h. Samples were withdrawn immediately after the AspAT addition (0 h) and after 24 h and analyzed by HPLC as described above.

**Assay of one-pot biocatalytic cascade synthesis of 4-hydroxy- $\alpha$ -amino acid derivatives with substrate recycling BCAT/L-Glu/L-Asp/AspAT.**

The reaction (500 μL total volume) was conducted in Eppendorf tubes (1.5 mL). A solution of BCAT and AspAT (28 and 42 μL of stock solution 18 and 12 mg protein mL<sup>-1</sup> in 50 mM sodium phosphate buffer pH 7.0 containing 100 mM NaCl, 0.1 mM PLP, and 50% (v/v) of glycerol, 0.003 U mL<sup>-1</sup> of BCAT and 0.18 U mL<sup>-1</sup> of AspAT. 1 mg protein mL<sup>-1</sup> of each one in the reaction), containing sodium pyruvate (2.5, 12.5, 22.5, and 25.0 μL, depending on the experiment of a 2 M aqueous stock solution, adjusted to pH 7.0, 10, 50, 90, and 100 mM final concentration in the reaction), L-Asp (45, 25, 5 and 100 μL, depending on the experiment of a 1.0 M stock solution 250 mM sodium phosphate buffer pH 8.0, (90, 50, 10 and 100 mM final concentration in the reaction, respectively), L-Glu (10 μL of a 1.0 M stock solution 250 mM sodium phosphate buffer pH 8.0, containing 25 mM PLP) and aldehyde **1b** (10 μL, 100 mM in the reaction). The reaction was started by adding HBPA (125 μL of a stock solution 0.029 U mL<sup>-1</sup>, 4 mg mL<sup>-1</sup> in 50 mM TEA buffer, 50 mM NaCl, 0.5 mM EDTA and 50% (v/v) of glycerol, 0.007 U mL<sup>-1</sup>, 1 mg protein mL<sup>-1</sup> final concentration in the reaction). The necessary volume of 50 mM phosphate buffer pH 7.0 to complete 500 μL after adding the enzyme was added in each case. The reaction mixtures were placed in a vortex mixer (1000 rpm) at 25 °C for 24 h. Samples were withdrawn immediately after the HBPA addition (0 h) and after 24 h and analyzed by HPLC as described above (**Figure S25**).



A



B

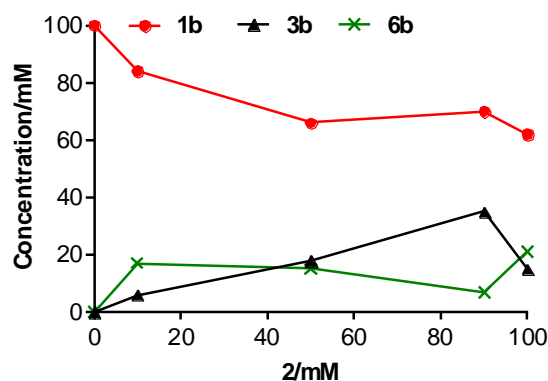
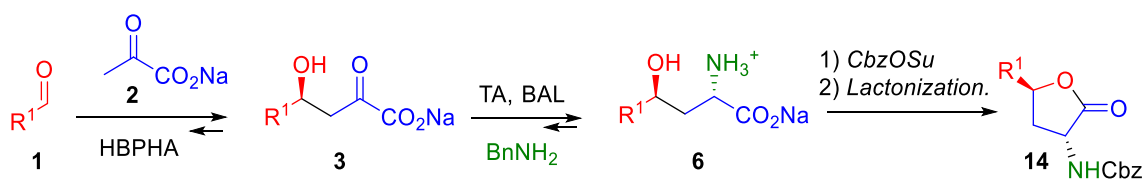


**Figure S25.** A) One-pot biocatalytic cascade synthesis of 4-hydroxy- $\alpha$ -amino acid derivative **6b** with substrate **2** recycling, starting from aldehyde **1b** (100 mM) and the amine donor **5** (100 mM). B) Concentration of the components after 24 h of reaction as a function of the initial concentration of pyruvate using HBPA/BCAT/AspAT transaminases catalysts.

### Synthesis of 4-hydroxy- $\alpha$ -amino acids by tandem HBPA/transaminase and conversion to $\alpha$ -amino- $\gamma$ -butyrolactone derivatives.

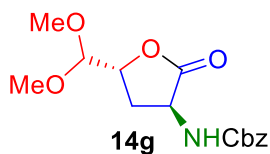
The aldol addition catalyzed by HBPA, transamination reaction, Cbz protection and the subsequent lactonization was carried as follows:



**NOTE: For convenience, the order of the compounds in the SI follows the order in which they were obtained which is different from that of the main text.**

**Benzyl ((3*S*,5*R*)-5-(dimethoxymethyl)-2-oxotetrahydrofuran-3-yl)carbamate (**14g**);**

Typical Procedure.



The precursor **3g** was prepared following the procedure described for *R*-**4a**. Reaction volume was 29 mL. Starting from **1g** (437  $\mu\text{L}$  of a 6.6 M commercial aqueous solution, 2.9 mmol, 1 eq, 0.1 M) and sodium pyruvate **2** (0.32 g, 2.9 mmol, 1 eq, 0.1 M). When the aldol adduct **3g** formed was maximum, the transamination reaction was initiated.

**Transamination and Cbz protection:** to the mixture of the aldol reaction (2.9 mmol of aldol adduct in 29 mL), benzylamine (**7**) (2.2 mL, of 1 M stock solution in 50 mM sodium phosphate pH 8.0, 4.3 mmol, 1.5 eq), PLP (10.2 mg, 1 mM final concentration in the reaction), ThDP (0.3 mg, 0.015 mM final concentration in the reaction),  $\text{MgSO}_4$  (24 mg, 2.5 mM final concentration in the reaction), and BAL (136  $\mu\text{L}$  of 2826  $\text{U mL}^{-1}$  stock solution in 50 mM buffer TEA containing 50 mM NaCl, 0.5 mM EDTA and 50% (v/v) of glycerol, 5.0  $\text{U mL}^{-1}$  final concentration in the reaction) were added. Reaction was started by adding the transaminase (T039, 76 mg of 0.1243  $\text{U mg}^{-1}$  lyophilized solid, dissolved in 50 mM sodium phosphate pH 7.0 (5 mL), 0.783  $\text{U mL}^{-1}$ , 6 mg protein  $\text{mL}^{-1}$  final concentration in the reaction). The mixture was placed in an orbital shaker (250 rpm) at 25  $^\circ\text{C}$  for 24 h. Formation of **6g** was estimated by measuring the aldol adduct **3g** consumed. For both enzymatic reactions, samples were withdrawn immediately after the enzyme addition (0 h) and after 24 h and analyzed by HPLC using pre-column derivatization as described above. When the consumption of **3g** reached a maximum (24 h), methanol (10 volumes) was added. The mixture was filtered through Celite® and the filter cake washed with methanol (3 x 50 mL). The filtrates were pooled and evaporated under vacuum, until all MeOH was removed. The aqueous residue was diluted with  $\text{NaHCO}_3$  20% w/v solution (50 mL). To this solution, Cbz-OSu (1.6 g dissolved in 50 mL 2-MeTHF, 2.2 eq) was added. The reaction was stirred at 25  $^\circ\text{C}$  during 12 h. Then, the aqueous phase was first extracted with EtOAc (3 x 50 mL). After that, the pH of aqueous solution was adjusted to 3.5 with 5 M HCl, and extracted with EtOAc (3 x 100 mL). The organic phase was dried over anhydrous  $\text{MgSO}_4$ , and the solvent removed under vacuum

and the residue submitted to intramolecular lactonization using three different procedures as follows:

**Procedure 1:** 471 mg of **6g** (1.4 mmol, 1eq) from the previous step was suspended in anhydrous DMF (60 mL) under N<sub>2</sub> atmosphere. To this solution, EDAC (414.3 mg, 2.2 mmol, 1.5 eq) and DMAP (5.3 mg, 43.2 μmol, 0.03 eq) were added. The reaction was stirred from 4 °C to rt overnight. Then, EtOAc (300 mL) was added and washed with H<sub>2</sub>O (3 x 100 mL), aqueous NaHCO<sub>3</sub> 20% w/v (3 x 100 mL) and brine (3 x 100 mL). The organic phase was dried over anhydrous MgSO<sub>4</sub>, absorbed onto silica gel (100 mL) and loaded on a column (AFORA, 5880/2, 47x4.5) packed with silica gel (100 g, 35-70 μm, 200-500 mesh, Merck). Product was eluted with a step gradient of hexane:EtOAc: 100:0, 500 mL, 90:10, 200 mL, 80:20, 200 mL, 70:30, 200 mL, 60:40, 2 L. Pure fractions were pooled, and the solvent removed under vacuum affording the compound **14g** as a white solid (dr: >95:5, 121 mg, 27%) (**Table S8**).  $[\alpha]_{20}^D = -20$  ( $c = 1$ , in CHCl<sub>3</sub>). <sup>1</sup>H NMR (400 MHz, CDCl<sub>3</sub>) δ 7.61 - 6.80 (m, 5H), 5.10 (s, 2H), 4.54 (d,  $J = 9.3$  Hz, 1H), 4.47 (td,  $J = 2 \times 10.0$ , 6.8 Hz, 1H), 4.38 (d,  $J = 2.7$  Hz, 1H), 3.47 (s, 3H), 3.46 (s, 3H), 2.77 (dd,  $J = 13.1$ , 9.7 Hz, 1H), 2.19 (d,  $J = 10.9$  Hz, 1H). <sup>13</sup>C NMR (101 MHz, CDCl<sub>3</sub>) δ 175.0, 155.7, 136.8, 104.9, 76.7, 67.3, 57.4, 56.3, 50.2, 29.3. ESI-TOF  $m/z$ : Calcd for [M+H<sup>+</sup>] C<sub>15</sub>H<sub>20</sub>NO<sub>6</sub><sup>+</sup>: 310.1321, found [M+H<sup>+</sup>]: 310.1291.

**Procedure 2:** 472 mg of **6g** (1.4 mmol, 1eq) from the previous reaction was suspended in anhydrous DMF (60 mL) under N<sub>2</sub> atmosphere. To this solution, HOBt (292 mg, 2.2 mmol, 1.5 eq) and EDAC (414.3 mg, 2.2 mmol, 1.5 eq) were added. The reaction was stirred overnight from 4 °C to rt. Work up and purification was performed as described for **procedure 1**, affording the compound **14g** (**Table S8**).

**Procedure 3:** 265 mg of **6g** (810.4 μmol, 1eq) from the previous reaction was suspended in anhydrous CH<sub>2</sub>Cl<sub>2</sub> (60 mL) under N<sub>2</sub> atmosphere. To this solution, HOBt (164.3 mg, 1.2 mmol, 1.5 eq), EDAC (233 mg, 1.2 mmol, 1.5 eq) and Et<sub>3</sub>N (164 mg, 1.6 mmol, 2 eq) were added. The reaction was stirred overnight from 4 °C to rt. Work up and purification was performed as described for **procedure 1**, affording the compound **14g** (**Table S8**).

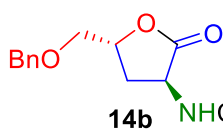
**Table S8.** Intramolecular lactonization conditions.

Procedure	Aldol Conv./(%) <sup>a</sup>	Transamination Conv./(%) <sup>b</sup>	Yield (%) <sup>c</sup>	[ $\alpha$ ] <sup>d</sup>
1	80	98	27	-20
2	86	90	35	-21
3	87	94	52	-20

<sup>a</sup> Percentage of aldol adduct (**3g**) formed after 24h. <sup>b</sup> Percentage of transaminated product (**6g**) formed after 24h. <sup>c</sup> Isolated yield (**14g**). <sup>d</sup>  $c=1$  in CHCl<sub>3</sub>.

### Benzyl ((3*S*,5*R*)-5-((benzyloxy)methyl)-2-oxotetrahydrofuran-3-yl)carbamate

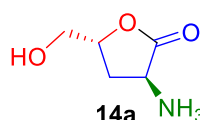
(**14b**).



Precursor **3b** was prepared following the procedure described above *R-4b*, starting from **1b** (0.5 g, 3.3 mmol, 0.1 M final concentration in the reaction) and sodium pyruvate **2** (0.37 g, 3.3 mmol, 1 eq). The reaction yielded 69% of **3b**. Transamination reaction was conducted in an Erlenmeyer (100 mL) using the BCAT/L-Glu/L-Asp/AspAT system. To the aldol reaction mixture (33 mL), L-Glu (1.2 mL of a 0.5 M stock solution in 250 mM sodium phosphate buffer pH 8.0, 10 mM, containing 25 mM PLP, 1 mM final concentration in the reaction), L-Asp (3 mL of a 1 M stock solution in 250 mM sodium phosphate buffer pH 8.0, 50 mM) were added. The reaction was started by adding BCAT (2.3 mL of a stock solution 0.0538 U mL<sup>-1</sup>, 18 mg mL<sup>-1</sup> in 50 mM NaH<sub>2</sub>PO<sub>4</sub> buffer pH 7.0, NaCl (100 mM), PLP (0.01 mM), glycerol (50% v/v), 0.003 U mL<sup>-1</sup>, 1 mg mL<sup>-1</sup> protein final concentration in the reaction), and AspAT (3.5 mL of a stock solution 2.1615 U mL<sup>-1</sup>, 12 mg mL<sup>-1</sup> in 50 mM NaH<sub>2</sub>PO<sub>4</sub> buffer pH 7.0, NaCl (100 mM), PLP (0.01 mM) and glycerol (50% v/v), 0.18 U mL<sup>-1</sup>, 1 mg mL<sup>-1</sup> protein final concentration in the reaction). The mixture was placed in an orbital shaker (250 rpm) at 25 °C for 24 h. Samples were withdrawn immediately after the enzyme addition (0 h) and after 24 h as described above, reaction was monitored by HPLC. When the reaction was completed (49% product formed), the enzymes were precipitated by adding methanol (10 volumes, 600 mL). The mixture was filtered through Celite® and the filter cake washed with methanol (3 x 50 mL). The filtrates were pooled and the solvent removed under vacuum, until all MeOH was evaporated and only the aqueous solution remained. Cbz protection and conversion to  $\alpha$ -amino- $\gamma$ -butyrolactone derivative **14b** were performed following the **procedure 3**. Product was eluted with a step gradient of hexane:EtOAc: 100:0, 500 mL, 90:10, 200 mL, 80:20, 200 mL, 70:30, 500 mL, 60:40, 1 L. The title compound **14b** was obtained as yellow oil (dr: >95:5, 222 mg, 26%). [ $\alpha$ ]<sub>20</sub><sup>D</sup> = -18 ( $c = 1$ , in CHCl<sub>3</sub>). <sup>1</sup>H NMR (400 MHz,

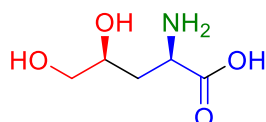
CDCl<sub>3</sub>)  $\delta$  7.39 – 7.23 (m, 10H), 5.10 (s, 2H), 4.70 (d,  $J = 9.2$  Hz, 1H), 4.66 – 4.46 (m, 2H), 4.10 (q,  $J = 3 \times 7.1$ , Hz, 1H), 3.70 (d,  $J = 8.0$  Hz, 1H), 3.54 (d,  $J = 7.9$  Hz, 1H), 2.68 (d,  $J = 11.3$  Hz, 1H), 2.38 (dd,  $J = 18.1, 9.9$  Hz, 1H). <sup>13</sup>C NMR (101 MHz, CDCl<sub>3</sub>)  $\delta$  128.5, 76.6, 73.8, 71.1, 70.9, 67.4, 50.4, 31.8. ESI-TOF  $m/z$ : Calcd for [M+H<sup>+</sup>] C<sub>20</sub>H<sub>22</sub>NO<sub>5</sub><sup>+</sup>: 356.1506, found [M+H<sup>+</sup>]: 356.1498.

**(3*S*,5*R*)-5-(Hydroxymethyl)-2-oxotetrahydrofuran-3-aminium chloride (14a).**



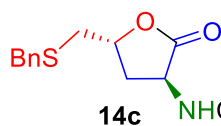
Compound **(14a)** was prepared by dissolving **14b** (50 mg, 140.7  $\mu$ mol, 1 eq.) in MeOH (15 mL). Then, HCl (156  $\mu$ L of 1 M stock solution, 1.1 eq) and Pd/C (1.50 mg, 10 mol%, 10% Pd, 50% humidity) were added. The suspension was stirred at room temperature for 2 hours under H<sub>2</sub> atmosphere. The reaction mixture was filtered through Celite<sup>®</sup> and the pellet was washed with MeOH (3x50 mL). Then, the solvent was removed *in vacuo* obtaining the title compound as a yellow oil (dr >95:5, 14 mg, 59%). (3*S*,5*R*)-5-(Hydroxymethyl)-2-oxotetrahydrofuran-3-aminium chloride, **14a**: <sup>1</sup>H NMR (400 MHz, CD<sub>3</sub>OD)  $\delta$  4.82 (m, 1H), 4.45 (dd,  $J = 10.7, 9.5$  Hz, 1H), 3.86 (dd,  $J = 12.4, 2.4$  Hz, 1H), 3.69 (dd,  $J = 12.4, 2.4$  Hz, 1H), 2.72 (dd,  $J = 13.0, 9.6$  Hz, 1H), 2.47 (ddd,  $J = 13.0, 10.7, 9.1$  Hz, 1H). <sup>13</sup>C NMR (101 MHz, CD<sub>3</sub>OD)  $\delta$  172.1, 78.7, 62.7, 47.8, 28.3.

The spectra of the sample changed with the time and it was because of the cyclic lactone is hydrolyzed leading to the acyclic carboxylate compound namely (2*S*,4*R*)-2-amino-4,5-



**dihydroxypentanoic acid**: <sup>1</sup>H NMR (400 MHz, CD<sub>3</sub>OD)  $\delta$  4.23 (dd,  $J = 8.0, 4.8$  Hz, 1H), 3.92 (dd,  $J = 5.8, 4.0$  Hz, 1H), 3.51 (m, 2H), 2.23 (ddd,  $J = 14.8, 4.9, 3.0$  Hz, 1H), 1.89 (ddd,  $J = 14.7, 10.2, 8.0$  Hz, 1H). <sup>13</sup>C NMR (101 MHz, CD<sub>3</sub>OD)  $\delta$  169.3, 68.8, 65.3, 50.4, 32.5.

**Benzyl ((3*S*,5*R*)-5-((benzylthio)methyl)-2-oxotetrahydrofuran-3-yl)carbamate (14c).**

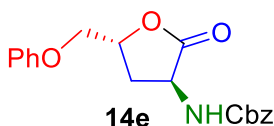


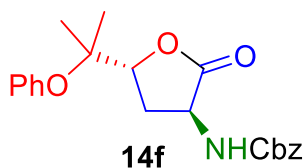
The synthesis of aldol intermediate **3c** was conducted in an Erlenmeyer flask (50 mL). The reaction volume was 15 mL. 2-(Benzylthio)acetaldehyde (**1c**) (0.25 g, 1.5 mmol, 1 eq, 0.1 M final concentration in the reaction) was dissolved in DMF (3 mL, 20% (v/v) in the reaction) and sodium pyruvate **2** (165.5 mg, 1.5 mmol, 1 eq, 0.1 M final concentration in

the reaction) dissolved in water (6.6 mL) was added. Finally, the reaction was started by adding the enzyme HBPA H205A (5.4 mL of a stock solution 0.009 U mL<sup>-1</sup>, 2.8 mg mL<sup>-1</sup> in 50 mM TEA buffer, 50 mM NaCl, 0.5 mM EDTA and 50% (v/v) of glycerol, 0.00324 U mL<sup>-1</sup>, 1 mg mL<sup>-1</sup> protein final concentration in the reaction). The reaction was placed in an orbital shaker (250 rpm) at 25 °C for 24h. Samples were withdrawn immediately after the enzyme addition (0 h) and after 24 h as described above. The reaction yielded 66% of **3c**. Enzymatic transamination of **3c** using BCAT/L-Glu/L-Asp/AspAT system yielded 66% of **6c**. Cbz protection and conversion to  $\alpha$ -amino- $\gamma$ -butyrolactone derivative **14c** were performed following the **procedure 3**. Product was eluted with a step gradient of hexane:EtOAc: 100:0, 500 mL, 90:10, 200 mL, 80:20, 200 mL, 70:30, 1.5 L, affording the compound **14c** as a solid (dr: >95:5, 124 mg, 22%).  $[\alpha]_{20}^D = -32$  ( $c = 1$ , in CHCl<sub>3</sub>). <sup>1</sup>H NMR (400 MHz, CDCl<sub>3</sub>)  $\delta$  7.68 – 6.78 (m, 10H), 5.11 (s, 2H), 4.73 (s, 1H), 4.49 (d,  $J = 6.5$  Hz, 1H), 3.75 (s, 2H), 2.65 (d,  $J = 5.3$  Hz, 2H), 2.52 (d,  $J = 10.6$  Hz, 1H), 2.31 (d,  $J = 12.9$  Hz, 1H). <sup>13</sup>C NMR (101 MHz, CDCl<sub>3</sub>)  $\delta$  174.4, 155.7, 128.5, 77.2, 67.6, 49.9, 36.9, 35.3, 33.4. ESI-TOF  $m/z$ : Calcd for [M+H<sup>+</sup>] C<sub>20</sub>H<sub>22</sub>NO<sub>4</sub>S<sup>+</sup>: 372.1288, found [M+H<sup>+</sup>]: 372.1270.

#### Benzyl ((3*S*,5*R*)-2-oxo-5-(phenoxy)methyl)tetrahydrofuran-3-yl)carbamate (**14e**).

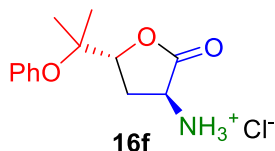
The precursor **3e** was prepared following the procedure described for *R*-**4e**. Reaction volume was 18 mL. Starting from **1e** (0.25 g, 1.8 mmol, 0.1M) and sodium pyruvate **2** (202.1 mg, 1.8 mmol, 1 eq), the reaction yielded 80% of **3e**. Transamination of **3e** using BCAT/L-Glu/L-Asp/AspAT system rendered 71% of **6e**. Cbz protection and conversion to  $\alpha$ -amino- $\gamma$ -butyrolactone derivative **14e** were performed following the **procedure 3**. Product was eluted with a step gradient of hexane:EtOAc: 100:0, 500 mL, 90:10, 200 mL, 80:20, 200 mL, 70:30, 500 mL, 60:40, 2 L affording the title compound **14e** as solid (dr: >95:5, 182 mg, 29%).  $[\alpha]_{20}^D = -35$  ( $c = 1$ , in CHCl<sub>3</sub>). <sup>1</sup>H NMR (400 MHz, CDCl<sub>3</sub>)  $\delta$  7.40 – 7.22 (m, 7H), 7.02 – 6.81 (m, 3H), 5.12 (s, 2H), 4.91 (d,  $J = 8.6$  Hz, 1H), 4.72 (td,  $J = 2 \times 10.0$ , 6.5 Hz, 1H), 4.23 (d,  $J = 10.5$  Hz, 1H), 4.05 (d,  $J = 10.3$  Hz, 1H), 2.80 (d,  $J = 13.0$  Hz, 1H), 2.48 (d,  $J = 11.7$  Hz, 1H). <sup>13</sup>C NMR (101 MHz, CDCl<sub>3</sub>)  $\delta$  174.7, 155.4, 128.9, 121.9, 114.9, 75.4, 69.3, 67.4, 50.2. ESI-TOF  $m/z$ : Calcd for [M+H<sup>+</sup>] C<sub>19</sub>H<sub>20</sub>NO<sub>5</sub><sup>+</sup>: 342.1359, found [M+H<sup>+</sup>]: 3421341.



**Benzyl ((3*S*,5*R*)-2-oxo-5-(2-phenoxypropan-2-yl)tetrahydrofuran-3-yl)carbamate (14f).**

The precursor **3f** was prepared following the procedure described above for *R*-**4f**. Reaction volume was 24 mL. Starting from **1f** (0.4 g, 2.4 mmol, 0.1 M) and sodium pyruvate **2** (268.1 mg, 2.4 mmol, 1 eq), the reaction afforded 63% of **3f**.

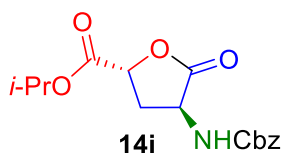
Transamination of **3f** was performed using the BCAT/L-Glu/L-Asp/AspAT system, rendering 56% of **6f**. Cbz protection and conversion to  $\alpha$ -amino- $\gamma$ -butyrolactone derivative **14f** were performed following the **procedure 3**. Product was eluted with a step gradient of hexane:EtOAc: 100:0, 500 mL, 90:10, 200 mL, 80:20, 2.5 L, affording the title compound **14f** as a yellow oil (dr: >95:5, 98 mg, 11%).  $[\alpha]_{20}^D = -26$  ( $c = 1$ , in  $\text{CHCl}_3$ ).  $^1\text{H NMR}$  (400 MHz,  $\text{CDCl}_3$ )  $\delta$  7.46 – 6.76 (m, 10H), 5.11 (s, 2H), 4.64 (td,  $J = 2 \times 9.9$ , 6.3 Hz, 1H), 4.42 (s, 1H), 4.10 (q,  $J = 3 \times 7.2$ , Hz, 1H), 3.01 (d,  $J = 10.3$  Hz, 1H), 2.37 (d,  $J = 10.8$  Hz, 1H), 1.31 (s, 3H), 1.29 (s, 3H).  $^{13}\text{C NMR}$  (101 MHz,  $\text{CDCl}_3$ )  $\delta$  175.2, 155.7, 153.3, 129.1, 128.5, 124.2, 123.8, 83.7, 80.5, 67.3, 50.3, 30.3, 23.5, 22.6. ESI-TOF  $m/z$ : Calcd for  $[\text{M}+\text{H}^+]$   $\text{C}_{21}\text{H}_{24}\text{NO}_5^+$ : 370.1686, found  $[\text{M}+\text{H}^+]$ : 370.1654.

**Cbz removal of 14f. Synthesis of (3*S*,5*R*)-2-oxo-5-(2-phenoxypropan-2-yl)tetrahydrofuran-3-aminium chloride (16f).**

To compound **14f** (50 mg, 135.4  $\mu\text{mol}$ , 1 eq) in MeOH (15 mL), HCl (270  $\mu\text{L}$  of 1 M stock solution, 2 eq) and Pd/C (1.34 mg, 10 mol%, 10% Pd, 50% humidity) were added. The suspension was stirred at room temperature for 1 hour under  $\text{H}_2$

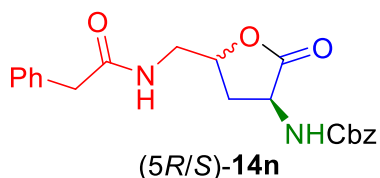
atmosphere. Reaction mixture was filtered through Celite<sup>®</sup> and the pellet was washed with MeOH (3 x 50 mL). Then, the solvent was removed *in vacuo* obtaining the title compound **16f** as a solid (18 mg, 49%)  $^1\text{H NMR}$  (400 MHz,  $\text{CD}_3\text{OD}$ )  $\delta$  7.28 (t,  $J = 7.7$  Hz, 2H), 7.11 (t,  $J = 7.4$  Hz, 1H), 6.97 (d,  $J = 7.9$  Hz, 2H), 4.67 (d,  $J = 9.0$  Hz, 1H), 4.41 (t,  $J = 2 \times 10.0$  Hz, 1H), 3.06 (dd,  $J = 13.4$ , 9.5 Hz, 1H), 2.44 (dt,  $J = 13.3$ ,  $2 \times 9.8$  Hz, 1H), 1.35 (s, 3H), 1.28 (s, 3H).  $^{13}\text{C NMR}$  (101 MHz,  $\text{CD}_3\text{OD}$ )  $\delta$  172.3, 153.5, 84.3, 81.0, 22.1, 21.5.

**Isopropyl (2*R*,4*S*)-4-(((benzyloxy)carbonyl)amino)-5-oxotetrahydrofuran-2-carboxylate (14i).**



The precursor **3i** was prepared following the procedure described for **R-4i**. Reaction volume was 16 mL. Starting from **1i** (190 mg, 1.6 mmol, 0.1M) and sodium pyruvate **2** (180.1 mg, 1.6 mmol, 1 eq), the reaction yielded 95% of **3i**. Transamination of **3i** was conducted using the T039/BnNH<sub>2</sub> system rendering 42% of **6i**. Cbz protection and conversion to  $\alpha$ -amino- $\gamma$ -butyrolactone derivative **14i** were performed following the **procedure 3**. Product was eluted with a step gradient of hexane:EtOAc: 100:0, 100 mL, 95:5, 100 mL, 90:10, 100 mL, 85:15, 100 mL, 80:20, 100 mL, 75:25, 100 mL, 70:30 1L affording the title compound **14i** as a solid (dr: >95:5, 179 mg, 34%).  $[\alpha]_{20}^D = -24.3$  ( $c = 1$ , in CHCl<sub>3</sub>). <sup>1</sup>H NMR (400 MHz, CDCl<sub>3</sub>)  $\delta$  7.39 – 7.23 (m, 5H), 5.11 (s, 3H), 4.93 (d,  $J = 9.5$  Hz, 1H), 4.46 (ddd,  $J = 11.4, 8.9, 6.0$  Hz, 1H), 2.79 (dd,  $J = 13.0, 8.8$  Hz, 1H), 2.53 (q,  $J = 3 \times 11.6$ , Hz, 1H), 1.27 (dt,  $J = 6.3, 2 \times 3.1$ , Hz, 6H). <sup>13</sup>C NMR (101 MHz, CDCl<sub>3</sub>)  $\delta$  175.2, 168.7, 155.7, 128.7, 73.8, 70.5, 67.4, 48.9, 33.3, 21.6. ESI-TOF  $m/z$ : Calcd for  $[M+H^+]$  C<sub>16</sub>H<sub>20</sub>NO<sub>6</sub><sup>+</sup>: 322.1284, found  $[M+H^+]$ : 322.1291.

**(3*S*,5*S*)- and (3*S*,5*R*)-Benzyl (-2-oxo-5-((2-phenylacetamido)methyl)tetrahydrofuran-3-yl)carbamate ((5*R*/*S*)-14n) as a diastereomeric mixture.**

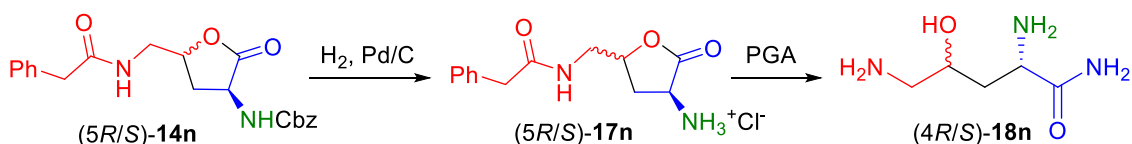


The precursor **3n** was prepared following the procedure described for **16b**. Reaction volume was 28 mL. Starting from **1n** (0.5 g, 2.8 mmol, 0.1M) and sodium pyruvate **2** (310.5 mg, 2.8 mmol, 1 eq) the reaction afforded 80% of **3n**. Transamination of **3n** was performed using the T039/BnNH<sub>2</sub> system, yielding 56% of **6n**. Cbz protection and conversion to  $\alpha$ -amino- $\gamma$ -butyrolactone derivatives (**4*R*/*S*)-14n**) were performed following procedure 3. Product was eluted with a step gradient of pentane: EtOAc: 100:0, 500 mL, 90:10, 200 mL, 80:20, 200 mL, 70:30, 200 mL, 60:40, 200 mL, 50:50, 200 mL, 40:60, 200 mL, 30:70, 200 mL, 20:80, 2.2 L, affording the compound **(5*R*/*S*)-14n** as a distereomeric mixture (dr 50:50 (**3*S*,5*S***):(**3*S*,5*R***)), as a yellow oil (266 mg, 25%).  $[\alpha]_{20}^D = -11.2$  ( $c = 1$ , in CHCl<sub>3</sub>). **Benzyl ((3*S*,5*R*)-2-oxo-5-((2-phenylacetamido)methyl)tetrahydrofuran-3-yl)carbamate, (**3*S*,5*R*)-14n**): <sup>1</sup>H NMR (400 MHz, CD<sub>3</sub>OD)  $\delta$  5.50 (s, 2H), 4.69 (dq,  $J = 9.3, 2 \times 5.0, 4.9$  Hz, 1H), 4.28 (t,  $J = 2 \times 9.7$  Hz, 1H), 3.50 (s, 2H), 3.43 (d,  $J = 5.6$  Hz, 2H), 2.30 (m, 2H). <sup>13</sup>C NMR (101 MHz, CD<sub>3</sub>OD)  $\delta$  176.0, 173.0, 156.9, 76.7, 66.4, 49.5 42.5, 42.4, 30.3. **Benzyl ((3*S*,5*S*)-2-oxo-5-((2-phenylacetamido)methyl)tetrahydrofuran-3-yl)carbamate, (**3*S*,5*S*)-14n**): <sup>1</sup>H****



NMR (400 MHz, CD<sub>3</sub>OD)  $\delta$  5.50 (s, 2H), 4.53 (dtd,  $J = 9.9, 2 \times 5.9, 3.6$  Hz, 1H), 4.45 (dd,  $J = 11.7, 9.1$  Hz, 1H), 3.52 (d,  $J = 3.5$  Hz, 1H), 3.50 (s, 2H), 3.42 (d,  $J = 5.6$  Hz, 1H), 2.50 (ddd,  $J = 12.3, 9.1, 5.8$  Hz, 1H), 1.97 (q,  $J = 2 \times 11.8, 11.6$  Hz, 1H). <sup>13</sup>C NMR (101 MHz, CD<sub>3</sub>OD)  $\delta$  175.1, 173.0, 156.9, 75.9, 66.4, 48.4, 42.5, 42.4, 27.4.

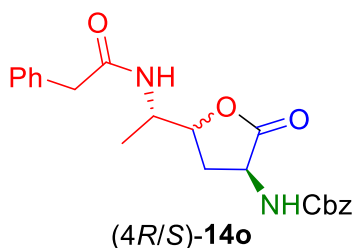
#### Selective deprotection of (5*R/S*)-14n mixture.



A portion of (5*R/S*)-14n mixture (100 mg, 261.5  $\mu\text{mol}$ , 1 eq) in MeOH (28 mL), HCl (500  $\mu\text{L}$  of 1 M stock solution) and Pd/C (2.8 mg, 10 mol%, 10% Pd, 50% humidity) were mixed. The suspension was stirred at room temperature for 1 hour under H<sub>2</sub> atmosphere. Reaction mixture was filtered through Celite<sup>®</sup> and the pellet was washed with MeOH (3 x 50 mL). Then, the solvent was removed *in vacuo* obtaining (5*R/S*)-17n as solid (68 mg, 91%). (5*R*)-17n: <sup>1</sup>H NMR (400 MHz, CD<sub>3</sub>OD)  $\delta$  4.76 (dddd,  $J = 9.1, 6.0, 4.9, 2.1$  Hz, 1H), 4.02 (t,  $J = 2 \times 10.1$  Hz, 1H), 3.52 (s, 2H), 3.49 (d,  $J = 2.3$  Hz, 2H), 2.52 (ddd,  $J = 13.5, 9.7, 2.1$  Hz, 1H), 2.32 (ddd,  $J = 13.5, 10.4, 9.0$  Hz, 1H). <sup>13</sup>C NMR (101 MHz, CD<sub>3</sub>OD)  $\delta$  173.6, 171.8, 78.4, 48.4, 42.4, 42.2, 28.4. (5*S*)-17n: <sup>1</sup>H NMR (400 MHz, CD<sub>3</sub>OD)  $\delta$  4.64 (dddd,  $J = 13.5, 10.4, 9.0$  Hz, 1H), 4.39 (dd,  $J = 12.0, 8.9$  Hz, 1H), 3.59 (d,  $J = 4.0$  Hz, 1H), 3.52 (s, 2H), 3.42 (d,  $J = 2.3$  Hz, 1H), 2.71 (ddd,  $J = 12.5, 8.8, 5.4$  Hz, 1H), 1.96 (m, 1H). <sup>13</sup>C NMR (101 MHz, CD<sub>3</sub>OD)  $\delta$  173.3, 171.5, 78.1, 50.5, 42.4, 42.1, 30.3. The hydrogenated compound obtained (60 mg, 210  $\mu\text{mol}$ ) was re-suspended in a volume of 155 mM sodium phosphate buffer (2.4 mL) and Penicillin G Amidase (PGA) from Roche diagnostics GmbH, Mannheim (226  $\mu\text{L}$  of a stock solution 1140 U mL<sup>-1</sup>, 100 U mL<sup>-1</sup> final concentration in the reaction) were added. The reaction was stirred (1000 rpm) at 25 °C. Reaction monitoring was carried out by HPLC immediately after the enzyme addition (0 h) and after 24 h in the conditions described above. When the reaction was completed the enzyme was precipitate by adding 100 mM HCO<sub>2</sub>H (3 mL) and centrifuged. The pellet was washed with 100 mM HCO<sub>2</sub>H (3 x 3 mL). Aqueous solution was adjusted to 30 mL and was purified by ionic exchange chromatography, was performed on Macro-Prep<sup>®</sup> High S Media (25 mL, Bio-Rad) (packed into a glass column (C16/20, GE HealthcareLife Science), equilibrated with 1 M SO<sub>4</sub>(NH<sub>4</sub>)<sub>2</sub> (500 mL). Crude fraction was loaded onto the column at 1 mL min<sup>-1</sup>. Colored impurities were washed away

with water (90 mL) at 3 mL min<sup>-1</sup>. Product was eluted with a gradient of 1 M NH<sub>4</sub>OH (420 mL) at 3 mL min<sup>-1</sup>, typical fraction size was 30 mL. Fractions were lyophilized and the (4*R/S*)-**18n** mixture was obtained as a solid (28 mg, 60%). (4*R*)-**18n**: <sup>1</sup>H NMR (400 MHz, D<sub>2</sub>O) δ 4.00 (dddd, *J* = 10.6, 8.8, 6.5, 3.4 Hz, 1H), 3.90 (dd, *J* = 6.2, 5.3 Hz, 1H), 3.09 (dd, *J* = 3.3, 2.3 Hz 1H), 2.90 (dd, *J* = 8.4, 4.8 Hz, 1H), 2.00 (m, 2H). <sup>13</sup>C NMR (101 MHz, D<sub>2</sub>O) δ 173.7, 64.9, 52.1, 44.4, 33.8. (4*S*)-**18n**: <sup>1</sup>H NMR (400 MHz, D<sub>2</sub>O) δ 4.12 (ddt, *J* = 10.4, 8.8, 2x3.1 Hz, 1H), 3.82 (t, *J* = 2x6.8 Hz, 1H), 3.09 (ddd, *J* = 3.4, 2.25 Hz, 1H), 2.90 (dd, *J* = 8.3, 4.8 Hz, 1H), 2.06 (ddd, *J* = 14.7, 6.6, 2.9 Hz, 1H), 1.80 (ddd, *J* = 14.7, 6.9, 10.4 Hz, 1H). <sup>13</sup>C NMR (101 MHz, D<sub>2</sub>O) δ 173.7, 65.9, 52.6, 44.4, 34.7.

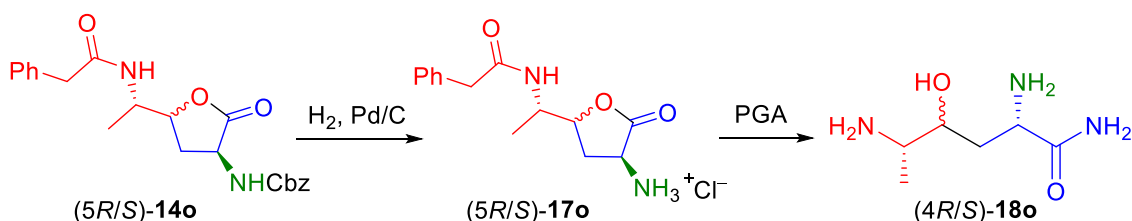
**(3*S*,5*S*)- and (3*S*,5*R*)-Benzyl (2-oxo-5-((*S*)-1-(2-phenylacetamido)ethyl)tetrahydrofuran-3-yl)carbamate ((5*R/S*)-**14o**) as a diastereomeric mixture.**



The precursor **3o** was prepared following the procedure described above **14c**. Reaction volume was 26 mL. The reaction was started by adding the enzyme HBPA H205A (9.2 mL of a stock solution 0.009 U mL<sup>-1</sup>, 2.8 mg mL<sup>-1</sup> in 50 mM TEA buffer, 50 mM NaCl, 0.5 mM EDTA and 50% (v/v) of glycerol, 0.00318 U mL<sup>-1</sup>, 1 mg protein mL<sup>-1</sup> final concentration in the reaction) to a solution of **1o** (0.5 g, 2.6 mmol, 0.1 M) and sodium pyruvate **2** (287.7 mg, 1 eq). This rendered 75% of **3o**. Transamination of **3o** was conducted using the BCAT/L-Glu/L-Asp/AspAT system, affording 50% of **6o**. Cbz protection and conversion to  $\alpha$ -amino- $\gamma$ -butyrolactone derivatives (5*R/S*)-**14o** were performed following procedure 3. Product was eluted with a step gradient of pentane:EtOAc: 100:0, 500 mL, 90:10, 200 mL, 80:20, 200 mL, 70:30, 200 mL, 60:40, 200 mL, 50:50, 200 mL, 40:60, 200 mL, 30:70, 3 L, affording a diastereomeric mixture (5*R/S*)-**14o** (dr 50:50 as a yellow oil (257 mg, 20%). [ $\alpha$ ]<sub>20</sub><sup>D</sup> = -22 (*c* = 1, in CHCl<sub>3</sub>). (5*R*)-**14o**: <sup>1</sup>H NMR (400 MHz, CDCl<sub>3</sub>) δ 5.47 (d, *J* = 8.9 Hz, 1H), 5.35 (d, *J* = 5.4 Hz, 1H), 5.10 (s, 2H), 4.54 (m, 1H), 4.22 (m, 1H), 4.14 (d, *J* = 8.6 Hz, 1H), 3.58 (s, 1H), 3.48 (s, 1H), 2.42 (t, *J* = 2x12.6 Hz, 1H), 2.29 (m, 1H), 1.08 (d, *J* = 6.8 Hz, 3H). <sup>13</sup>C NMR (101 MHz, CDCl<sub>3</sub>) δ 175.1, 170.6, 155.7, 80.1, 67.5, 49.7, 47.8, 43.8, 30.8, 14.8. (5*S*)-**14o**: <sup>1</sup>H NMR (400 MHz, CDCl<sub>3</sub>) δ 5.71 (d, *J* = 9.2 Hz, 1H), 5.10 (s, 2H), 5.02 (d, *J* = 7.1 Hz, 1H), 4.35 (m, 1H), 4.33 (m, 1H), 4.23 (m, 1H), 3.58 (s, 1H), 3.48 (s, 1H), 2.54 (ddd, *J* =

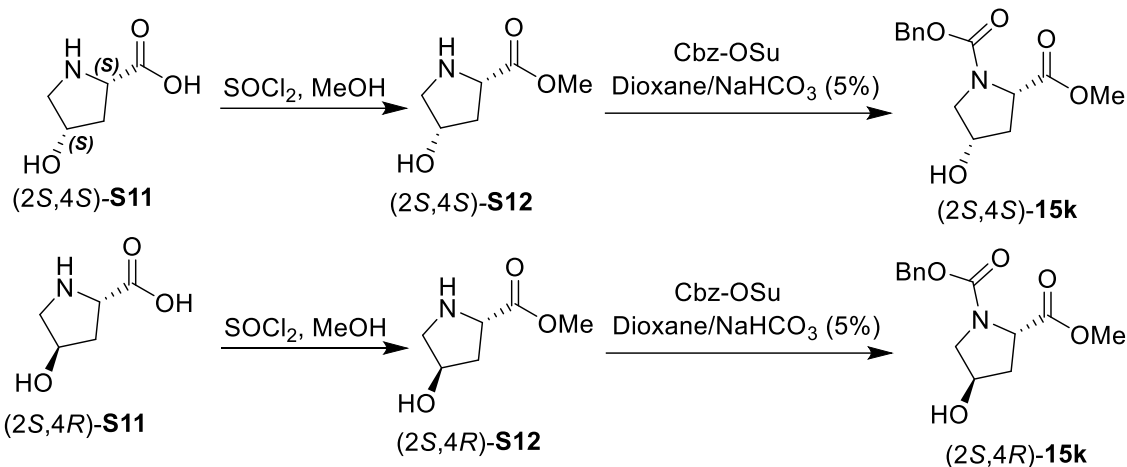
12.9, 9.1, 5.8 Hz, 1H), 1.78 (q,  $J = 3 \times 11.8$ , 1H), 1.24 (d,  $J = 7.1$  Hz, 3H).  $^{13}\text{C}$  NMR (101 MHz,  $\text{CDCl}_3$ )  $\delta$  173.8, 171.3, 155.7, 79.7, 67.5, 51.2, 46.0, 43.9, 31.7, 18.2.

### Selective deprotection of (5*R/S*)-14o mixture.



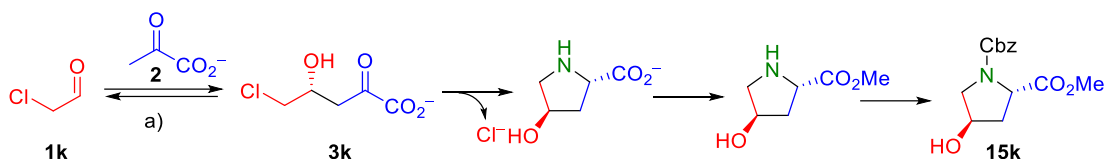
The selective deprotection of the PheAc and Cbz groups was conducted following the procedure described for (5*R/S*)-14n, starting from the (4*R/S*)-14o' mixture (120 mg, 302.3  $\mu\text{mol}$ ) yielding (5*R/S*)-17o as a solid (90 mg, >99%). (5*R*)-17o:  $^1\text{H}$  NMR (400 MHz,  $\text{CD}_3\text{OD}$ )  $\delta$  4.59 (dt,  $J = 23.7, 2 \times 6.6$  Hz, 1H), 4.42 (m, 1H), 4.15 (m, 1H), 3.52 (s, 2H), 2.69 (t,  $J = 10.6$  Hz, 1H), 2.03 (t,  $J = 11.2$  Hz, 1H), 1.22 (m, 3H).  $^{13}\text{C}$  NMR (101 MHz,  $\text{CD}_3\text{OD}$ )  $\delta$  172.7, 171.5, 80.2, 49.4, 46.9, 42.3, 29.9, 15.3. (5*S*)-17o:  $^1\text{H}$  NMR (400 MHz,  $\text{CD}_3\text{OD}$ )  $\delta$  4.55 (dd,  $J = 15.8, 7.8$  Hz, 1H), 4.24 (t,  $J = 2 \times 9.8$  Hz, 1H), 4.10 (m, 1H), 3.52 (s, 2H), 2.56 (dd,  $J = 13.4, 9.4$  Hz, 1H), 2.31 (dt,  $J = 13.6, 2 \times 10.2$  Hz, 1H), 1.21 (m, 3H).  $^{13}\text{C}$  NMR (101 MHz,  $\text{CD}_3\text{OD}$ )  $\delta$  172.8, 171.8, 80.6, 47.3, 46.8, 42.3, 27.9, 15.1. After removal the PheAc as described for (4*R/S*)-18n gave (4*R/S*)-18o (58 mg, 81%). (4*R*)-18o:  $^1\text{H}$  NMR (400 MHz,  $\text{D}_2\text{O}/\text{HCO}_2\text{H}$  (0.1M))  $\delta$  4.04 (t,  $J = 2 \times 2.9$  Hz, 1H), 3.77 (t,  $J = 2 \times 6.7$  Hz, 1H), 3.32 (tt,  $J = 2 \times 6.7, 2 \times 3.3$  Hz, 1H), 1.97 (d,  $J = 4.0$  Hz, 1H), 1.72 (dd,  $J = 7.3, 3.7$  Hz, 1H), 1.11 (d,  $J = 6.9$  Hz, 3H).  $^{13}\text{C}$  NMR (101 MHz,  $\text{D}_2\text{O}$ )  $\delta$  173.3, 68.6, 52.5, 51.2, 32.5, 11.4. (4*S*)-18o:  $^1\text{H}$  NMR (400 MHz,  $\text{D}_2\text{O}/\text{HCO}_2\text{H}$  (0.1M))  $\delta$  3.89 (dd,  $J = 7.3, 3.8$  Hz, 1H), 3.65 (ddd,  $J = 10.1, 7.0, 2.9$  Hz, 1H), 3.19 (p,  $J = 4 \times 6.8$  Hz, 1H), 2.02 (m, 1H), 1.93 (m, 1H), 1.16 (d,  $J = 6.8$  Hz, 3H).  $^{13}\text{C}$  NMR (101 MHz,  $\text{D}_2\text{O}$ )  $\delta$  173.6, 69.2, 51.8, 32.7, 14.6.

**Chemical synthesis of 1-Benzyl 2-methyl (2*S*,4*R*)- and (2*S*,4*S*)-4-hydroxypyrrolidine-1,2-dicarboxylate ((2*S*,4*R*)-**15k** and (2*S*,4*S*)-**15k**).**



To a separate solutions of commercial diastereomers (2*S*,4*R*)-**S11** and (2*S*,4*S*)-**S11** (0.5 g, 3.8 mmol) in anhydrous MeOH (50 mL) at  $-80\text{ }^{\circ}\text{C}$ ,  $\text{SOCl}_2$  (1.8 g, 15.3 mmol, 4 eq) was slowly added stirring. When the addition was finished the solution was allow to warm up to rt. After stirring for 24 h, the excess acid generated was removed under vacuum affording **S12** (0.55 g, quantitative). **S12** (3.7 mmol, 1 eq), was diluted with  $\text{NaHCO}_3$  20% w/v (60 mL) and Cbz-OSu (0.93 g, 3.7 mmol, 1 eq, dissolved in dioxane (60 mL)) was then added. The reactions were stirred at  $25\text{ }^{\circ}\text{C}$  for 12 h. The products were extracted with EtOAc (3 x 100 mL) and washed with  $\text{H}_2\text{O}$  (3 x 100 mL), brine (3 x 100 mL). Then, the organic phases were dried over anhydrous  $\text{MgSO}_4$  and concentrated under vacuum yielding the compound (2*S*,4*R*)-**15k** as a solid (1.1 g, >99%) and (2*S*,4*S*)-**15k** as an oil (1.1 g, >99%). (2*S*,4*R*)-**15k**: 2-rotamers double signal NMR:  $^1\text{H}$  NMR (401 MHz,  $\text{CDCl}_3$ )  $\delta$  7.40-7.29 (m, 5H), 5.23 – 5.02 (m, 2H), 4.52 (m, 2H), 3.77 (s, 1H), 3.56 (s, 1H), 3.73 – 3.69 (m, 3H), 2.32 (m, 1H), 2.11 (m, 1H).  $^{13}\text{C}$  NMR (101 MHz,  $\text{CDCl}_3$ )  $\delta$  173.2 (rot 1), 173.0 (rot 2), 155.0 (rot 1), 154.5 (rot 2), 70.2 (rot 1), 69.5 (rot 2), 67.2 (rot 1), 67.1 (rot 2), 54.7 (rot 1), 55.3 (rot 2), 52.4 (rot 1), 52.2 (rot 2), 39.2 (rot 1), 38.4 (rot 2). 1-Benzyl 2-methyl (2*S*,4*S*)-4-hydroxypyrrolidine-1,2-dicarboxylate, (2*S*,4*S*)-**15k**: 2-rotamers double signal NMR:  $^1\text{H}$  NMR (401 MHz,  $\text{CDCl}_3$ )  $\delta$  7.40 – 7.29 (m, 5H), 5.23-5.06 (m, 2H), 4.46 (m, 1H), 4.41 (dt,  $J = 5.7, 2 \times 3.0$  Hz, 1H) 3.82 (s, 1H), 3.79 (s, 1H), 3.79-3.60 (m, 3H), 3.60 (d,  $J = 4.4$ , Hz, 1H) 2.33 (tdd,  $J = 2 \times 14.3, 9.8, 4.6$  Hz, 1H), 2.16 (dd,  $J = 14.2, 5.0$  Hz 1H).  $^{13}\text{C}$  NMR (101 MHz,  $\text{CDCl}_3$ )  $\delta$  175.3 (rot 1), 175.0 (rot 2), 155.0 (rot 1), 154.2 (rot 2), 71.3 (rot 1), 70.3 (rot 2), 67.4 (rot 1), 67.3 (rot 2), 58.2 (rot 1), 57.7 (rot 2), 52.8 (rot 1), 52.6 (rot 2), 38.7 (rot 1), 37.8 (rot 2).

### Chemoenzymatic synthesis of 1-benzyl-2-methyl (2*S*,4*R*)-4-hydroxypyrrolidine-1,2-dicarboxylate (**15k**).



The precursor 4-hydroxy-2-oxoacid (**3k**) was prepared following the procedure described for **14c**. Reaction volume was 38 mL. To a solution of **1k** (490  $\mu\text{L}$  of a 7.9 M commercial aqueous solution, 3.8 mmol, 1 eq, 0.1 M) and sodium pyruvate **2** (0.42 g, 3.8 mmol, 1 eq), HBPA H205A (14 mL of a stock solution 0.009 U  $\text{mL}^{-1}$ , 2.8  $\text{mg mL}^{-1}$  in 50 mM TEA buffer, 50 mM NaCl, 0.5 mM EDTA and 50% (v/v) of glycerol, 0.00324 U  $\text{mL}^{-1}$ , 1  $\text{mg mL}^{-1}$  of protein final concentration in the reaction) was added. This rendered 64% of **3k**. Transamination of **3k** was conducted using the BCAT/L-Glu/L-Asp/AspAT system, affording 81% of *trans*-4-hydroxy-L-proline. The *trans*-4-hydroxy-L-proline was formed by an intramolecular nucleophilic substitution of the terminal chloro at C5 by the amine group after the transamination reaction. The derivative **15k** (yellow oil, 611 mg, 51%) was prepared following the procedure described for the mixture (2*S*,4*R*)-**15k**:(2*S*,4*S*)-**15k**. Product **15k** was eluted with a step gradient of pentane:EtOAc: 100:0, 500 mL, 90:10, 200 mL, 80:20, 200 mL, 70:30, 200 mL, 60:40, 200 mL, 50:50, 200 mL, 40:60, 2.2 L (611 mg, 51%). The NMR spectra showed the presence of two rotamers,  $^1\text{H}$  NMR (400 MHz,  $\text{CDCl}_3$ )  $\delta$  7.45 – 7.14 (m, 5H), 5.13 (dt,  $J = 24.0, 2 \times 12.3$  Hz, 1H), 5.00 (d,  $J = 12.4$  Hz, 1H), 4.49 (m, 1H), 3.73-3.68 (m, 3H), 3.67 (m, 1H), 3.64 (dd,  $J = 4.2, 2.3$  Hz, 2H), 3.53 (s, 1H), 2.30 (m, 1H), 2.28 (m, 1H), 2.09 (d,  $J = 1.7$  Hz, 1H), 2.07 (d,  $J = 1.7$  Hz, 1H).  $^{13}\text{C}$  NMR (101 MHz,  $\text{CDCl}_3$ )  $\delta$  173.1 (rot 1), 172.3 (rot 2), 155.0 (rot 1), 154.5 (rot 1), 70.2 (rot 1), 69.4 (rot 1), 67.3, 57.9 (rot 1), 57.7 (rot 2), 55.2 (rot 1), 54.6 (rot 2), 52.4 (rot 1), 52.1 (rot 2), 39.2 (rot 1), 38.4 (rot 2).  $[\alpha]_{20}^{\text{D}} = -55.4$  ( $c = 1$ , in MeOH). ESI-TOF  $m/z$ : Calcd for  $[\text{M}+\text{H}^+]$   $\text{C}_{14}\text{H}_{18}\text{NO}_5^+$ : 280.1193, found  $[\text{M}+\text{H}^+]$ : 380.1185.

## Analysis of the diastereomeric excess of **15k**

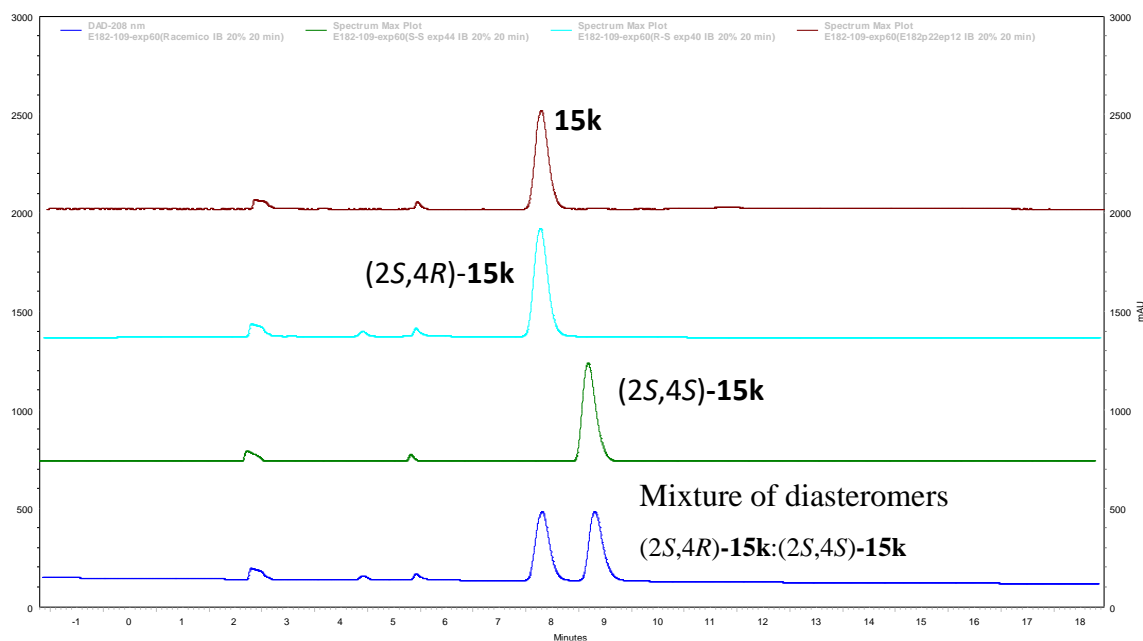
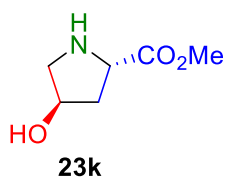


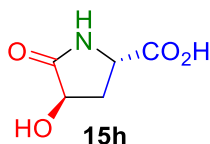
**Figure S26:** Chiral HPLC analysis chromatogram of **15k** synthesized by HBPA H205A and BCAT/L-Glu/L-Asp/AspAT transamination system. Conditions: CHIRALPACK® IB 46 x 250 mm column, 5  $\mu\text{m}$ , flow rate 1 mL min<sup>-1</sup> at 25 °C and UV detection (208 nm). Isocratic elution hexane:<sup>t</sup>PrOH 80:20 (v/v).

### Synthesis of *trans*-4-hydroxy-L-proline methyl ester (**23k**)



A portion of (2*S*,4*R*)-**15k** (50 mg, 158.4  $\mu\text{mol}$ , 1 eq.) in MeOH (16 mL), HCl (500  $\mu\text{L}$  of 1 M stock solution) Pd/C (1.7 mg, 10 mol%, 10% Pd, 50% humidity) were mixed. The suspension was stirred at rt for 1 hour under H<sub>2</sub> atmosphere. The reaction mixture was filtered through Celite® and the pellet was washed with MeOH (3 x 50 mL). Then, the solvent was removed *in vacuo* obtaining methyl (2*S*,4*R*)-4-hydroxypyrrolidine-2-carboxylate, **23k** as an oil (38 mg, quantitative). <sup>1</sup>H NMR (400 MHz, CD<sub>3</sub>OD)  $\delta$  4.63 – 4.54 (m, 2H), 3.43 (d, *J* = 10.0 Hz, 1H), 3.30 (d, *J* = 7.9 Hz, 1H), 2.40 (dd, *J* = 13.4, 7.5 Hz, 1H), 2.18 (t, *J* = 10.5, 10.5 Hz, 1H). <sup>13</sup>C NMR (101 MHz, CD<sub>3</sub>OD)  $\delta$  169.2 69.2, 58.0, 52.6, 37.2.

### (2*S*,4*R*)-4-Hydroxy-5-oxopyrrolidine-2-carboxylic acid (**15h**).



The precursor **3h** was prepared following the procedure described for *R-4h*. The reaction volume was 20 mL. Starting from **1h** (400  $\mu$ L of a 4.9 M commercial aqueous solution, 2.0 mmol, 1 eq, 0.1 M) and sodium pyruvate **2** (216 mg, 2.0 mmol, 1 eq), the reaction yielded 82% of **3h**. Transamination of **3h** using BCAT/L-Glu/L-Asp/AspAT system rendered 38% of **6h**. When the reaction was completed, the enzymes were precipitate by adding methanol (10 volumes, 260 mL). Then, the reaction was filtered through Celite® and the filter cake washed with methanol (3x50 mL). The filtrates were pooled and the solvent removed under vacuum, until all MeOH was evaporated and only the aqueous solution remained. The residue, was diluted with NaHCO<sub>3</sub> 20% w/v (50 mL). The reaction was stirred at 25 °C for 12 h. Then, the aqueous phase was concentrated up to 25 mL and after that, it was adjusted to pH 10.0 with a NaOH solution. The title compound (**15h**) was partially purified by ionic exchange chromatography, in a Macro-Prep® High Q Media (25 mL, Bio-Rad) stationary phase in H<sup>+</sup> form, packed into a glass column (C16/20, GE HealthcareLife Science). The stationary phase was equilibrated with 1 M HCO<sub>2</sub>Na. Crude fraction at pH 10.0 (25 mL) was loaded onto the column at 1 mL min<sup>-1</sup>. Colored impurities were washed away with water (75 mL) at 3 mL min<sup>-1</sup>. Product was eluted with a gradient from 0 to 100% HCO<sub>2</sub>H (1 M) in 50 min at 3 mL min<sup>-1</sup>, typical fraction size was 25 mL. Fractions were lyophilized and the title compound **15h** was obtained as a yellow solid (65.4 mg, 9%). <sup>1</sup>H NMR (500 MHz, D<sub>2</sub>O)  $\delta$  4.46 (dd,  $J = 10.1, 3.6$  Hz, 1H), 3.99 (dt,  $J = 8.0, 2 \times 4.0$  Hz, 1H), 2.50 (ddd,  $J = 15.0, 5.2, 3.6$  Hz, 1H), 2.06 (m, 1H). <sup>13</sup>C NMR (126 MHz, D<sub>2</sub>O)  $\delta$  177.3, 173.2, 68.8, 52.8, 33.9. The final material contains L-Asp and L-Glu as main impurities coming from the transamination reaction.

## Chromatograms of the HPLC analysis on chiral stationary phases

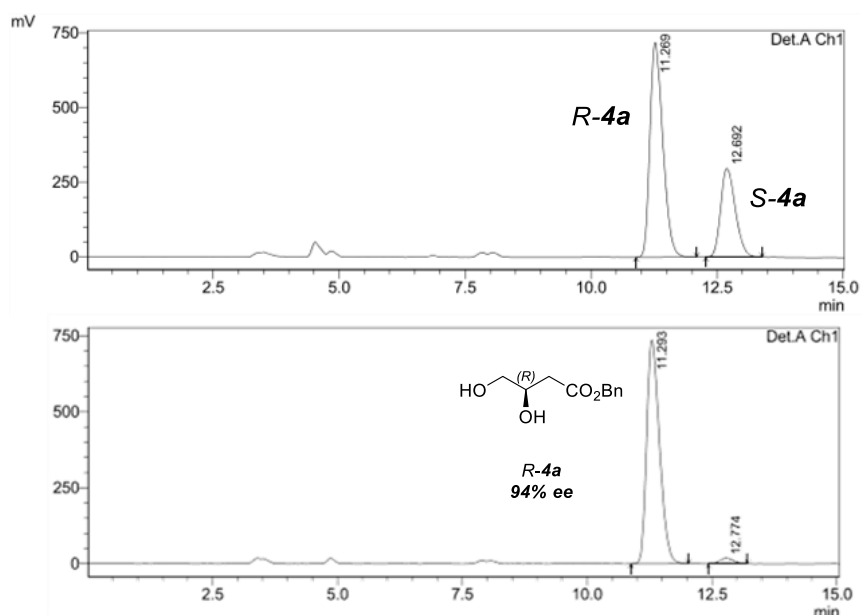


**Figure S74:** Chiral HPLC analysis chromatogram of *R-4a* synthesized with HBPA *wild-type* (down) and *rac-4a* synthesized with MBP-YFAU( $\text{Ni}^{2+}$ ) *wild-type* (see section Chiral HPLC analysis of 4-hydroxyesters). Conditions: CHIRALPACK® ID 46 x 250 mm column, 5  $\mu\text{m}$ , flow rate 1 mL  $\text{min}^{-1}$  at 25 °C and UV detection (254 nm). Isocratic elution hexane:*i*PrOH 80:20 (v/v).

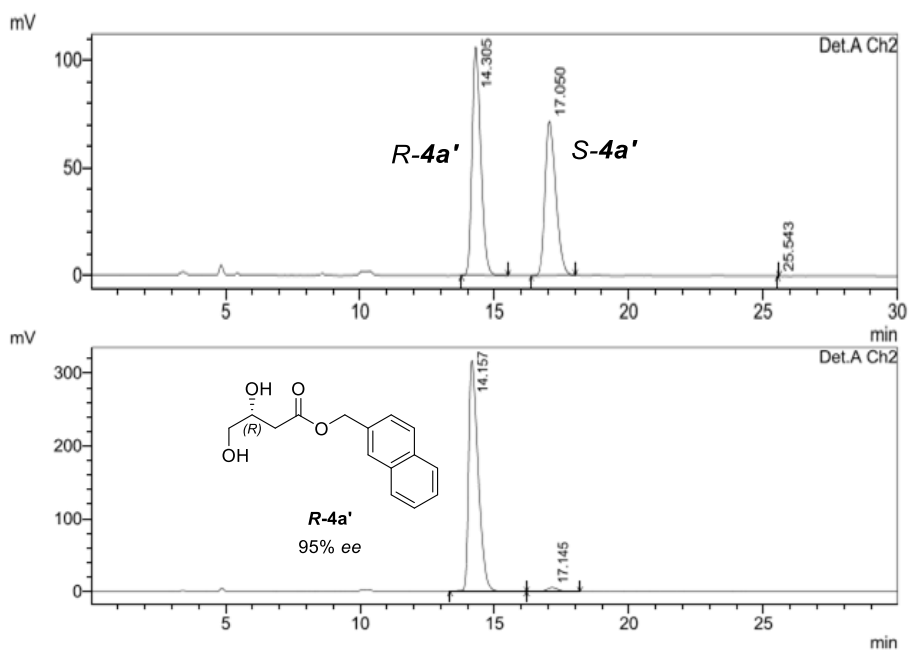


**Figure S75:** Chiral HPLC analysis chromatogram of *R-4a'* synthesized with HBPA *wild-type* (down) and *rac-4a'* synthesized with MBP-YFAU( $\text{Ni}^{2+}$ ) *wild-type* (see section



Chiral HPLC analysis of 4-hydroxyesters). Conditions: CHIRALPACK® ID 46 x 250 mm column, 5  $\mu\text{m}$ , flow rate 1 mL  $\text{min}^{-1}$  at 25 °C and UV detection (254 nm). Isocratic elution hexane:*i*PrOH 80:20 (v/v).

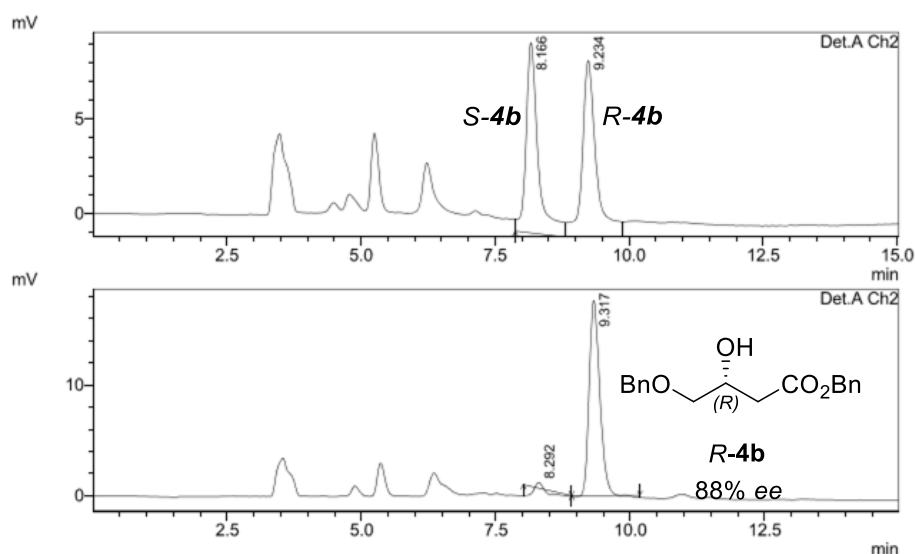


**Figure S76:** Chiral HPLC analysis chromatogram of *R*-**4b** synthesized with HBPA *wild-type* (down) and *rac*-**4b** synthesized with MBP-YFAU( $\text{Ni}^{2+}$ ) *wild-type* type (see section Chiral HPLC analysis of 4-hydroxyesters). Conditions: CHIRALPACK® IB 46 x 250 mm column, 5  $\mu\text{m}$ , flow rate 1 mL  $\text{min}^{-1}$  at 25 °C and UV detection (254 nm). Isocratic elution hexane:*i*PrOH 80:20 (v/v).

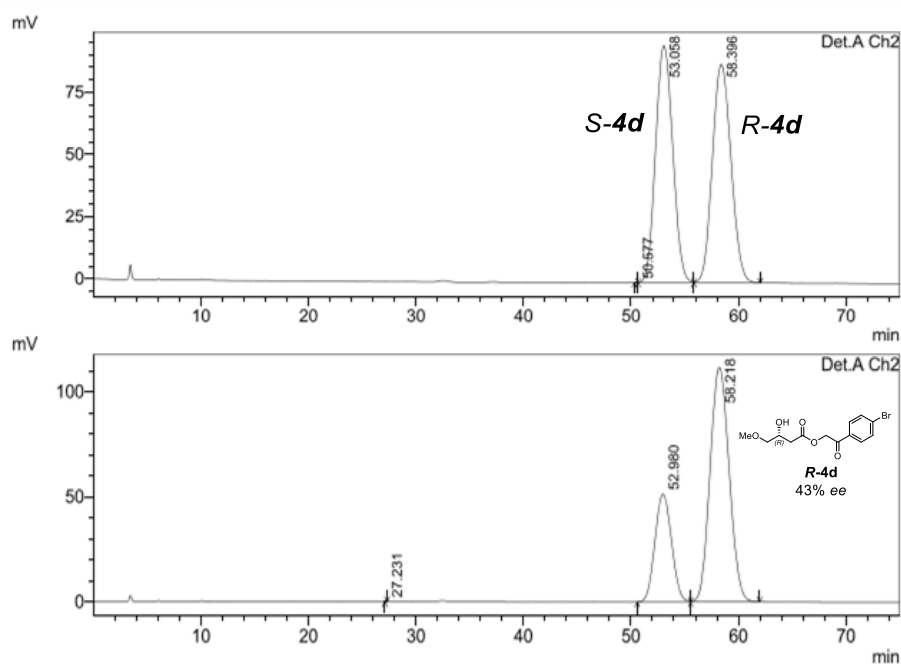


**Figure S77:** Chiral HPLC analysis chromatogram of *R*-**4d** synthesized with HBPA *wild-type* (down) and *rac*-**4d** synthesized with MBP-YFAU( $\text{Ni}^{2+}$ ) *wild-type* type (see section

Chiral HPLC analysis of 4-hydroxyesters). Conditions: CHIRALPACK® IC 46 x 250 mm column, 5  $\mu\text{m}$ , flow rate 1 mL  $\text{min}^{-1}$  at 25 °C and UV detection (254 nm). Isocratic elution hexane:<sup>i</sup>PrOH 80:20 (v/v).

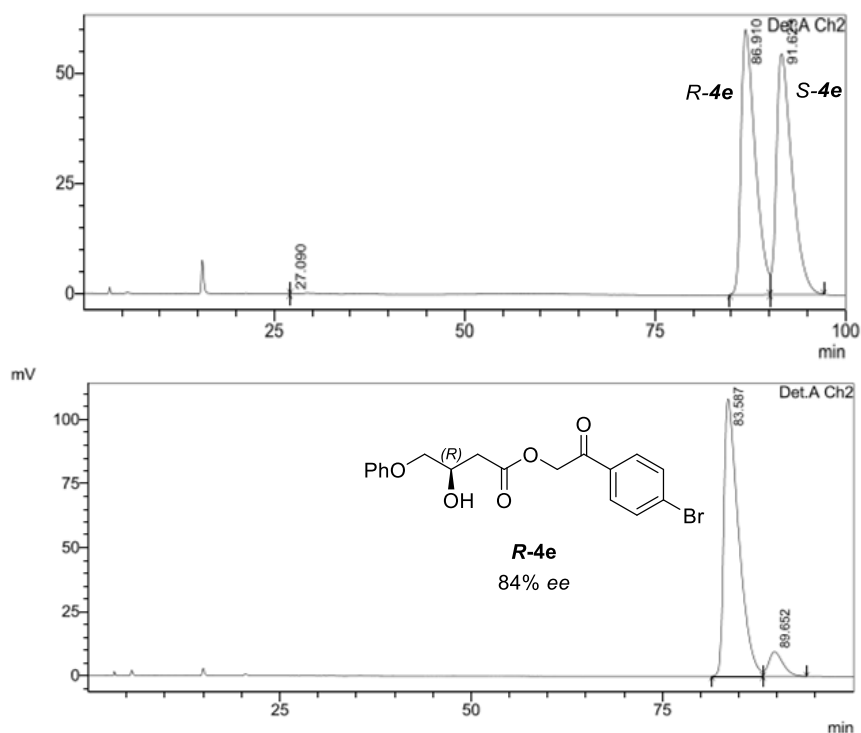


**Figure S78:** Chiral HPLC analysis chromatogram of *R-4e* synthesized with HBPA *wild-type* (down) and *rac-4e* synthesized with MBP-YFAU( $\text{Ni}^{2+}$ ) *wild-type* type (see section Chiral HPLC analysis of 4-hydroxyesters). Conditions: CHIRALPACK® IB 46 x 250 mm column, 5  $\mu\text{m}$ , flow rate 1 mL  $\text{min}^{-1}$  at 25 °C and UV detection (254 nm). Isocratic elution hexane:<sup>i</sup>PrOH 95:5 (v/v).

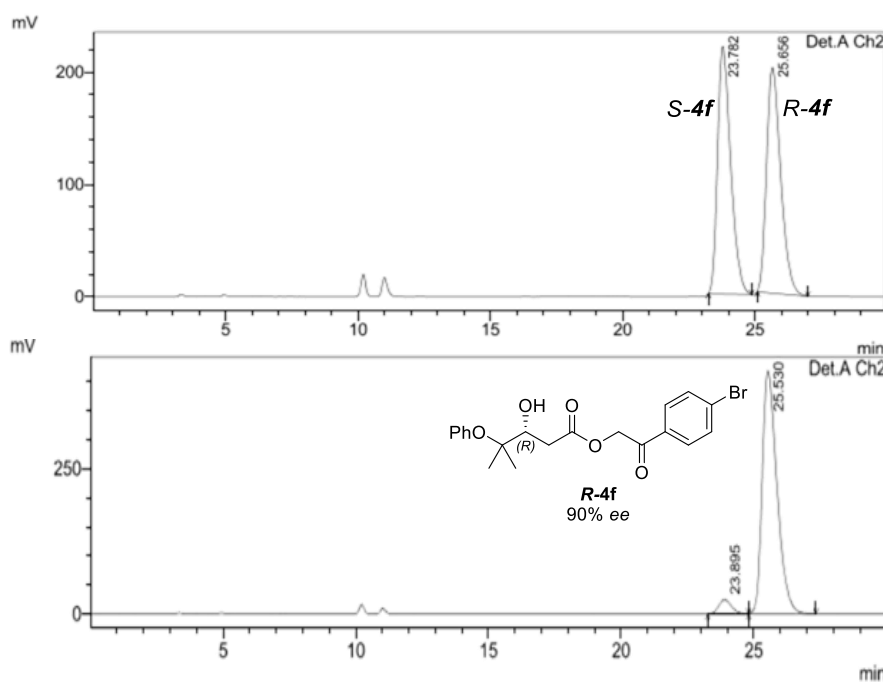


**Figure S79:** Chiral HPLC analysis chromatogram of *R-4f* synthesized with HBPA *wild-type* (down) and *rac-4f* synthesized with MBP-YFAU(Ni<sup>2+</sup>) *wild-type* type (see section Chiral HPLC analysis of 4-hydroxyesters). Conditions: CHIRALPACK® IB 46 x 250 mm column, 5  $\mu$ m, flow rate 1 mL min<sup>-1</sup> at 25 °C and UV detection (254 nm). Isocratic elution hexane:<sup>i</sup>PrOH 90:10 (v/v).

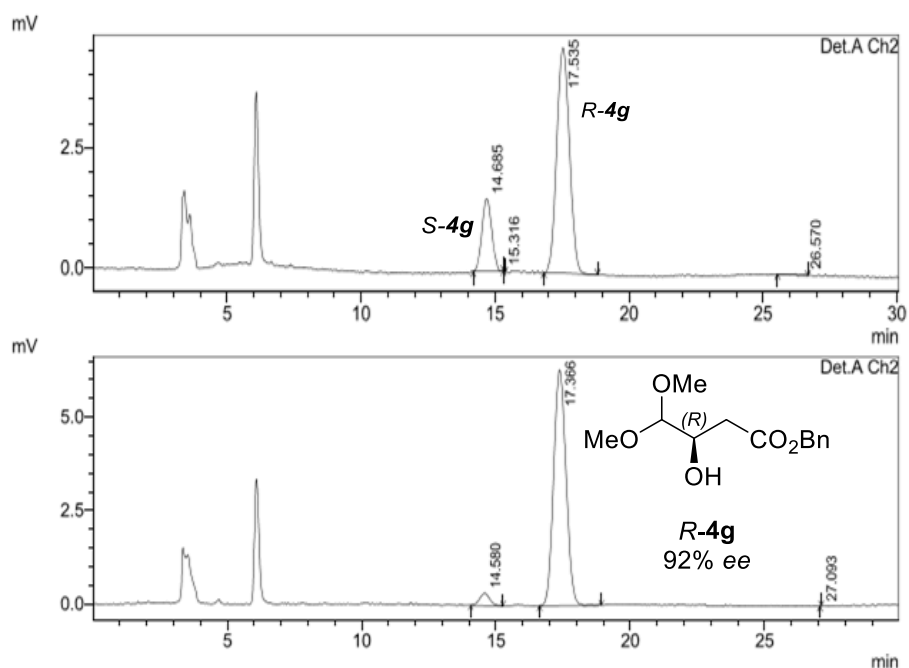


**Figure S80:** Chiral HPLC analysis chromatogram of *R-4g* synthesized with HBPA *wild-type* (down) and *rac-4g* synthesized with MBP-YFAU(Ni<sup>2+</sup>) *wild-type* type (see section Chiral HPLC analysis of 4-hydroxyesters). Conditions: CHIRALPACK® IC 46 x 250

mm column, 5  $\mu\text{m}$ , flow rate 1 mL  $\text{min}^{-1}$  at 25 °C and UV detection (254 nm). Isocratic elution hexane:*i*PrOH 80:20 (v/v).

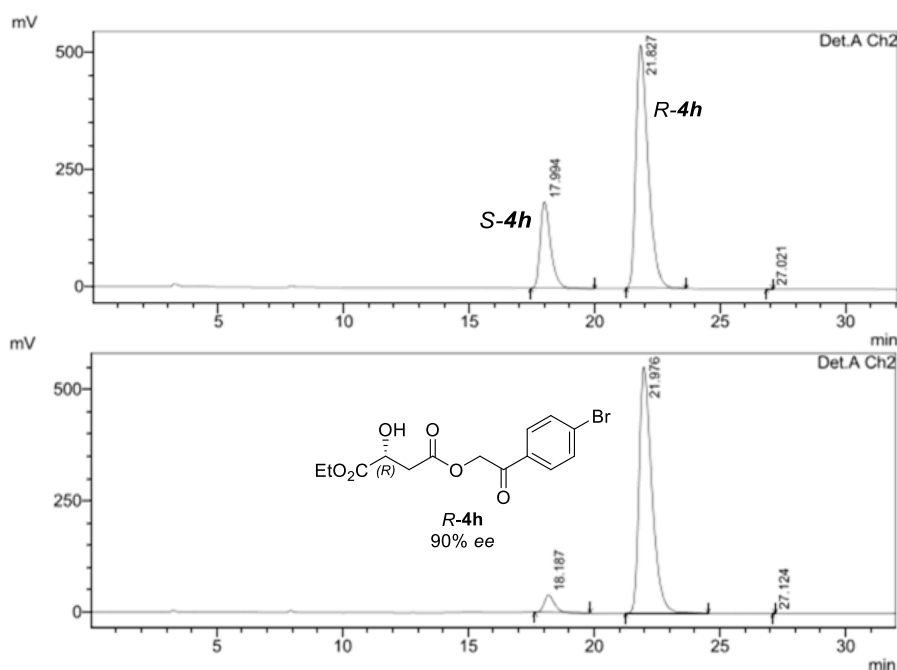


**Figure S81:** Chiral HPLC analysis chromatogram of *R*-4h synthesized with HBPA *wild-type* (down) and *rac*-4h synthesized with MBP-YFAU( $\text{Ni}^{2+}$ ) *wild-type* type (see section Chiral HPLC analysis of 4-hydroxyesters). Conditions: CHIRALPACK® IB 46 x 250 mm column, 5  $\mu\text{m}$ , flow rate 1 mL  $\text{min}^{-1}$  at 25 °C and UV detection (254 nm). Isocratic elution hexane:*i*PrOH 80:20 (v/v).

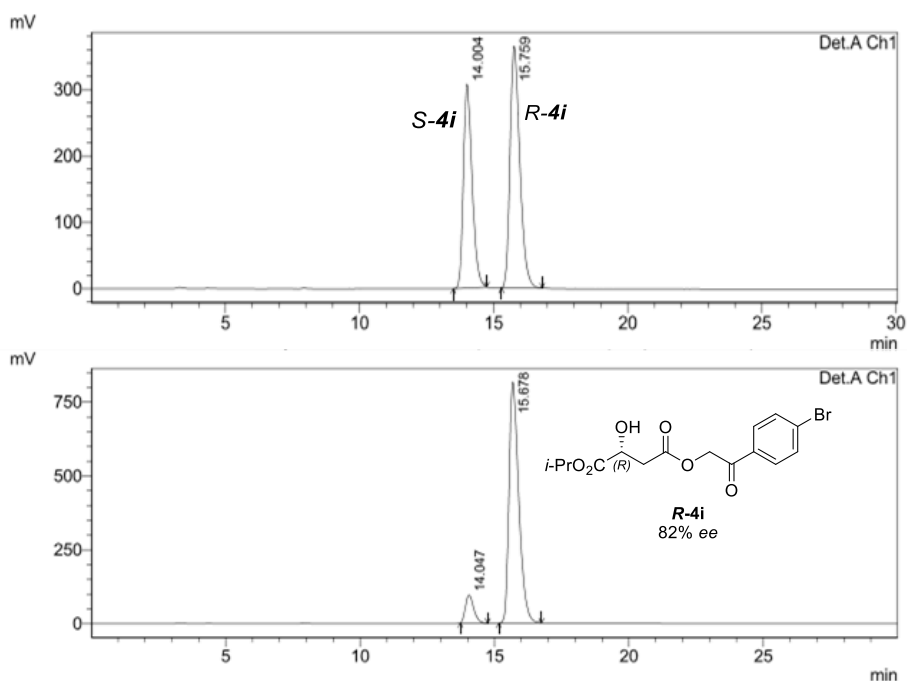


**Figure S82:** Chiral HPLC analysis chromatogram of *R*-4i synthesized with HBPA *wild-type* (down) and *rac*-4i synthesized with MBP-YFAU( $\text{Ni}^{2+}$ ) *wild-type* type (see section

Chiral HPLC analysis of 4-hydroxyesters). Conditions: CHIRALPACK® IB 46 x 250 mm column, 5  $\mu\text{m}$ , flow rate 1 mL  $\text{min}^{-1}$  at 25 °C and UV detection (254 nm). Isocratic elution hexane:*i*PrOH 80:20 (v/v).

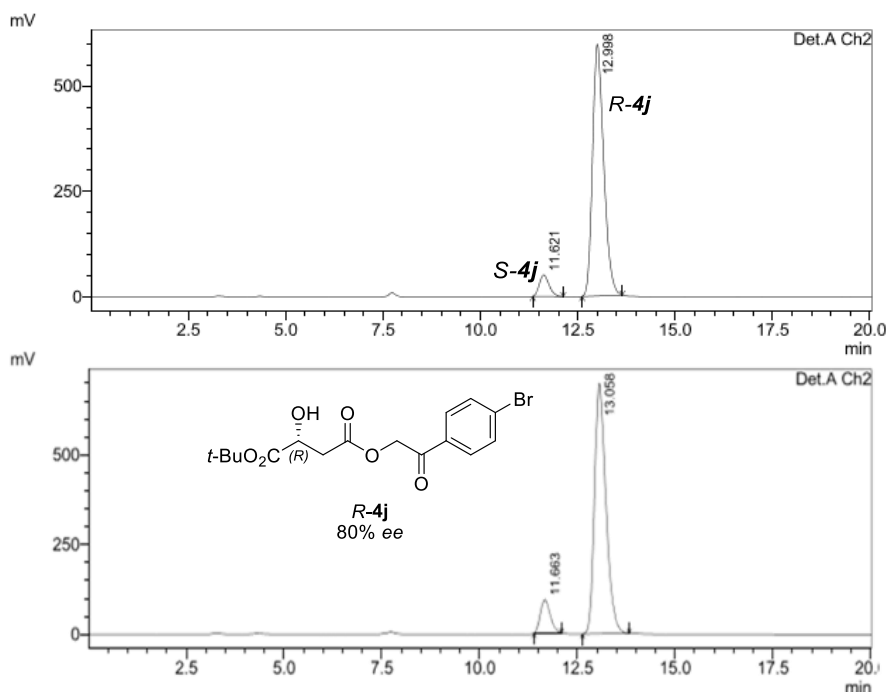


**Figure S83:** Chiral HPLC analysis chromatogram of *R-4j* synthesized with HBPA *wild-type* (down) and *rac-4j* synthesized with MBP-YFAU( $\text{Ni}^{2+}$ ) *wild-type* type (see section Chiral HPLC analysis of 4-hydroxyesters). Conditions: CHIRALPACK® IB 46 x 250 mm column, 5  $\mu\text{m}$ , flow rate 1 mL  $\text{min}^{-1}$  at 25 °C and UV detection (254 nm). Isocratic elution hexane:*i*PrOH 80:20 (v/v).

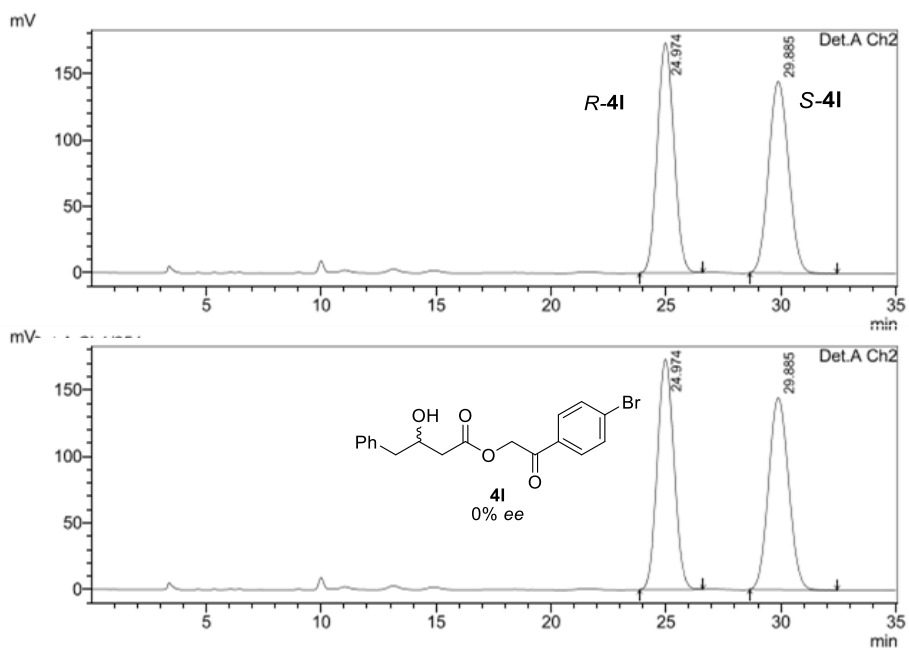


**Figure S84:** Chiral HPLC analysis chromatogram of *racemic* **4I** synthesized with HBPA *wild-type* (down) and *rac*-**4I** synthesized with MBP-YFAU(Ni<sup>2+</sup>) *wild-type* type (see section Chiral HPLC analysis of 4-hydroxyesters). Conditions: CHIRALPACK® IC 46 x 250 mm column, 5 μm, flow rate 1 mL min<sup>-1</sup> at 25 °C and UV detection (254 nm). Isocratic elution hexane:*i*PrOH 80:20 (v/v).

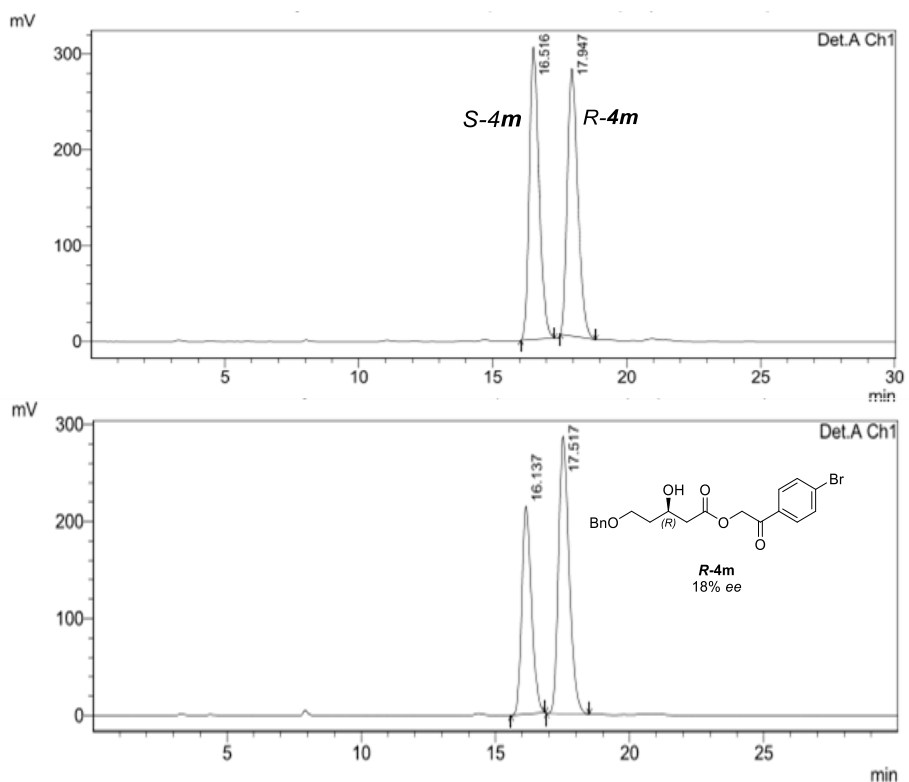


**Figure S85:** Chiral HPLC analysis chromatogram of *R*-**4m** synthesized with HBPA *wild-type* (down) and *rac*-**4m** synthesized with MBP-YFAU(Ni<sup>2+</sup>) *wild-type* type (see section Chiral HPLC analysis of 4-hydroxyesters). Conditions: CHIRALPACK® IB 46 x 250 mm column, 5 μm, flow rate 1 mL min<sup>-1</sup> at 25 °C and UV detection (254 nm). Isocratic elution hexane:<sup>i</sup>PrOH 80:20 (v/v).

## Computational Modeling

The crystal structure of HBPA has recently been solved (PDB 6DAO) together with the structure of its homolog *trans*-*o*-carboxybenzylidene pyruvate hydratase-aldolase (CBPA), the later crystalized alone (PDB 6DAN) and in complex with a substrate molecule (PDB 6DAQ).<sup>14</sup> The HBPA active site is located inside of a relatively deep and narrow cavity, where the ε-amino group of the essential Lys183 is at about 11 Å from the surface, with several aromatic residues flanking the entrance (H205, W224, F269 and F277) and predominantly polar residues (G64, T65, G67, Y155, N157 and N281) at the deeper end, close to the catalytic lysine (**Figure S86A, B**).

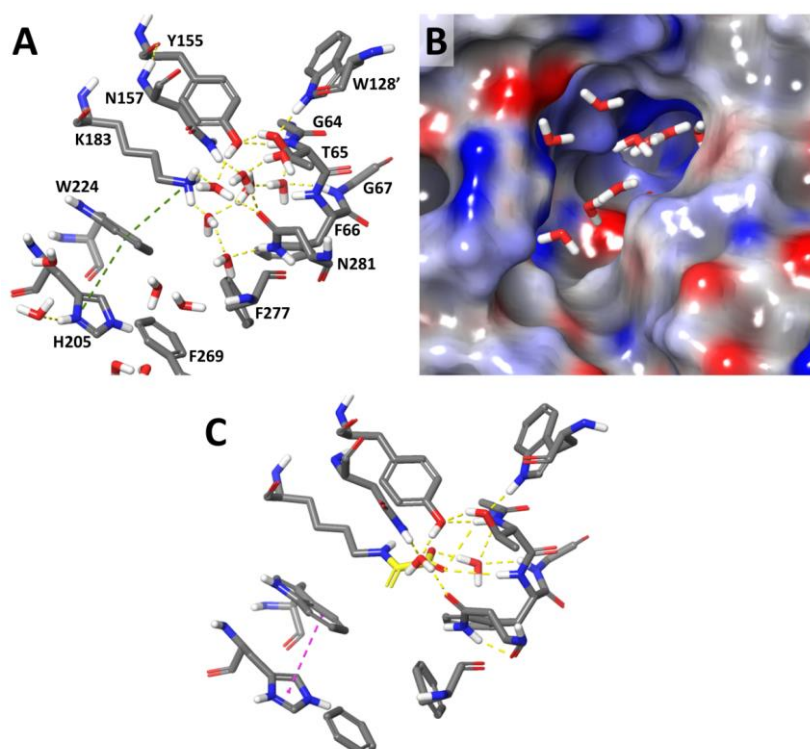


**Figure S86.** (A) Crystal structure of the active site of HBPA (chain A, PDB 6DAO<sup>14</sup>), showing the essential Lys residue (K183) and the residues that conform the cavity, and (B) its electrostatic potential mapped surface. (C) Model of the enamine pyruvate HBPA

covalent complex. The pyruvate enamine is highlighted with yellow C-atoms. Two water molecules are also shown: one of them H-bond to the pyruvate carboxylate and the second one to residues Y155 and N157.

The structure of the CBPA complex (PDB 6DAQ) allows proposing that the covalently bound pyruvate enamine intermediate in HBPA adopts a similar configuration, with its carboxylate moiety oriented towards the pyruvoyl carboxylate binding motif (GXXGE, G<sup>64</sup>TFGE<sup>68</sup> in HBPA), stabilized by H-bonds with the backbone amide NH groups of residues Thr65 and Phe66, and with a conserved water molecule which in turn is hydrogen bonded to the backbone amides of Gly64 and Gly67 (**Figure S86C**). The proposed enzymatic mechanism for HBPA (**Figure S87**) implies that Tyr155 could be the acid/base catalyst that protonates the carbonyl oxygen of the aldehyde electrophile, once the C-C bond is formed.<sup>14</sup> Therefore, the incoming aldehyde should displace a water molecule that is H-bonded to Tyr155 and Asn157 in the HBPA crystal structure (Figure S85C), and adequately locate its carbonyl oxygen for protonation by Tyr155. Based on this hypothesis, structural models of the pre-reactive complexes of pyruvate-enamine bound HBPA, *wild-type* and H205A variant, with the different electrophiles assayed, approaching the enamine from its *re*- and *si*-faces, were built (Figures S87-S92). Similarly, models were built for the corresponding aldol adduct intermediates bound as imines to residue Lys183 (Figures S93-S98). According to the mechanism (Figure S87), these models have the Lys183  $\epsilon$ -nitrogen atom protonated and the phenol group of Tyr155 unprotonated.

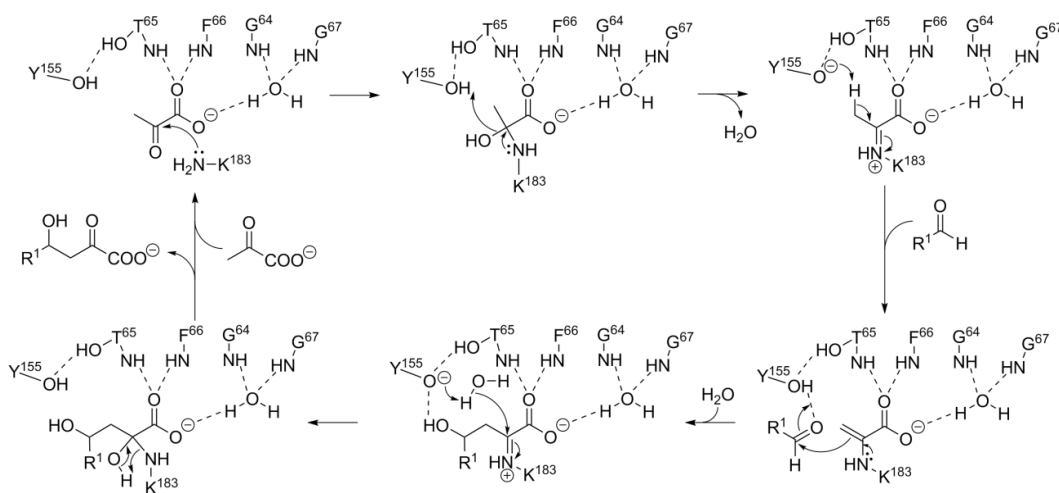


**Figure S87.** Proposed mechanism for HBPA.



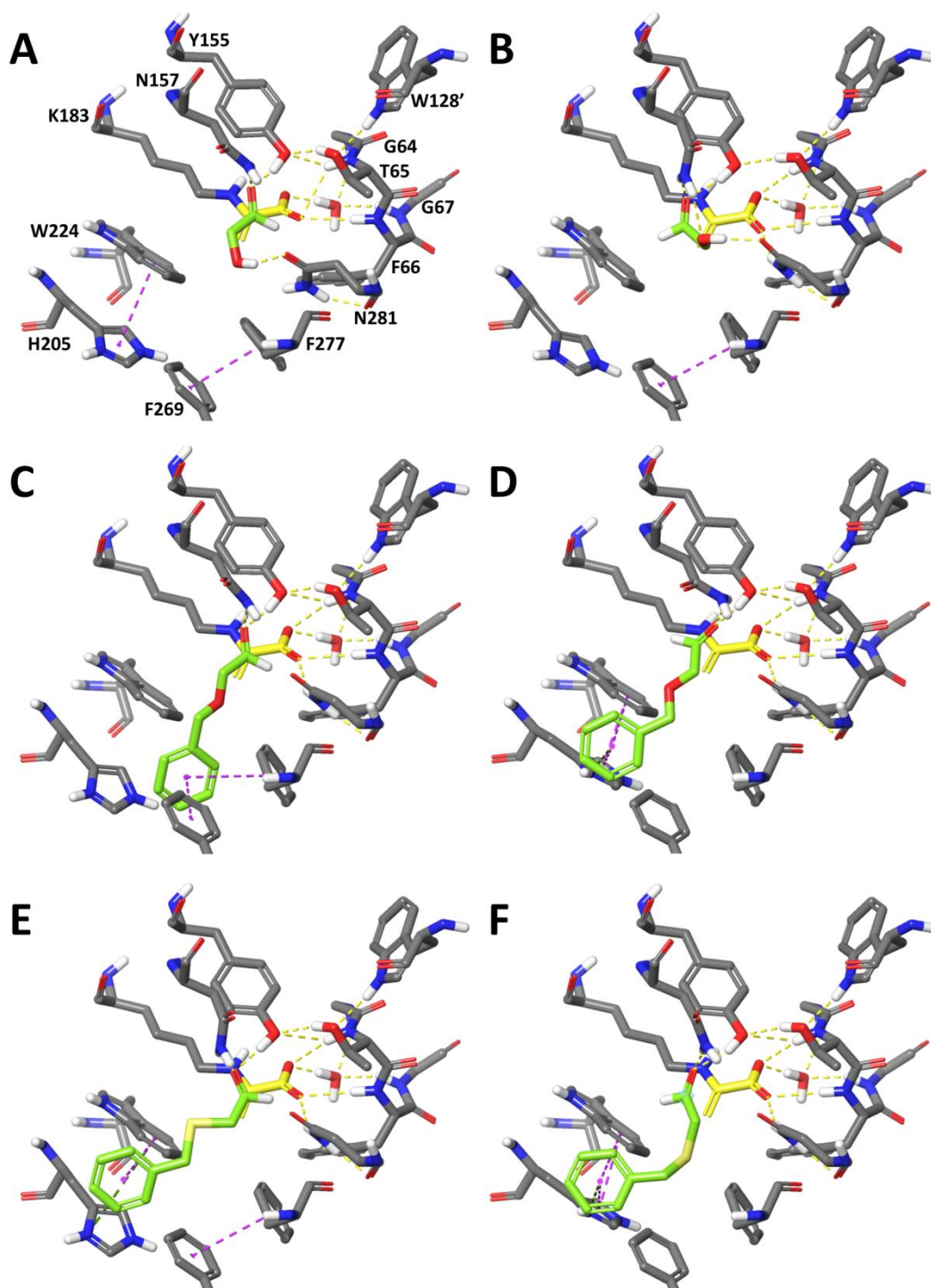


**Figure S88.** Models of the pre-reactive complexes of pyruvate-enamine bound *wild-type* HBPA with (A,B) **1a**, (C,D) **1b** and (E,F) **1c**. Electrophiles **1a-c** are shown approaching the enamine from their *re*- (A,C,E) or *si*-face (B,D,F). The pyruvate-enamine is shown with yellow C-atoms, the electrophile molecules with green C-atoms, and the interactions with dashed lines: H-bond in yellow,  $\pi$ - $\pi$  stacking in magenta and  $\pi$ -cation in green.

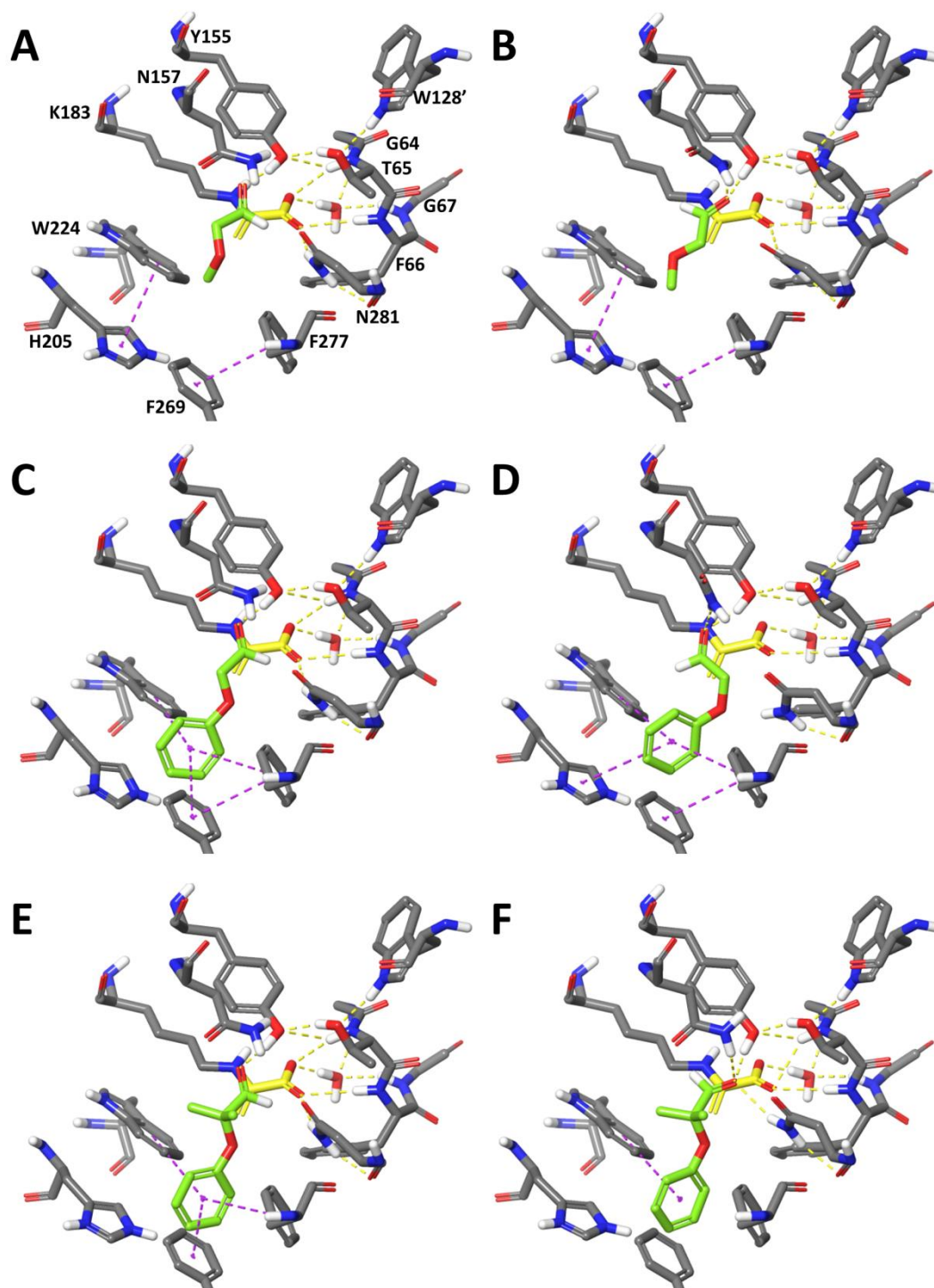


**Figure S89.** Models of the pre-reactive complexes of pyruvate-enamine bound *wild-type* HBPA with (A,B) **1d**, (C,D) **1e** and (E,F) **1f**. Electrophiles **1d-f** are shown approaching the enamine from their *re*- (A,C,E) or *si*-face (B,D,F). Representation details as in Figure S88.

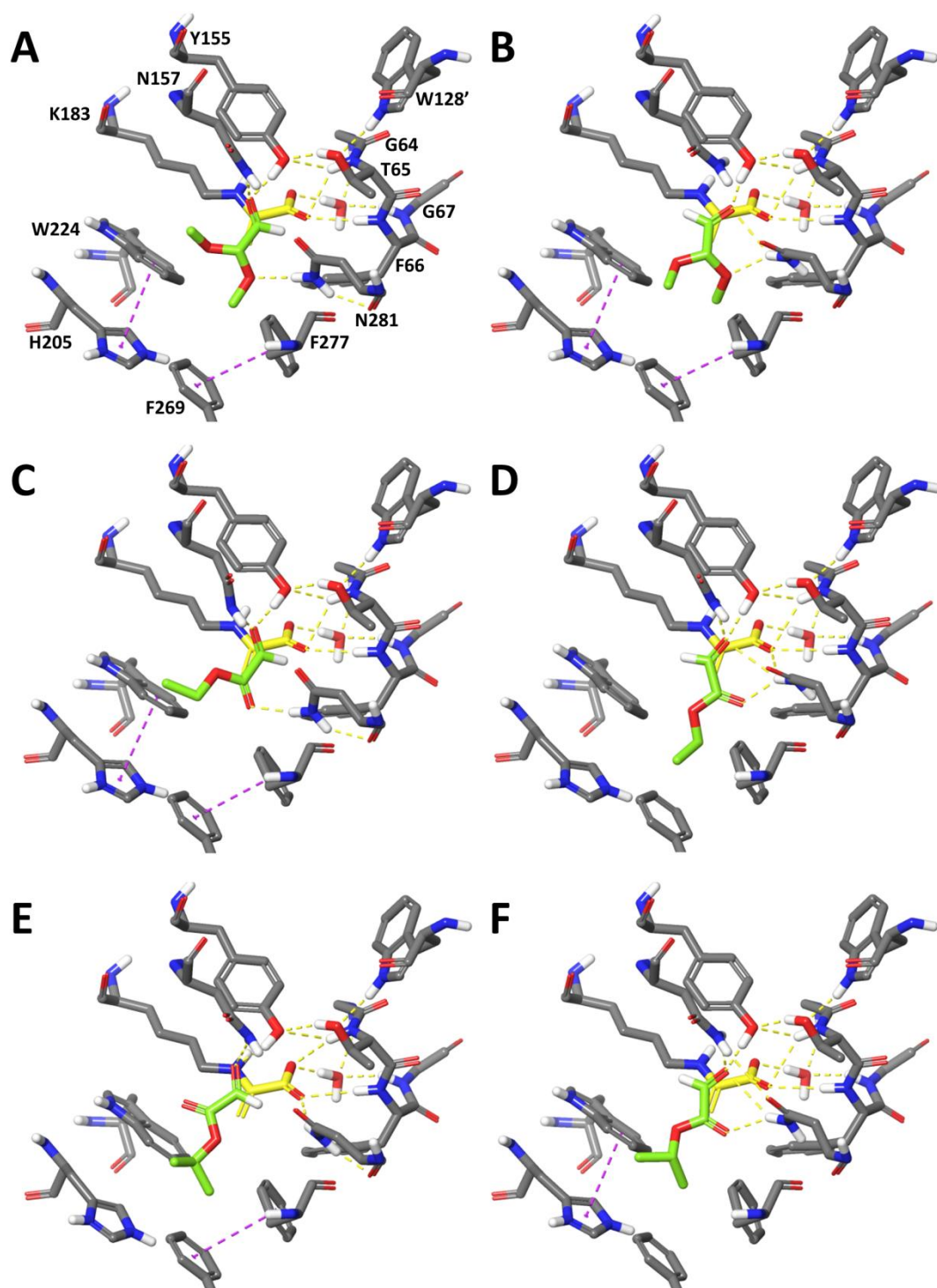


**Figure S90.** Models of the pre-reactive complexes of pyruvate-enamine bound *wild-type* HBPA with (A,B) **1g**, (C,D) **1h** and (E,F) **1i**. Electrophiles **1g-i** are shown approaching the enamine from their *re*- (A,C,E) or *si*-face (B,D,F). Representation details as in Figure S88.

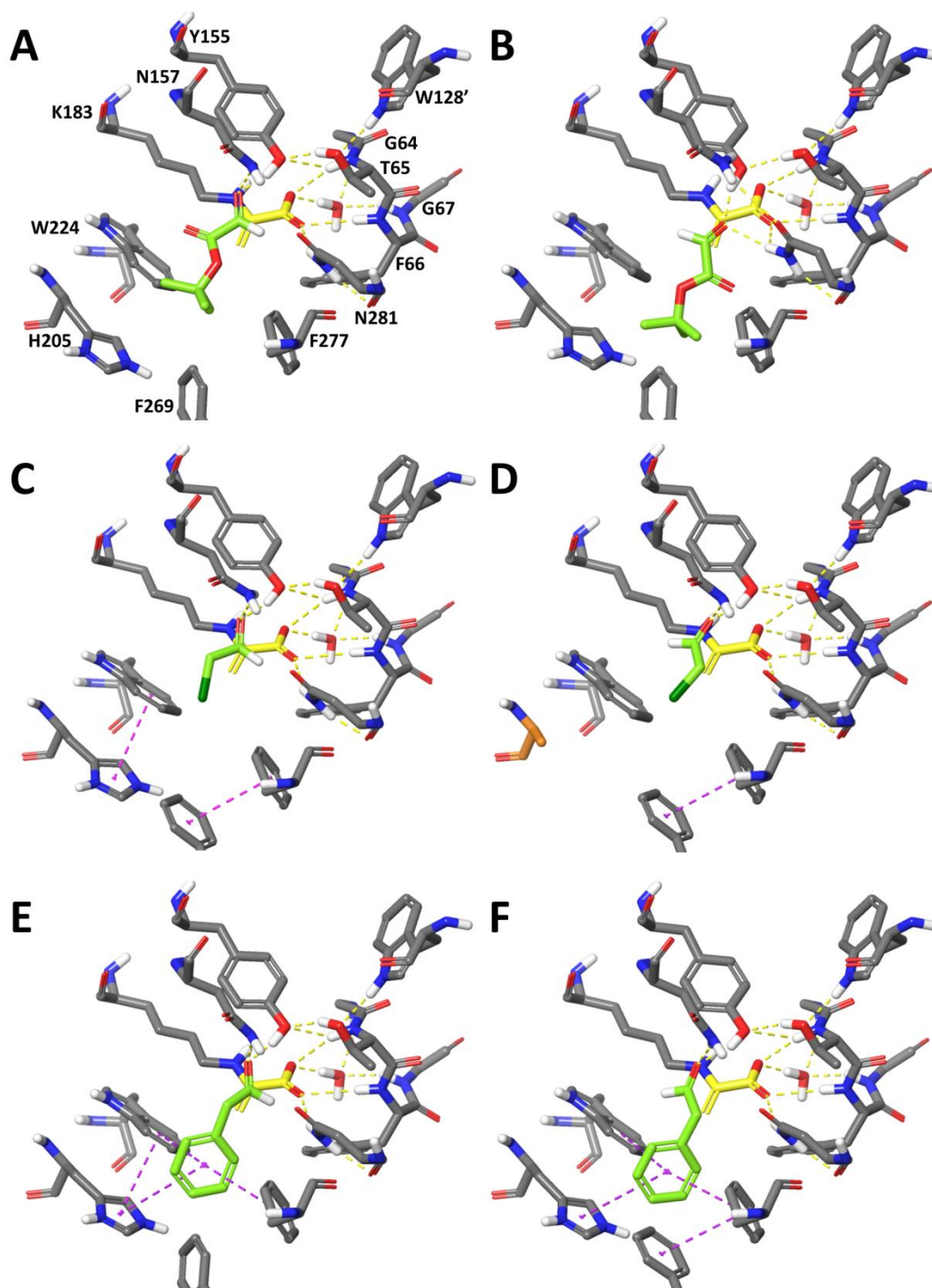


**Figure S91.** Models of the pre-reactive complexes of pyruvate-enamine bound *wild-type* HBPA with (A,B) **1j**, (C,D) **1k** and (E,F) **1l**. Electrophiles **1j-l** are shown approaching the enamine from their *re*- (A,C,E) or *si*-face (B,D,F). Representation details as in Figure S88.

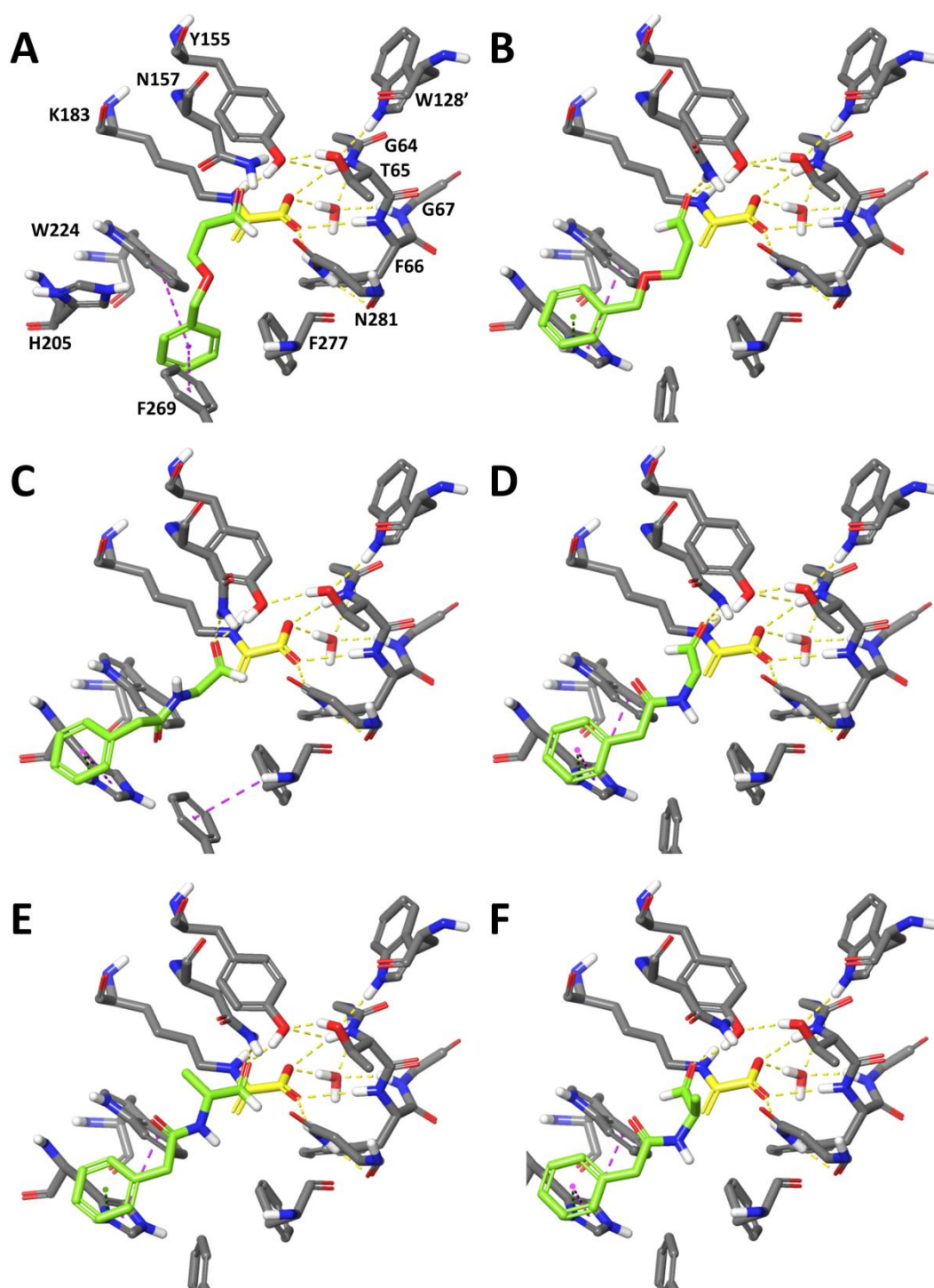


**Figure S92.** Models of the pre-reactive complexes of pyruvate-enamine bound *wild-type* HBPA with (A,B) **1m**, (C,D) **1n** and (E,F) **1o**. Electrophiles **1m-o** are shown approaching the enamine from their *re*- (A,C,E) or *si*-face (B,D,F). Representation details as in Figure S88.

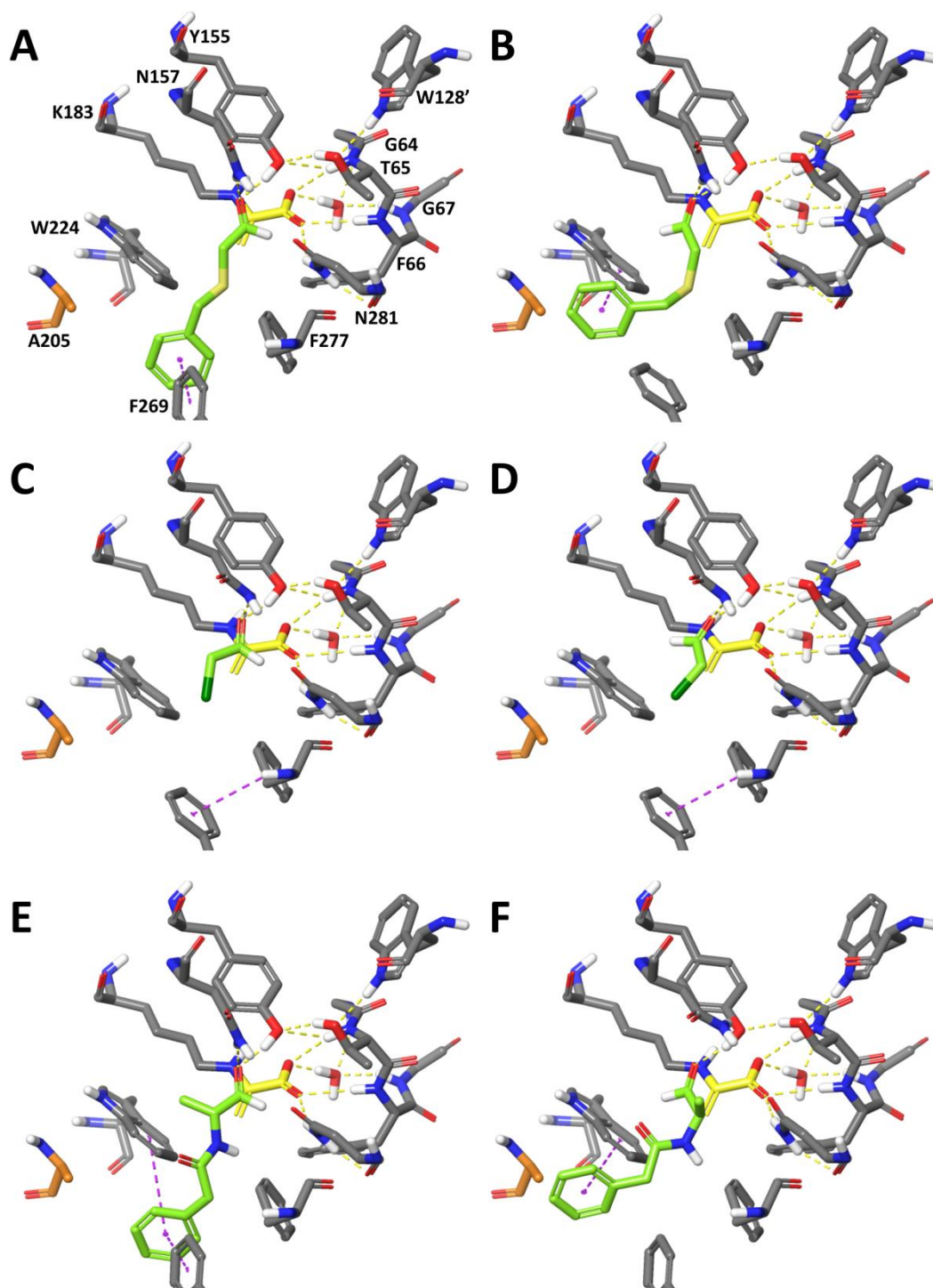


**Figure S93.** Models of the pre-reactive complexes of pyruvate-enamine bound HBPA H205A with (A,B) **1c**, (C,D) **1k** and (E,F) **1o**. Electrophiles **1m-o** are shown approaching the enamine from their *re*- (A,C,E) or *si*-face (B,D,F). The mutated residue A205 is highlighted in orange. The rest of representation details as in Figure S88.

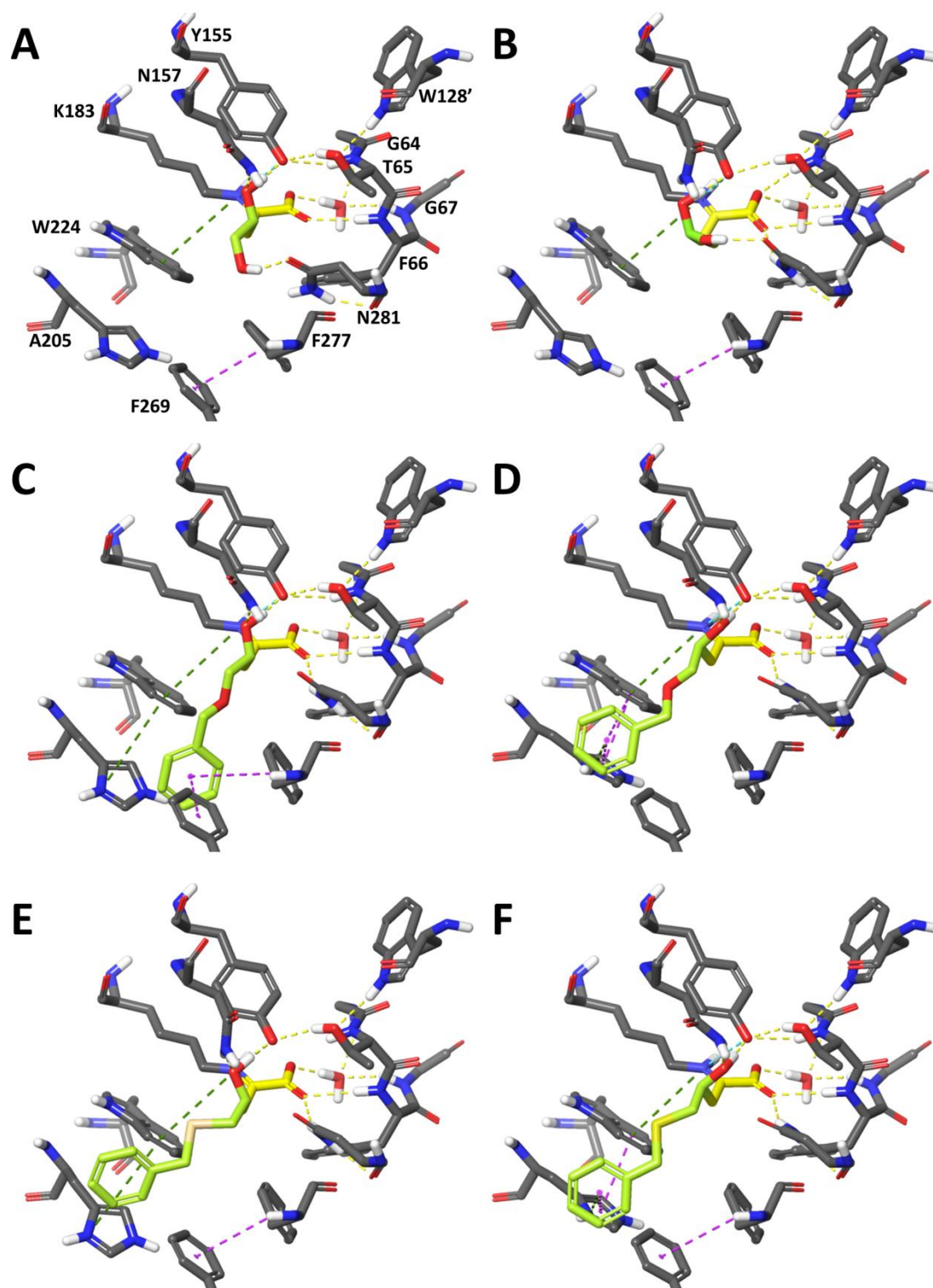


**Figure S94.** Models of HBPA complexes with the K183-bound aldol adduct imines derived from (A) (*R*)-**3a**, (B) (*S*)-**3a**, (C) (*R*)-**3b**, (D) (*S*)-**3b**, (E) (*R*)-**3c** and (F) (*S*)-**3c**. The pyruvate-derived moiety is shown with yellow C-atoms, the electrophile-derived moieties with green C-atoms, and the interactions with dashed lines: H-bond in yellow, salt bridges in cyan,  $\pi$ - $\pi$  stacking in magenta and  $\pi$ -cation in green.

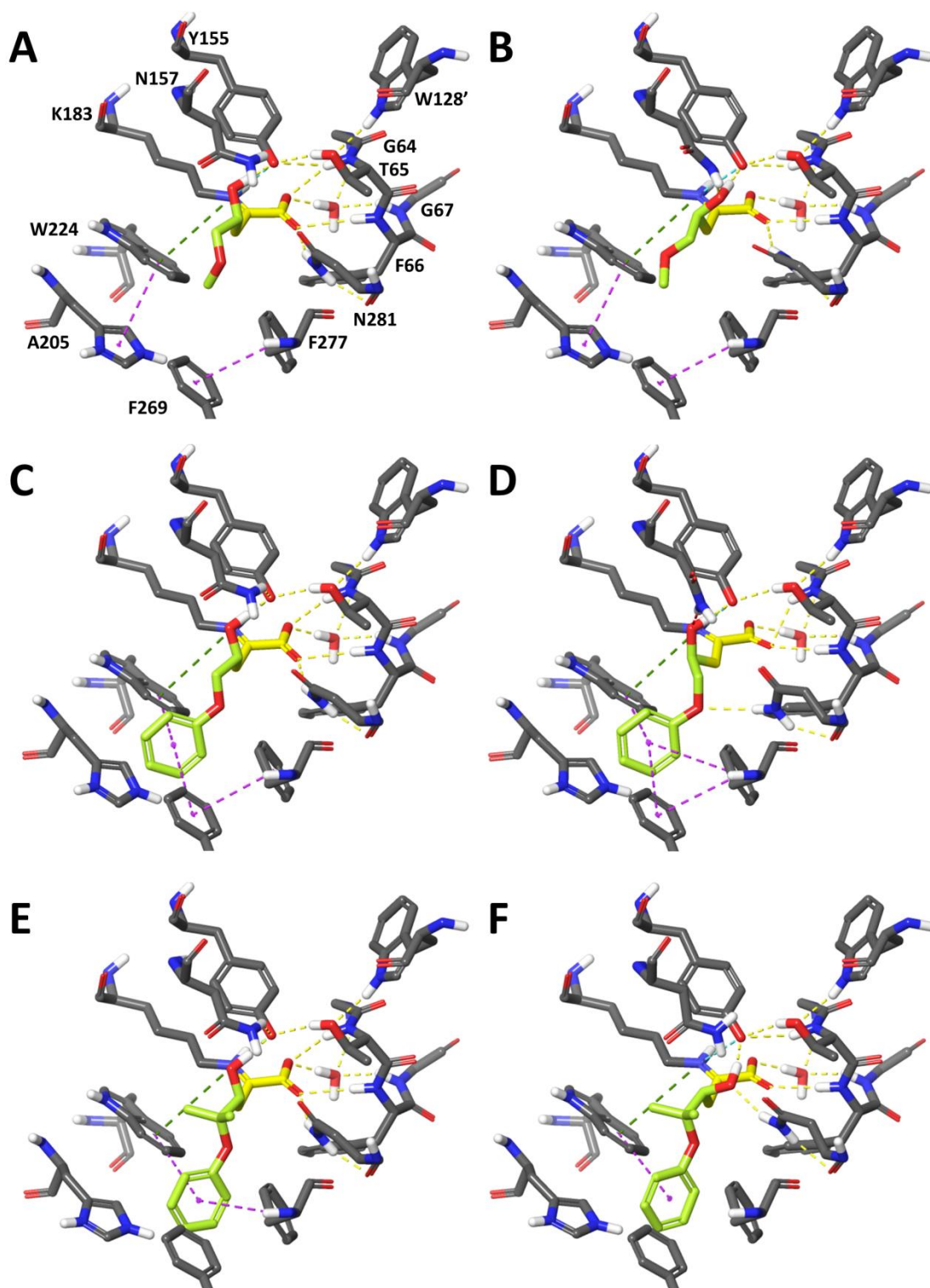


**Figure S95.** Models of HBPA complexes with the K183-bound aldol adduct imines derived from (A) *(R)*-3d, (B) *(S)*-3d, (C) *(R)*-3e, (D) *(S)*-3e, (E) *(R)*-3f and (F) *(S)*-3f. Representation details as in Figure S94.



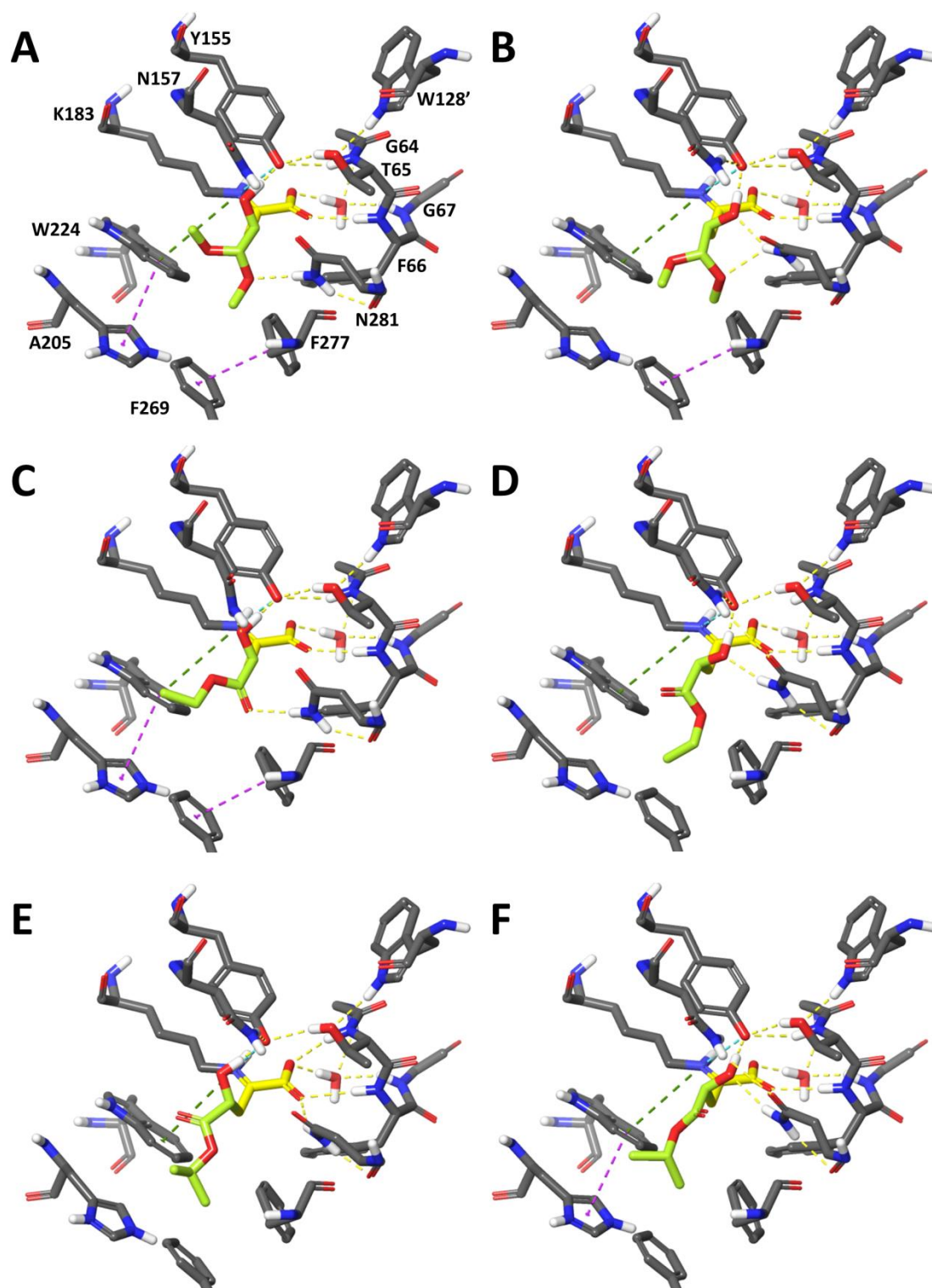


**Figure S96.** Models of HBPA complexes with the K183-bound aldol adduct imines derived from (A) (*R*)-**3g**, (B) (*S*)-**3g**, (C) (*R*)-**3h**, (D) (*S*)-**3h**, (E) (*R*)-**3i** and (F) (*S*)-**3i**. Representation details as in Figure S94.

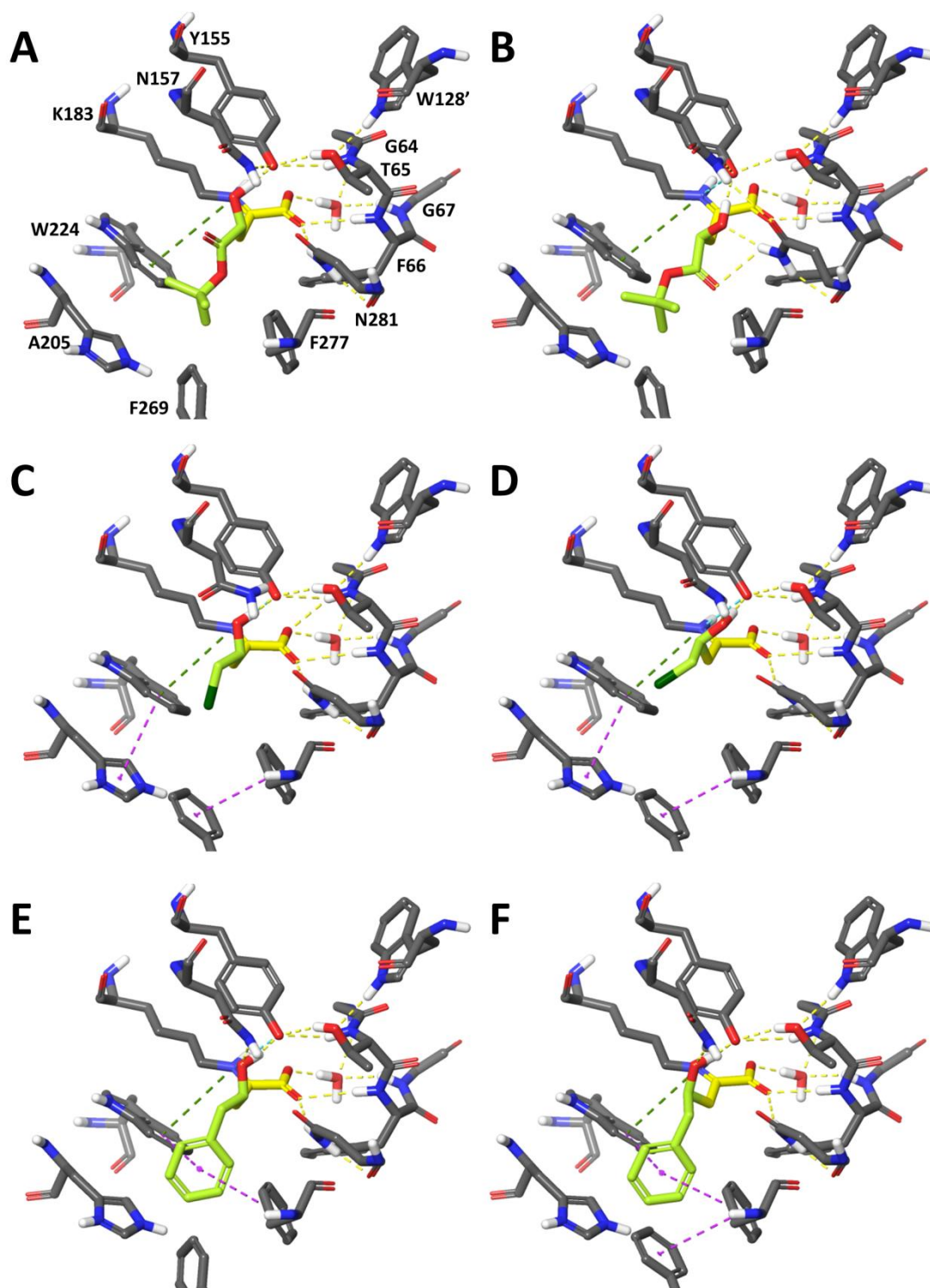


**Figure S97.** Models of HBPA complexes with the K183-bound aldol adduct imines derived from (A) (*R*)-**3j**, (B) (*S*)-**3j**, (C) (*R*)-**3k**, (D) (*S*)-**3k**, (E) (*S*)-**3l** and (F) (*R*)-**3l**. Representation details as in Figure S94.

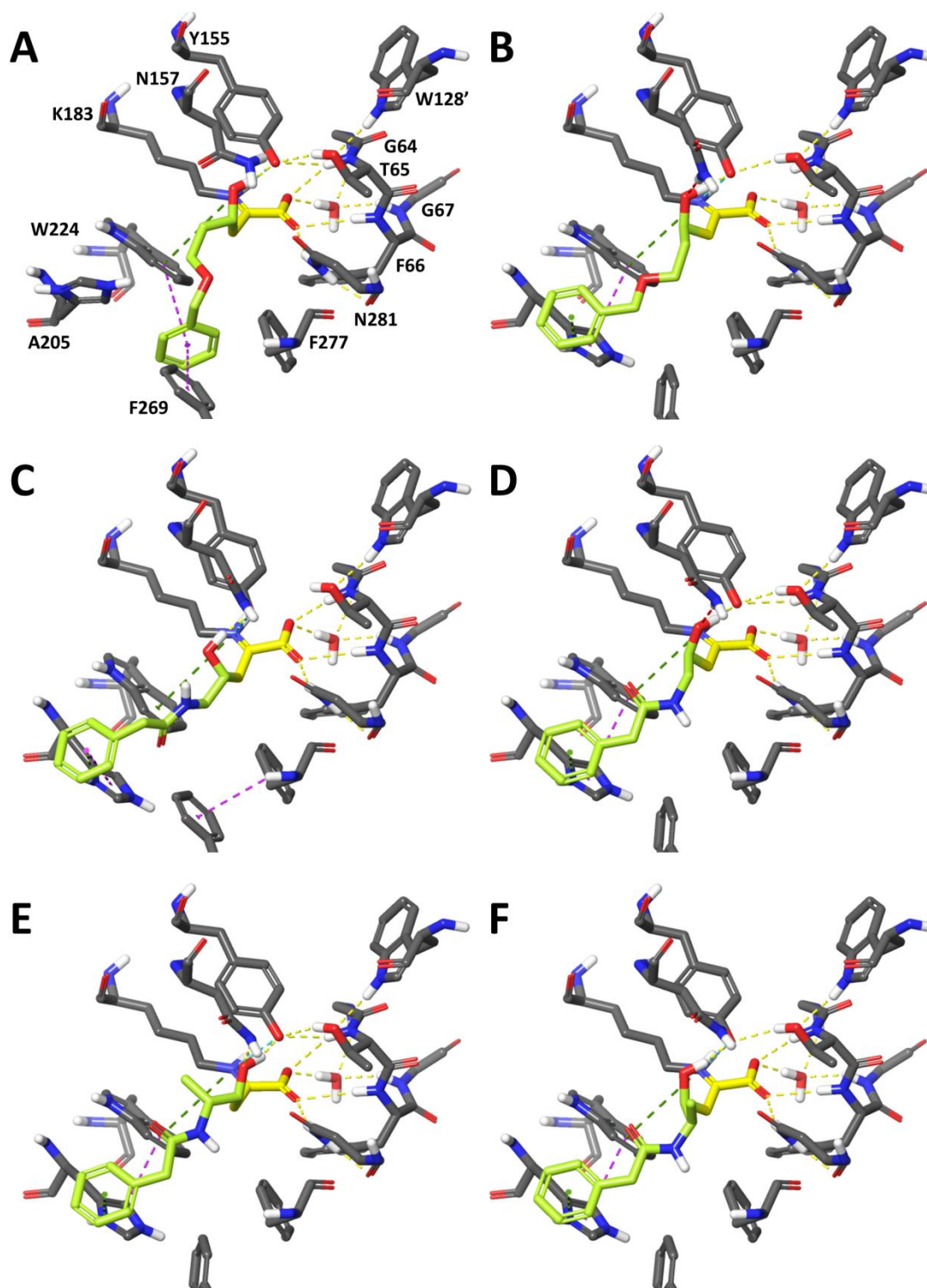


**Figure S98.** Models of HBPA complexes with the K183-bound aldol adduct imines derived from (A) (*R*)-**3m**, (B) (*S*)-**3m**, (C) (*R*)-**3n**, (D) (*S*)-**3n**, (E) (*R*)-**3o** and (F) (*S*)-**3o**. Representation details as in Figure S94.

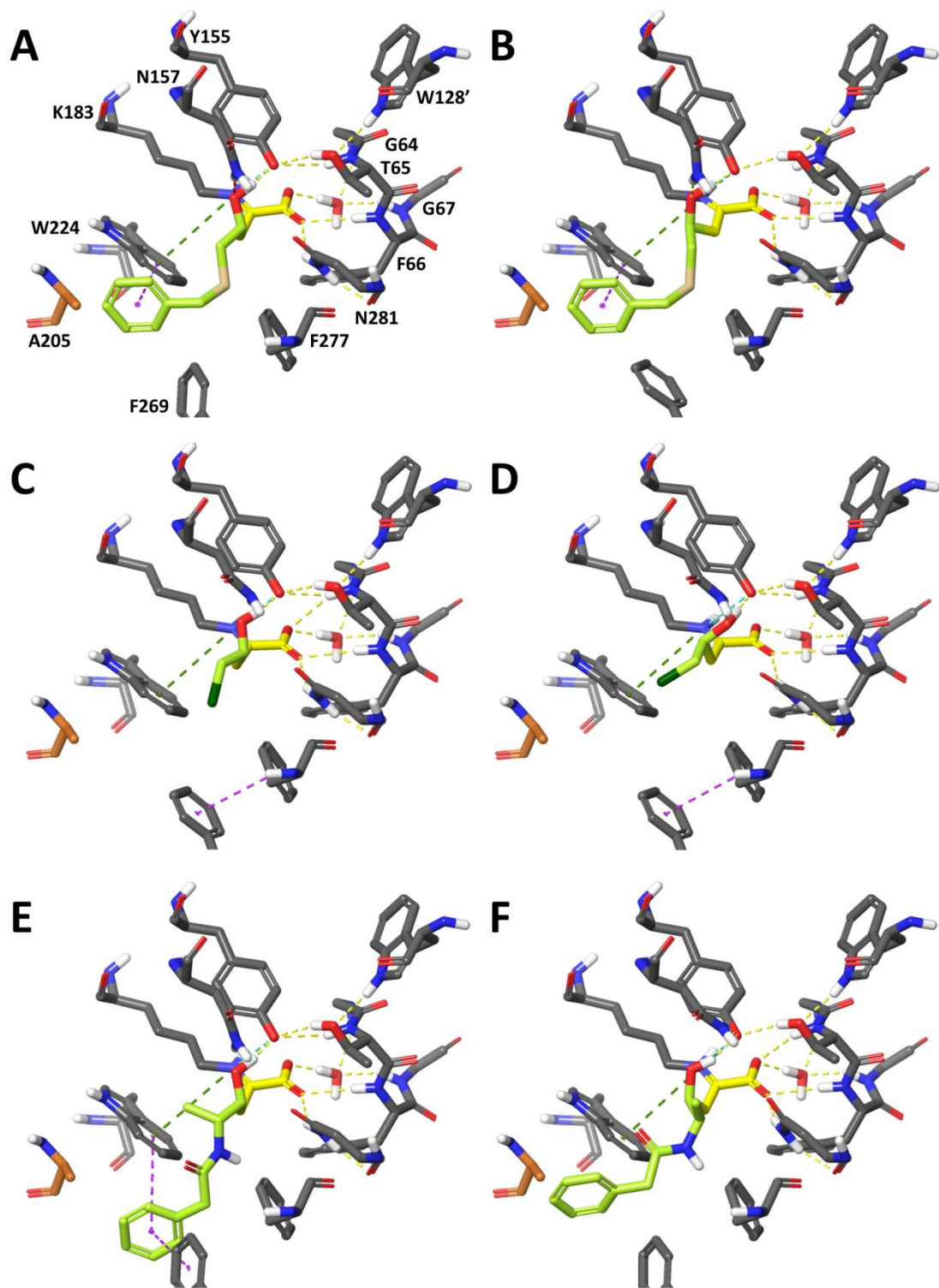


**Figure S99.** Models of HBPA H205A complexes with the K183-bound aldol adduct imines derived from (A) *(R)*-3c, (B) *(S)*-3c, (C) *(R)*-3k, (D) *(S)*-3k, (E) *(R)*-3o and (F) *(S)*-3o. The mutated residue A205 is highlighted in orange. The rest of representation details as in Figure S94.

## Computational Methods.

Protein complexes were modeled with the package Schrödinger Suite 2020-2,<sup>15</sup> through its graphical interface Maestro.<sup>16</sup> The Protein Preparation Wizard<sup>17</sup> included in Maestro was used to prepare the protein structure by removing solvent molecules and ions, adding hydrogens, setting protonation states<sup>18</sup> and running a restrained minimization using the OPLS3 force-field.<sup>19</sup> The program MacroModel<sup>17a</sup> with the same force field and GB/SA water solvation conditions<sup>20</sup> was used for further molecular mechanics calculations. The program QSite<sup>21</sup> was used for the QM/MM calculations.

Molecular models of the pre-reactive pyruvate-enamine intermediate with the electrophiles bound into the active site of the HBPA protein were generated starting from the HBPA crystal structure (PDB 6DAO).<sup>14</sup> Mutations were introduced within Maestro, followed by restrained minimization. The structures of the bound pyruvate and electrophiles were built within Maestro, based on the structure of the ligand bound into the active site of the homolog CBPHA protein (PDB 6DAQ). The pyruvate was modeled as enamine bound to the essential K183 residue. The electrophiles were modeled approaching the enamine from their *re*- and *si*-faces. For that purpose, they were manually placed in the active site of HBPA and adequately oriented to satisfy the conditions of (i) having its C-atom at approximately 2.4 Å of the reactive enamine C-atom of pyruvate, and (ii) establishing a hydrogen bond interaction between the aldehyde O-atom and the phenol and amide groups of Y155 and N157, respectively. The structures of the complexes were minimized with QSite at the DFT B3LYP/6-31G\*\* level of theory, establishing a distance constraint between the two reactive C-atoms to keep them at a distance of 2.4 Å. The QM/MM boundary was defined by placement of hydrogen caps between the C $\alpha$  and C $\beta$  atoms of residues Y155, N157, K183 and N281 of HBPA. The pyruvate-enamine, a water molecule that is H-bound to the pyruvate carboxylate, and the electrophile molecules were also included as part of the QM region. All residues with atoms within 6 Å of the QM region were simultaneously optimized using the OPLS3 force-field,<sup>19</sup> while residues which were further away were kept frozen. A distance dependent dielectric ( $\epsilon = 78$ ) was used for calculating the electrostatic component of the MM energy. Furthermore, to find the best bound conformations for the more flexible electrophiles, a conformational search was performed using the mixed MCMM/LMCS method<sup>22</sup> implemented in MacroModel to find the best poses for the aldehyde R<sup>1</sup> substituents, while the carbonyl group and the rest of the system were kept frozen. Then,

the best conformers detected by this search were QM/MM reoptimized as above. Finally, the optimized structures were used to build the corresponding aldol adducts, bound as imines to residue Lys183. According to the mechanism, after C-C bond formation, the resulting intermediates should have the Lys183  $\epsilon$ -nitrogen atom protonated and the phenol group of Tyr155 unprotonated. These structural modifications were performed within Maestro and the resulting model structures were QM/MM reoptimized as above.

## References.

1. (a) Calveras, J.; Egido-Gabás, M.; Gómez, L.; Casas, J.; Parella, T.; Joglar, J.; Bujons, J.; Clapés, P., Dihydroxyacetone phosphate aldolase-catalyzed synthesis of structurally diverse polyhydroxylated pyrrolidine derivatives and evaluation of their glycosidase inhibitory properties. *Chem. Eur. J.* **2009**, *15*, 7310-7328; (b) Concia, A. L.; Lozano, C.; Castillo, J. A.; Parella, T.; Joglar, J.; Clapés, P., D-Fructose-6-phosphate aldolase in organic synthesis: cascade chemical-enzymatic preparation of sugar-related polyhydroxylated compounds. *Chem. Eur. J.* **2009**, *15*, 3808-3816; (c) Garrabou, X.; Gomez, L.; Joglar, J.; Gil, S.; Parella, T.; Bujons, J.; Clapés, P., Structure-guided minimalist redesign of L-fuculose-1-phosphate aldolase active site. Expedient synthesis of novel polyhydroxylated pyrrolizidines and their inhibitory properties against glycosidases and intestinal disaccharidases *Chem. Eur. J.* **2010**, *16*, 10691-10706.
2. Hernández, K.; Parella, T.; Joglar, J.; Bujons, J.; Pohl, M.; Clapés, P., Expedient Synthesis of C-Aryl Carbohydrates by Consecutive Biocatalytic Benzoin and Aldol Reactions. *Chem. Eur. J.* **2015**, *21*, 3335-3346.
3. Hernández, K.; Gómez, A.; Joglar, J.; Bujons, J.; Parella, T.; Clapés, P., 2-Keto-3-Deoxy-L-Rhamnonate Aldolase (YfaU) as Catalyst in Aldol Additions of Pyruvate to Amino Aldehyde Derivatives. *Adv. Synth. Catal.* **2017**, *359*, 2090-2100.
4. Ferreira, T.; Rasb, W., ImageJ user guide: IJ 1.46 r. **2012**.
5. Eaton, R. W., trans-o-Hydroxybenzylidenepyruvate Hydratase-Aldolase as a Biocatalyst. *Appl. Environ. Microbiol.* **2000**, *66*, 2668-2672.
6. Mironov, G. G.; St-Jacques, A. D.; Mungham, A.; Eason, M. G.; Chica, R. A.; Berezovski, M. V., Bioanalysis for Biocatalysis: Multiplexed Capillary Electrophoresis–Mass Spectrometry Assay for Aminotransferase Substrate Discovery and Specificity Profiling. *J. Am. Chem. Soc.* **2013**, *135*, 13728-13736.
7. Keiko, N. A.; Stepanova, L. G.; Verochkina, E. A.; Chuvashov, Y. A., Synthesis and properties of alkylthioethanals. *ARKIVOC (Gainesville, FL, U. S.)* **2011**, 127-138.
8. Hon, Y.-S.; Wong, Y.-C.; Chang, C.-P.; Hsieh, C.-H., Tishchenko reactions of aldehydes promoted by diisobutylaluminum hydride and its application to the macrocyclic lactone formation. *Tetrahedron* **2007**, *63*, 11325-11340.
9. Kumar, S.; Pearson, A. L.; Pratt, R. F., Design, synthesis, and evaluation of  $\alpha$ -ketoheterocycles as class C  $\beta$ -lactamase inhibitors. *Bioorg. Med. Chem.* **2001**, *9*, 2035-2044.
10. Zhang, P.-l.; Wang, G.; Liu, J.-s.; Xu, F.-q.; Zhao, Z.-z.; Wang, W.-x.; Wang, J.-t.; Wang, G.-k.; Wu, P.-y., Three new metabolites from the endophytic fungus

*Climacocystis montana* isolated from the root bark of *Paeonia ostia*. *Phytochemistry Letters* **2018**, *26*, 50-54.

11. Espelt, L.; Parella, T.; Bujons, J.; Solans, C.; Joglar, J.; Delgado, A.; Clapés, P., Stereoselective aldol additions catalyzed by dihydroxyacetone phosphate dependent aldolases in emulsion systems: preparation and structural characterization of linear and cyclic aminopolyols from aminoaldehydes. *Chem. Eur. J.* **2003**, *9*, 4887-4899.
12. White, J. D.; Hansen, J. D., Total Synthesis of (-)-7-Epicylindrospermopsin, a Toxic Metabolite of the Freshwater Cyanobacterium *Aphanizomenon ovalisporum*, and Assignment of Its Absolute Configuration. *J. Org. Chem.* **2005**, *70*, 1963-1977.
13. Sheldrick, G., A short history of SHELX. *Acta Crystallogr. Sect. A* **2008**, *64*, 112-122.
14. LeVieux, J. A.; Medellin, B.; Johnson, W. H.; Erwin, K.; Li, W.; Johnson, I. A.; Zhang, Y. J.; Whitman, C. P., Structural Characterization of the Hydratase-Aldolases, NahE and PhdJ: Implications for the Specificity, Catalysis, and N-Acetylneuraminatase Lyase Subgroup of the Aldolase Superfamily. *Biochemistry* **2018**, *57*, 3524-3536.
15. Schrödinger *Release 2020-2: Schrödinger Suite 2020-2 Protein Preparation Wizard; Epik, Schrödinger, LLC, New York, NY, 2020; Impact, Schrödinger, LLC, New York, NY, 2020; Prime, Schrödinger, LLC, New York, NY, 2020.*, 2020.
16. Schrödinger *Release 2020-2: Maestro*, Schrödinger, LLC: New York, NY, 2020.
17. (a) Schrödinger *Release 2020-2: Macromodel*, Schrödinger, LLC: New York, NY, 2020; (b) Sastry, G. M.; Adzhigirey, M.; Day, T.; Annabhimoju, R.; Sherman, W., Protein and ligand preparation: parameters, protocols, and influence on virtual screening enrichments. *J. Comput. Aided Mol. Des.* **2013**, *27*, 221-234.
18. Olsson, M. H. M.; Søndergard, C. R.; Rostkowski, M.; Jensen, J. H., PROPKA3: Consistent Treatment of Internal and Surface Residues in Empirical pKa predictions. *J. Chem. Theor. Comput.* **2011**, *7*, 525-537.
19. Harder, E.; Damm, W.; Maple, J.; Wu, C.; Reboul, M.; Xiang, J. Y.; Wang, L.; Lupyan, D.; Dahlgren, M. K.; Knight, J. L.; Kaus, J. W.; Cerutti, D. S.; Krilov, G.; Jorgensen, W. L.; Abel, R.; Friesner, R. A., OPLS3: A Force Field Providing Broad Coverage of Drug-like Small Molecules and Proteins. *J Chem Theory Comput* **2016**, *12*, 281-296.
20. Still, W. C.; Tempczyk, A.; Hawley, R. C.; Hendrickson, T., Semianalytical Treatment of Solvation for Molecular Mechanics and Dynamics. *J. Am. Chem. Soc.* **1990**, *112*, 6127-6129.
21. (a) Schrödinger *Release 2020-2: QSite*, Schrödinger, LLC: New York, NY, 2020; (b) Murphy, R. B.; Philipp, D. M.; Friesner, R. A., A mixed quantum mechanics/molecular mechanics (QM/MM) method for large-scale modeling of chemistry in protein environments. *J. Comp. Chem.* **2000**, *21*, 1442-1457; (c) Philipp, D. M.; Friesner, R. A., Mixed ab initio QM/MM modeling using frozen orbitals and tests with alanine dipeptide and tetrapeptide. *J. Comp. Chem.* **1999**, *20*, 1468-1494.
22. Kolossvary, I.; Guida, W. C., Low-mode conformational search elucidated: application to C<sub>39</sub>H<sub>80</sub> and flexible docking of 9-deazaguanine inhibitors into PNP. *J. Comput. Chem.* **1999**, *20*, 1671-1684.

**Materiales y métodos.**  
**Capítulo 3.2**



## Supporting Information

### **Biocatalytic synthesis of homochiral 2-hydroxy-4-butyrolactone derivatives by tandem aldol addition and carbonyl reduction.**

Carlos J. Moreno<sup>a</sup>, Karel Hernández<sup>a</sup>, Samantha Gittings<sup>b</sup>, Michael Bolte<sup>c</sup>, Jesús Joglar<sup>a</sup>,  
Jordi Bujons<sup>a</sup>, Teodor Parella<sup>d</sup>, Pere Clapés<sup>\*a</sup>

<sup>a</sup>Catalonia Institute for Advanced Chemistry, Dept. Chemical Biology & Molecular Modelling, IQAC-CSIC, Spain.

<sup>b</sup>Prozomix Ltd. West End Industrial Estate, Haltwhistle, Northumberland, NE49 9HA, UK.

<sup>c</sup>Institut für Anorganische Chemie, J.-W.-Goethe-Universität, Frankfurt/Main, Germany.

<sup>d</sup>Servei de Ressonància Magnètica Nuclear. Universitat Autònoma de Barcelona, Bellaterra, Spain.

\*Corresponding author: pere.clapes@iqac.csic.es

### **Table of Contents**

Materials. ....	2
Methods. ....	4
Protein production and purification. ....	5
Thin layer chromatography (TLC) analysis. ....	7
Specific rotation. ....	7
HPLC analysis. ....	7
NMR analysis. ....	8
Activity determination of DpkA <sub>Psyrin</sub> . ....	8
Activity determination of KPR <sub>Ecoli</sub> . ....	9
Activity determination of glucose dehydrogenase (GDH). ....	10
Biocatalytic aldol addition of 2-oxoacid (2) to formaldehyde (1). Analytical scale. ....	11
One-pot two-step stereoselective synthesis of 2-hydroxy-4-butyrolactone derivatives (5). ....	13
One-pot enzymatic cascade for the stereoselective synthesis of 2-hydroxy-4-butyrolactones derivatives (5a,b). ....	24
Strategy for enantiomeric excess determination of products 5 (a, j-n). ....	25
Biocatalytic aldol addition of sodium pyruvate (2a) to aldehydes (1b-g). Analytical scale. ....	33
One-pot two-step stereoselective synthesis of 4-substituted-2-hydroxy-4-butyrolactones 8 by tandem biocatalytic aldol-reduction reactions catalyzed by HBPA <sub>Pputida</sub> and DpkA <sub>Psyrin</sub> . ....	35
Kinetic Studies. ....	39

X-Ray structures .....	52
NMR spectra.....	56
Computational Methods.....	148

## Materials.

Formaldehyde (**1**), glycolaldehyde dimer (**1b**), 2,2-dimethoxyacetaldehyde (**1c**), chloroacetaldehyde (**1c**), benziloxiacetaldehyde (**1d**), sodium pyruvate (**2a**), 2-oxobutyric acid (**2b**), 2-oxopentanoic acid (**2c**), 4-Methyl-2-oxovaleric acid (**2f**), sodium 3-methyl-2-oxobutyrate (**2j**), were purchased from Sigma-Aldrich. The rest of aldehyde and 2-oxoacids used in this study were synthesized in our lab using procedure described in previous works<sup>1-3</sup>. Stock solutions of 2-oxoacids were prepared in H<sub>2</sub>O, pH adjusted to 7.0 with 1 M NaOH and stored at 4 °C. Under these conditions precipitation of sodium salt compounds (**2g-n**) was observed. Before using, these solutions were carefully treated with the heat gun under stirring until a clear solution was obtained (Table S1).

**Table S1: Substrates (2a-n) stock solution.**

2-oxoacids ( <b>2</b> )	Stock concentration/M
<b>2a</b>	2.0
<b>2b</b>	1.0
<b>2c</b>	1.8
<b>2d</b>	2.0
<b>2e</b>	1.0
<b>2f</b>	0.65
<b>2g</b>	1.5
<b>2h</b>	1.0
<b>2i</b>	0.8
<b>2j</b>	1.0
<b>2k</b>	1.0
<b>2l</b>	1.0
<b>2m</b>	0.65
<b>2n</b>	0.44

The 3-benzyloxyamine hydrochloride, D-(-)-pantolactone and (*R*)-(+)- $\alpha$ -Hydroxy- $\gamma$ -butyrolactone were purchased from Sigma-Aldrich. Sodium borohydride DL-(-)-pantolactone and 4-bromobenzoyl chloride were purchased from TCI chemical. NADPH was purchased from CARL ROTH. Glucose dehydrogenase (GDH) as a cell

free extract powder and NADP<sup>+</sup> were provided by Prozomix Ltd (PRO-GDH(001)). All reagent for Molecular Biology were supplied from ThermoFischer Scientific.

Synthetic oligonucleotides were purchased from Eurofins Genomics. All reagents for molecular biology were from Life Thermo Scientific. Culture media components for *E. coli* were from Pronadisa (Madrid, Spain). Antibiotics and IPTG were from Carl Roth. Nickel Sepharose<sup>TM</sup> High Performance was from Cytiva<sup>TM</sup>. Water for analytical HPLC was obtained from an Arium pro ultrapure water purification system (Sartorius Stedim Biotech) and the rest of solvents used in this work were of analytical grade or HPLC grade. Bacterial strains, oligonucleotides and plasmids used in this study are listed in Table S2.

**Table S2.** Strains, plasmids and oligonucleotides used in this study.

<b>Strains</b>	<b>Relevant genotype</b>
<i>E. coli</i> Nova Blue (Novagen <sup>®</sup> ) (used for plasmid preparation).	<i>endA1</i> , <i>hsdR17</i> (rB <sup>+</sup> , mB <sup>+</sup> ), <i>supE44</i> , <i>thi1</i> , <i>recA1</i> , <i>gyrA96</i> , <i>relA1</i> , <i>lac F'</i> [proA <sup>+</sup> B <sup>+</sup> , <i>lacI</i> <sup>q</sup> ZΔM15::Tn10] ( <i>Tet</i> <sup>R</sup> ).
<i>E. coli</i> M15 [pREP4] (used for protein expression).	<i>nal</i> <sup>s</sup> , <i>str</i> <sup>s</sup> , <i>rif</i> <sup>s</sup> , <i>thi</i> <sup>-</sup> , <i>lac</i> <sup>-</sup> , <i>ara</i> <sup>+</sup> , <i>gal</i> <sup>+</sup> , <i>mlt</i> <sup>-</sup> , F <sup>-</sup> , <i>recA</i> <sup>+</sup> , <i>uvr</i> <sup>+</sup> , <i>lon</i> <sup>+</sup> , Km <sup>R</sup> . <sup>4</sup>
<i>E. coli</i> B121-A1 (used for protein expression)	F <sup>-</sup> <i>ompT gal dcm lon hsdS<sub>B</sub>(r<sub>B</sub><sup>-</sup>m<sub>B</sub><sup>-</sup>)[malB<sup>+</sup>]<sub>K-12</sub>(λ<sup>S</sup>) <i>araB:T7RNAP-tetA</i></i>
<b>Oligonucleotides</b>	<b>Sequences</b>
Primer dpka <sub><i>P.syrin</i></sub> (53)	Forward: 5' ATTATAAT <b>CCATGG</b> GCTGTCCGCCAGCCACGCTGACCAGCCC 3' <i>NcoI</i>
Primer dpka <sub><i>P.syrin</i></sub> (35)	Reverse: 3' ATTATAAT <b>AGATCT</b> GTGGCCTGCCAGCTCTTGCAAAC 5' <i>BglII</i>
Primer panE <sub><i>E.coli</i></sub> (53)	Forward: 5' ATATATAT <b>GGATCC</b> ATGAAAATTACCGTATTGGGATGC 3' <i>BamHI</i>
Primer panE <sub><i>E.coli</i></sub> (35)	Reverse: 5' ATATATAT <b>AAGCTT</b> CTACCAGGGGCGAGGCAAACC 3' <i>HindIII</i>
<b>Plasmids</b>	<b>Relevant genetic characteristics</b>
pQE-60	The vector encodes one multiple cloning site preceded by a T5 promoter, <i>lac</i> operator and ribosome binding site. The vector also carries the ColE1 replicon and ampicillin resistance gene <sup>4</sup> .
pQE-40	The vector encodes one multiple cloning site preceded by a T5 promoter, <i>lac</i> operator and ribosome binding site. The vector also carries the ColE1 replicon and ampicillin resistance gene <sup>4</sup> .
pQE-40- <i>panE</i>	<i>panE</i> gene (912 bp) from <i>E. coli K-12</i> (NCBI data base accession number CP015085.1) cloned in pQE40 ( <i>BamHI</i> and <i>HindIII</i> ).
pQE-60- <i>dpka</i>	<i>dpka</i> gene (1032 bp) from <i>Pseudomonas syringae</i> (NCBI data base accession DSM50315) cloned in pQE60 ( <i>NcoI</i> and <i>BglII</i> ).
pQE60 <i>panB wt</i> pQE60 <i>panB I202A</i> pQE60 <i>panB I212A</i>	Previous work. <sup>1-2</sup>
pQE40 <i>malE-rmhA wt</i>	Previous work. <sup>5-6</sup>
pQE40 <i>malE-rmhA W23V</i>	Previous work. <sup>7</sup>
pETDuet-1- <i>HBPA</i>	Previous work. <sup>3</sup>
pETDuet-1- <i>HBPA H205A</i>	Previous work. <sup>3</sup>

## Methods.

### Genes cloning.

The *dpka* gene (NCBI data base accession number DQ017704.1) was amplified from genomic DNA of *Pseudomonas syringae* van Hall 1902 (DSM No: 50315) using de primers: *dpka*<sub>*P*syrin</sub> (53) and *dpka*<sub>*P*syrin</sub> (35). The amplicon (1032 bp) was cloned in the into a pQE 60 plasmid with the restriction enzymes FastDigest™ *Nco*I and *Bg*III. All DNA manipulation were performed using routine procedures of molecular biology according to the manufacturer's protocols (Sequence S01 and Sequence S02).

**SEQUENCE S01.** Base sequence of the *dpka* gene(blue) insert into a pQE-60.

*Nco*I

```
CCATGGATGGGCATGTCCGCCAGCCACGCTGACCAGCCCACTCAAACCGTTTCTTACCCGCAACTGATCGACCTGCTG
CGCCGGATTTTCGTGGTCCACGGGACCTCACGGAGGTCGCCGATGTACTCGCTGAAAACCTGCGCCAGTGCCACGCG
CGACGGTTCGCACAGTCATGGCATCTTTCGCATTCCCGGCTATCTGTCTTCGTTGGCCAGCGGTTGGGTGGATGGCAA
GGCGGTGCCGGTGGTCGAGGATGTCCGGCGCGCATTTGTCAAGGTCGATGCTTGCAACGGCTTTCGCCAGCCGGCAC
TGGCGGCGGCCAGGTCAGTGTGATCGATAAGGCGCGCAGTGCCGGGGTTGCGATTCTGGCCATTCGGGGCTCGCAT
CATTTCGCCGCGCTGTGGCCAGATGTGCAACCGTTTGCCGAGCAGGGGCTGGTTGCGCTGAGCATGGTCAACAGCAT
GACCTGCGTGTACCCACGGGTGCTCGGCAGCCCTTGTTCGGCACCAACCCGATCGCCTTCGGTGCGCCGCGCGCAGG
TGGCGAGCCCATCGTTTTTGACCTGGCCACCAGCGCCATTGCCACGGTGACGTGACAGATTGCTGCGCGTGAAGGGC
GGTTGCTGCCGGCGGGCATGGGTGTTGATCGTGACGGGCTGCCGACGCAGGAGCCTCGCGCCATTCTCGACGGCGGG
GCGCTGTTGCCGTTCCGGCGGCACAAGGGCTCGGCATTGTGCGATGATGGTCGAGTTGCTGGCGGCAGGGCTGACCGG
TGGCAATTTCTCGTTCGAGTTCGACTGGTTCGAAGCATCCCGGCGCACAGACGCCCTGGACCGGCCAGTTGCTGATCGT
CATTGATCCCGACAAAGGTGCCGGTCCAGCACTTTCGCGAGCGCAGCGAGGAAGTGGTGCGCCAGCTTACAGGGGTCG
GCCAGGAACGATTGCCCGCGACAGGGGTTACCTGGAGCGGGCACGCTCGATGGCGCACGGAATAGTCATTGCCAG
GCCGACCTTGAGCGTTTGCAAGAGCTGGCAGGCCACAGATCTCATCACCATCACCATCACTAA
```

*Bg*III

**SEQUENCE S02.** Amino acid sequence of protein construct. Starting methionine incorporated by open reading frame in pQE-60,  $\Delta$ 1-pyrroline-2-carboxylate reductase (*DpkA*<sub>*P*syrin</sub>, EC 1.5.1.21) and 6x His tag (red).

```
MGMSASHADQPTQTVSYPQLIDLLRRIFVVHGTSPEVADVLAENCASAQRDGS
HSHGIFRIPGYLSSLASGWVDGKAVPVVEDVGAFFVRVDACNGFAQPALAAAR
SLLIDKARSAGVAILAIRGSHHFAALWPDVEPFQGLVALSMVNSMTCVVPH
GARQPLFGTNPFIAGAPRAGGEPVFDLATSIAIHGDVQIAAREGRLLPAGMGV
DRDGLPTQEPRAILDGGALLPFGGHKGSALSMMVELLAAGLTGGNFSFEFDWS
KHPGAQTPWTGQLLIVIDPKGAGQHFAQRSEELVRQLHGVGQERLPGDRRYL
ERARSMAGVIAQADLERLQELAGHRSHHHHHH*
```

The *panE* gene (NCBI data base accession number CP015085.1) was amplified from genomic DNA of *E. coli* K-12 using de primers: *panE*<sub>*E*coli</sub> (53) and *panE*<sub>*E*coli</sub> (35). The amplicon (912 bp) was cloned into a pQE-40 plasmid with the restriction enzymes FastDigest™ *Bam*HI and *Hind*III. All DNA manipulation were performed using routine procedures of molecular biology according to the manufacturer's protocols (Sequence S03 and Sequence S04).

### SEQUENCE S03. Bases sequence of the *panE* gene (blue) insert in pQE-40

*Bam*HI

ATGAGAGGATCGCATCACCATCACCATCACGGATCCATGAAAATTACCGTATTGGGATGCGGTGCCTTAGGGCAATT  
ATGGCTTACAGCACTTTGTAACACAGGGTCACGCGTTTCAGGGCTGGCTGCGCGTACCGCCAACCTTATTGTAGTGTGAA  
TCTGGTTGAGACAGATGGTTCGATATTTAATGAATCGCTGACCGCCAACGATCCCGATTTTCTGCCACCAGCGATCT  
GCTCCTGGTGACGCTGAAAGCATGGCAGGTTTCCGATGCCGTCAAAGCCTCGCGTCCACACTGCCTGTAACCACGC  
CAATACTGTTAATTCACAACGGCATGGGCACCATCGAAGAGTTGCAAAACATTTCAGCAGCCATTACTGATGGGCACC  
ACCACCCATGCCGCCCGCCGCGACGGCAATGTCATTATTCATGTGGCAAACGGTATCACGCATATTGGTCCGGCACG  
GCAAACAGGACGGCGATTACAGTTATCTGGCGGATATTTGCAAACCGTATTGCCTGACGTGCGGTGGCATAACAATA  
TTCGCGCCGAGCTGTGGCGCAAGCTGGCAGTCAACTGTGTGATTAATCCACTGACCGCCATCTGGAATTGCCCGAATG  
GTGAATTACGTCATCATCCGCAAGAAATTATGCAGATATGCGAAGAAGTCGCGGCAGTGATCGAACCGGAAGGGCAT  
CATACTCAGCAGAAGATTTGCGTGATTACGTGATGCAGGTGATTGATGCAACAGCGGAAATATCTCGTCGATGTT  
GCAGGATATCCGCGCGCTGCGCCACCCGAAATCGACTATATCAATGGTTTTCTTTACGCCGCGCCCGCGCGCATGG  
GATTGCCGTACCGGAAAACACCCGCTGTTTGAATGGTAAAAAGAAAGGAGAGTGAATATGAGCGCATCGGCACT  
GGTTTGCCTCGCCCCTGGTAGAAGCTT

*Hind*III

**SEQUENCE S04.** Amino acid sequence of protein construct. Starting methionine incorporated by the open reading frame in pQE-40, ketopantoate reductase ( $KPR_{Ecoli}$ , EC 1.1.1.169, blue) and 6x His tag (red).

MRGSHHHHHHGS MKITVLGCGALGQLWLTALCKQGH DVQGWLRVPQPYCSV  
NLVETDGSIFNESLTANDPDLFATS DLLLVTLKAWQVSDAVKSLASTLPVTTPI  
LIHNGMG TIEELQNIQQPLLMGTTTHAARRDGNVHHVANGITHIGPARQQDGD  
YSYLADILQTVLPDVAWHNNIRAE LWRKLA VNCVINPLTAIWNCPNGELRHHP  
QEIMQICEEVA AVIEREGHHTSAEDLRDYVMQVIDATAENISSMLQDIRALRHT  
EIDYINGFLLRRARAHGIAVPENTRLFEMVKRKESEYERIGTGLPRPW\*

### Protein production and purification.

**General procedure for  $DpkA_{Psynin}$  and  $KPR_{Ecoli}$ :** Home-made chemically competent cells (*E. coli* M-15[pREP-4] strain from QIAGEN)<sup>8</sup> were transformed with the corresponding plasmid and grown in LB plate with ampicillin ( $100 \mu\text{g mL}^{-1}$ ) plus kanamycin ( $25 \mu\text{g mL}^{-1}$ ) at  $37^\circ\text{C}$  overnight. A bacterial plaque scraping was transferred into a baffled shaker flask (100 mL) containing LB medium (30 mL) plus ampicillin ( $100 \mu\text{g mL}^{-1}$ ) and kanamycin ( $25 \mu\text{g mL}^{-1}$ ), and grown at  $37^\circ\text{C}$  on a rotary shaker at 200 rpm overnight ( $OD_{600} \approx 2-3$  after the growth). An aliquot of the pre-culture (20 mL) was transferred into a baffled shaker flask (2 L) containing LB medium (1 L) plus ampicillin ( $100 \mu\text{g mL}^{-1}$ ), kanamycin ( $25 \mu\text{g mL}^{-1}$ ) and antifoam SE-15 (0.02% v/v). The culture was incubated at  $37^\circ\text{C}$  with shaking at 200 rpm. During the middle exponential phase growth ( $DO_{600} \approx 0.5-0.8$ ), the temperature was lowered and proteins expression were induced with IPTG (1 mM). After 12-16 h, the culture (5 L) were centrifuged ( $2500 g$  for 45 min at  $4^\circ\text{C}$ ) and the pellet of cells (16-22 g) was re-suspended in the lysis buffer (400 mL, 50 mM  $\text{NaH}_2\text{PO}_4$  buffer pH 8.0, 300 mM NaCl, and 10 mM imidazole). Cells were lysed using a cell disrupter (Constant Systems) and cellular debris were removed by centrifugation ( $35000 g$  for 45 min at  $4^\circ\text{C}$ ). The clear supernatant was applied to a cooled HR 16/40 column (Cytiva<sup>TM</sup>) packed with Nickel

Sepharose™ High Performance (50 mL bed volume, Cytiva™) at 3 mL min<sup>-1</sup> and washed with lysis buffer (400 mL) at 6 mL min<sup>-1</sup>. The protein was eluted with elution buffer (200 mL, 50 mM NaH<sub>2</sub>PO<sub>4</sub> buffer pH 8.0, 300 mM NaCl, and 500 mM imidazole) at a flow rate of 6 mL min<sup>-1</sup> (Figure S1A and B). The purified protein was dialyzed against dialysis buffer (3x1 L 24 h each, 20 mM TEA buffer pH 6.5, 100 mM NaCl, and 50% (v/v) of glycerol). The dialyzed solution obtained (95-135 mL) was stored at -20 °C. Protein concentrations were determined by absorption at 280 nm using extinction coefficients calculated by ProtParam (<https://web.expasy.org/protparam/>), DpkA<sub>*P\_syrin*</sub> (Abs 0.1% (= 1 g L<sup>-1</sup>) 0.709), and KPR<sub>*E\_coli*</sub> (Abs 0.1% (= 1 g L<sup>-1</sup>) 1.35) assuming all Cys residues are reduced (Table S3).

**General procedure for GDH:** The enzyme, provided by Prozomix Ltd (PRO-GDH(001)) as a cell free extract powder (6 g), was re-suspended in the lysis buffer (400 mL, 50 mM NaH<sub>2</sub>PO<sub>4</sub> buffer pH 8.0, 300 mM NaCl, and 10 mM imidazole). Cellular debris was removed by centrifugation (35000 g for 45 min at 4 °C). The enzyme was purified following the protocol indicated above (Figure S1C) The purified protein was dialyzed against dialysis buffer (3x1 L 24 h each, 10 mM HEPES buffer pH 6.5, 100 mM NaCl, and 50% (v/v) of glycerol). The dialyzed solution obtained (90-120 mL) was stored at -20 °C. Protein concentration was determined using Pierce® 660 nm Protein Assay Reagent (Thermo Scientific) in 96 wells plate according to the manufacturer's protocols (Table S3).

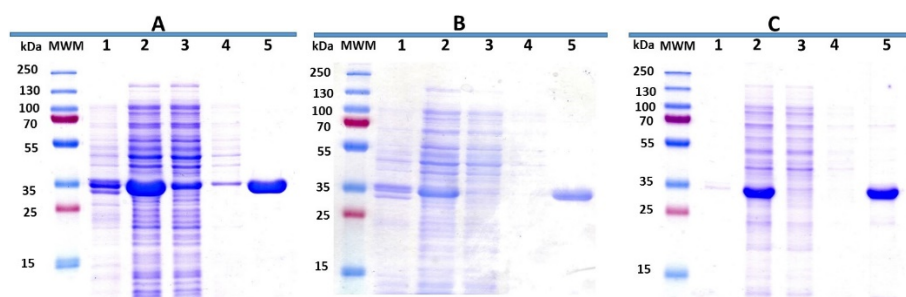


**Figure S1:** Analysis of enzyme purification steps by Coomassie Blue-stained SDS-PAGE. DpkA<sub>*P\_syrin*</sub> (A), KPR<sub>*E\_coli*</sub> (B), GDH (C). In each case, the gel was loaded with samples from pellet after lysis (lane 1), supernatant of lysis (lane 2), flow-through fraction (lane 3), wash fraction (lane 4) and elution fraction (lane 5). The molecular masses of the proteins in the Standard Molecular Weight Marker are as indicated. The predicted molecular mass of DpkA<sub>*P\_syrin*</sub> and KPR<sub>*E\_coli*</sub> are 37.6 kDa and 35.3 kDa respectively.

General procedure for YfaU<sub>Ecoli</sub>, HBPA<sub>Pputida</sub> and KPHMT<sub>Ecoli</sub> expression and purification were performed as describe in previous works <sup>1,3,5</sup>

**Table S3. Typical enzyme concentration obtained in this work.**

Enzymes	Concentration/ mg mL <sup>-1</sup>
KPHMT <sub>Ecoli</sub> wt	9.3
KPHMT <sub>Ecoli</sub> I202A	7.7
KPHMT <sub>Ecoli</sub> I212A	8.5
MBP-YfaU <sub>Ecoli</sub> wt	0.5 <sup>a</sup>
MBP-YfaU <sub>Ecoli</sub> W23V	0.5 <sup>a</sup>
HBPA <sub>Pputida</sub>	4.0 (0.029 U mL <sup>-1</sup> U mL <sup>-1</sup> ) <sup>b</sup>
HBPA <sub>Pputida</sub> H205A	3.8 (0.009 U mL <sup>-1</sup> U mL <sup>-1</sup> ) <sup>b</sup>
DpkA <sub>Psyrin</sub>	4.0 (2.6 10 <sup>-2</sup> U mL <sup>-1</sup> ) <sup>c</sup>
KPR <sub>Ecoli</sub>	4.0 (52 U mL <sup>-1</sup> ) <sup>c</sup>
GDH	5.2 (20.8 U mL <sup>-1</sup> ) <sup>c</sup>

<sup>a</sup>mg protein mL<sup>-1</sup> lyophilized powder. <sup>b</sup>Enzyme activity assays were described in previous work<sup>3</sup>. <sup>c</sup>Enzyme activity assays are described below

### Thin layer chromatography (TLC) analysis.

TLC analysis was performed using precoated silica gel plates with or without fluorescent indicator UV254 (Macherey-Nagel GmbH & Co. KG, Kieselgel 60). TLC without fluorescent visualization was stained using ceric ammonium molybdate or potassium permanganate.

### Specific rotation.

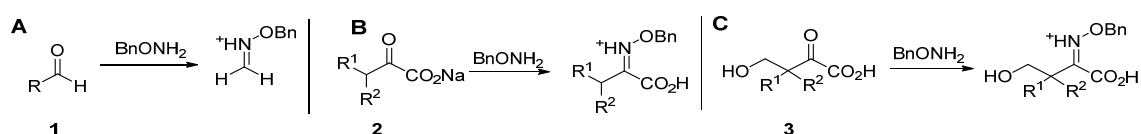
Specific rotation values were measured with a Perkin Elmer Model 341 (Überlingen, Germany) (Na Lamp, 589 nm). Products (5 to 20 mg) were dissolved in MeOH (1.5 mL) and the samples were analyzed at room temperature 1.0 dm cell with polarized light (Na D line 589 nm) at 25 °C. Rotation values are described in each compound.

### HPLC analysis.

a) HPLC analysis was performed on a RP-HPLC XBridge® C18, 5 μm, 4.6 × 250 mm column (Waters). The solvent system used was: solvent (A): 0.1% (v/v)

trifluoroacetic acid (TFA) in H<sub>2</sub>O and solvent (B): 0.095% (v/v) TFA in CH<sub>3</sub>CN/H<sub>2</sub>O 4:1, flow rate 1 mL min<sup>-1</sup>, detection at 215 nm and column temperature at 30 °C.

The amount of substrates and products were quantified from the peak areas using an external standard methodology. Reaction monitoring for formaldehyde (**1**), ketoacids (**2**) and aldol adduct (**3**) (**Scheme S1**) were carried out as follows: samples were withdrawn from the reaction mixture (10 μL) and mixed with a solution of BnONH<sub>2</sub> (50 μL of a 0.13 M stock solution in pyridine:methanol:water 33:15:2), and then diluted with methanol (500 μL). After centrifugation, samples were analyzed by HPLC. Elution conditions: gradient from 10 to 100% B over 30 min (reaction with compounds **2a-l**) and 10 to 100% B over 60 min (reaction with compounds **2m, n**).



Area = 10<sup>6</sup> C(1a/mM), R<sup>2</sup>=0.99, λ = 215nm Area = 10<sup>6</sup> C(2a/mM), R<sup>2</sup>=0.99, λ = 215nm

**Scheme S1.** Pre-column derivatization of substrates (**A** and **B**) and products (**C**) bearing carbonyl groups with *O*-benzylhydroxylamine.

**b)** Enantiomeric excesses were analyzed by HPLC on a CHIRALPAK<sup>®</sup> ID, column (46 x 250 mm, 5 μm). The solvent system used was: solvent (A): Hexane and solvent (B): Isopropanol, detection by diode array detection (215-350 nm) and column temperature at 30 °C.

### NMR analysis.

Routine <sup>1</sup>H (400 MHz) and <sup>13</sup>C (101 MHz) NMR spectra of compounds were recorded with a Varian Mercury-400 spectrometer. Full characterization of the described compounds was performed using typical gradient-enhanced 2D experiments: COSY, HSQC, NOESY and HMBC recorded under routine conditions.

### Activity determination of DpkA<sub>Psyrin</sub>.

The ketoreductase activity of the DpkA<sub>Psyrin</sub> was determined in a continuous assay method monitoring the oxidation of NADPH to NADP<sup>+</sup> at 340 nm (NADPH ε<sub>340</sub> = 6.22 mM<sup>-1</sup> cm<sup>-1</sup>) using sodium pyruvate as substrate. The reactions were monitored during 15 min measuring each 30 s. The assay mixture (0.3 mL) consisted of 50 mM Tris-HCl



buffer pH 8.0, containing NADPH (0.16 mM), sodium pyruvate (40 mM) and appropriate amounts of enzyme (0.19 mg mL<sup>-1</sup> to 3.0 mg mL<sup>-1</sup>). One unit of activity was defined as the amount of DpkA<sub>Psyrin</sub> that catalyzes the formation of 1 μmol NADP<sup>+</sup> per min at 30 °C (Figure S2). Units: 6.5 10<sup>-3</sup> U mg<sup>-1</sup>.

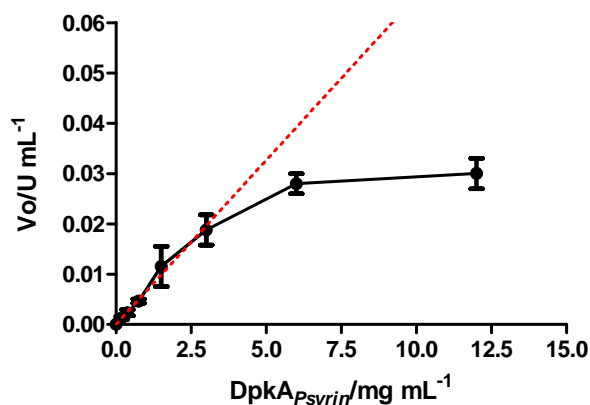


**Figure S2.** Variation of the ketoreductase activity of the DpkA<sub>Psyrin</sub> with the enzyme concentrations. Enzymatic specific activity (typically 6.5 10<sup>-3</sup> U mg<sup>-1</sup>) was calculated as the slope of the plot of V<sub>0</sub> vs. [DpkA<sub>Psyrin</sub>] in the linear region. One unit of activity was defined as the amount of DpkA<sub>Psyrin</sub> that catalyzes the formation of 1 μmol NADP<sup>+</sup> per min at 30 °C.

#### Activity determination of KPR<sub>Ecoli</sub>.

The ketoreductase activity of the KPR<sub>Ecoli</sub> was determined in a continuous assay method monitoring the oxidation of NADPH to NADP<sup>+</sup> at 340 nm (NADPH ε<sub>340</sub> = 6.22 mM<sup>-1</sup> cm<sup>-1</sup>) using sodium 4-hydroxy-3,3-dimethyl-2-oxobutanoate as substrate (synthesized as described below). The reactions were monitored during 15 min measuring each 30 s. The assay mixture (0.3 mL) consisted of 50 mM Tris-HCl buffer pH 8.0, containing NADPH (0.16 mM), sodium 4-hydroxy-3,3-dimethyl-2-oxobutanoate (50 mM) and appropriate amounts of enzyme (0.48 μg mL<sup>-1</sup> to 7.81 μg mL<sup>-1</sup>). One unit of activity was defined as the amount of KPR<sub>Ecoli</sub> that catalyzes the formation of 1 μmol NADP<sup>+</sup> per min at 30 °C (Figure S3). Units: 13 U mg<sup>-1</sup>.

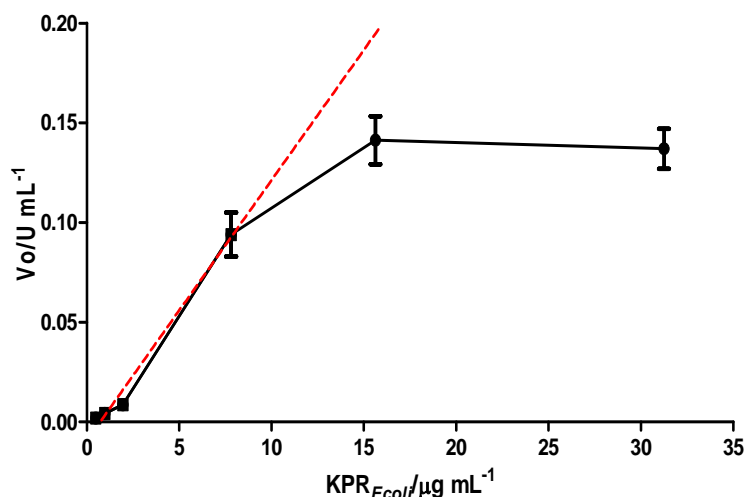


**Figure S3.** Variation of the ketoreductase activity of the KPR<sub>Ecoli</sub> with the enzyme concentrations. Enzymatic specific activity (typically 13 U mg<sup>-1</sup>) was calculated as the slope of the plot of  $V_0$  vs. [KPR<sub>Ecoli</sub>] in the linear region. One unit of activity was defined as the amount of KPR<sub>Ecoli</sub> that catalyzes the formation of 1 μmol NADP<sup>+</sup> per min at 30 °C.

#### Activity determination of glucose dehydrogenase (GDH).

The dehydrogenase activity of the purified GDH (PRO-GDH (001)) was determined in a continuous assay method monitoring the reduction of NADP<sup>+</sup> to NADPH at 340 nm (NADPH  $\epsilon_{340} = 6.22 \text{ mM}^{-1} \text{ cm}^{-1}$ ) using glucose as substrate. The reactions were monitored during 15 min measuring each 30 s. The assay mixture (0.3 mL) consisted of 100 mM Tris-HCl buffer pH 8.0, containing NADP<sup>+</sup> (0.25 mM), glucose (30 mM) and appropriate amounts of enzyme (1.9 μg mL<sup>-1</sup> to 62.5 μg mL<sup>-1</sup>). One unit of activity was defined as the amount of GDH that catalyzes the formation of 1 μmol NADPH per min at 30 °C (Figure S4). Units: 4 U mg<sup>-1</sup>.

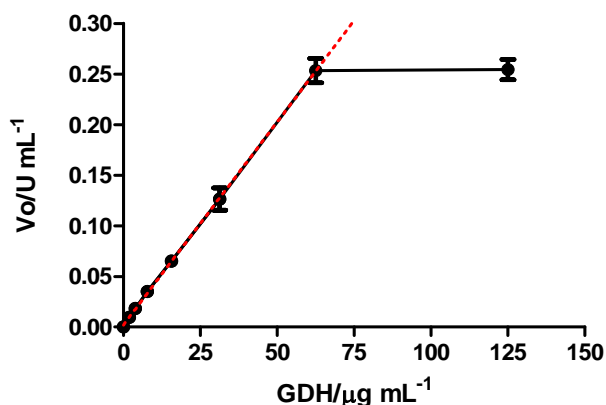
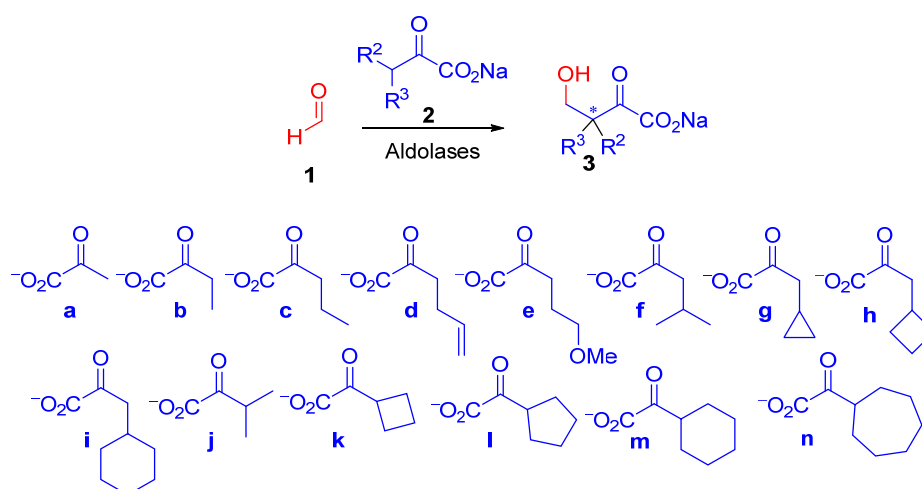


**Figure S4.** Variation of the dehydrogenase activity of the GDH with the enzyme concentrations. Enzymatic specific activity (typically 4 U mg<sup>-1</sup>) was calculated as the slope of the plot of  $V_0$  vs. [GDH] in the linear region. One unit of activity was defined as the amount of GDH that catalyzes the formation of 1 μmol NADPH per min at 30 °C.

#### Biocatalytic aldol addition of 2-oxoacid (2) to formaldehyde (1). Analytical scale



**Scheme S2.** Biocatalytic aldol addition of 2-oxoacids (**2a-n**) to formaldehyde (**1a**) catalyzed by YfaU<sub>Ecoli</sub> and KPHMT<sub>Ecoli</sub>.

#### Aldol addition of 2a-i to 1<sup>9</sup> catalyzed by S-stereoselective YfaU<sub>Ecoli</sub> wt and YfaU<sub>Ecoli</sub> W23V.

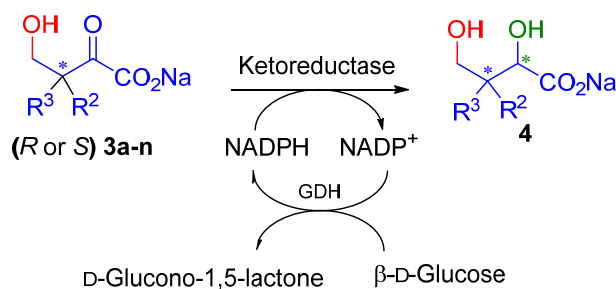
Reactions were carried out at analytic level as follows: The reactions (500 μL total volume) were conducted in Eppendorf tubes (1.5 mL) and placed in a vortex mixer (100 rpm) at 25°C. To a solution of YfaU<sub>Ecoli</sub> wt or YfaU<sub>Ecoli</sub> W23V enzymes (4 mg of lyophilized powder at 0.5 mg protein mg<sup>-1</sup> lyophilized powder, 2 mg of protein, 2 mg protein mL<sup>-1</sup> final concentration in the reaction,) in plain water, NiCl<sub>2</sub> (5 μL of a 0.1 M

stock solution in water, 1 mM in the reaction), and the 2-oxoacids (**2a-i**, 0.5-2 M stock solution in water pH 7.0, 1 mmol, 1 eq, 0.1 M in the reaction) were added. Reactions were started by adding formaldehyde (**1a**, 50  $\mu\text{L}$  of a 1 M in water solution, 1 eq, 0.1 M in the reaction). Samples were withdrawn immediately after the addition of formaldehyde (0 h) and at 24 h and analyzed by HPLC as described above.

**Aldol addition of 2a-n to 1<sup>9-10</sup> catalyzed by R-stereoselective KPHMT<sub>Ecoli</sub> and variants.**

Reactions were carried out at analytic level as follows: The reactions (500  $\mu\text{L}$  total volume) were conducted in Eppendorf tubes (1.5 mL) and placed in a vortex mixer (100 rpm) at 25°C. To a solution of KPHMT<sub>Ecoli</sub> wt or variants (1 mg protein mL<sup>-1</sup> in the reaction, from a protein stock solutions in 20 mM TEA buffer pH 7.0, 100 mM NaCl, and 50% (v/v) of glycerol) in plain water, CoCl<sub>2</sub> (5  $\mu\text{L}$  of a 0.1 M stock solution, 1 mM in the reaction), and the 2-oxoacids (**2a-n**, 0.5-2 M stock solution in water pH 7.0, 1 mmol, 1 eq, 0.1 M in the reaction) were added. The reaction was started by adding formaldehyde (**2**, 50  $\mu\text{L}$  of a 1 M in water solution, 1 eq, 0.1 M in the reaction). Samples were withdrawn immediately after the formaldehyde addition (0 h) and after 24 h and analyzed by HPLC as described above.

**Biocatalytic reduction of 4-hydroxy-2-oxoacids (3a-n). Substrate scope of ketoreductases. Analytical scale.**

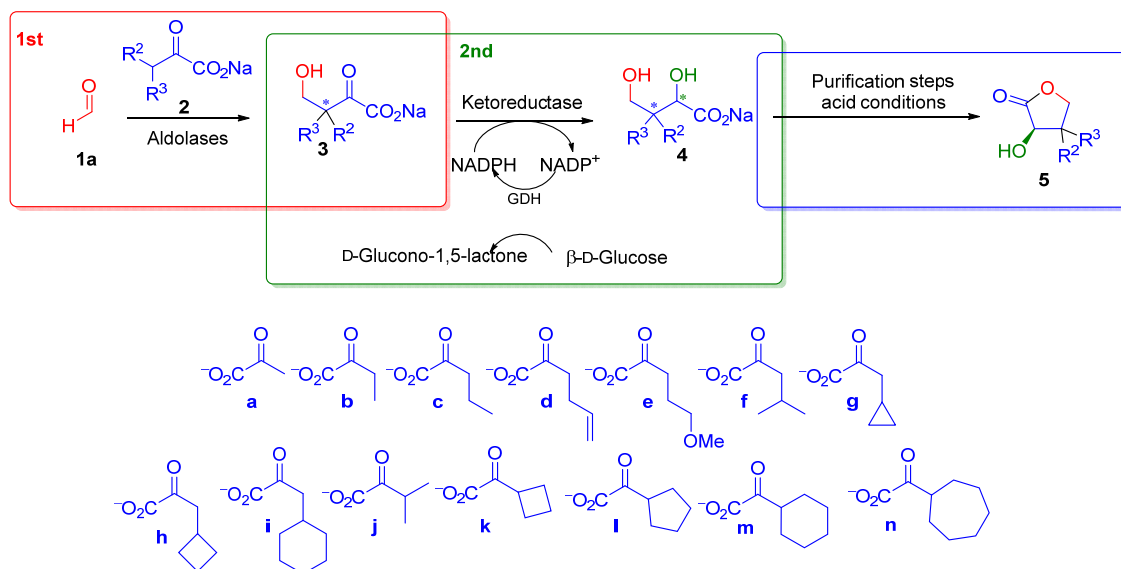


**Scheme S3.** Biocatalytic reduction of aldol adducts (*R* or *S*) **3a-n** catalyzed by DpkA<sub>Psyrin</sub> and KPR<sub>Ecoli</sub>.

**Biocatalytic reduction catalyzed by KPR<sub>Ecoli</sub> or DpkA<sub>Psyrin</sub>:** Reactions were carried out at analytic level as follows: The reactions (500  $\mu\text{L}$  total volume) were conducted in Eppendorf tubes (1.5 mL) and placed in a vortex mixer (100 rpm) at 25 °C. The reduction mixture solutions (250  $\mu\text{L}$ ) were prepared by adding; KPR<sub>Ecoli</sub> (125  $\mu\text{L}$  of a

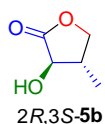
stock solution of 52 U mL<sup>-1</sup>, 4 mg mL<sup>-1</sup> in 20 mM TEA buffer pH 7.0, 100 mM NaCl, and 50% (v/v) of glycerol, 13 U mL<sup>-1</sup> final concentration in the reaction) or DpkA<sub>Psyrin</sub> (125 μL of a stock solution of 2.6 10<sup>-2</sup> U mL<sup>-1</sup>, 4 mg mL<sup>-1</sup> in 20 mM TEA buffer pH 7.0, 100 mM NaCl, and 50% (v/v) of glycerol, 6.5 10<sup>-3</sup> U mL<sup>-1</sup> final concentration in the reaction), EDTA (5 μL of a 0.5M stock solution in 20 mM TEA buffer pH 8.0, 5 mM final concentration in the reaction), GDH (83 μL of a stock solution 20.8 U mL<sup>-1</sup>, 5.2 mg mL<sup>-1</sup> in 10 mM HEPES buffer pH 6.5, 50 mM NaCl, and 50% (v/v) of glycerol, 3.5 U mL<sup>-1</sup> final concentration in the reaction), glucose (18 mg, 4 eq, 0.2 M final concentration in reaction) and NADP<sup>+</sup> (1.9 mg, 5 mM in reaction). The reactions were started by the addition of a sample of the corresponding aldol reaction (250 μL), containing adducts **3a-n** (≈ 100 mM as the basis of calculation) (Scheme S3). Samples were withdrawn immediately after the addition of aldol substrate (0 h) and after 24 h and analyzed by HPLC as described above.

### One-pot two-step stereoselective synthesis of 2-hydroxy-4-butyrolactone derivatives (**5**).



**Scheme S4.** One-pot two-step stereoselective synthesis of 2-hydroxy-4-butyrolactones derivatives (**5**) combining aldolases (YfaU<sub>Ecoli</sub> and KPHMT<sub>Ecoli</sub>) and ketoreductases (DpkA<sub>Psyrin</sub> and KPR<sub>Ecoli</sub>).

The reactions combining YfaU<sub>Ecoli</sub> and KPR<sub>Ecoli</sub> were carried out as follows:

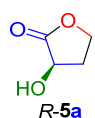


Synthesis of (2*R*,3*S*)-3-methyl-2-hydroxy-4-butyrolactone (2*R*,3*S*-**5b**). Typical procedure (Scheme S4): **Aldol addition (1<sup>st</sup>)**: The reaction (1 mmol scale, 10 mL total volume) was conducted in a round-bottom flask (100 mL) at 25 °C and magnetically stirred with a bar at 250 rpm. To a solution of YfaU<sub>Ecoli</sub> wt (60 mg of lyophilized powder at 0.5 mg protein mg<sup>-1</sup> lyophilized powder, 30 mg of protein, 3 mg protein mL<sup>-1</sup> final concentration in the reaction) in plain water (4 mL), 2-oxobutyric acid (**2b**) (1 mL of a 1 M stock solution in water pH 7.0, 1 mmol, 1 eq, 0.1 M in the reaction) and NiCl<sub>2</sub> (100 μL of a 0.1 M stock solution in water, 10 μmol, 1 mM in the reaction) were added. The reaction was started by adding formaldehyde (**1a**, 1 mL of a 1 M stock solution in water, 1 mmol, 1 eq, 0.1 M in the reaction). The reaction was monitored by HPLC as described in the analytical scale reactions.

**Aldol reduction (2<sup>nd</sup>)**. After 24h, the reduction reaction (20 mL final volume) was carried out adding EDTA (200 μL, of 0.5 M stock solution in 50 mM TEA buffer pH 8.0, 5 mM in the reaction), glucose (721 mg, 4.0 mmol, 4 eq, 0.2 M final concentration in the reaction), GDH (3.30 mL of a stock solution 20.8 U mL<sup>-1</sup>, 5.2 mg mL<sup>-1</sup> in 10 mM HEPES buffer pH 6.5, 50 mM NaCl, and 50% (v/v) of glycerol, 3.4 U mL<sup>-1</sup> final concentration in the reaction), and KPR<sub>Ecoli</sub> (1.8 mL of a stock solution 52 U mL<sup>-1</sup>, 4 mg mL<sup>-1</sup> in 20 mM TEA buffer pH 7.0, 100 mM NaCl, and 50% (v/v) of glycerol, 4.7 U mL<sup>-1</sup> final concentration in the reaction). The reaction was started by adding a solution of NADP<sup>+</sup> (4.7 mL of stock solution 21 mM in 350 mM sodium phosphate buffer pH 8.0, 5 mM final concentration in the reaction). The mixture reaction was stirred at room temperature and the reaction was monitored by HPLC as described in the analytical scale reactions. After no aldol adduct was detected by HPLC (24 h), methanol (200 mL) was added under stirring. The mixture was filtered through Celite<sup>®</sup> and the filter cake washed with methanol (3 x 50 mL). The organic solvent was removed and the pH of the remaining aqueous solution was adjusted to 9.0 with 1 M NaOH. Then, water was added up to a final volume of 40 mL. The product purification was started with anion exchange chromatography (DOWEX 1X8 ion exchange resin (50-100 mesh) in HCO<sub>2</sub><sup>-</sup> form, column: 44 cm, Ø = 1,6 cm). The sample was loaded onto the column and the resin was washed with plain water (90 mL). The bound fractions with the compound were eluted with a solution of 1 M HCO<sub>2</sub>H (fraction volume 30 mL). Fractions containing the product were pooled freeze-dried, dissolved in methanol (30 mL), absorbed in silica and purified by column chromatography on silica with a step gradient

of hexane:EtOAc: 100:0, 200 mL, 75:25, 200 mL, 50:50, 200 mL and 25:75, 500 mL. Pure fractions were pooled and the solvent removed under vacuum affording the lactone **2R,3S-5b** as a yellow oil (43 mg, 45%). During the freeze drying under acid conditions the lactonization of the compound **4b** took place. <sup>1</sup>H NMR (400 MHz, D<sub>2</sub>O) δ 4.50 (dd, *J* = 9.0, 7.9 Hz, 1H), 4.23 (d, *J* = 11.1 Hz, 1H), 3.94 (dd, *J* = 10.8, 9.0 Hz, 1H), 2.61 – 2.46 (m, 1H), 1.20 (d, *J* = 6.6 Hz, 3H). <sup>13</sup>C NMR (101 MHz, D<sub>2</sub>O) δ 180.1, 73.3, 71.5, 38.5, 12.8. Selected NMR signals for the minor diastereomer: <sup>1</sup>H NMR (400 MHz, D<sub>2</sub>O) δ 4.42 (t, *J* = 8.5 Hz, 1H), 4.21 – 4.11 (m, 1H), 3.86 (dd, *J* = 10.8, 9.0 Hz, 1H), 2.51 – 2.35 (m, 1H), 1.12 (dd, *J* = 6.8, 1.6 Hz, 4H). <sup>13</sup>C NMR (101 MHz, D<sub>2</sub>O) δ 72.8, 69.9, 34.7, 10.9.  $[\alpha]_{20}^D = + 58.7$  (*c* = 1, in MeOH). ESI-TOF *m/z*: Calcd for [M+Na<sup>+</sup>] C<sub>5</sub>H<sub>8</sub>O<sub>3</sub>Na<sup>+</sup>:139.0366, found [M+Na<sup>+</sup>]: 139.0364.

#### (*R*)-2-hydroxy-4-butyrolactone (*R*-5a).



The title compound was prepared as described for **2R,3S-5b**. Starting from **2a** ([**2a**] = [**1a**] = 1 M in the reaction,  $V_{\text{aldol reaction}} = 1$  mL. The aldol reaction was diluted with plain water (9 mL) before starting the reduction reaction  $V_{\text{reduction reaction}} = 20$  mL), **R-5a** was obtained as a white solid (15 mg, 30%). In this case the product was eluted with a step gradient of Hexane:EtOAc: 100:0, 200 mL, 90:10, 200 mL, 80:20, 200 mL and 70:30, 500 mL on column chromatography on silica. <sup>1</sup>H NMR (400 MHz, CDCl<sub>3</sub>) δ 4.51 (dd, *J* = 11.5, 9.6 Hz, 1H), 4.44 (td, *J* = 2x9.0, 1.9 Hz, 1H), 4.23 (ddd, *J* = 10.5, 9.3, 6.0 Hz, 1H), 2.67 – 2.56 (m, 1H), 2.29 (dtd, *J* = 12.7, 2x10.4, 8.8 Hz, 1H). <sup>13</sup>C NMR (101 MHz, CDCl<sub>3</sub>) δ 178.0, 67.6, 65.3, 31.0. The NMR data matched that reported in the literature.<sup>11</sup>  $[\alpha]_{20}^D = + 34.1$  (*c* = 1, in MeOH), in our hands, commercial (*R*)-3-Hydroxydihydrofuran-2(3*H*)-one (Sigma Aldrich 444286). ee: ≥99% (see below),  $[\alpha]_{20}^D = + 34.8$  (*c* = 1, in MeOH). ESI-TOF *m/z*: Calcd for [M+Na<sup>+</sup>] C<sub>4</sub>H<sub>6</sub>NaO<sub>3</sub><sup>+</sup>:125.0209, found [M+Na<sup>+</sup>]: 125.0215.

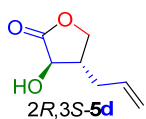
#### (2*R*,3*S*)-3-ethyl-2-hydroxy-4-butyrolactone (2*R*,3*S*-5c).



The title compound was prepared using YfaU<sub>Ecoli</sub> W23V variant with the procedure described for **2R,3S-5b**. Starting from **2c** ([**2c**] = [**1a**] = 100 mM), the major lactone **2R,3S-5c** was obtained as a yellow oil (57 mg, 44%). <sup>1</sup>H NMR (400 MHz, D<sub>2</sub>O) δ 4.55 (dd, *J* = 9.0, 8.1 Hz, 1H), 4.32 (d, *J* = 10.9 Hz, 1H), 4.00 (dd, *J* = 10.7, 9.1 Hz, 1H), 2.44 (tt, *J* = 2x10.8, 8.1, 8.0, 6.0 Hz, 1H),

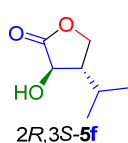
1.75 (ddd,  $J = 13.6, 7.6, 6.0$  Hz, 1H), 1.56 (dt,  $J = 13.7, 2 \times 7.6$  Hz, 1H), 0.97 (t,  $J = 2 \times 7.6$  Hz, 3H).  $^{13}\text{C}$  NMR (101 MHz,  $\text{D}_2\text{O}$ )  $\delta$  180.5, 72.1, 70.6, 44.7, 22.6, 10.5. Minor lactone key selected signals:  $^1\text{H}$  NMR (400 MHz,  $\text{D}_2\text{O}$ )  $\delta$  4.64 (d,  $J = 7.5$  Hz, 1H), 4.35 (m, 1H), 4.20 (d,  $J = 2.4$  Hz, 0H), 2.53 (dddd,  $J = 12.8, 7.4, 5.2, 2.4$  Hz, 1H), 1.22 (m, 1H).  $^{13}\text{C}$  NMR (101 MHz,  $\text{D}_2\text{O}$ )  $\delta$  69.3, 41.2, 18.2, 10.3.  $[\alpha]_{20}^{\text{D}} = +44.5$  ( $c = 1$ , in MeOH). ESI-TOF  $m/z$ : Calcd for  $[\text{2M}+\text{Na}^+]$   $\text{C}_{12}\text{H}_{20}\text{NaO}_6^+$ :283.1152, found  $[\text{2M}+\text{Na}^+]$ : 283.1165.

**(2*R*,3*S*)-3-Allyl-2-hydroxy-4-butyrolactone (2*R*,3*S*-5*d*).**



The title compound was prepared using YfaU<sub>Ecoli</sub> W23V variant with the procedure described for 2*R*,3*S*-5*b*. Starting from **2d** ( $[\text{2d}] = [\text{1a}] = 100$  mM), 2*R*,3*S*-5*d* was obtained as a yellow oil (41 mg, 29%).  $^1\text{H}$  NMR (400 MHz,  $\text{CDCl}_3$ )  $\delta$  5.96 – 5.62 (m, 1H), 5.20 – 5.08 (m, 2H), 4.42 (dd,  $J = 9.3, 7.7$  Hz, 1H), 4.14 (d,  $J = 10.0$  Hz, 1H), 3.87 (dd,  $J = 10.2, 9.3$  Hz, 1H), 2.65 – 2.50 (m, 2H), 2.26 (tdd,  $J = 9.4, 9.4, 7.3, 4.1$  Hz, 1H).  $^{13}\text{C}$  NMR (101 MHz,  $\text{CDCl}_3$ )  $\delta$  177.2, 133.5, 117.8, 71.8, 69.1, 43.0, 34.3. Selected NMR signals for the minor diastereomer:  $^1\text{H}$  NMR (400 MHz,  $\text{CDCl}_3$ )  $\delta$  4.45 (dd,  $J = 9.3, 7.7$  Hz, 1H), 4.16 (d,  $J = 10.0$  Hz, 1H), 3.90 (dd,  $J = 10.2, 9.2$  Hz, 1H), 2.36 – 2.22 (m, 1H).  $^{13}\text{C}$  NMR (101 MHz,  $\text{CDCl}_3$ )  $\delta$  133.7, 118.01, 72.0, 43.2, 34.5. The NMR data matched that reported in the literature.<sup>12</sup>  $[\alpha]_{20}^{\text{D}} = +3.8$  ( $c = 1$ , in MeOH). ESI-TOF  $m/z$ : Calcd for  $[\text{M}+\text{Na}^+]$   $\text{C}_7\text{H}_{10}\text{NaO}_3^+$ :165.0522, found  $[\text{M}+\text{Na}^+]$ : 165.0527.

**(2*R*,3*S*)-3-isopropyl-2-hydroxy-4-butyrolactone (2*R*,3*S*-5*f*).**

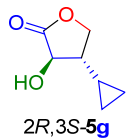


The title compound was prepared using YfaU<sub>Ecoli</sub> W23V variant with the procedure described for 2*R*,3*S*-5*b*. Starting from **2f** ( $[\text{2f}] = [\text{1a}] = 100$  mM), 2*R*,3*S*-5*f* was obtained as a white solid (36 mg, 25%). Major diastereomer (2*R*,3*S*-5*f*)  $^1\text{H}$  NMR (400 MHz,  $\text{CDCl}_3$ )  $\delta$  4.42 (dd,  $J = 9.2, 8.2$  Hz, 1H), 4.16 (d,  $J = 10.4$  Hz, 1H), 3.89 (dd,  $J = 10.6, 9.2$  Hz, 1H), 2.24 (tt,  $J = 2 \times 10.5, 2 \times 8.4$  Hz, 1H), 1.79 (dp,  $J = 8.6, 4 \times 6.7$  Hz, 1H), 1.11 (d,  $J = 6.7$  Hz, 3H), 0.95 (d,  $J = 6.7$  Hz, 3H).  $^{13}\text{C}$  NMR (101 MHz,  $\text{CDCl}_3$ )  $\delta$  178.2, 71.8, 68.9, 50.1, 30.9, 20.7, 20.2. Selected NMR signals for the minor diastereomer:  $^1\text{H}$  NMR (400 MHz,  $\text{CDCl}_3$ )  $\delta$  4.36 (dd,  $J = 9.2, 6.8$  Hz, 1H), 4.26 (dd,  $J = 9.3, 5.9$  Hz, 1H), 2.42 – 2.32 (m, 3H), 2.13 (q,  $J = 6.8$  Hz, 1H).  $^{13}\text{C}$  NMR (101 MHz,  $\text{CDCl}_3$ ) no signal detected. The NMR data matched that reported in the



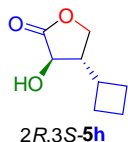
literature.<sup>13</sup>  $[\alpha]_{20}^D = + 31.4$  ( $c = 1$ , in MeOH). ESI-TOF  $m/z$ : Calcd for  $[M+Na^+]$   $C_7H_{12}NaO_3^+$ :167.0679, found  $[M+Na^+]$ : 167.0686.

#### (2*R*,2*S*)-3-Cyclopropyl--2-hydroxy-4-butyrolactone (2*R*,3*S*-5*g*).



The title compound was prepared using YfaU<sub>Ecoli</sub> W23V variant with the procedure described for 2*R*,3*S*-5*b*. Starting from **2g** ( $[2g] = [1a] = 100$  mM), 2*R*,3*S*-5*g* was obtained as a yellow oil (66 mg, 46%). <sup>1</sup>H NMR (400 MHz, CDCl<sub>3</sub>)  $\delta$  4.42 (dd,  $J = 9.2, 8.1$  Hz, 1H), 4.22 (dd,  $J = 10.4, 2.1$  Hz, 1H), 3.96 (dd,  $J = 10.5, 9.2$  Hz, 1H), 1.95 (tt,  $J = 2 \times 10.4, 2 \times 8.2$  Hz, 1H), 0.85 – 0.73 (m, 1H), 0.66 – 0.50 (m, 2H), 0.50 – 0.38 (m, 1H), 0.21 (dtd,  $J = 9.5, 5.6, 5.4, 4.5$  Hz, 1H). <sup>13</sup>C NMR (101 MHz, CDCl<sub>3</sub>)  $\delta$  177.6, 72.4, 69.2, 48.2, 10.5, 2.3 (d,  $J = 9.5$  Hz). Selected NMR signals for the minor diastereomer: <sup>1</sup>H NMR (400 MHz, CDCl<sub>3</sub>)  $\delta$  4.32 (dd,  $J = 9.3, 5.6$  Hz, 1H), 4.12 (d,  $J = 8.7$  Hz, 1H), 3.85 – 3.79 (m, 1H), 2.62 – 2.44 (m, 1H). <sup>13</sup>C NMR (101 MHz, CDCl<sub>3</sub>) No signals detected.  $[\alpha]_{20}^D = + 30.0$  ( $c = 1.3$  in MeOH). ESI-TOF  $m/z$ : Calcd for  $[2M+Na^+]$   $C_{14}H_{20}O_6Na^+$ :307.1152, found  $[2M+Na^+]$ : 307.1166.

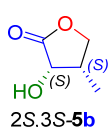
#### (2*R*,3*S*)-3-Cyclobutyl-2-hydroxy-4-butyrolactone (2*R*,3*S*-5*h*).



The title compound was prepared using YfaU<sub>Ecoli</sub> W23V variant with the procedure described 2*R*,3*S*-5*b*. Starting from **2h** ( $[2h] = [1a] = 100$  mM), 2*R*,3*S*-5*h* was obtained as a yellow oil (73 mg, 46%). <sup>1</sup>H NMR (400 MHz, CDCl<sub>3</sub>)  $\delta$  4.40 (dd,  $J = 9.1, 7.7$  Hz, 1H), 4.38 (dd,  $J = 10.0, 9.1$  Hz, 1H), 4.13 (dd,  $J = 9.7, 2.3$  Hz, 1H), 2.56 (ddd  $J = 10.0, 8.1, 2.0$  Hz, 1H), 2.51 (dd,  $J = 8.1, 2.3$  Hz, 1H), 2.14 – 1.97 (m, 2H), 2.09 – 1.83 (m, 2H), 1.83 – 1.79 (m, 2H). <sup>13</sup>C NMR (101 MHz, CDCl<sub>3</sub>)  $\delta$  177.9, 71.4, 68.1, 48.1, 36.0, 25.6 (d,  $J = 4.6$  Hz), 18.9. No other diastereomer was detected within the limits of detection by high-field <sup>1</sup>H and <sup>13</sup>C NMR ( $\leq 3\%$ ).  $[\alpha]_{20}^D = + 47.4$  ( $c = 1.2$ , in MeOH). ESI-TOF  $m/z$ : Calcd for  $[2M+Na^+]$   $C_{16}H_{24}O_6Na^+$ :335.1461, found  $[2M+Na^+]$ : 335.1451.

**The reactions combining YfaU<sub>Ecoli</sub> and DpkA<sub>Psyrin</sub> were carried out as follows:**

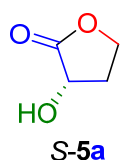
#### (2*S*,3*S*)-4-Methyl-2-hydroxy-4-butyrolactone (2*S*,3*S*-5*b*).



Synthesis of aldol intermediate 2*S*-3*b*, was performed as described for 2*R*,3*S*-5*b*, starting from **2b** ( $[2b] = [1a] = 100$  mM). After 24 h, the reduction

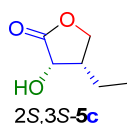
reaction (20 mL final volume) was carried out as follows: to the aldol reaction mixture were added EDTA (200  $\mu\text{L}$ , of 0.5 M stock solution in 50 mM TEA buffer pH 8.0, 5 mM in the reaction), glucose (721 mg, 4 mmol, 4 eq, 0.2 M final concentration in the reaction), GDH (3.30 mL of a stock solution 20.8 U  $\text{mL}^{-1}$ , 5.2 mg  $\text{mL}^{-1}$  in 10 mM HEPES buffer pH 6.5, 50 mM NaCl, and 50% (v/v) of glycerol, 3.4 U  $\text{mL}^{-1}$  final concentration in the reaction) and DpkA<sub>Psyrin</sub> (5.0 mL of a stock solution 2.6  $10^{-2}$  U  $\text{mL}^{-1}$ , 4 mg  $\text{mL}^{-1}$  in 20 mM TEA buffer pH 7.0, 100 mM NaCl, and 50% (v/v) of glycerol, 6.5  $10^{-3}$  U  $\text{mL}^{-1}$  final concentration in the reaction). The reaction was started by adding a solution of NADP<sup>+</sup> (1.5 mL of stock solution 67 mM in 1 M sodium phosphate buffer pH 8.0, 5 mM final concentration in the reaction). The purification was performed as described for 2*R*,3*S*-**5b** and lactone 2*S*,3*S*-**5b** was obtained as a yellow oil (40 mg, 35%). <sup>1</sup>H NMR (400 MHz, D<sub>2</sub>O)  $\delta$  4.74 (d,  $J = 7.2$  Hz, 1H), 4.47 (dd,  $J = 9.3, 5.3$  Hz, 1H), 4.16 (dd,  $J = 9.3, 1.7$  Hz, 1H), 2.95 – 2.67 (m, 1H), 1.05 (dd,  $J = 7.2, 1.7$  Hz, 3H). <sup>13</sup>C NMR (101 MHz, D<sub>2</sub>O)  $\delta$  179.8, 72.8, 69.9, 34.7, 10.9. Minor diastereoisomer key selected signals: <sup>1</sup>H NMR (400 MHz, D<sub>2</sub>O)  $\delta$  3.86 (dd,  $J = 10.7, 9.0$  Hz, 1H), 2.50 – 2.39 (m, 1H), 1.12 (d,  $J = 6.7$  Hz, 3H). <sup>13</sup>C NMR (101 MHz, D<sub>2</sub>O)  $\delta$  71.5, 38.5, 12.8.  $[\alpha]_{20}^{\text{D}} = + 30.9$  ( $c = 1$ , in MeOH). ESI-TOF  $m/z$ : Calcd for  $[\text{M}+\text{Na}^+]$  C<sub>5</sub>H<sub>8</sub>O<sub>3</sub>Na<sup>+</sup>:139.0366, found  $[\text{M}+\text{Na}^+]$ : 139.0359.

#### (*S*)-2-Hydroxy-4-butyrolactone (*S*-**5a**).



The title compound was prepared as described for 2*S*,3*S*-**5b**. Starting from **2a** ( $[\mathbf{2a}] = [\mathbf{1a}] = 1$  M in the reaction,  $V_{\text{aldol reaction}} = 1$  mL. The aldol reaction was diluted with plain water (9 mL) before starting the reduction reaction,  $V_{\text{reduction reaction}} = 20$  mL). The purification was performed as described for *R*-**5a**, and the title compound *S*-**5a** was obtained as a yellow oil (20 mg, 20%). NMR spectra were indistinguishable from that of *R*-**5a**.  $[\alpha]_{20}^{\text{D}} = - 23.3$  ( $c = 1$ , in MeOH). In our hands, commercial (*R*)-3-hydroxydihydrofuran-2(3*H*)-one (Sigma Aldrich 444286). ee:  $\geq 99\%$  (see below),  $[\alpha]_{20}^{\text{D}} = + 35$  ( $c = 1$ , in MeOH). ESI-TOF  $m/z$ : Calcd for  $[\text{M}+\text{Na}^+]$  C<sub>4</sub>H<sub>6</sub>O<sub>3</sub>Na<sup>+</sup>:125.0210, found  $[\text{M}+\text{Na}^+]$ : 125.0205.

#### (2*S*,3*S*)-3-Ethyl-2-hydroxy-4-butyrolactone (2*S*,3*S*-**5c**).

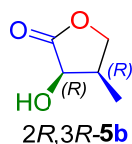


Synthesis of aldol adduct 2*S*-**3c** was prepared using YfaU<sub>Ecoli</sub> W23V variant with the procedure described 2*S*,3*S*-**5b** and starting from **2c** ( $[\mathbf{2c}] = [\mathbf{1a}] =$

100 mM). Lactone **2S,3S-5c** was obtained as a yellow oil (22 mg, 17%).  $^1\text{H}$  NMR (400 MHz,  $\text{D}_2\text{O}$ )  $\delta$  4.74 (d,  $J = 7.5$  Hz, 1H), 4.44 (dd,  $J = 9.5, 5.6$  Hz, 1H), 4.31 (dd,  $J = 9.5, 2.4$  Hz, 1H), 2.74 – 2.46 (m, 1H), 1.64 (dtd,  $J = 14.9, 7.5, 7.4, 5.1$  Hz, 1H), 1.31 (ddt,  $J = 16.4, 14.4, 7.3, 7.3$  Hz, 1H), 0.96 (t,  $J = 2 \times 7.5$  Hz, 3H).  $^{13}\text{C}$  NMR (101 MHz,  $\text{D}_2\text{O}$ )  $\delta$  180.1, 70.6, 69.3, 41.2, 18.2, 10.3. Minor lactone key selected signals:  $^1\text{H}$  NMR (400 MHz,  $\text{D}_2\text{O}$ )  $\delta$  4.46 (t,  $J = 8.6$  Hz, 1H), 3.92 (m, 1H), 2.36 (m, 1H), 1.73 – 1.61 (m, 1H).  $^{13}\text{C}$  NMR (101 MHz,  $\text{D}_2\text{O}$ )  $\delta$  180.5, 72.1, 44.7, 22.6, 10.5.  $[\alpha]_{20}^{\text{D}} = + 0.8$  ( $c = 1$ , in MeOH). ESI-TOF  $m/z$ : Calcd for  $[\text{2M}+\text{Na}^+]$   $\text{C}_{12}\text{H}_{20}\text{O}_6\text{Na}^+$ :283.1152, found  $[\text{2M}+\text{Na}^+]$ : 283.1149.

**The reactions combining  $\text{KPHMT}_{E.coli}$ , and  $\text{KPR}_{E.coli}$  were carried out as follows:**

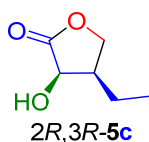
**(2R,3R)-3-methyl-2-hydroxy-4-butyrolactone (2R,3R-5b).**



**Aldol addition (1<sup>st</sup>):** The reaction (1 mmol scale, 10 mL total volume) was conducted in a round-bottom flask (100 mL) at 25 °C and magnetically stirred with a bar at 250 rpm. To a solution of  $\text{KPHMT}_{E.coli}$  wt (1.1 mL of 9.3 mg  $\text{mL}^{-1}$  stock solution 20 mM TEA buffer pH 7.0, 100 mM NaCl, and 50% (v/v) of glycerol, 1 mg protein  $\text{mL}^{-1}$  in the reaction) in plain (6.8 mL) water,  $\text{CoCl}_2$  (100  $\mu\text{L}$  of a 0.1 M stock solution, 1 mM in the reaction), and **2b** (1 mL of a 1 M stock solution in water pH 7.0, 1 mmol, 1 eq, 0.1 M in the reaction) were added. The reaction was started by adding formaldehyde (**1a**, 1 mL of a 1 M in water solution, 1 eq, 0.1 M in the reaction). The reaction was monitored by HPLC as described in the analytical scale reactions.

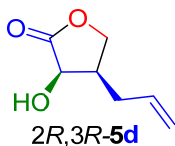
**Aldol reduction (2<sup>nd</sup>):** The reduction of aldol adduct with  $\text{KPR}_{E.coli}$  and final lactone purification was performed as describe for **2R,3S-5b**. Final product **2R,3R-5b** was obtained as a yellow oil (43 mg, 37%).  $^1\text{H}$  NMR (400 MHz,  $\text{D}_2\text{O}$ )  $\delta$  4.51 (t,  $J = 2 \times 8.4$  Hz, 1H), 4.24 (d,  $J = 11.1$  Hz, 1H), 3.95 (dd,  $J = 10.8, 9.0$  Hz, 1H), 2.61 – 2.34 (m, 1H), 1.21 (d,  $J = 6.5$  Hz, 3H).  $^{13}\text{C}$  NMR (101 MHz,  $\text{D}_2\text{O}$ )  $\delta$  180.1, 73.3, 71.5, 38.5, 12.8. Minor diastereoisomer key selected signals:  $^1\text{H}$  NMR (400 MHz,  $\text{D}_2\text{O}$ )  $\delta$  4.15 (d,  $J = 11.2$  Hz, 1H), 3.91 – 3.82 (m, 1H), 2.44 (tdd,  $J = 12.4, 9.2, 6.3$  Hz, 1H), 1.12 (d,  $J = 6.5$  Hz, 1H).  $^{13}\text{C}$  NMR (101 MHz,  $\text{D}_2\text{O}$ )  $\delta$  73.3, 71.5, 38.5, 12.8.  $[\alpha]_{20}^{\text{D}} = - 41.7$  ( $c = 1$ , in MeOH). ESI-TOF  $m/z$ : Calcd for  $[\text{M}+\text{Na}^+]$   $\text{C}_5\text{H}_8\text{O}_3\text{Na}^+$ :139.0366, found  $[\text{M}+\text{Na}^+]$ : 139.0371.

**(2R,3R)-3-Ethyl-2-hydroxy-4-butyrolactone (2R,3R-5c).**



The synthesis of the title compound was performed as described for 2R,3R-5b. Starting from **2c** ( $[2c] = [1a] = 100$  mM), 2R,3R-5c was obtained as a yellow oil (23 mg, 25%).  $^1\text{H}$  NMR (400 MHz,  $\text{D}_2\text{O}$ )  $\delta$  4.74 (d,  $J = 7.4$  Hz, 1H), 4.44 (dd,  $J = 9.5, 5.6$  Hz, 1H), 4.31 (dd,  $J = 9.5, 2.4$  Hz, 1H), 2.63 (ddd,  $J = 7.3, 5.3, 2.2$  Hz, 1H), 1.64 (dtd,  $J = 15.0, 7.6, 7.5, 5.0$  Hz, 1H), 1.31 (ddq,  $J = 14.5, 9.0, 3 \times 7.4$  Hz, 1H), 0.96 (t,  $J = 2 \times 7.5$  Hz, 3H).  $^{13}\text{C}$  NMR (101 MHz,  $\text{D}_2\text{O}$ )  $\delta$  180.1, 70.6, 69.3, 41.1, 18.2, 10.3. Minor lactone key selected signals:  $^1\text{H}$  NMR (400 MHz,  $\text{D}_2\text{O}$ )  $\delta$  4.46 (t,  $J = 8.6$  Hz, 1H), 3.92 (m, 1H), 2.36 (m, 1H), 1.73 – 1.61 (m, 1H).  $^{13}\text{C}$  NMR (101 MHz,  $\text{D}_2\text{O}$ )  $\delta$  180.5, 72.1, 44.7, 22.6, 10.5.  $[\alpha]_{20}^{\text{D}} = -2.0$  ( $c = 1$ , in MeOH). Calcd for  $[2\text{M}+\text{Na}^+]$   $\text{C}_{12}\text{H}_{20}\text{O}_6\text{Na}^+$ : 283.1152, found  $[2\text{M}+\text{Na}^+]$ : 283.1159.

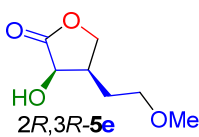
**(2R,3R)-3-Allyl-2-hydroxy-4-butyrolactone (2R,3R-5d).**



The title compound was prepared using KPHMT<sub>Ecoli</sub> I212A variant and following the procedure described for 2R,3R-5b. Starting from **2d** ( $[2d] = [1a] = 100$  mM), 2R,3R-5d was obtained as a yellow oil (36 mg, 25%).

$^1\text{H}$  NMR (400 MHz,  $\text{CDCl}_3$ ) 5.87 – 5.63 (m, 1H), 5.26 – 5.07 (m, 2H), 4.56 (d,  $J = 7.4$  Hz, 1H), 4.25 (d,  $J = 2.3$  Hz, 1H), 2.78 – 2.63 (m, 1H), 2.58 – 2.49 (m, 1H), 2.04 (dt,  $J = 14.5, 2 \times 9.0$  Hz, 1H).  $^{13}\text{C}$  NMR (101 MHz,  $\text{CDCl}_3$ )  $\delta$  177.3, 134.6, 118.2, 69.4, 68.9, 39.5, 29.9. Selected NMR signals for the minor diastereomer:  $^1\text{H}$  NMR (400 MHz,  $\text{CDCl}_3$ )  $\delta$  5.86 – 5.81 (m, 1H), 5.17 (dq,  $J = 6.1, 1.6, 1.5, 1.5$  Hz, 2H), 4.42 (dd,  $J = 9.3, 7.7$  Hz, 1H), 4.27 (ddd,  $J = 9.4, 5.4, 0.7$  Hz, 3H), 4.14 (d,  $J = 10.0$  Hz, 1H), 2.64 – 2.56 (m, 1H), 2.32 – 2.20 (m, 1H).  $^{13}\text{C}$  NMR (101 MHz,  $\text{CDCl}_3$ )  $\delta$  177.1, 133.5, 117.8, 71.8, 69.1, 43.0, 34.3.  $[\alpha]_{20}^{\text{D}} = -20.0$  ( $c = 0.6$ , in MeOH). ESI-TOF  $m/z$ : Calcd for  $[\text{M}+\text{Na}^+]$   $\text{C}_7\text{H}_{10}\text{O}_3\text{Na}^+$ : 165.0522, found  $[\text{M}+\text{Na}^+]$ : 165.0528.

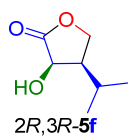
**(2R,3R)-3-(3-methoxypropyl)-2-hydroxy-4-butyrolactone (2R,3R-5e).**



The title compound was prepared using KPHMT<sub>Ecoli</sub> I212A variant and following the procedure described for 2R,3R-5b. Starting from **2e** ( $[2e] = [1a] = 100$  mM), 2R,3R-5e was obtained as a yellow oil (64 mg, 40%).  $^1\text{H}$  NMR (400 MHz, DMSO)  $\delta$  4.35 (dd,  $J = 7.0, 6.0$  Hz, 1H), 4.26 (dd,  $J = 8.9, 6.1$  Hz, 1H), 4.07 (dd,  $J = 9.0, 4.2$  Hz, 1H), 3.39 (td,  $J = 2 \times 6.4, 4.4$  Hz, 2H), 3.23 (s,

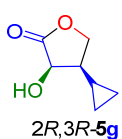
3H), 2.57 – 2.45 (m, 1H), 1.81 (ddd,  $J = 14.3, 7.1, 5.6$  Hz, 1H), 1.39 (ddd,  $J = 14.0, 10.7, 6.5$  Hz, 1H).  $^{13}\text{C}$  NMR (101 MHz, DMSO)  $\delta$  176.9, 69.9, 69.5, 68.0, 57.9, 37.5, 25.2. Minor lactone key selected signals:  $^1\text{H}$  NMR (400 MHz, DMSO)  $\delta$  3.83 (dd,  $J = 10.6, 8.9$  Hz, 1H), 2.31 (m, 1H), 1.72 – 1.59 (m, 1H).  $^{13}\text{C}$  NMR (101 MHz, DMSO)  $\delta$  71.9, 70.5, 69.3, 42.2, 30.4.  $[\alpha]_{20}^{\text{D}} = +2.8$  ( $c = 1$ , in MeOH). ESI-TOF  $m/z$ : Calcd for  $[\text{M}+\text{Na}^+]$   $\text{C}_7\text{H}_{12}\text{O}_4\text{Na}^+$ : 183.0628, found  $[\text{M}+\text{Na}^+]$ : 183.0635.

**(2*R*,3*R*)-3-isopropyl-2-hydroxy-4-butyrolactone (2*R*,3*R*-5*f*).**



The title compound was prepared using KPHMT<sub>Ecoli</sub> I202A variant and following the procedure described for 2*R*,3*R*-5*b*. Starting from **2f** (**[2f]** = **[1a]** = 100 mM), 2*R*,3*R*-5*f* was obtained as a yellow oil (52 mg, 36%).  $^1\text{H}$  NMR (400 MHz,  $\text{CDCl}_3$ )  $\delta$  4.42 (dd,  $J = 7.1, 1.9$  Hz, 1H), 4.36 (dd,  $J = 9.2, 6.9$  Hz, 1H), 4.26 (dd,  $J = 9.3, 5.9$  Hz, 1H), 2.35 (qd,  $J = 7.0, 7.0, 7.0, 5.9$  Hz, 1H), 2.13 (h,  $J = 6.8$  Hz, 1H), 1.04 (d,  $J = 6.8$  Hz, 3H), 0.91 (d,  $J = 6.8$  Hz, 3H).  $^{13}\text{C}$  NMR (101 MHz,  $\text{CDCl}_3$ )  $\delta$  177.6, 69.2, 68.3, 46.3, 24.6, 20.8, 18.6. Selected NMR signals for the minor diastereomer  $^1\text{H}$  NMR (400 MHz,  $\text{CDCl}_3$ )  $\delta$  3.92 (dd,  $J = 10.7, 9.2$  Hz, 1H), 2.26 (ddd,  $J = 10.5, 8.4, 2.1$  Hz, 1H), 1.86 – 1.75 (m, 1H), 1.13 (d,  $J = 6.7$  Hz, 1H), 0.97 (d,  $J = 6.7$  Hz, 1H).  $^{13}\text{C}$  NMR (101 MHz,  $\text{CDCl}_3$ )  $\delta$  (very small signals) 71.7, 68.8, 49.9, 20.5, 20.1. The NMR data matched that reported in the literature.<sup>13</sup>  $[\alpha]_{20}^{\text{D}} = +42.4$  ( $c = 1.1$ , in MeOH). ESI-TOF  $m/z$ : Calcd for  $[\text{M}+\text{Na}^+]$   $\text{C}_7\text{H}_{12}\text{O}_3\text{Na}^+$ : 167.0679, found  $[\text{M}+\text{Na}^+]$ : 167.0674.

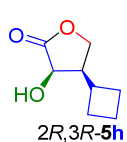
**(2*R*,3*R*)-3-Cyclopropyl-2-hydroxy-4-butyrolactone (2*R*,3*R*-5*g*).**



The title compound was prepared as described for 2*R*,3*R*-5*b*. Starting from **2g** (**[2g]** = **[1]** = 100 mM), 2*R*,3*R*-5*g* was obtained as a white solid (40 mg, 28%).  $^1\text{H}$  NMR (400 MHz,  $\text{CDCl}_3$ )  $\delta$  4.51 (d,  $J = 7.2$  Hz, 1H), 4.32 (dd,  $J = 9.3, 5.5$  Hz, 1H), 4.22 (dd,  $J = 9.3, 2.5$  Hz, 1H), 2.06 – 1.93 (m, 1H), 0.95 – 0.83 (m, 1H), 0.71 (dddd,  $J = 9.2, 8.2, 5.7, 4.8$  Hz, 1H), 0.58 – 0.51 (m, 1H), 0.32 (ddd,  $J = 10.5, 9.5, 5.0$  Hz, 1H), 0.17 (dddd,  $J = 14.2, 9.5, 5.5, 4.7$  Hz, 1H).  $^{13}\text{C}$  NMR (101 MHz,  $\text{CDCl}_3$ )  $\delta$  177.2, 70.3, 70.2, 45.5, 7.9, 4.2, 2.0. Selected NMR signals for the minor diastereomer  $^1\text{H}$  NMR (400 MHz,  $\text{CDCl}_3$ )  $\delta$  4.42 (dd,  $J = 9.3, 8.0$  Hz, 1H), 3.96 (dd,  $J = 10.5, 9.2$  Hz, 1H), 0.79 (tdd,  $J = 8.3, 4.8, 3.3$  Hz, 1H), 0.44 (dq,  $J = 9.3, 4.9$  Hz, 1H).  $^{13}\text{C}$  NMR (101 MHz,  $\text{CDCl}_3$ )  $\delta$  72.4, 69.2, 48.2, 10.5, 2.3, 2.2.  $[\alpha]_{20}^{\text{D}} = -2.9$  ( $c = 1.3$ , in

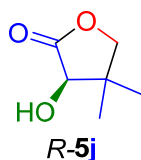
MeOH). ESI-TOF m/z: Calcd for  $[2M+Na^+]$   $C_{14}H_{20}O_6Na^+$ : 307.1152, found  $[2M+Na^+]$ : 307.1166.

**(2*R*,3*R*)-3-Cyclobutyl-2-hydroxy-4-butyrolactone (2*R*,3*R*-5*h*).**



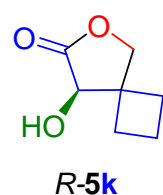
The title compound was prepared using KPHMT<sub>Ecoli</sub> I202A variant and following the procedure described for 2*R*,3*R*-5*b*. Starting from **2h** (**[2h]** = **[1a]** = 100 mM), 2*R*,3*R*-5*h* was obtained as a white solid (30 mg, 30%). <sup>1</sup>H NMR (400 MHz, CDCl<sub>3</sub>) δ 4.54 (d, *J* = 7.1 Hz, 1H), 4.26 (dd, *J* = 9.4, 5.3 Hz, 1H), 4.14 (d, *J* = 1.9 Hz, 1H), 2.65-2.59 (m, 1H), 2.58-2.51 (m, 1H), 2.18-2.13 (m, 1H), 2.09-2.02 (m, 1H), 1.96-1.98 (m, 1H), 1.87-1.84 (m, 2H), 1.73-1.64 (m, 1H). <sup>13</sup>C NMR (101 MHz, CDCl<sub>3</sub>) δ 177.6, 70.1, 68.2, 45.6, 33.0, 28.1, 26.2, 19.0. Selected NMR signals for the minor diastereomer: <sup>1</sup>H NMR (400 MHz, CDCl<sub>3</sub>) δ 4.39 (dd, *J* = 9.1, 7.8 Hz, 1H), 4.13 – 4.07 (m, 1H), 3.84 (t, *J* = 2x9.6 Hz, 1H), 2.58-2.51 (m, 1H), 2.50-2.46 (m, 1H), 1.97-1.90 (m, 3H), 1.88-1.81 (m, 3H). <sup>13</sup>C NMR (101 MHz, CDCl<sub>3</sub>) 177.8, 71.5, 68.2, 48.0, 36.0, 25.6, 25.6, 18.9.  $[\alpha]_{20}^D = +2$  (*c* = 0.8 in MeOH). ESI-TOF m/z: Calcd for  $[M+Na^+]$   $C_8H_{10}O_3Na^+$ : 179.0678, found  $[M+Na^+]$ : 179.0671.

**(*R*)-3,3-dimethyl-2-hydroxy-4-butyrolactone (*R*-5*j*).**



The title compound was prepared as described for 2*R*,3*R*-5*b*. Starting from **2j** (**[2j]** = **[1a]** = 100 mM), *R*-5*j* was obtained as a white solid (66 mg, 51%). <sup>1</sup>H NMR (400 MHz, CDCl<sub>3</sub>) δ 4.12 (s, 1H), 4.03 (d, *J* = 8.9 Hz, 1H), 3.94 (dd, *J* = 8.9, 0.8 Hz, 1H), 1.23 (s, 3H), 1.08 (s, 3H). <sup>13</sup>C NMR (101 MHz, CDCl<sub>3</sub>) δ 177.6, 76.5, 75.9, 41.0, 23.1, 18.9. The NMR data matched that reported in the literature<sup>14</sup>. ee: ≥99% (see below),  $[\alpha]_{20}^D = -22.5$  (*c* = 1 in MeOH), In our hands, commercial D-(–)-pantolactone (Sigma Aldrich 237817)  $[\alpha]_{20}^D = -28.0$  (*c* = 1 in MeOH). ESI-TOF m/z: Calcd for  $[M+Na^+]$   $C_6H_{10}O_3Na^+$ : 153.0522, found  $[M+Na^+]$ : 153.0527.

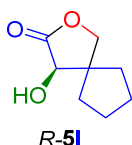
**(*R*)-8-Hydroxy-6-oxaspiro[3.4]octan-7-one (*R*-5*k*).**



The title compound was prepared as described for 2*R*,3*R*-5*b*. Starting from **2k** (**[2k]** = **[1a]** = 100 mM), *R*-5*k* was obtained as a white solid (58 mg, 40%). <sup>1</sup>H NMR (400 MHz, CDCl<sub>3</sub>) δ 4.41 (d, *J* = 9.1 Hz, 1H), 4.18

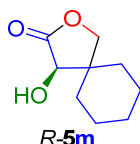
(s, 1H), 4.10 (d,  $J = 9.1$  Hz, 1H), 2.54 (dd,  $J = 14.6, 5.5$  Hz, 1H), 2.31 (dtd,  $J = 9.9, 8.5, 8.1, 2.0$  Hz, 1H), 2.01 (dp,  $J = 8.5, 2 \times 2.4, 2 \times 2.2$  Hz, 1H), 1.98 – 1.88 (m, 2H), 1.83 – 1.73 (m, 1H).  $^{13}\text{C}$  NMR (101 MHz,  $\text{CDCl}_3$ )  $\delta$  177.0, 75.4, 73.1, 46.7, 26.3, 25.1, 15.8. The NMR data matched that reported in the literature.<sup>14</sup> ee:  $\geq 99\%$  (see below),  $[\alpha]_{20}^{\text{D}} = +20.1$  ( $c = 1$  in MeOH). ESI-TOF  $m/z$ : Calcd for  $[\text{M}+\text{Na}^+]$   $\text{C}_7\text{H}_{10}\text{O}_3\text{Na}^+$ : 165.0522, found  $[\text{M}+\text{Na}^+]$ : 165.0533.

**(R)-4-Hydroxy-2-oxaspiro[4.4]nonan-3-one (R-5l).**



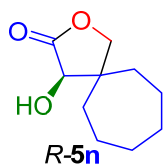
The title compound was prepared using KPHMT<sub>Ecoli</sub> I202A variant and following the procedure described for 2*R*,3*R*-5b. Starting from **2l** (**[2l]** = **[1a]** = 100 mM), **R-5l** was obtained as a white solid (63 mg, 40%).  $^1\text{H}$  NMR (400 MHz,  $\text{CDCl}_3$ )  $\delta$  4.28 (s, 1H), 4.13 (d,  $J = 8.9$  Hz, 1H), 4.02 (dd,  $J = 8.9, 1.0$  Hz, 1H), 2.06 – 1.95 (m, 1H), 1.94 – 1.84 (m, 1H), 1.83 – 1.75 (m, 1H), 1.75 – 1.68 (m, 1H), 1.68 – 1.60 (m, 3H), 1.48 – 1.37 (m, 1H).  $^{13}\text{C}$  NMR (101 MHz,  $\text{CDCl}_3$ )  $\delta$  177.5, 76.1, 73.9, 51.8, 33.8, 29.3, 25.2, 25.1. The NMR data matched that reported in the literature.<sup>15</sup> ee:  $\geq 99\%$  (see below). The optical rotation values  $[\alpha]$  was determined for **R-10l** (see below). ESI-TOF  $m/z$ : Calcd for  $[\text{2M}+\text{Na}^+]$   $\text{C}_{16}\text{H}_{24}\text{O}_6\text{Na}^+$ : 335.1465, found  $[\text{2M}+\text{Na}^+]$ : 335.1461.

**(R)-4-Hydroxy-2-oxaspiro[4.5]decan-3-one (R-5m).**



The title compound was prepared using KPHMT<sub>Ecoli</sub> I212A variant and following the procedure described for 2*R*,3*R*-5b. Starting from **2m** (**[2m]** = **[1a]** = 100 mM), **R-5m** was obtained as a yellow solid (26 mg, 15%).  $^1\text{H}$  NMR (400 MHz,  $\text{CDCl}_3$ )  $\delta$  4.35 (d,  $J = 9.1$  Hz, 1H), 4.07 (s, 1H), 3.88 (dd,  $J = 9.2, 1.5$  Hz, 1H), 1.83 – 1.68 (m, 2H), 1.69 – 1.55 (m, 4H), 1.50 – 1.35 (m, 2H), 1.34 – 1.18 (m, 2H).  $^{13}\text{C}$  NMR (101 MHz,  $\text{CDCl}_3$ )  $\delta$  177.4, 75.6, 73.4, 44.0, 33.6, 25.7, 25.2, 22.8, 21.6. The NMR data matched that reported in the literature.<sup>15</sup> ee: 98% (see below). The optical rotation values  $[\alpha]$  was determined for **R-10m** (see below). ESI-TOF  $m/z$ : Calcd for  $[\text{2M}+\text{Na}^+]$   $\text{C}_{18}\text{H}_{28}\text{O}_6\text{Na}^+$ : 363.1778, found  $[\text{2M}+\text{Na}^+]$ : 363.1769.

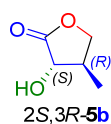
**(R)-4-Hydroxy-2-oxaspiro[4.6]undecan-3-one (R-5n).**



The title compound was prepared using KPHMT<sub>Ecoli</sub> I202A variant and following the procedure described for 2*R*,3*R*-5b. Starting from **2n** (**[2n]** =

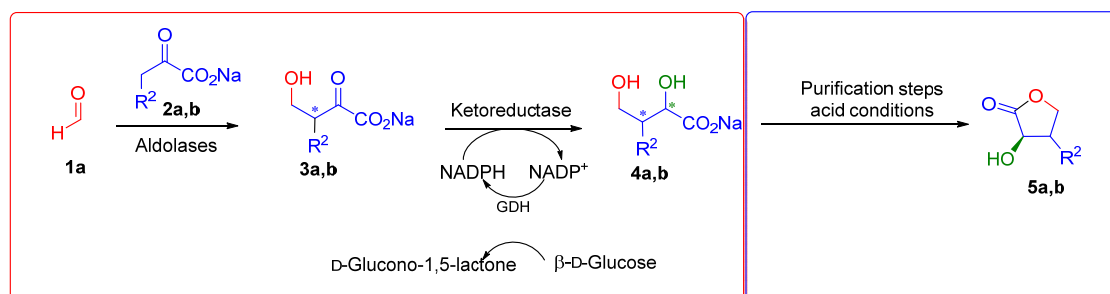
[**1a**] = 100 mM), **R-5n** was obtained as a yellow solid (20 mg, 11%). <sup>1</sup>H NMR (400 MHz, CDCl<sub>3</sub>) δ 4.16 (s, 1H), 4.14 (s, 1H), 3.85 (dd, *J* = 9.0, 1.5 Hz, 1H), 1.97 – 1.76 (m, 2H), 1.77 – 1.56 (m, 5H), 1.57 – 1.36 (m, 5H). <sup>13</sup>C NMR (101 MHz, CDCl<sub>3</sub>) δ 177.9, 77.8, 75.1, 47.4, 37.0, 30.2, 30.1, 29.3, 23.4, 22.9. The NMR data matched that reported in the literature.<sup>15</sup> ee: 98% (see below). The optical rotation values [ $\alpha$ ] was determined for **R-10n** (see below). ESI-TOF *m/z*: Calcd for [M+Na<sup>+</sup>] C<sub>10</sub>H<sub>16</sub>O<sub>3</sub>Na<sup>+</sup>: 207.0992, found [M+Na<sup>+</sup>]: 207.0981.

**The reactions combining KPHMT<sub>Ecoli</sub>, and DpkA<sub>Psyrin</sub> were carried out as follows:**  
**(2*S*,3*R*)-3-Methyl-2-hydroxy-4-butyrolactone (2*S*,3*R*-5b).**



The title compound was prepared as follows. The aldol reaction ([**2b**] = [**1**] = 100 mM) was performed as described for **2*R*,3*R*-5b**, and then was submitted to reduction with DpkA<sub>Psyrin</sub> catalysis using the procedure described for **2*S*,3*S*-5b**. Compound **2*S*,3*R*-5b** was obtained as a yellow oil (61 mg, 53%). <sup>1</sup>H NMR (400 MHz, D<sub>2</sub>O) δ 4.5 (t, *J* = 2x8.5 Hz, 1H), 4.2 (d, *J* = 11.1 Hz, 1H), 3.9 (dd, *J* = 10.8, 9.0 Hz, 1H), 2.6 – 2.4 (m, 1H), 1.2 (d, *J* = 6.5 Hz, 3H). <sup>13</sup>C NMR (101 MHz, D<sub>2</sub>O) δ 180.1, 73.3, 71.5, 38.5, 12.8. Selected NMR signals for the minor diastereomer: <sup>1</sup>H NMR (400 MHz, D<sub>2</sub>O) δ 4.67 – 4.64 (m, 1H), 4.10 – 4.03 (m, 1H), 2.79 – 2.68 (m, 1H), 0.97 (d, *J* = 7.1 Hz, 3H). <sup>13</sup>C NMR (101 MHz, D<sub>2</sub>O) δ 72.8, 69.9, 34.7, 10.9. [ $\alpha$ ]<sub>20</sub><sup>D</sup> = – 53.4 (*c* = 1 in MeOH). ESI-TOF *m/z*: Calcd for [M+Na<sup>+</sup>] C<sub>5</sub>H<sub>8</sub>O<sub>3</sub>Na<sup>+</sup>: 139.0366, found [M+Na<sup>+</sup>]: 139.0375.

**One-pot enzymatic cascade for the stereoselective synthesis of 2-hydroxy-4-butyrolactones derivatives (5a,b).**

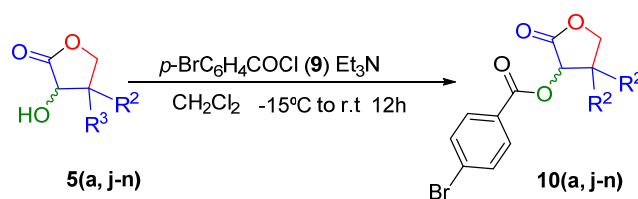


**Scheme S5.** One-pot enzymatic cascade for the stereoselective synthesis of 2-hydroxy-4-butyrolactones derivatives (**5a,b**) combining aldolases (YfaU<sub>Ecoli</sub> and KPHMT<sub>Ecoli</sub>) and ketoreductases (DpkA<sub>Psyrin</sub> and KPR<sub>Ecoli</sub>).



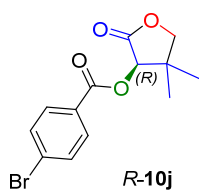
The reaction (1 mmol scale, 10 mL total volume) was conducted in a round-bottom flask (100 mL) at 25 °C and magnetically stirred with a bar at 250 rpm. To a solution of aldolase (YfaU<sub>Ecoli</sub> wt, 60 mg of lyophilized powder at 0.5 mg protein mg<sup>-1</sup> lyophilized powder, 30 mg of protein, 3 mg protein mL<sup>-1</sup> final concentration in the reaction or KPHMT<sub>Ecoli</sub> wt, 1.1 mL of 9.3 mg mL<sup>-1</sup> stock solution 20 mM TEA buffer pH 7.0, 100 mM NaCl, and 50% (v/v) of glycerol, 1 mg protein mL<sup>-1</sup> in the reaction) in sodium phosphate buffer pH 8.0 (83 mM in the reaction), 2-oxoacid (**2a** or **2b**) (stock solution in water pH 7.0, 1 mmol, 1 eq, 0.1 M in the reaction) and MCl<sub>2</sub> (100 μL of a 0.1 M stock solution in water, 10 μmol, 1 mM in the reaction, M<sup>2+</sup> = Ni<sup>2+</sup> or Co<sup>2+</sup> for YfaU<sub>Ecoli</sub> wt and KPHMT<sub>Ecoli</sub> wt respectively) were added. Then, ketoreductase (KPR<sub>Ecoli</sub>, 0.9 mL of a stock solution 52 U mL<sup>-1</sup>, 4 mg mL<sup>-1</sup> in 20 mM TEA buffer pH 7.0, 100 mM NaCl, and 50% (v/v) of glycerol, 4.7 U mL<sup>-1</sup> final concentration in the reaction or DpkA<sub>psyrin</sub>, 2.5 mL of a stock solution 2.6 10<sup>-2</sup> U mL<sup>-1</sup>, 4 mg mL<sup>-1</sup> in 20 mM TEA buffer pH 7.0, 100 mM NaCl, and 50% (v/v) of glycerol, 6.5 10<sup>-3</sup> U mL<sup>-1</sup> final concentration in the reaction), glucose (721 mg, 4.0 mmol, 4 eq, 0.4 M final concentration in the reaction), GDH (1.6 mL of a stock solution 20.8 U mL<sup>-1</sup>, 5.2 mg mL<sup>-1</sup> in 10 mM HEPES buffer pH 6.5, 50 mM NaCl, and 50% (v/v) of glycerol, 3.4 U mL<sup>-1</sup> final concentration in the reaction) and NADP<sup>+</sup> (42 mg, 0.05 mmol, 5 mM final concentration in the reaction) were added. The reaction was started by adding formaldehyde (**1**, 1 mL of a 1 M stock solution in water, 1 mmol, 1 eq, 0.1 M in the reaction). The reaction was monitored by HPLC (see above in the description of analytical scale reactions) and the purification was performed as described for *2R,3S-5b* and *R-5a*. Products: *R-5a*, *S-5a*, *2R,3S-5b*, *2S,3S-5b*, *2R,3R-5b* and *2S,3R-5b* were obtained with 30, 20, 57, 33, 37 and 57 % of isolated yield respectively. The physical and chemical properties of the products were indistinguishable from the lactones obtained in one pot two steps strategy.

#### Strategy for enantiomeric excess determination of products **5** (a, j-n).



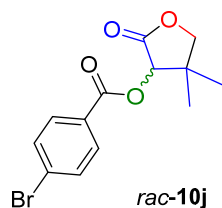
**Scheme S6.** Chemical modification of lactones **5** (a, j-n) for enantiomeric excess determination.

**(R)-4,4-Dimethyl-2-oxotetrahydrofuran-3-yl 4-bromobenzoate (*R*-10j)**



Typical procedure: A dried three-necked round bottomed flask was charged with anhydrous  $\text{CH}_2\text{Cl}_2$  (20 mL) under  $\text{N}_2$  atmosphere. Then, *R*-5j (100 mg, 0.8 mmol, 1.0 eq) was added and the mixture was cooled at  $-15$  °C. The reaction was started by addition of 4-bromobenzoyl chloride (**9**) (219 mg, 1.0 mmol, 1.3 eq) and  $\text{Et}_3\text{N}$  (161  $\mu\text{L}$ , 117 mg, 1.2 mmol, 1.5 eq). The mixture was stirred 1h at  $-15$  °C and 15 h at r.t. The reaction was diluted with  $\text{CH}_2\text{Cl}_2$  (200 mL), transferred to a separation funnel and extracted with 1 M HCl (200 mL), 5%  $\text{NaHCO}_3$  (3 x 100 mL) and brine (3 x 100 mL). The organic phase was dried over anhydrous magnesium sulfate, filtered and the solvent was removed under vacuum. The product was loaded onto a silica column chromatography and eluted with a step gradient of Hexane:EtOAc: 100:0, 200 mL, 90:10, 200 mL and 80:20, 700 mL. Pure fractions were pooled and the solvent was removed under vacuum affording the title compound (*R*-10j) as a white solid (172 mg, 72%).  $^1\text{H}$  NMR (400 MHz,  $\text{CDCl}_3$ )  $\delta$  7.95 (d,  $J = 8.5$  Hz, 1H), 7.62 (d,  $J = 8.5$  Hz, 1H), 5.60 (s, 1H), 4.11 (d,  $J = 3.8$  Hz, 2H), 1.28 (s, 3H), 1.22 (s, 3H).  $^{13}\text{C}$  NMR (101 MHz,  $\text{CDCl}_3$ )  $\delta$  172.6, 165.2, 132.4, 132.0, 129.5, 128.1, 76.7, 76.2, 41.0, 23.6, 20.5. ee:  $\geq 99\%$ .  $[\alpha]_{20}^{\text{D}} = +16.9$  ( $c = 1$  in MeOH).

***rac*-4,4-Dimethyl-2-oxotetrahydrofuran-3-yl 4-bromobenzoate (*rac*-10j).**



Synthesis of *rac*-10j was performed as described for *R*-10j. Starting from commercial DL-pantolactone (100 mg, TCI EUROPE P0010), affording *rac*-10j as a white solid (54 mg, 22%). NMR spectra were indistinguishable from that of *R*-10j.

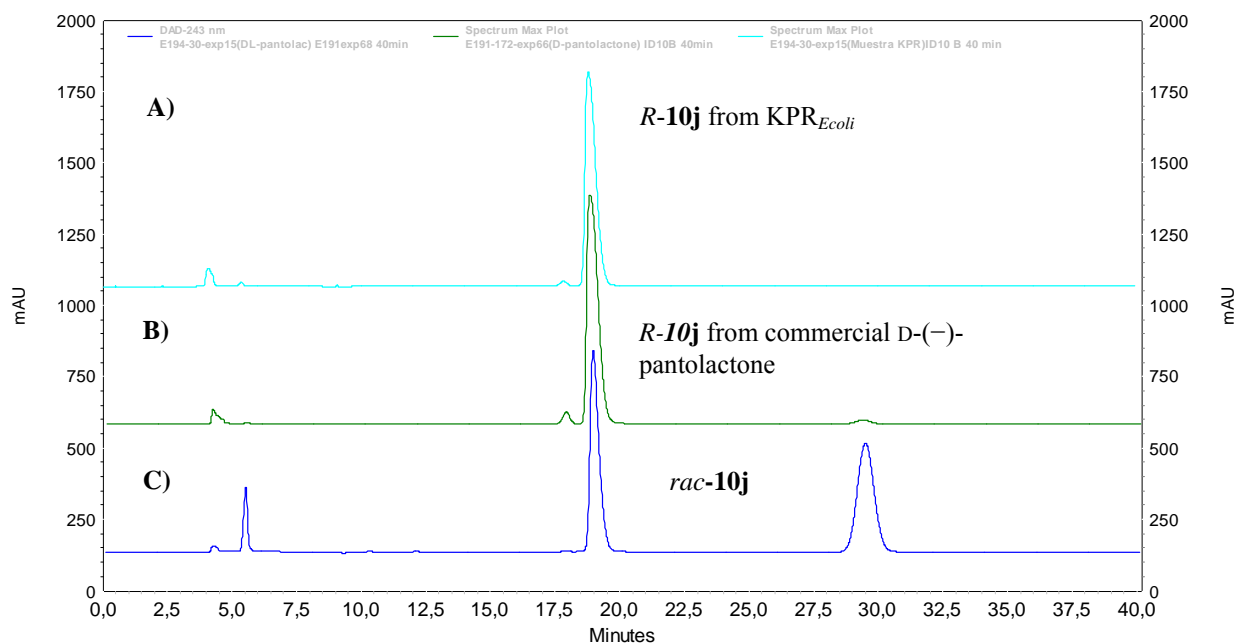
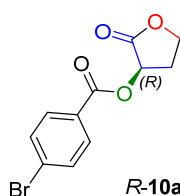


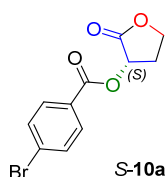
**Figure S5.** HPLC analysis on chiral stationary phase (CPHPLC) of *R*-**10j** from KPR<sub>Ecoli</sub> catalysis (**A**), *R*-**10j** from commercial D(-)-pantolactone (Sigma-Aldrich 237817) (**B**) and *rac*-**10j** from commercial D,L-pantolactone (TCI EUROPE P0010) (**C**). The analyte *R*-**10j** was identified by comparing retention time to that of a commercial standard. Conditions: CHIRALPACK® ID, flow rate 1 mL min<sup>-1</sup> at 30 °C and detection at 254 nm. Isocratic elution Hexane:<sup>i</sup>PrOH 90:10 (v/v). tr (*R*) = 19.7 min, tr (*S*) = 29.6 min.

**(*R*)-2-Oxotetrahydrofuran-3-yl 4-bromobenzoate (*R*-10a).**



The synthesis of *R*-**10a** was performed as described for *R*-**10j**. Starting from a solution of *R*-**5a** (30 mg) in anhydrous acetonitrile (5 mL), *R*-**10a** was obtained as a yellow oil (64 mg, 76%). <sup>1</sup>H NMR (400 MHz, CDCl<sub>3</sub>) δ 7.94 (d, *J* = 8.6 Hz, 1H), 7.61 (d, *J* = 8.6 Hz, 1H), 5.64 (dd, *J* = 9.7, 8.6 Hz, 1H), 4.55 (td, *J* = 2x9.1, 2.5 Hz, 1H), 4.37 (td, *J* = 2x9.6, 6.5 Hz, 1H), 2.90 – 2.77 (m, 1H), 2.43 (dtd, *J* = 12.9, 2x9.8, 9.0 Hz, 1H). <sup>13</sup>C NMR (101 MHz, CDCl<sub>3</sub>) δ 172.9, 165.3, 132.4, 132.0, 129.5, 128.1, 68.8, 65.5, 29.6. ee: ≥99%. [α]<sub>20</sub><sup>D</sup> = +15.6 (*c* = 1.2 in MeOH).

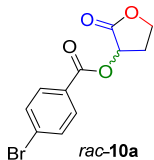
**(*S*)-2-Oxotetrahydrofuran-3-yl 4-bromobenzoate (*S*-10a).**



The synthesis of *S*-**10a** was performed as described for *R*-**10j**. Starting from a solution *S*-**5a** (30 mg) in anhydrous acetonitrile (5 mL), *S*-**10a** was obtained as a yellow oil (20 mg, 20%). NMR spectra were

indistinguishable from that of *R*-**10a**. ee:  $\geq 99\%$ .  $[\alpha]_{20}^D = -14.7$  ( $c = 1$  in MeOH).

#### *rac*-2-Oxotetrahydrofuran-3-yl 4-bromobenzoate (*rac*-**10a**).



The aldol precursor **3a** was prepared following the procedure described for *2R,3S*-**5b**. Starting from sodium pyruvate **2a** (440 mg, 4 mmol, 1 eq, 1 M concentration in the reaction) and **1a** (120 mg, 4 mmol, 1 eq, 1 M in the reaction). **Chemical reduction**: after 24 h of the aldol reaction, NaBH<sub>4</sub> (756 mg, 20 mmol, 5 eq) was added to the mixture and stirred at 25 °C for 1 h. Formation of *rac*-**4a** was estimated by measuring the aldol adduct **3a** consumed by HPLC as described above and product purification was performed as described for *R*-**5a** (*rac*-**5a**, 89 mg, 22%). The synthesis of title compound was performed as described for *R*-**10j**, starting from a solution of *rac*-**5a** (30 mg) in acetonitrile (5 mL), afforded *S*-**10a** as a white solid (39 mg, 47%). NMR spectra were indistinguishable from *R*-**10a**.

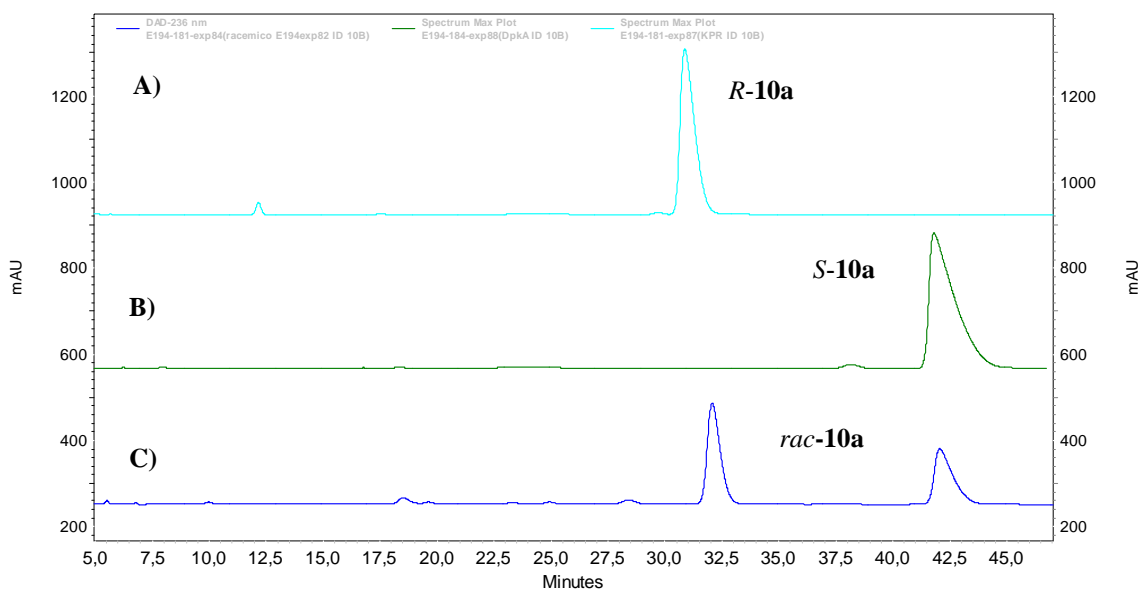
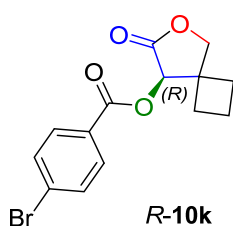


**Figure S6.** CPHPLC chromatogram of *R*-**10a** from KPR<sub>Ecoli</sub> catalysis (**A**), *S*-**10a** from DpkA<sub>Psyrin</sub> catalysis (**B**) *rac*-**10a** (**C**). Conditions: CHIRALPACK® ID, flow rate 1 mL min<sup>-1</sup> at 30 °C and detection at 254 nm. Isocratic elution hexane:<sup>i</sup>PrOH 90:10 (v/v). tr (*R*) = 32.9 min, tr (*S*) = 43.0 min.

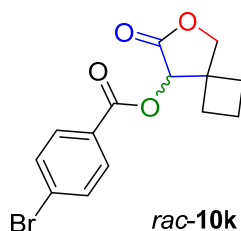
#### (*R*)-7-Oxo-6-oxaspiro[3.4]octan-8-yl 4-bromobenzoate (*R*-**10k**).



Synthesis of title compound was performed as described for *R*-**10j** starting from *R*-**5k** (66 mg). *R*-**10k** was obtained as a white solid (115 mg, 76% yield). <sup>1</sup>H NMR (400 MHz, CDCl<sub>3</sub>)  $\delta$  8.02 (d,  $J =$

8.5 Hz, 1H), 7.66 (d,  $J = 8.5$  Hz, 1H), 5.70 (s, 1H), 4.53 (d,  $J = 9.2$  Hz, 1H), 4.30 (d,  $J = 9.3$  Hz, 1H), 2.62 – 2.47 (m, 1H), 2.44 – 2.26 (m, 1H), 2.17 – 1.77 (m, 4H).  $^{13}\text{C}$  NMR (101 MHz,  $\text{CDCl}_3$ )  $\delta$  171.7, 164.9, 132.0, 131.6, 129.1, 127.7, 45.9, 27.1, 26.6, 15.9. ee:  $\geq 99\%$ .  $[\alpha]_{20}^{\text{D}} = +44.7$  ( $c = 1.5$  in MeOH).

***rac*-7-Oxo-6-oxaspiro[3.4]octan-8-yl 4-bromobenzoate (*rac*-10k).**



The aldol precursor **3k** was prepared following the procedure described for *2R,3S*-**5b**, starting from **2k** (150 mg, 1 eq, 0.1 M concentration in the reaction) and **1a** (30 mg, 0.1 M concentration in the reaction). Chemical reduction of aldol adduct was prepared as described for *rac*-**10a**. Benzoylation of *rac*-**5k** (30 mg) was performed as describe for *R*-**10j**. The title

compound was obtained as a yellow oil (32 mg, 47%). NMR spectra were indistinguishable from that of *R*-**10k**.

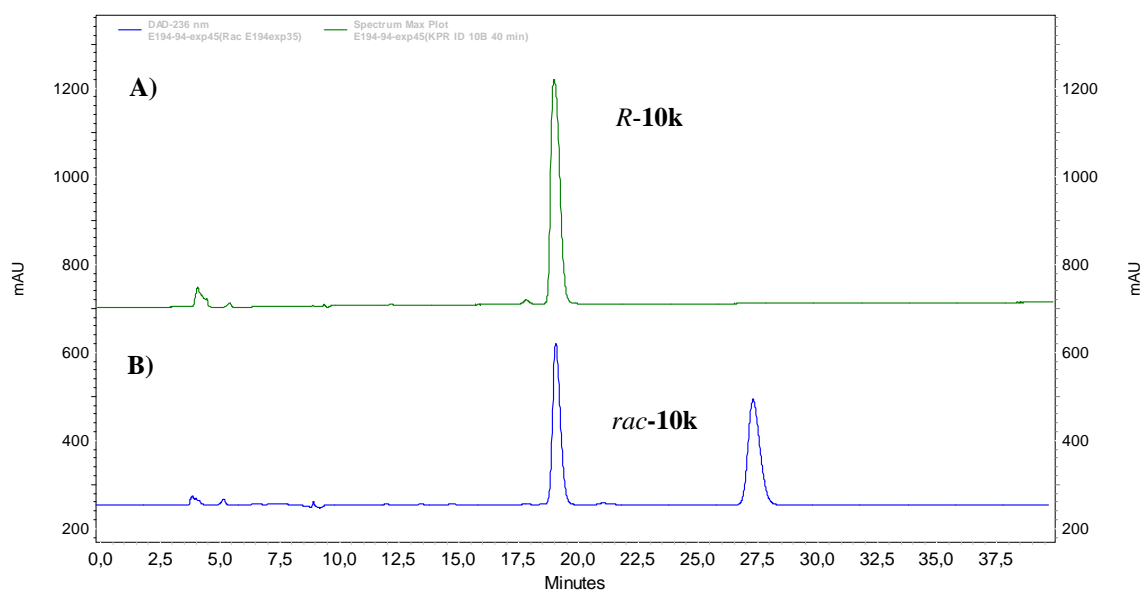
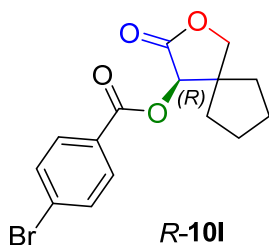


**Figure S7.** CPHPLC chromatogram of *R*-**10k** from  $\text{KPR}_{Ecoli}$  catalysis (A) and *rac*-**10k** (B). Conditions: CHIRALPACK<sup>®</sup> ID, flow rate  $0.8 \text{ mL min}^{-1}$  at  $30 \text{ }^\circ\text{C}$  and detection at 254 nm. Isocratic elution hexane:*i*PrOH 90:10 (v/v).  $\text{tr} (R) = 19.2$  min and  $\text{tr} (S) = 27.8$  min.

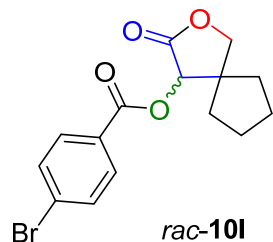
**(*R*)-3-Oxo-2-oxaspiro[4.4]nonan-4-yl 4-bromobenzoate (*R*-10l).**



Synthesis of title compound was performed as described for *R*-**10j** starting from *R*-**5l** (65 mg). *R*-**10l** was obtained as a yellow oil (96

mg, 68% yield).  $^1\text{H}$  NMR (400 MHz,  $\text{CDCl}_3$ )  $\delta$  7.95 (d,  $J = 8.6$  Hz, 2H), 7.62 (d,  $J = 8.6$  Hz, 2H), 5.75 (s, 1H), 4.23 (d,  $J = 9.0$  Hz, 1H), 4.17 (d,  $J = 9.9$  Hz, 1H), 2.08 – 1.90 (m, 1H), 1.78 – 1.53 (m, 7H).  $^{13}\text{C}$  NMR (101 MHz,  $\text{CDCl}_3$ )  $\delta$  172.3, 164.8, 132.2, 131.6, 129.2, 127.8, 76.0, 74.0, 51.3, 33.8, 30.9, 24.9, 24.9. ee:  $\geq 99\%$ .  $[\alpha]_{20}^{\text{D}} = +35.1$  ( $c = 1$  in MeOH).

***rac*-3-Oxo-2-oxaspiro[4.4]nonan-4-yl 4-bromobenzoate (*rac*-10l).**



The aldol precursor **3l** was prepared as described for **2R,3S-5b**, starting from **2l** (164 mg, 1 eq, 0.1 M concentration in the reaction) and **1a** (30 mg, 1 eq, 0.1 M concentration in the reaction). Chemical reduction was carried out as described for ***rac*-10a**. Benzoylation of ***rac*-5l** (35 mg) was performed as describe for ***R*-10j**. The title compound was obtained as a yellow oil (39 mg, 51%). NMR spectra were indistinguishable from that of ***R*-10l**.

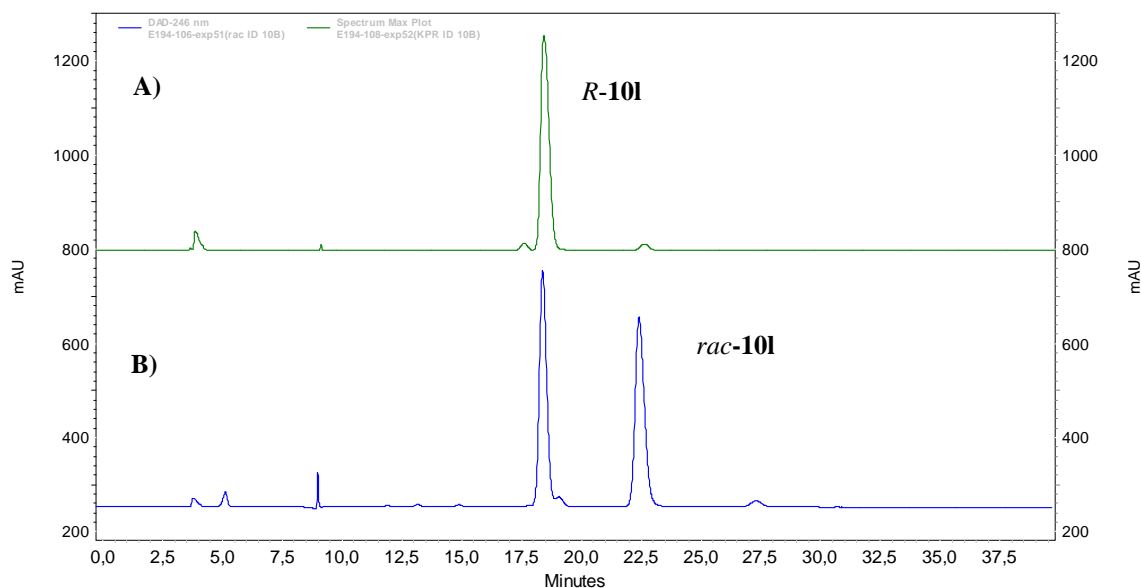
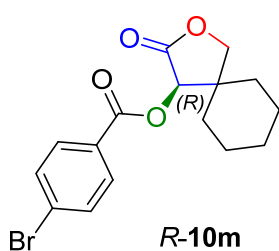


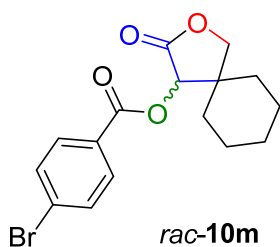
**Figure S8.** CPHPLC chromatogram of ***R*-10l** from  $\text{KPR}_{Ecoli}$  catalysis (A) and ***rac*-10l** (B). Conditions: CHIRALPACK<sup>®</sup> ID, flow rate  $0.8 \text{ mL min}^{-1}$  at  $30 \text{ }^\circ\text{C}$  and detection at 254 nm. Isocratic elution Hexane:<sup>*i*</sup>PrOH 90:10 (v/v).  $\text{tr}(\text{R}) = 18.8 \text{ min}$  and  $\text{tr}(\text{S}) = 22.8 \text{ min}$ .

**(R)-3-Oxo-2-oxaspiro[4.4]nonan-4-yl 4-bromobenzoate (*R*-10m).**



***R*-10m** Synthesis of title compound was performed as described for *R*-10j starting from *R*-5m (26 mg) in acetonitrile (5 mL). *R*-10m was obtained as a yellow oil (9 mg, 17% yield). <sup>1</sup>H NMR (400 MHz, CDCl<sub>3</sub>) δ 7.95 (d, *J* = 8.6 Hz, 1H), 7.62 (d, *J* = 8.6 Hz, 1H), 5.59 (s, 1H), 4.44 (d, *J* = 9.3 Hz, 1H), 4.07 (dd, *J* = 9.3, 1.3 Hz, 1H), 1.80 – 1.32 (m, 10H). <sup>13</sup>C NMR (101 MHz, CDCl<sub>3</sub>) δ 172.3, 164.7, 132.0, 131.5, 129.1, 127.7, 75.5, 73.4, 43.8, 33.7, 29.7, 27.2, 25.2, 22.7. ee: 98%. [α]<sub>20</sub><sup>D</sup> = +12.7 (*c* = 0.75 in MeOH).

***rac*-3-oxo-2-oxaspiro[4.5]decan-4-yl 4-bromobenzoate (*rac*-10m).**



The aldol precursor **3m** was prepared following the procedure described for *2R,3S*-5b, starting from **2m** (156 mg, 1 eq, 0.1 M concentration in the reaction) and **1a** (30 mg, 1 eq, 0.1 M concentration in the reaction). Chemical reduction was performed as described for *rac*-7a. Benzoylation of *rac*-10m was performed as describe for *R*-10j. The title compound was obtained as a yellow oil (26 mg, 17%). NMR spectra were indistinguishable from that of *R*-10m.

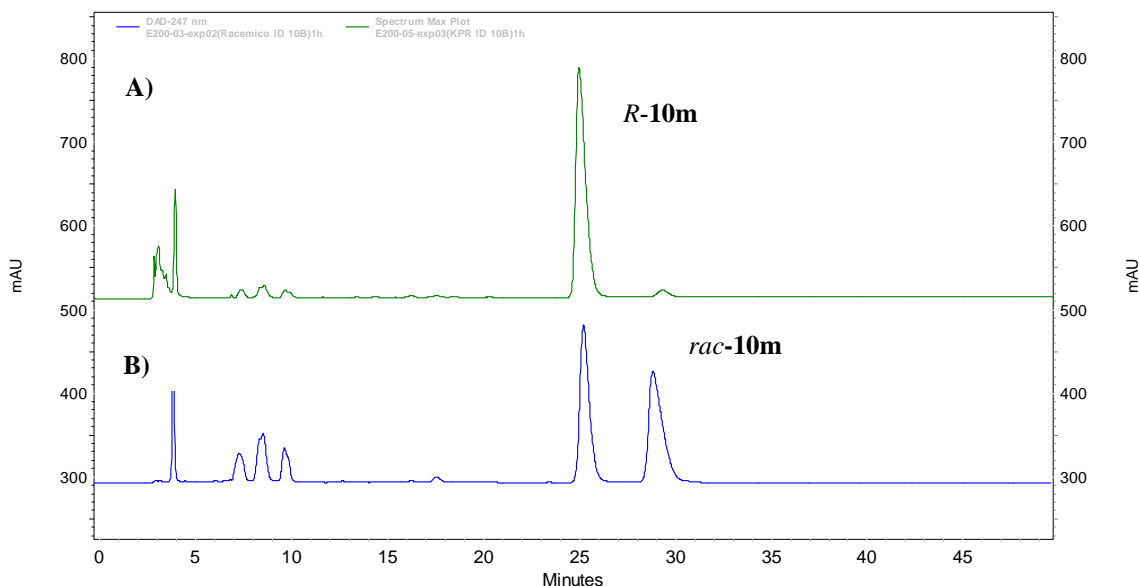
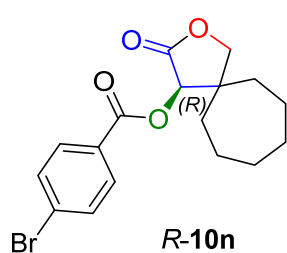


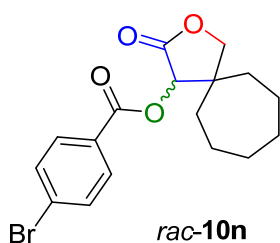
**Figure S9.** CPHPLC chromatogram of *R*-10m from KPR<sub>Ecoli</sub> catalysis (A) and *rac*-10m (B). Conditions: CHIRALPACK<sup>®</sup> ID, flow rate 1 mL min<sup>-1</sup> at 30 °C and detection at 254 nm. Isocratic elution Hexane:<sup>i</sup>PrOH 90:10 (v/v). tr (*R*) = 25.6 min, tr (*S*) = 29.2 min.

**(R)-3-oxo-2-oxaspiro[4.6]undecan-4-yl 4-bromobenzoate (*R*-10n).**



Synthesis of title compound was performed as described for *R*-10j starting from *R*-5n (20 mg) in acetonitrile (5 mL). *R*-10n was obtained as a yellow oil (9 mg, 23% yield). <sup>1</sup>H NMR (400 MHz, CDCl<sub>3</sub>) δ 7.95 (dd, *J* = 8.7, 2.3 Hz, 2H), 7.70 – 7.58 (m, 2H), 5.63 (s, 1H), 4.26 (d, *J* = 9.1 Hz, 1H), 4.04 (d, *J* = 9.1 Hz, 1H), 2.4 – 2.3 (m, 1H), 2.10 – 1.85 (m, 1H), 1.80 – 1.24 (m, 10H). <sup>13</sup>C NMR (101 MHz, CDCl<sub>3</sub>) δ 172.9, 165.1, 132.5, 132.0, 129.5, 128.2, 77.6, 75.4, 47.3, 36.9, 31.2, 30.5, 30.3, 23.7, 23.3. ee: 98%. [α]<sub>20</sub><sup>D</sup> = + 31.2 (*c* = 0.4 in MeOH).

**rac-3-oxo-2-oxaspiro[4.6]undecan-4-yl 4-bromobenzoate (*rac*-10n).**



The aldol precursor **3n** was prepared following the procedure described for *2R,3S*-5b, starting from **2n** (283.4 mg, 1 eq, 0.1 M concentration in the reaction) and **1a** (50 mg, 1 eq, 0.1 M concentration in the reaction). Chemical reduction was performed as described for *rac*-7a. Benzoylation of *rac*-10n was performed as describe for *R*-10j. The title compound was obtained as a yellow oil (20 mg, 7%). NMR spectra were indistinguishable from that of *R*-10n.

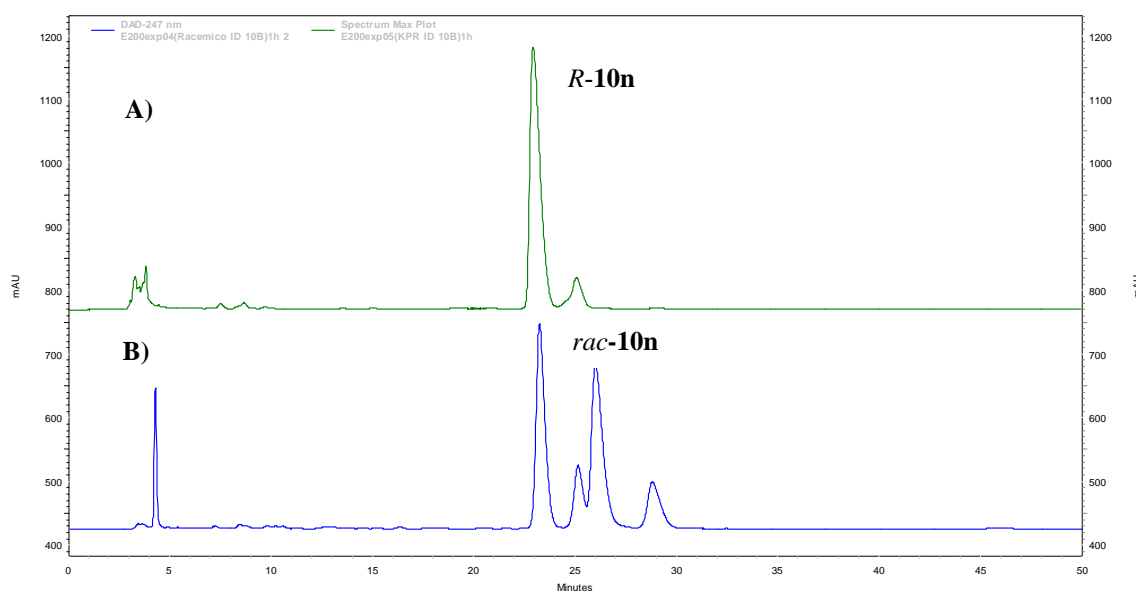
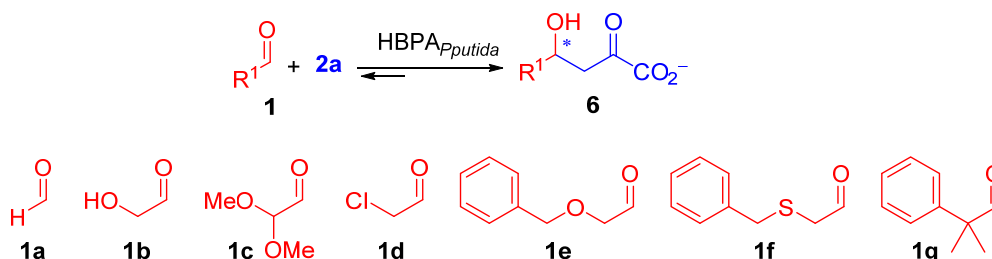


**Figure S10.** CPHPLC chromatogram of *R*-10n from KPR<sub>Ecoli</sub> catalysis (A) and *rac*-10n (B). Conditions: CHIRALPACK® ID, flow rate 1 mL min<sup>-1</sup> at 30 °C and detection at



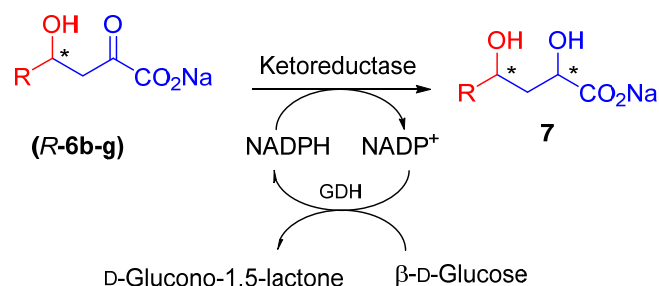
254 nm. Isocratic elution Hexane:PrOH 90:10 (v/v).  $t_r$  (*R*) = 22.9 min,  $t_r$  (*S*) = 25.9 min.

### Biocatalytic aldol addition of sodium pyruvate (**2a**) to aldehydes (**1b-g**). Analytical scale



Reactions were carried out at analytic level as follows: The reactions (500  $\mu\text{L}$  total volume) were conducted in Eppendorf tubes (1.5 mL) and placed in a vortex mixer (1000 rpm) at 25°C. To a solution of the aldehyde (**1b-g**) (dissolved in 50 mM sodium phosphate buffer pH 7.0, 100 mM final concentration in the reaction; in case of partial water solubility, DMF (20% v/v in the reaction was used), a solution of sodium pyruvate (**2a**) (25  $\mu\text{L}$  of a 2.0 M aqueous stock solution, pH 6.5-7.0, 100 mM final concentration in the reaction, (*Caution: The solution of sodium pyruvate has to be freshly prepared before use!*)) was added. The reaction was started by adding of HBPA<sub>*Pputida*</sub> wild-type (125  $\mu\text{L}$  of a stock solution 0.029 U mL<sup>-1</sup>, 4 mg mL<sup>-1</sup> in 50 mM TEA buffer, 50 mM NaCl, 0.5 mM EDTA and 50% (v/v) of glycerol, 0.007 U mL<sup>-1</sup>, 1 mg protein mL<sup>-1</sup> final concentration in the reaction, for enzyme reactions with **1b-c**, and **1e**). Or HBPA<sub>*Pputida*</sub> H205A (132  $\mu\text{L}$  of a stock solution 0.009 U mL<sup>-1</sup>, 3.8 mg mL<sup>-1</sup> in 50 mM TEA buffer, 50 mM NaCl, 0.5 mM EDTA and 50% (v/v) of glycerol, 0.00324 U mL<sup>-1</sup>, 1 mg mL<sup>-1</sup> protein final concentration in the reaction, for enzyme reactions with **1d**, **1f**, and **1g**). The reaction mixture was placed in a vortex mixer (1000 rpm) at 25 °C for 24 h. Samples were withdrawn immediately after the enzyme addition (0 h) and after 24 h and analyzed by HPLC as described above.

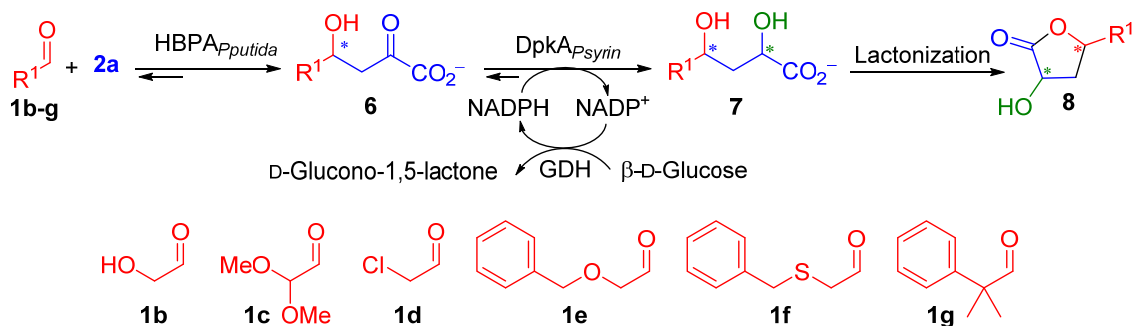
### Biocatalytic reduction of 4-hydroxy-2-oxoacids (**6b-g**). Substrate scope of ketoreductases. Analytical scale.



**Scheme S7.** Biocatalytic reduction of aldol adducts (**R-6b-g**) catalyzed by  $\text{DpkA}_{P_{\text{Syrin}}}$  and  $\text{KPR}_{E_{\text{coli}}}$ .

**Biocatalytic reduction catalyzed by  $\text{KPR}_{E_{\text{coli}}}$  or  $\text{DpkA}_{P_{\text{Syrin}}}$ :** Reactions were carried out at analytic level as follows: The reactions (500  $\mu\text{L}$  total volume) were conducted in Eppendorf tubes (1.5 mL) and placed in a vortex mixer (100 rpm) at 25  $^{\circ}\text{C}$ . The reduction mixture solutions (250  $\mu\text{L}$ ) were prepared by adding;  $\text{KPR}_{E_{\text{coli}}}$  (125  $\mu\text{L}$  of a stock solution of 52  $\text{U mL}^{-1}$ , 4  $\text{mg mL}^{-1}$  in 20 mM TEA buffer pH 7.0, 100 mM NaCl, and 50% (v/v) of glycerol, 13  $\text{U mL}^{-1}$  final concentration in the reaction) or  $\text{DpkA}_{P_{\text{Syrin}}}$  (125  $\mu\text{L}$  of a stock solution of  $2.6 \cdot 10^{-2}$   $\text{U mL}^{-1}$ , 4  $\text{mg mL}^{-1}$  in 20 mM TEA buffer pH 7.0, 100 mM NaCl, and 50% (v/v) of glycerol,  $6.5 \cdot 10^{-3}$   $\text{U mL}^{-1}$  final concentration in the reaction), GDH (83  $\mu\text{L}$  of a stock solution 20.8  $\text{U mL}^{-1}$ , 5.2  $\text{mg mL}^{-1}$  in 10 mM HEPES buffer pH 6.5, 50 mM NaCl, and 50% (v/v) of glycerol, 3.5  $\text{U mL}^{-1}$  final concentration in the reaction), glucose (18 mg, 4 eq, 0.2 M final concentration in reaction) and  $\text{NADP}^+$  (1.9 mg, 5 mM in reaction). The reactions were started by the addition of a sample of the corresponding aldol reaction (250  $\mu\text{L}$ ), containing adducts **6b-g** ( $\approx 100$  mM as the basis of calculation). Samples were withdrawn immediately after the addition of aldol substrate (0 h) and after 24 h and analyzed by HPLC as described above.

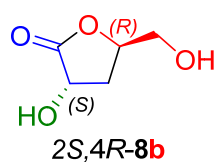
**One-pot two-step stereoselective synthesis of 4-substituted-2-hydroxy-4-butyrolactones **8** by tandem biocatalytic aldol-reduction reactions catalyzed by HBPA<sub>Pputida</sub> and DpkA<sub>Psyrin</sub>.**



**Scheme 8.** One-pot two-step synthesis of 4-substituted-2-hydroxy-4-butyrolactones **8** by tandem biocatalytic aldol-reduction reactions catalyzed by HBPA<sub>Pputida</sub> and DpkA<sub>Psyrin</sub>.

The reactions combining HBPA<sub>Pputida</sub> and DpkA<sub>Psyrin</sub> were carried out as follows:

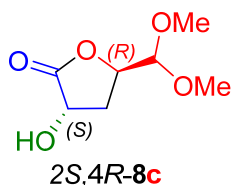
(2*S*,4*R*)-4-(hydroxymethyl)-2-(hydroxy)-4-butyrolactone (2*S*,4*R*-**8b**).



**Aldol addition (1<sup>st</sup>):** The reaction (1 mmol scale, 8.3 mL total volume) was conducted in a round-bottom flask (100 mL) at 25 °C for 24 h and orbitally stirred at 250 rpm. Sodium pyruvate **2b** (91.6 mg, 1 mmol, 1 eq, 0.1 M in the reaction) and glycolaldehyde dimer **1b** (50 mg, 1 mmol monomer, 1 eq, 0.1 M in the reaction) were dissolved in 5.9 mL of water. Finally, reaction was started by adding the enzyme (HBPA *wild-type*, 2 mL of a stock solution 0.029 U mL<sup>-1</sup>, 4 mg mL<sup>-1</sup> in 50 mM TEA buffer, 50 mM NaCl, 0.5 mM EDTA and 50% (v/v) of glycerol, 0.007 U mL<sup>-1</sup>, 1 mg protein mL<sup>-1</sup> final concentration in the reaction). Reaction was monitored by HPLC and samples were withdrawn immediately after the enzyme addition (0 h) and after 24 h as described above. **Aldol reduction (2<sup>nd</sup>).** After 24 h, the reduction reaction (16.6 mL final volume) was carried out as follows: to the aldol reaction mixture were added glucose (598 mg, 4 mmol, 4 eq, 0.2 M final concentration in the reaction), GDH (2.75 mL of a stock solution 20.8 U mL<sup>-1</sup>, 5.2 mg mL<sup>-1</sup> in 10 mM HEPES buffer pH 6.5, 50 mM NaCl, and 50% (v/v) of glycerol, 3.4 U mL<sup>-1</sup> final concentration in the reaction) and DpkA<sub>Psyrin</sub> (4.15 mL of a stock solution 2.6 10<sup>-2</sup> U mL<sup>-1</sup>, 4 mg mL<sup>-1</sup> in 20 mM TEA buffer pH 7.0, 100 mM NaCl, and 50%

(v/v) of glycerol,  $6.5 \cdot 10^{-3} \text{ U mL}^{-1}$  final concentration in the reaction). The reaction was started by adding a solution of  $\text{NADP}^+$  (1.4 mL of stock solution 69 mM in 1 M sodium phosphate buffer pH 8.0, 5 mM final concentration in the reaction). The mixture reaction was stirred at room temperature and the reaction was monitored by HPLC as described above. After no aldol adduct was detected by HPLC (24 h), methanol (200 mL) was added under stirring. The mixture was filtered through Celite<sup>®</sup> and the filter cake washed with methanol (3 x 50 mL). The organic solvent was removed and the pH of the remaining aqueous solution was adjusted to 9.0 with 1 M NaOH. Then, water was added up to a final volume of 40 mL. The product purification was started with anion exchange chromatography (DOWEX 1X8 ion exchange resin (50-100 mesh) in  $\text{HCO}_2^-$  form, column: 44 cm,  $\text{Ø} = 1,6$  cm). The sample was loaded onto the column and the resin was washed with plain water (90 mL). The bound fractions with the compound were eluted with a solution of 1 M  $\text{HCO}_2\text{H}$  (fraction volume 30 mL). Fractions containing the product were pooled freeze-dried, dissolved in methanol (30 mL), absorbed in silica and purified by column chromatography on silica with a step gradient of hexane:EtOAc: 100:0, 200 mL, 0:100, 300 mL. Pure fractions were pooled and the solvent removed under vacuum affording the lactone **2S,4R-8b** as a yellow oil (30 mg, 27%).  $^1\text{H}$  NMR (400 MHz,  $\text{D}_2\text{O}$ )  $\delta$  4.83 (ddt,  $J = 8.9, 4.4, 2 \times 2.7$  Hz, 1H), 4.73 (t,  $J = 2 \times 8.9$  Hz, 1H), 3.85 (dd,  $J = 12.9, 2.7$  Hz, 1H), 3.68 (dd,  $J = 12.9, 4.5$  Hz, 1H), 2.54 (ddd,  $J = 13.5, 9.0, 2.9$  Hz, 1H), 2.34 (dt,  $J = 13.5, 2 \times 8.9$  Hz, 1H).  $^{13}\text{C}$  NMR (101 MHz,  $\text{D}_2\text{O}$ )  $\delta$  180.0, 79.5, 67.0, 62.9, 31.9. Minor diastereomer selected key signals  $^1\text{H}$  NMR (400 MHz,  $\text{D}_2\text{O}$ )  $\delta$  4.50 (dd,  $J = 3.0, 0.9$  Hz, 1H), 3.83 (dd,  $J = 13.0, 2.6$  Hz, 1H).  $^{13}\text{C}$  NMR (101 MHz,  $\text{D}_2\text{O}$ ) peaks detected by HSQC experiment:  $\delta$  73.1, 62.1.  $[\alpha]_{20}^{\text{D}} = -49.6$  ( $c = 1$ , in MeOH), dr: 98:2. ESI-TOF  $m/z$ : Calcd for  $[\text{M}+\text{Na}^+]$   $\text{C}_5\text{H}_8\text{O}_4\text{Na}^+$ : 155.0315, found  $[\text{M}+\text{Na}^+]$ : 155.0319.

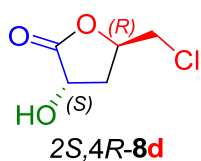
#### (2S,4R)-4-(dimethoxymethyl)-2-(hydroxy)-4-butyrolactone (**2S,4R-8c**)



The title compound was prepared as described for **2S,4R-8b**. Starting from **1c** ( $[\mathbf{1c}] = [\mathbf{2a}] = 100$  mM in the reaction,  $V_{\text{aldol reaction}} = 10,6$  mL). **2S,4R-8c** was obtained as a yellow oil (54 mg, 29%). In this case the product was eluted with a step gradient of Hexane:EtOAc: 100:0, 200 mL, 75:25, 200 mL, 50:50, 200 mL and 25:75, 500 mL on column chromatography on silica.  $^1\text{H}$  NMR (400 MHz, MeOD)  $\delta$  4.42 (ddd,  $J = 8.9, 3.2, 2.2$  Hz, 1H), 4.32 (t,  $J = 2 \times 8.8$  Hz, 1H), 4.26 (d,  $J = 3.2$  Hz, 1H),

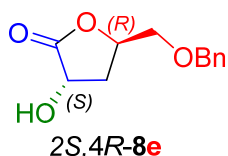
3.32 (s, 3H), 3.31 (s, 3H), 2.43 (ddd,  $J = 13.4, 8.9, 2.3$  Hz, 1H), 1.93 (dt,  $J = 13.4, 2 \times 8.8$  Hz, 1H).  $^{13}\text{C}$  NMR (101 MHz, MeOD)  $\delta$  179.5, 106.2, 77.7, 67.7, 57.4, 56.7, 32.2. No signals were detected from minor diastereomers  $[\alpha]_{20}^{\text{D}} = -35.7$  ( $c = 0.5$ , in MeOH), dr: 98:2. ESI-TOF  $m/z$ : Calcd for  $[\text{M}+\text{Na}^+]$   $\text{C}_7\text{H}_{12}\text{O}_5\text{Na}^+$ : 199.0577, found  $[\text{M}+\text{Na}^+]$ : 199.0566.

**(2*S*,4*R*)-4-(chloromethyl)-2-(hydroxy)-4-butyrolactone (2*S*,4*R*-8*d*).**



Synthesis of aldol adduct **6d** was prepared using HBPA<sub>*Pputida*</sub> H205A variant with the procedure described 2*S*,4*R*-8*d*, starting from **1d** (**1d** = **2a**) = 100 mM in the reaction,  $V_{\text{aldol reaction}} = 7,6$  mL). 2*S*,4*R*-8*d* was obtained as a yellow oil (30 mg, 26%). In this case the product was eluted with a step gradient of Hexane:EtOAc: 100:0, 200 mL, 75:25, 200 mL and 50:50, 750 mL on column chromatography on silica.  $^1\text{H}$  NMR (400 MHz,  $\text{CDCl}_3$ )  $\delta$  4.92 (ddt,  $J = 8.7, 4.5, 2 \times 3.4$  Hz, 1H), 4.68 (dd,  $J = 8.9, 7.7$  Hz, 1H), 3.78 (dd,  $J = 12.1, 4.5$  Hz, 1H), 3.67 (dd,  $J = 12.1, 3.4$  Hz, 1H), 2.58 (ddd,  $J = 13.8, 8.9, 3.3$  Hz, 1H), 2.42 (ddd,  $J = 13.8, 8.6, 7.7$  Hz, 1H).  $^{13}\text{C}$  NMR (101 MHz,  $\text{CDCl}_3$ )  $\delta$  177.1, 76.5, 67.5, 46.8, 33.5. Minor diastereomer selected key signals  $^1\text{H}$  NMR (400 MHz,  $\text{CDCl}_3$ )  $\delta$  4.42 (dd,  $J = 7.4, 4.1$  Hz, 1H), 3.76 (dd,  $J = 5.2, 1.3$  Hz, 1H), 3.60 (dd,  $J = 7.4, 5.3$  Hz, 2H), 2.20 – 2.12 (m, 1H), 1.94 (ddd,  $J = 14.4, 9.4, 7.4$  Hz, 1H).  $^{13}\text{C}$  NMR (101 MHz,  $\text{CDCl}_3$ ) peaks detected by HSQC experiment:  $\delta$  68.8, 49.4. The NMR data matched that reported in the literature.<sup>16</sup>  $[\alpha]_{20}^{\text{D}} = -59.7$  ( $c = 0.5$ , in MeOH), dr: 94:6. ESI-TOF  $m/z$ : Calcd for  $[\text{M}+\text{Na}^+]$   $\text{C}_5\text{H}_7\text{ClO}_3\text{Na}^+$ : 172.9976, found  $[\text{M}+\text{Na}^+]$ : 245.0779.

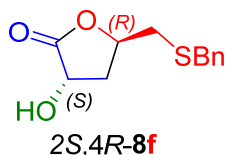
**(2*S*,4*R*)-4-((benzyloxy)methyl)-2-(hydroxy)-4-butyrolactone (2*S*,4*R*-8*e*).**



The synthesis of aldol intermediate **6b** was conducted in an Erlenmeyer (50 mL). Reaction volume was 5.3 mL. Benzyloxyacetaldehyde (**1e**) (80.0 mg, 5.3 mmol, 1 eq, 0.1 M in the reaction) was dissolved in DMF (1.1 mL, 20% (v/v) final concentration in the reaction) and sodium pyruvate **2a** (58.6mg, 5.3 mmol, 1 eq, 0.1 M final concentration in the reaction) dissolved in water (2.9 mL) was added. Finally, reaction was started by adding the enzyme (HBPA *wild-type*, 1.3 mL of a stock solution 0.029 U mL<sup>-1</sup>, 4 mg mL<sup>-1</sup> in 50 mM TEA buffer, 50 mM NaCl, 0.5 mM EDTA and 50% (v/v) of glycerol, 0.007 U mL<sup>-1</sup>, 1 mg protein mL<sup>-1</sup> final concentration in the

reaction). Reaction was monitored by HPLC and samples were withdrawn immediately after the enzyme addition (0 h) and after 24 h as described above. **Aldol reduction**, the reduction of aldol adduct with DpkA<sub>Psyrin</sub> was performed as describe for 2*S*,4*R*-**8b**. In this case, the product was obtained after anion exchange purification as a white solid (41 mg, 30%). Containing: (2*S*,4*R*)-5-(benzyloxy)-2,4-dihydroxypentanoic acid (2*S*,4*R*-**7e**): <sup>1</sup>H NMR (400 MHz, D<sub>2</sub>O) δ 7.49 – 7.06 (m, 5H), 4.53 (s, 2H), 4.27 (dd, *J* = 6.6, 5.4 Hz, 1H), 4.05 – 3.94 (m, 1H), 3.51 (dd, *J* = 10.7, 3.7 Hz, 1H), 3.44 (dd, *J* = 10.7, 6.9 Hz, 1H), 1.93 (dt, *J* = 14.5, 2x5.1 Hz, 1H), 1.80 (ddd, *J* = 14.7, 8.1, 6.6 Hz, 1H). <sup>13</sup>C NMR (101 MHz, D<sub>2</sub>O) δ 177.6, 137.3, 128.7, 128.7, 128.5, 128.4, 73.0, 73.3, 66.7, 67.4, 37.0, and (2*S*,4*R*-**8e**) <sup>1</sup>H NMR (400 MHz, D<sub>2</sub>O) δ 7.49 – 7.17 (m, 5H), 4.80 (ddt, *J* = 9.0, 5.4, 2x2.8 Hz, 1H), 4.64 – 4.55 (m, 1H), 4.52 (s, 2H), 3.71 (dd, *J* = 11.7, 2.7 Hz, 1H), 3.60 (dd, *J* = 11.7, 5.0 Hz, 1H), 2.41 (ddd, *J* = 13.4, 8.9, 2.9 Hz, 1H), 2.23 (dt, *J* = 13.4, 2x8.9 Hz, 1H). <sup>13</sup>C NMR (101 MHz, D<sub>2</sub>O) δ 179.8, 137.3, 128.7, 128.7, 128.5, 128.4, 78.0, 73.0, 70.9, 66.6, 32.2. [α]<sub>20</sub><sup>D</sup> = – 33.3 (*c* = 0.5, in MeOH), dr: 94:6. ESI-TOF *m/z*: Calcd for [M+Na<sup>+</sup>] C<sub>12</sub>H<sub>14</sub>O<sub>4</sub>Na<sup>+</sup>: 245.0784, found [M+Na<sup>+</sup>]: 245.0779.

**(2*S*,4*R*)-4-((benzylthio)methyl)-2-(hydroxy)-4-butyrolactone (2*S*,4*R*-**8f**).**

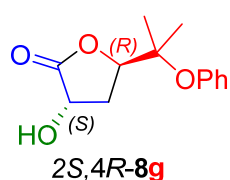


Synthesis of aldol adduct **6f** was prepared using HBPA<sub>Pputida</sub> H205A variant with the procedure described 2*S*,4*R*-**8e**, starting from **1f** ([**1f**] = [**2a**] = 100 mM in the reaction, V<sub>aldol reaction</sub> = 10.2 mL). The **Aldol reduction** with DpkA<sub>Psyrin</sub> was performed as describe for 2*S*,4*R*-**8b**. After no aldol adduct was detected by HPLC (24 h), methanol (200 mL) was added under stirring. The mixture was filtered through Celite<sup>®</sup> and the filter cake washed with methanol (3 x 50 mL). The solvent was removed under vacuum. The residue was re-suspended in toluene (200 mL) and *p*-toluene-sulfonic acid (19.5 mg, 0.01 eq) was added. The mixture was heated to reflux for 16h, using a dean-stark apparatus. This is to promote the formation of lactone.

After which it was cooled, 5% NaHCO<sub>3</sub> (100 mL) was added, toluene was removed and the aqueous solution was extracted with CH<sub>2</sub>Cl<sub>2</sub> (3 × 50 mL). Aqueous phase was then acidified to pH 2 with 3 M HCl and extracted with EtOAc (3 × 50 mL). The organic layer was washed with water (3 × 50 mL) and brine (3 × 50 mL), and dried over MgSO<sub>4</sub>. The sample was absorbed in silica and purified by column chromatography on silica with a step gradient of hexane:EtOAc: 100:0, 200 mL, 75:25, 200 mL, 50:50,

200mL and 75:25, 500 mL. Pure fractions were pooled and the solvent removed under vacuum affording the lactone **2S,4R-8f** as a brown oil (92 mg, 38%). <sup>1</sup>H NMR (400 MHz, CDCl<sub>3</sub>) δ 7.40 – 7.22 (m, 5H), 4.76 (dtd, *J* = 7.9, 2x5.4, 3.9 Hz, 1H), 4.61 (td, *J* = 2x8.1, 2.2 Hz, 1H), 3.76 (d, *J* = 2.9 Hz, 2H), 2.66 (d, *J* = 5.5 Hz, 2H), 2.42 – 2.27 (m, 2H). <sup>13</sup>C NMR (101 MHz, CDCl<sub>3</sub>) δ 176.9, 137.4, 129.1, 128.7, 127.4, 77.5, 67.3, 37.1, 35.3, 34.6. Minor diastereomer selected key signals: <sup>1</sup>H NMR (400 MHz, CDCl<sub>3</sub>) δ 4.56 – 4.42 (m, 1H), 2.01 (dt, *J* = 12.7, 10.3 Hz, 1H). <sup>13</sup>C NMR (101 MHz, CDCl<sub>3</sub>) δ no signals detected.  $[\alpha]_{20}^D = -30.4$  (*c* = 0.5, in MeOH), dr: 87:13. ESI-TOF *m/z*: Calcd for  $[M+Na^+]$  C<sub>12</sub>H<sub>14</sub>SO<sub>3</sub>Na<sup>+</sup>: 261.0556, found  $[M+Na^+]$ : 261.0551.

**(2S,4R)-4-(2-phenoxypropan-2-yl)-2-(hydroxy)-4-butyrolactone (2S,4R-8g).**



Synthesis of aldol adduct **6g** was prepared as described for **2S,4R-8e**. Starting from **1g** ( $[1g] = [2a] = 100$  mM in the reaction,  $V_{\text{aldol reaction}} = 6$  mL). The **Aldol reduction** with DpkA<sub>psyrin</sub> was performed as describe for **2S,4R-8b**. Lactonization reaction and purification were carried out as described for **2S,4R-8f** was obtained as a white solid (52 mg, 34%). <sup>1</sup>H NMR (400 MHz, CDCl<sub>3</sub>) δ 7.32 – 7.22 (m, 2H), 7.16 – 7.06 (m, 1H), 6.92 (dd, *J* = 8.6, 1.1 Hz, 2H), 4.76 (t, *J* = 2x8.7 Hz, 1H), 4.45 (dd, *J* = 9.0, 2.2 Hz, 1H), 2.90 (ddd, *J* = 13.4, 9.0, 2.3 Hz, 1H), 2.39 – 2.27 (m, 1H), 1.32 (s, 3H), 1.29 (s, 3H). <sup>13</sup>C NMR (101 MHz, CDCl<sub>3</sub>) δ 178.0, 153.9, 129.2, 124.2, 123.8, 83.7, 80.3, 67.3, 31.4, 23.6, 22.6. No signals were detected from minor diastereomers.  $[\alpha]_{20}^D = -47.2$  (*c* = 0.5, in MeOH), dr: 98:2. ESI-TOF *m/z*: Calcd for  $[M+Na^+]$  C<sub>13</sub>H<sub>16</sub>O<sub>4</sub>Na<sup>+</sup>: 259.0941, found  $[M+Na^+]$ : 259.0958.

**Kinetic Studies.**

**Substrates (3a-m) and (6b-g) stock solution preparation.**

Stock solutions of aldol adduct (**3a-m**) in H<sub>2</sub>O pH 7.0 were prepared using the best 2-oxoacid aldolase variant as described above. Likewise for stock solutions of aldol adduct (**6b-g**) was prepared in 50 mM phosphate buffer pH 7.0 using the best HBPA variant as described above (Table S4). In both cases, enzymes were removed from the mixture using Amicon Ultra-15, PLBC Ultracel-PL membrane, 3 KDa cutoff.

**Table S4.** Adduct aldol stock solutions in water.

Substrate <b>3</b>	Aldolases	Concentration/mM <sup>a</sup>	ee <sup>b</sup> /%
<b>3a</b>	YfaU <sub>Ecoli</sub> wt	85	-
<b>3S-3b</b>	YfaU <sub>Ecoli</sub> W23V	92	98
<b>3S-3c</b>		95	99
<b>3S-3d</b>		88	98
<b>3S-3f</b>		89	99
<b>3S-3g</b>		98	98
<b>3S-3h</b>		98	94
<b>3R-3b</b>		KPHMT <sub>Ecoli</sub> wt	94
<b>3R-3c</b>	KPHMT <sub>Ecoli</sub> wt	98	95
<b>3R-3d</b>	KPHMT <sub>Ecoli</sub> I212A	97	96
<b>3R-3e</b>	KPHMT <sub>Ecoli</sub> I212A	82	- <sup>c</sup>
<b>3R-3g</b>	KPHMT <sub>Ecoli</sub> wt	84	87
<b>3R-3h</b>	KPHMT <sub>Ecoli</sub> I202A	80	75
<b>3j</b>	KPHMT <sub>Ecoli</sub> wt	88	- <sup>d</sup>
<b>3k</b>	KPHMT <sub>Ecoli</sub> wt	80	- <sup>d</sup>
<b>3l</b>	KPHMT <sub>Ecoli</sub> wt	96	- <sup>d</sup>
<b>4R-6b</b>	HBPA <sub>Pputida</sub> wt	82	94
<b>4R-6c</b>	HBPA <sub>Pputida</sub> wt	85	87

<sup>a</sup>Concentration was estimated on the basis of the conversion percentage of the aldol addition at 24h. <sup>b</sup>Determined by HPLC on a chiral stationary phase in our lab using procedure published in previous works <sup>9</sup>. <sup>c</sup>Not determined. <sup>d</sup>Not applicable.

### Steady-State Kinetic Studies of ketoreductases.

The kinetic parameters for KPR<sub>Ecoli</sub> and DpkA<sub>Psyrin</sub> were determined in a continuous assay method monitoring the oxidation of NADPH to NADP<sup>+</sup> at 340 nm (NADPH  $\epsilon_{340} = 6.22 \text{ mM}^{-1} \text{ cm}^{-1}$ ) using aldol adduct as substrates (Table S4). The reactions were monitored during 15 min measuring each 30 s. The assay mixture (0.3 mL) consisted of 50 mM Tris-HCl buffer pH 8.0, containing NADPH (0.16 mM), aldol adducts (1-60 mM) and appropriate amounts of enzymes (optimal range of enzyme concentration determined for each substrate, see S11-S32). One unit of activity was defined as the amount of ketoreductases that catalyzes the formation of 1  $\mu\text{mol}$  NADP<sup>+</sup> per min at 30 °C. Measurements were carried out in triplicate independent experiments. To determine the kinetic parameters, data were fitted to the Michaelis-Menten kinetic model using the software GraphPad Prism version 5.0.



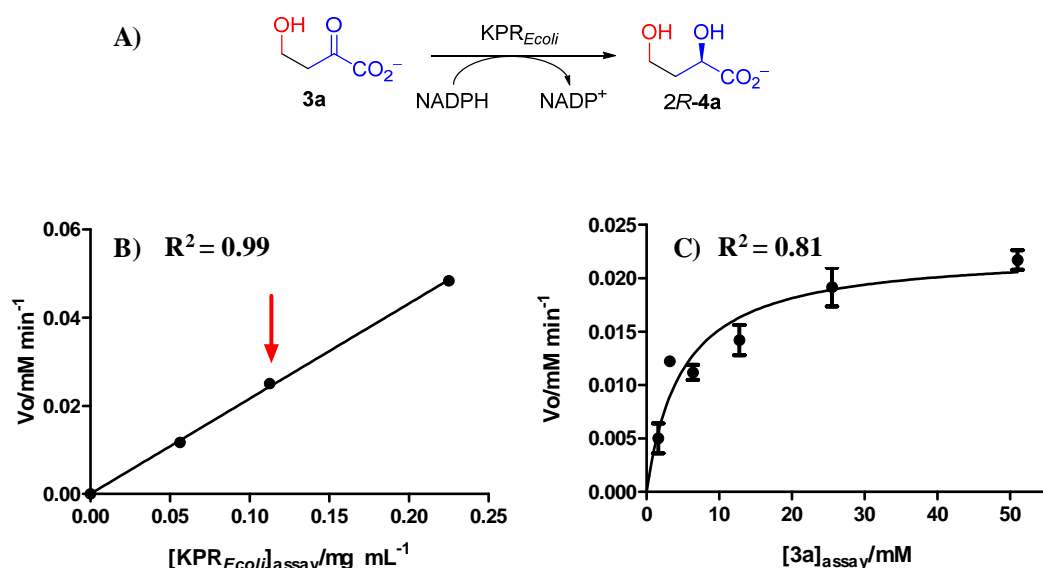


**Figure S11.** Reduction of **3a** to **2R-4a** catalyzed by  $KPR_{Ecoli}$ . (A). Initial reaction rate ( $V_o$ ) vs the enzyme concentration. The arrow shows the enzyme concentration selected to perform the enzyme assay (B) and  $V_o$  vs substrate concentration ( $0.2 (K_m^{app}) \leq [S] \leq 20.2 (K_m^{app})$ ), adjusted to a Michaelis-Menten model by non-linear regression method (C). Each point is the mean of three independent experiments.

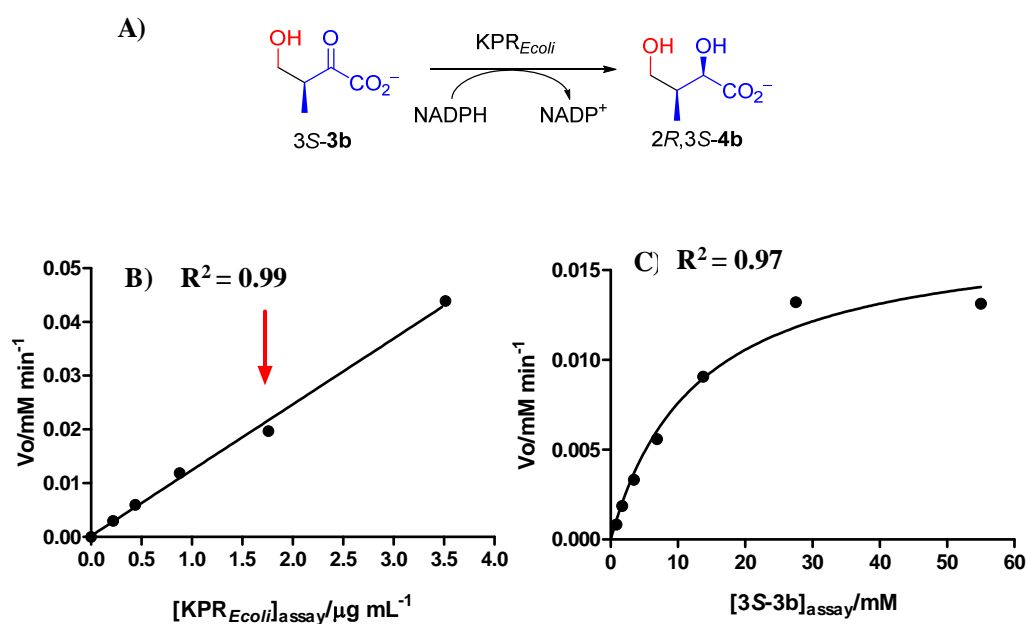


**Figure S12.** Reduction of **3S-3b** to **2R,3S-4b** catalyzed by  $KPR_{Ecoli}$ . (A). Initial reaction rate ( $V_o$ ) vs the enzyme concentration. The arrow shows the enzyme concentration selected to perform the enzyme assay (B) and  $V_o$  vs substrate concentration ( $0.07 (K_m^{app}) \leq [S] \leq 4.5 (K_m^{app})$ ), adjusted to a Michaelis-Menten model by non-linear regression method (C). Each point is the mean of three independent experiments.

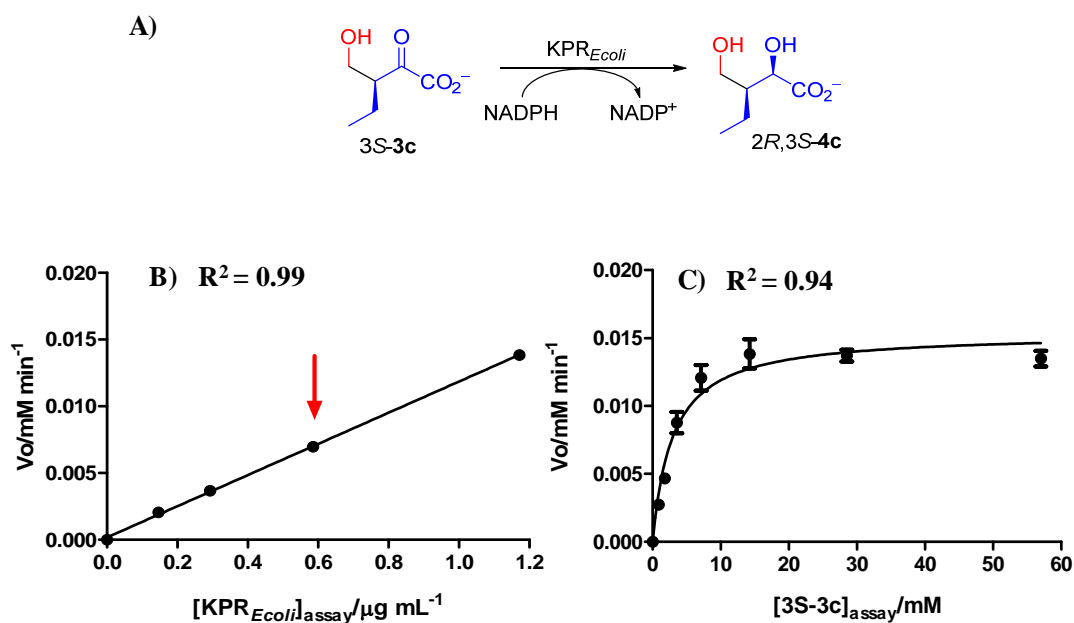


**Figure S13.** Reduction of 3S-3c to 2R,3S-4c catalyzed by  $KPR_{Ecoli}$ . (A). Initial reaction rate ( $V_0$ ) vs the enzyme concentration. The arrow shows the enzyme concentration selected for the enzyme assay (B) and  $V_0$  vs substrate concentration ( $0.3 (K_m^{app}) \leq [S] \leq 19.3 (K_m^{app})$ ), adjusted to a Michaelis-Menten model by non-linear regression method (C). Each point is the mean of three independent experiments.

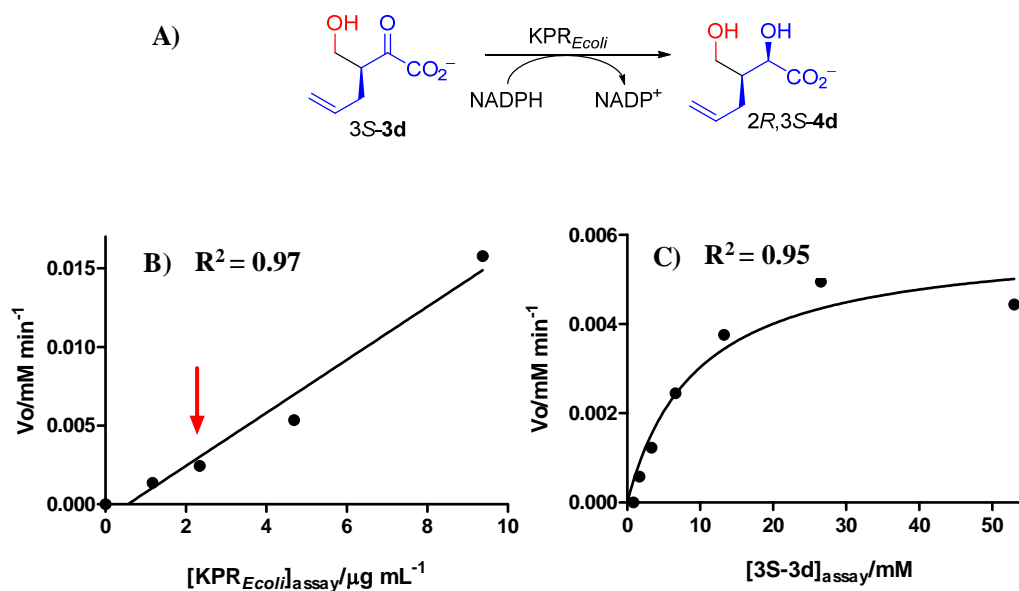


**Figure S14.** Reduction of 3S-3d to 2R,3S-4d catalyzed by  $KPR_{Ecoli}$ . (A). Initial reaction rate ( $V_0$ ) vs the enzyme concentration. The arrow shows the enzyme concentration selected for the enzyme assay (B) and  $V_0$  vs substrate concentration ( $0.11 (K_m^{app}) \leq [S]$

$\leq 5.8$  ( $K_m^{app}$ ), adjusted to a Michaelis-Menten model by non-linear regression method (C). Each point is the mean of three independent experiments.

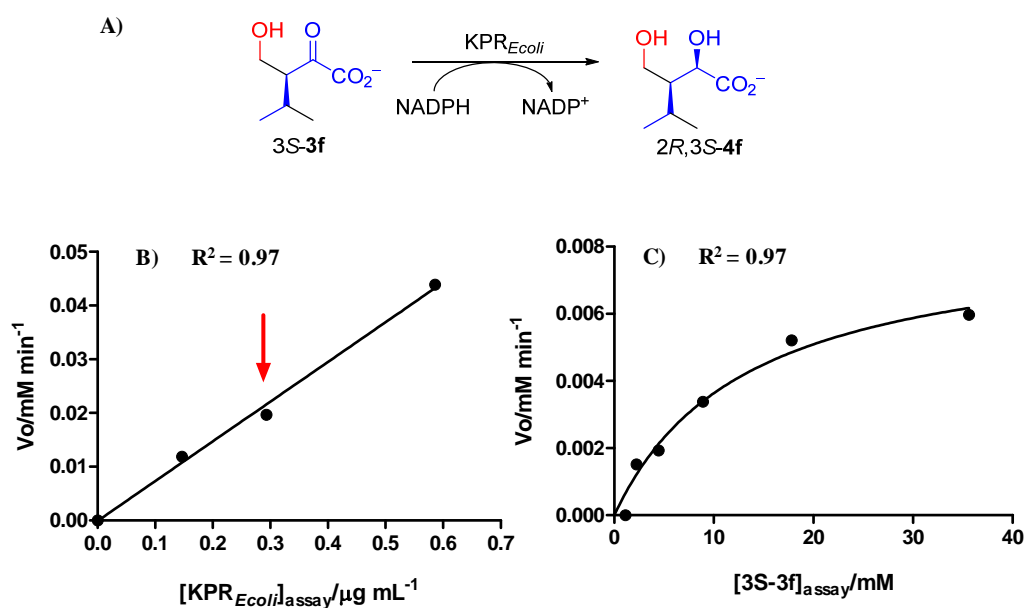


**Figure S15.** Reduction of 3S-3f to 2R,3S-4f catalyzed by KPR<sub>Ecoli</sub>. (A). Initial reaction rate ( $V_0$ ) vs the enzyme concentration. The arrow shows the enzyme concentration selected for the enzyme assay (B) and  $V_0$  vs substrate concentration ( $0.08$  ( $K_m^{app}$ )  $\leq$   $[S]$   $\leq 2.8$  ( $K_m^{app}$ )), adjusted to a Michaelis-Menten model by non-linear regression method (C). Each point is the mean of three independent experiments.

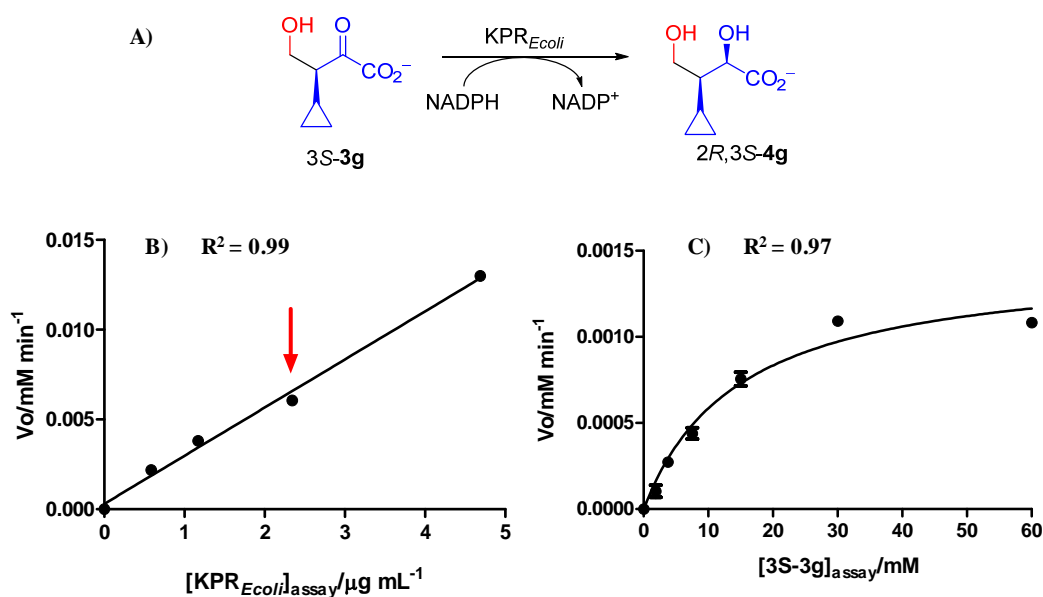


**Figure S16.** Reduction of 3S-3g to 2R,3S-4g catalyzed by KPR<sub>Ecoli</sub>. (A). Initial reaction rate ( $V_0$ ) vs the enzyme concentration. The arrow shows the enzyme concentration

selected for the enzyme assay (**B**) and  $V_o$  vs substrate concentration ( $0.07(Km^{app}) \leq [S] \leq 4(Km^{app})$ ), adjusted to a Michaelis-Menten model by non-linear regression method (**C**). Each point is the mean of three independent experiments.

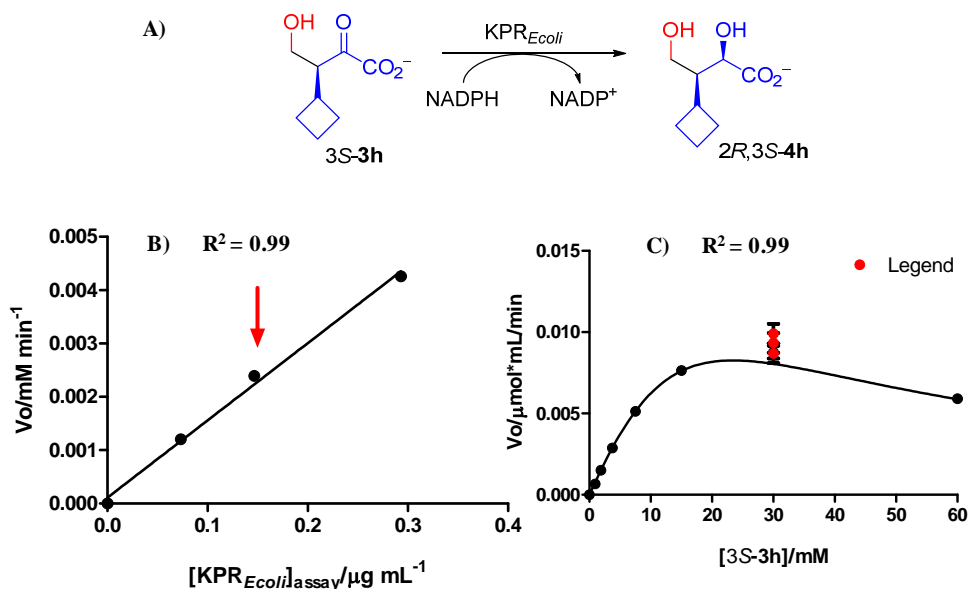


**Figure S17.** Reduction of 3S-3h to 2R,3S-4h catalyzed by KPR<sub>Ecoli</sub>. (**A**). Initial reaction rate ( $V_o$ ) vs the enzyme concentration. The arrow shows the enzyme concentration selected for the enzyme assay (**B**) and  $V_o$  vs substrate concentration ( $0.015 (Km^{app}) \leq [S] \leq 0.9 (Km^{app})$ ), adjusted to a Michaelis-Menten model by non-linear regression method (**C**). Each point is the mean of three independent experiments. The data were fitted to a substrate inhibition model using statistical analysis in GraphPad Prism 5 software. Comparison of fits between Michaelis-Menten: null hypothesis, and substrate inhibition: alternative hypothesis. For a  $P < 0.0001$ , the conclusion ( $\alpha = 0.05$ ) was: reject null hypothesis, and the preferred model was substrate inhibition. The outlier point is shown in red.

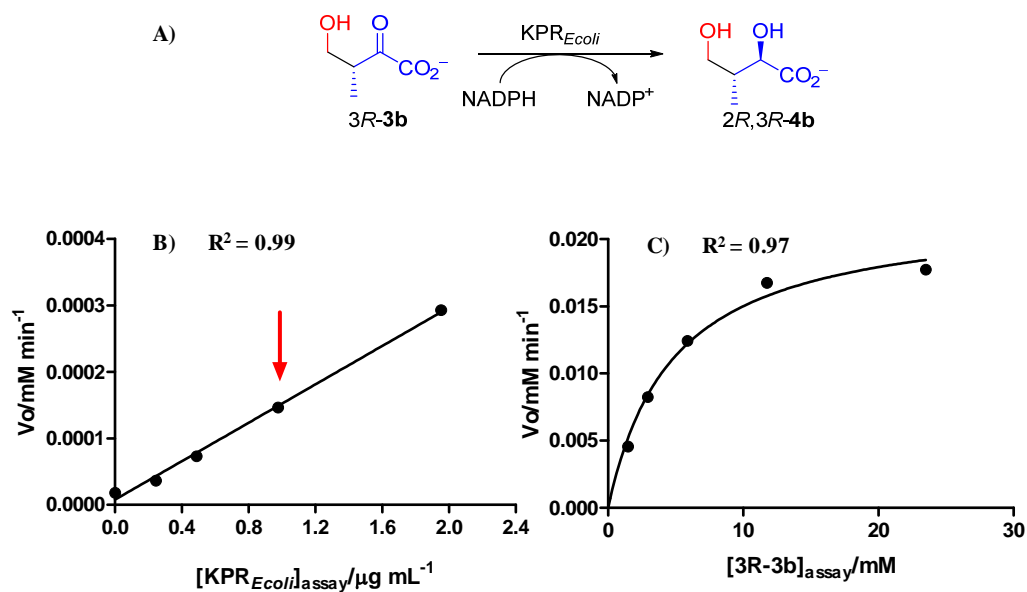


**Figure S18.** Reduction of 3R-3b to 2R,3R-4b catalyzed by KPR<sub>Ecoli</sub>. (A). Initial reaction rate ( $V_0$ ) vs the enzyme concentration. The arrow shows the enzyme concentration selected for the enzyme assay (B) and  $V_0$  vs substrate concentration ( $0.2 (K_m^{app}) \leq [S] \leq 5(K_m^{app})$ ), adjusted to a Michaelis-Menten model by non-linear regression method (C). Each point is the mean of three independent experiments.

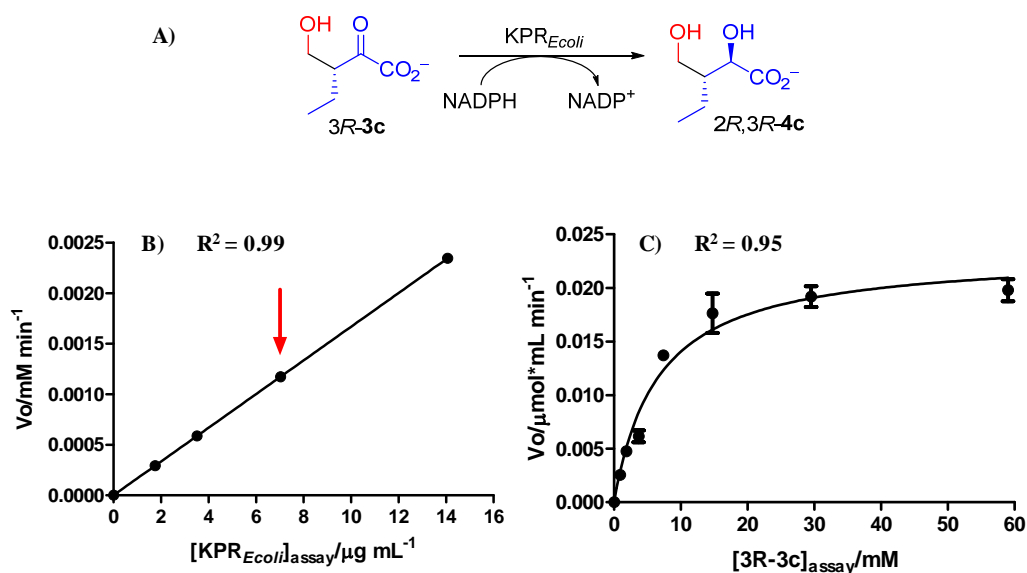


**Figure S19.** Reduction of 3R-3c to 2R,3R-4c catalyzed by KPR<sub>Ecoli</sub>. (A). Initial reaction rate ( $V_0$ ) vs the enzyme concentration. The arrow shows the enzyme concentration selected for the enzyme assay (B) and  $V_0$  vs substrate concentration ( $0.14 (K_m^{app}) \leq [S] \leq 8.6 (K_m^{app})$ ), adjusted to a Michaelis-Menten model by non-linear regression method (C). Each point is the mean of three independent experiments.

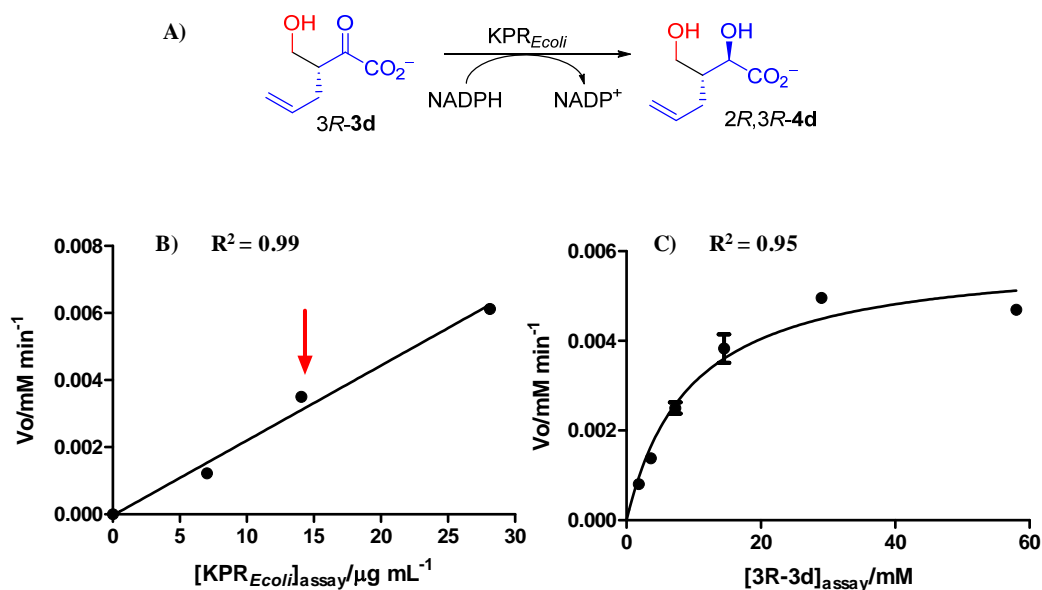


**Figure S20** Reduction of 3R-3d to 2R,3R-4d catalyzed by  $KPR_{Ecoli}$ . (A). Initial reaction rate ( $V_0$ ) vs the enzyme concentration. The arrow shows the enzyme concentration selected for the enzyme assay (B) and  $V_0$  vs substrate concentration ( $0.11 (K_m^{app}) \leq [S] \leq 6.1 (K_m^{app})$ ), adjusted to a Michaelis-Menten model by non-linear regression method (C). Each point is the mean of three independent experiments.

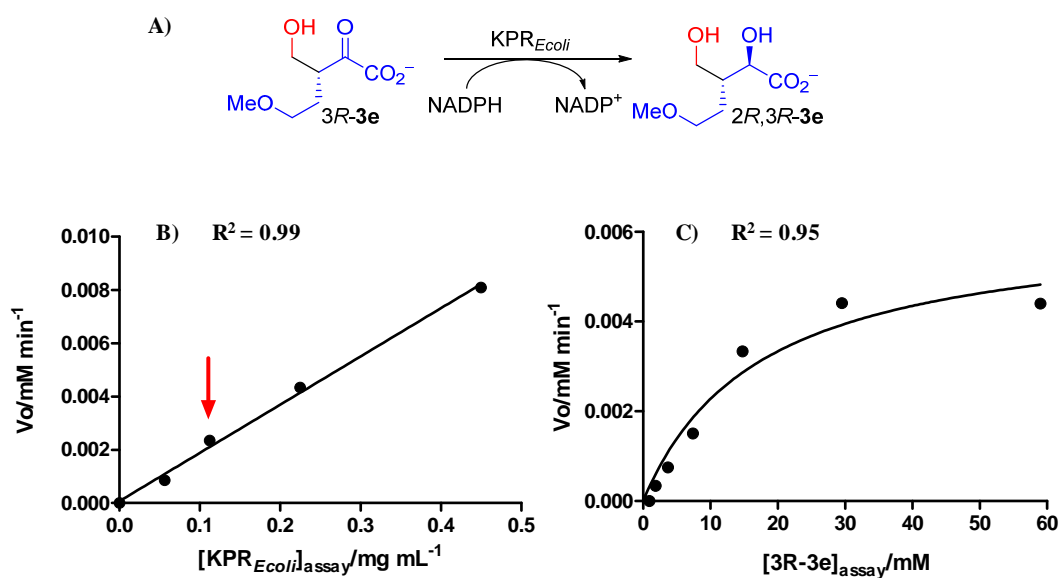


**Figure S21.** Reduction of 3R-3e to 2R,3R-4e catalyzed by  $KPR_{Ecoli}$ . (A). Initial reaction rate ( $V_0$ ) vs the enzyme concentration. The arrow shows the enzyme concentration selected for the enzyme assay (B) and  $V_0$  vs substrate concentration ( $0.05 (K_m^{app}) \leq [S] \leq 3.3 (K_m^{app})$ ), adjusted to a Michaelis-Menten model by non-linear regression method (C). Each point is the mean of three independent experiments.

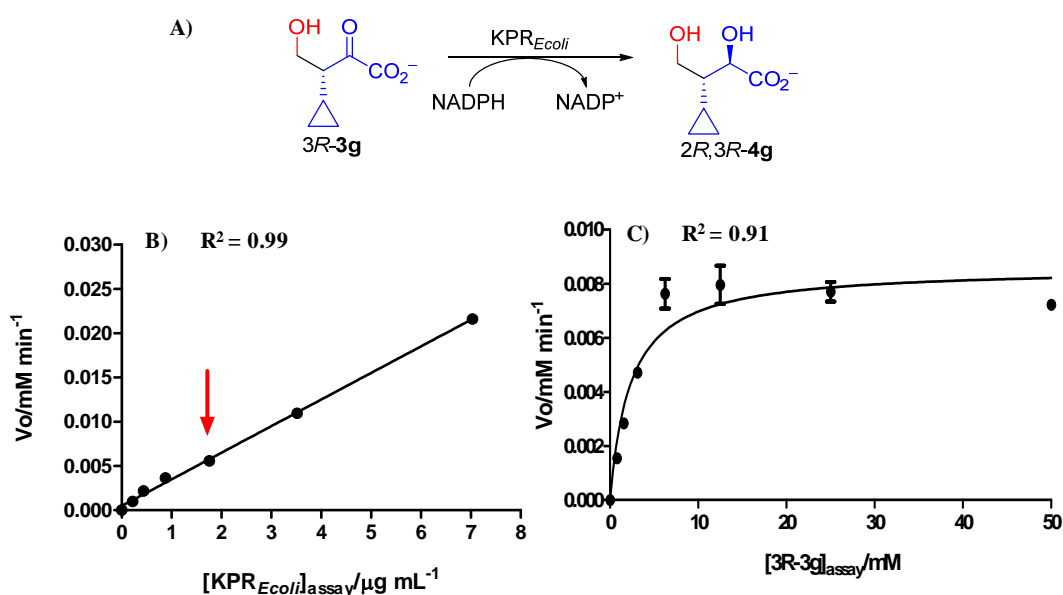


**Figure S22.** Reduction of 3R-3g to 2R,3R-4g catalyzed by  $KPR_{Ecoli}$ . (A). Initial reaction rate ( $V_0$ ) vs the enzyme concentration. The arrow shows the enzyme concentration selected for the enzyme assay (B) and  $V_0$  vs substrate concentration ( $0.4 (K_m^{app}) \leq [S] \leq 21.7 (K_m^{app})$ ), adjusted to a Michaelis-Menten model by non-linear regression method (C). Each point is the mean of three independent experiments.

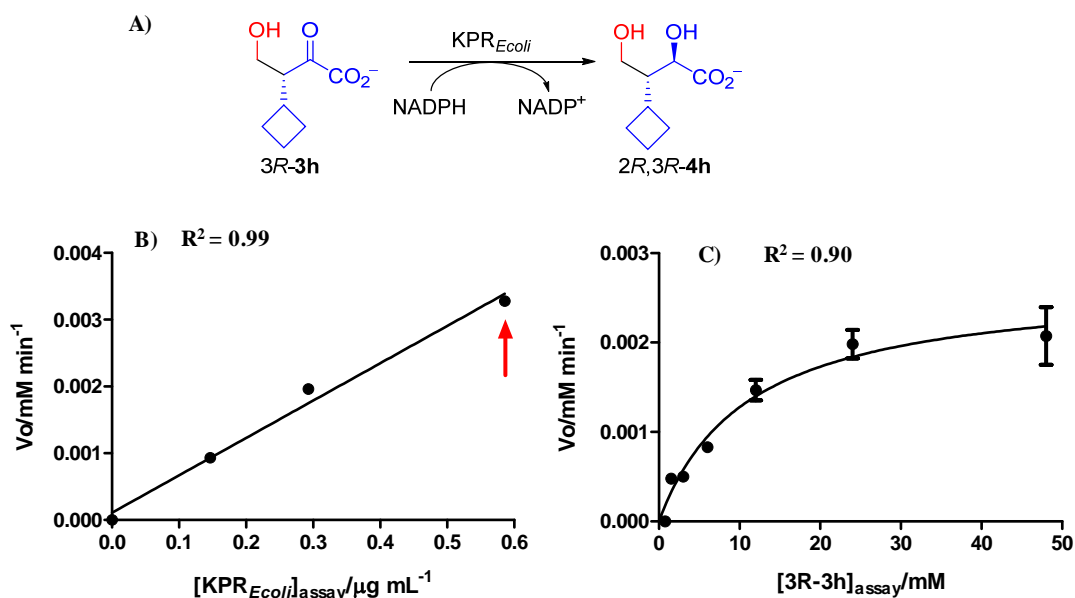


**Figure S23.** Reduction of 3R-3h to 2R,3R-4h catalyzed by  $KPR_{Ecoli}$ . (A). Initial reaction rate ( $V_0$ ) vs the enzyme concentration. The arrow shows the enzyme concentration selected for the enzyme assay (B) and  $V_0$  vs substrate concentration ( $0.09(K_m^{app}) \leq [S] \leq 4.4 (K_m^{app})$ ), adjusted to a Michaelis-Menten model by non-linear regression method (C). Each point is the mean of three independent experiments.

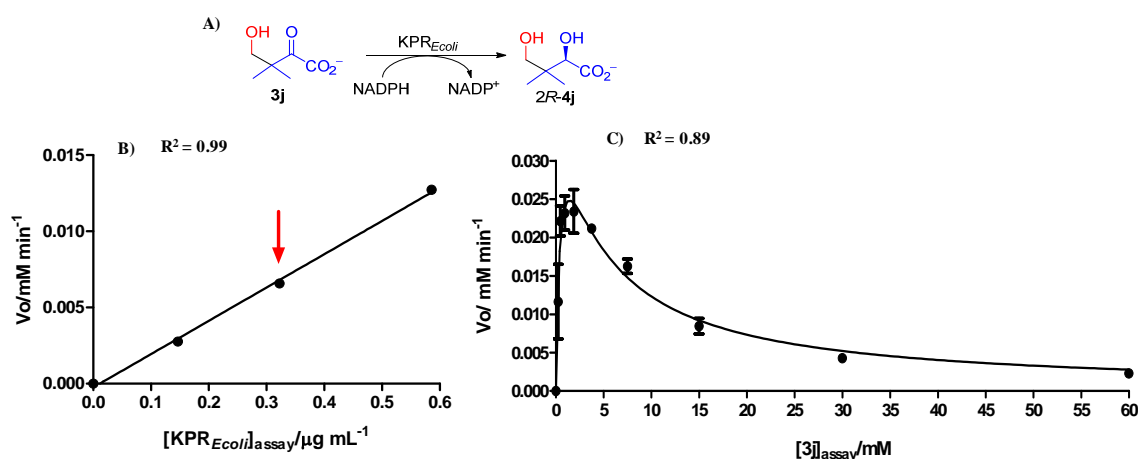


**Figure S24.** Reduction of **3j** to **2R-4j** catalyzed by  $KPR_{Ecoli}$ . (A). Initial reaction rate ( $V_0$ ) vs the enzyme concentration. The arrow shows the enzyme concentration selected for the enzyme assay (B) and  $V_0$  vs substrate concentration ( $2.5(Km^{app}) \leq [S] \leq 150(Km^{app})$ ), adjusted to a Michaelis-Menten model by non-linear regression method (C). Each point is the mean of three independent experiments.

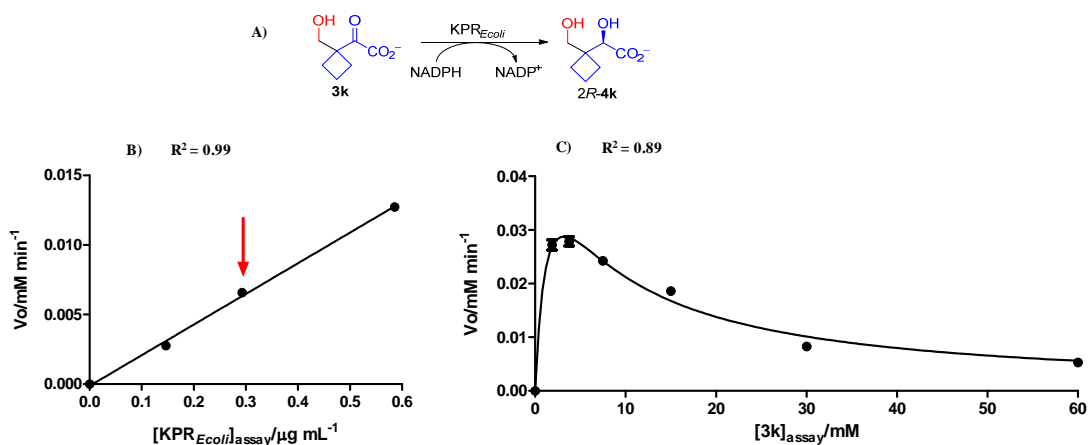


**Figure S25.** Reduction of **3k** to **2R-4k** catalyzed by  $KPR_{Ecoli}$ . (A). Initial reaction rate ( $V_0$ ) vs the enzyme concentration. The arrow shows the enzyme concentration selected for the enzyme assay (B) and  $V_0$  vs substrate concentration ( $0.7(Km^{app}) \leq [S] \leq 40(Km^{app})$ ), adjusted to a Michaelis-Menten model by non-linear regression method (C). Each point is the mean of three independent experiments.



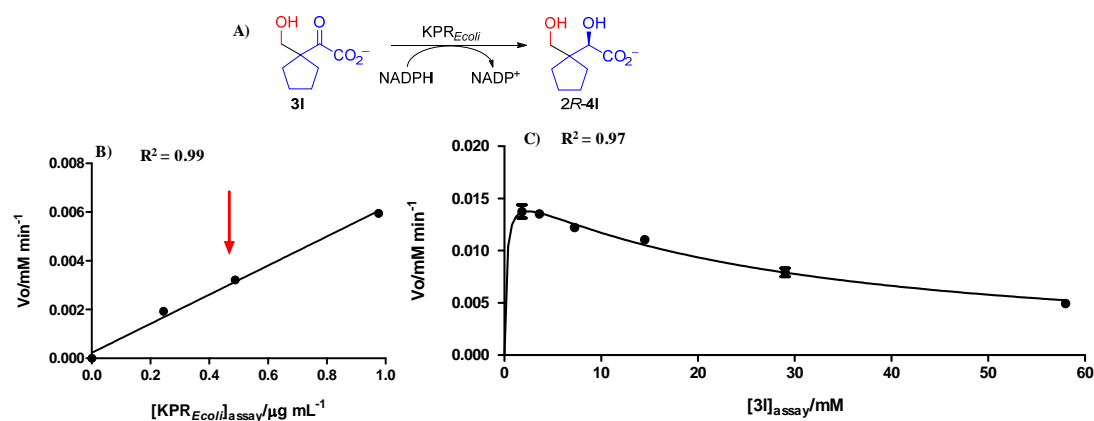


**Figure S26.** Reduction of **3I** to **2R-4I** catalyzed by  $KPR_{Ecoli}$ . (A). Initial reaction rate ( $V_0$ ) vs the enzyme concentration. The arrow shows the enzyme concentration selected for the enzyme assay (B) and  $V_0$  vs substrate concentration ( $5(Km^{app}) \leq [S] \leq 290 (Km^{app})$ ), adjusted to a Michaelis-Menten model by non-linear regression method (C). Each point is the mean of three independent experiments.

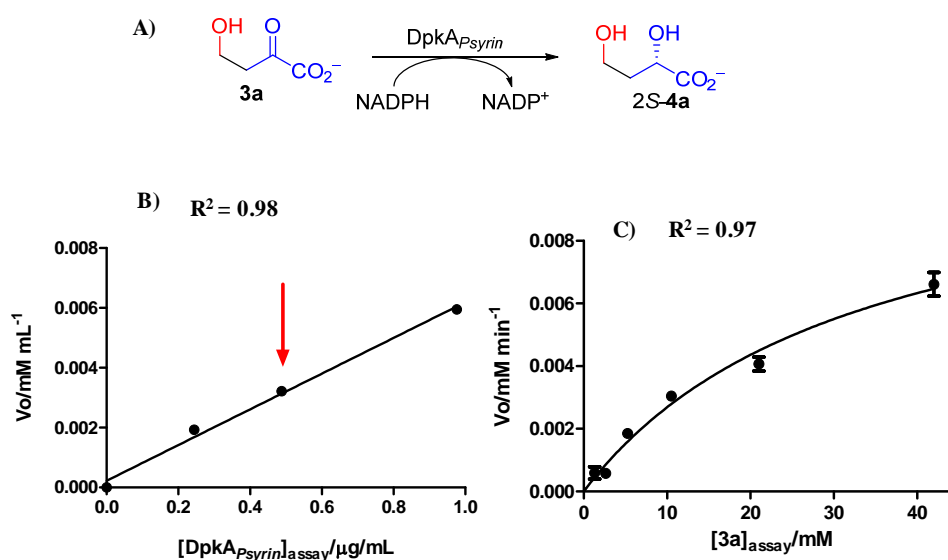


**Figure S27.** Reduction of **3a** to **2S-4a** catalyzed by  $DpkA_{Psyrrin}$ . (A). Initial reaction rate ( $V_0$ ) vs the enzyme concentration. The arrow shows the enzyme concentration selected for the enzyme assay (B) and  $V_0$  vs substrate concentration ( $0.03(Km^{app}) \leq [S] \leq 1.3 (Km^{app})$ ), adjusted to a Michaelis-Menten model by non-linear regression method (C). Each point is the mean of three independent experiments.

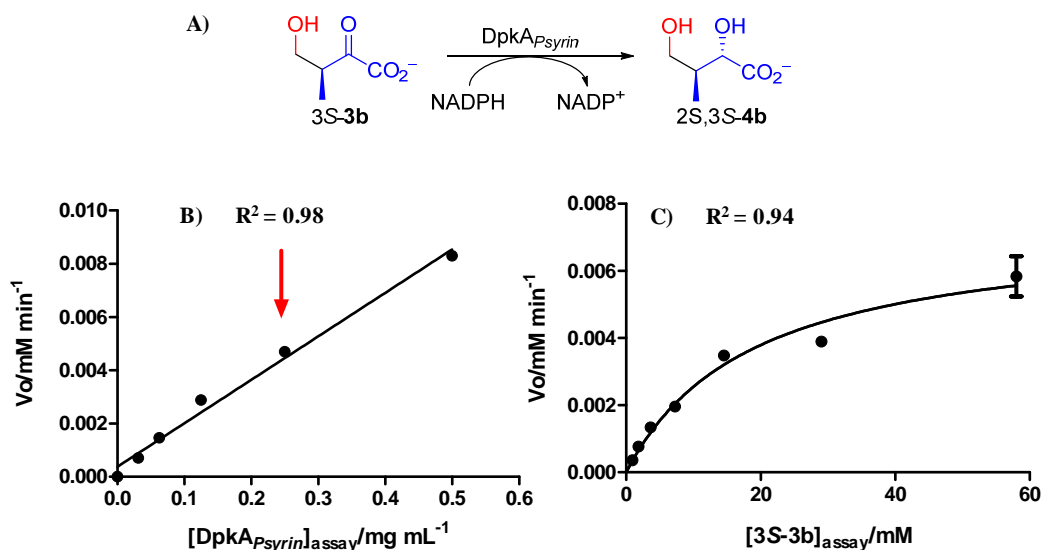


**Figure S28.** Reduction of 3S-3b to 2S,3S-4b catalyzed by DpkA<sub>Psytrin</sub>. (A). Initial reaction rate ( $V_0$ ) vs the enzyme concentration. The arrow shows the enzyme concentration selected for the enzyme assay (B) and  $V_0$  vs substrate concentration ( $0.05(Km^{app}) \leq [S] \leq 3 (Km^{app})$ ), adjusted to a Michaelis-Menten model by non-linear regression method (C). Each point is the mean of three independent experiments.

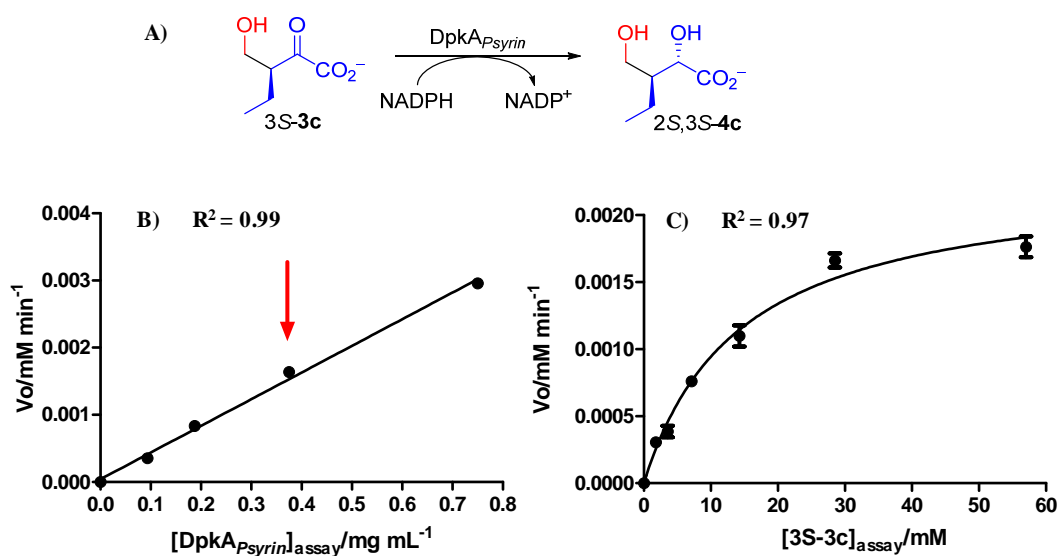


**Figure S29.** Reduction of 3S-3c to 2S,3S-4c catalyzed by DpkA<sub>Psytrin</sub>. (A). Initial reaction rate ( $V_0$ ) vs the enzyme concentration. The arrow shows the enzyme concentration selected for the enzyme assay (B) and  $V_0$  vs substrate concentration ( $0.07(Km^{app}) \leq [S] \leq 4.1 (Km^{app})$ ), adjusted to a Michaelis-Menten model by non-linear regression method (C). Each point is the mean of three independent experiments.

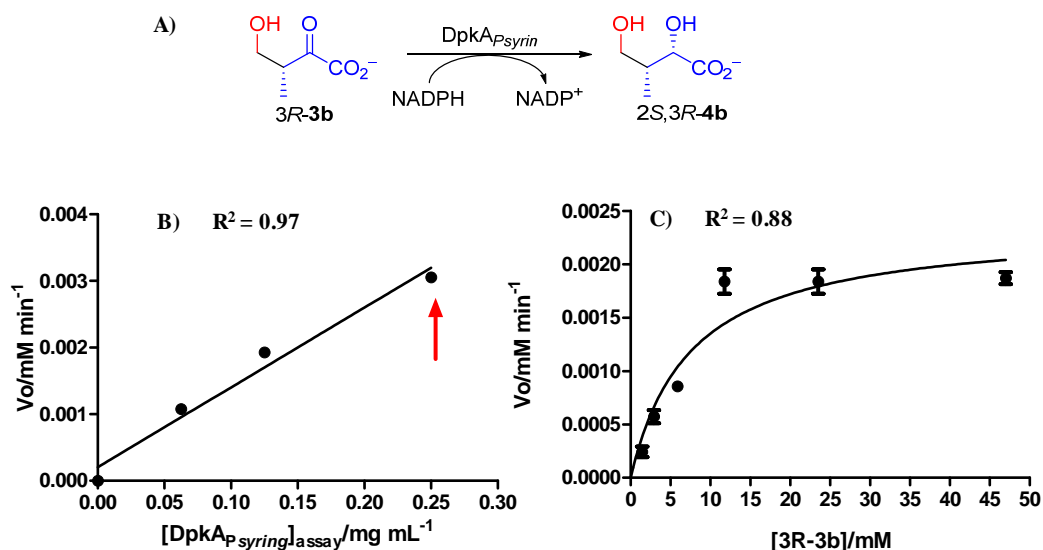


**Figure S30.** Reduction of 3R-3b to 2S,3R-4b catalyzed by DpkA<sub>Psyryn</sub>. (A). Initial reaction rate ( $V_0$ ) vs the enzyme concentration. The arrow shows the enzyme concentration selected for the enzyme assay (B) and  $V_0$  vs substrate concentration ( $0.13(Km^{app}) \leq [S] \leq 6.3 (Km^{app})$ ), adjusted to a Michaelis-Menten model by non-linear regression method (C). Each point is the mean of three independent experiments.

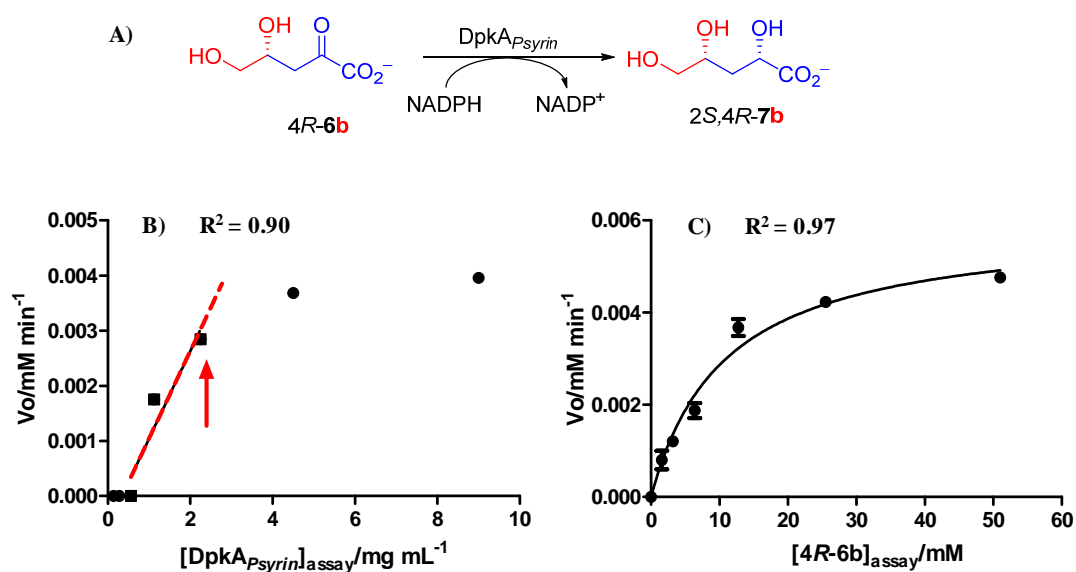


**Figure S31.** Reduction of 4R-6b to 2S,4R-7b catalyzed by DpkA<sub>Psyryn</sub>. (A). Initial reaction rate ( $V_0$ ) vs the enzyme concentration. The arrow shows the enzyme concentration selected for the enzyme assay (B) and  $V_0$  vs substrate concentration ( $0.09(Km^{app}) \leq [S] \leq 4.6 (Km^{app})$ ), adjusted to a Michaelis-Menten model by non-linear regression method (C). Each point is the mean of three independent experiments.

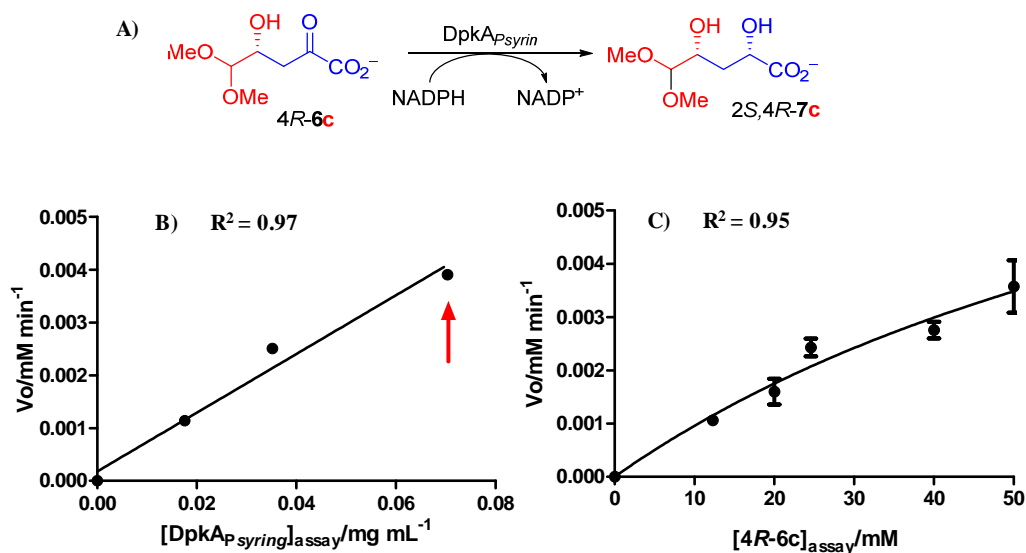


**Figure S32.** Reduction of 4R-6c to 2S,4R-7c catalyzed by DpkA<sub>P<sub>syryn</sub></sub>. (A). Initial reaction rate ( $V_0$ ) vs the enzyme concentration. The arrow shows the enzyme concentration selected for the enzyme assay (B) and  $V_0$  vs substrate concentration ( $0.01(Km^{est}) \leq [S] \leq 0.6(Km^{est})$ ), adjusted to a Michaelis-Menten model by non-linear regression method (C). Each point is the mean of three independent experiments.

### X-Ray structures

Suitable single crystals for X-ray structural analysis of *R*-51 were obtained at room temperature. Compound *R*-51 (40 mg) was dissolved in Hexane:methanol 3:1 (v/v) (5 mL). Crystals were obtained by evaporation in glass vials (6 mL, 3.5 cm, Ø 1.4 cm) after 48 h at 25 °C. The X-ray diffraction analysis on the *R*-51 indicates that KPR<sub>Ecoli</sub> rendered *R*-51 having *R* configuration (**Figure S33**).

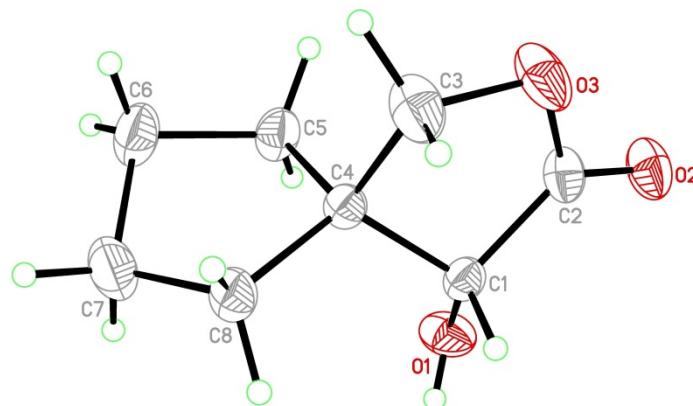


**Figure S33.** X-ray structure of *R*-51. ORTEP-type plot displaying one molecule with 50% probability ellipsoids. The data can be obtained free of charge from The Cambridge Crystallographic Data Centre via [www.ccdc.cam.ac.uk/data\\_request/cif](http://www.ccdc.cam.ac.uk/data_request/cif)

Data were collected on a STOE IPDS II two-circle diffractometer with a Genix Microfocus tube with mirror optics using MoK $\alpha$  radiation ( $\lambda = 0.71073 \text{ \AA}$ ). The data were scaled using the frame scaling procedure in the X-Area program system (Software X-Area - STOE & Cie GmbH. <https://www.stoe.com/product/software-x-area>). The structures was solved by direct methods using the program SHELXS and refined against  $F^2$  with full-matrix least-squares techniques using the program SHELXL<sup>17</sup> (Table S5 and S6).

**Table S5.** Crystal data and structure refinement for *R-5I*.

Identification code	<i>R-5I</i>	
CCDC number	2208404	
Empirical formula	C <sub>8</sub> H <sub>12</sub> O <sub>3</sub>	
Formula weight	156.18	
Temperature	173(2) K	
Wavelength	0.71073 $\text{\AA}$	
Crystal system	Orthorhombic	
Space group	P 21 21 21	
Unit cell dimensions	a = 5.9887(4) $\text{\AA}$	$\alpha = 90^\circ$
	b = 9.1619(6) $\text{\AA}$	$\beta = 90^\circ$
	c = 14.1820(7) $\text{\AA}$	$\gamma = 90^\circ$
Volume	778.14(8) $\text{\AA}^3$	
Z	4	
Density (calculated)	1.333 Mg/m <sup>3</sup>	
Absorption coefficient	0.101 mm <sup>-1</sup>	
F(000)	336	
Crystal color, shape	colorless needle	
Crystal size	0.280 x 0.120 x 0.110 mm <sup>3</sup>	
Theta range for data collection	3.633 to 27.182 $^\circ$ .	
Index ranges	$-7 \leq h \leq 7, -11 \leq k \leq 11, -18 \leq l \leq 17$	
Reflections collected	10506	
Independent reflections	1713 [R(int) = 0.0447]	
Completeness to theta = 25.000 $^\circ$	99.3 %	
Absorption correction	Semi-empirical from equivalents	
Max. and min. transmission	1.000 and 0.310	
Refinement method	Full-matrix least-squares on $F^2$	

Data / restraints / parameters	1713 / 0 / 104	
Goodness-of-fit on $F^2$	1.177	
Final R indices [ $I > 2\sigma(I)$ ]	R1 = 0.0433, wR2 = 0.1068	
R indices (all data)	R1 = 0.0443, wR2 = 0.1077	
Absolute structure parameter	-0.3(9)	
Extinction coefficient	n/a	
Largest diff. peak and hole	0.209 and -0.147 e.Å <sup>-3</sup>	

**Table S6** Atomic coordinates ( $\times 10^4$ ) and equivalent isotropic displacement parameters ( $\text{Å}^2 \times 10^3$ ) for *R-5I*.  $U(\text{eq})$  is defined as one third of the trace of the orthogonalized  $U^{ij}$  tensor.

	x	y	z	U(eq)
O(1)	4931(4)	7397(2)	4334(1)	33(1)
O(2)	2558(3)	5162(2)	5316(1)	35(1)
O(3)	4827(4)	3606(2)	4601(2)	41(1)
C(1)	5909(4)	6032(2)	4491(2)	22(1)
C(2)	4222(4)	4952(3)	4856(2)	27(1)
C(3)	6880(5)	3694(3)	4029(2)	37(1)
C(4)	6871(4)	5239(2)	3630(2)	20(1)
C(5)	5373(4)	5368(3)	2748(2)	30(1)
C(6)	6993(5)	5350(4)	1924(2)	37(1)
C(7)	8943(5)	6236(4)	2285(2)	40(1)
C(8)	9213(4)	5740(3)	3306(2)	28(1)

In addition, Cu K- $\alpha$  radiation ( $\lambda = 1.5406 \text{ Å}$ ) was employed at room temperature to assess the absolute stereochemistry of *R-5I*. The Flack-x-parameter was determined to be -0.04(16) (Table S7).

**Table S7.** Crystal data and structure refinement for *R-5I* with Cu K- $\alpha$  radiation.

Identification code	<i>R-5I</i> c13_cu	
CCDC number	2208405	
Empirical formula	C <sub>8</sub> H <sub>12</sub> O <sub>3</sub>	
Formula weight	156.18	
Temperature	293(2) K	
Wavelength	1.54178 Å	
Crystal system	Orthorhombic	

Space group	P 21 21 21	
Unit cell dimensions	a = 6.0593(5) Å	$\alpha = 90^\circ$ .
	b = 9.2089(7) Å	$\beta = 90^\circ$ .
	c = 14.3338(11) Å	$\gamma = 90^\circ$ .
Volume	799.82(11) Å <sup>3</sup>	
Z	4	
Density (calculated)	1.297 Mg/m <sup>3</sup>	
Absorption coefficient	0.820 mm <sup>-1</sup>	
F(000)	336	
Crystal colour, shape	colorless needle	
Crystal size	0.280 x 0.120 x 0.110 mm <sup>3</sup>	
Theta range for data collection	5.710 to 68.675°.	
Index ranges	-7<=h<=7, -11<=k<=11, -16<=l<=16	
Reflections collected	13027	
Independent reflections	1427 [R(int) = 0.1262]	
Completeness to theta = 68.000°	98.3 %	
Absorption correction	Semi-empirical from equivalents	
Max. and min. transmission	1.000 and 0.239	
Refinement method	Full-matrix least-squares on F <sup>2</sup>	
Data / restraints / parameters	1427 / 0 / 104	
Goodness-of-fit on F <sup>2</sup>	1.785	
Final R indices [I>2sigma(I)]	R1 = 0.1178, wR2 = 0.3220	
R indices (all data)	R1 = 0.1419, wR2 = 0.3904	
Absolute structure parameter	-0.04(16)	
Extinction coefficient	n/a	
Largest diff. peak and hole	0.325 and -0.750 e.Å <sup>-3</sup>	

## Computational Methods.

Protein complexes were modeled with the package Schrödinger Suite 2022-2,<sup>18</sup> through its graphical interface Maestro.<sup>19</sup> The Protein Preparation Wizard<sup>20</sup> included in Maestro was used to prepare the protein structure by removing solvent molecules and ions, adding hydrogens, setting protonation states<sup>21</sup> and running a restrained minimization using the OPLS4 force-field.<sup>22</sup> The program MacroModel<sup>23</sup> with the same force field and GB/SA water solvation conditions<sup>24</sup> was used for further molecular mechanics calculations. The program QSite<sup>19, 25-26</sup> was used for the QM/MM calculations.

Molecular models of the pre-reactive 4-hydroxy-2-oxoacids bound into the active sites of KPR<sub>Ecoli</sub> and DpkA<sub>Psyrin</sub> were generated from the reported crystal structures of both enzymes.<sup>27-28</sup> In particular, KPR<sub>Ecoli</sub> was modeled from chain B of PDB structure 2OFP,<sup>27</sup> which is in the closed form and includes the NADP cofactor and a molecule of pantoate. On the other hand, all the modeling with DpkA<sub>Psyrin</sub> was performed on the active site of chain A of PDB structure 2CWH,<sup>28</sup> although both chains A and B, which show quite similar overall structures, were taken into account for the calculations since the enzyme naturally functions as a dimer and the active site cavity on each subunit also involves residues from the neighboring one. Substrates **3** were built within Maestro, based on the structure of the ligands bound in each case. The structures of the complexes were minimized with QSite at the DFT B3LYP/6-31G\*\* level of theory. For KPR<sub>Ecoli</sub> the QM/MM boundary was defined by placement of hydrogen caps between the C $\alpha$  and C $\beta$  atoms of residues Lys176, Asn184, Asn194 and Asn241, as well as between the C4' and C5' atoms of the ribose ring bound to the nicotinamide moiety of the NADPH cofactor (Figure S68A). For DpkA<sub>Psyrin</sub> the boundary was established through hydrogen caps between the C $\alpha$  and C $\beta$  atoms of residues His54, Arg58 and Thr166, and the C4' and C5' atoms of the same ribose ring of NADPH (Figure S68B). In both cases the substrate molecule was also part of the QM region. All residues with atoms within 6 Å of the substrate and the NADPH molecules were simultaneously optimized using the default OPLS2005 force-field,<sup>29</sup> while residues which were further away were kept frozen. Furthermore, to find the best bound conformations for the more flexible substrates, a conformational search was performed using the mixed MCM/ LMCS method<sup>30</sup> implemented in MacroModel to find the best poses for the C-3 substituents (R<sup>1</sup> and R<sup>2</sup> substituents in Scheme 2 of the main text), while the rest of the system was kept frozen. Then, the best conformers detected by this search were



QM/MM reoptimized as above. All complexes were characterized as minima by running frequency analysis calculations and confirming that they had no imaginary frequencies.

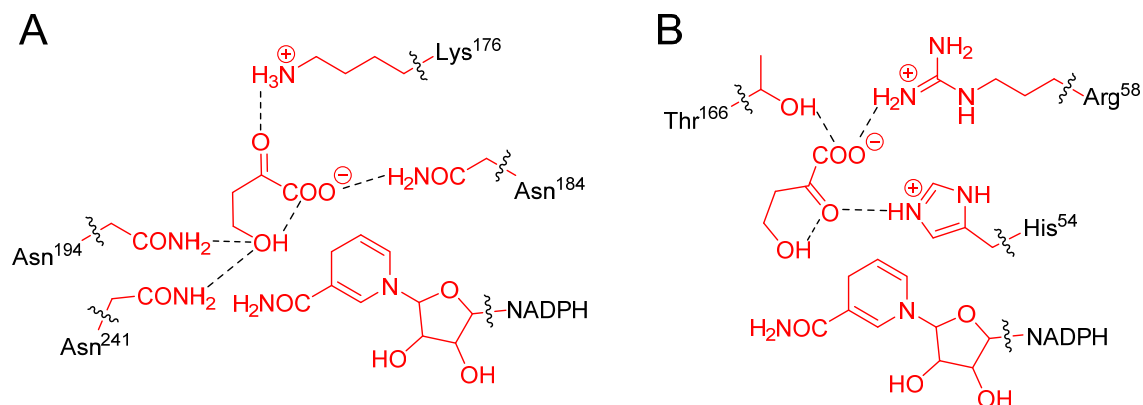
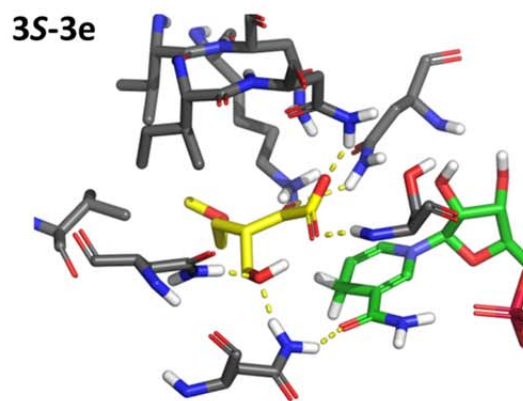
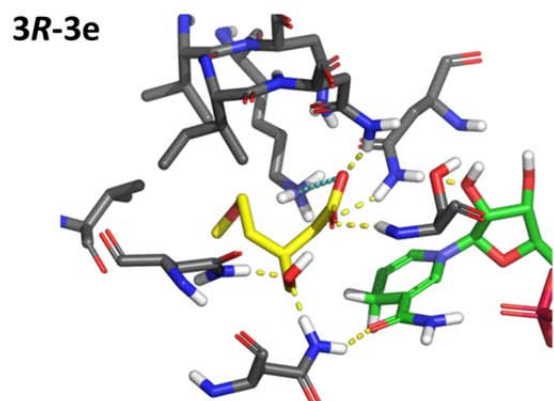
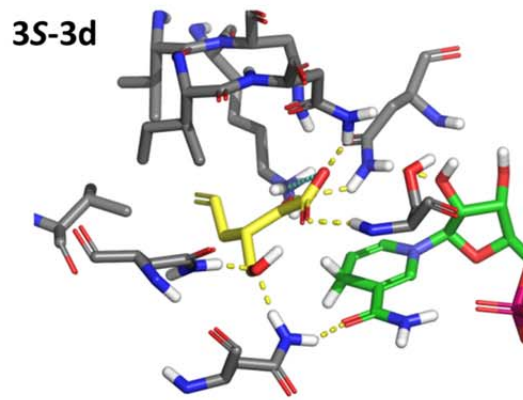
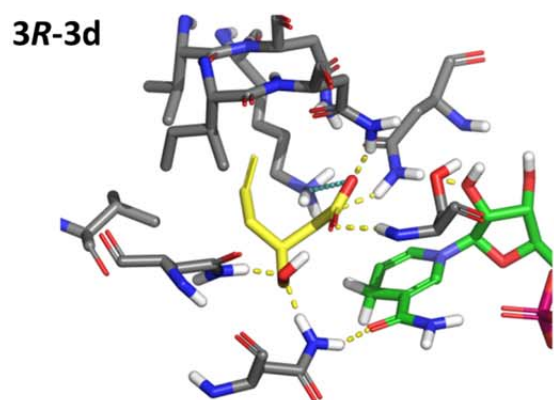
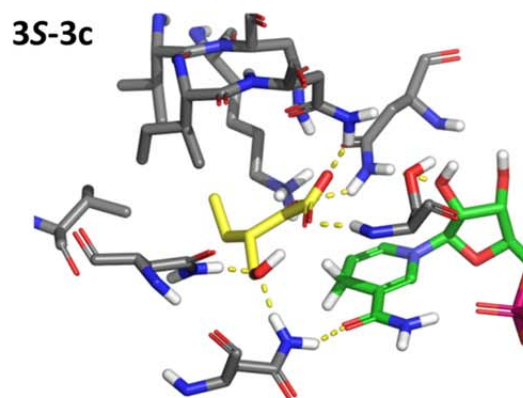
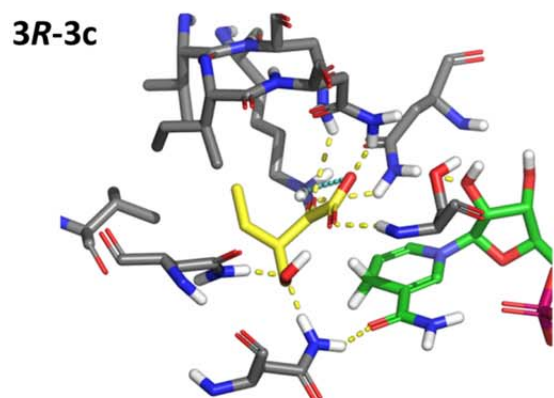
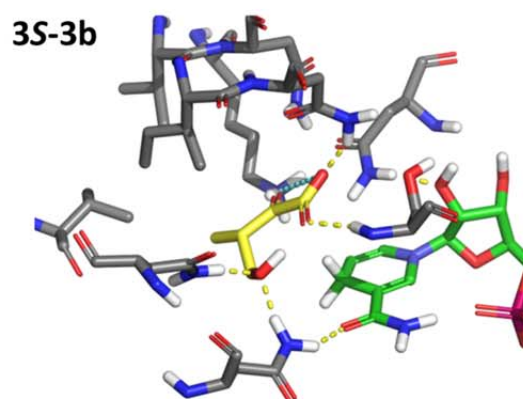
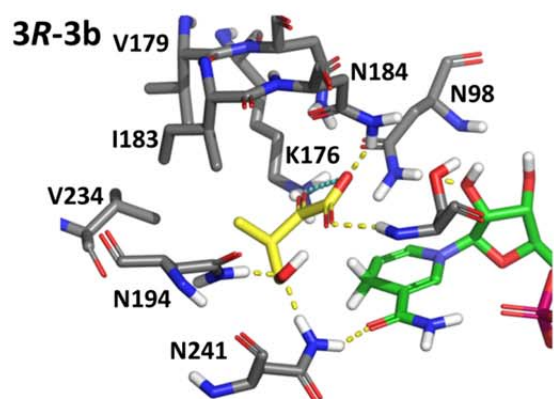
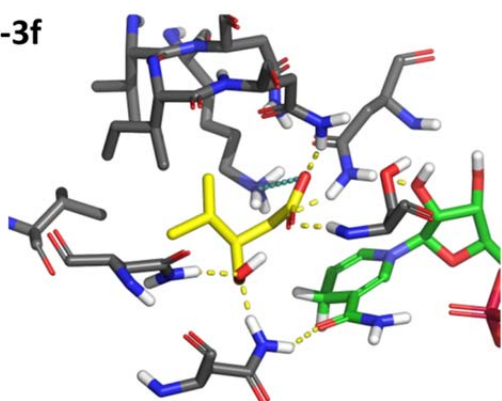


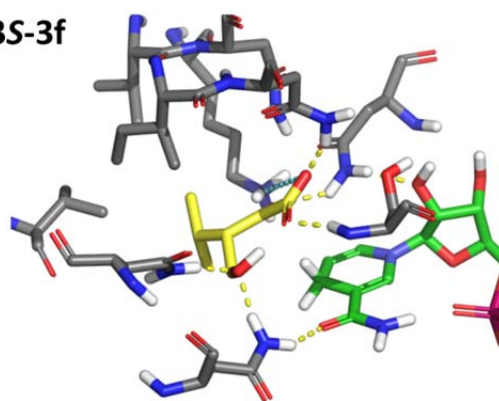
**Figure S68.** Active sites of KPR<sub>Ecoli</sub> (A) and DpkA<sub>Psyrrin</sub> (B) with bound **3a**, as example substrate, and atoms that constitute the QM region (red atoms) in each case. Wavy lines denote where the hydrogen caps were placed; dashed lines represent hydrogen bonds.



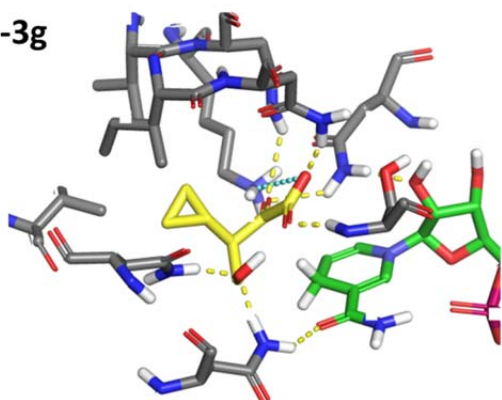
3R-3f



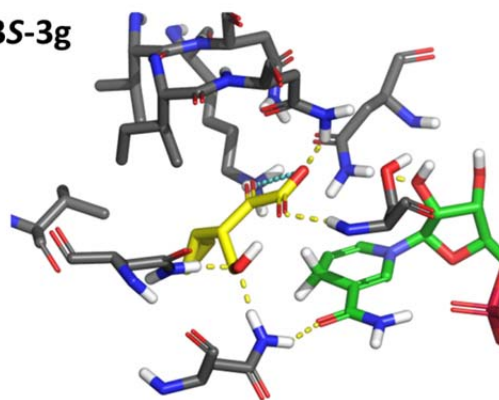
3S-3f



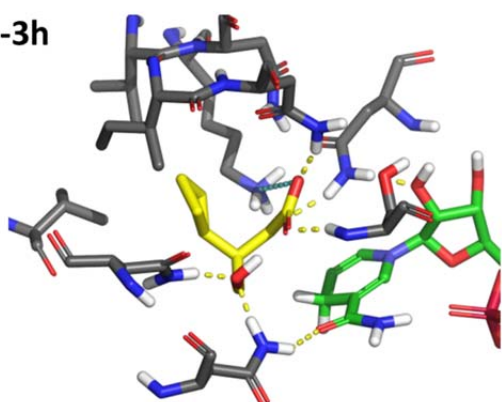
3R-3g



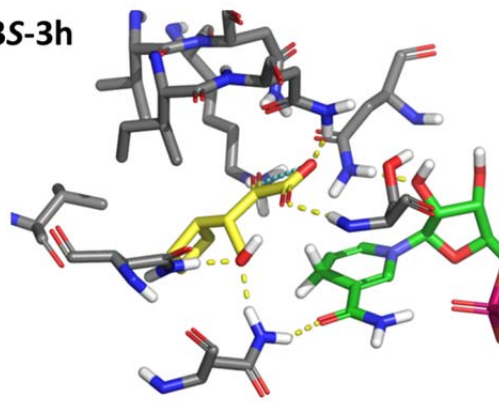
3S-3g



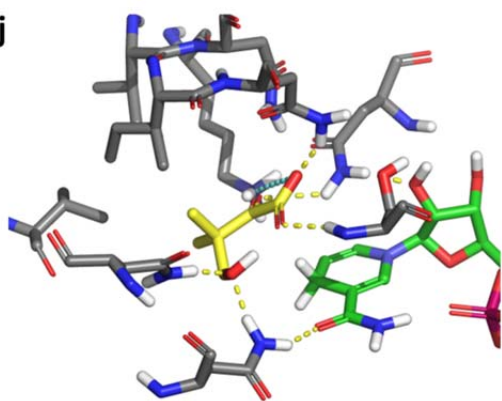
3R-3h



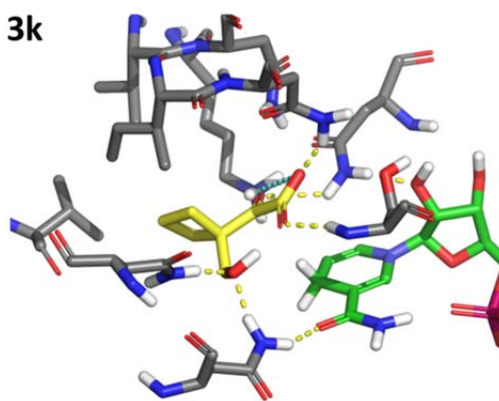
3S-3h

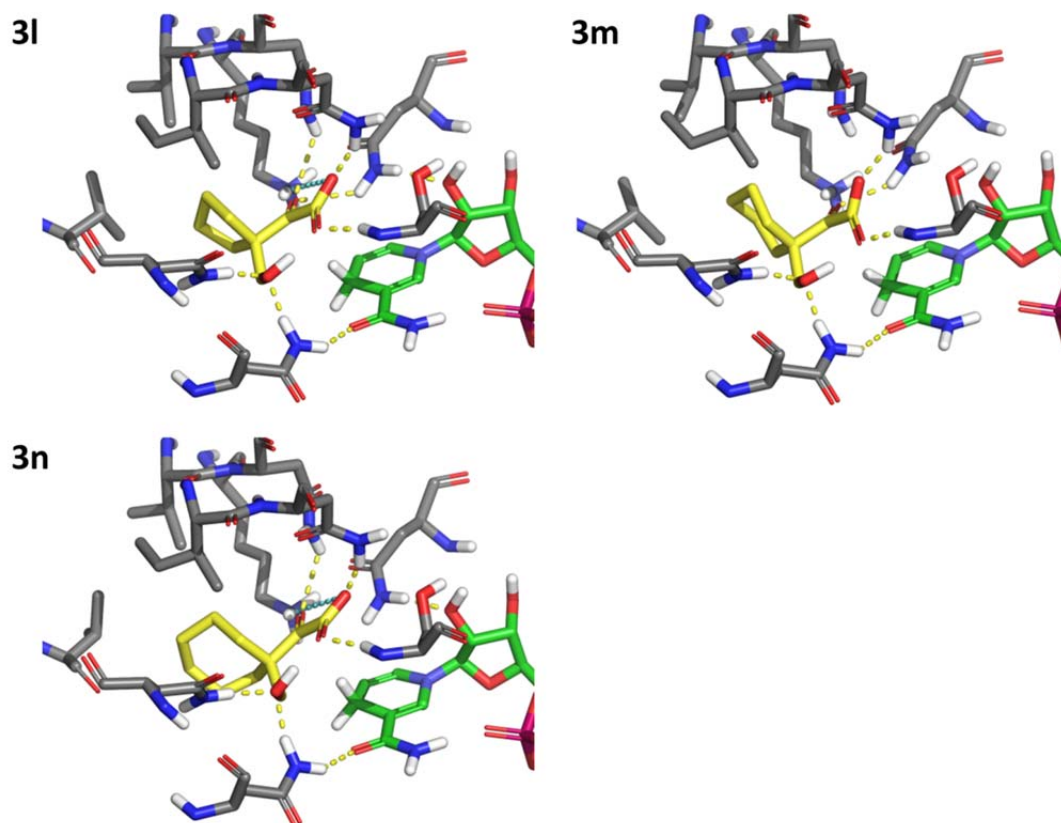


3j

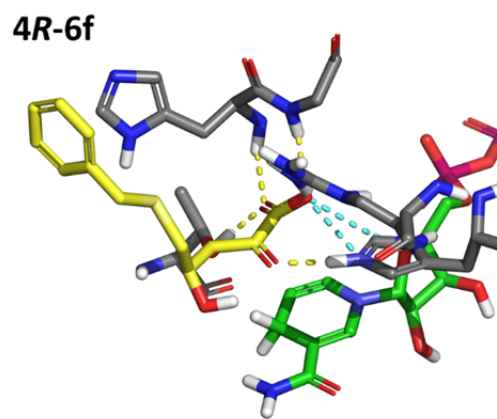
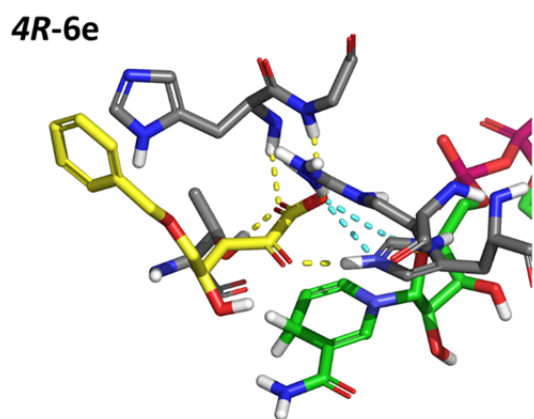
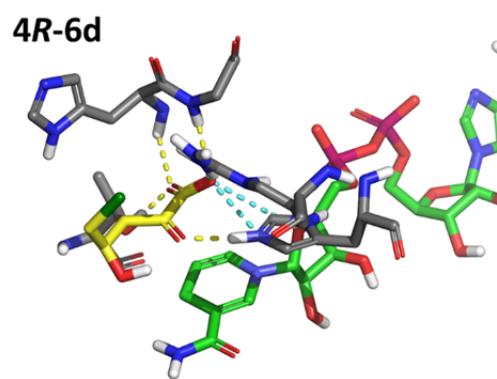
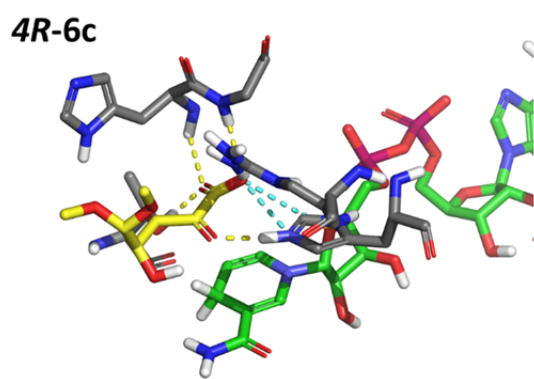
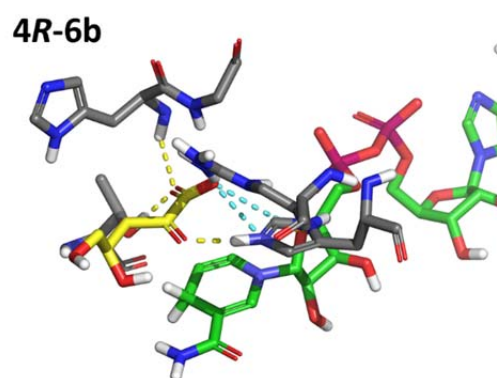
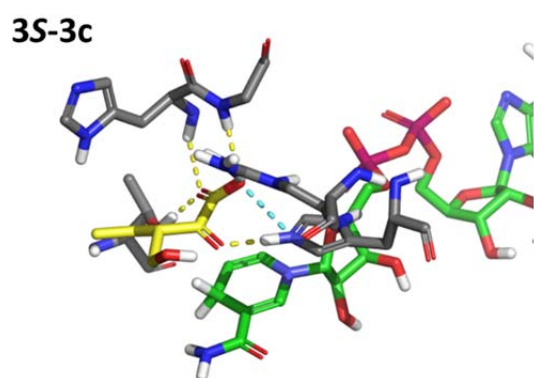
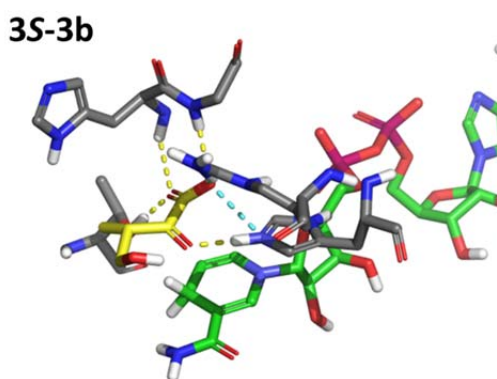
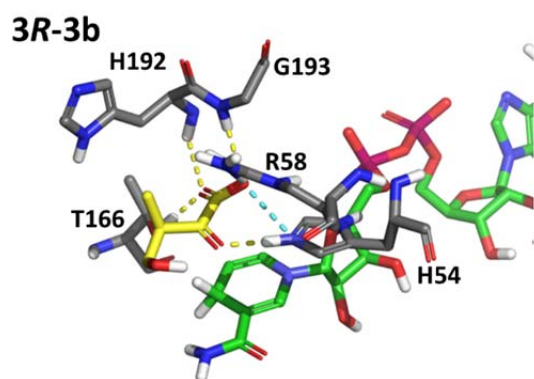


3k





**Figure S69.** Molecular models of substrates **3** bound into the active site of KPR<sub>Ecoli</sub>. These models were built starting from PDB structure 2OFP and they were optimized by QM/MM methods as described. The substrate, NADPH and close protein residues are shown with yellow, green and gray C-atoms; H-bonds and salt bridges are shown with yellow and cyan dashed lines.



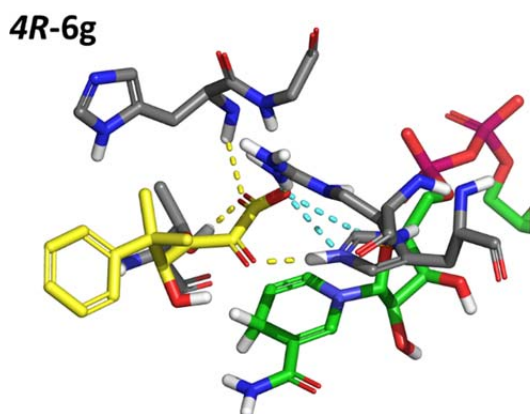


**Figure S70.** Molecular models of substrates **3** and **6** bound into the active site of DpkA<sub>Psyrin</sub>. These models were built starting from PDB structure 2CWH and they were optimized by QM/MM methods as described. The substrate, NADPH and close protein residues are shown with yellow, green and gray C-atoms; H-bonds and salt bridges are shown with yellow and cyan dashed lines.

## References

1. Marín-Valls, R.; Hernández, K.; Bolte, M.; Joglar, J. s.; Bujons, J.; Clapes, P., Chemoenzymatic hydroxymethylation of carboxylic acids by tandem stereodivergent biocatalytic aldol reaction and chemical decarboxylation. *ACS Catalysis* **2019**, *9* (8), 7568-7577.
2. Marín-Valls, R.; Hernández, K.; Bolte, M.; Parella, T.; Joglar, J. s.; Bujons, J.; Clapés, P., Biocatalytic construction of quaternary centers by aldol addition of 3, 3-disubstituted 2-oxoacid derivatives to aldehydes. *Journal of the American Chemical Society* **2020**, *142* (46), 19754-19762.
3. Moreno, C. J.; Hernández, K.; Charnok, S. J.; Gittings, S.; Bolte, M.; Joglar, J.; Bujons, J.; Parella, T.; Clapés, P., Synthesis of  $\gamma$ -hydroxy- $\alpha$ -amino acid derivatives by enzymatic tandem aldol addition–transamination reactions. *ACS catalysis* **2021**, *11* (8), 4660-4669.
4. QIAexpressionist, A., A handbook for high-level expression and purification of 6xhis-tagged proteins. *Qiagen. p1-125* **2002**.
5. Hernandez, K.; Bujons, J.; Joglar, J. s.; Charnock, S. J.; Dominguez de Maria, P.; Fessner, W. D.; Clapés, P., Combining aldolases and transaminases for the synthesis of 2-amino-4-hydroxybutanoic acid. *ACS Catalysis* **2017**, *7* (3), 1707-1711.
6. Hernández, K.; Gómez, A.; Joglar, J.; Bujons, J.; Parella, T.; Clapés, P., 2-Keto-3-Deoxy-L-Rhamnonate Aldolase (YfaU) as Catalyst in Aldol Additions of Pyruvate to Amino Aldehyde Derivatives. *Adv. Synth. Catal.* **2017**, *359* (12), 2090-2100.
7. Hernández, K.; Joglar, J.; Bujons, J.; Parella, T.; Clapés, P., Nucleophile promiscuity of engineered class II pyruvate aldolase YfaU from *E. coli*. *Angewandte Chemie International Edition* **2018**, *57* (14), 3583-3587.
8. Green, M. R.; Sambrook, J., The Hanahan method for preparation and transformation of competent *Escherichia coli*: high-efficiency transformation. *Cold Spring Harbor Protocols* **2018**, *2018* (3), pdb. prot101188.
9. Marín-Valls, R.; Hernández, K.; Bolte, M.; Joglar, J.; Bujons, J.; Clapés, P., Chemoenzymatic Hydroxymethylation of Carboxylic Acids by Tandem Stereodivergent

- Biocatalytic Aldol Reaction and Chemical Decarboxylation. *ACS Catal.* **2019**, *9* (8), 7568-7577.
10. Marín-Valls, R.; Hernández, K.; Bolte, M.; Parella, T.; Joglar, J.; Bujons, J.; Clapés, P., Biocatalytic Construction of Quaternary Centers by Aldol Addition of 3,3-Disubstituted 2-Oxoacid Derivatives to Aldehydes. *J. Am. Chem. Soc.* **2020**, *142* (46), 19754-19762.
  11. Yamaguchi, S.; Motokura, K.; Sakamoto, Y.; Miyaji, A.; Baba, T., Tin-catalyzed conversion of biomass-derived triose sugar and formaldehyde to  $\alpha$ -hydroxy- $\gamma$ -butyrolactone. *Chem. Commun.* **2014**, *50* (35), 4600-4602.
  12. Magnani, J. L.; Peterson, J. M.; Zierke, M.; Smiesko, M.; Ernst, B., E-Selectin Antagonists Modified by Macrocyclic Formation to the Galactose. Google Patents: 2016.
  13. Scheffler, U.; Mahrwald, R., Histidine-catalyzed asymmetric aldol addition of enolizable aldehydes: Insights into its mechanism. *The Journal of organic chemistry* **2012**, *77* (5), 2310-2330.
  14. Nakata, K.; Gotoh, K.; Ono, K.; Futami, K.; Shiina, I., Kinetic Resolution of Racemic 2-Hydroxy- $\gamma$ -butyrolactones by Asymmetric Esterification Using Diphenylacetic Acid with Pivalic Anhydride and a Chiral Acyl-Transfer Catalyst. *Org. Lett.* **2013**, *15* (6), 1170-1173.
  15. Bourgeois, F.; Medlock, J. A.; Bonrath, W.; Sparr, C., Catalyst repurposing sequential catalysis by harnessing regenerated prolinamide organocatalysts as transfer hydrogenation ligands. *Organic letters* **2019**, *22* (1), 110-115.
  16. Vugts, D. J.; Aktas, H.; Al-Mafraji, K.; De Kanter, F. J.; Ruijter, E.; Groen, M. B.; Orru, R. V., Synthesis of 3'-Deoxyribolactones using a Hydrolysis-Induced Lactonization Cascade Reaction of Epoxy Cyanohydrins. Wiley Online Library: 2008.
  17. Sheldrick, G., A short history of SHELX. *Acta Crystallogr. Sect. A* **2008**, *64* (1), 112-122.
  18. Schrödinger Release 2022-2, Schrödinger, LLC: New York, NY, 2022.
  19. Philipp, D. M.; Friesner, R. A., Mixed ab initio QM/MM modeling using frozen orbitals and tests with alanine dipeptide and tetrapeptide. *J. Comp. Chem.* **1999**, *20*, 1468-1494.
  20. Sastry, G. M.; Adzhigirey, M.; Day, T.; Annabhimoju, R.; Sherman, W., Protein and ligand preparation: parameters, protocols, and influence on virtual screening enrichments. *J. Comput. Aided Mol. Des.* **2013**, *27* (3), 221-34.
  21. Olsson, M. H. M.; Søndergard, C. R.; Rostkowski, M.; Jensen, J. H., PROPKA3: Consistent Treatment of Internal and Surface Residues in Empirical pKa predictions. *J. Chem. Theor. Comput.* **2011**, *7*, 525-537.
  22. Lu, C.; Wu, C.; Ghoreishi, D.; Chen, W.; Wang, L.; Damm, W.; Ross, G. A.; Dahlgren, M. K.; Russell, E.; Von Bargen, C. D.; Abel, R.; Friesner, R. A.; Harder, E. D., OPLS4: Improving Force Field Accuracy on Challenging Regimes of Chemical Space. *J Chem Theory Comput* **2021**.
  23. Schrödinger Release 2022-2: *Macromodel*, Schrödinger, LLC: New York, NY, 2022.
  24. Still, W. C.; Tempczyk, A.; Hawley, R. C.; Hendrickson, T., Semianalytical Treatment of Solvation for Molecular Mechanics and Dynamics. *J. Am. Chem. Soc.* **1990**, *112* (16), 6127-6129.
  25. Schrödinger Release 2022-2: *QSite*, Schrödinger, LLC: New York, NY, 2022.
  26. Murphy, R. B.; Philipp, D. M.; Friesner, R. A., A mixed quantum mechanics/molecular mechanics (QM/MM) method for large-scale modeling of chemistry in protein environments. *J. Comp. Chem.* **2000**, *21*, 1442-1457.

27. Ciulli, A.; Chirgadze, D. Y.; Smith, A. G.; Blundell, T. L.; Abell, C., Crystal Structure of *Escherichia coli* Ketopantoate Reductase in a Ternary Complex with NADP<sup>+</sup> and Pantoate Bound: substrate recognition, conformational change, and cooperativity. *J. Biol. Chem.* **2007**, 282 (11), 8487-8497.
28. Goto, M.; Muramatsu, H.; Mihara, H.; Kurihara, T.; Esaki, N.; Omi, R.; Miyahara, I.; Hirotsu, K., Crystal Structures of  $\Delta^1$ -Piperideine-2-carboxylate/ $\Delta^1$ -Pyrroline-2-carboxylate Reductase Belonging to a New Family of NAD(P)H-dependent Oxidoreductases: Conformational Change, Substrate Recognition, and Stereochemistry of the Reaction. *J. Biol. Chem.* **2005**, 280 (49), 40875-40884.
29. Harder, E.; Damm, W.; Maple, J.; Wu, C.; Reboul, M.; Xiang, J. Y.; Wang, L.; Lupyan, D.; Dahlgren, M. K.; Knight, J. L.; Kaus, J. W.; Cerutti, D. S.; Krilov, G.; Jorgensen, W. L.; Abel, R.; Friesner, R. A., OPLS3: A Force Field Providing Broad Coverage of Drug-like Small Molecules and Proteins. *J Chem Theory Comput* **2016**, 12 (1), 281-96.
30. Kolossvary, I.; Guida, W. C., Low-mode conformational search elucidated: application to C<sub>39</sub>H<sub>80</sub> and flexible docking of 9-deazaguanine inhibitors into PNP. *J. Comput. Chem.* **1999**, 20 (Copyright (C) 2013 American Chemical Society (ACS). All Rights Reserved.), 1671-1684.



# **Materiales y métodos.**

## **Capítulo 3.3**

## Supporting Information

### Expanding synthetic applications of $\Delta^1$ -Piperidine-2-carboxylate/ $\Delta^1$ -pyrroline-2-carboxylate reductase from *Pseudomonas syringae* (DpkA<sub>Psyrin</sub>). Biocatalytic asymmetric synthesis of (S,E)-2-hydroxy-4-arylbut-3-enoic acid derivatives.

Carlos J. Moreno,<sup>a‡</sup> Samantha Gittings,<sup>b</sup> Dieter Schollmeyer,<sup>c</sup> Jesús Joglar,<sup>a</sup> Jordi Bujons,<sup>a</sup> Karel Hernández,<sup>a\*</sup> Pere Clapés<sup>a\*</sup>

<sup>a</sup>Catalonia Institute for Advanced Chemistry, Dept. Chemical Biology & Molecular Modelling, IQAC-CSIC, Spain.

<sup>b</sup>Prozomix Ltd. West End Industrial Estate, Haltwhistle, Northumberland, NE49 9HA, UK.

<sup>c</sup>Institut für Anorganische Chemie, J.-W.-Goethe-Universität, Frankfurt/Main, Germany.

<sup>d</sup>Servei de Ressonància Magnètica Nuclear. Universitat Autònoma de Barcelona, Bellaterra, Spain.

\*Corresponding authors:

[pere.clapes@iqac.csic.es](mailto:pere.clapes@iqac.csic.es)

[khsqbm@cid.csic.es](mailto:khsqbm@cid.csic.es)

## Table of Contents

Materials. ....	2
Methods. ....	2
HPLC analysis. ....	2
NMR analysis. ....	3
Biocatalytic aldol addition of 2 to aldehydes (1a-p), catalyzed by HBPA <sub>pputida</sub> and variant. ....	3
Biocatalytic reduction of arylbut-3-enoic acids (3a-p) catalyzed by DpkA <sub>Psyrin</sub> . Analytical scale...	4
Synthesis of arylbut-3-enoic acids (3). ....	6
Synthesis of (S,E)-2-hydroxy-4-arylbut-3-enoic acid derivatives (S-4). ....	10
Synthesis of S-3a in a one-pot two-step system. ....	12
X-Ray structures ....	21
Steady-state kinetic studies of DpkA <sub>Psyrin</sub> for sodium pyruvate. ....	20
NMR spectra* ....	
References. ....	22

\*Se encuentra como material electrónico

## Materials.

Benzaldehyde (**1a**), 2-nitrobenzaldehyde (**1b**), 2-fluorobenzaldehyde (**1c**), 2-chlorobenzaldehyde (**1d**), 2-iodobenzaldehyde (**1f**), 2,6-fluorobenzaldehyde (**1g**), 2-chloro-6-fluorobenzaldehyde (**1h**), thiophene-3-carboxaldehyde (**1i**), 3-nitrobenzaldehyde (**1j**), 4-nitrobenzaldehyde (**1k**), 3-chlorobenzaldehyde (**1l**), 4-chlorobenzaldehyde (**1m**), 2-Hydroxy-3-methoxybenzaldehyde (**1n**), *trans*-Cinnamaldehyde (**1o**), fluorene-2-carboxaldehyde (**1p**), indole-3-carboxaldehyde (**1q**) and sodium pyruvate (**2a**) were purchased from Sigma-Aldrich. 2-bromobenzaldehyde (**1e**), sodium borohydride were purchased from TCI chemical. NADPH was purchased from CARL ROTH. Glucose dehydrogenase (GDH) as a cell free extract powder and NADP<sup>+</sup> were provided by Prozomix Ltd (PRO-GDH(001)). Water for analytical HPLC was obtained from an Arium pro ultrapure water purification system (Sartorius Stedim Biotech) and the rest of solvents used in this work were of analytical grade or HPLC grade.

## Methods.

General procedure for HBPA<sub>Pputida</sub>, GDH and DpkA<sub>Psyrin</sub> expression, purification and activity determination were performed as describe in previous works (**Table S1**).<sup>1-2</sup>

**Table S1. Typical enzyme concentration obtained in this work.**

Enzymes	Concentration/ mg mL <sup>-1</sup>
HBPA <sub>Pputida</sub>	4.0 <sup>a</sup> (0.029 U mL <sup>-1</sup> U mL <sup>-1</sup> ) <sup>b</sup>
HBPA <sub>Pputida</sub> H205A	3.8 <sup>a</sup> (0.009 U mL <sup>-1</sup> U mL <sup>-1</sup> ) <sup>b</sup>
DpkA <sub>Psyrin</sub>	4.0 <sup>a</sup> (2.6 10 <sup>-2</sup> U mL <sup>-1</sup> ) <sup>b</sup>
GDH	5.2 <sup>a</sup> (20.8 U mL <sup>-1</sup> ) <sup>b</sup>

<sup>a</sup>mg protein mL<sup>-1</sup> lyophilized powder. <sup>b</sup>Enzyme activity assays were described in previous work.<sup>1-2</sup>

## HPLC analysis.

- a) HPLC analysis was performed on a RP-HPLC XBridge® C18, 5 μm, 4.6 × 250 mm column (Waters). The solvent system used was: solvent (A): 0.1% (v/v) trifluoroacetic acid (TFA) in H<sub>2</sub>O and solvent (B): 0.095% (v/v) TFA in CH<sub>3</sub>CN/H<sub>2</sub>O 4:1, flow rate 1 mL min<sup>-1</sup>, detection at 215 nm and column

temperature at 30 °C. The amount of substrates and products were quantified from the peak areas using an external standard methodology. Reaction monitoring for benzaldehyde (**1a**), aldol adduct (**3**) and reduced product (**4**) were carried out as follows: samples were withdrawn from the reaction mixture (25  $\mu$ L) and diluted with methanol (500  $\mu$ L). After centrifugation, samples were analyzed by HPLC. Elution conditions: gradient from 10 to 100% B over 30 min.

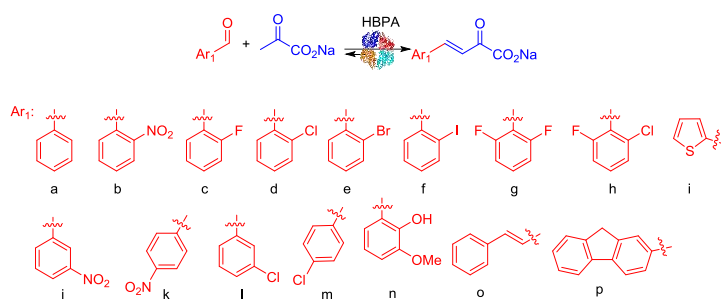
- b) Enantiomeric excesses were analyzed by HPLC on a CHIRALPAK® ID, column (46 x 250 mm, 5  $\mu$ m). The solvent system used was: solvent (A): Hexane + 0,1%TFA and solvent (B): Isopropanol + 0,1%TFA, detection by diode array detection (215-350 nm) and column temperature at 30 °C.

### NMR analysis.

Routine  $^1\text{H}$  (400 MHz) and  $^{13}\text{C}$  (101 MHz) NMR spectra of compounds were recorded with a Varian Mercury-400 spectrometer. Full characterization of the described compounds was performed using typical gradient-enhanced 2D experiments: COSY, HSQC, and NOESY recorded under routine conditions.

### Biocatalytic aldol addition of **2** to aldehydes (**1a-p**), catalyzed by HBPA<sub>*Pputida*</sub> and variant.

Analytical scale: The reaction (total volume 500  $\mu$ L) was carried out in 1.5 mL Eppendorf tubes. To a solution of the aldehydes (**1a-p**) dissolved in DMF (20% v/v in the reaction), a solution of sodium pyruvate (**2**) (25  $\mu$ L of a 2.0 M aqueous stock solution, pH 6.5-7.0, final concentration 100 mM) was added in the reaction. The reaction was initiated with the addition of HBPA (125  $\mu$ L of a 0.029 U mL<sup>-1</sup> stock solution, 4 mg mL<sup>-1</sup> in 50 mM TEA buffer, 50 mM NaCl, 0.5 mM EDTA and 50% (v/v) glycerol, 0.007 U mL<sup>-1</sup>, 1 mg mL<sup>-1</sup> protein mL<sup>-1</sup> final concentration in the reaction) (**Table S1**). The reaction mixture was placed on a vortex mixer (1000 rpm) at 25 °C for 24 h. Samples were extracted immediately after enzyme addition (0 h) and after 24 h and analyzed by HPLC as described above.

**Table S1.** Aldol condensation of sodium pyruvate to aromatic aldehydes catalyzed by HBPA *wt.*

Aldehyde	Aldol adduct <b>3</b>	Aldol conversion at 24 (%) <sup>a</sup> Sodium pyruvate 1eq.
<b>1a</b>	<b>3a</b>	50
<b>1b</b>	<b>3b</b>	90
<b>1c</b>	<b>3c</b>	70
<b>1d</b>	<b>3d</b>	94
<b>1e</b>	<b>3e</b>	70
<b>1f</b>	<b>3f</b>	85
<b>1g</b>	<b>3g</b>	>95
<b>1h</b>	<b>3h</b>	>95
<b>1i</b>	<b>3i</b>	85
<b>1j</b>	<b>3j</b>	78
<b>1k</b>	<b>3k</b>	70
<b>1l</b>	<b>3l</b>	81
<b>1m</b>	<b>3m</b>	64
<b>1n</b>	<b>3n</b>	59
<b>1o</b>	<b>3o</b>	40
<b>1p</b>	<b>3p</b>	20

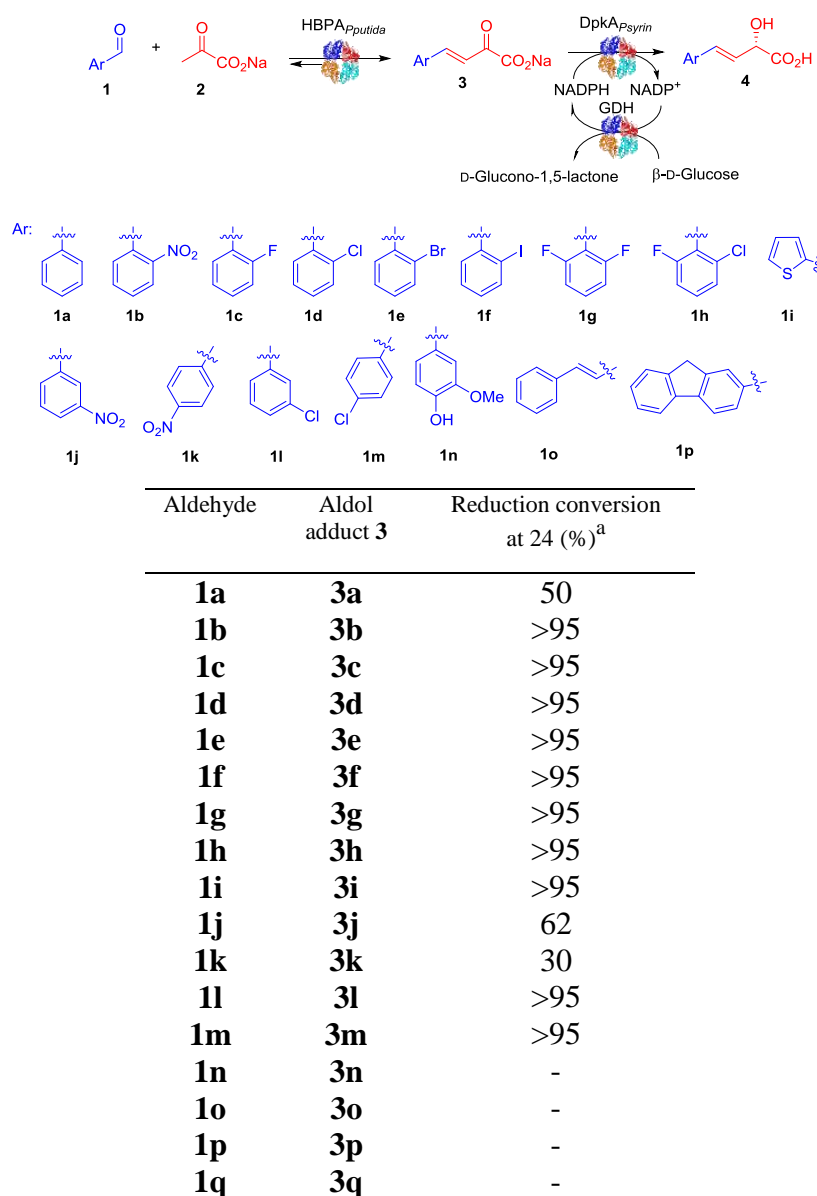
<sup>a</sup>Aldol conversion measured by HPLC using 1eq of pyruvate. <sup>b</sup>Aldol conversion measured by HPLC using 3eq of pyruvate. <sup>c</sup>Not performed.

### **Biocatalytic reduction of arylbut-3-enoic acids (**3a-p**) catalyzed by DpkA<sub>Psyrin</sub>. Analytical scale.**

Reactions were carried out at analytic level as follows: The reactions (500  $\mu\text{L}$  total volume) were conducted in Eppendorf tubes (1.5 mL) and placed in a vortex mixer (1000 rpm) at 25  $^{\circ}\text{C}$ . To a solution of the aldehydes (**1a-p**) dissolved in DMF (20% v/v in the reaction), a solution of sodium pyruvate (**2**) (25  $\mu\text{L}$  of a 2.0 M aqueous stock solution, pH 6.5-7.0, final concentration 100 mM), DpkA<sub>Psyrin</sub> (125  $\mu\text{L}$  of a stock solution of  $2.6 \cdot 10^{-2}$  U  $\text{mL}^{-1}$ , 4 mg  $\text{mL}^{-1}$  in 20 mM TEA buffer pH 7.0, 100 mM NaCl, and 50% (v/v) of glycerol,  $6.5 \cdot 10^{-3}$  U  $\text{mL}^{-1}$  final concentration in the reaction), GDH (83  $\mu\text{L}$  of a stock solution  $20.8$  U  $\text{mL}^{-1}$ , 5.2 mg  $\text{mL}^{-1}$  in 10 mM HEPES buffer pH 6.5, 50 mM NaCl, and

50% (v/v) of glycerol, 3.5 U mL<sup>-1</sup> final concentration in the reaction), a solution of NADP<sup>+</sup> y glucose (42 μL, NADP<sup>+</sup> stock solution 60 mM, 5mM final concentration in the reaction, glucose stock solution 2.4M, 200mM in reaction, dissolved in 1M sodium phosphate buffer pH 8.0, 84 mM final concentration in the reaction). The reaction was initiated with the addition of HBPA (125 μL of a 0.029 U mL<sup>-1</sup> stock solution, 4 mg mL<sup>-1</sup> in 50 mM TEA buffer, 50 mM NaCl, 0.5 mM EDTA and 50% (v/v) glycerol, 0.007 U mL<sup>-1</sup>, 1 mg mL<sup>-1</sup> protein mL<sup>-1</sup> final concentration in the reaction) (**Table S2**). Samples were withdrawn immediately after the addition of aldol substrate (0 h) and after 24 h and analyzed by HPLC as described above.

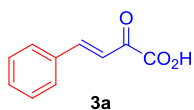
**Table S2.** Biocatalytic reduction of aldol adducts **3a-p** catalyzed by DpkA<sub>P<sub>sy</sub>rin</sub>.



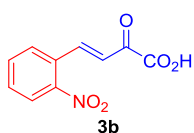
<sup>a</sup>measured by HPLC

## Synthesis of arylbut-3-enoic acids (3).

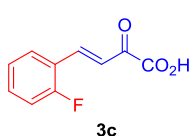
### (*E*)-2-oxo-4-phenylbut-3-enoic acid (3a).



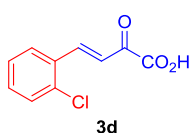
Synthesis of (*E*)-2-oxo-4-phenylbut-3-enoic acid (**3a**). Typical procedure: The reaction (0,5 mmol scale, 20 mL total volume) was conducted in an erlenmeyer at 25 °C and an orbital shaker (250 rpm). To a solution of the aldehyde (**1a**, 110mg, 1.04 mmol, 50mM in reaction) dissolved in DMF (20% v/v in reaction), a solution of sodium pyruvate (**2**) (1.5 mL of a 2.0 M concentrated solution, pH 6.5-7.0, 3.12 mmol, 150 mM in reaction, 3eq) was added. The reaction was initiated with the addition of enzyme (HBPA wt, 5 mL of a 0.029 U mL<sup>-1</sup> stock solution, 4 mg mL<sup>-1</sup> in 50 mM TEA buffer, 50 mM NaCl, 0.5 mM EDTA and 50% (v/v) glycerol, 0.007 U mL<sup>-1</sup>, 1 mg mL<sup>-1</sup> protein mL<sup>-1</sup> final concentration in reaction). The mixture was placed on an orbital shaker (250 rpm) at 25 °C for 24 h. The reaction was monitored by HPLC. The reaction was monitored by HPLC and samples were extracted immediately after enzyme addition (0 h) and after 24 h as described above. After completion of the reaction the enzyme component was precipitated with MeOH (10 volumes) filtered over Celite® the filtrate was washed with 5% NaHCO<sub>3</sub>, (3x100 mL), the organic solvent was evaporated and the aqueous phase was extracted with AcOEt (3x100 mL). The pH of the aqueous phase was adjusted to pH 2.0 with 3M HCl. The compound was extracted with AcOEt (3x100 mL). This organic phase was washed with pure H<sub>2</sub>O (3x100 mL), then with saturated NaCl solution (3 x 100 mL), dried over anhydrous MgSO<sub>4</sub> and concentrated under vacuum. The solid was adsorbed on a KP-C18-HS SNAP Cartridge and purified by Biotage Isolera with gradient (solvent system used was A: H<sub>2</sub>O+0.1% HCO<sub>2</sub>H and B: CH<sub>3</sub>CN+0.1% HCO<sub>2</sub>H), from 0 to 100% of B, 20 VC and 100%B 10 VC. After purification, the pure fractions were collected and the organic solvent was removed by vacuum, the compound was extracted from the acidic aqueous phase with AcOEt (3x50 mL), washed with pure H<sub>2</sub>O (3x 50 mL), then with saturated NaCl solution (3x50 mL), dried over anhydrous MgSO<sub>4</sub> and concentrated under vacuum, to afford compound **3a** as a yellow solid (161 mg, 81%). <sup>1</sup>H NMR (400 MHz, DMSO) δ 7.88 – 7.78 (m, 2H), 7.76 (d, *J* = 16.3 Hz, 1H), 7.56 – 7.40 (m, 3H), 7.30 (d, *J* = 16.3 Hz, 1H). <sup>13</sup>C NMR (101 MHz, DMSO) δ 186.6, 164.9, 148.0, 134.3, 132.0, 129.6, 122.0. The spectral properties of this product agreed with those reported in the literatura.<sup>3-4</sup>

**(E)-4-(2-nitrophenyl)-2-oxobut-3-enoic acid (3b).**

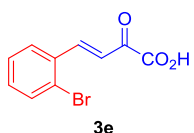
The title compound was prepared as described for **3a**. Starting from **1b** (**[1b]** = 150mg, 50 mM and **[2]** = 328mg, 150 mM in the reaction), **3b** was obtained as an orange solid (184 mg, 84%). <sup>1</sup>H NMR (400 MHz, DMSO)  $\delta$  8.12 (dd,  $J$  = 8.1, 1.3 Hz, 1H), 8.04 (d,  $J$  = 16.2 Hz, 1H), 8.00 (d,  $J$  = 8.0 Hz, 1H), 7.82 (td,  $J$  = 7.7, 7.3, 0.7 Hz, 1H), 7.73 (ddd,  $J$  = 8.8, 7.5, 1.4 Hz, 1H), 7.27 (d,  $J$  = 16.1 Hz, 1H). <sup>13</sup>C NMR (101 MHz, DMSO)  $\delta$  185.7, 163.9, 148.6, 142.1, 134.1, 131.7, 129.3, 125.2. The spectral properties of this product matched those reported in the literatura.<sup>4</sup>

**(E)-4-(2-fluorophenyl)-2-oxobut-3-enoic acid (3c).**

The title compound was prepared as described for **3a**. Starting from **1c** (**[1c]** = 110mg, 50 mM and **[2]** = 293, mg, 150 mM in the reaction), **3c** was obtained as a yellow solid (88 mg, 51%). <sup>1</sup>H NMR (400 MHz, DMSO)  $\delta$  7.60 (td,  $J$  = 7.9, 7.8, 1.7 Hz, 1H), 7.31 (qd,  $J$  = 7.2, 7.2, 7.2, 1.8 Hz, 1H), 7.23 – 7.14 (m, 2H), 6.82 (dd,  $J$  = 16.1, 1.9 Hz, 1H), 6.48 (dd,  $J$  = 16.0, 5.2 Hz, 1H), 4.72 (dd,  $J$  = 5.2, 1.9 Hz, 1H). <sup>13</sup>C NMR (101 MHz, DMSO)  $\delta$  174.0, 160.0 (d,  $J$  = 247.2 Hz), 131.4 (d,  $J$  = 4.7 Hz), 129.9 (d,  $J$  = 8.5 Hz), 128.2 (d,  $J$  = 3.6 Hz), 125.2 (d,  $J$  = 3.2 Hz), 124.2 (d,  $J$  = 11.8 Hz), 122.5 (d,  $J$  = 3.7 Hz), 116.2 (d,  $J$  = 21.9 Hz), 71.3.<sup>4</sup>

**(E)-4-(2-chlorophenyl)-2-oxobut-3-enoic acid (3d).**

The title compound was prepared as described for **3a**. Starting from **1d** (**[1d]** = 150mg, 50 mM and **[2]** = 352, mg, 150 mM in the reaction), **3d** was obtained as a yellow solid (179 mg, 80%). <sup>1</sup>H NMR (400 MHz, DMSO)  $\delta$  8.03 (dd,  $J$  = 7.1, 2.4 Hz, 1H), 8.02 (d,  $J$  = 16.8 Hz, 1H), 7.59 (dd,  $J$  = 8.0, 1.4 Hz, 1H), 7.52 (td,  $J$  = 8.0, 7.6, 1.7 Hz, 1H), 7.44 (td,  $J$  = 2x7.8, 0.9 Hz, 1H), 7.37 (d,  $J$  = 16.2 Hz, 1H). <sup>13</sup>C NMR (101 MHz, DMSO)  $\delta$  185.7, 164.0, 141.6, 134.6, 132.9, 131.4, 130.2, 128.6, 128.0, 124.2. The spectral properties of this product matched those reported in the literatura.<sup>4</sup>

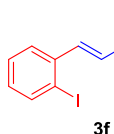
**(E)-4-(2-bromophenyl)-2-oxobut-3-enoic acid (3e).**

The title compound was prepared as described for **3a**. Starting from **1e** (**[1e]** = 150mg, 50 mM and **[2]** = 268 mg, 150 mM in the reaction), **3d** was obtained as a yellow solid (184 mg, 89%). <sup>1</sup>H NMR (400 MHz,



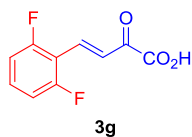
DMSO)  $\delta$  8.02 (d,  $J = 1.9$  Hz, 1H), 7.98 (d,  $J = 16.0$  Hz, 1H), 7.76 (dd,  $J = 7.9, 1.4$  Hz, 1H), 7.48 (td,  $J = 2 \times 7.6, 1.4$  Hz, 1H), 7.42 (td,  $J = 7.6, 7.4, 1.8$  Hz, 1H), 7.33 (d,  $J = 16.2$  Hz, 1H).  $^{13}\text{C}$  NMR (101 MHz, DMSO)  $\delta$  186.2, 164.5, 144.8, 134.0, 133.6, 133.5, 129.2, 129.0, 126.1, 124.8.

**(E)-4-(2-iodophenyl)-2-oxobut-3-enoic acid (3f).**



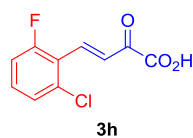
The title compound was prepared as described for **3a**. Starting from **1f** (**[1f]** = 160mg, 50 mM and **[2]** = 228 mg, 150 mM in the reaction), **3f** was obtained as a yellow solid (160 mg, 77%).  $^1\text{H}$  NMR (400 MHz, DMSO)  $\delta$  8.00 (dd,  $J = 7.9, 1.2$  Hz, 1H), 7.94 (dd,  $J = 7.9, 1.6$  Hz, 1H), 7.87 (d,  $J = 16.1$  Hz, 1H), 7.48 (td,  $J = 7.7, 7.6, 1.1$  Hz, 1H), 7.24 (d,  $J = 16.1$  Hz, 1H), 7.22 (td,  $J = 7.6, 7.5, 1.6$  Hz, 1H).  $^{13}\text{C}$  NMR (101 MHz, DMSO)  $\delta$  185.8, 164.2, 149.6, 140.0, 136.2, 132.8, 129.0, 128.2, 124.2, 103.4. The spectral properties of this product matched those reported in the literature.<sup>4</sup>

**(E)-4-(2,6-difluorophenyl)-2-oxobut-3-enoic acid (3g).**

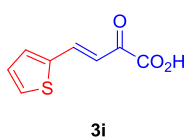


The title compound was prepared as described for **3a**. Starting from **1g** (**[1g]** = 150mg, 50 mM and **[2]** = 349 mg, 150 mM in the reaction), **3g** was obtained as a yellow solid (175 mg, 78%).  $^1\text{H}$  NMR (400 MHz, DMSO)  $\delta$  7.68 (d,  $J = 16.7$  Hz, 1H), 7.61 (t,  $J = 2 \times 8.5$  Hz, 1H), 7.46 (d,  $J = 16.6$  Hz, 1H), 7.28 (t,  $J = 2 \times 8.9$  Hz, 2H).  $^{13}\text{C}$  NMR (101 MHz, DMSO)  $\delta$  185.0, 163.4, 162.4 (d,  $J = 6.7$  Hz), 159.9 (d,  $J = 6.7$  Hz), 133.6 (t,  $J = 11.3, 11.3$  Hz), 131.7, 126.5 (t,  $J = 8.4, 8.4$  Hz), 112.7, 112.5.

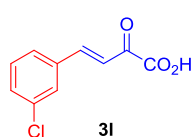
**(E)-4-(2-chloro-6-fluorophenyl)-2-oxobut-3-enoic acid (3h).**



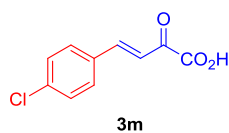
The title compound was prepared as described for **3a**. Starting from **1h** (**[1h]** = 150mg, 50 mM and **[2]** = 312 mg, 150 mM in the reaction), **3h** was obtained as a yellow solid (144 mg, 67%).  $^1\text{H}$  NMR (400 MHz, DMSO)  $\delta$  7.82 (d,  $J = 16.6$  Hz, 1H), 7.60 – 7.49 (m, 2H), 7.47 (d,  $J = 6.3$  Hz, 1H), 7.44 (d,  $J = 16.5$  Hz, 1H).  $^{13}\text{C}$  NMR (101 MHz, DMSO)  $\delta$  185.1, 163.4, 162.8, 160.3, 135.6 (d,  $J = 2.0$  Hz), 133.0 (d,  $J = 10.6$  Hz), 127.6 (d,  $J = 14.2$  Hz), 126.5 (d,  $J = 3.2$  Hz), 120.5 (d,  $J = 14.0$  Hz), 115.8 (d,  $J = 22.9$  Hz).

**(E)-2-oxo-4-(thiophen-2-yl)but-3-enoic acid (3i).**

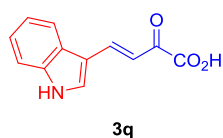
The title compound was prepared as described for **3a**. Starting from **1i** (**[1i]** = 120mg, 50 mM and **[2]** = 353 mg, 150 mM in the reaction), **3i** was obtained as a yellow solid (185 mg, 95%). <sup>1</sup>H NMR (400 MHz, DMSO) δ 7.94 (d, *J* = 16.0 Hz, 1H), 7.87 (d, *J* = 5.0 Hz, 1H), 7.72 (d, *J* = 0.6 Hz, 1H), 7.22 (dd, *J* = 5.0, 3.7 Hz, 1H), 6.97 (d, *J* = 15.9 Hz, 1H). <sup>13</sup>C NMR (101 MHz, DMSO) δ 184.9, 164.2, 139.9, 139.1, 134.6, 132.1, 129.1, 119.6.

**(E)-4-(3-chlorophenyl)-2-oxobut-3-enoic acid (3l).**

The title compound was prepared as described for **3a**. Starting from **1l** (**[1l]** = 150mg, 50 mM and **[2]** = 352 mg, 150 mM in the reaction), **3l** was obtained as a yellow solid (94 mg, 42%). <sup>1</sup>H NMR (400 MHz, DMSO) δ 7.94 (t, *J* = 2x1.9 Hz, 1H), 7.79 (dt, *J* = 7.6, 2x1.4 Hz, 1H), 7.72 (d, *J* = 16.3 Hz, 1H), 7.59 – 7.49 (m, 1H), 7.48 (t, *J* = 2x7.8 Hz, 1H), 7.36 (d, *J* = 16.3 Hz, 1H). <sup>13</sup>C NMR (101 MHz, DMSO) δ 186.4, 164.3, 145.5, 136.1, 133.9, 131.0, 130.9, 128.6, 127.6, 123.1.<sup>4</sup>

**(E)-4-(4-chlorophenyl)-2-oxobut-3-enoic acid (3m).**

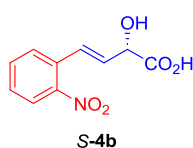
The title compound was prepared as described for **3a**. Starting from **1m** (**[1m]** = 150mg, 50 mM and **[2]** = 352 mg, 150 mM in the reaction), **3m** was obtained as a yellow solid (163 mg, 73%). <sup>1</sup>H NMR (400 MHz, DMSO) δ 7.85 (d, *J* = 8.6 Hz, 2H), 7.74 (d, *J* = 16.3 Hz, 1H), 7.53 (d, *J* = 8.5 Hz, 2H), 7.31 (d, *J* = 16.3 Hz, 1H). <sup>13</sup>C NMR (101 MHz, DMSO) δ 186.7, 164.9, 146.3, 136.5, 133.3, 131.6, 131.3, 129.6, 129.2, 122.8. The spectral properties of this product matched those reported in the literatura.<sup>4</sup>

**(E)-4-(1H-indol-3-yl)-2-oxobut-3-enoic acid (3q).**

The title compound was prepared as described for **3a**. Starting from **1q** (**[1q]** = 130mg, 50 mM and **[2]** = 296 mg, 150 mM in the reaction), **3q** was obtained as a yellow solid (130 mg, 67%). <sup>1</sup>H NMR (400 MHz, DMSO) δ 8.17 (d, *J* = 3.0 Hz, 1H), 8.00 (d, *J* = 16.0 Hz, 1H), 7.90 (dd, *J* = 6.5, 2.4 Hz, 1H), 7.51 (dd, *J* = 7.5, 1.7 Hz, 1H), 7.25 (tt, *J* = 2x7.2, 2x5.5 Hz, 2H), 7.10 (d, *J* = 16.0 Hz, 1H). <sup>13</sup>C NMR (101 MHz, DMSO) δ 166.0, 143.9, 138.2, 135.4, 125.4, 123.6, 122.2, 120.6, 115.3, 113.3.

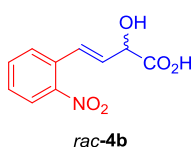
## Synthesis of (*S,E*)-2-hydroxy-4-arylbut-3-enoic acid derivatives (*S-4*).

### (*S,E*)-2-hydroxy-4-(2-nitrophenyl)but-3-enoic acid (*S-4b*).



**Typical procedure:** the reaction (0,5 mmol scale, 20 mL total volume) was conducted in a round-bottom flask (100 mL) at 25 °C and magnetically stirred with a bar at 250 rpm. To a solution of the aldehyde (**1b**, 150 mg, 1 mmol, 1 eq, 0.05 M in the reaction) dissolved in DMF (4,0 mL, 20% (v/v) in the reaction), a solution of sodium pyruvate (**2**) (500  $\mu$ L of a 2.0 M aqueous stock solution, pH 6.5-7.0, final concentration 0,05 mM), HBPA (5,0 mL of a 0.029 U mL<sup>-1</sup> stock solution, 4 mg mL<sup>-1</sup> in 50 mM TEA buffer, 50 mM NaCl, 0.5 mM EDTA and 50% (v/v) glycerol, 0.007 U mL<sup>-1</sup>, 1 mg mL<sup>-1</sup> protein mL<sup>-1</sup> final concentration in the reaction), glucose (721 mg, 2 mmol, 4 eq, 0.2 M final concentration in the reaction), GDH (3.30 mL of a stock solution 20.8 U mL<sup>-1</sup>, 5.2 mg mL<sup>-1</sup> in 10 mM HEPES buffer pH 6.5, 50 mM NaCl, and 50% (v/v) of glycerol, 3.4 U mL<sup>-1</sup> final concentration in the reaction) and DpkA<sub>Psyrin</sub> (5.0 mL of a stock solution 2.6 10<sup>-2</sup> U mL<sup>-1</sup>, 4 mg mL<sup>-1</sup> in 20 mM TEA buffer pH 7.0, 100 mM NaCl, and 50% (v/v) of glycerol, 6.5 10<sup>-3</sup> U mL<sup>-1</sup> final concentration in the reaction) were adding. The reaction was started by adding a solution of NADP<sup>+</sup> (6,2 mL of stock solution 16 mM in 0,4 M sodium phosphate buffer pH 8.0, 5 mM final concentration in the reaction). Samples were withdrawn immediately after the addition of aldol substrate (0 h) and after 24 h and analyzed by HPLC as described above. The purification was done following the protocol described for **3a**. *S-4b* was obtained as a white solid (152 mg, 69%). <sup>1</sup>H NMR (400 MHz, DMSO)  $\delta$  7.94 (dd,  $J = 8.1, 1.3$  Hz, 1H), 7.80 (dd,  $J = 7.9, 1.4$  Hz, 1H), 7.69 (td,  $J = 7.7, 7.6, 1.4$  Hz, 1H), 7.53 (td,  $J = 7.8, 7.4, 1.4$  Hz, 1H), 6.99 (dd,  $J = 15.8, 2.0$  Hz, 1H), 6.51 (dd,  $J = 15.7, 4.9$  Hz, 1H), 4.77 (dd,  $J = 4.9, 2.0$  Hz, 1H). <sup>13</sup>C NMR (101 MHz, DMSO)  $\delta$  173.2, 147.9, 133.5, 133.3, 130.6, 128.7, 128.2, 124.1, 123.9, 70.6.

### (*E*)-2-hydroxy-4-(2-nitrophenyl)but-3-enoic acid (*rac-4b*).



The aldol precursor **3b** was prepared and purified as described for **3a**, starting from **1b** (150 mg, 1 eq, 0.1 M concentration in the reaction) and **2** (109 mg, 1 eq, 0.1 M concentration in the reaction). **Chemical reduction** was carried out as follows: **Typical procedure:** A dried three-necked round bottomed flask was charged with anhydrous MeOH (25 mL) under N<sub>2</sub> atmosphere. Then, CeCl<sub>3</sub>\*7H<sub>2</sub>O (6.6 g, 17,2 mmol, 39.2.0 eq) was dissolved, and

added a portion of **3b** (100 mg, 0,45 mmol, 1.0 eq) after 30 minutes on magnetic stirring (300 rpm) at rt. The chemical reduction was initiated by adding NaBH<sub>4</sub> (17.1 mg, 0,45 mmol, 1.0 eq), the mixture was stirred at 25 °C for 10 min. Formation of *rac*-**4b** was estimated by measuring the aldol adduct **3b** consumed by HPLC. When the conversion was maximized, a solution 5% NaHCO<sub>3</sub> (50 mL) was add to stop the reaction. After that, the solvent was evaporated under vacuum. Aqueous phase was adjusted to pH 2.0 with a 3M HCl solution and extracted with AcOEt (3 x 50 mL). The organic phases were combined, washed with water (3x100 mL), brine (3 x 100 mL) and dried over anhydrous magnesium sulfate. The solvent removed under vacuum affording (*E*)-2-hydroxy-4-(2-nitrophenyl)but-3-enoic acid (*rac*-**4b**) as brown solid (85 mg, 85%). NMR spectra were indistinguishable from that of *S*-**4b**.

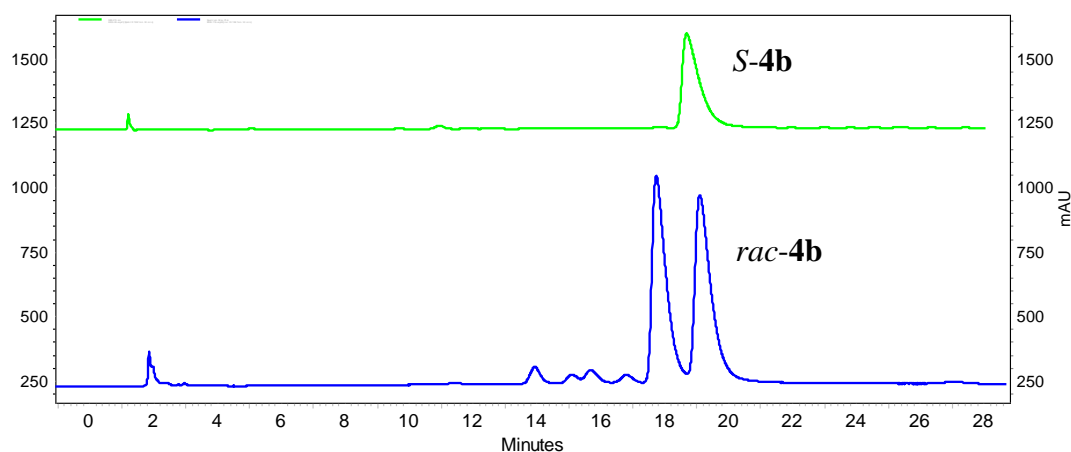
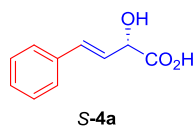


**Figure S1.** CPHPLC chromatogram of *S*-**4b** from DpkA<sub>Pyrrin</sub> catalysis (A) *rac*-**4b**. (B). Conditions: CHIRALPACK® ID, flow rate 1 mL min<sup>-1</sup> at 30 °C and detection at 254 nm. Isocratic elution hexane + 0,1% TFA: <sup>i</sup>PrOH + 0,1% TFA 85:15 (v/v), tr (*R*) = 19.0 min, tr (*S*) = 20.3 min.

**(*S,E*)-2-hydroxy-4-phenylbut-3-enoic acid (*S*-**4a**).**

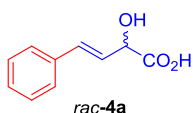


The title compound was prepared as described for *S*-**4b** starting from **1a** (150 mg). The (*3a* and *S*-**4a** mixture) was obtained as a yellow solid (90 mg, 40%). **3a** <sup>1</sup>H NMR (400 MHz, DMSO) δ 7.88 – 7.78 (m, 2H), 7.76 (d, *J* = 16.3 Hz, 1H), 7.56 – 7.40 (m, 3H), 7.30 (d, *J* = 16.3 Hz, 1H). <sup>13</sup>C NMR (101 MHz, DMSO) δ 186.6, 164.9, 148.0, 134.3, 132.0, 129.6, 122.0. *S*-**4a** <sup>1</sup>H NMR (400 MHz, DMSO) δ 7.43 (d, *J* = 6.9 Hz, 1H), 7.33 (t, *J* = 2x7.6 Hz, 2H), 7.25 (t, *J* = 2x7.3 Hz, 1H), 6.69 (dd, *J* = 16.0, 1.8 Hz, 1H), 6.35 (dd, *J* = 15.9, 5.6 Hz, 1H), 4.68 (dd, *J* = 5.6, 1.8 Hz,

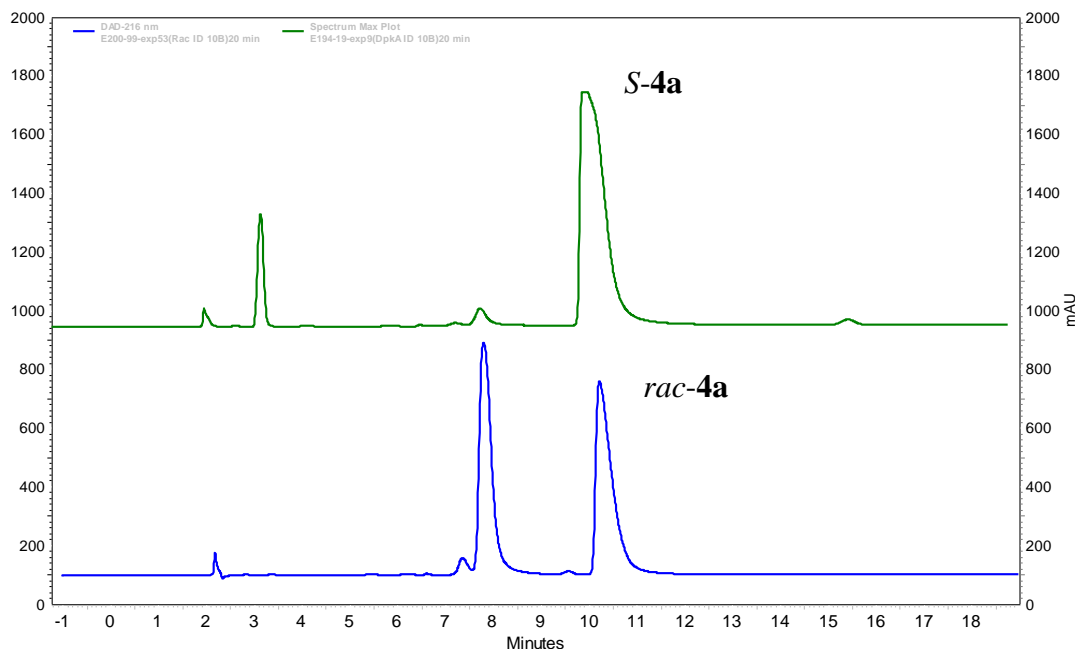
1H).  $^{13}\text{C}$  NMR (101 MHz, DMSO)  $\delta$  173.8, 136.2, 130.2, 128.7, 127.9, 127.7, 126.4, 70.9.

### Synthesis of *S*-**3a** in a one-pot two-step system.

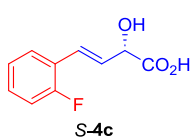
**Aldol addition (1<sup>st</sup>):** Synthesis of **3a**. The reaction (1 mmol scale, 14 mL total volume) was conducted in an erlenmeyer at 25 °C and an orbital shaker (250 rpm). To a solution of the aldehyde (**1a**, 150mg, 1.4 mmol, 100 mM in reaction) dissolved in DMF (20% v/v in reaction), a solution of sodium pyruvate (**2**) (700  $\mu\text{L}$  of a 2.0 M concentrated solution, pH 6.5-7.0, 3.12 mmol, 100 mM in reaction, 1eq) was added. The reaction was initiated with the addition of enzyme (HBPA *wt*, 3.5 mL of a 0.029 U mL<sup>-1</sup> stock solution, 4 mg mL<sup>-1</sup> in 50 mM TEA buffer, 50 mM NaCl, 0.5 mM EDTA and 50% (v/v) glycerol, 0.007 U mL<sup>-1</sup>, 1 mg mL<sup>-1</sup> protein mL<sup>-1</sup> final concentration in reaction). The mixture was placed on an orbital shaker (250 rpm) at 25 °C for 24 h. The reaction was monitored by HPLC. The reaction was monitored by HPLC and samples were extracted immediately after enzyme addition (0 h) and after 24 h as described above. **Aldol reduction (2<sup>nd</sup>):** After 24h, the reduction reaction (28 mL final volume) was carried out adding glucose (1 g, 4.0 mmol, 4 eq, 0.2 M final concentration in the reaction), GDH (4.6 mL of a stock solution 20.8 U mL<sup>-1</sup>, 5.2 mg mL<sup>-1</sup> in 10 mM HEPES buffer pH 6.5, 50 mM NaCl, and 50% (v/v) of glycerol, 3.4 U mL<sup>-1</sup> final concentration in the reaction), and DpkA<sub>Psyrin</sub> (7.0 mL of a stock solution 2.6 10<sup>-2</sup> U mL<sup>-1</sup>, 4 mg mL<sup>-1</sup> in 20 mM TEA buffer pH 7.0, 100 mM NaCl, and 50% (v/v) of glycerol, 6.5 10<sup>-3</sup> U mL<sup>-1</sup> final concentration in the reaction) were adding. The reaction was started by adding a solution of NADP<sup>+</sup> (2.4 mL of stock solution 58.3 mM in 1M sodium phosphate buffer pH 8.0, 5 mM final concentration in the reaction). Samples were withdrawn immediately after the addition of aldol substrate (0 h) and after 24 h and analyzed by HPLC as described above. The purification was done following the protocol described for **3a**. the compound *S*-**4a** was obtained as a white solid (176 mg, 62%).  $^1\text{H}$  NMR (400 MHz, DMSO)  $\delta$  7.43 (d,  $J$  = 6.9 Hz, 1H), 7.33 (t,  $J$  = 2x7.6 Hz, 2H), 7.25 (t,  $J$  = 2x7.3 Hz, 1H), 6.69 (dd,  $J$  = 16.0, 1.8 Hz, 1H), 6.35 (dd,  $J$  = 15.9, 5.6 Hz, 1H), 4.68 (dd,  $J$  = 5.6, 1.8 Hz, 1H).  $^{13}\text{C}$  NMR (101 MHz, DMSO)  $\delta$  173.8, 136.2, 130.2, 128.7, 127.9, 127.7, 126.4, 70.9.

**(E)-2-hydroxy-4-phenylbut-3-enoic acid (*rac*-3a).**

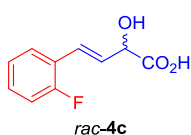
Synthesis of title compound was performed as described for *rac*-4b starting from **3a** (100 mg), *rac*-4a was obtained as a white solid (90 mg, 90%). NMR spectra were indistinguishable from that of *S*-4a.



**Figure S2.** CPHPLC chromatogram of *S*-4a from DpkA<sub>*Psyrin*</sub> catalysis (A) *rac*-4a. (B). Conditions: CHIRALPACK® ID, flow rate 1 mL min<sup>-1</sup> at 30 °C and detection at 254 nm. Isocratic elution hexane + 0,1%TFA: *i*PrOH + 0,1%TFA 90:10 (v/v). tr (*R*) = 7.9 min, tr (*S*) = 10.4 min.

**(*S,E*)-4-(2-fluorophenyl)-2-hydroxybut-3-enoic acid (*S*-4c).**

The title compound was prepared as described for *S*-4b, starting from **1c** (110 mg) *S*-4c was obtained as a white solid (138 mg, 72%). <sup>1</sup>H NMR (400 MHz, DMSO) δ 7.60 (t, *J* = 7.3, 7.3 Hz, 1H), 7.31 (dd, *J* = 9.9, 3.9 Hz, 1H), 7.19 (q, *J* = 7.8, 7.8, 7.2 Hz, 1H), 6.82 (d, *J* = 16.1 Hz, 0H), 6.48 (dd, *J* = 16.1, 5.2 Hz, 1H), 4.72 (dd, *J* = 5.1, 1.4 Hz, 1H). <sup>13</sup>C NMR (101 MHz, DMSO) δ 173.5, 159.5 (d, *J* = 247.2 Hz), 130.9 (d, *J* = 4.7 Hz), 129.4 (d, *J* = 8.5 Hz), 127.7 (d, *J* = 3.6 Hz), 124.7 (d, *J* = 3.3 Hz), 123.7 (d, *J* = 11.9 Hz), 122.0 (d, *J* = 3.7 Hz), 115.7 (d, *J* = 21.9 Hz), 70.8.

**(*E*)-4-(2-fluorophenyl)-2-hydroxybut-3-enoic acid (*rac*-4c).**

Synthesis of title compound was performed as described for *rac*-4b starting from **3c** (70 mg). *rac*-4c was obtained as a white solid (59 mg, 84%). NMR spectra were indistinguishable from that of *S*-4c.

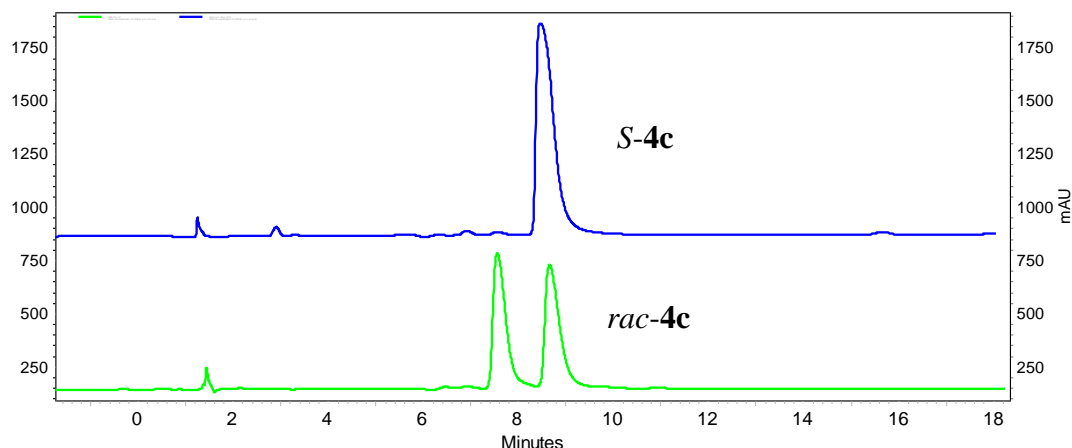
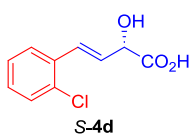


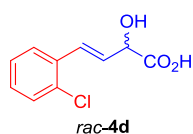
**Figure S3.** CPHPLC chromatogram of *S*-**4c** from DpkA<sub>Psyrin</sub> catalysis (A) *rac*-**4c** (B). Conditions: CHIRALPACK® ID, flow rate 1 mL min<sup>-1</sup> at 30 °C and detection at 254 nm. Isocratic elution hexane + 0,1% TFA: *i*PrOH + 0,1% TFA 90:10 (v/v), tr (*R*) = 9.5 min, tr (*S*) = 10.4 min.

**(*S,E*)-4-(2-chlorophenyl)-2-hydroxybut-3-enoic acid (*S*-**4d**).**



The title compound was prepared as described for *S*-**4b**, starting from **1d** (130 mg). *S*-**4d** was obtained as a white solid (138 mg, 71%). <sup>1</sup>H NMR (400 MHz, DMSO) δ 7.68 (dd, *J* = 7.5, 2.0 Hz, 1H), 7.45 (dd, *J* = 7.5, 1.8 Hz, 1H), 7.30 (pd, *J* = 4x7.3, 1.8 Hz, 2H), 7.03 (dd, *J* = 15.9, 1.9 Hz, 1H), 6.45 (dd, *J* = 15.8, 5.1 Hz, 1H), 4.75 (dd, *J* = 5.1, 2.0 Hz, 1H). <sup>13</sup>C NMR (101 MHz, DMSO) δ 173.4, 134.0, 131.9, 131.3, 129.6, 129.2, 127.5, 127.1, 125.3, 70.7.

**(*E*)-4-(2-chlorophenyl)-2-hydroxybut-3-enoic acid (*rac*-**4d**).**



Synthesis of title compound was performed as described for *rac*-**4b** starting from **3d** (100 mg). *rac*-**4d** was obtained as a white solid (95 mg, 95%). NMR spectra were indistinguishable from that of *S*-**4d**.

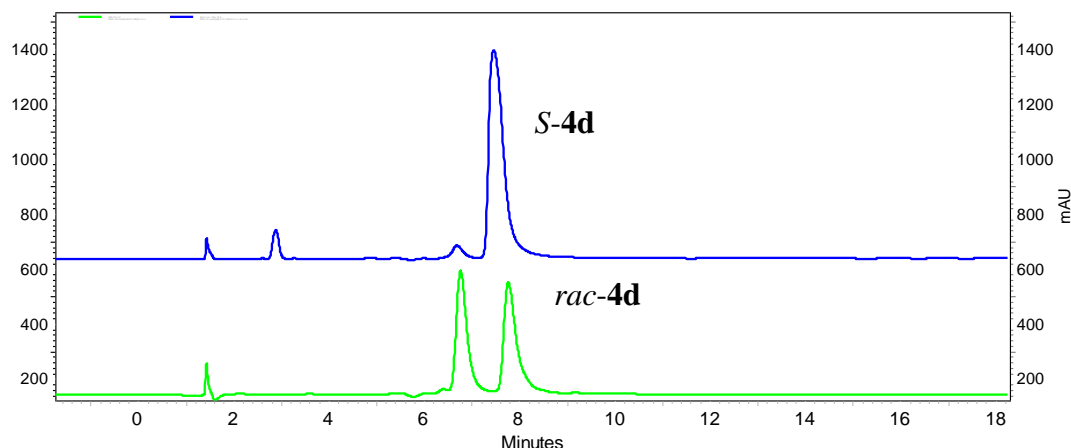
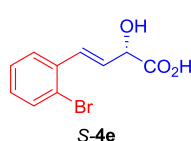


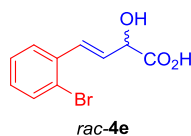
**Figure S4.** CPHPLC chromatogram of *S*-4d from DpkA<sub>psyrin</sub> catalysis (A) *rac*-4d (B). Conditions: CHIRALPACK® ID, flow rate 1 mL min<sup>-1</sup> at 30 °C and detection at 254 nm. Isocratic elution hexane + 0,1% TFA: *i*PrOH + 0,1% TFA 90:10 (v/v), tr (*R*) = 8.3 min, tr (*S*) = 9.3 min.

**(*S,E*)-4-(2-bromophenyl)-2-hydroxybut-3-enoic acid (*S*-4e).**



The title compound was prepared as described for *S*-4b, starting from **1e** (150 mg). *S*-4e was obtained as a white solid (163 mg, 78%). <sup>1</sup>H NMR (400 MHz, DMSO) δ 7.66 (d, *J* = 6.2 Hz, 1H), 7.62 (d, *J* = 8.0 Hz, 1H), 7.36 (t, *J* = 2x6.9, Hz, 1H), 7.20 (td, *J* = 7.7, 7.6, 1.7 Hz, 1H), 6.99 (dd, *J* = 15.8, 1.9 Hz, 1H), 6.41 (dd, *J* = 15.8, 5.1 Hz, 1H), 4.75 (dd, *J* = 5.2, 2.0 Hz, 1H). <sup>13</sup>C NMR (101 MHz, DMSO) δ 173.4, 135.7, 132.9, 131.4, 129.5, 128.1, 128.0, 127.2, 122.9, 70.6.

**(*E*)-4-(2-bromophenyl)-2-hydroxybut-3-enoic acid (*rac*-4e).**



Synthesis of title compound was performed as described for *rac*-4b starting from **3e** (100 mg). *rac*-4e was obtained as a white solid (90 mg, 90%). NMR spectra were indistinguishable from that of *S*-4e.



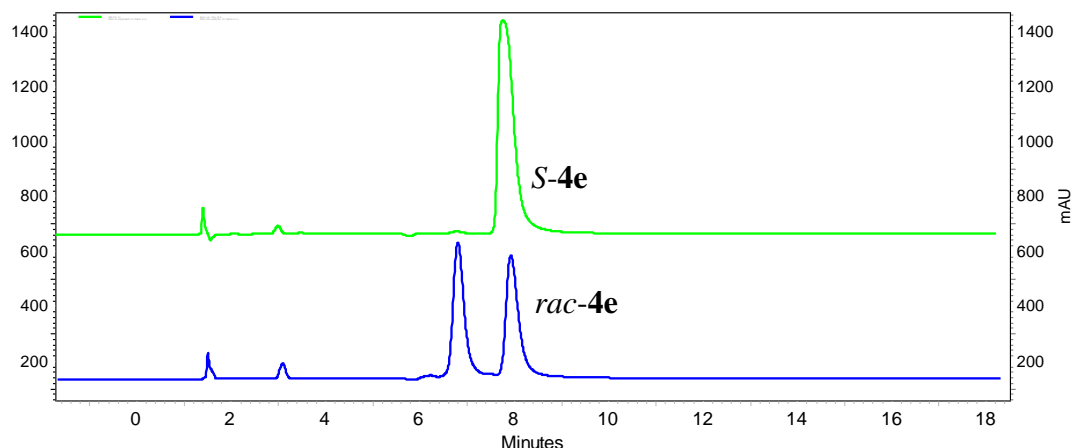
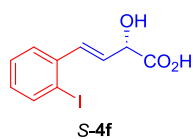


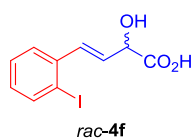
**Figure S5.** CPHPLC chromatogram of *S*-**4e** from DpkA<sub>Psyrim</sub> catalysis (A) *rac*-**4e** (B). Conditions: CHIRALPACK® ID, flow rate 1 mL min<sup>-1</sup> at 30 °C and detection at 254 nm. Isocratic elution hexane + 0,1% TFA: *i*-PrOH + 0,1% TFA 90:10 (v/v). tr (*R*) = 7.4 min, tr (*S*) = 8.4 min.

**(*S,E*)-2-hydroxy-4-(2-iodophenyl)but-3-enoic acid (*S*-**4f**).**



The title compound was prepared as described for *S*-**4b**, starting from **3f** (160 mg). *S*-**4f** was obtained as a white solid (158 mg, 75%). <sup>1</sup>H NMR (400 MHz, DMSO) δ 7.87 (dd, *J* = 7.9, 1.3 Hz, 1H), 7.59 (dd, *J* = 7.9, 1.7 Hz, 1H), 7.37 (td, *J* = 2x7.6, 1.3 Hz, 1H), 7.02 (td, *J* = 2x7.6, 1.6 Hz, 1H), 6.86 (dd, *J* = 15.7, 1.9 Hz, 1H), 6.33 (dd, *J* = 15.7, 5.1 Hz, 1H), 4.74 (dd, *J* = 5.1, 2.0 Hz, 1H). <sup>13</sup>C NMR (101 MHz, DMSO) δ 173.4, 139.4, 138.9, 133.0, 131.2, 129.5, 128.7, 126.6, 100.2, 70.5.

**(*E*)-2-hydroxy-4-(2-iodophenyl)but-3-enoic acid (*rac*-**4f**).**



Synthesis of title compound was performed as described for *rac*-**4b** starting from **3f** (100 mg). *rac*-**4f** was obtained as a white solid (98 mg, 98%). NMR spectra were indistinguishable from that of *S*-**4f**.

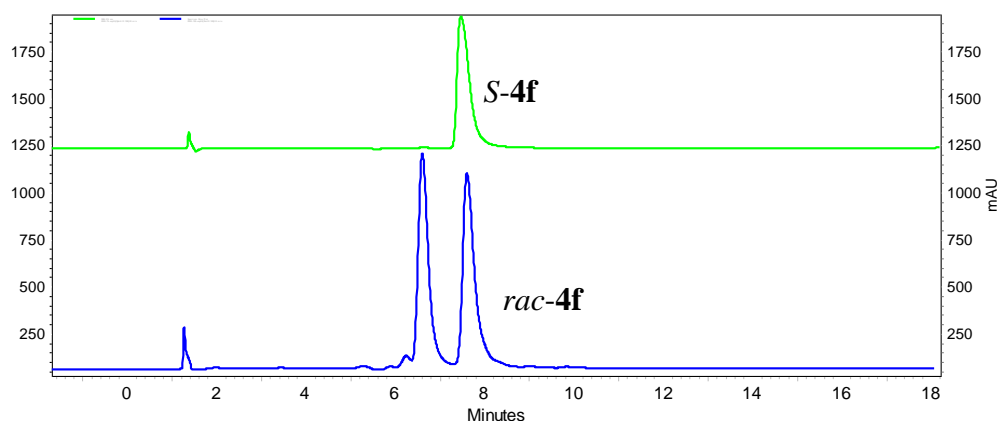
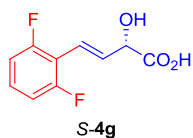


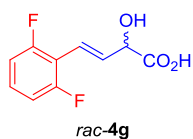
**Figure S6.** CPHPLC chromatogram of *S*-**4f** from DpkA<sub>Psyrin</sub> catalysis (A) *rac*-**4f** (B). Conditions: CHIRALPACK® ID, flow rate 1 mL min<sup>-1</sup> at 30 °C and detection at 254 nm. Isocratic elution hexane + 0,1% TFA: *i*PrOH + 0,1% TFA 90:10 (v/v). tr (*R*) = 8.4 min, tr (*S*) = 9.3 min.

**(*S,E*)-4-(2,6-difluorophenyl)-2-hydroxybut-3-enoic acid (*S*-**4g**).**



The title compound was prepared as described for *S*-**4b**, starting from **1g** (130 mg). *S*-**4g** was obtained as a white solid (138 mg, 70%). <sup>1</sup>H NMR (400 MHz, DMSO) δ 7.36 (tt, *J* = 8.5, 8.5, 6.5, 6.5 Hz, 1H), 7.13 (t, *J* = 8.6, 8.6 Hz, 2H), 6.73 (dd, *J* = 16.3, 1.8 Hz, 1H), 6.61 (dd, *J* = 16.4, 4.7 Hz, 1H), 4.77 (dd, *J* = 4.7, 1.8 Hz, 1H). <sup>13</sup>C NMR (101 MHz, DMSO) δ 173.3, 161.3 (d, *J* = 8.0 Hz), 158.8 (d, *J* = 7.8 Hz), 135.1 (t, *J* = 7.6, 7.6 Hz), 129.3 (t, *J* = 10.9, 10.9 Hz), 115.8, 113.1, 112.1 (d, *J* = 6.3 Hz), 111.9 (d, *J* = 6.2 Hz).

**(*E*)-4-(2,6-difluorophenyl)-2-hydroxybut-3-enoic acid (*rac*-**4g**).**



Synthesis of title compound was performed as described for *rac*-**4b** starting from **3g** (100 mg). *rac*-**4g** was obtained as a yellow solid (90 mg, 90%). NMR spectra were indistinguishable from that of *S*-**4g**.

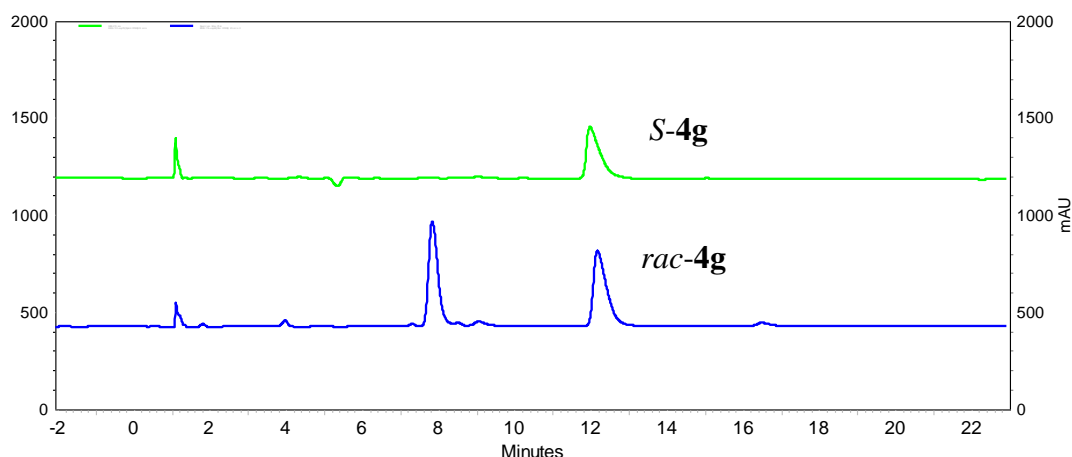
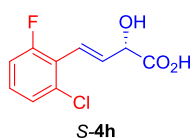


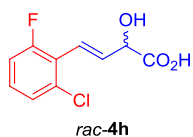
**Figure S7.** CPHPLC chromatogram of *S*-**4g** from DpkA<sub>Psyrim</sub> catalysis (A) *rac*-**4g** (B). Conditions: CHIRALPACK® ID, flow rate 1 mL min<sup>-1</sup> at 30 °C and detection at 254 nm. Isocratic elution hexane + 0,1% TFA: *i*PrOH + 0,1% TFA 90:10 (v/v). tr (*R*) = 9.9 min, tr (*S*) = 14.0 min.

**(*S,E*)-4-(2-chloro-6-fluorophenyl)-2-hydroxybut-3-enoic acid (*S*-**4h**).**



The title compound was prepared as described for *S*-**4b**, starting from **1g** (130 mg). *S*-**4h** was obtained as a white solid (160 mg, 85%). <sup>1</sup>H NMR (400 MHz, DMSO) δ 7.36 (td, *J* = 7.9, 7.8, 2.1 Hz, 2H), 7.33 – 7.22 (m, 1H), 6.83 (dd, *J* = 16.3, 2.0 Hz, 1H), 6.57 (ddd, *J* = 16.3, 4.7, 1.1 Hz, 1H), 4.78 (dd, *J* = 4.8, 2.0 Hz, 1H). <sup>13</sup>C NMR (101 MHz, DMSO) δ 173.3, 161.7, 159.2, 136.0 (d, *J* = 11.8 Hz), 129.4 (d, *J* = 10.4 Hz), 125.9 (d, *J* = 3.4 Hz), 122.6 (d, *J* = 14.7 Hz), 119.7, 115.2 (d, *J* = 23.4 Hz), 70.8.

**(*E*)-4-(2-chloro-6-fluorophenyl)-2-hydroxybut-3-enoic acid (*rac*-**4h**).**



Synthesis of title compound was performed as described for *rac*-**4b** starting from **3h** (100 mg). *rac*-**4h** was obtained as a white solid (90 mg, 90%). NMR spectra were indistinguishable from that of *S*-**4h**.

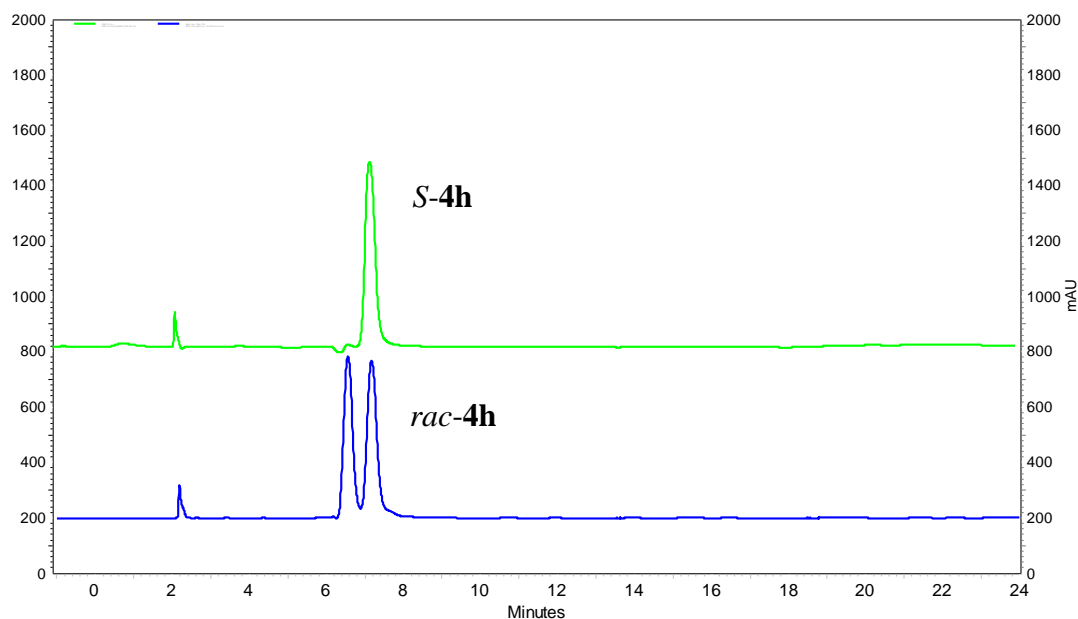
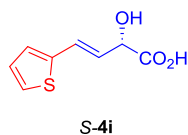


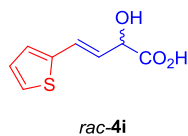
**Figure S8.** CPHPLC chromatogram of *S-4h* from  $DpkA_{P_{\text{Syrin}}}$  catalysis (A) *rac-4h* (B). Conditions: CHIRALPACK® ID, flow rate 1 mL min<sup>-1</sup> at 30 °C and detection at 254 nm. Isocratic elution hexane + 0,1% TFA: *i*-PrOH + 0,1% TFA 90:10 (v/v), tr (*R*) = 7.7 min, tr (*S*) = 8.2 min.

**(*S,E*)-2-hydroxy-4-(thiophen-2-yl)but-3-enoic acid (*S-4i*).**



The title compound was prepared as described for *S-4b*, starting from **3f** (100 mg). *S-4i* was obtained as a white solid (94 mg, 57%). <sup>1</sup>H NMR (400 MHz, DMSO) δ 7.42 (d, *J* = 5.0 Hz, 0H), 7.11 (d, *J* = 3.5 Hz, 1H), 7.01 (dd, *J* = 5.1, 3.5 Hz, 1H), 6.85 (dd, *J* = 15.7, 1.8 Hz, 1H), 6.08 (dd, *J* = 15.7, 5.6 Hz, 1H), 4.64 (dd, *J* = 5.6, 1.8 Hz, 1H). <sup>13</sup>C NMR (101 MHz, DMSO) δ 173.6, 141.1, 127.8, 127.2, 126.5, 125.2, 123.7, 70.5.

**(*E*)-2-hydroxy-4-(thiophen-2-yl)but-3-enoic acid (*rac-4i*).**



Synthesis of title compound was performed as described for *rac-4b* starting from **3i** (45 mg). *rac-4i* was obtained as a white solid (43 mg, 96 %). NMR spectra were indistinguishable from that of *S-4i*.

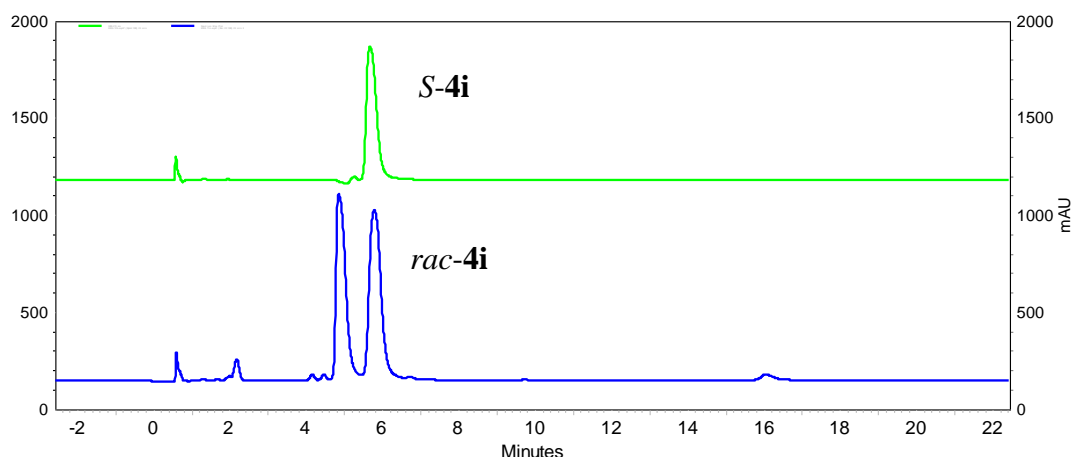


**Figure S9.** CPHPLC chromatogram of *S-4i* from  $DpkA_{P_{syrin}}$  catalysis (A) *rac-4i* (B). Conditions: CHIRALPACK® ID, flow rate 1 mL min<sup>-1</sup> at 30 °C and detection at 254 nm. Isocratic elution hexane + 0,1% TFA: *i*-PrOH + 0,1% TFA 90:10 (v/v).  $t_r$  (*R*) = 7.5 min,  $t_r$  (*S*) = 8.3 min.

### Steady-state kinetic studies of $DpkA_{P_{syrin}}$ for sodium pyruvate.

The kinetic parameters for  $DpkA_{P_{syrin}}$  were determined in a continuous assay method monitoring the oxidation of NADPH to NADP<sup>+</sup> at 340 nm (NADPH  $\epsilon_{340} = 6.22 \text{ mM}^{-1} \text{ cm}^{-1}$ ) using sodium pyruvate as substrates (**Figure S10A**). The reaction was monitored during 15 min measuring each 30 s. The assay mixture (0.3 mL) consisted of 50 mM Tris-HCl buffer pH 8.0, containing NADPH (0.16 mM), sodium pyruvate (1-60 mM) and appropriate amounts of enzymes (optimal range of enzyme concentration determined for each substrate, **Figure S10B**). One unit of activity was defined as the amount of enzyme that catalyze the formation of 1  $\mu\text{mol}$  NADP<sup>+</sup> per min at 30 °C. Measurements were carried out in triplicate independent experiments. To determine the kinetic parameters, data were fitted to the Michaelis-Menten kinetic model using the software GraphPad Prism version 5.0 (**Figure S10C**).

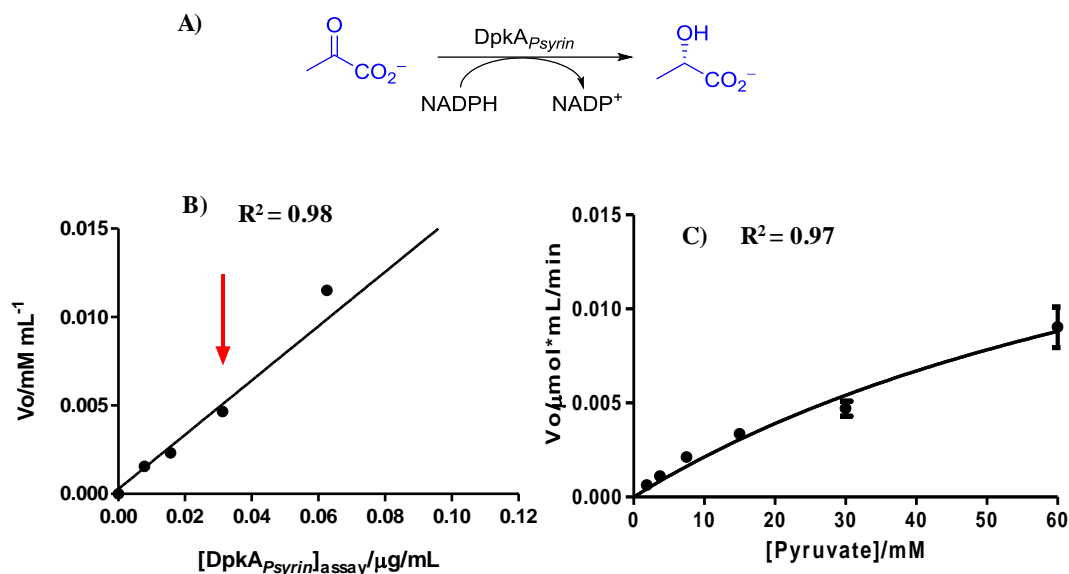


**Figure S10.** Reduction of **3a** to **2R-4a** catalyzed by  $KPR_{Ecoli}$ . (A). Initial reaction rate ( $V_o$ ) vs the enzyme concentration. The arrow shows the enzyme concentration selected to perform the enzyme assay (B) and  $V_o$  vs substrate concentration ( $0.01 (K_m^{app}) \leq [S] \leq 0.6 (K_m^{app})$ ), adjusted to a Michaelis-Menten model by non-linear regression method (C). Each point is the mean of three independent experiments.

### X-Ray structures

Suitable single crystals for X-ray structural analysis of (*S*)-**4c**, (*S*)-**4d**, and (*S*)-**4e** were obtained at room temperature. Compounds (*S*)-**4c**, (50mg), (*S*)-**4d** (30 mg), and (*S*)-**4e** (50 mg) were dissolved in Hexane:Et<sub>2</sub>O 2:1 (v/v) (3 mL). Crystals were obtained by evaporation in glass vials (6 mL, 3.5 cm, Ø 1.4 cm) after 48 h at 25 °C. The X-ray diffraction analysis indicates that  $DpkA_{Psytrin}$  having *S* configuration (Table S3).

**Table S3.** X-ray Crystallographic partial data.

Identification code	<i>S</i> - <b>4c</b>	<i>S</i> - <b>4d</b>	<i>S</i> - <b>4e</b>
CCDC number			
Bond precisión C-C	0.0084 Å	0.0088 Å	0.0162 Å
Wavelength	1.54178	0.71073	0.71073
Cell	a=3.9579(2) b=5.8045(3) c=38.6073(17) $\alpha=90 \beta=90 \gamma=90$	a=9.4407(4) b=10.4356(6) c=20.2586(9) $\alpha=90 \beta=90 \gamma=90$	a=9.5962(3) b=10.4564(4) c=20.4188(9) $\alpha=90 \beta=90 \gamma=90$
Temperature	120 K	120 K	120 K
Volume	886.95(8)	1995.87(17)	2048.86(14)
Space group	P 21 21 21	P 21 21 21	P 21 21 21

Hall group	P 2ac 2ab	P 2ac 2ab	P 2ac 2ab
Moiety formula	C <sub>10</sub> H <sub>9</sub> F O <sub>3</sub>	C <sub>10</sub> H <sub>9</sub> Cl O <sub>3</sub>	C <sub>10</sub> H <sub>9</sub> Br O <sub>3</sub>
Sum formula	C <sub>10</sub> H <sub>9</sub> F O <sub>3</sub>	C <sub>10</sub> H <sub>9</sub> ClO <sub>3</sub>	C <sub>10</sub> H <sub>9</sub> Br O <sub>3</sub>
Mr	196.17	212.62	257.07
Dx,g cm-3	1.469	1.415	1.667
Z	4	8	8
Mu (mm-1)	1.044	0.359	3.990
F000	408.0	880.0	1024.0
F000'	409.56	881.63	1022.26
h,k,lmax	4,6,46	12,13,26	12,13,26
Nref	1605[1011]	4887[2776]	4923[2795]
Tmin,Tmax	0.829,0.930	0.933,0.986	0.419,0.595
Tmin'	0.701	0.879	0.384
Data completeness	1.53/0.96	1.73/0.98	1.75/0.99
Theta(max)	67.713	Theta(max)= 28.128	27.927
S	1.108	1.107	1.114
wR2(reflections)	0.2173(1544))	0.1332(4789)	0.2176(4886)
R(reflections)=	0.0716(1291)	0.0637( 3589)	0.0807(4180)

## References

1. Moreno, C. J.; Hernández, K.; Charnok, S. J.; Gittings, S.; Bolte, M.; Joglar, J.; Bujons, J.; Parella, T.; Clapés, P., Synthesis of  $\gamma$ -hydroxy- $\alpha$ -amino acid derivatives by enzymatic tandem aldol addition–transamination reactions. *ACS catalysis* **2021**, *11* (8), 4660-4669.
2. Moreno, C. J.; Hernández, K.; Gittings, S.; Bolte, M.; Joglar, J. s.; Bujons, J.; Parella, T.; Clapés, P., Biocatalytic Synthesis of Homochiral 2-Hydroxy-4-butyrolactone Derivatives by Tandem Aldol Addition and Carbonyl Reduction. *ACS Catalysis* **2023**, *13*, 5348-5357.
3. Eaton, R. W., trans-o-Hydroxybenzylidenepyruvate Hydratase-Aldolase as a Biocatalyst. *Applied and environmental microbiology* **2000**, *66* (6), 2668-2672.
4. Fansher, D. J.; Ngwira, N.; Salehi, A. R.; Woods, J.; Cascao, A.; Palmer, D. R., Biocatalytic Synthesis of  $\alpha$ ,  $\beta$ -Unsaturated 2-Keto Acids and Derivatives Using the Promiscuous Aldolase, NahE. *Synthesis* **2023**, *55* (01), 75-89.